BRAIN STIMULATION
MODELS, EXPERIMENTS AND OPEN QUESTIONS
HIVE DELIVERABLE D1.1

P. C. MIRANDA
F. WENDLING
G. RUFFINI (ED)
I. MERLET
B. MOLAEE-ARDEKANI
S. DUNNE
A. SORIA-FRISCH
D. WHITMER

hiVE

HYPER
INTERACTION
VIABILITY
EXPERIMENTS

HYPER
INTERACTION
VIABILITY
EXPERIMENTS

HIVE: Hyper Interaction Viability Experiments
EU FP7 FET OPEN - 222079

Brain Stimulation: models, experiments and open questions

WORK PACKAGE: WP1 – Biophysical models

DELIVERABLE D1.1
Review of state-of-the-art in currents distribution and effects

P. C. Miranda (FFCUL), F. Wendling, I. Merlet,
B. Molaee-Ardekani (INSERM), G. Ruffini (Ed.),
S. Dunne, A. Soria-Frisch and D. Whitmer (Starlab)

EXECUTIVE SUMMARY

This document is a deliverable of WP1 of HIVE, and more concretely of Activity A1.1—*Review of the state-of-the-art in currents distribution and effects modeling.* It is a companion to D3.1, the *Review of the state of the art in human stimulation.*

The expected results of WP1 are better models for current propagation in the brain resulting from multisite stimulation, better characterization of biological effects of electrical currents on neurons, neuronal ensembles and the brain as a whole, and improved understanding of potential safety issues in current stimulation. The initial part of this work, and the subject of the current document, is to carry out a review of the science and technology in the modeling of stimulation-induced current distributions and the electric field in the brain (animal or human). It will also review modern paradigms for brain function and the interaction of induced currents with neurons and neuronal populations.

In this deliverable we analyze the state of the art in biophysical modeling of transcranial electrical and magnetic brain stimulation. The focus of this work is a review of models of currents and fields induced by stimulation, and a review of the effects of the induced electric fields on neurons and neuronal ensembles.

The analysis starts with a review of the basic physics of the problem: the Poisson equation in conductive media, the quasi-static and steady-state approximations, dielectric properties of the the brain tissues, and the currents and fields induced by tDCS and TMS stimulation technologies.

Then we focus on with the interaction of the induced fields on single neurons and on neuronal ensembles. We cover both modeling aspects at the single neuron and assembly level and experimental findings both in vitro and at the global brain scale using tDCS and TMS. Transcranial stimulation variants such as tACS and tRNS are discussed, and we also provide an overview of the relevance of resonance concepts to the interaction of fields with neuronal circuits at different scales.

Finally, we review what we know and what we don't know about transcranial brain stimulation, and provide suggestions for future modeling and experimental work on the project.

DELIVERABLE IDENTIFICATION SHEET

IST Project No.	FP7 – FET Open – 222079
Acronym	**HIVE**
Project URL	http://www.hive-eu.org/
EU Project Officer	Aymard De-Touzalin

Deliverable	**D1.1– Review of state-of-the-art in currents distribution and effects**
Work Package	**WP1– Biophysical models**

Date of delivery	**Contractual**	M4	**Actual**	09 June, 2009
Status	v1.3		Reviewed by QCB	
Nature	Report			
Dissemination	Public			

Authors (Partner)	P. C. Miranda (FFCUL), F. Wendling, I. Merlet, B. Molaee-Ardekani (INSERM), G. Ruffini (Ed.), S. Dunne, A. Soria-Frisch and D. Whitmer (Starlab)			
Responsible Author	G. Ruffini (Ed.)	**Email**	giulio.ruffini@starlab.es	
	Partner	Starlab	**Phone**	+34 93 254 03 62

Abstract (for dissemination)	We analyze the state of the art in biophysical modeling of transcranial electrical and magnetic brain stimulation. We review models of currents and field models by stimulation, and of the effects of the induced electric fields on neurons and neuronal ensembles. We start with a review of the basic physics of the problem: the Poisson equation in conductive media, the quasi-static and steady-state approximations, dielectric properties of the the brain tissues, and the currents and fields induced by tDCS and TMS stimulation technologies. Then we focus on with the interaction of the induced fields on single neurons and on neuronal ensembles. We cover both modeling aspects at the single neuron and assembly level and experimental findings both in vitro and at the global brain scale using tDCS and TMS. Transcranial stimulation variants such as tACS and tRNS are discussed, and we also provide an overview of the relevance of resonance concepts to the interaction of fields with neuronal circuits at different scales.
Keywords	Biophysics, Computational Neuroscience

Version Log				
Issue date	**Rev. No.**	**Author**	**Actual**	**Change**
09 June, 2009	v1.3	G. Ruffini (Ed.)	09 June, 2009	Final Version

Contents

Chapter 1

INTRODUCTION

1 About HIVE

Could computers someday interact directly with the human brain?

The vision of this four-year project is that in the next 50 years we will witness the coming of age of technologies for fluent brain-computer and computer-mediated brain-to-brain inter-action. While recent research has delivered important breakthroughs in brain-to-computer transmission, little has been achieved in the other direction : computer-controlled brain stimulation. The project's goals is to research stimulation paradigms to design, develop and test a new generation of more powerful and controllable non-invasive brain stimulation technologies. Starting from current distribution and multi-scale neuron-current interaction modeling and stimulation experiments using tDCS, TMS, EEG and fMRI in different scenarios, the project will develop multisite transcranial current stimulation technologies implementing real time EEG monitoring and feedback. It will explore high-level communication using stimulation, stimulation during different states of consciousness, stimulation and therapy, as well as sense synthesis, that is, the construction of new perceptions deriving from sensors interacting directly with brains through stimulation systems—all with the goal of probing the limits of non-invasive computer-to-brain interfaces. The project will develop biophysical models for multisite stimulation, carry out stimulation experiments with animals and humans, and integrate the results to develop and test new multisite technologies for interaction. Given the fundamental role of interaction in human experience, advances in this area can deliver breakthrough information society technologies of great value in addition to advancing the state-of-the-art in fundamental neuroscience research, neurology diagnosis and therapy.

2 The biophysics and physiology of stimulation

This document is a deliverable from of WP1 of HIVE, and more concretely of Activity A1.1—*Review of the state-of-the-art in currents distribution and effects modeling.* WP1 is to develop better models for current propagation in the brain resulting from multisite stimulation, better characterization of biological effects of electrical currents on neuron, neuronal ensembles and the brain and improved understanding of potential safety issues in current stimulation and recommendations. As the initial part of this work and the subject of the current document, this activity will carry out a review of science and technology in the modeling of stimulation-induced current distributions and the electric field in the brain (animal or human). It will

also review the current understanding of the interaction of induced currents with neurons and neuronal populations.

Chapter 1 focuses on the electric field generated by stimulation, starting from a description of the basic equations (the Poisson equation for conductive media), the quasi-static approximation, steady-state condition and dielectric properties of tissues, and then technical aspects of tCS (tDCS, tACS and tRNS) and TMS. Chapter 2 describes modeling and experimental aspects of the interaction of electric fields with neurons and populations of neurons, including resonance effects. The Appendices provide more examples and provide and in-depth analysis of some electromagnetic aspects.

This report is the result of an intense and rewarding interdisciplinary collaboration in the project. Chapter and/or section editors are identified by their initials. Figures from other papers have been taken for this report without requesting permission from their authors.

Chapter 2

THE ELECTRIC FIELD

1 The Poisson equation [GR]

We are interested here in electromagnetic brain stimulation. This is achieved by imposing some external field on brain tissues. Such fields give rise to currents in brain tissues, and these, in turn, give rise to charge accumulations. As we will see, charges accumulate wherever there is a change in conductivity (e.g., at tissue boundaries, or at the scalp-air interface).

Regardless of the origin, the result of endogenous activity or externally forcing is an electromagnetic field. This field is what will change brain activity by coupling to neurons. In fact, due to the low frequencies and intensities of interest here, it is the electric field that dominates this interaction.

Natural (endogenous) or artificial electric fields in a conductive medium (such as the interior or exterior of the cell) produce Ohmic currents of the form $J^\Omega = \sigma E$. In general we can express the current[1] as a sum of Ohmnic and non-Ohmnic parts,

$$J = J^I + \sigma E, \tag{2.1}$$

where σ is the conductivity and J^I is the non-Ohmnic current component (the 'I' superscript refers to the sometimes used term 'impressed current'). The units of E are V/m, those of J are A/m^2, those of σ are 1/(Ohm m).

The continuity equation (charge conservation) is

$$\nabla \cdot J + \frac{\partial \rho}{\partial t} = 0. \tag{2.2}$$

where ρ is the charge density. If we assume that we are in a near steady-state situation,

$$\frac{\partial \rho}{\partial t} = 0,$$

J is proportional to the curl of the magnetic field—that is, we assume the displacement current is small. Then, we can write

$$\nabla \cdot J = 0$$

and therefore

$$\nabla \cdot J^I + \nabla \cdot (\sigma E) = 0. \tag{2.3}$$

---

[1]See the Appendices for some background EM theory.

which is known as Poisson's equation when expressed as a function of the potential ($E = -\nabla\varphi$). This is fully equivalent to the continuity equation under steady state. If we assume a constant conductivity σ, and using $\nabla \cdot E = 4\pi\rho/\epsilon$ we can write

$$\nabla \cdot J^I + 4\pi\frac{\sigma}{\epsilon}\rho = 0, \tag{2.4}$$

or

$$\rho = -\frac{\epsilon}{4\pi\sigma}\nabla \cdot J^I. \tag{2.5}$$

This equation indicates that associated to the impressed currents there is a charge density. More specifically, *charges arise where impressed current density field lines are born or die.* Thus, in order to compute the resulting fields in the scalp we can already state that the impressed current sources or sinks will give rise to local charges, which are the ultimate sources of the electric potential. This may seem surprising, but is in fact the mechanism behind phenomena like the voltage drop across a resistor.

1.1 Variable conductivity and charge density

So far we have assumed a constant conductivity. Here we show directly that spatial variations in conductivity lead to charge accumulations. Recall that

$$0 = \nabla \cdot J^I + \nabla \cdot (\sigma E) = \nabla \cdot J^I + \sigma\nabla \cdot E + E \cdot \nabla\sigma, \tag{2.6}$$

hence

$$\rho = -\frac{\epsilon}{4\pi\sigma}\left(\nabla \cdot J^I + E \cdot \nabla\sigma\right). \tag{2.7}$$

So, we see that, in addition to the those associated to the divergence of impressed currents, there will be charges accumulating proportionally to the dot product of the ohmic current density and the gradient of the conductivity. Both phenomena are associated to the finite conductivity of the medium and its spatial behavior: we have charge traffic jams, so to speak. We can make this point clearer by using again Ohm's law and the definition of resistivity ($r = 1/\sigma$),

> *Under steady state, spatial conductivity variations lead to charge accumulations, which then lead to E fields and potentials. When the resistivity increases along the current, positive charge density appears (and vice versa):*
>
> $$\rho = \frac{\epsilon}{4\pi}\left(J \cdot \nabla r - r\nabla \cdot J^I\right). \tag{2.8}$$

Indeed, we can rewrite (ignoring impressed currents)

$$\rho = -\frac{\epsilon}{4\pi\sigma}E \cdot \nabla\sigma$$

in terms of current and resistivity as

$$\rho = \frac{\sigma\epsilon}{4\pi}E \cdot \nabla\left(\frac{1}{\sigma}\right) = \frac{\epsilon}{4\pi}J \cdot \nabla r.$$

An intuition for the physics of the Poisson equation is best developed through the analysis of simple toy models. See the Appendix (Section 4) for some examples.

	10 Hz	100 Hz	1000 Hz	10000 Hz
Lung	0.15	0.025	0.05	0.14
Fatty tissue		0.01	0.03	0.15
Liver	0.2	0.035	0.06	0.2
Heart muscle	0.1	0.04	0.015	0.32

Table 2.1 – Averages of ratio of capacitive to resistive currents for various frequencies and body tissues (from [Plonsey:1969aa])

1.2 TMS vs. tDCS

In the case of brain stimulation we are not concerned with 'micro'-impressed currents, and we simply model the electric field as (Equation 2.3)

$$\nabla \cdot (\sigma E) = 0. \tag{2.9}$$

This equation applies whether we are concerned with tCS or TMS. In the first case, tDCS, this equation is solved by imposing boundary conditions (no outward current at the scalp, conditions at the electrodes, etc.). If a step function model is used for the conductivity, i.e., the conductivity is assumed constant at each of the layers, the equation to solve is Laplace's

$$0 = \nabla \cdot E = -\nabla^2 \varphi$$

with the addition of boundary conditions at each boundary layer.

The case of TMS is solved by dividing first the field as a sum of the external 'primary' field (which can be calculated from coil parameters and expressed from the vector potential) and the 'secondary' field (expressed as the gradient of a potential)

$$E = -\partial_t A - \nabla \varphi. \tag{2.10}$$

and the equation for the fields becomes

$$0 = \nabla \cdot (\sigma \left[\partial_t A + \nabla \varphi \right]). \tag{2.11}$$

Again, if constant conductivity is assumed, the situation reverts to Laplace's equation (which holds for each region of constant conductivity for the secondary potential, which is Coulombic in nature)

$$0 = \nabla \cdot (\partial_t A + \nabla \varphi) = \nabla \cdot \partial_t A + \nabla^2 \varphi.$$

More generally, if we work in the Coulomb gauge, $\nabla \cdot A = 0$, we can write Equation 2.9 as

$$0 = \nabla \cdot (\sigma(\partial_t A + \nabla \varphi)) = \partial_t A \cdot \nabla \sigma + \nabla(\sigma \nabla \varphi) = \partial_t A \cdot \nabla \sigma - \nabla(\sigma E_s). \tag{2.12}$$

2 The quasistatic approximation [PCM, GR]

The frequencies involved in transcranial magnetic and electric stimulation lie in the range DC-10 kHz. At the lower frequency end we have tDCS and at the higher frequency end we have monophasic TMS pulses [Kammer:2001aa] whose frequency spectrum peaks at about 3

kHz. Given the low frequencies involved and the dielectric properties of the head's tissues (conductivity $\sigma < 1$ S/m and relative permittivity $\varepsilon_r \sim 10^5$), several approximations can be made which simplify the determination of the electric field distribution [Plonsey:1967aa, Sarvas:1987aa, Roth:1991aa, Heller:1992aa]

The first approximation consists in neglecting propagation effects and is justified by the fact that the wavelength associated with the low frequencies used in transcranial stimulation is several orders of magnitude larger than the dimensions of the human head. This means that the electric field varies with no significant phase differences throughout the brain. The second approximation is related to the fact that the effect of the magnetic field produced by the currents in the tissue is negligible both in electric and magnetic stimulation. In the third approximation, capacitive effects are neglected and the tissue is treated as purely resistive. Then, charge accumulation at tissue boundaries can be considered to occur instantaneously.

The main consequences of the quasistatic approximation are that the spatial and the temporal variations of the electric field can be described separately and that the time variation of the total electric field in the brain is determined by the stimulus waveform. Also, for TMS, the contribution of the induced currents to the total magnetic field can be neglected.

A more detailed analysis of the quasi-static assumption is provided in the Appendices.

3   Low frequency dielectric properties of brain tissues [PCM]

The dielectric properties of the tissues used in the head models will have a significant impact on the computation of the electric field distribution in the brain during transcranial stimulation. The choice of the correct values for these parameters is more critical for transcranial electrical stimulation than for transcranial magnetic stimulation. As far as the electric field is concerned, only the ratio of the different conductivity values is relevant.

The frequency dependence of the electrical conductivity, σ, and of the relative permittivity, ε_r, of a typical biological tissue is illustrated in Figure 2.1. In general, the relationship between the applied electric field, $\vec{E}$, and the total current density, $\vec{J}$, is given by $\vec{J} = \sigma\vec{E}$, where $\sigma = \sigma + j\omega\,\varepsilon_0\varepsilon_r$ is the complex conductivity of the tissue. Below 10 kHz, the conductivity is approximately constant whereas the relative permittivity tends to increase by one or two orders of magnitude. Even so, biological tissues are predominantly resistive in this frequency range, i.e. $\omega\,\varepsilon_0\varepsilon_r < \sigma$.

One of the earliest references for low frequency resistive properties of biological tissues is the compilation by [Geddes:1967aa], which was updated later in [Geddes:1989aa]. In 1979, [Foster:1979aa] reviewed the data available on the dielectric properties of brain tissue between 0.01 and 10 GHz and later summarized some general principles and data in a chapter entitled "Dielectric properties of tissues" in [Polk:1996aa]. Other reviews were presented by [Stuchly:1980aa] and [Duck:1990aa]. A comprehensive study of the dielectric properties of tissues was reported by Gabriel et al. in a series of three papers [Gabriel:1996aa, Gabriel:1996ab, Gabriel:1996ac]. Experimental data were fitted across a wide frequency range for many different tissues and the results are available on-line[2]. A meta-analysis of the electric conductivity of human tissues was performed by [Faes:1999aa]. Many of the measurements reported in the literature were performed on animal tissues.

For a given tissue, the low frequency data in the literature present a wide range of values, reflecting both physiological variability in tissue properties and differences in measurement
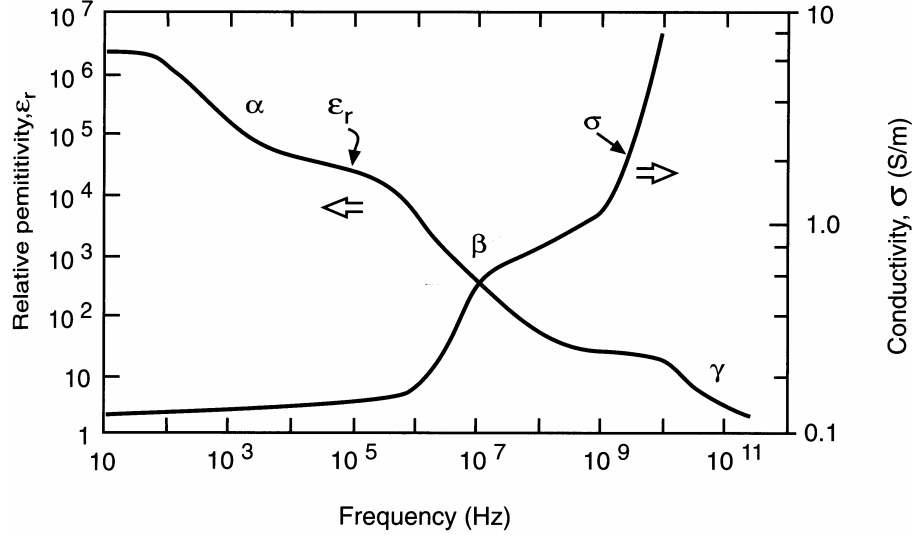
---

[2] http://niremf.ifac.cnr.it/tissprop

Figure 2.1 – Frequency variation of dielectric properties of typical soft tissue (from [Reilly:1998aa])

conditions and methods. Here, the data for the main brain tissues are reviewed with the aim of obtaining average conductivity values to use in a realistic head model with a limited number of tissue types. Reported data were obtained at frequencies ≤ 10 kHz and were obtained in normal tissues since pathology will affect conductivity [Crile:1922aa, Akhtari:2006aa]. In more sophisticated models, *in-vivo* patient specific conductivity values may be derived from diffusion tensor MRI [Tuch:2001aa].

3.1 Scalp

The scalp is made up mainly of three different tissues: skin, fat and muscle. Because of its heterogeneous nature and the anisotropy of muscle, the local conductivity within the scalp can vary by as much as a factor of 20.

The conductivity of muscle is strongly influenced by the direction of its fibres. In the longitudinal direction, reported conductivity values vary between 0.333 S/m and 0.935 S/m, with an average value of 0.624 S/m. In the perpendicular direction, the conductivity values vary between 0.043 and 0.350 with an average value of 0.131 S/m [Burger:1961aa, Rush:1963aa, Epstein:1983aa, Gielen:1984aa, Gielen:1986aa, Gabriel:1996ac, Zheng:1984aa, Faes:1999aa].

Fat has a low conductivity, ranging from 0.026 S/m to 0.046 S/m, with an average value of 0.036 S/m [Hemingway:1932aa, Schwan:1956aa, Rush:1963aa, Geddes:1967aa, Rigaud:1994aa, Gabriel:1996ac]. A high proportion of fat may have a significant impact on the scalp's conductivity.

The skin's deeper layers have a high conductivity, 0.5263 S/m, but the dry superficial skin is very resistive, 0.0001 S/m [Yamamoto:1976aa, Yamamoto:1976ab]. Dead and dry skin should be removed by abrasion before attaching electrodes.

As for a conductivity value representative of the scalp, some authors use an average value of skin and muscle of 0.336 S/m [Wolters:1999aa]. However, the most often used value is 0.435 S/m, measured *in vivo* using DC and a 4-electrode method by [Burger:1961aa]. Moreover, [Rush:1968aa] used a similar value of 0.45 S/m. Recently, [Goncalves:2003aa] used

an electrical impedance tomography based method together with a realistic head model with 3 tissues to deduce the effective conductivity values of scalp, skull and brain at 60 Hz. The average scalp conductivity value from six subjects was 0.332 S/m at 60 Hz.

3.2 Skull

Bone generally consists of a harder layer of cortical bone that surrounds a softer part, the cancellous bone. The conductivity of cancellous bone is approximately 4 times higher than that of cortical bone: 0.081 S/m vs 0.020 S/m [Gabriel:1996ab]. These values are almost constant in the frequency range DC to 10 kHz. The permittivity is also low so capacitive effects can be neglected, except perhaps for cancellous bone at frequencies below 100 Hz.

In the case of the skull there are three layers: 2 outer cortical layers that enclose a central cancellous layer, which means that the conductivity of the skull is anisotropic. Another important factor is the conductivity of the skull is not uniform due to the variation of its thickness in different parts of the head. Finally, the existence of sutures and natural openings provide localized low resistance paths for current [Law:1993aa].

Despite the limitations involved in estimating an average conductivity value for the skull, several measurements have been reported for human skulls. The average of the values reported by Law is 0.013 S/m [Law:1993aa]. [Oostendorp:2000aa] measured the conductivity of a skull specimen *in vitro*. They estimated the conductivity of the skull by combining measurements with a model of the head and report a value of 0.015 S/m. [Akhtari:2002aa] measured the conductivity of the 3 skull layers in skull flaps excised from four patients undergoing intracranial surgery . The average bulk conductivity was 0.010 S/m. [Hoekema:2004aa] measured unusually high values ranging from 0.032 S/m to 0.080 S/m in samples temporarily removed during epilepsy surgery. [Goncalves:2003aa] estimated an average value of 0.008 S/m using the method already described in the previous section. These values are higher than the value of 0.0056 S/m originally introduced by [Rush:1968aa].

3.3 CSF

There are few measurements of the conductivity of CSF [Crile:1922aa, Radvan-Ziemnowicz:1964aa]. [Baumann:1997aa] report a value of 1.79 S/m at 37 $^\text{o}$C that is constant in the range 10 Hz to 10 kHz.

3.4 Grey matter

Cortical grey matter is usually considered to be homogeneous and isotropic. This is known to be an oversimplification [Hoeltzell:1979aa], but is probably a reasonable approximation for the bulk conductivity at the mm scale. Most measurements yielded values between 0.161 S/m and 0.450 S/m in the frequency range of 1 to 10 kHz [Crile:1922aa, Freygang:1955aa, Ranck:1963aa, Van-Harreveld:1963aa, Robillard:1977aa]. Lower values were reported by [Gabriel:1996aa], [Gabriel:1996ab, Gabriel:1996ac], ranging from 0.03 to 0.116 S/m for frequencies of 10 Hz up to 10 kHz. More recently, [Logothetis:2007aa] reported an average value of 0.404 S/m that is practically frequency independent in the range 1 Hz to 10 kHz.

Slightly different values were measured in the cerebellum [Crile:1922aa, Nicholson:1975aa, Okada:1994aa] , the hippocampus [Ranck:1966aa] and the caudate nucleus [Robillard:1977aa].

A value of 0.33 S/m is widely used for grey matter in modeling studies.

3.5 White matter

White matter is anisotropic, with a longitudinal conductivity (along the direction of the fibres) that is 5-10 times greater than its transverse conductivity (perpendicular to the direction of the fibres) [Nicholson:1965aa, Ranck:1965aa]. The longitudinal conductivity of white matter is greater than that of grey matter and its transverse conductivity is lower. Some studies report a single conductivity value that is lower than of grey matter [Crile:1922aa, Freygang:1955aa, Van-Harreveld:1963aa, Robillard:1977aa]. The average value of these "isotropic" conductivity values is 0.18 S/m [Nicholson:1965aa] reports average transverse and longitudinal conductivity values of 0.13 S/m and 1.13 S/m.

3.6 Brain

In the simplest models, the brain may be represented by a single conductivity value. In this case, the value measured by [Goncalves:2003aa] using electric impedance tomography and a 3-layer realistically shaped head model seems appropriate: 0.33 S/m.

3.7 Conclusions

For TMS modeling, there is sufficient conductivity data in the range 1-10 kHz to build a table of conductivity values. Capacitive effects can be ignored because relative permittivities are sufficiently low.

In contrast, there is little DC conductivity data to be used in tDCS calculations. There is even less data in the frequency range 1-100 Hz, which may be the relevant range for tACS. It is generally agreed that the conductivity of biological tissues is relatively constant or decreases slightly at low frequencies [Reilly:1998aa]. This suggests that conductivity values adopted for TMS may be used as a reasonable approximation for values at lower frequencies down to DC.

According to [Gabriel:1996ab], the relative permittivity of several tissues may reach values approaching 10^7 for frequencies below 100 Hz, in which case capacitive effects may no longer be negligible. This is not a problem for finite element packages since the relative permittivity of the tissues can be taken into account, but correct values have to be specified in the model. At the end of their paper, the authors point out that given the lack of data at low frequencies, the fitted data must be used with caution.

Tissue	σ (S/m)
Scalp	0.45
Skull	0.013
CSF	1.8
Grey matter	0.33
White matter – "isotropic"	0.18
White matter - longitudinal	1.1
White matter - transverse	0.13

Table 2.2 – Conductivity values for use in TMS calculations

4 tCS [PCM]

The interest in the application of direct currents (DC) to the human scalp was renewed by the recent demonstration that weak DC currents (typically < 1 mA) have a clear modulatory effect on cortical excitability [Priori:1998aa, Nitsche:2000aa]. The effect can outlast the stimulus, depending on stimulus duration; it can last for 90 min after stimulation when a current of 1 mA is applied for 13 min [Nitsche:2001aa]. These neuromodulatory effects open new possibilities in terms cognitive research and potential therapeutic applications [Nitsche:2008aa].

4.1 Electric field and current density distribution

A necessary first step in understanding the effect of the electric field on the neurons is to determine the spatial distribution of the electric field created in the brain. As we will show later, it is also important to know the orientation of the electric field relative to the neurons.

The potential difference applied to the two electrodes used in tDCS creates an electric field that sets free charges in a conductive tissue in coherent motion. The electric field, $\vec{E}$, is given by minus the gradient of the electric potential, φ , i.e. $\vec{E} = -\nabla\varphi$. The current density, $\vec{J}$, and the electric field, are related by $\vec{J} = \sigma\,\vec{E}$, where σ is the electric conductivity of the tissue and assuming that $\omega\,\varepsilon_0\varepsilon_r < \sigma$. In the steady state, the electric potential in a conductor obeys the current continuity equation

$$\nabla \cdot \vec{J} = -\nabla \cdot (\sigma\,\nabla\varphi) = 0, \tag{2.13}$$

which has a unique solution given appropriate boundary conditions.

These are $(\sigma\,\nabla\varphi) \cdot \vec{n} = 0$ where $\vec{n}$ is the vector normal to the domain boundary (i.e. no current flow perpendicular to the skin), except at the electrodes where the boundary condition is $\varphi =$ const. At internal boundaries both the potential, φ , and the normal current density, $(\sigma\,\nabla\varphi) \cdot \vec{n}$, are continuous. These boundary conditions also hold for time-varying potentials, provided that the frequencies involved are low enough for the quasistatic approximation to remain valid. Analytical solutions can be obtained in some simple cases, but numerical methods have to be used complex geometries are involved. Once the electric potential is known, the electric field and the current density can be computed.

[Rush:1968aa, Rush:1969aa] obtained an analytical solution for the potential variation in the mid-sagittal slice of a three-layer spherical head model (scalp, skull and brain) due to two point electrodes on the scalp and in that plane. They investigated the effect of electrode separation on the current density distribution and estimated that if the electrodes were placed on the occipital and frontal bones then as much as 45% of the injected current would penetrate into the brain. [Saypol:1991aa] used this model to compare and contrast the electric field distribution during transcranial electric and magnetic stimulation. [Ferdjallah:1996aa] extended the solution to 4 layers (scalp, skull, CSF and brain) and used it to validate numerical solutions obtained using a finite difference method.

A limitation of the above studies is that they deal with point electrodes whereas electrodes currently used in tDCS are rather large, about 25-35 cm^2 and this will certainly influence the current density distribution in the cortex near the electrode. [Stecker:2005aa] extended Rush and Driscoll's analytical solution to electrodes of finite size and investigated the effect of electrode size on the current distribution. [Miranda:2006aa] implemented a spherical head model using the finite element method to investigate the current density distribution taking into account large electrode sizes. They found that the current density on the scalp is highest

in a narrow band under the perimeter of the electrodes. In the brain, the current density under the electrode was much weaker and more uniform due the attenuating and blurring effect of the skull. Forty to 60% of the injected current penetrated into the brain, depending on the distance between electrodes. The current direction in the brain was predominantly radial under the electrode and tangential between electrodes.

[Wagner:2007aa] developed a more realistic head FE model based on MR images which included 5 tissue types: scalp, skull, CSF, grey and white matter. Using this model, they investigated the effect of electrode position, electrode size and the presence of cortical lesions. They concluded that the magnitude of the current density in the brain depends on where the electrode is positioned on the scalp because the underlying structure is different. Also, in tDCS the magnitude of the current density seems to be sufficient to alter ongoing cortical neural activity.

[Lu:2007aa] compared the magnitude of the electric field and current density during TMS and tDCS in a realistic head model based the impedance method.

[Datta:2008aa] also used a FE spherical head model to look at the focality of different combinations of disc and ring electrodes. They found that increasing electrode proximity improved focality but increased shunting through the scalp. Use of more than two disc electrodes or of ring electrodes allowed to increase focality in the sense that the current density could be made higher under one electrode and lower under the others.

4.2 Electrode montages, electrode sizes

The usual setup for tDCS is to place an "active" electrode over the region to be affected and a "reference" electrode over a region where the effect of the current is thought to be minimal. For example, the "active" electrode may be placed over the primary motor cortex and the "reference" electrode over the contralateral eyebrow [Nitsche:2000aa]. If both electrodes have the same area then the magnitude current density in the brain will be similar under both electrodes (only the direction of the current is reversed) so there isn't really an active and a reference electrode. This nomenclature is used only for convenience, but it should be borne in mind that when both electrodes have the same area then anodal stimulation under one of the electrodes implies cathodal stimulation under the other and vice-versa [Nitsche:2007aa].

A comprehensive synopsis of all tDCS studies published between 1998 and early 2008, including electrode positions, was compiled by [Nitsche:2008aa]. Stimulated areas include the motor cortex (M1, hand area, leg area, C3/C4, premotor cortex), the somatosensory cortex (S1), the visual cortex (Oz, left V5), the frontal cortex (DLPFC, F3, F4, Fp3), the parietal cortex (P6, P8, CP5), the parietotemporal cortex (P3-T5, P4-T6) and the cerebellum. The reference electrode was usually positioned over the contralateral eyebrow but other positions have also been used, such as Cz, the contralateral DLPFC for DLPFC stimulation, both mastoids, chin, neck, right deltoid.

The pairs of electrodes used in tDCS usually have areas of 35 cm^{2}each (e.g. [Fregni:2005aa]) or 25cm^{2}each (e.g. [Iyer:2005aa]). The use of large electrodes is perceived as being safer as it would produce lower current densities. This is an issue that needs to be examined in detail bearing in mind that what determines tDCS effect is current density in the brain, amongst other factors. Recently, the use of "active" electrodes with smaller areas was shown to achieve more focal stimulation and, conversely, the use of larger "reference" electrodes was shown to render them ineffective [Nitsche:2007aa]. In this study, combinations of electrodes with areas of 3.5 cm^2, 35 cm^2 and 100 cm^2 were used.

Clearly, electrode position and electrode size will have a major impact on the electric field distribution. In order to calculate the electric field in the brain, the electrode positions on the scalp must be faithfully reproduced in the model used to calculate the electric field distribution. One way of doing this is to use the 10/20 or the 10/10 EEG system [Jurcak:2007aa] to place the electrodes on the subject's head and to represent these positions in a realistic model of the same subject's head. The use of circular electrodes will also make this job easier since only the position of the centre of the electrode and its radius needs to be specified, whereas for a rectangular electrode its orientation would also have to be known. The use of rectangular electrodes should be avoided also because the current density on the scalp is highest at the electrode corners [Miranda:2006aa].

4.3 Intensity and polarity

The most often used current intensity is 1 mA but in some studies this value was pushed to 2 mA [Nitsche:2008aa]. Polarity is an important factor on the outcome of stimulation since it determines the direction of the current relative to the stimulated neurons. In the motor cortex, anodal stimulation increases cortical excitability whereas cathodal stimulation decreases it [Nitsche:2000aa].

Changing the injected current intensity by a certain factor, e.g. doubling it, for a given electrode montage does not affect the spatial distribution the electric field or the current density but changes its magnitude by that same factor. Changing the stimulus polarity merely reverses the direction of the electric field and of the current density.

The current density in the brain during tDCS is largely unknown. There are few measurements done using implanted electrodes and they have two major disadvantages: only a component of the electric field is measured (in the direction determined by the positions of the two electrodes between which the potential difference is being measured) and the fact that the skull is no longer intact likely increases the amount of current that penetrates the brain, particularly near the opening. [Dymond:1975aa] report values for the electric field of 0.6 to 1.6 V/m for a current intensity of 1 mA; the stimulation electrodes were placed bilaterally over the frontal pole and the mastoids and the recording electrodes were implanted near the hippocampus.

4.4 Other waveforms: tACS, tRNS

Transcranial electric stimulation using weak alternating currents (AC) has also been shown to influence brain function. The underlying idea is that the frequency used in the electric stimulation should match the brain waves or rhythms that are characteristic of the brain function to be influenced. Marshall et al. were able to boost slow oscillations during sleep and to enhance declarative memory by applying tACS over the frontal cortex at 0.75 Hz, which is the peak frequency of slow oscillations that are associated with long term memory consolidation [Marshall:2006aa]. Kanai et al. were able to induce phosphenes in subjects in darkness by stimulating their visual cortex with tACS at frequencies in the alpha band (10-12 Hz) [Kanai:2008aa]. When the subjects sat in an illuminated room, phosphenes were most easily elicited by stimulating the occipital cortex at frequencies in beta band (14-20 Hz). Thus, it seems possible to influence ongoing brain activity in specific frequency bands in specific locations and hence to influence behavioural responses. On a different note, [Terney:2008aa] showed that stimulation with a current whose amplitude varied randomly in time with a

frequency spectrum of 100-640 Hz, increased motor cortical excitability. The advantage of this type of stimulation is that the average charge transfer during stimulation tends to zero. The calculation of the electric field distribution in tACS and random waveform stimulation is not fundamentally different from the tDCS case, because the quasistatic approximation holds in both instances. The dielectric properties have to be set according to the stimulation frequency.

4.5   Stimulation depth

All tDCS studies so far have targeted superficial cortical areas or the cerebellum [Nitsche:2008aa]. The authors are not aware of any studies reporting successful modulation of deep brain structures.

The possibility of placing the reference electrode far from the active electrode, even as far as the right deltoid, should provide a means to steer the current through deep brain regions. The limitation is that the current density decreases with distance from the electrodes, so it will be lower in depth. The use of multiple electrodes to optimize both the magnitude and the direction of the current density in depth should be investigated using numerical methods and simple head models.

4.6   Multichannel systems

As far as the authors are aware, there are no studies on the use of multichannel or multi-electrode system for transcranial electric stimulation. Recently, [Datta:2008aa] investigated the use of a small number of disc and ring electrodes to control focality during tDCS, as already mentioned in section 4.1.

The rationale for designing a multichannel system may be different depending on whether the electrode positions are fixed in advance or whether they can be chosen freely. In the latter case, the issue is how to place the electrodes on the scalp and in what number in order to stimulate the target(s) optimally. In the former case, the stimulation electrodes can be placed in standard positions, e.g. using a 10/10 EEG electrode cap, and the potential at each electrode in the array set so as to optimize stimulation of the target(s). The advantage of this method is that the 10/20 system EEG positions in the 10/10 EEG cap can be used to record the EEG and the other positions are free to place stimulation electrodes.

5   TMS [PCM]

TMS took off in 1985 when [Barker:1985aa] demonstrated a compact and practical device at the 11th International Congress of Electroencephalography and Clinical Neurophysiology in London and at the Physiological Society in Oxford. Today, it is a well-established technique with applications in basic neurophysiology, clinical investigation and cognitive neuroscience. There are potential therapeutic applications in psychiatry, for example in depression. Several books have been written on this topic [Chokroverty:1990aa, Mills:1999aa, George:2000aa, Pascual-Leone:2002aa, Walsh:2003aa, Hallet:2005aa, Wasserman:2008aa].

TMS pulses can be applied in a variety of temporal sequences, with repetition rates as high as 50 Hz. It follows from the quasistatic approximation that during a TMS pulse the relative spatial distribution of the electric field is constant and the time course of its magnitude follows exactly the waveform of the pulse. In a sequence of pulses, the time course of the electric

field follows the time course of each pulse in the sequence. For the sake of completeness, we refer here the main TMS application modes:

1. Single pulse: the amplitudes of the electromyographic (EMG) potentials evoked by consecutive TMS pulses are thought to be independent of each other if separated by an interval of at least 5 s. This technique can be used to measure cortical excitability (see definition of threshold in [Rossini:1994aa]) or for brain mapping [Cohen:1991ab]. It can also be used to provoke reversible "brain lesions" that can be used to establish a causal link between brain activity and task performance and to explore brain connectivity [Pascual-Leone:1999ab].

2. Paired-pulse TMS: Two pulses are delivered through the same coil within a few milliseconds. For inter-stimulus intervals below 5 ms, the effect of the first (subthreshold) stimulus is to reduce the amplitude of the motor evoked response (MEP) to the second (suprathreshold) stimulus. For inter-stimulus intervals above 5 ms, the effect on the MEP is the opposite [Awiszus:1999aa]. The effect is called short intracortical inhibition or facilitation. This technique probes intra-cortical neuron connections.

3. Paired associative stimulation (PAS): electric stimuli at the median nerve are delivered at the same time as suprathreshold TMS pulses at the cortex, resulting in an increase in the amplitude of the response to a test TMS stimulus. This effect is thought to reflect associative long-term potentiation of cortical synapses [Stefan:2000aa].

4. Repetitive TMS: a train of pulses is delivered at a frequency, f, greater than 0.2 Hz. rTMS has long lasting effects on brain function. The effect of slow rTMS (0.2 Hz < f < 1 Hz) is to decrease brain excitability whereas the effect of fast rTMS ($f > 5$ Hz) is to increase excitability [Hallett:2007aa]. Several therapeutic applications of rTMS are being pursued, for example in the treatment of depression or of pain [Lefaucheur:2006aa].

5. Theta bursts: bursts of high frequency rTMS (e.g., 3 pulses at 50 Hz) are delivered at 5 Hz, a frequency which falls within the theta band of the EEG [Huang:2005aa]. It produces "consistent, rapid, and controllable electrophysiological and behavioral changes in the function of the human motor system that outlast the period of stimulation by more than 60 min."

Here, again, the importance of frequency in determining the effect of stimulation is clear, as it was already in the case of tACS. Also, associative paired stimulation may provide a possible exogenous mechanism for targeting stimulation.

5.1 Electric field and current density distribution

The spatial distribution of the electric field induced in the brain during TMS is very different from that created by electric stimulation due to the fact that the electric field is produced by a time-varying current in the stimulation coil and that no current crosses the skin. Because the quasistatic approximation also holds in TMS, the time course of the electric field is determined solely by the time course of the current in the coil.

In TMS, the primary source of electric field is the time-varying current in the coil, as described by Faraday's law of electromagnetic induction. Writing the Maxwell-Faraday equation in terms of the magnetic vector potential, $\vec{A}$, instead of the magnetic flux density,

$\vec{B} = \nabla \times \vec{A}$, we have, to within the gradient of a scalar function [Jackson:1962aa]

$$\vec{E} = -\frac{\partial \vec{A}}{\partial t}.$$

For a current I, in a coil, the magnetic vector potential is given by [Griffiths:1999aa]

$$\vec{A} = \frac{\mu_0\,I}{4\,\pi} \int \frac{1}{r}\,d\vec{l},$$

where r is the distance from a point P on the coil to the field point and $d\vec{l}$ is a vector tangent to the coil at point P. The integral is performed over the length of the coil. In a TMS experiment, only the current changes with time so

$$\vec{E} = -\frac{\mu_0}{4\,\pi}\frac{\mathrm{dI}}{\mathrm{dt}} \int \frac{1}{r}\,d\vec{l}.$$

The minus sign indicates that the direction of the induced electric field is opposite to that of the current when the current is increasing with time. This formula gives the electric field induced in an unbounded isotropic medium, such as air, and shows that its spatial distribution is determined solely by the coil shape. It has been used to calculate the electric field induced by different coils [Cohen:1990aa, Grandori:1991aa, Esselle:1992aa]. In particular, an analytical solution is available for circular coils [Smythe:1989aa, Jackson:1962aa]. In this case, the electric field is zero along a line perpendicular to the plane of the coil and passing through the centre of the coil. Also, in terms of cylindrical coordinates, the electric field points in the tangential direction with no radial or axial component. The induced electric field is strongest close to the current-carrying wires, decreases rapidly with distance and generally follows the shape of the coil.

In the presence of a bounded volume conductor such as the head, electric charge will build up at the boundary and also on internal interfaces separating tissues with different electrical conductivities so as to ensure current continuity. This surface charge gives rise to a secondary electric field that can be expressed as $-\nabla\varphi$, giving a total electric field [Jackson:1962aa]

$$\vec{E} = -\frac{\partial \vec{A}}{\partial t} - \nabla\varphi. \tag{2.14}$$

On the boundary of the volume conductor, i.e. the skin, the charge builds up so as to produce an electric field that exactly cancels the normal component of the primary electric field, i.e.

$$\frac{\partial \vec{A}}{\partial t} \cdot \vec{n} = -\left(\nabla\varphi\right) \cdot \vec{n}. \tag{2.15}$$

Since the field due to this charge accumulation opposes the primary electric field, the total induced electric field inside the volume conductor will be less than it would have been in air. For a homogeneous isotropic volume conductor and in the Coulomb gauge, Equation 2.11 reduces to Laplaces equation for the electric potential, that must be solved subject to the above mentioned boundary condition. In addition, when the volume conductor is heterogeneous then both the potential, φ, and the normal current density, σE, must be continuous at the interfaces. Since air, the coil materials and the head tissues have a relative magnetic permeability, μ_r, very close to 1, this problem does not involve any boundaries as far as the

magnetic field is concerned. Once the magnetic vector potential and the electric potential are known then the total electric field can be calculated using Equation 2.15.

The approach outlined above has been used to obtain analytical solutions for the electric field induced in a spherical head model and some numerical solutions too. [Eaton:1992aa] derived a set of formulae to calculate the electric field distribution induced in a spherical head model by an arbitrarily shaped coil. The formulae indicate that in the quasistatic limit, the radial component of the induced electric field is zero. This implies that the electric field induced in a spherical head model made up of several concentric layers with different conductivities is the same as that induced in a homogeneous sphere, since no current crosses the spherical interfaces. These formulae are also very useful to validate numerical calculations.[Esselle:1994aa] derived an analytical solution for the field induced in a cylindrical conductor. The axial electric field was found to be zero along the axis of the cylinder, as predicted theoretically [Cohen:1991aa].

In terms of numerical solutions, [Tofts:1990aa] calculated the electric field induced in a semi-infinite volume conductor bounded by an infinite planar surface. He found that the component of the induced electric field perpendicular to the boundary was zero, even when the coil was placed perpendicular to the boundary. [Roth:1990aa, Roth:1990ab, Roth:1991aa, Roth:1991ab] calculated the electric field induced in a sphere and in a cylinder and also found that the radial component of the electric field in a sphere and the axial component of the electric field along the axis of a cylinder are equal to zero.

The finite element method has been used to calculate the electric field distribution in heterogeneous or anisotropic media. [Wang:1994aa] considered an anisotropic slab and found the current density to be increased along the direction corresponding to the highest conductivity eigenvalue. Conversely, the electric field was increased along the direction corresponding to the lowest conductivity eigenvalue. In a heterogeneous model, the current density was highest in the high conductivity region and the electric field was highest in the low conductivity region. In the first case, these effects are due to the appearance of a volume charge density in the anisotropic medium and in the second case they are due to surface charge density on the interfaces separating regions with different conductivities. Liu and Ueno used the finite element method to calculate the effect of a planar interface on the electric field and electric field gradient [Liu:2000aa]. They found that the presence of the interface could lead to the activation of a neuron that ran parallel and close to the interface.[Miranda:2003aa] also used the finite element method to investigate the effect of heterogeneity and anisotropy on the distribution of the electric field induced in a sphere [Miranda:2003aa]. The results show that for realistic conductivity values and anisotropy ratios, there are significant changes in the electric field distribution relative to that in a homogeneous isotropic sphere. It was also pointed out that in an anisotropic sphere, the radial component of the electric field is not necessarily zero at the boundary but the radial component of the current density is.

Other authors have used the reciprocity theorem (see [Rush:1969aa]) to obtain analytic expressions for the electric field induced during TMS. [Heller:1992aa] derived an expression for the electric field induced in a sphere by an external magnetic dipole (current loop). This approach was also used to calculate the electric field induced in unbounded, semi-infinite, spherical and cylindrical media by circular coils [Ruohonen:1995aa] and by figure of eight coils [Ravazzani:1996ab] (see below for a definition of the various coil shapes). [Thielscher:2002aa] computed the electric field induced in a sphere by realistic models of commercial coils made by Medtronics and by Magstim.

5.2 Coil shapes and coil positioning

The coils most often used in TMS are the circular coil and the figure of eight, or butterfly, coil. The figure of eight coil consists of two circular coils (the wings) next to and touching each other. In the region where the two coils touch (the junction), the current flows in the same direction in both coils so the electric field induced under this region is twice as strong as it is under the wings. Under the junction, the induced field is tangential to both coils and perpendicular to the line joining the centres of the two wings. Several authors have calculated the spatial distribution of the electric field induced by these and other coils in air, e.g., [Cohen:1990aa], [Grandori:1991aa], [Esselle:1992aa], or for simple geometries of the volume conductor [Roth:1990aa, Roth:1990ab, Roth:1991aa, Roth:1990ab, Esselle:1994aa, Ruohonen:1995aa, Ravazzani:1996ab, Thielscher:2004aa]. The figure of eight coil is often preferred because it provides more focal stimulation.

The position of the coil on the scalp is an important factor in determining the electric field distribution in the brain. In the case of the motor cortex, the best position is determined by maximizing the amplitude of the motor evoked potential (MEP) and for other brain regions the coil is positioned relative to standard reference points such as Cz. The coil is held tangential to the skull. In the case of the figure of eight coil, the direction of the electric field induced under the junction can be rotated by rotating the whole coil. For monophasic pulses, lowest threshold stimulation is achieved when the induced electric field points in the posterior-anterior (PA) direction, approximately perpendicular to the central sulcus [Mills:1992aa][Pascual-Leone:1994aa, Pascual-Leone:1994ab, Werhahn:1994aa, Kaneko:1996aa, Niehaus:2000aa, Kammer:2001aa]. For biphasic pulses, the lowest threshold is observed when the electric field initially points in the anterior-posterior direction (AP), because it is the 2nd phase of the pulse that is more efficient in depolarizing cells [Corthout:2001aa, Kammer:2001aa]. The characteristics of monophasic and biphasic pulses are described in more detail in the section on waveforms.

A variety of other coils have been proposed but they were never made available commercially. For TMS, the slinky coil [Ren:1995aa] [Zimmermann:1996aa] and the 3D differential coil [Hsu:2001aa] were proposed as alternatives to the figure of eight coil. The 4-leaf coil [Roth:1994ab] and the toroidal coil [Carbunaru:2001aa] were specifically designed for peripheral nerve stimulation.

Recently, interest in stimulation of deep frontal regions for psychiatric applications, particularly for the treatment of depression, has led to the development of new coils. One such coil, developed by Neuronetics Inc. (http://www.neuronetics.com) has now been cleared by the FDA for the treatment of depression [OReardon:2007aa]. The coil includes a ferromagnetic core to increase field strength in depth, presumably as outlined in [Davey:2005aa, Davey:2006aa]. Brainsway, Inc (http://www.brainsway.com) is another company offering a TMS system for the treatment of depression. This coil is based on a complex winding pattern that minimizes the electric field's decay rate with depth [Roth:2002aa, Zangen:2005aa, Levkovitz:2007aa, Roth:2007aa].

5.3 Stimulation intensity

Stimulation intensity is usually specified as a percentage of maximum stimulator output (MSO). It is usually set relative to the subject's motor threshold, e.g. 10% above motor threshold. Even though these guidelines are sufficient for clinical practice they do not give

any information about the electric field actually induced in the brain nor about the rate of change of the current in the coil. The rate of change of the current is a measure of stimulus intensity that is needed to predict the electric field magnitude in absolute terms.

[McRobbie:1984aa] estimated that a current density of 5.5 Am^{-2} is required for stimulation of peripheral nerve (human forearm) using long stimuli (rheobase), which corresponds to an electric field of 33 V/m given that a value of 0.15 Sm^{-1} was used for the conductivity. Based on numerical modeling, [Kowalski:2002aa] calculated that the rheobase current density required to stimulate the primary motor cortex to be 2.5 Am^{-2}. For typical TMS pulse durations, the current densities may have to be 2-3 times higher than this.

[Wagner:2004aa] measured the current density induced by TMS in a patient with implanted depth electrodes for epilepsy monitoring. For safety reasons, the coil to electrode distance was approximately 8.3 cm and stimulation was performed at a low intensity of 7% MSO. A maximum current density of 0.12 Am^{-2} was measured.

Information regarding the rate of change of the current in the coil can be obtained by combining the average relative threshold values reported in [Kammer:2001aa] with the fact that for the Magstim 200 (monophasic pulse), the maximum rate of change of the current (100% of MSO) is about 171x10^6 A/s [Thielscher:2002aa]. The motor threshold for stimulation of the motor cortex using the Magstim 200 with the induced current flowing in the posterior anterior direction was found to be 39.3 %, which corresponds to a peak current rate of change of 67x10^6 A/s.

5.4   Waveforms

The term waveform refers to the temporal variation of the induced electric field, which is determined by the temporal variation of the rate of change of the current in the coil with time, $\frac{dI}{dt}$. The most common waveforms are the monophasic and the biphasic waveforms, illustrated below [Kammer:2001aa]. The time to the first zero-crossing is typically around 100 μs for the monophasic waveform and about 200-250 μs to the second zero-crossing for the biphasic waveform. The intensity required for stimulation (threshold) is lowest when the induced electric field during the initial phase of the waveform points in the posterior-anterior (PA) direction for the monophasic pulse and in the anterior-posterior (AP) direction for the biphasic waveform.

The change in membrane depolarization is greatest near the first zero-crossing for monophasic waveform and near the second zero-crossing for biphasic waveforms. The reason why the second phase of the biphasic waveform is more effective than the first one is attributed to a reversal of Na$^+$ inactivation during the hyperpolarizing first phase [Maccabee:1998aa] or, more simply, to the finite time constant of the membrane [Davey:2000aa, Corthout:2001aa]. In any case, this explains why the optimal electric field direction is opposite for these two waveforms. Whether the change in membrane potential is greatest for the monophasic or the biphasic waveform depends on the device used [Kammer:2001aa], but biphasic waveforms are inherently more efficient that monophasic ones [Davey:2000aa].

5.5   Multichannel systems

[Ruohonen:1998aa] proposed a multichannel system for transcranial magnetic stimulation and for peripheral nerve stimulation [Ruohonen:1999aa]. The main aim of the multichannel system is to increase focality. It also has the advantages that it is possible to stimulate different
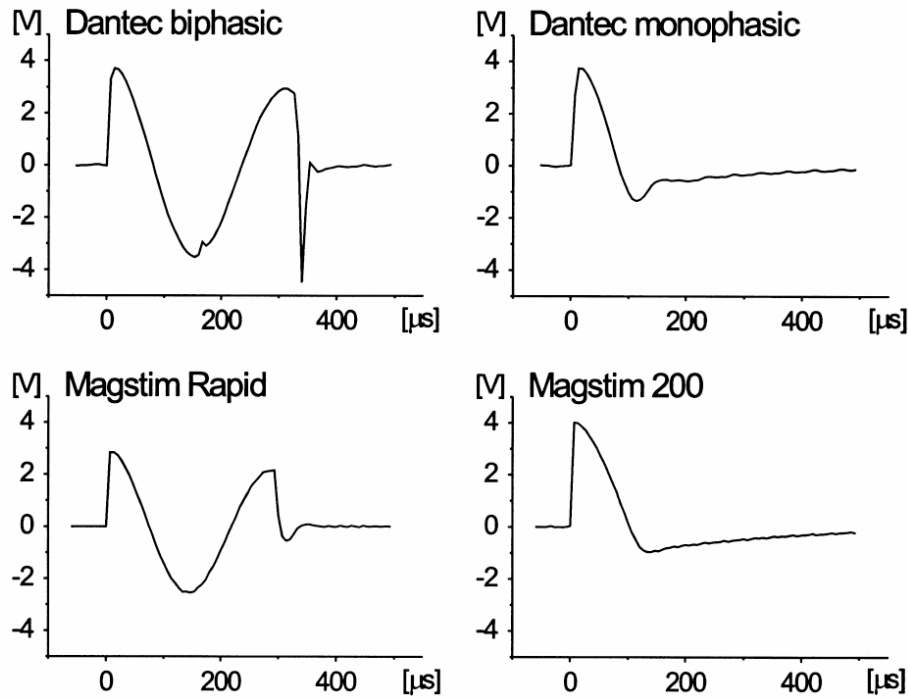
Figure 2.2 – Monophasic and biphasic waveforms for two common TMS devices (from [Kammer:2001aa]).

locations without moving the array of coils or to stimulate a few different sites simultaneously. The multichannel system cannot focus the field in depth. The proposed system has not yet been built.

5.6   Stimulation depth

The typical circular or figure of eight coil is used to stimulate the more superficial cortex. In the case of the motor cortex, stimulation is thought to occur at a depth of 18-20 mm below the scalp surface [Epstein:1990aa] [Rudiak:1994aa]. Slightly deeper targets, such as the representation of the lower limbs in the walls of the interhemispheric fissure, stimulation can be achieve at higher stimulation intensities or using large coils, for which the electric field decays more slowly with depth. One such coil is the double cone coil produced by Magstim[3]. This is a figure of eight coil with large wings that are angled at approximately 90°. The stimulated region is located in-between the two wings and can be 3–4 cm deep. It has been used, for example, to stimulate the anterior cingulated cortex [Hayward:2007aa] and the brainstem [Lo:2007aa].

5.7   Realistic head models

The limitations of the spherical model and the need for more realistic head models have long been recognized in the EEG source localization literature. For example, a realistic model of the head was used to establish more accurately the relationship between the electrical

---

[3] See http://www.magstim.com/magneticstimulators/magstimacc/12493.html.

sources in the brain and the potential distribution on the scalp [Yan:1991aa] or to account for and remove the blurring effect of the skull on the potential distribution on the scalp [Le:1993aa]. Given the geometrical complexity of anatomical structures and the heterogeneity of their dielectric properties, numerical methods must be used to solve Maxwell's equations in these realistic models. More often than not, the boundary element (BE) method was used to build such models, e.g. [Hamalainen:1989aa] or [Roth:1997aa]. This method is much lighter computationally than the finite element (FE) method but does not allow for the specification of anisotropic properties. See [Johnson:1997aa] for a review of numerical methods in bioelectric field problems.

The models used to calculate electric field and current density distributions in transcranial electric and magnetic stimulation are the same as those used in EEG and MEG, except that the field sources are located on or outside the scalp. Since the anisotropic properties of some brain tissues, such as white matter and the skull, will have a significant impact on the electric field and current density distribution in the brain [Miranda:2003aa], we have chosen the FE method for this project. In a future project we intend to use data from diffusion tensor MRI (DT-MRI) to specify tissue conductivity in our models. Here we review only studies using realistic head models based on the FE method.

The main steps in constructing a realistic FE head model are image segmentation, tissue classification and mesh generation. For TMS or tDCS, the stimulation coil or the electrodes must also be represented in the model. As a final step, the appropriate dielectric properties must be assigned to each element based on the tissue classification results, and suitable boundary conditions and loads applied.

In some studies models are created using hexahedral finite elements whose dimensions are taken directly from the voxels of the MR image, which makes the mesh generation step straightforward. These models were used to investigate the influence of volume currents and extended sources on the MEG [Haueisen:1997aa] or to estimate the effect of tissue anisotropy on the electric field induced during TMS [De-Lucia:2007aa].

Most studies have used tetrahedral finite elements: the main advantage is that it is possible to represent smooth curved surfaces more accurately and the disadvantage is the increased complexity in mesh generation (given that the hexahedral mesh is already defined by the image). In most cases, only the brain envelope is represented and the number of different tissues considered is small. One interesting study used a simple realistic head model (scalp, skull and brain) to demonstrate the influence of skull anisotropy on the EEG forward and inverse problem [Marin:1998aa]. Another study used a slightly more realistic model (6 tissues, including CSF) to re-examine the importance of volume currents in MEG [Van-Uitert:2003aa]. Wagner et al. also used a simple realistic model (5 tissues, element type not specified) to calculate the spatial distribution of the electric field during TMS [Wagner:2004ab] and tDCS [Wagner:2007aa]. [Holdefer:2006aa] used a 2D model to predict the current distribution in a coronal slice during electric stimulation and to investigate the effect of white matter anisotropy. The folding of cortical grey matter was faithfully represented.

The most complex model was implemented by [Wolters:2006aa] who created a 3D tetrahedral mesh using the program CURRY. It was a five-tissue model, which includes CSF and a realistic representation of the cortical sheet. The anisotropy of the skull was taken into account and DT-MRI was used to estimate the electrical conductivity of white matter. This model was used to study the influence of tissue conductivity anisotropy on EEG/MEG field and return current computation.

In a recent communication, [Chen:2007aa] outlined a method to produce a detailed finite element of the human head using the program MIMICS for mesh generation.

The desirable features for a good realistic head model for transcranial neural stimulation are the following:

1. A realistic representation of the cortical sheet, defined by the "CSF – grey matter" and the "grey matter – white matter" interfaces. The inclusion of these surfaces has two advantages. The effect of tissue heterogeneity on the applied electric field is taken into account and the link with cell orientation is established since most neurons lie perpendicular to the cortical sheet. The second aspect is essential to model the effect of the electric field on neurons. This requires defining a mesh with enough geometrical detail using a number of elements that is small enough so that the problem can be solved in a reasonable CPU time.

2. The CSF compartment should also be represented with reasonable accuracy. It is a thin compartment but due to the high conductivity of CSF, current will be shunted through it and affect the current density distribution. In order to segment the CSF, the usual high-resolution T1 images are not sufficient so another image of the same subject is required. The preference goes for a CT image that will give a good mask for the skull, the CSF being obtained by subtraction of the skull mask from the "skull+CSF" mask from the T1 image. Alternatively, the CSF mask can be obtained from a T2 or a proton density image.

3. The skull has a low conductivity, which means that the spatial distribution of the electric field in the brain during electric stimulation is much broader than on the scalp. A correct representation of the skull in the model will quantify this blurring effect, and automatically include the effect of openings and skull thickness variation. The effect of the skull sutures is much more difficult to model. Skull anisotropy is due to its layered structured, with two layers of low conductivity cortical bone encasing a more conducting inner layer of cancellous bone. Temporal bones do not have this tri-layered structure [Law:1993aa]. These properties are likely to enhance the blurring effect and make its dependence on skull thickness more complex.

4. White matter will also have an impact on the electric field distribution [Wolters:2006aa, De-Lucia:2007aa] and this may be particularly relevant in the white matter adjacent to the grey matter. To model this effect, DT-MRI data would have to be incorporated into the FE model. This requires a continuous description of the diffusion/conductivity tensor so as to map it onto the FE mesh [Pajevic:2002aa].

5.8 Safety

Safety guidelines in TMS and tDCS are based on past clinical experience with no significant contribution from modeling. The current guidelines for TMS consider single pulse TMS safe and prescribe maximum limits for repetitive TMS (rTMS) at various frequencies in the form of a table [Wassermann:1998aa]. An update to these guidelines also included recommendations regarding inter-train intervals [Chen:1997ab]. Note that the guidelines resulted from a meeting in 1996 but were published only in 1998 whereas the update was published in 1997.

There are no guidelines for tDCS, but all studies that looked into safety considered the application of 1 mA through an electrode with 35 cm^2 to be free of adverse effects[Nitsche:2003ab, Iyer:2005aa, Poreisz:2007aa]. The longest application time reported is 20 min [Iyer:2005aa].

Chapter 3

INTERACTION WITH NEURONAL SYSTEMS

1 The electric field and single neurons [PCM, GR]

The effect of applied electric field on single neurons has been reviewed several times from different perspectives. The review by Ranck [Ranck:1975aa] deals with extracellular neural stimulation. From the point of view of transcranial stimulation, the most important point is that it is the component of the electric field parallel to the axon that causes stimulation, as shown by Rushton in 1927 [Rushton:1927aa]. This review also contains some useful information regarding strength-duration relations. Rall presented a comprehensive overview of cable theory applied to neurons [Rushton:1927aa]. The cable equation is derived, steady-state and transient analytical solutions for many special cases are given and the cable properties of the neuron are discussed. The effect of fibre termination, branching and tapering on membrane potential is examined. Particular attention is paid to the description of the dendrites. Coburn also reviewed neural modeling in electric stimulation by remote electrodes, with an emphasis on the properties of analytic solutions, for subthreshold and suprathreshold conditions [Coburn:1989aa]. Lumped circuit elements for myelinated fibres and the effect of fibre bending and branching were also considered. More recently, Roth [Roth:1994aa] and then Basser and Roth [Basser:2000aa] reviewed the mechanisms whereby applied electric fields, including those induced during transcranial magnetic stimulation (TMS), interact with excitable cells and tissues. The stimulation of cortical tissue was considered explicitly. Jefferys reviewed non-synaptic interactions between neurons, including the effect of endogenous and applied weak electric fields [Jefferys:1995aa], which may be particularly relevant for understanding the effects of transcranial DC stimulation (tDCS).

From the point of view of transcranial neural stimulation, TMS and tDCS are currently the most promising techniques. However, these two techniques have two fundamental differences. The first one is the great difference in the spatial distribution of the applied electric field [Saypol:1991aa]. The second important one, in terms of modeling neural stimulation, is that (suprathreshold) TMS raises the membrane potential above its stimulation threshold whereas tDCS does not: TMS stimulates neurons and tDCS modulates neural excitability [Nitsche:2008aa]. Given that TMS pulses are much shorter than the time constant of the membrane in the cell soma and dendritic tree, TMS most likely depolarizes the axon, including the axon hillock and initial segment. In tDCS, the mechanisms whereby tissue excitability is

altered are not yet well understood [Ardolino:2005aa] so changes in transmembrane potential of all parts of the cell should be investigated, particularly the soma and the dendritic tree. These differences should be borne in mind when modeling the effect of the electric field on the neurons.

1.1 The cable equation - passive response [PCM]

The subthreshold response of a uniform, straight and infinitely long fibre to an applied electric field $\vec{E}$ is given by the cable equation [Rattay:1986aa, Roth:1990aa]

$$\tau \frac{\partial V}{\partial t} - \lambda^2 \frac{\partial^2 V}{\partial x^2} + V = -\lambda^2 \frac{\partial E_x}{\partial x}$$

where V is the deviation of the transmembrane potential from its resting value, τ and λ are the membrane's time and space constants and E_x is the component of the applied electric field along the fibre's direction. This equation assumes that the relation between the transmembrane current and transmembrane potential is linear. The total applied electric field is given by $\vec{E} = -\frac{\partial \vec{A}}{\partial t} - \nabla \varphi$, where $\vec{A}$ is the magnetic vector potential and φ is the extracellular electric potential. The term on the right is the "driving" or "activating" function, which in the absence of significant time-varying currents reduces to $\lambda^2 \frac{\partial^2 \varphi}{\partial x^2}$.

In an axon, the time and space constant are related to the electrical properties of the cell by

$$\lambda = \sqrt{\frac{r_m}{r_i}} \quad \text{and} \quad \tau = r_m c_m,$$

respectively, where r_m is the resistance of the membrane times unit length, c_m is the capacitance of the membrane per unit length and r_i is the intracellular axial resistance per unit length [Roth:1990aa]. The time constant is independent of axon size whereas the space constant varies with the square root of the radius of the axon [Nicholls:1992aa].

This continuous cable equation can be used to model magnetic or electric stimulation of non-myelinated fibres and also of myelinated fibres when the characteristic length of the applied electric field is larger than the membrane's space constant. In the latter case, homogenised parameters should be used for the time and space constants [Basser:1993aa]. This equation can be used estimate changes in membrane potential in some simple cases, provided the spatial distribution of the applied electric field is known.

Some passive steady-state solutions for axons   Subthreshold responses are useful because they are a good indicator of the region where stimulation begins[Plonsey:1995aa] and they are easily obtained.

When the transmembrane potential varies slowly over distances comparable to the membrane space constant and a steady-state has been reached, then the first two terms in the cable equation are negligible and the change in transmembrane potential is given approximately by the activating function [Rattay:1986aa]

$$V(x) = -\lambda^2 \frac{\partial E_x}{\partial x}.$$

This implies that a long straight fibre, as may be found in a peripheral nerve, will be stimulated near the point where the component of the electric field along the fibre is decreasing

most rapidly, as was shown experimentally [Nilsson:1992aa]. In this case, no depolarization occurs in a uniform applied electric field.

If a fibre terminates with a "sealed end" boundary condition, the intracellular current must be zero at this point and current is forced to flow through the membrane in its vicinity. If a terminated fibre of length 2L is subject to a uniform electric field, the steady-state change in transmembrane potential is given by [Plonsey:1988aa]

$$V(x) = E_x \ \lambda \frac{\sinh(x/\lambda)}{\cosh(L/\lambda)}.$$

If $L >> \lambda$, the transmembrane potential changes significantly only at the ends and $V(L) = E_x \ \lambda$. If $L << \lambda$, $V(L) = E_x \ L$ and the potential varies approximately linearly between the two ends. Excitation at neural terminations may be an important mechanism in transcranial neural stimulation, where $E_x \ \lambda$ is potentially much larger than $-\lambda^2 \frac{\partial E_x}{\partial x}$.

Neurons that bend sharply in a uniform electric field can also be depolarized. The steady-state change in transmembrane potential at a sharp bend is given [Roth:1994aa] by

$$V = E_x \ \lambda \sin\left(\frac{\theta_1 + \theta_2}{2}\right) \sin\left(\frac{\theta_1 - \theta_2}{2}\right)$$

where θ_1 and θ_2 are the angles that the straight sections make with the direction of the applied electric field (x-axis). For a fibre that is parallel to the electric field and then bends through 90°, the depolarization is given by $\lambda E_x / 2$. Abdeen and Stuchly investigated the effect of the bend shape on the activation function [Abdeen:1994aa]. Fibre bending may be an important stimulation mechanism in subcortical white matter where fibres bend away from the gray matter into the white matter. Preferential stimulation at a bend has been demonstrated experimentally [Amassian:1992aa, Maccabee:1993aa].

The electric field is discontinuous at the interface separating two tissues with different electric conducties and this discontinuity can depolarize the axon. At the interface, the change in membrane potential is given by $\lambda \Delta E_x / 2$, where ΔE_x is the jump in the normal component of the electric field multiplied by the cosine of the angle between the direction of the axon and the normal to the interface [Miranda:2007aa]. This stimulation mechanism may be relevant when axons cross from the grey matter into the white matter.

Fibre branching and non-uniformity in its diameter are another two situations that can lead to a change in membrane potential in a uniform electric field [Roth:1994aa].

Cell polarization In the preceding section, attention was focussed on the axon and the information presented is particularly relevant for TMS. In the case of tDCS, subthreshold polarization of other parts of the cell, such as the soma and dendritic tree may also be important.

Analytical results are available for simple cell shapes such as spherical or the cylindrical cells [Plonsey:1988aa]. Tranchina and Nicholson calculated the effect of an applied electric field on the transmembrane potential of a neuron model that included a straight myelinated axon, the soma and a dendrite described by an "equivalent cylinder" [Tranchina:1986aa]. The net polarization at the soma resulted from the contributions by the axon and by the dendritic tree. These, in turn, depended on simple combinations of the parameters describing the neuron. They concluded that the soma is "a likely site for action potential initiation when the field is strong enough". However, if the axon has a bend then the bend is "another likely site of for action potential initiation".

In general, an electric field that points from the dendritic tree towards the axon of a cell hyperpolarizes the dendritic tree and depolarizes the axon or the soma [Ranck:1975aa]. If the field is strong enough an action potential can be generated. If the field points in the opposite direction then the soma and the axon are hyperpolarized. This is probably why stimulation of neurons in cortical gyri using surface electrodes is excitatory when the electrode is an anode and inhibitory when the electrode is a cathode.

1.2 The cable equation - active response [PCM]

Analytical solutions for the cable equation can only be achieved by considering several simplifications for the neuron model and for the temporal and spatial variation of the electric field along the neurons. The first set of simplifications assumes that the current that goes through the neuron's membrane has a linear relation with the transmembrane's potential. While this is valid for some neuronal sections, excitable membranes also contain voltage gated ionic channels for which the relation between the current and the transmembrane potential is highly non-linear. Regarding the applied electric field, it is often assumed that it is constant along the neuron and that its duration is long enough for a steady-state to be reached. These assumptions are not generally true in transcranial stimulation: the field along the neurons may vary rapidly due to bends and terminations and the stimulus duration may be comparable to the membrane time constant.

In order to solve the cable equation without taking into account the aforementioned simplifications, numerical methods must be employed. These methods often solve a spatially and temporally discretized form of the cable equation instead of the usual partial differential equation [McNeal:1976aa, Rattay:1986aa]. Recently, Manola *et al.* combined the calculation of the electric field distribution in a model of the central sulcus and prefrontal gyrus with an implementation of a discretized cable equation to study anodal and cathodal stimulation of the motor cortex using epidural electrodes [Manola:2007aa]. They concluded that neural elements perpendicular to the electrode surface are preferentially excited by anodal stimulation while cathodal stimulation excites those parallel to its surface.

1.2.1 Spatially discretized cable equation

Following [Nagarajan:1993aa], the cable equation can be written as:

$$C_n \frac{\mathrm{dV}_n}{\mathrm{dt}} + \mathrm{I_{ionic,n}} = \mathrm{G}_a(V_{n-1} - 2V_n + V_{n+1}) + \mathrm{G}_a \left(\int_{x(n-1)}^{x(n)} E_x(s)\mathrm{ds} - \int_{x(n)}^{x(n+1)} E_x(s)\mathrm{ds} \right) \qquad (3.1)$$

where C_n is the capacitance of the neuron's membrane, G_a is the axial conductance and E_x is the total electric field along the neuron. Equation 3.1 is a continuity equation, stating that the difference between the axial current that enters and leaves a given section n of the discretized neuron (right-hand side) is equal to the current that goes through the neuron's membrane (left-hand side). The latter is the sum of two contributions: a capacitive current ($C_n \, dV_n/dt$), due to charge that accumulates on both sides of the membrane, and an ionic current ($I_{ionic,n}$), accounting for the current that flows through the channels of the membrane.

The ionic current term depends on the characteristics of the neuron's section being modelled. In myelinated internodes, the relation between the ionic current and the transmembrane

potential is linear. These are called passive compartments and for them the ionic current term is simply given by

$$I_{\text{ionic,n}} = \pi \ d_i g_L \Delta\mathrm{x}(V - V_r), \tag{3.2}$$

where d_i is the section's diameter, Δx is the section's length, g_L is the membrane's conductance per unit area and V_r is the membrane's resting potential.

In the nodes of Ranvier, there is a non-linear relation between the current and the transmembrane voltage, due to the existence of voltage gated ionic channels. There are several different models that describe the behaviour of these so-called active compartments, from the classical descriptions of Hodgkin and Huxley [Hodgkin:1952aa] to the more recent models based on human sensory fibres data [Wesselink:1999aa]. For the latter model, the ionic current term is given by

$$I_{\text{ionic,n}} = \pi \ d_i \delta[\mathrm{g}_{\text{Na}} m^3 h(V_n - E_{\text{Na}}) + \mathrm{g}_K n^4(V_n - E_K) + \mathrm{g}_L(V_n - E_L)], \tag{3.3}$$

where δ is the length of the compartment, the first term on the right describes the contribution of voltage gated sodium channels, the second term the contribution of potassium channels and the last term refers to leakage current (ionic current that flows passively through the membrane). The parameters g_{Na} and g_K are the maximum value of the membrane's conductance (per unit area) to sodium and potassium ions, respectively. The time-dependent functions m, h and n are dimensionless variables that are obtained solving the following ordinary differential equations:

$$\begin{aligned}
\frac{dm}{dt} &= \alpha_m(1-m) - \beta_m m \\
\frac{dh}{dt} &= \alpha_h(1-h) - \beta_h h \\
\frac{dn}{dt} &= \alpha_n(1-n) - \beta_n n
\end{aligned} \tag{3.4}$$

In these equations, the functions α and β depend on the membrane's voltage. See, e.g., [Wesselink:1999aa] for a complete description.

1.2.2 Temporal discretization

Finding the temporal variation of the transmembrane potential for each compartment requires that we solve n equations of the form of Equation 3.1, one for each compartment of the discretized neuron. For active compartments, Equation 3.1 is coupled with Equations 3.4. In this section we describe some of the methods that allow for this calculation to be performed efficiently.

There are several possible ways to temporally discretize the above equations. The simplest one, known as the forward Euler method, provides a direct way of solving the equations, by using the value of the ionic-current in the previous time-step, t, to find the transmembrane voltage at the new time-step, $t+1$. In this method, Equation 3.1 is discretized in the following way:

$$C_n \frac{V_n^{\text{t}+1} - V_n^t}{\Delta\mathrm{t}} + \mathrm{I}_{\text{ionic,n}}^t = \mathrm{G}_a(V_{n-1}^t - 2\mathrm{V}_n^t + \mathrm{V}_{n+1}^t) + \mathrm{G}_a \left(\int\limits_{x(n-1)}^{x(n)} E_x^t(s)\mathrm{ds} - \int\limits_{x(n)}^{x(n+1)} E_x^t(s)\mathrm{ds} \right) \tag{3.5}$$

where Δt is the temporal grid step. Equations 3.4 can be discretized in a similar manner. This method is very straightforward and easy to implement computationally, however it has been shown to be very unstable and inaccurate [Mascagni:1998aa].

The forward Euler method is an explicit method because the value of the transmembrane potential at each time step depends only on the value of the ionic current in the previous time step. There are also implicit methods, for which the solution of the potential at each time step requires knowledge about the ionic current at both the new time step and the previous one. These methods are somewhat harder to implement computationally but are often more stable and accurate. One that is usually used is the Crank-Nicolson method, for which the temporal discretization of the cable equation is given by

$$
\begin{aligned}
C_n \frac{V_n^{t+1} - V_n^t}{\Delta t} + \frac{I_{\text{ionic,n}}^{t+1} + I_{\text{ionic,n}}^t}{2} \;=\; & \frac{G_a}{2}(V_{n-1}^t - 2V_n^t + V_{n+1}^t) \\
+\; & \frac{G_a}{2}(V_{n-1}^{t+1} - 2V_n^{t+1} + V_{n+1}^{t+1}) \\
+\; & \frac{G_a}{2}\left(\int_{x(n-1)}^{x(n)} E_x^t(s)\mathrm{d}s - \int_{x(n)}^{x(n+1)} E_x^t(s)\mathrm{d}s \right) \\
+\; & \frac{G_a}{2}\left(\int_{x(n-1)}^{x(n)} E_x^{t+1}(s)\mathrm{d}s - \int_{x(n)}^{x(n+1)} E_x^{t+1}(s)\mathrm{d}s \right) \quad (3.6)
\end{aligned}
$$

As before, these equations can be discretized in a similar manner. From the previous equation we see that the Crank-Nicolson method simply averages the ionic current term and the axial current term (right hand side of the cable equation) at time steps t and $t+1$. This approach, however, has the downside that the solution for the ionic current term at the time step $t+1$ requires knowledge about the transmembrane potential at the same time step, which is unknown. To solve this problem several iterative approaches have been employed which successfully approximate the term $I_{\text{ionic,n}}^{t+1}$ until Equation 3.6 is fulfilled (see [Cooley:1966aa] for a corrector-predictor approach to this problem). Another alternative approach has been devised which avoids iteration of the non-linear equations (see [Mascagni:1998aa] and [Hines:1984aa] for a complete description). This is accomplished by staggering the temporal grids used to calculate m, h and n and the one used to calculate the transmembrane potential. It is possible to show that this method produces a $o(\Delta t^2)$ solution avoiding iteration.

1.2.3 Software packages [FW]

Different software packages are now available to build detailed models of single neurons and networks of neurons and to perform simulations from these models. The two more popular ones are called "*Neuron*" [Hines:1984aa, Hines:2001aa, Hines:2003aa, Hines:2007aa] and "*Genesis*" [Bower:1998aa, Bower:2003aa, Bower:2007aa] (see Figure 3.20), although there exist some others. Most of the available softwares are based on compartmental modeling which introduces a spatial discretization of neurons to simplify the equations describing, in time and space, the dynamics of ion-specific channels, the synaptic interactions between cells and propagation properties of membrane potentials. They can also account for the neuron morphology that can highly vary from one structure to another. Software packages mainly differ in the organization of the user interface, in the level of physiological detail that can be added

to model neurons and in the way integration methods are implemented. Detailed neuron models may now have more than one thousand compartments with multiple channels. At the cell level, some packages can handle this complexity. However, for network simulations, although tremendous progress has been achieved on computer speed, parallel-computing is still required. An interesting alternative is to use simplified or "reduced" neuron models in large networks as described in [Pinsky:1994aa].

In most packages, standard numerical methods are available to solve the set of differential equations that govern a given neuron model (like forward, backward or exponential Euler methods). In some packages the method developed by [Hines:1984aa] is available. It provides an efficient way to solve differential equations and may be used to speed up simulations in the case where the coupled equations describe a branching tree-like structure (such as the dendrites of a neuron) without closed loops. This brief paragraph can only give a short idea on available neuronal modeling software. For readers who wish more details about the respective functionalities of these software packages, the comparative review by [De-Schutter:1992aa] is very informative, although written more than 10 years ago. More recently, new computer languages are being developed for description and simulation of neural systems, e.g., NSL – Neural Simulation Language [Weitzenfeld:2002aa]. One should also mention a software package called "neuroConstruct" [Gleeson:2007aa]. It has been designed to help the development of complex networks of biologically realistic neurons (incorporating dendritic morphologies and realistic cell membrane conductances). It is compliant with NEURON and GENESIS simulators.

1.3 Single cell interaction models [GR]

In this section we provide a short review of the state of the art in neuron-stimulation field interaction.

In [Rattay:1986aa] the **excitation of active axons with extracellular electrodes** is analyzed using a discretized 1D model (difference equations). This model is really based on prior work for sub-threshold stimulation [McNeal:1976aa], where the approximation that the extracellular potential determined only by the external field is justified by the small size of fibers and because the period of interest is that prior to excitation. In the discussion below we show that this condition can be relaxed somewhat. Further studies of this modeling approach for the case of stimulation using extracellular electrodes are carried out in [Rattay:1989aa]. The essence of these papers is to mode the externally induced field as a potential, and in this sense they are limited to electrical stimulation. These papers are not explicit about the role of boundary conditions at the terminations, nor of fiber bends, and the discussion is at the level of difference (compartment) models including active Hodgkin-Huxley elements.

In [Rattay:1998aa] a compartmental model of the excitation of a neuron is presented, and it shown that the most likely place for excitation is the myelinated neuron.

The generalization to **magnetic stimulation** is carried out in [Roth:1990aa], under similar assumptions as in [McNeal:1976aa]: 1) a 1D case with the axoplasm acting as a b) an Ohmic conductor and with c) negligible extracellular secondary potential. In this paper the 1D **passive cable equation** for a fiber of radius a and thickness δ is derived,

$$\lambda^2 \frac{\partial^2 V}{\partial x^2} - V = \tau \frac{\partial V}{\partial t} + \lambda^2 \frac{\partial E_x^p}{\partial x}$$

with the axial spatial scale constant

$$\lambda = \sqrt{r_m/r_i}$$

where $r_m = R_m^s/(2\pi a) = \rho_m \delta/(2\pi a)$ and the **time constant** [Plonsey:2007aa]

$$\tau = c_m r_m = C_m R_m = C_m^s R_m^s$$

and where R_m and C_m are the resistance and capacitance of a membrane of length L and radius a and thickness δ, $r_m = R_m^s/(2\pi a)$ (resistance times unit length) and $c_m = C_m^s 2\pi a$ (capacitance per unit length), R_m^s and C_m^s are the "specific" resistance times area and capacitance per area of the membrane (i.e., quantities associated to one unit of area) and where a is the cable radius and δ its membrane thickness. Also, $r_i = \rho_i/(\pi a^2)$ is the intracellular resistance per unit length. We can refer to the following definition of resistivity, $R = \rho L/A$.

Although membrane resistance and capacitance are a function of the area patch considered, the time constant are not. Therefore, the time constant does not depend on cell dimensions. It depends only on membrane properties. The specific capacitance of the membrane is close to $\sim 1\mu F/cm^2$. However, the specific resistance R_m varies among cell types (the density of open channels opened at rest varies) and the time constant is therefore also variable, ranging from 1 to several hundred ms [Bower:2003aa]. The time constant provides a measure of the time window of input integration (a memory of sorts).

The greek letter ρ will refer to resistivity (resistance per unit length and times area),

$$\rho = \frac{R\,dA}{dL}$$

but we also use the "specific resistivity" R_m (resistance times unit area of the membrane, by multiplying resistivity by membrane thickness δ)

$$R_m = \rho_m \delta$$

and the complementary resistance per unit length (intracellular)

$$r_i = \rho_i/(\pi a^2)$$

Using these expressions, we can rewrite Ohm's law across the membrane, $V = IR$, as $V = J_\rho R_m$, for example.

Note that using these expression we can express the **space constant** λ in terms of the fiber radius a and its thickness δ as

$$\lambda = a\sqrt{\pi \frac{\delta}{2\pi a}\frac{\rho_m}{\rho_i}} = \sqrt{a\frac{\delta}{2}\frac{\rho_m}{\rho_i}} \tag{3.7}$$

Therefore, and in contrast to τ_m, the space constant does depend on cell dimensions (on the diameter).

A follow up paper ([Basser:1992aa]) generalizes slightly the work in [Roth:1990aa] while maintaining axial symmetry requirement, again with the same end result of an activation function proportional to the derivative of the along-axis stimulating electric field. In this latter work, there is a nice discussion on how the magnetic and electric stimulation cases are
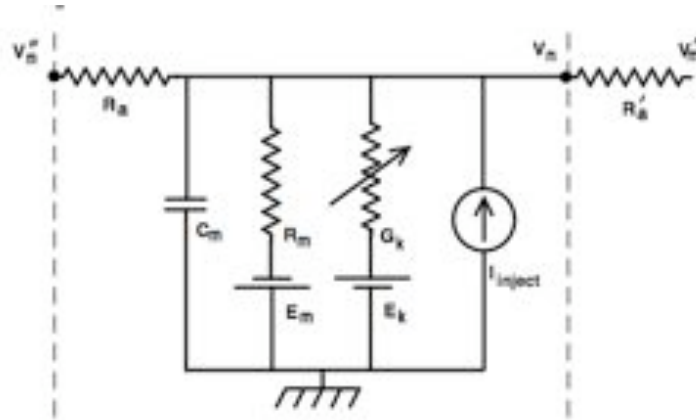
Figure 3.1 – Figure from [Bower:2003aa] showing an equivalent circuit for a generic neural compartment.

essentially the same if the results are analyzed in terms of the induced electric field (either directly or through induction). The role of boundary conditions or fiber bends is not discussed.

The role of **boundary conditions** (e.g., sealed terminations) is emphasized and treated in [Nagarajan:1993aa] using a compartment model. Compartment models are discussed in more detail in [Segev:1999aa], and the appropriate conditions at branching points are terminations are discussed (although not under stimulation)—see Figure 3.1.

In [Nagarajan:1995aa] the **role of the tissue surrounding the axon** is analyzed (the axon is located at the center of a nerve bundle) under axial symmetry assumptions. It is shown that nerve bundle anisotropy and the presence of perineurium can affect the transmembrane response.

The **neuron bend** case is nicely discussed in [Basser:1992aa] and [Abdeen:1994aa], where the fact is highlighted that it is the along axis directional derivative of the field component along axis that appears, and that there are several terms that fall out, some proportional to the field derivative, and some to the field itself.

In [Ruohonen:1995aa], [Ruohonen:1996aa] and [Ruohonen:1998aa] it is argued that the primary field radial component also plays an important role in stimulation, based on work by [Cartee:1992aa]. In reality, the mechanism that is is alluded to is the same one that acts along axis due to terminations. The radial component of the field induces a transmembrane potential change proportional to the external field and the radius of the fiber. However, there is a factor of 2 in the expression given in [Ruohonen:1996aa] ($\Delta V_m = 2RE_\rho$) which seems wrong (see Toy model 4 above). The overall potential drop imposed by the external field is carried by one side of the fiber (depolarizing, say), and the other half by the other side (hyperpolarizing).

With regards to brain stimulation, the characteristic dimension of the shapes of cortical neurons are small compared to the spatial scales of field variation ([Ruohonen:1998aa] and [Wagner:2007aa]). Hence the primary mechanisms for activation are terminations and bends, where the "effective" gradient of the field will be great. Therefore, the activation will occur at the locus of the maximum of the external field magnitude rather than its gradient (see Figure 3.2), and that not only the strength of the field, but also its direction is relevant in determining the locus and strength of the activation. Furthermore, TMS is thought to excite

axons rather than cell bodies or other parts.

In [Ruohonen:1998aa], [Nagarajan:1993aa] and [Hsu:2003aa] we find a discussion on strength-duration relationship for TMS stimulation. Since the membrane acts like a leaky capacitor (a capacitor and resistor in series) with with time constant of about 150 μs, the shorter the pulse, the less energy is needed. It is also stated that the pulse duration should not be inferior to the chronaxie time of the neuron (the minimum time over which an electric current double the strength of the rheobase needs to be applied, in order to stimulate a muscle fiber or nerve cell).

The role of bends and terminations is further discussed in [Miranda:2007aa] and references therein, where polarization at terminations and bends is shown to be proportional to λE_x. This is a natural result, since the natural scale in the fiber is provided by λ (typically with a value of 2 mm). In this paper other important points are made, including the fact that of all the possible mechanisms for polarization it is this one that is of greatest impact for TMS and tDCS (where the external field gradients are small): **the main mechanism (or lowest threshold) will take place where axons bend or end, and is simply proportional to field strength**. The role of tissue conductivity heterogeneity is also discussed in this paper as a possible source of polarization: as an axon crosses an internal conductivity boundary in the surrounding medium, where charges will accumulate upon stimulation.

The current propagation models for tDCS described in [Miranda:2006aa] and in [Wagner:2007aa] indicate that the low field intensities in tDCS do not actively stimulate the cortex, but **modulate excitability by modifying the polarization state of the membrane, altering firing rates**.

In [Manola:2007aa] a simulation of cortical stimulation (Motor Cortex Stimulation via epidural implant) using a compartmental models describing a myelinated axon, soma and dendritic trunk is carried out, aiming at more accurate simulation of **pyramidal neurons**—see Figures 3.3 and 3.4. The simulations include the "embedding" of the neurons in grey and white matter, CSF, etc. In this paper, the role of the varying diameter of neurons is also discussed—the bigger the axon diameter, the greater the excitation (which falls from from current conservation). Modeling results confirmed experimental findings that anodal (+) stimulation depolarizes the axonal part of neurons perpendicular to the electrode while hyperpolarizing their dendritic part,and that neurons with their dendritic trees pointing towards the anode (+) are preferentially excited—see Figure 3.5. Axonal nodes near loci of surrounding tissue conductivity change (boundary between gray and white matter) are also preferential excitation sites, as discussed at length in [Miranda:2007aa].
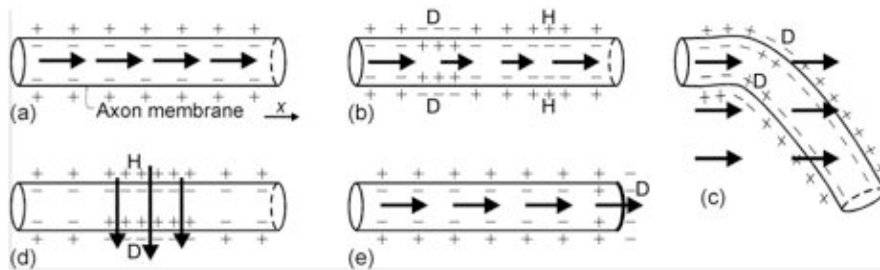

Figure 3.2 – Figure 4 in [Ruohonen:1998aa] showing polarization and depolarization associated to real or effective (bends, terminations, etc.) field gradients in neuron fibers.
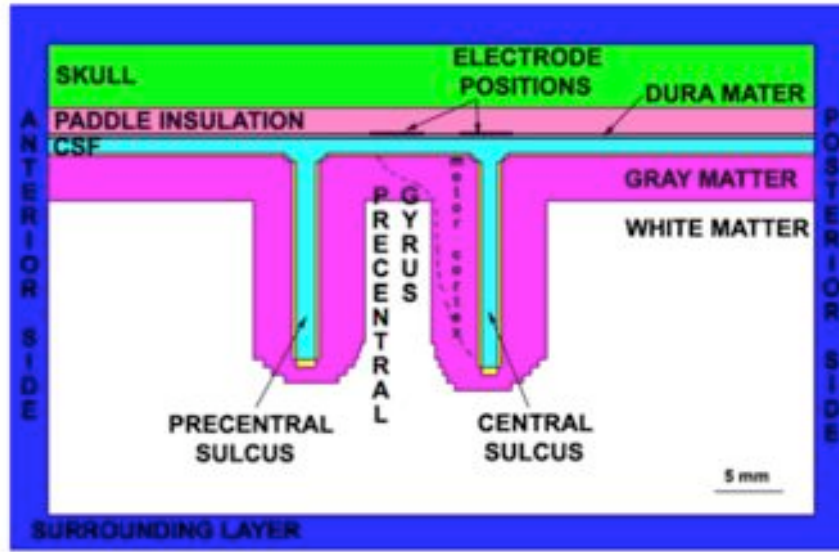
Figure 3.3 – Figure 1 in [Manola:2007aa] showing the anterior-posterior cross-section of the 3D conductivity model.
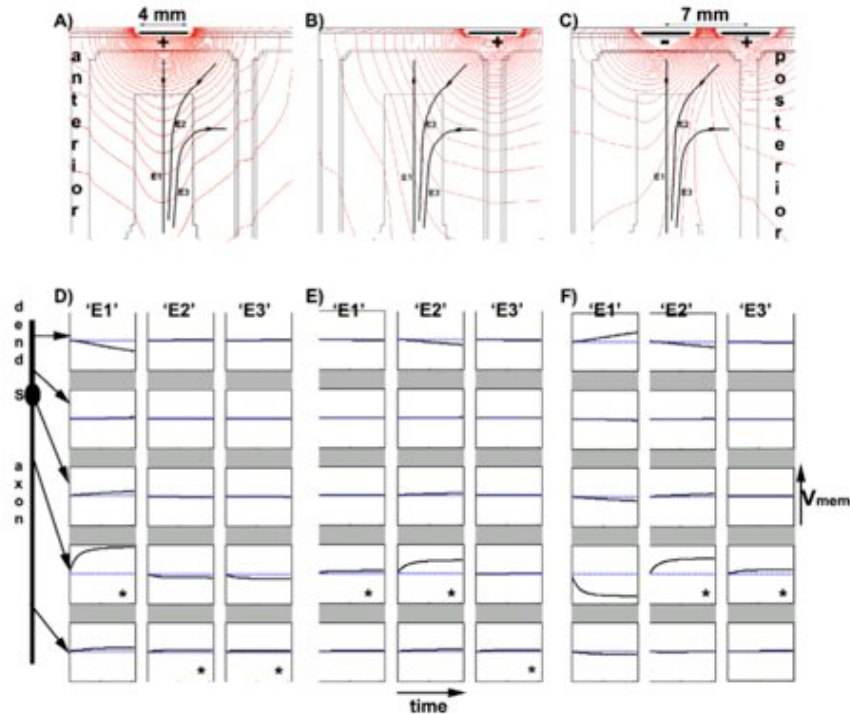

Figure 3.4 – Figure 4 in [Manola:2007aa] showing iso-potential lines from stimulation in different configurations and membrane polarization time histories at different neuron locations during the stimulus pulse.

The **relative orientations of neurons and the external fields**, as well as other micro-architecture need to be further studied in order to predict stimulation locus and strength—see Figure 3.6. While TMS exploits a neuro-stimulation mechanism as well as neuro-modulatory, tDCS is clearly neuro-modulatory: tDCS currents modify the transmembrane potential of neurons, and thus modify the level of excitability and the firing rates of individual neurons [Wagner:2007aa].
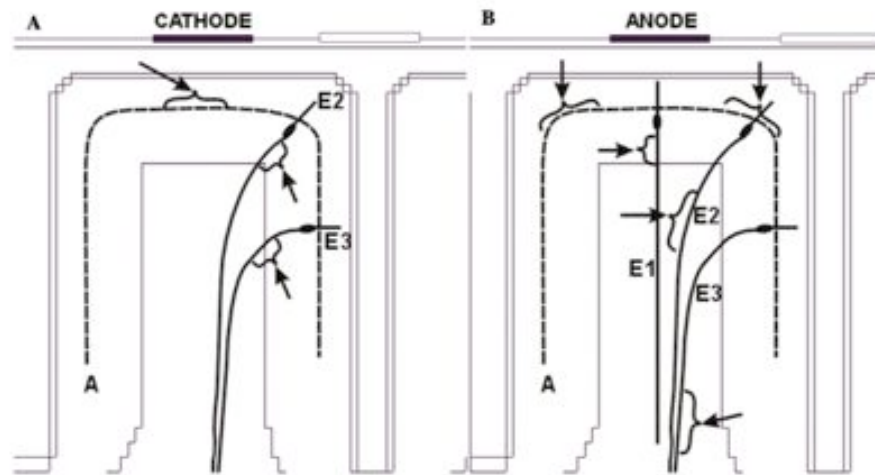
Figure 3.5 – Figure 6 in [Manola:2007aa] preferential sites of excitation for cathodal (-) and anodal (+) stimulation.
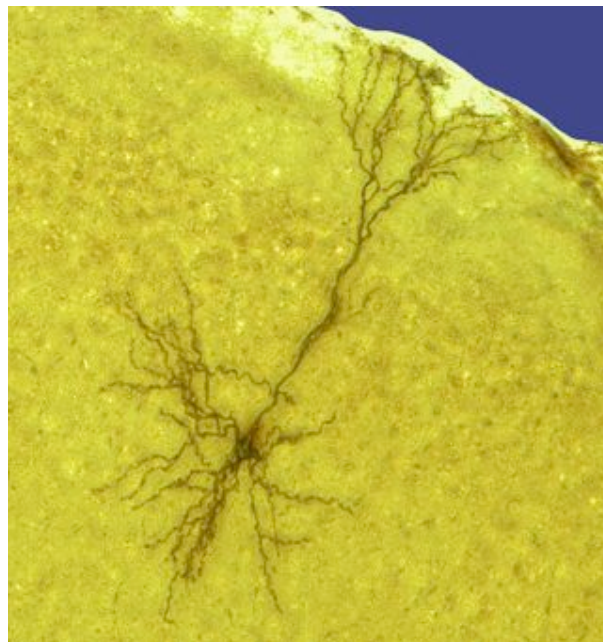
Figure 3.6 – Mouse Somatosensory Cortex Pyramidal Neuron from Norman Atkins Jr., Neuronal Pattern Analysis Group, Beckman Institute, http://www.itg.uiuc.edu/exhibits/iotw/2002-01-17/, illustrating the orientation of cells in the cortex.

These points are further emphasized in [Been:2007aa] and references therein (e.g., [Ardolino:2005aa], and more recently in [Antal:2008aa], which state that, anodal tDCS typically has an excitatory effect on the local cerebral cortex by depolarizing neurons (and vice-versa in the cathode). The effects of tDCS last up to hour after stimulation, with mechanisms involving the membrane function through local changes in ionic concentration, alteration in transmembrane proteins and electrolysis-related charges in hydrogen ion concentration induced by exposure to a can electric field. It is stated also that the mechanism of action of tDCS is not completely clear but "appear to involve a combination of hyper and de-polarizing effects on neuronal axons as well as alterations in synaptic function."

It is concluded in [Ardolino:2005aa] that the long lasting effects of cathodal tDCS may arise from non-synaptic mechanisms, possibly involving alterations in transmembrane protein and changes in pH. The same points regarding the relation of protein-synthesis and long lasting effects are made in [Nitsche:2008aa], as well as with modifications of intracellular cAMP and calcium levels (relating to work in [Gartside:1968aa]).

In addtion, in [Nitsche:2008aa] it is reported that tDCS induces focal reversible shifts of prolonged cortical excitability, although does not induce neuronal action potentials: polarization changes in the membrane are not strong or rapid enough (unless the stimulation circuits are rapidly switched on or off, in which case neuronal firing can take place). Hence **tDCS is neuromodulatory** in character. The stimulated tissue is polarized and hyper or de polarization of the membrane take place. Moreover, besides field intensity, stimulation duration plays an important role in the establishment of after effects. Based on this observations, it appears as if in tDCS there are two types of time scales and associated phenomena: short time scales (membrane polarization) and long time scales (non-synaptic mechanisms, protein or pH effects). Short applications do not lead to after effects, only excitability shifts during stimulation.

Already in [Bindman:1964aa] the effects of brief passage of polarizing currents through the cerebral cortex of the rat were studied, and it was observed that surface-positive current (anodal) stimulation enhances firing rate and the size of evoked potentials, while negative currents had the opposite effect. Also, if the currents were maintained for 5-10 minutes, a persistent after-erfect the same direction was produced, lasting steadily for at least 1-5 hours. It was hypothesized that the mechanism for long-term effects can be associated directly to the changes in firing rates.

Finally, in [Terney:2008aa] a tDCS variant called tRNS (for transcranial random noise stimulation) is presented, with similar effects to tDCS (increase of corticospinal excitability) and it is argued that since no DC component is present there must be a different mechanism at play (since reversing polarity in tDCS changes the effects, while this does not affect tRNS). It is argued that similarly to tACS there may be interference with natural oscillatory activity. It has been suggested that synaptic activity can be boosted by noise, and stochastic resonance may be associated. Another mechanism accounting for non-linearity and therefore stochastic resonance in mentioned, "rectification" of high-frequency currents at the membrane. It is stated that "a pure DC stimulus can open the Na^+ channels only once, whereas repeated pulses (tRNS) can induce multiple ionic influxes, and achieve substantially heightened effects". An important difference with tDCS, it is argued, is that tRNS is only excitatory effect (not hyperpolarization, only depolarization).
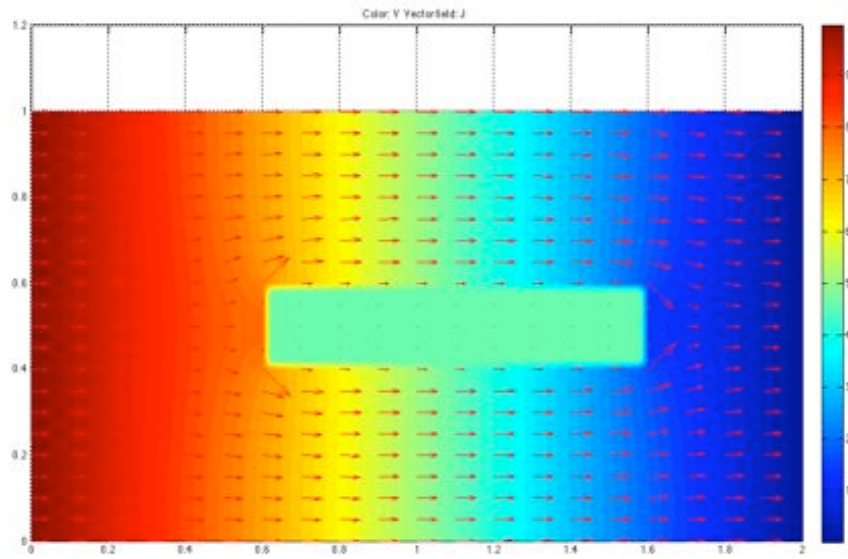
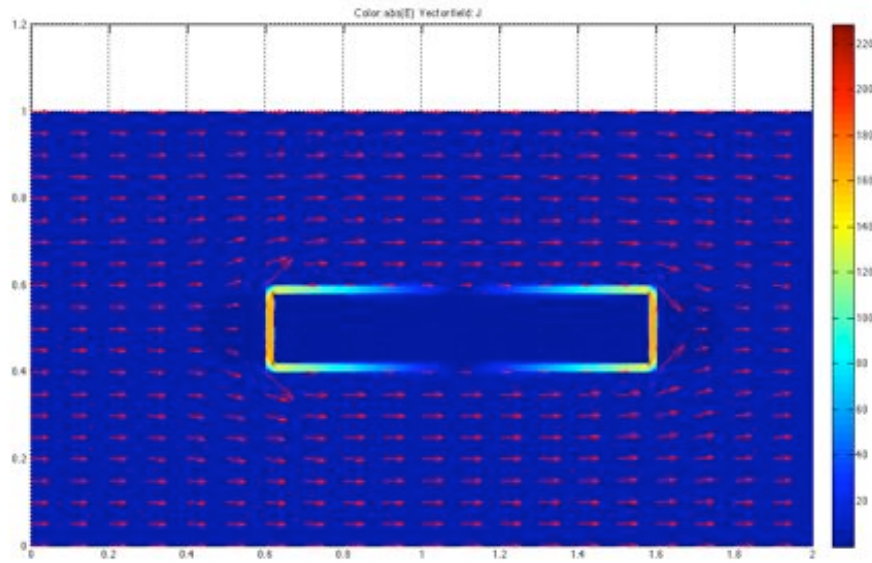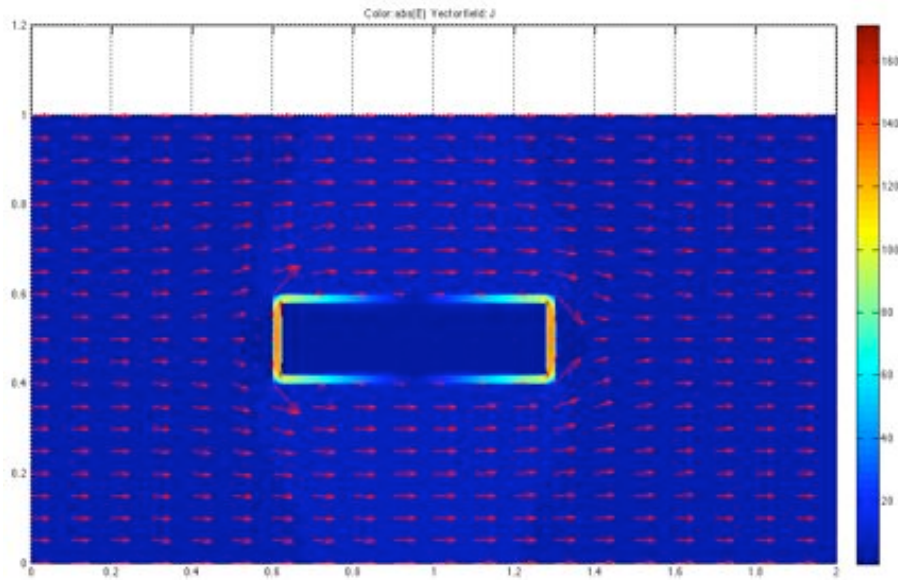**Figure 3.7** – Sealed neuron in a conductive bath and with two parallel plates at 10 and 0 V. The potential is shown in color, and the current density by arrows. The potential inside the neuron is constant (zero field).

1.4 A simple model for a passive neuron under stimulation (2D) [GR]

The following provides a simulation of a single neuron, modeled as a filled, hollow cylinder in a conductive bath and with a very low conductivity membrane (and in steady-state and no capacitance). The interior of the neuron is conductive as well. An external electric field is created by two parallel plates (on each side, at 10 and 0 V). Since the interior is effectively sealed due to a low conductivity membrane, there can be no electric field inside. The membrane polarizes both on the terminations and on the sides.

Such simulations can be directly relevant to in-vitro experimental work, in which a 2D approach may suffice.

The larger the neuron spatial constant is, the higher the polarization will be. The potential inside the neuron is constant (zero electric field), but the transmembrane potential drop is very different at different neuron sites (as can be inferred by the field in the membrane, see Figures 3.8, 3.11 and 3.12. In 2D the neuron has an impact on the current distribution (currents are forced around it), but in 3D this will play a much smaller role. A long neuron aligned with the field "sees" a higher potential difference from one end to the other, and will be much more polarized.

Figure 3.8 – Sealed neuron in a conductive bath and with two parallel plates at 10 and 0 V. The magnitude of the field is shown in color, and the current density by arrows.
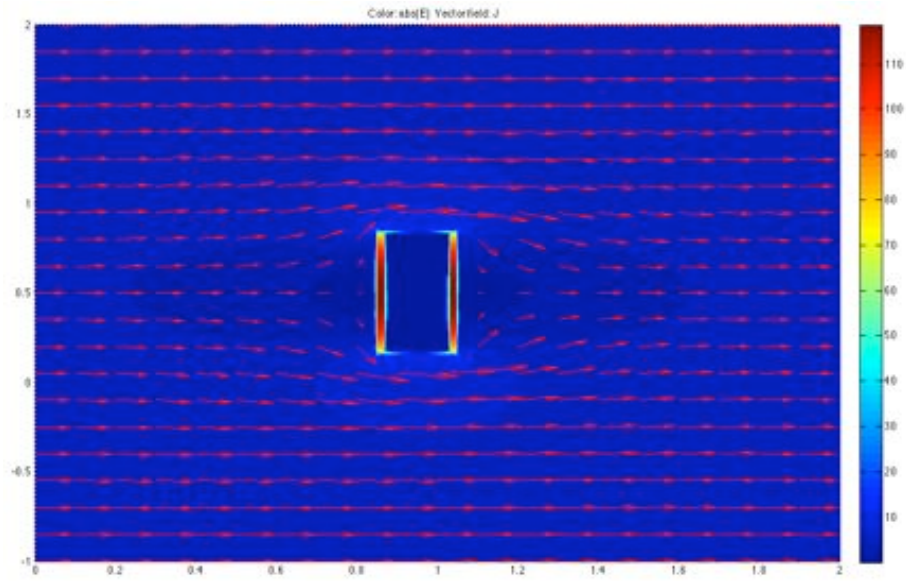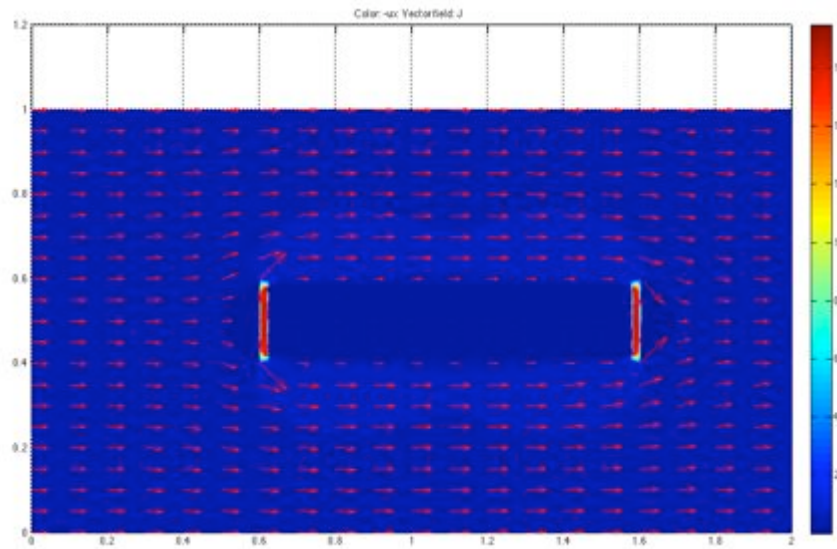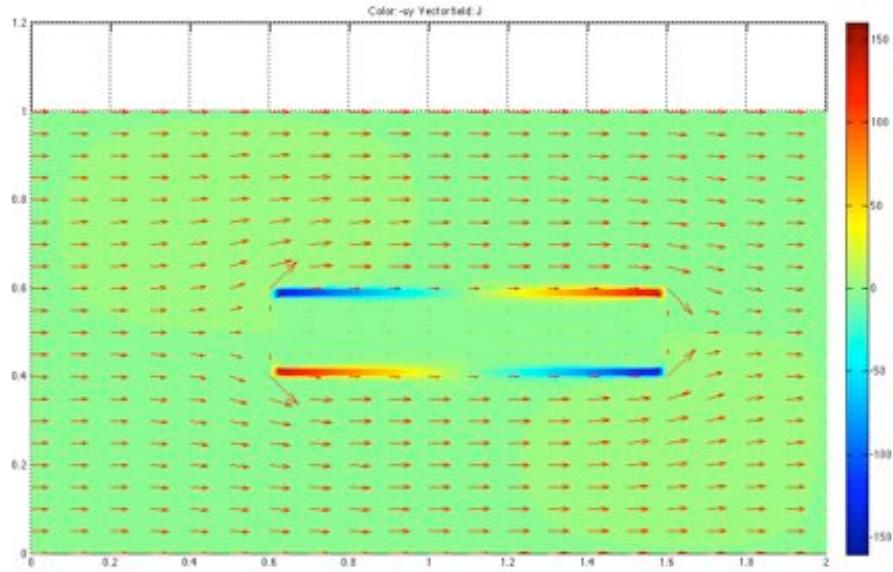

Figure 3.9 – Sealed shorter neuron in a conductive bath and with two parallel plates at 10 and 0 V. The magnitude of the field is shown in color, and the current density by arrows. The electric field magnitude is overall smaller than for the longer neuron case. Since the resistivity in the membrane is the same as in the other case, this means that there is less current flowing into the neuron, which is expected, as the potential difference across the neuron terminations depends on the length of the neuron.

Figure 3.10 – Sealed shorter neuron rotated 90 degrees in a conductive bath and with two parallel plates at 10 and 0 V. The magnitude of the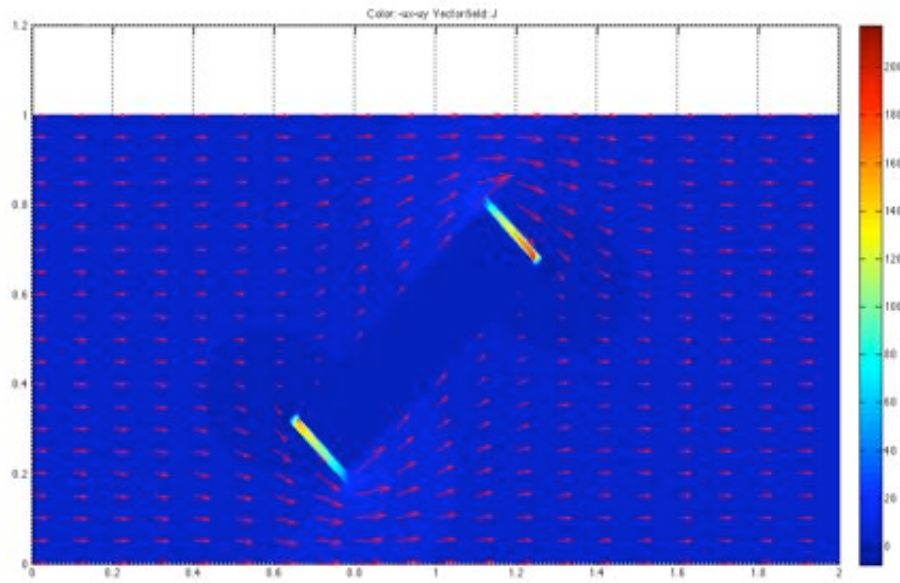 field is shown in color, and the current density by arrows. The electric field magnitude is overall smaller than for the other cases. Since the resistivity in the membrane is the same as in the other case, this means that there is less current flowing into the neuron, which is expected, as the potential difference across the neuron terminations depends on the length of the neuron.

Figure 3.11 – Sealed neuron in a conductive bath and with two parallel plates at 10 and 0 V. The x-component of the field is shown in color, and the current density by arrows.
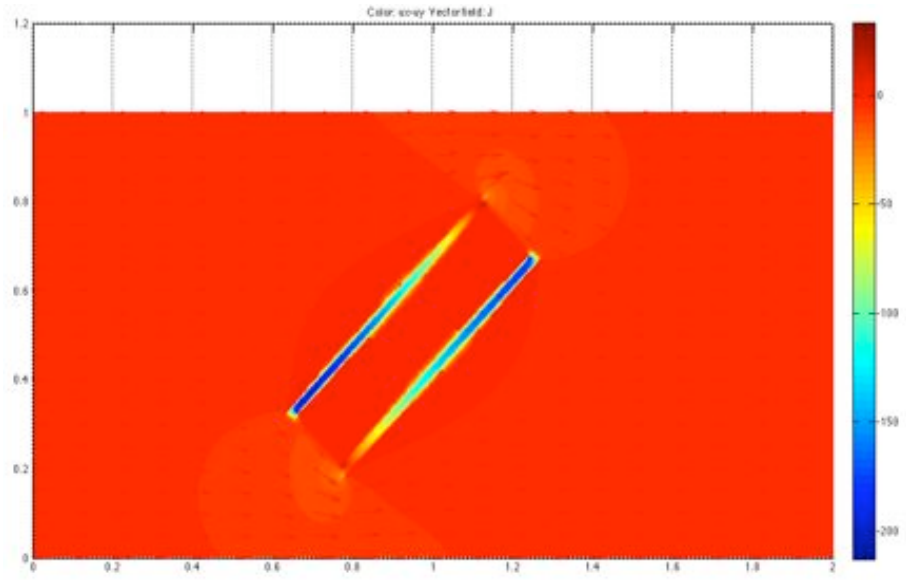
Figure 3.12 – Sealed neuron in a conductive bath and with two parallel plates at 10 and 0 V. The y-component of the field is shown in color, and the current density by arrows.
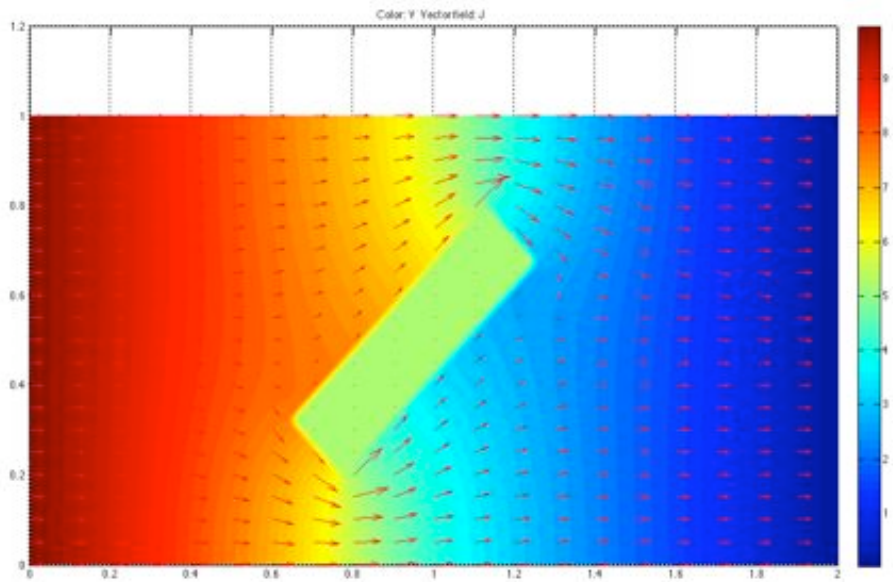
Figure 3.13 – Sealed neuron in a conductive bath and with two parallel plates at 10 and 0 V. The potential is shown in color, and the current density by arrows. The potential inside the neuron is constant (zero field).
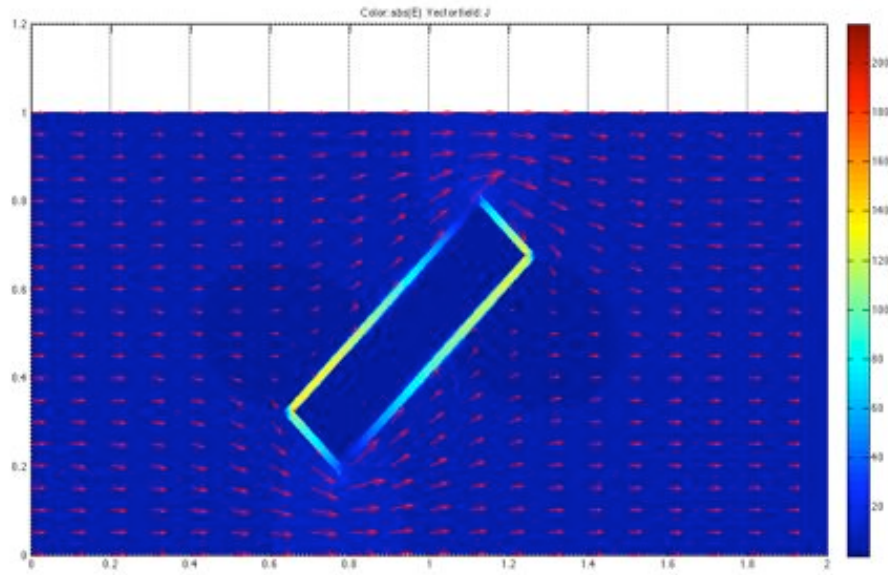
Figure 3.14 – Sealed neuron in a conductive bath and with two parallel plates at 10 and 0 V. The magnitude of the field is shown in color, and the current density by arrows.

Figure 3.15 – Sealed neuron in a conductive bath and with two parallel plates at 10 and 0 V. The x'-component (rotated x component) of the field is shown in color, and the current density by arrows.

Figure 3.16 – Sealed neuron in a conductive bath and with two parallel plates at 10 and 0 V. The y'-component (rotated y component) of the field is shown in color, and the current density by arrows.

1.5 The un-stimulated neuron: neuron models [GR]

In this section we will provide a short review of the state of the art in neuron modeling.

Before discussing stimulation per se, we should mention the basic models for the generation and propagation of actions potentials. The polarization state and ionic conductances at a given point in the membrane are described by the Hodgkin-Huxley (HH) equations as a function of an external current $I(t)$ [Trappenberg:2002aa]. These equations are rooted on conservation of charge (a recurring theme) and read

$$C\frac{\partial V}{\partial t} = -g_K n^4(V - E_k) - g_{N_a} m^3 h(V - E_{N_a}) - g_L(V - E_L) + I(t)$$

$$\tau_n \dot{n} = -[n - n_0(V)]$$
$$\tau_m \dot{m} = -[m - m_0(V)]$$
$$\tau_h \dot{h} = -[h - h_0(V)] \tag{3.8}$$

(see [Trappenberg:2002aa] for details). In order to have propagating action potentials, these equations have to be coupled using a cable propagation equation that is given by ([Trappenberg:2002aa] see section 2.5.2 and also in [Wagner:2007aa] and [Bower:2003aa], and the discussion in [Roth:1990aa] is particularly lucid)

$$\lambda^2 \frac{\partial^2 V_m(x,t)}{\partial x^2} - \tau \frac{\partial V_m(x,t)}{\partial t} - V_m(x,t) + V_{\text{rest}} = -4dR_m I_{\text{inj}}(V_m(x,t), t) \tag{3.9}$$

Such compartment models are also discussed, including the role of boundary conditions, in greater detail in [Dayan:2001aa] (Chapter 6).

In [Bower:2003aa] we have the compartamental version of this equation, which we write here to display in a clearer way the continuity relation,

$$\frac{V_m' - V_m}{R_a'} + \frac{V_m'' - V_m}{R_a} + I_{inject} = C_m \frac{dV_m}{dt} + \frac{V_m - E_m}{R_m} + \sum_k g_k(V_m)(V_m - E_k) \tag{3.10}$$

The main point for combining the Hodgkin-Huxley equations with the cable model is to include the HH variable membrane conductance into the cable model (modifying the last term in Equation 3.17).

1.6 The passive cable equation for a cylindrical but possibly bent neuron [GR]

Here we analyze and generalize somewhat the cable equation under stimulation.

In the following we refer to Figure 3.18. Consider a cylindrical but possible bent cable immersed in a very conductive fluid and under the influence of an external "primary" electric field E. This primary field creates an overall induced electric field which is the sum of the primary and secondary field due to charge distribution. Let x denote the axial coordinate of this cable (not necessarily a straight cable, so this coordinate refers to the along axis distance in a generally bent cylinder), and ρ the radial one. We now demonstrate that for any given point along the cable, the transmembrane potential $V(x,t)$ (to be defined) satisfies the passive cable equation (here x is the axial coordinate and ρ will denote the radial coordinate)

$$\lambda^2 \frac{\partial^2 V}{\partial x^2} = \tau \frac{\partial V}{\partial t} + \frac{V}{r_m} + f(x,t) \tag{3.11}$$

The cable equation just states that under (local[1]) steady state the delta of axial current per unit length must flow out across the membrane (capacitively or resistively)—see Figure 3.17:

$$\int dA \, \frac{\partial J_x}{\partial x} = -a \int d\phi \, J_\rho \tag{3.12}$$

This is the equation of conservation of charge/current under steady state $\nabla \cdot J = 0$ (i.e., when $\dot{\rho} = 0$ inside the cell). The negative sign defines the axial current positive direction to be out of the membrane (if J_x increases, current must be flowing in, and thus negative). This equation is applicable to a straight cylinder, or a bent one.

Let

$$\langle f(x, \rho, \phi) \rangle_\phi \equiv \frac{1}{2\pi} \int d\phi \, f(x, \rho, \phi)$$

Then we can write,

$$\int dA \, \frac{\partial J_x}{\partial x} = -2\pi a \langle J_\rho \rangle_\phi$$

If we further assume that σ_i is constant,

$$\sigma_i \int dA \, \frac{\partial E_x}{\partial x} = -2\pi a \langle J_\rho \rangle_\phi$$

and using an analog defintion for the the cross-section (c.s.) average,

$$\pi a^2 \sigma_i \partial_x \langle E_x \rangle_{c.s.} = -2\pi a \langle J_\rho \rangle_\phi$$

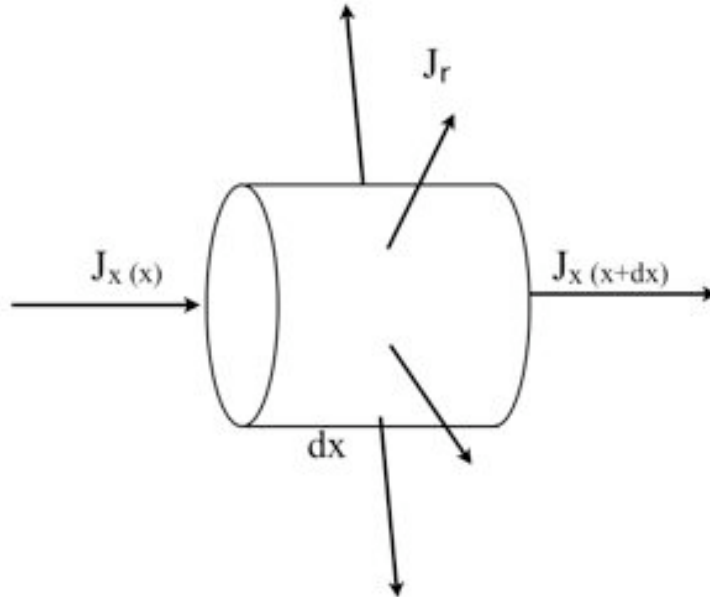[1] Charges do accumulate at the membrane, but here we are inside.

Figure 3.17 – Conservation of current in a cylinder sub-section.
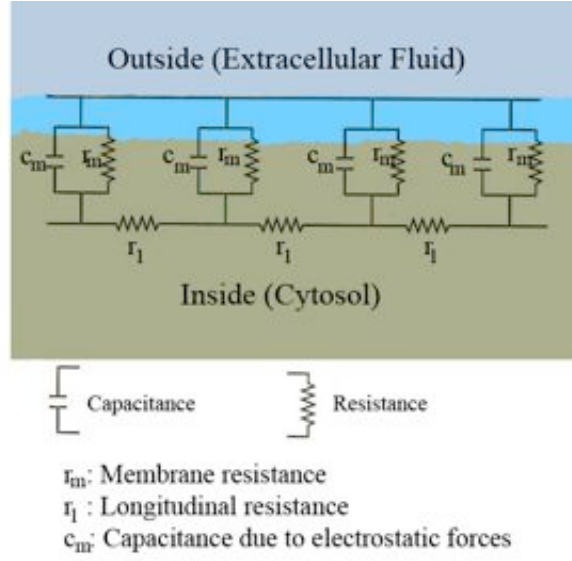
Figure 3.18 – Schematic overview of cable theory's simplified view of a piece of neuronal fiber. The outside potential is 0, the inside potential is $V(x,t)$—and therefore equal to the transmembrane potential ($V_m = V = V_i - V_o$). When an electrical current is moving along the inside of a fiber the cytosol exerts a resistance (rl). Simultaneously current will escape through the phospholipid bilayer (with resistance rm) to the outside; and due to electrostatic forces a buildup of charge (cm) will take place along the bilayer (from Wikipedia, public domain image).

or

$$\pi a^2 \sigma_i \partial_x \langle E_x \rangle_{c.s.} = -c_m \partial_t \langle \Phi_{tm} \rangle_\phi - \frac{\langle \Phi_{tm} \rangle_\phi}{r_m}$$

or,

$$\lambda^2 \, \partial_x \langle E_x \rangle_{c.s.} = -\tau \, \partial_t \langle \Phi_{tm} \rangle_\phi - \langle \Phi_{tm} \rangle_\phi \tag{3.13}$$

We will return to this expression in a moment.

We can proceed further if we make here the important **assumption of homogeneity** across axis. That is, we assume that $J_x = J_x(x)$ only (not ϕ or ρ) and the problem reduces to 1D. Then

$$\int dA \, \frac{\partial J_x}{\partial x} = \pi a^2 \frac{\partial J_x}{\partial x}$$

and

$$-a \int d\phi \, J_\rho = -2\pi a J_\rho$$

and

$$\pi a^2 \frac{\partial J_x}{\partial x} = -2\pi a J_\rho \tag{3.14}$$

As mentioned above, the bent case is nicely discussed in [Basser:1992aa] and [Abdeen:1994aa], where the fact is highlighted that it is the along axis directional derivative of the field component along axis that appears, and that there are several terms that fall out, some proportional to the field derivative, and some to the field itself. Let u_L be a the unit vector field along the axis. Then,

$$E_l = u_l \cdot E$$

and the desired quantity is[2]

$$u_l \cdot \nabla(E_l) = u_l \cdot \nabla(u_l \cdot E)$$

Now, the current densities in question are proportional to the local electric field—the total one. We can however separate the total field into an external driving current (or primary as some papers call it), and a secondary (driven) one:

$$E = E^p + E^s \tag{3.15}$$

The primary electric field is due to an external forcing, and is assumed to be not affected directly by what happens in the conducting medium (the external apparatus sets up the macroscopic field regardless of what happens in the conducting medium, there is no feedback). The conducting medium reacts to this forcing, and under equilibrium adds a secondary field. The simulations in the previous section provide a particular solution to the cable equation under steady-state. For example, the secondary field is constructed so that inside a sealed conductor (e.g., a neuron with a sealed membrane), the total field is zero.

Continuing with a point inside the membrane, we can rewrite Equation 3.14 using $J = \sigma_i E$,

$$\pi a^2 \sigma_i \frac{\partial E_x}{\partial x} = -2\pi a \sigma_i E_\rho \tag{3.16}$$

We can now express the secondary field as a potential (as it is due to charge redistributions and is therefore "coulombic" in nature),

$$E^s = -\nabla V^s$$

and rewrite the LHS of Equation 3.16

$$\pi a^2 \sigma_i \frac{\partial E_x^p}{\partial x} - \pi a^2 \sigma_i \frac{\partial^2 V^s}{\partial x^2} = -2\pi a \sigma_i E_\rho$$

We now express the RHS in terms of the EMF Φ_{tm} associated to the axial current (due to the total electric field, primary plus secondary) and the resistivity and capacitance of the membrane,

$$\pi a^2 \sigma_i \frac{\partial E_x^p}{\partial x} - \pi a^2 \sigma_i \frac{\partial^2 V^s}{\partial x^2} = -c_m \frac{\partial \Phi_{tm}}{\partial t} - \frac{\Phi_{tm}}{r_m} \tag{3.17}$$

or (since $\pi a^2 \sigma_i = 1/r_i$)

$$\partial_x E_x^p - \partial_x^2 V^s = -c_m r_i \partial_t \Phi_{tm} - \frac{r_i}{r_m} \Phi_{tm}$$

or

$$\lambda^2 \, \partial_x E_x^p - \lambda^2 \, \partial_x^2 V^s = -\tau \, \partial_t \Phi_{tm} - \Phi_{tm} \tag{3.18}$$

This equation is the same as the one derived in [Nagarajan:1996aa] (equation (16) in p. 306).

Most papers on stimulation separate the external primary field (electric or magnetic), and concentrate on the secondary field associated to the response of the system to the applied field. This is what is represented by the potential V or Φ in some papers—in a very confusing way. We must keep in mind that what drives ion gates are the *total* local electric fields.

---

[2]We can see that there are many terms that fall out if we make use of the vector formula $\nabla(a \cdot b) = (a \cdot \nabla)b + (b \cdot \nabla)a + a \times (\nabla \times b) + b \times (\nabla \times a)$.

So, although it may make sense mathematically to work with the secondary field through the associated potential, one must remember that, in principle, to connect back to biological effects, the total field in the membrane must be considered in the end, because this is the physical quantity of interest.

As stated in [Roth:1990aa] (p. 590, top), however, at the membrane the primary electric field E will be much smaller in comparison to the secondary one (charge accumulation across a very thin membrane provides a huge local field). Therefore, we can approximate $\Phi_{tm} \approx V^s - V_o^s$, the difference in secondary internal and external potential

$$\lambda^2 \frac{\partial E_x^p}{\partial x} - \lambda^2 \frac{\partial^2 V^s}{\partial x^2} = -\tau \frac{\partial}{\partial t}(V^s - V_o^s) - (V^s - V_o^s)$$

or, if we assume $\partial_x V_o^s \approx 0$, we can finally write

$$\lambda^2 \frac{\partial E_x^p}{\partial x} - \lambda^2 \frac{\partial^2 \Phi_{tm}}{\partial x^2} = -\tau \frac{\partial \Phi_{tm}}{\partial t} - \Phi_{tm} \tag{3.19}$$

In the (2D) bent case, recall we would have both in the LHS and in the RHS a radial average, in this case the average radial potential (field, current and potential are all linearly related), as we saw above. We can write

$$\lambda^2 \frac{\partial E_x^p}{\partial x} - \lambda^2 \frac{\partial^2 \langle \Phi_{tm} \rangle}{\partial x^2} = -\tau \frac{\partial \langle \Phi_{tm} \rangle}{\partial t} - \langle \Phi_{tm} \rangle \tag{3.20}$$

In a steady state situation we have

$$\lambda^2 \frac{\partial E_x^p}{\partial x} - \lambda^2 \frac{\partial^2 \langle \Phi_{tm} \rangle}{\partial x^2} = -\langle \Phi_{tm} \rangle$$

1.7 The role of boundary conditions [GR]

Just as important as this PDE are its **boundary conditions**. The "termination" boundary conditions for a neuron are that at $x = 0$, L there are no current flows axially, and therefore, or $E_x = -\nabla V = 0$, or

$$E_x^p - \partial_x V^s = 0. \tag{3.21}$$

Thus, we see that the impact of stimulation will be through either the stimulation term $\partial_x E_x^p$ in the PDE, and the termination boundary conditions.

Consider a simple example. Steady-state in a neuron with two terminations (one at each end) and under a constant electric field (and therefore with zero gradient). The equation to solve is

$$\pi a^2 \sigma_i \frac{\partial^2 V^s}{\partial x^2} - \frac{V^s}{r_m} = 0$$

or, with $\lambda = a\sqrt{\pi \sigma_i r_m}$,

$$\lambda^2 \frac{\partial^2 V^s}{\partial x^2} - V^s = 0$$

which has the general solution

$$V^s(x) = Ae^{x/\lambda} + Be^{-x/\lambda}$$

The "termination" boundary conditions are that at $x = 0$, L there are no current flows axially, and therefore, or $E_x = -\nabla V = 0$, or $E_x^p - \partial_x V^s = 0$, or

$$E_x^p = \partial_x V^s(x) = \frac{A}{\lambda} e^{x/\lambda} - \frac{B}{\lambda} e^{-x/\lambda}$$

at each point:

$$E_x^p = \frac{A}{\lambda} - \frac{B}{\lambda}, \ \ E_x^p = \frac{A}{\lambda} e^{L/\lambda} - \frac{B}{\lambda} e^{-L/\lambda}$$

which yields,

$$A = \frac{E_x^p \lambda}{2 \cosh(L/\lambda)} (1 - e^{-L/\lambda})$$

$$B = -\frac{E_x^p \lambda}{2 \cosh(L/\lambda)} (1 - e^{L/\lambda})$$

or

$$V^s(x) = \frac{E_x^p l}{2 \cosh(L/\lambda)} (1 - e^{-L/\lambda}) e^{x/l} - \frac{E_x^p l}{2 \cosh(L/\lambda)} (1 - e^{L/\lambda}) e^{-x/\lambda}$$

and rearranging a bit, we finally obtain the 1D transmembrane potential (see Figure 3.19)

$$V^s(x) = \frac{E_x^p \lambda}{\cosh(L/\lambda)} [\sinh(x/\lambda) + \sinh((x - L)/\lambda)] \tag{3.22}$$

At $x = L$ we find

$$V^s(L) = E_x^p \lambda \tanh(L/\lambda) \longrightarrow E_x^p \lambda$$

for long fibers.

1.8 Stimulation in compartmental models [GR]

As discussed above, in [Bower:2003aa] we have the compartamental version of the cable equation already considering stimulation,

$$\frac{V_m'' - V_m}{R_a} - \frac{V_m - V_m'}{R_a} + I_{inject} = C_m \frac{dV_m}{dt} + \frac{V_m - E_m}{R_m} + \sum_k g_k(V_m)(V_m - E_k)$$
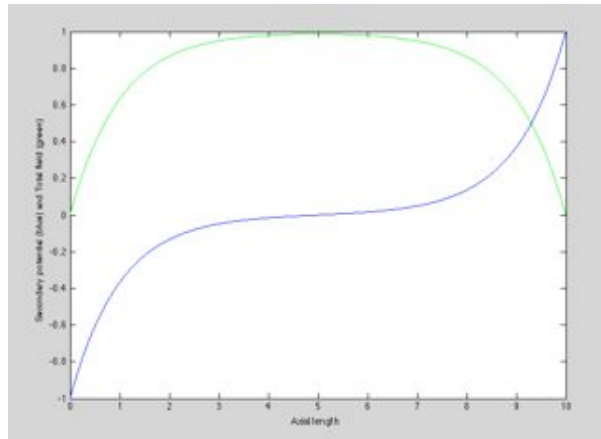

Figure 3.19 – Solution to 1D problem ($l = 1$, $L = 10$ and $E_x^p = 1$) in steady state, see Equation 3.22. In blue the secondary transmembrane potential is provided, and in green the total axial field, which satisfies the termination boundary conditions.

In order to make connection with our work here, we simply set

$$I_{inject} = -\frac{\partial E_l^p}{\partial x}\frac{L_c^2}{R_a} \equiv \frac{\delta E_m}{R_m}$$

Thus, we can interpret the stimulation as a shift in the resting potential of the form

$$\delta E_m = -R_m \frac{\partial E_l^p}{\partial x}\frac{L_c^2}{R_a}$$

As was discussed before, this shift will be of the order of $\delta E_m \sim \lambda E_l$ in terminations or bends. Simumation environments like GENESIS [Bower:2003aa] can provide a useful testing ground for stimulation.

1.9 Summary [GR]

As a summary of this analysis we provide the following points:

- Under electromagnetic stimulation in the quasi-static regime, stimulation affects neuron function through electric field coupling.

- The electric field alters membrane polarization and therefore ion channel function and firing rates.

- The main factors affecting membrane polarization are a) the field strength along axis, b) the field gradient strength along the fiber axis, c) the axial scale λ: the larger the better (and this is proportional to fiber the square root of fiber radius).

- Fiber bends and fiber terminations are key aspects to consider. Stimulation will be most effective in those places.

- At the low frequencies considered here it is not possible to focalize the electric field inside a constant conductivity medium so that a local maximum or minimum is attained.
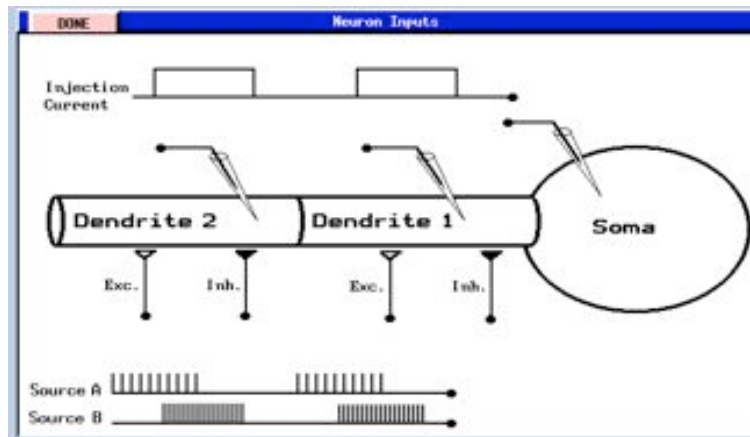

Figure 3.20 – The Genesis simulation environment.

- On stimulation, the electric field is amplified in regions where the conductivity changes, and in particular at membranes. A simple rule of thumb is that it will focus on the membrane in terminations and bends, and that it will be of the order of $\sim E_l\, \lambda/\delta$ —that is, proportional to the along axis field strength times the spatial constant and inversely proportional to membrane thickness.

- The effects will be to de- or hyper-polarize the membrane, shifting the membrane resting potential, and as result impact the firing rates of neurons (probability of firing).

- While TMS exploits a neuro-stimulation mechanism, initiating action potentials in axons (in addition to a neuro-modulatory one), tDCS is clearly neuro-modulatory: tDCS currents modify the transmembrane potential of neurons, and thus modify the level of excitability and the firing rates of individual neurons.

- tDCS does not actively stimulate the cortex, but modulates excitability by modifying the polarization state of the membrane, altering firing rates.

- There are important differences in short and time scale effects from tDCS. Short time scales effects are clearly mediated by membrane polarization changes.

- With regards to long term scales, the effects of tDCS last up to hour after stimulation, with mechanisms involving altering the membrane function through local changes in ionic concentration, alteration in transmembrane proteins and electrolysis-related charges in hydrogen ion concentration induced by exposure to a can electric eld. Short applications do not lead to after effects, only excitability shifts during stimulation.

2   The electric field and neuronal assemblies [FW, AS-F]

2.1   Detailed large-scale neural network models [FW]

Compared with the large number of modeling studies related to the effects of external fields on single neurons, the number of studies dealing with the effects of fields on detailed large-scale neural networks is very limited. Before the year 2005, when [Esser:2005aa] presented the first detailed model to simulate the effects of TMS on different layers of cortical circuits, modeling was only limited to exploring the distribution of magnetic fields in cortical structures [Ravazzani:1996ab, Miranda:2003aa, Nadeem:2003aa, Wagner:2004ab] and their effects on single neurons [Nagarajan:1993aa, Ruohonen:1996ab, Hsu:2000aa, Hsu:2003aa]. To our knowledge, the same situation exists for electric fields ([Svirskis:1997aa, Rattay:1998aa, McIntyre:1999aa] or [Manola:2005aa, Manola:2007aa, Wagner:2007aa]).

However, [Anderson:2007aa] was the first to use a realistic simulation of the cortex to examine the effects of external electrical stimulation.

These detailed models can lead us to gain a better understanding of brain activities in different cortical layers in response to applied electric or magnetic fields. In the following the main features and insights of these studies are summarized.

2.1.1   Topology of detailed models

Detailed models usually study the behaviour of a few mm² of a cortical patch. The basic constructing element of these models is called "macrocolumn" or simply "column". Basically a 2D array of columns forms the cortical patch. Each column is represented by a few number of cortical cells (of various types) that make intra/inter connections within/between cortical columns. In reality, each column consists of 10^4-10^5 neurons. However, in detailed models the number of neurons is much less than this value. Esser et al. used a cylindrical column (D: 300 µm) containing 225 neurons, and Arderson et al. used a cubic column (L: 25 µm) including 16 neurons. In Esser's model, each column was segmented into a 5x5 group of topographic elements in three cortical layers L2/L3, L5 and L6 (two excitatory and one inhibitory cell in each topographic element). The model included two 8x8 arrays of interlaced columns having opposite preferred directions, and the total size of the motor cortex patch (MP) was 5.5x5.5 mm. MP received inputs from premotor (PM), sensory cortex (SI), and thalamus. PM and SI were modelled as 40x40 grids of randomly firing neurons (mean firing rate was 1 Hz). Thalamus was consisted of two 40x40 grids of neurons representing reticular and thalamocortical cells. Anderson's model was formed from a 32x32 array of columns. It consisted four layers (L2/L3, L4, L5 and L6) including pyramidal, basket, double bouquet, stellate and chandelier cells. The size of the cortical patch was 0.8x0.8 mm.

Basically, in large-scale models, connections within/between cortical columns are established by four types of synapses (GABA$_A$, GABA$_B$, AMPA and NMDA). The structure and the number of connections are supposed to be in accordance with the physiological data given in different neurophysiology literatures (such as [Kang:1994aa, Thomson:1997aa, Somogyi:1998aa, Kaneko:2000aa, Okhotin:2002aa] or [Thomson:2003aa, Bannister:2005aa, Watts:2005aa]). Intrinsic properties of neurons (ion channels) are described by various ionic currents such as noninactivating hyperpolarization-activated cation current, low-threshold calcium current, persistent sodium current, and, depolarization-activated potassium current. Schematic diagrams showing the topology of Anderson's and Esser's models are given in Figure 3.21.
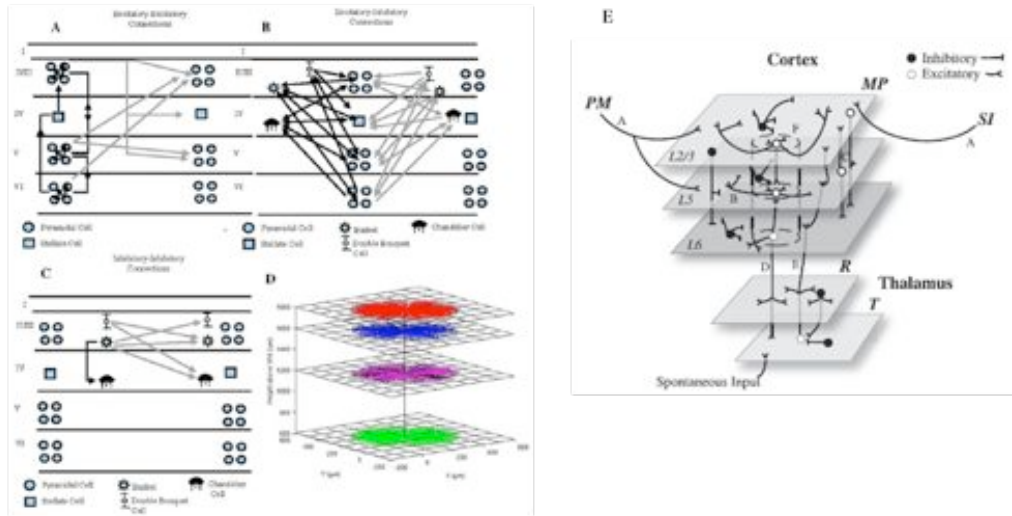
Figure 3.21 – (A-C) Schematic diagram of the neurons locating in different simulated cortical layers in Anderson et al. model. Intra/enter connections within/between columns are represented by dark/light shaded lights. (D) Spatial size scale of axonal arborisation pattern from representative layer 2/3. (E) Schematic diagram of different included cortical areas. Taken from [Esser:2005aa]. For this report, permission has not been requested.

2.1.2 Simulating the effects of externally-applied electric/magnetic fields [FW]

To study the responses of cortical circuits to external fields, one should first simulate the applied external field. Esser et al. simulated TMS pulses by activating synchronously a given fraction of fibre terminals throughout the MP cortex. This procedure is consistent with experimental studies indicating that peripheral nerves are most easily stimulated at terminations [Maccabee:1993aa]. This is also supported by nerve modeling studies indicating that a neuron is most likely to be activated by TMS where a geometric discontinuity, such as fiber termination (e.g., dendrites or synapses) occur [Abdeen:1994aa, Ruohonen:1996ab].

In Anderson's model, the external field was assumed to be generated by either one or two circular disks with radii of 1mm. The medium was assumed to be homogenous having a conductivity equal to the gray matter conductive value ($\sigma = 0.3$ S/m). For a homogenous medium it is straightforward to obtain the spatial potential distribution from a single or double disk receiving a given amount of current. Anderson et al. used the second difference of the voltage (Δ^2V) along initial segments of axons and along nodes of Ranvier (located in the middle of horizontal axon branches) as a parameter by which they determined whether an action potential should be generated in neurons in response to the stimulation. Thresholds for Δ^2V along initial segments and nodes of Ranvier were set to 3 mV and 8 mV, respectively, according to neuronal modeling studies [McIntyre:1999aa, McIntyre:2004aa].

2.1.3 Insights from detailed models

Detailed models have the ability to reproduce electrical activities of single cells in small cortical patches. One of the advantages of these models is that a field potential can be obtained from single neuronal activities. This field potential can be compared with electrical activities that

are recorded experimentally by field electrodes. This led detailed models to be good candidates for the validation or rejection of new hypotheses about the underlying mechanisms of brain responses to external stimulations. Some of these mechanisms are difficult to understand from experimental analysis. For instance, on the basis of detailed modeling, Esser et al. proposed a possible mechanism by which I-waves could be generated in different neocortical layers in response to single or paired TMS pulses [Esser:2005aa]. Although many experimental studies have been previously conducted to characterize I-waves, [Sakai:1997aa][Terao:2000aa] [Di-Lazzaro:2001aa], little was known about the detailed mechanism by which these waves are generated. As another example, Anderson et al. could infer from their modeling study how electrical stimulations affect seizure activities [Anderson:2007aa]. In the following, some of the most important insights obtained from these two models are presented.

The model by [Esser:2005aa] indicates that TMS induces the generation of a volley of I-waves in layer 5 of the cortex where cortico-spinal fibres are emitted. The activities of these descending fibres (I-waves) can be recorded in the epidural area. It was shown that the number of I-waves in the volley was a function of TMS strength. At 15 and 25% of full strength, TMS could generate volleys of two and three I-waves, respectively.

At 25% of maximal strength, the TMS pulse directly activates a large number of cortical fibre terminals in all cortical layers. However, due to strong synapses made by neurons from layers 2/3 and 5, TMS initially elicits a response from layers 2/3 and 5, that subsequently propagates to layer 6 and then to the thalamus. Neurons in layer 5 spike multiple times (three times in this case), whereas other neurons spike only once. This is mainly due to strong net depolarizing currents and high ratio of excitatory to inhibitory synapses that exist in layer 5, and not in other layers. The net depolarization in layer 5 changes with the amount of excitatory pulses targeting this layer (especially from layer 2/3). Strength of TMS determines the amount of firing, net depolarization and thereby, the number of I-waves generated in layer 5. Figure 3.22 shows the simulated response of 40 representative inhibitory and excitatory neurons in different layers of the model to a TMS pulse at 25% strength.

Using the model, [Esser:2005aa] also studied the effects of paired-pulse TMS on I-waves. Both sub-/supra-threshold and supra-/sub-threshold paradigms were investigated. In the first paradigm, the epidural responses could be inhibited or facilitated according to TMS interstimulus intervals (ISIs). Inhibition was obtained for ISIs smaller than 8 ms, while facilitation was obtained for ISIs between 9 to 12 ms. In the second paradigm, the response was facilitated (115% to 125%). The enhancement followed a wavelike pattern with peaks at ISIs of 1, 3.2 and 4.6 ms as those observed in humans. Such effects have been directly explored clinically on I-waves and/or indirectly on motor-evoked potentials (MEP) [Ziemann:1998aa, Ziemann:1996aa, Di-Lazzaro:1998aa].

A detailed study of neuronal activities in different cortical layers of the model suggests the following mechanism for sub-/supra-threshold stimulation. First, the sub-threshold TMS pulse activates a small number of cortical fibre terminals in all cortical layers. Since the sensitivity to depolarizing inputs is higher for inhibitory neurons than for excitatory neurons, hyperpolarizing synaptic currents are induced in all cortical layers. When the suprathreshold TMS pulse is delivered at a short ISI, these hyperpolarizing currents prevent firing of excitatory cells (especially in layer 2/3). On the other hand, neurons in layer 5 fire, because of the high ratio of excitatory to inhibitory synapses in this layer. However, without receiving enough subsequent excitatory inputs from layer 2/3, most layer 5 neurons do not spike many times as described before for a single TMS pulse. At a longer ISI (>9 ms), the inhibitory effect induced by the subthreshold pulse fades as $GABA_A$ synaptic channels close.
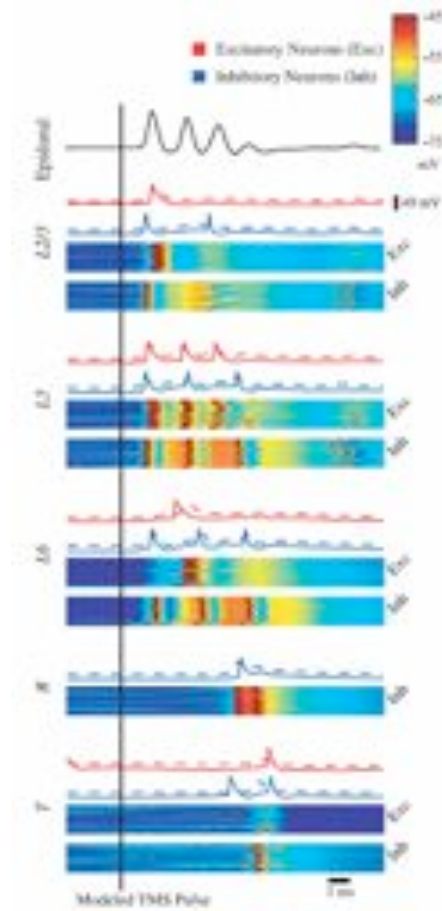
Figure 3.22 – Responses of different neuronal layers of the model to a 25% TMS pulse. Top trace: simulated epidural response showing a volley of four I-waves. Bellow: cell responses in different layers. For each layer, the top traces are excitatory and inhibitory cell membrane potentials. Solid lines depict single-cell membrane potentials, whereas the dashed lines depict average membrane potentials for the population (offset by 20 mV from the single-cell trace for clarity). Membrane potential plots show membrane potentials for 40 neighbouring excitatory or inhibitory cells. Taken from [Esser:2005aa]. For this report, permission has not been requested.

The model proposed by [Anderson:2007aa] made the first framework for studying the evolution of seizure activities in response to stimulations with different parameters. They used monopolar or dipolar electrodes emitting a single pulse or a train of rectangle pulses (duration of pulse 200 µs) in a frequency range from 60 to 200 Hz. They also varied the overall levels of excitatory and inhibitory connections in the model using some multiplicative factors acting on synaptic gains.

Simulations showed that a 0.1 s external field induced by the monopolar electrode could cease the seizure activity and could delay the next population spike for about 0.6 s. This phenomenon was studied in five overall levels of excitatory and inhibitory connections. The delay increased with the frequency of stimulating pulses. Figure 3.23 illustrates how 200 Hz stimulating pulses may stop the seizure in each of the studied connectivity levels. The influence of the frequency on the time that the network returns to seizure activity is also illustrated in this figure.
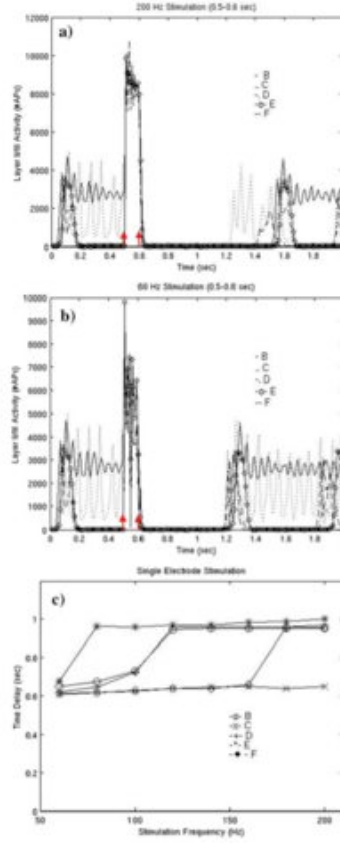
Figure 3.23 – Stimulation effects as a function of frequency and connectivity. (a-b) Trains of rectangular pulses at 200 and 50 Hz from 0.5 s to 0.6 s suppress the seizure activity in all the networks with different connectivity patterns. (c) Delay to return of activity as a function of frequency for five tested connectivity patterns (B-F). Taken from [Anderson:2007aa]. [For this report, permission has not been requested]

In their model, [Anderson:2007aa] also studied the effects of the polarity and the orientation of stimulations. They emulated a longer cortical network by connecting opposite corners of the described cortical patch in Section 2.1.1. This connection was especially including pyramidal cells in layers 2/3 and 5. Stimulation of this extended cortical patch by dipole electrodes indicated that if the orientation of stimulation is parallel to the orientation of connections (in both polarities), the effects of stimulations on stopping the seizure increases. Finally, by the means of single-pulse stimulation protocol, they showed that the time alignment between the stimulation and the peak activity of the network could modify the time duration after which seizure activity reappears. Altogether, the simulations described below (i.e. the effect of frequency, orientation, time alignment, etc.) increase our knowledge about the response of brain circuits to stimulations and leads us to further optimize stimulation parameters for a desired action.

2.2   Lumped-parameter neuronal population models [FW]

Two complementary modeling approaches were developed over the past decades in order to analyze and interpret the activity generated by networks of neurons.

In the first one, referred to as "detailed", single neurons are accurately modeled regarding their structural components (dendrites, soma, axon) and functional properties such as passive or active channels. Neuronal networks are then built from the interconnection of a sufficiently large number (i.e. several thousands) of principal neurons and different types of interneurons with appropriate synaptic interactions. In these networks, the field activity is reconstructed from the summated post-synaptic potentials of pyramidal cell membranes. The influence of various parameters such as the types of neurons introduced in the network, network size, connectivity patterns, and conduction delays can then be studied. The first models were developed by [Rall:1968aa] to represent passive electrical properties. Then, in order to add active properties and to test some hypotheses about differences in impulse responses at the soma and at the axon, Dodge and colleagues [Dodge:1979aa, Dodge:1973aa] proposed a computer simulation of a motoneuron in which thresholds in these regions could be altered by using different sets of values for the voltage sensitive rate constants (in the HH equations) for the soma and axon. Whole cell models were proposed by Traub and colleagues for neocortical and hippocampal pyramidal cells [Traub:1979ab, Traub:1979aa, Traub:1982aa]. In such models, the ionic channels in each compartment are represented by differential equations describing their properties (whether voltage-gated, ligand-gated, or second messenger-activated properties).

In the second approach, referred to as "macroscopic" or "lumped", a higher level of organization, i.e. the neuronal population level, is considered. It starts from the fact that neurons form populations and that field oscillations (LFPs, EEG) are caused by ensemble dynamics rising from macroscopic statistical interactions between interconnected neuronal sub-populations (pyramidal cells and interneurons). The macroscopic modeling approach has developed since the 1960's. It conceptually differs from the detailed approach briefly described above in the sense that it emphasizes the properties of populations of cells instead of those of individual neurons. In considered populations, cells are assumed to be spatially close and their interconnections are assumed to be random but dense enough so that the probability for any two cells in the population to be connected (either directly or via interneurons) is high. Based on these assumptions, population models represent the temporal dynamics of the aggregates while the spatial interactions between cells are neglected. This implies that the relevant variable of these models is not the single spike but rather the spike frequency, or firing-rate, computed from the total current delivered by synaptic inputs (which sum linearly according to the mean-field approximation) into the soma. During the past decades, this class of models has been used in numerous theoretical and experimental studies, mainly related to interpretation of neurophysiological data.

Pioneer works on models of localized populations of neurons started in the early 1970's with Wilson and Cowan [Wilson:1972aa] who put the theoretical bases of these models. Authors started from works of [Mountcastle:1997aa] and [Hubel:1965aa, Hubel:1963aa] who brought physiological evidence for the existence of such populations: a high degree of local redundancy is present within relatively small volumes of cortical tissue as many cells have nearly identical responses to identical stimulus. They also used a crucial assumption, considered, at that time, as an axiom: all neural processes depend upon the interaction of excitatory and inhibitory cells. Therefore, they considered a population as being composed of two subpopulations, one excitatory and the other one inhibitory and proposed an approach based on two variables, namely $E(t)$ and $I(t)$, representing the proportion of excitatory and inhibitory cells firing per unit time respectively. Following the same approach, Freeman and colleagues developed a comprehensive model of the olfactory system since the

early 1960's [Freeman:1973aa, Freeman:1968aa, Freeman:1963aa]. Similar ideas developed at the same time by Lopes da Silva and collaborators [Suffczynski:2001aa] led to the development of a lumped-parameter population model able to explain the alpha rhythm of the EEG observed in dog. Later, Zetterberg and colleagues [Zetterberg:1978aa] studied the performances of this model in terms of stability. Interestingly, they imitated both background EEG activity and certain types of paroxysmal activity and reached a conclusion that epileptic spikes are generated by populations of neurons that operate close to instability. Works were also pursued on the mechanisms of transition between normal EEG activity (i.e. non-epileptiform) and epileptiform paroxysmal activity. Model predictions were compared with results obtained in different types of epilepsy, including patients with absence seizures and allowed for generation of hypotheses about pathophysiological mechanisms of ictal transitions [Suffczynski:2006aa, Suffczynski:2001aa]. The lumped parameter model of alpha rhythm generation they proposed was also the starting point in the design of a model of cortical column used to simulate visual evoked potentials computed from spontaneous EEG signals [Jansen:1995aa, Jansen:1993aa]. An interesting feature of this study is that authors proposed a simplified generic model for cortical activity generation that was studied and extended by Wendling et al. [Wendling:2005aa, Wendling:2002aa, Wendling:2000aa] in the context of model-based interpretation of intracerebral EEG signals in epilepsy. Finally, it is also important to underline that the recent past years have witnessed a large increase of interest for neural mass models [David:2004aa, David:2003aa, Zavaglia:2006aa].

2.2.1 Mean-field models: basic assumptions and principles

In the simplest form of the neuronal population model, a cluster of neurons is considered. As displayed in Figure 3.24-a, this cluster contains two subsets. The first subset is composed of the principal cells (i.e. pyramidal cells). The second subset is composed of local interneurons (i.e. other nonpyramidal cells, stellate or basket cells). Pyramidal cells receive excitatory input from other pyramidal cells (collateral excitation) or inhibitory input from interneurons. These latter cells receive excitatory input only from pyramidal cells.

As illustrated in Figure 3.24-b, each subset is characterized by two functions, respectively named as the "pulse-to-wave function" and the "wave-to-pulse function" by [Freeman:1992aa]. The former is a linear transfer function that changes presynaptic information (i.e. the average density of afferent action potentials) into postsynaptic information (i.e. an average excitatory or inhibitory postsynaptic membrane potential, respectively EPSP or IPSP, Figure 3.24-c). The latter is a static nonlinear function that relates the average level of membrane potential of the neurons in the considered subset to an average pulse density of potentials fired by these neurons (Figure 3.24-d). This nonlinear function mimics the integrating action that takes place at the soma (threshold and saturation effects).

2.2.2 From generic to specific models at neuronal population level

An interesting feature of neuronal population models is that they can be adapted to specific brain structures based on available data about the organization of subsets of neurons and interneurons within considered structures. Following this "macroscopic" approach, Freeman and colleagues developed a comprehensive model of the olfactory system since the early 1960's [Freeman:1973aa, Freeman:1968aa, Freeman:1963aa]. Based on histological and physiological analytic methods conducted in animal models (cat), their model reproduces the
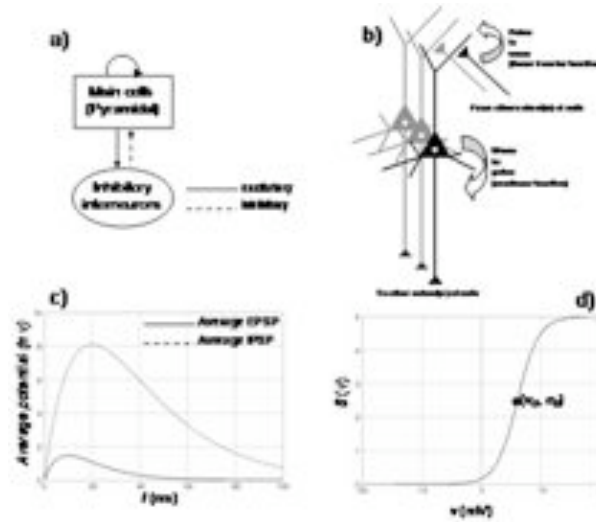
Figure 3.24 – a) Structure of the generic neuronal population model representing a cluster of neurons composed of two subsets: main cells (i.e. pyramidal cells) and local interneurons (i.e. other nonpyramidal cells, stellate or basket cells). Pyramidal cells receive excitatory input from other pyramidal cells (collateral excitation) or inhibitory input from interneurons. These latter cells receive excitatory input only from pyramidal cells. b) Each subset is characterized by two functions, respectively named as the "pulse-to-wave function" and the "wave-to-pulse function". The former changes presynaptic information (average density of afferent action potentials) into postsynaptic information (average excitatory or inhibitory postsynaptic membrane potential, respectively EPSP or IPSP). The latter relates the average level of membrane potential of the neurons to an average pulse density of potentials fired by these neurons. c) Impulse response of the "pulse-to-wave function" approximating actual average excitatory (dotted line) or inhibitory (solid line) postsynaptic potentials. d) Shape of the "wave-to-pulse" function. Nonlinear sigmoid shape accounts for the integrating action that takes place at the soma (threshold and saturation effects). Taken from [Wendling:2008aa].

global organization of the olfactory system. Its structure includes the olfactory receptor neurons (model input) as well as main components like the olfactory bulb (OB), the anterior olfactory nucleus (AON), and the prepyriform cortex (PC). Each part (OB, AON and PC) contains four subsets of cells (two excitatory and two inhibitory). Authors showed that the model produces realistic EEG signals that approximate those experimentally recorded in the same structures [Freeman:1987aa]. Similar ideas developed at the same time by Lopes da Silva and collaborators [Suffczynski:2001aa]z led to the development of a lumped-parameter population model able to explain the alpha rhythm of the EEG observed in dog. The model was based on two interacting populations of neurons representing a subset of excitatory thalamocortical relay cells (TCR) and a subset of inhibitory interneurons (IN) connected to the former subset through a negative feedback loop. Model predictions were compared with results obtained in different types of epilepsy, including patients with absence seizures and allowed for generation of hypotheses about pathophysiological mechanisms of ictal transitions [Suffczynski:2006aa, Suffczynski:2001aa]. In line with these previous studies, Wendling and co-workers [Wendling:2002aa, Wendling:2000aa] designed a the model of hippocampal activity, starting from recent results about i) the role of inhibitory interneurons in hippocampal or neocortical networks in the generation of gamma frequency oscillations

[Jefferys:1996aa, Whittington:2000aa], ii) the non-uniform alteration of GABAergic inhibition in experimental models of temporal epilepsy (reduced dendritic inhibition and increased somatic inhibition) [Cossart:2001aa], and iii) the possible depression of $GABA_{A,fast}$ circuit activity by $GABA_{A,slow}$ inhibitory post-synaptic currents in the hippocampus [Banks:2000aa]. The model was designed to represent the hippocampal cellular organization of interacting subsets of principal neurons and interneurons, as summarized in Figure 3.25. It consists in three subsets of neurons, namely the main cells (i.e. pyramidal cells), the slow dendritic-projecting inhibitory interneurons ($GABA_{A,slow}$ receptors) and the fast somatic-projecting inhibitory interneurons ($GABA_{A,fast}$ receptors). Three key model parameters are directly related to excitatory, slow inhibitory and fast inhibitory synaptic interactions between subsets of cells. The main results showed that he the model can produce strikingly realistic activities compared to depth-EEG signals for relevant modifications of excitation/inhibition-related parameters. The model predicted a dis-inhibition process during the transition from interictal to ictal activity and a key role of interneurons projecting to the soma of pyramidal cells during the fast onset activity. Interestingly, these model-based hypoteses were recently confirmed experimentally [Gnatkovsky:2008aa].

2.2.3 Simulation of electrical stimulation effects in a macroscopic model of hippocampus

The first attempt to reproduce electrical stimulation effects in macroscopic models was published recently [Suffczynski:2008aa]. In order to obtain a deeper insight into the nature of the EEG changes leading to an ictal transition and into the reasons why a stimulation or "active" paradigm may be superior to a "passive" analysis, the authors investigated these processes using a computational approach. They used the model of a hippocampal network presented in Section 2.2.2 in which they reproduced the effects of electrical stimulation induced with clinical depth-electrodes. Regarding the effect of this external stimulation performed by an extracellular bipolar electrode, authors assumed an "additive model": the change of membrane potential is proportional to the generated extracellular current in all three subpopulations represented in the model although in real tissue it would depend on the relative position of neurons with respect to the electrode. The simulated stimulation consisted of square, monophasic pulses of 1 ms duration at the frequency of 10 Hz, delivered during 60 s, as in the protocol used in epileptic patients.

Using this simplified model of stimulation in a macroscopic computational model, authors were able to investigate functional links between physiological parameters controlling excitability of the hippocampal network, on the one hand, and EEG quantities measured from passive observations or from the responses to active stimulations, on the other hand.

2.3 Other methodologies for EEG simulation [AS-F]

This section deals with the description of two different methodologies for the simulation of EEG signals based on a certain modeling of neural activity. On the one hand [Cosandier2007] and [Cosandier2008] describe a model at the neuronal network level in order to approximate EEG recordings both on scalp and intra-cerebral electrodes. This methodology is described below. On the other hand, an integrative connectionist approach [Kasabov2008] is taken into account. This one combines modeling work at different levels of abstraction in order to simulate EEG recorded with scalp electrodes. Section 2.3.2 deals with this second approach.
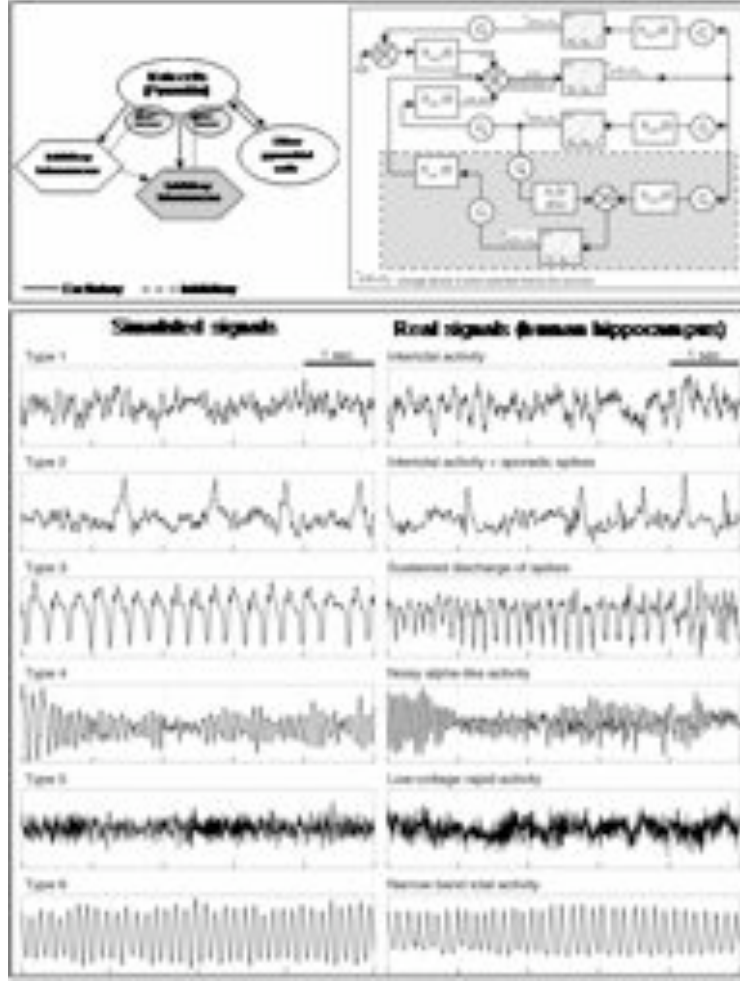
Figure 3.25 – Neuronal population model based on the cellular organization of the hippocampus. a) Schematic representation. A whole population of neurons is considered inside which a subset of principal cells (pyramidal cells) project to and receive feedback from other local cells. Input to interneurons is excitatory (AMPA receptor-mediated). Feedback to pyramidal cells is either excitatory (recurrent excitation) or inhibitory (dendritic-projecting interneurons with slow synaptic kinetics - $GABA_{A,slow}$ - and somatic-projecting interneurons (grey color) with faster synaptic kinetics - $GABA_{A,fast}$ -). As described in (Banks et al. 2000), dendritic interneurons project to somatic ones. b) Corresponding block diagram representation. The introduction of an additional subset of interneurons with fast synaptic kinetics adds a fast feedback inhibitory loop (grey rectangle) to the generic model. The three main parameters of the model respectively correspond to the average excitatory synaptic gain (EXC), to the average slow inhibitory synaptic gain (SDI) and to the average fast inhibitory synaptic gain (FSI). See table 3 for other model parameters.

2.3.1   Application of the Extended Source Model

The model presented in [Cosandier2007] and further employed in [Cosandier2008] is first based on combining a model of the spatial distribution of electrical sources together with the temporal evolution of this activity. This model is denoted as Extended Source Model. Once the sources are modeled the methodology proposes the resolution of the forward problem for simulating EEG signals recorded by both scalp and intra-cerebral electrodes (see Fig. 3.26).
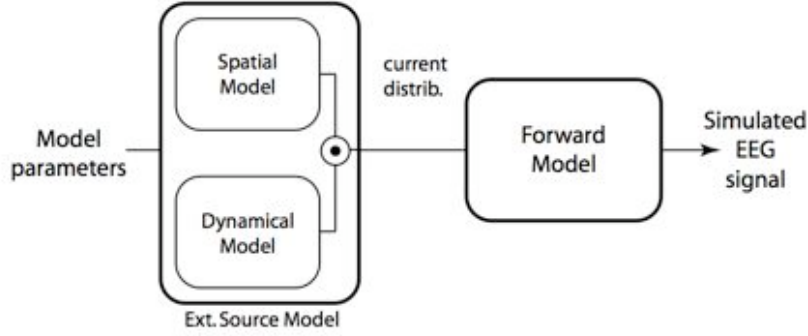
Figure 3.26 – Block diagram of the employment of the Extended Source Model for the simulation of the EEG signals.

The Extended Source Model is explained in [Cosandier2007]. It is based on a 3D model of current distribution denoted in matrix form as $\mathbf{I}$. This matrix with elements $I_{ij} = I(\mathbf{x}_i, t_j)$ synthesizes the linear superposition of N electrical sources in 3D positions $\mathbf{x}_i$ at times $t_j = 1, \ldots, T$. The model supposes therefore a discretization in the space and time domains.

In the space domain a segmentation of the neocortical surface S is first undertaken, whereby a grid of N surfaces of area s_i mm^2 is created. An elementary dipole moment is placed in each of these surfaces in order to model the electrical activity of the underlaying neural population in the spatial domain. As known a dipole moment is characterized by position, orientation and magnitude. Each dipole moment is placed in the center of mass of the surface s_i and with a normal orientation to this surface [Cosandier2007][Cosandier2008]. The magnitude of the dipole moment $q(x_i)$ is computed assuming an average volume current density in the cerebral cortex of 175 nA/mm^2 and an average cortical thickness of 3 mm, which results in:

$$q(\mathbf{x}_i) = s_i \cdot 525 \ [nA \cdot mm]. \tag{3.23}$$

In the temporal domain, the temporal dynamics of the neural populations involved in the generation of neural activity is modeled. The resulting model is described in detail in [Wendling:2000aa] and can be classified as a lumped model (see Sec. 2.2). In this Section we just give an overview of this system based on the block diagram depicted in Fig. ??. We can observe that different populations are modeled in its own and the coupling among them is modeled by a constant K. Although this coupling can be individualized by taking into account the coupling between particular pairs (i, j) of neural populations through a constant K_{ij}, it has been considered constant all over population pairs through a unique K (see Fig. 3.26) in the model.

In each neuronal population the modeling is done on the global current activity within the neuronal assembly. As expected, there are two types of current contributions denoted as excitatory and inhibitory. The coupling of other neural populations contributes to the excitatory post-synaptic membrane potential. To this excitatory afferent activity contribute as well a global representation of the average density of afferent action potentials denoted as $p(t)$. Both the excitatory and the inhibitory activities go through two linear transfer functions, respectively $h_e(t)$ and $h_i(t)$, which transform the average pre-synaptic pulse density of action
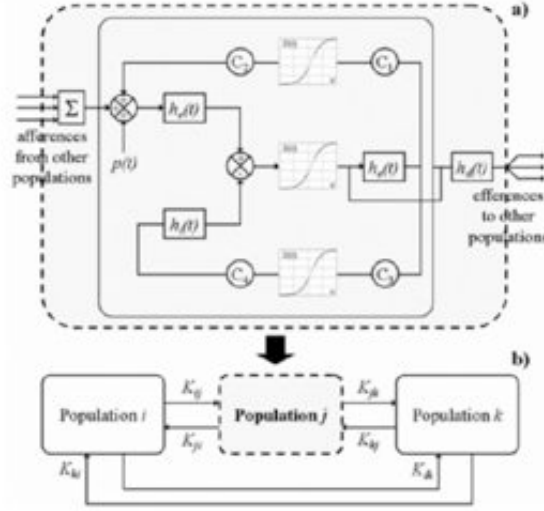
Figure 3.27 – Block diagram of the Lumpen-parameters Model used for the simulation of the interaction of neural populations in the time domain. Taken from [Cosandier2007].

potentials into a post-synaptic membrane potential either excitatory or inhibitory. Once its interaction result has been computed by subtracting the inhibitory from the excitatory activity, this goes through a non-linear function that transforms the post-synaptic membrane potential into an average density of potentials fired by the neurons of the population and that presents an excitatory effect thus going again through the non-linear transfer function $h_e(t)$. Moreover it returns in a feedback loop to the input of the neural population both excitatory and inhibitory after going again through two non-linear functions that transform average density of potentials into average post-synaptic potential. The global output of each neural population is computed after going through a third transfer function $h_d(t)$, which delivers $\alpha_i(t)$, a representation of the local field potential (LFP) generated by the neural population i. The output $\alpha_i(t)$ is lastly used as the input to the excitatory activity in other populations through K.

The models in the space and temporal domains described above are thence combined through the following equation:

$$I(\mathbf{x}_i, t) = q(\mathbf{x_i}) \cdot \alpha_i(t), \tag{3.24}$$

where $q(\mathbf{x}_i)$ denotes the result of eq. (3.23). After discretizing in the time domain for samples $t_j = 1, \ldots, T$, we obtain the components I_{ij} of the matrix $\mathbf{I}$ used for modeling the current distribution depicted in Fig. 3.26 as a result of the extended source model. For simulating the EEG signal generation we need thence to solve the forward model that transforms the neural activity into the electrical potentials $\mathbf{V}$ behind the EEG signals. The EEG is expressed in matrix form $\mathbf{V}$ of dimensions $M \times T$. Each element of this matrix denote the potential of one of the M sensors with respect to a point placed at infinity, i.e. this is the point of electrical reference, in time t_j. The forward model can be therefore expressed as a product of matrices

$$\mathbf{V} = \mathbf{GI}, \tag{3.25}$$

where $\mathbf{G}$ a $M \times N$ matrix, where G_{ki} denotes the influence of the dipole in cell i to the signal recorded at sensor $k = 1, \ldots, M$.

The coefficients of the matrix $\mathbf{G}$ are set up by solving the forward problem. For this purpose, it is necessary to count on the dipole parameters (i.e. the position and orientation computed heretofore) the sensor position, and a head model. No propagation effects are taken into account in [Cosandier2008], so that no delay is accounted between the currents in $\mathbf{I}$ and the measures at the electrodes. Further consequences of this simplification are not stated in the reference work. Taking these facts into account, the only element to be computed is the head model. Two different approaches are followed for the simulation of intracerebral electrode signals and scalp ones. In the first case a spherical model, where brain, skull, and scalp, are modeled through 3 concentric spheres, is supposed. In case of the scalp electrode signals a more realistic head model is employed.

The realistic model is based on the consideration of three nested homogeneous volumes, whose surface geometry is extracted from 3D MRI data. The extraction is based on a surface segmentation and triangulation processes undertaken with the ASA software[3]. The forward computations are computed through a numerical method denoted as boundary element method, which is included in the same software package. Having used external software for the resolution of the forward model, very few details are clear on the completion of this step.

2.3.2   Integrative Connectionist Systems

Integrative connectionist systems constitute a novel paradigm in the biologically plausible modeling of neuronal functions through the integration in the same system of neuronal models and principles of evolutionary computation [Kasabov2008]. In this context different frameworks have been proposed for different application fields. We are interested herein in the application of integrative connectionist systems for the simulation of EEG signals. This has been achieved through a so called computational neurogenetic model (CNGM)[Benuskova2008][Kasabov2008]. This type of models try to characterize the interaction between a connectionist system, i.e. neural network, and a genetic network, which models the relationships among several genes. This fact is motivated by the wish to model the neural function at a molecular level as well, i.e. below the neural modeling level. At the molecular level the model is supposed to lay on the modeling of the genetic interactions.

Using a CNGM, the simulation of the EEG generation will be achieved herein through the interaction of a neural model and a genetic one. In contrast to the Extended Response Model (see Sec. 2.3.1), where the current signals are modeled for a neural ensemble, the neural model used herein described the currents in each of the neurons forming part of a neural ensemble. For this purpose a Spike Neural Network is used. These type of neural networks models the spikes generated by each of the artificial neurons and the interaction among them within the network. Different spiking neuronal models have been proposed, being the most relevant ones the Integrate-and-Fire, the Hodgkin-Huxely Model, and the Simple Response Model [Gerstner2002][Izhikevich2003]. The CGNM uses the Simple Response Model (SRM), from which a simplified version known as simple zero order SRM exists, for the EEG simulation. SRM and its simplification are described in the following.

Simple 'zero order' Spike Response Model

The simplified Spike Response Model [Gerstner2002] (Chapter 1), denoted as SMR_0, presents two main points. The first one describes the effect of spikes in a post-synaptic

---

[3]Demo available at http://www.ant-neuro.com/products/asa

neuron. When different trains of spikes coming from different neurons arrive at the neuron we want to characterize, they generate a potential difference between the inner and the outer part of the neuron cell i denoted as membrane potential $u_i(t)$. Before the spike trains arrive at neuron i the membrane potential is at its basis level denoted as $u_{rest}(t)$ (normally taken to be $-65mV$). The incoming spike adds some potential to this basis level due to the so called post-synaptic potential $\varepsilon_{ij}(t)$ from neuron j. This can be characterized by equation:

$$u_i(t) = \varepsilon_{ij}(t) + u_{rest}(t). \tag{3.26}$$

The process is graphically described in Fig. **??**A. As it can be observed the process is further characterized by the instant of time when neuron j fires the spike k, which is denoted as $t_j^{(k)}$. It is worth mentioning that the PSP can be excitatory, i.e. $\varepsilon_{ij} > 0$, or inhibitory, respectively denoted as EPSP or IPSP. The excitatory behavior results in a depolarization of the membrane potential, whereas the inhibitory one in its so-called hyper-polarization, i.e. the potential decreases below $u_{rest}(t)$.
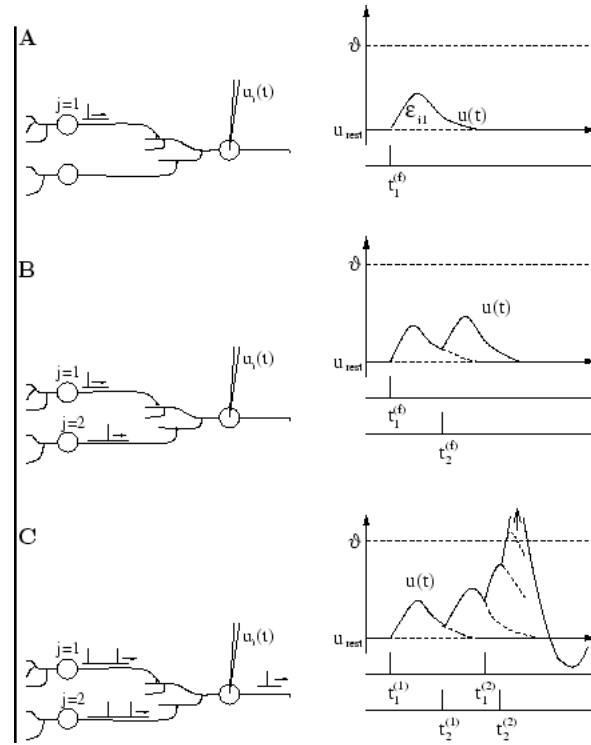
Figure 3.28 – Schematic description of the effect of PSPs in the membrane potential $u_i(t)$ of a neuron, which can be measured in the soma through an electrode. A: Arriving from just one neurons. B: Arriving from two neurons. C: Repeatedly arriving from two neurons and making $u_i(t)$ reaching a threshold γ whereby an outgoing spike is generated. Taken from [Gerstner2002].

If more than one incoming spike train is taken into consideration, the resulting membrane potential results from the superposition of the different PSPs (see Fig. **??**B). Since the process is repeated for each spike fired at $t_j^{(k)}$, it can be modeled through the following expression:

$$u_i(t) = \sum_j \sum_k \varepsilon_{ij}(t - t_j^{(k)}) + u_{rest}(t). \tag{3.27}$$

The superposition of the incoming spikes over all neurons and firing times can make the membrane potential reaching a firing threshold γ if several spike trains arrive in a short time interval. At this time point the neuron stops behaving following the linear superposition and generates a pulse-like potential denoted as action potential, which will become the PSP of the neurons with incoming connections from neuron i (see Fig. **??**C).

The second main point of the model is the waveform of the outgoing action potential. The action potential presents a short duration pulse reaching peak values of $100 mV$. After this pulse the potential return to the basis membrane potential. However it does not stop at this level but goes under it, undergoing an hyper-polarization of the membrane potential which is called spike-afterpotential. Once reached the minimum potential level, the membrane potential returns to basis level $u_{rest}(t)$ following an exponential waveform. The overall waveform has been modeled as $\eta(t)$ through the expression:

$$\eta(t - t_i^{(k)}) = \begin{cases} 1/\Delta t & \text{for } 0 < t - t_i^{(k)} < \Delta t \\ -\eta_0 \exp(-\frac{t - t_i^{(k)}}{\tau}) & \text{otherwise} \end{cases}, \tag{3.28}$$

where $\eta_0, \tau, \Delta t > 0$. If Δt is sufficiently small the pulse approaches a Dirac delta, which is placed at the firing time of neuron i denoted therefore as $t_i^{(k)}$

$$\eta(t - t_i^{(k)}) = \delta(t - t_i^{(k)}) - \eta_0 \exp(-\frac{t - t_i^{(k)}}{\tau}) \quad \forall t \geq t_i^{(k)} . \tag{3.29}$$

Figure **??** synthesizes the former explanation. If $\eta_0 \ggg \gamma$, this parameter models the neuronal refractoriness, whereby it is more difficult that the neuron i fires two spikes, one immediately after the other. In a more general form of refractoriness model [Kandel2000] (p. 157) the refractory period is divided in two time periods, the absolute and the relative ones. While in the first one it is impossible to fire a spike, in the second one it is just more difficult. This differentiation is not taken into account in the simplified model described herein.
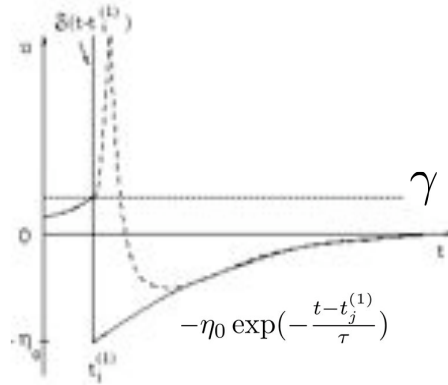
Figure 3.29 – The action potential generated by the membrane potential when passing over the threshold γ. Dashed line: Actual form of the action potential. Continuous line: Modeling through a Dirac delta and an exponential charging into u_{rest}, which has been set here to reference 0. Modified from [Gerstner2002].

Putting together the two points formerly described we can model the neuronal dynamics by setting up the value of the membrane potential of neuron i through the expression:

$$u_i(t) = \eta(t - \hat{t}_i) + \sum_j \sum_k \varepsilon_{ij}(t - t_j^{(k)}) + u_{rest}(t), \tag{3.30}$$

where $\hat{t}_i$ is the last firing time of neuron i, i.e.

$$\hat{t}_i = \max_k\{t_i^{(k)}\} \mid t_i^{(k)} < t, \tag{3.31}$$

η expression comes from eq. (3.29), and ε_{ij} states for the response of neuron i to the spike train from neuron j. Neuron i fires whenever its value reaches the threshold γ from below, setting up the values of the firing times $t_i^{(k)}$

$$u_i(t) = \gamma \;\wedge\; \frac{du_i(t)}{dt} > 0 \;\Rightarrow\; t \doteq t_i^{(k)}. \tag{3.32}$$

The model formerly described presents some limitations. They can be consulted in [Gerstner2002][4].

Full Spike Response Model

A generalization of the model described in the former section has been set up and denoted as full SRM. In my opinion the most charactering traits of the model can be summarized in two points: a generalization of the membrane potential expression by taking into account other effects than the PSPs, and changing the way of modeling the refractoriness with respect to the one used in the simplified model. In the full model the refractoriness is modeled through a time dependent value of the firing threshold.

In SRM the basis level of potential of the neurons is first set to 0

$$u_{rest}(t) = 0 \tag{3.33}$$

in order to simplify a bit the notation. The full SRM establishes a generalized form of the membrane potential of neuron i, which substitutes eq. (3.30) of the simplified model with

$$u_i(t) = \eta(t - \hat{t}_i) + \int_0^\infty \kappa(t - \hat{t}_i, s) I^{ext}(t - s) ds, \tag{3.34}$$

where $s = t - t_j^{(k)}$ states for the time gap from the firing of the neuron j indexed by k. In this equation two different terms can be distinguished. These two terms are characterized by the kernels denoted as η, and κ. As in the simplified SRM model, η states for the waveform of the action potential in the modeled neurons. An equation like the one in (3.29) can be taken for that. However the exact waveform of η is not so important, but the definition of a firing time $t_i^{(k)}$. This time instant plays the same role as the resetting time in the integrate-and-fire model [Gerstner2002][5]. The integrate-and-fire model can therefore be seen a particular case of the SRM model.

Kernel κ states for the 'impulse response' of neuron i to any external current, which can be generated by other neurons or by external current sources. Thus the second term of eq. (3.34) is similar to a filter convolution expression, where κ plays the role of the filter impulse response. If we consider as current sources other neurons than the one being modeled, the convolution of the current function generated by them and κ results in a third kernel denoted as ε. Kernel ε states for the effect of the PSP currents from incoming neurons j in the modeled neuron i.

$$u_i(t) = \eta(t - \hat{t}_i) + \sum_j v_{ij} \sum_k \varepsilon_{ij}(t - \hat{t}_i, s) + \int_0^\infty \kappa(t - \hat{t}_i, s) I^{ext}(t - s) ds, \tag{3.35}$$

---

[4]Or in http://icwww.epfl.ch/~gerstner/SPNM/node5.html#SECTION01132000000000000000.
[5]http://icwww.epfl.ch/~gerstner/SPNM/node26.html#SECTION02311000000000000000

The kernels ε and κ are therefore closely related. Actually they are used along [Gerstner2002] in a very confusing manner. As already mentioned ε results, in an ideal world since it is not described this way in any of the consulted reference works, from the convolution of the current signal coming from the neuron j once having traversed the synapse with the 'impulse response' kernel κ. Kernel κ represents therefore the linear response of the membrane potential to an input current. In this context v_{ij} states for the synaptic efficiency between neurons i and j. In case of no external stimulation, kernel κ drops out from the expression. It is worth pointing out that all kernels are expressed as a function of $t - \hat{t}_i$, where $\hat{t}_i$ is defined in (3.32).

As mentioned above the second main trait of the SRM model is the existence of a time varying threshold

$$\gamma \rightarrow \gamma(t - \hat{t}_i), \tag{3.36}$$

i.e. again a function of $\hat{t}_i$, the last firing time of neuron i. This time variation is a way of modeling the refractoriness period, when the neuron firing is more difficult or even impossible [Fuortes1962]. This is not the only way to model refractoriness within SRM. Hence we could also model it through ε and/or κ so that input current pulses after $\hat{t}_i$ present an amplitude proportional to the distance to this time point. Moreover refractoriness can be modeled through the kernel η. Indeed the exponential part of (3.28) models it within the simplified SRM.

In Figure **??** refractoriness has been modeled by three concurrent traits. The first one is an exponentially varying threshold with a previous absolute refractory period, where the threshold value after the firing $\hat{t}_i$ presents a constant value larger than the spike peak. The absolute refractory time period is sometimes denoted as Δ^{abs}. Second refractoriness is modeled through the hyperpolarization period of the membrane represented within the kernel η. Lastly the firing of other incoming neuron spikes after $\hat{t}_i$, represented by kernel κ, presents a time-dependent maximum value. The more distance the firing time is from $\hat{t}_i$, the larger is the amplitude value.
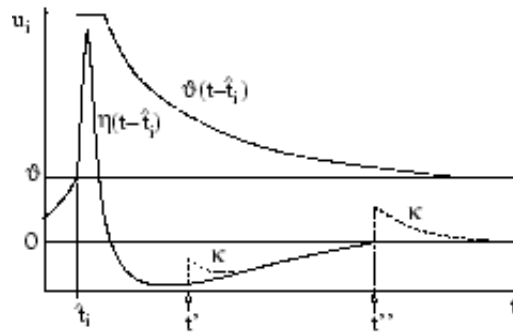
Figure 3.30 – Modeling of refractoriness through a time-dependent threshold (here represented by υ instead of γ used in text), and through kernels η and κ. The firing time of neuron i is represented by $\hat{t}_i$. The firing times of two consecutive incoming neuron spikes by t' and t''. Taken from [Gerstner2002].

Spiking Neural Network

The full SRM model is taken as starting point for the Spiking Neural Network (SNN) that models the system information processing level of brain processes analysis in [Benuskova2008]. At this analysis level the information processing undertaken by neuronal ensembles is modeled.

We first comment the used neuron model, whereby the membrane potential is defined in the SNN through the expression

$$u_i(t) = \sum_k \delta(t - t_i^{(k)}) + \sum_j v_{ij} \sum_m \varepsilon_{ij}(t - t_j^{(m)} - \Delta_{ij}^{ax}), \tag{3.37}$$

where the kernel of the action potential η has been modeled through a delta, and the membrane potential induced by the currents coming from the incoming neurons j is modeled through the kernel ε and weighted by the synaptic efficiency between neuron j and i represented by v_{ij}. The term Δ_{ij}^{ax} states for the delay introduced by the physical distance between neurons i and j. This term is proportional to the Euclidean distance between both neuron positions in the network, whose model will be commented below.

The post-synaptic potential kernel ε (PSP) is modeled through the combination of two exponential functions in the form

$$\varepsilon_{ij}^{type}(s) = A^{type} \left[\exp\left(-\frac{s}{\tau_{decay}^{type}} \right) - \exp\left(-\frac{s}{\tau_{rise}^{type}} \right) \right], \tag{3.38}$$

where *type* denotes the type of synaptic connection, which can be set up among *fast excitation*, *slow excitation*, *fast inhibition*, or *slow inhibition*. This type definition affects the definition of the time constants τ, both in the rise and decay phases, and the amplitude of the PSP.

As it can be seen the refractoriness is not modeled through the kernel η but through an exponentially varying threshold of the form

$$\gamma(t - t_i^{(k)}) = B \cdot \gamma_0 \exp\left(-\frac{t - t_i^{(k)}}{\tau_{decay}^{\gamma}} \right), \tag{3.39}$$

with time constant τ_{decay}^{γ} and resting value, i.e. the value of the threshold when there are no previous spikes, of γ_0. Both absolute and relative refractory periods are modeled through these two values. A summary of all the neuron modeling can be observed in Fig. **??**a.

Based on the formerly described neuron model a SNN is set up, whereby a set of neurons is organized in a plane (see Fig. **??**b) with N neurons, where N has been set up to 120 [Benuskova2008]. Neurons are randomly placed and their excitatory or inhibitory nature is randomly defined maintaining a proportion of $10 - 25\%$ of inhibitory neurons. Connectivity is as well randomly defined with a probability of connection between two neurons of 0.5. With this probability the absence of connectivity is modeled setting up a value

$$v_{ij} = 0. \tag{3.40}$$

If two neurons are connected, the synaptic efficacy of the existing lateral connections between neuron i and j are modeled through v_{ij}, which is in this case a function of the Euclidean distance between the two neurons d_{ij} of the form

$$v_{ij}(d_{ij}) = \frac{J_0^{exc/inh}}{\sigma_{exc/inh}} \exp\left(-\frac{d_{ij}^2}{\sigma_{exc/inh}^2} \right) \tag{3.41}$$

A further effect in the membrane potential u_i due to connectivity is based on the influence of background noise or oscillations. These external inputs can come for instance from coupled
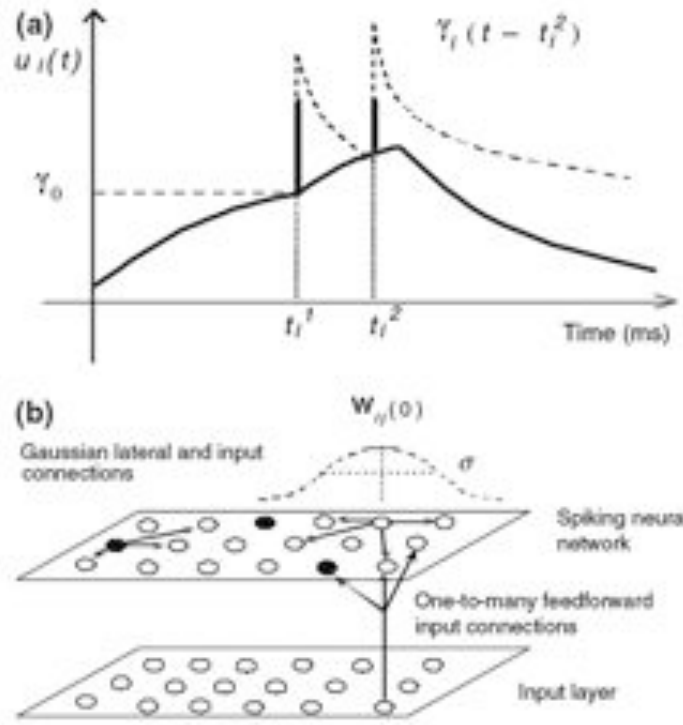
Figure 3.31 – a) Example of a signal generated by the neuron model that includes two spikes. b) Representation of the spike neural network used in the described framework. White circles represent excitatory neurons, whereas inhibitory are black. Taken from [Benuskova2008].

neuronal ensembles (see Fif. **??**b). They result in an additive term to be added to the general equation of the membrane potential in (3.37):

$$u_i^{ext}(t) = \sum_k v_{ik}^{ext} \varepsilon_{ik}(t). \tag{3.42}$$

No details beyond this equation are given on this aspect of the SNN either in [Benuskova2008] nor [Kasabov2008], but they could probably be modified in order to simulate external inputs from other sources, e.g. electric stimulation.

We have seen along the elucidation of the SNN that there are several parameters in the model. Actually its number is around 20. Table 2 in [Benuskova2008] summarizes the parameters and their range. The exact values of these parameters within the corresponding parameter range are supposed to be influenced by gene expression. The gene expression and this influence are therefore modeled through a so-called gene regulatory network.

Gene Regulatory Network

A gene regulatory network (GRN) is a model of the interaction of several genes. This is important since genes participate in procedures of memory and learning [Kasabov2008]. Moreover the mutation of genes can cause several brain diseases. In this context long-term potentiation and depression are basically molecular processes, where genetic expression presents a principal role (see [Kandel2001] for an introduction).

The gene expression influences cognitive systems through the modification of neuronal spiking parameters [Kasabov2008]. The following paragraphs explain how this influence is

modeled [Benuskova2008]. First the gene interaction within the GRN is modeled through a connectivity matrix $\mathbf{W}$, which expresses the connectivity among the genes of the set of genes that form part of the network. In the temporal domain the expression of a particular gene of the network g_j depends on the expression of the genes within the network through

$$g_j(t + \Delta t) = w_{j0} + \varsigma \left(\sum_{k=1}^{N_G} w_{jk} g_k(t) \right), \tag{3.43}$$

where N_G is the number of genes in the network, $\varsigma()$ denotes a sigmoid function, $w_{j0} \geq 0$ is the basal level of the exprtession of gene j, and w_{jk} are the components of the connectivity matrix $\mathbf{W}$. Normally normalized gene expression values are taken into account, i.e. $g_j(t) \in [0,1] \, \forall j$, with initial values in the range $[0, 0.1]$.

Once the gene expression level in the network is set up, a linear relationship between this level and the protein level is assumed. Therefore protein levels p_i are expressed through

$$p_i(t + \Delta t) = z_{i0} + \sum_{j=1}^{N_P} z_{ij} g_j(t), \tag{3.44}$$

where N_P is the number of protein subunits taken into account, $z_{i0} \geq 0$ the basal level of protein concentration, and $z_{ij} \geq 0$ the coefficient of proportionality between protein i and gene j expression. Once this value has been found the temporal evolution of neuronal parameters P_i can be found applying the simple expression

$$P_i(t) = P_i(0) p_i(t), \tag{3.45}$$

where $P_i(0)$ is the initial value of neuronal parameter i. This expression models a direct relationship between proteins and neuronal parameters, which links the neuronal with the genetic dynamics. Although each neuron in the network is supposed to be affected by a different GRN, the simplification of using a unique GRN is assumed in [Kasabov2008]. Moreover no feedback from the neuronal activity into the genetic one has been taken into account.

The main point of this model is the computation of a suitable connectivity matrix $\mathbf{W}$ that fits within the process we want to model. There are different methodological approaches for undertaking this step as reported in [Kasabov2008]. Genetic algorithms [Goldberg1989] are used in [Benuskova2008] for fulfilling this purpose as described in the following section (Sec. 2.3.2).

Computational Neurogenetic Modeling of Local Field Potential Generation

In this section the simulation of EEG generation is attained. For this purpose a framework formed by the coupling of a GRN and a SNN is used (see Fifg. **??**). This approach can be employed in the analysis of memory and learning processes, but as well for the analysis of different neurodegenerative diseases related to cognitive functions. The relationship among all the aforementioned and the genetic system has been shown in [Kandel2001] (the reader is referred to this paper for a deeper understanding of this relationship). The underlying idea is that plausible models of neuronal ensembles, e.g. SNN, should include models of gene interaction in it, e.g. GRN. Therefore the dynamics of the SNN is affected through the change in the neuronal parameters provoked by the gene interaction dynamics modeled through GRN.

The model is structured by a GRN coupled to a SNN. The interaction between these two pieces goes through the selection of an appropriate connectivity matrix in the genetic network
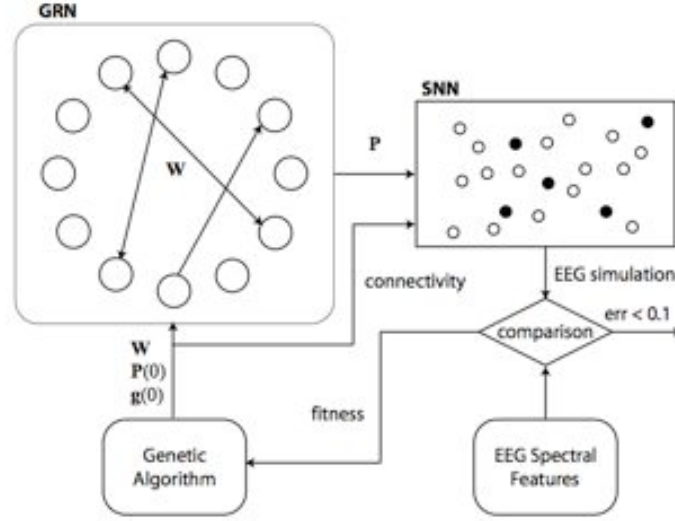
Figure 3.32 – Block diagram of the CNGM used for the simulation of the EEG signals.

W. As mentioned above the computation of this matrix is done through the application of Genetic Algorithms [Goldberg1989][Mitchell1998]. Therefore a population of possible CNGM is first initialized. This step includes the codification of the GRN parameters **W**, **g**(0), and **P**(0), and the connectivity within the SNN. This last parameter is expressed through the subindices i, j that make $v_{ij} = 0$ as expressed by (3.40), which substitute then the synaptic efficacy (3.41) in the network.

Once the population has been initialized, we apply first the temporal dynamics of the GRN for each individual in the CNGM population, expressed by eqs. (3.43) to (3.45). This process transforms gene expression level **g** into neuronal parameters **P** after a time T. With the neuronal parameter set for each time step we can apply thence the neuronal dynamics in the SNN, which are expressed by eqs. (3.37) to (3.43) given the connectivity codified in the genomes of the population. This process delivers the membrane potential $u_i(t)$ for each neuron in the SNN as a time function in $[0, \Delta t, \dots, T]$, where $T = 5$s in [Benuskova2008]. We can thence compute the local field potential LFP as the average of all membrane potentials in the network:

$$LFP = \frac{1}{N} \sum_{i=1}^{N} u_i(t). \tag{3.46}$$

Although LFP and EEG are not the same type of signal, [Kasabov2008] states that their frequency features are equivalent. Therefore the spectrum of the resulting LFP is computed in order to undertake its comparison with the EEG we want to approximate in the frequency domain. The error between the two spectra is taken as the fitness that drives the genetic algorithm, which iterates till the error is below 0.1 [Benuskova2008]. If this is not the case, the old population is transformed through the usual genetic operators, i.e. slection, crossover, and mutation [Mitchell1998], into the new one. The pseudocode of the algorithm[6] can be

---

[6]A software application implementing the model described herein can be found in `http://aratika.aut.ac.nz/adpgn_movies/KCIR/Computational%20Intelligence%20for%20neuroinformatics/`

found in Algorithm 1.

Algorithm 1 : Algorithm of the CNGM used for EEG simulation [Benuskova2008] (see Fig. **??**).

---

    construct population of CNGMs through random generation $\mathbf{W}$, $\mathbf{g}(0)$, $\mathbf{P}(0)$, $i, j \mid v_{ij} = 0$

    repeat
      for all individual $\in$ population **do**
        for t=0 to T **do**
5:          run CNGM, eqs. (3.37)-(3.45)
        end for
        LFP $\leftarrow (1/N) \sum u_i(t)$
        compute LFP spectral features
        individual fitness $\leftarrow$ error in frequency domain with recorded EEG
10:   **end for**
    apply genetic operators to generate new population
    until error ≤ 0.1
    analyze GRN for significant gene patterns

2.3.3 Conclusions

The Extended Source Model (see Sec. 2.3.1) does not model individual neurons, but ensembles. On the contrary, the Cognitive Neurogenetic Model (see Sec. 2.3.2) does model individual neurons. This is due to the inclusion of a Spiking Neural Network within this model. It is worth finding out if the model at the neuronal ensemble level used in the Extended Source Model is sufficient for the kind of research we want to undertake in brain stimulation. One important point in this context is that the best known electrical interaction resides at the neural level, where the response of a neuronal ensemble to an external stimulation is not so clear.

Furthermore it seems difficult to introduce a term that accounts for the external current sources within the Extended Source Model. On the contrary, it seems that the Cognitive Neurogenetic Model allows such a study by introducing a term within the each neuron's membrane potential expression for this purpose. However this point is worth further exploring, since no explicit further development of the used Spiking Neural Network is analyzed neither in [Benuskova2008] nor in [Kasabov2008].

Lastly the Extended Source Model ignores the molecular level of analysis. It may be investigated if this simplification is relevant for the application on hand. Although short term effects of electrical stimulation are well-known, not so much is known about the long-term effects. It can be therefore hypothesized that the long-term effects are related with this processing level in the brain.

If the aforementioned hypothesis fulfills, it is worth further investigating if the model described in Sec. 2.3.2 can serve the investigation of long term effects of brain electrical stimulation in the genetic response. In this sense it could be conducted an experiment whereby EEG is measured from a brain before electrical stimulation. The EEG generation will be

---

`Computational%20neuro-genetic%20modelling/introduction.htm`

thence modeled through a CNGM approach finding out the weight matrix of gene expression. After this the brain will be electrically stimulated and the EEG measured again after some time defining the long term. This new EEG generation will be again modeled through the CNGM. The changes in the weight matrix could indicate some hypothesis for undertaking genetic research on the achieved long term changes.

3 Effects of electric fields: in-vitro findings [FW]

In this section, we review some experimental studies performed at the level of single cells or 'small-scale' neural networks. The general and common objective of these studies is to progress in the understanding of the effects induced by applied electric fields on neuronal systems from experimental recordings performed at cellular or network level.

3.1 Stimulation and recording protocols

Most of the research work reviewed in this section is performed using in-vitro data using hippocampal slices. Indeed, this experimental model offers a lot of advantages. First the amount of knowledge accumulated on this structure over the past decades (nicely summarized in the "hippocampus book" [OKeefe:2006aa] is considerable. Second, technical and practical procedures required for recording from hippocampal slice preparations are now well controlled allowing for comparison of results obtained from different research groups. And finally, a number of experimental models based on hippocampal slice preparations have been described in order to study either normal or pathological processes. Some of these experimental models became "standard" and are now widely used across the world. Since the development of the first brain slice preparation [Yamamoto:1966aa, Yamamoto:1966ab], many disciplines benefited from this model including neurobiology, anatomy, neurophysiology, pharmacology, biophysics and computational neuroscience. The slice preparation is highly versatile and well suited to multi-faceted research strategies regarding the effects of external currents on neurons and networks. Despite the numerous advantages briefly described below, several drawbacks should also be kept in mind especially if the goal is to extrapolate in-vitro results to in-vivo situations. Indeed, although these points are very rarely discussed in papers, it should be mentioned that i) the complex relationship between oxygen delivery and energy demand/supply is strongly altered in slice preparations, ii) the composition of the artificial cerebrospinal fluid (ASCF) is an essential issue as real cerebrospinal fluid contains many metabolites that are not included in the ASCF and iii) many of the intrinsic and most of the extrinsic connections are severed in the slice model reducing the potential use in the interpretation of field effects on specific brain rhythms.

3.1.1 Typical experimental setup

A general description of the experimental setup is illustrated in Figure 3.33. Brain slices are usually thin sections of about 400 µm. They are maintained in viable conditions for extended periods (typically several hours) in an interface recording chamber with ACSF.

The slice preparation allows for application of electric fields generated across slices by passing current between two parallel wires (typically AgCl-coated silver) placed on the surface of the ACSF in the chamber. The orientation of the applied field with respect to the orientation of cells can be modified by rotating the parallel electrodes. The slice preparation offers an easy access to many features of the brain tissue that would be difficult to measure otherwise, particularly in the presence of exogenous electric fields, preserving, at the same time, the network organization of the tissue. It also allows for controlling the properties of the electric field (intensity and (non-)uniformity w.r.t. space) in the chamber with two recording electrodes separated by a defined distance (1 mm for instance) and calibrated to the current passed through the stimulating electrodes.
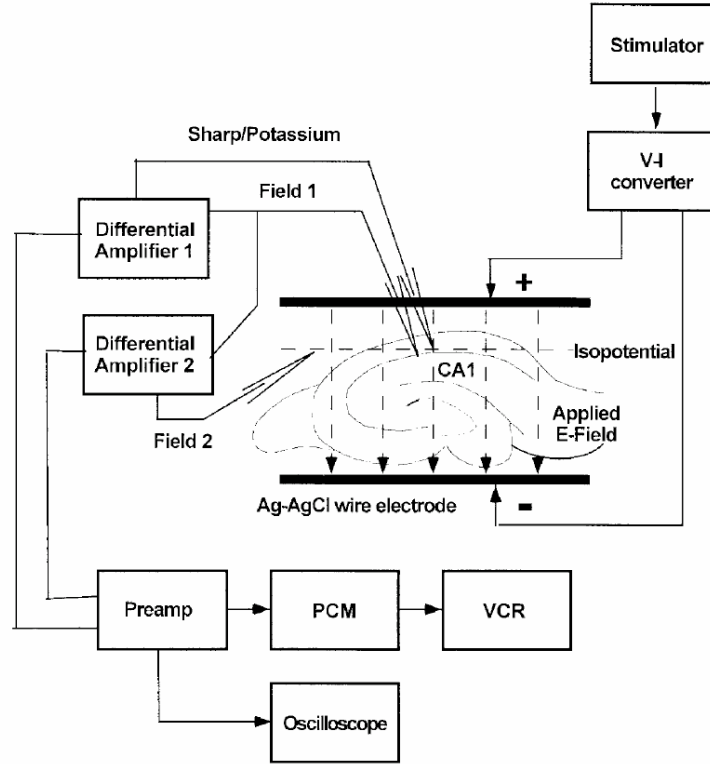
Figure 3.33 – An example of experimental setup used to study the effects of applied electric fields at the level of single cells or small networks in vitro, in slice preparations. Taken from [Bikson:2004aa]. For this report, permission has not been requested.

3.1.2   Recorded data

Most of *in vitro* studies reviewed in the following sections involve electrophysiological recordings, either extracellular or intracellular or both. Some studies also make use of more recent imaging techniques such as optical mapping of transmembrane potential changes based on voltage sensitive dies [Bikson:2004aa, Deans:2007aa]. Extracellular recordings are analyzed to study population responses including synaptic and firing parameters, during and after external stimulation. Intracellular recordings bring more microscopic information to characterize the synaptic responses or the properties of ion channels and receptors. Finally, microscopic imaging techniques (like two-photon imaging or optical imaging) are complementary to the aforementioned techniques. They allow for better assessment of the network function, providing a time-varying visualization of the activity in a population of cells with enhanced spatial resolution (compared to electrophysiology).

3.1.3   Features of applied electric fields

The main features of applied electric fields (AC versus DC, mono- versus bi-phasic stimulation, intensity and orientation with respect to the cell) can considerably vary from one study to another, depending on the general objective of the work. In order to provide, at least, some main features of stimulation parameters used in slice preparation, we summarized the information regarding the protocols in Table 3.1.

Study	Field	Frequency	Mag.	Direction / polarity of E	Location of stimulation	Recording	Animal
[Jefferys:1981aa]	DC	Duration: 25-250 msec	Up to 70 mV/mm	Perpendicular and parallel with granule cell layers in both polarities	Afferent fibers	Granule cell body layer (extra cellular)	guinea-pig
[Richardson:1984aa]	NA	NA	NA	NA	stratum radiatum or alveus to evoke CA1 cells orthodromically and antidromically, respectively (about 5-40 V)	CA1 pyramidal cells (extra and intra cellular)	Wistar rats (150-200 g)
[Taylor:1984aa, Taylor:1984ab]	NA	NA	NA	NA	stump of the fimbria (0.5-1 Hz) continuous intracellular injection of hyperpolarizing currency (1-4 nA)	CA2, CA3 (intracellular, extracellular)	Sprague – Dawley rats (250-300 g)
[Bawin:1984aa]	Sinusoidal (electrodes: two rows agar-filled tubes)	5, 60 Hz (duration: 5-30 s, 3-5 min)	2-7 mV/mm (p-p)	Perpendicular with CA1 cell layers.	stratum radiatum. 2) stratum Oriens 3) alveus (200 µs, 2-6 V, 0.2 Hz)	CA1 (extracellular)	Sprague – Dawley rats (40-100 days old)
[Ghai:2000aa]	DC	Duration: 8, 30 s	0-8 mV/mm	0, 45, 90, 135 and 180 deg in both polarities.	NA	CA1 (extracellular, Potassium)	Sprague – Dawley rats (125-175 g)
[Bikson:2001aa]	Sinusoidal Biphasic square waves: 100% duty cycle — Intracellular sinusoidal stimulation	20, 50, 500 and 5000 Hz — 20-50 Hz	From 25 to 200 mV/mm —3 nA (no tonic firing for <0.5 nA)	Perpendicular and parallel with CA1 and CA3 cell layers.	NA	CA1, CA3 Extracellular, intracellular, Potassium	Sprague – Dawley rats (75-250 g)
[Gluckman:2001aa]	A feedback electric field	Frequency content of the feedback field was restricted to <10Hz	5̃0 mV/mm	Perpendicular with CA1 cell layer in soma-dendritic orientation	NA	CA1 (extracellular)	Sprague – Dawley rats (125-150 g)

Study	Field	Frequency	Mag.	Direction / polarity of E	Location of stimulation	Recording	Animal
[Bikson:2004aa]	DC	Duration: 1 s	<200 mV/mm	Perpendicular and parallel with CA1 cell layers in both polarities	Stratum oriens or stratum lacunosum moleculare in CA1a (200 µs)	Extracellular, intracellular, optical imaging	Sprague-Dawley rats (180-225 g)
[Radman:2007aa]	DC Sinusoidal	0, 30 Hz	<30 mV/mm	Perpendicular with CA1 cell layers in both polarities	Intracellular current ramps (0.1-1.6 nA/s)	Intracellular, extracellular	Sprague Dawley rats (125-150 g)
[Deans:2007aa]	Sinusoidal	5-100 Hz (Duration: 1, 10 s)	0.5, 1, 2, 3, 5, 10 and 16 mV/mm (p-p)	Perpendicular with CA3c cell layers	NA	Extracellular, intracellular, optical imaging	Sprague-Dawley rats (150-250 g)

Table 3.1 – Main features of applied electric fields in studies performed on slice preparations.

3.2   Effects on cell and network excitability

Since the beginning of the last century, many authors have described some effects of imposed electric currents on the polarization of the neuron membrane. The first 'quantitative' study is probably that published by Terzuolo and Bullock in 1956 in which the authors claim that they "*have not seen in the literature, however, a quantitative evaluation of the sensitivity of nerve cells to electric fields in terms of voltage gradient across some appropriate dimension of the neuron*" [Terzuolo:1956aa]. At this time, although recording techniques were less sophisticated than they are now and although our knowledge about the properties of the excitable membrane was less advanced, the authors noticed some striking effects of polarizing electrodes on the firing of nerve cells in two experimental preparations in the peripheral nervous system (sensory neuron of Crustacea and cardiac ganglion of the lobster). In particular, they reported a modulation effect on the firing frequency, mainly on already active neurons, a preferential axis of polarization, and an acceleration of the frequency of the rhythmic bursts corresponding to heart beats for currents as low as 4.3×10^{-7} A. These observations led them to conclude that firing in nerve cells "*can be easily modulated in frequency by very low voltage gradients (0.1 mV/100 µm) measured in the external field across the whole soma, as compared to the voltage gradient necessary to stimulate a silent neuron*".

Later, in the cerebral cortex, [Bindman:1964aa] showed in an *in vivo* model (anaesthetized rat) that it was also possible to increase the firing rate of neocortical pyramidal cells with applied currents expected to depolarize their somata. Based on the recording of evoked potentials and unitary spikes, they discovered two major effects of cortical polarization, referred to as '*immediate effects*' and '*after-effects*'. Immediate effects were characterized by an alteration of the size and form of the evoked potentials due to the passage of polarizing current. As shown in Figure 3.34, immediate effects of a surface-positive polarization (in the order of 3 µA), resulted in i) a reduction in amplitude or in the suppression of the positive wave of the evoked potential and ii) an increase of a negative wave in amplitude and duration. Effects of surface-negative polarization were found to be less pronounced. After-effects were observed when the polarizing current was passed for about 5 min or longer. They were characterized by a persistent change in peak amplitude of the negative wave of the evoked response. This long-lasting change was in the same direction as that induced by the current produced by the surface-positive polarization, i.e. increased amplitude and duration.

Although authors could not technically characterize the current flow, they mention that it was highly probable that current flow was inwards through the dendritic processes and outwards via the soma. At this time, they also concluded that they were '*not in a position to discuss the way in which polarizing current acts on a neurone to alter its long-term excitability*'. Indeed, the term 'plasticity' is not explicitly mentioned in the paper, but it is very likely that the authors brought an early and clear evidence that such effects occur in the cerebral cortex under the influence of exogenous currents (see Section 3.4).

Following the early studies performed in the middle of the last century, significant progress on the quantification of electric field effects have been made during the past 40 years, in particular using slice preparation techniques that developed meanwhile.

3.2.1   Effects of orientation and polarity

In the eighties, Jefferys[Jefferys:1981aa] published a study where the issue of the control of the direction of the extracellular current in relation to the cell layers is addressed by careful
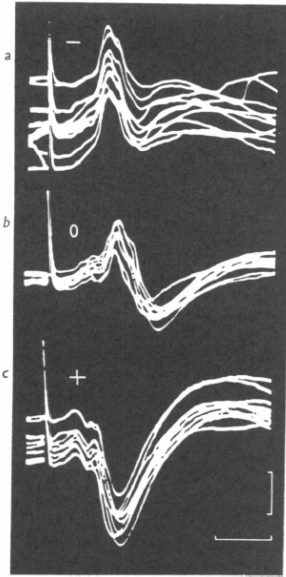
Figure 3.34 – Superimposed consecutive evoked potentials (anaesthetized rat, forepaw stimuli, recording from surface of contralateral somatosensory area.). (a) Effect of surface-negative polarization (3 µA total current flow). (b) Normal traces showing waves. (c) Effect of surface-positive polarization (3 µA).Voltage calibration = 1 mV; Time bar = 10 msec. Taken from [Bindman:1964aa]. For this report, permission has not been requested.

positioning of pairs of polarizing electrodes (Figure 3.35). In this study based on *in vitro* conventional electrophysiological recordings (evoked potentials, stimulation of afferent fibres) from hippocampal slices (guinea-pig, dentate area, granule cell) submitted to electric fields (controlled in direction and intensity), the mechanism of changes induced by polarization were studied by an analysis of the laminar evoked potentials.

The author showed that currents (pulses of 25 to 250 msec) parallel to the cell axis (so-called 'soma-depolarizing currents') and making the dendrites more positive than the cell body layer strongly enhanced the cell excitability, as shown by the important increase of the amplitude of the population spike and by the reduced time to its peak. Conversely, currents of equal strength but perpendicular to main cell axis were found to have no consistent effect on the responses. He suggested that the altered excitability was primarily due to a modification of the membrane potential at a spike trigger zone in the vicinity of the cell body. This modification was due to a fraction of current flowing intracellularly and thus, the predominant effect of applied fields was on the granule cells rather than on the presynaptic axons.

Twenty years after the first paper, the same group of research published a more comprehensive and quantified study on the effects of uniform state extracellular electric fields on neuronal excitability in rat hippocampal slices [Bikson:2004aa]. In this study, authors used both electrophysiological (intracellular and extracellular) and optical (voltage-sensitive dyes) investigation techniques in order to characterize the cellular and network activity in CA1 and CA3. Their objective was to re-visit some basic assumptions about field parameters: i) polarity and degree of cell polarization as a function of the orientation of the applied DC field, ii) dendrites versus soma polarization, iii) time variance or invariance in the efficacy of applied DC fields and iv) short-term after-effects of DC fields.

Regarding the field orientation, they found that electric fields parallel to the somato-
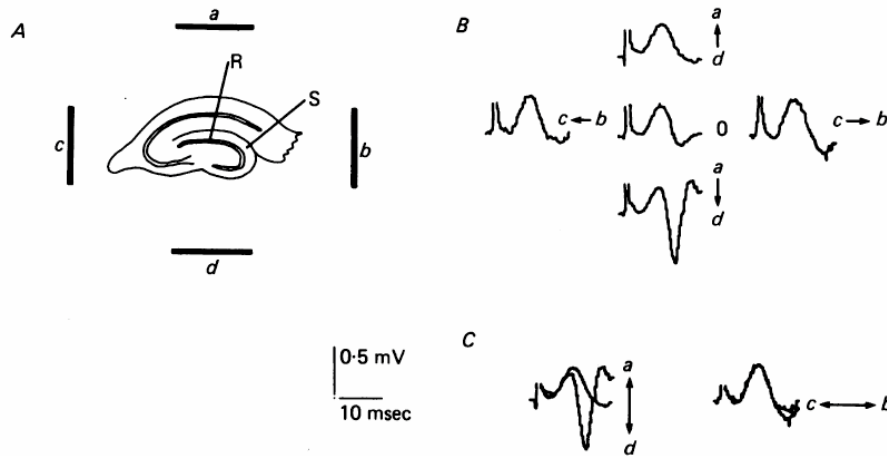
Figure 3.35 – Effect of direction of polarizing current. A) polarization currents were passed across a transverse slice, between gross electrodes positioned in the ACSF at sites a and d or b and c (S, stimulus, site; R, recording site). The polarization potential gradient was 17 mV/mm, measured over a 250 sum track in the slice. Responses to afferent volleys were recorded from the cell body layer and are labelled with the direction of conventional current (B). To aid comparison, responses under both directions of current have been superimposed for each electrode pair (C).

dendritic axis induced polarization of CA1 pyramidal cells. Electric fields perpendicular to the somato–dendritic axis did not induce somatic polarization. However, they modulated orthodromic responses. Authors suggested that this finding may indicate an effect on afferents. Regarding the polarity, negative (cathode on alveus side of CA1, inverted with respect to Figure 3.33) electric fields decreased the delay and increased the amplitude of population spikes evoked by oriens stimulation. Positive electric fields had an inverse effect, i.e. they increased the delay and decrease the amplitude of the population spike.

In terms of intensity, changes in the population spike amplitude starting to occur for polarizing gradients greater than 4.0 mV/mm were already reported in [Jefferys:1981aa]. However, the author mentions that the obtained results might have been affected by instrumental precision and that weaker fields might as well have an influence. Further studies [Francis:2003aa, Radman:2007aa] reviewed in the next section confirmed this hypothesis later on. This value also led the author to suggest that ephaptic interactions (through endogenous currents) between neighbouring granule cells (which are densely packed) could also play a role as fields of up to 20 mV/mm have been recorded during seizure activity and in the order of 0.5-4 mV/mm during normal slow wave activity. These effects are discussed in section below.

3.2.2 Effects of field intensity

Although a well-defined electric field threshold eliciting an action potential can hardly be determined, most of the studies mentioned that even very weak electric fields seem to modulate neuronal activity. In fact, the first experimental evidence that neuronal networks are detectably sensitive to electric fields lower than 1 mV/mm was published quite recently in [Francis:2003aa]. Using electrophysiological recordings in longitudinal hippocampal slices (maximizing the alignment of CA1 or CA3 neurons with the parallel electric field lines), the authors examined the effects of weak fields both on single neuron and network responses, with

a particular attention paid to synchronization quantified using peri-stimulus time histograms (PSTHs). The field waveform was designed to mimic the low frequency natural CA3 population extracellular fields. In CA3, at a field strength of 3.9 mV/mm rms (6.8 mV/mm peak), the stimulus (burst waveforms with a Gaussian profile, 26 msec full width at half-maximal, 1–2 Hz) was able to entrain the network once its phase came into close alignment with the population phase. In some cases, synchronization at smaller field strengths (560 µV/mm rms) was also obtained. In CA1, synchronization between network activity and electric field stimulus was obtained at 1.75 mV/mm rms. CA1 pyramidal cell networks were sensitive to fields with rms amplitudes as small as 140 µV/mm. At cellular level, most single units demonstrated burst firing activity. The CA1 networks were found to be more sensitive to electric fields than the CA3 networks. A possible explanation suggested by the authors is that the CA1 subfield in the hippocampus is more "homogenous" from the anatomical viewpoint, i.e. pyramidal cells are more regularly aligned (in their total dendritic lengths) across the CA1 area, in contrast to CA3. An interesting finding in this study is also that networks are more sensitive than the average single neuron threshold to field modulation.

Interestingly, from extracellular recordings, [Bikson:2004aa] plotted the amplitude of the population spike evoked by oriens stimulation as a function of the strength of the applied field. They found that small electric fields ($<|40|$ mV/mm), applied parallel to the somato-dendritic axis, induced polarization of CA1 pyramidal cells. This study revealed that the relationship between applied field and induced polarization was linear, as illustrated in Figure 3.36.

From intracellular recordings (effects on single pyramidal cells of CA1), authors confirmed that application of exogenous uniform electric fields parallel to the soma–dendritic axis result in changes in transmembrane potential (all recorded neurons). A summary of the main findings is provided in Figure 3.37. In brief, positive (respectively negative) fields resulted in somatic hyperpolarization (respectively depolarization). In the range of $[-40, +60]$ mV/mm, the polarization varied linearly with the strength of the applied electric field with an average sensitivity of 0.12 +/- 0.05 mV per mV/mm. As shown in Figure 3.37 A and B, positive extracellular applied fields increased the threshold of intracellular current needed for action potential generation. Negative fields decreased action potential threshold, and could polarize the neurons enough to elicit action potentials directly. Authors also investigated the effect of applied fields on action potential threshold in response to oriens (Figure 3.37 C) and LM stimulation (and Figure 3.37 D). In the latter case, fields affected action potential generation (increase with the field strength). When positive fields reduced the action potential threshold, they also increased the subthreshold EPSP amplitude, while negative fields had variable and inconsistent effects on EPSPs.

3.2.3   Effects of ephaptic interactions

As mentioned above, according to the sensitivity of spike initiation in granule cells as a function of extracellular fields, [Jefferys:1981aa] suggested that looking for ephaptic interactions between neighbouring cells might be a 'fruitful' approach.

Ephaptic interaction between nerve cells is the name given to the electrically-induced influence of currents by "active" neurons on neighbouring "passive" neurons. These currents are thought to play a role in the synchronization of neuronal networks.

In 1984, [Richardson:1984aa] examined the ephaptic interactions in a rat hippocampus slice. They showed that in both ortho- and antidromic stimulations of CA1 pyramidal cells, an induced negative intracellular wave (referenced to bath ground) can be recorded inside
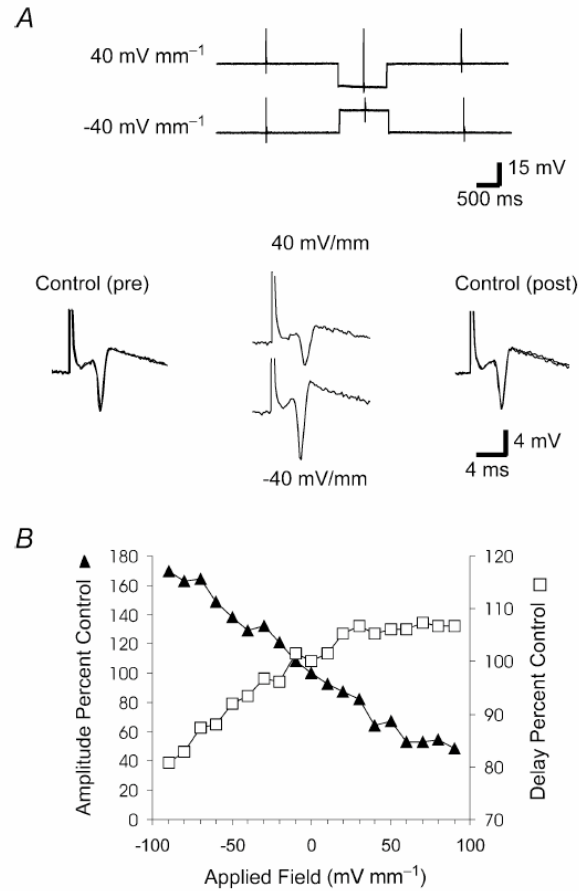
Figure 3.36 – Effect of applied uniform electric fields on population spikes evoked by oriens stimulation. A, top, stimulus protocol. Population spikes were evoked continuously at 0.5 Hz. One-second electric fields were applied 500 ms before the orthodromic pulse. Bottom, population spikes evoked before, during and after application of 40 mV mm−1 uniform electric fields. Pre- and post-traces are overlaid. In this and subsequent figures, the orthodromic stimulation artefact is clipped. B, effect of varied amplitude electric fields on population spike amplitude and delay. Taken from [Bikson:2004aa]. For this report, permission has not been requested.

those neurons that were not activated directly by the stimulations. Extracellular recordings indicated that this ground based intracellular response was coincident with the falling phase of the extracellular population spike and it could be observed even if synaptic transmissions were blocked by MnSO4 and CaCl2 blockers. This was an indication that the negative intracellular wave was generated ephapticaly in response to neural population activity.

Interestingly, calculating transmembrane potential (TMP) by the subtraction of extracellular potential from intracellular potential indicated that this negative intracellular wave is observed as a depolarizing wave across the membrane in the vicinity of soma (i.e. it is a depolarizing TMP). In fact, although there was a transient drop in the intracellular potential due to ephaptic effect, the TMP was increased near the soma.

Authors suggested a mechanism for this depolarizing TMP. They stated that the action potential in a given firing cell (active cell) generates a local extracellular negativity and a current sink in the vicinity of the soma. The sink is at the origin of ephaptic interactions
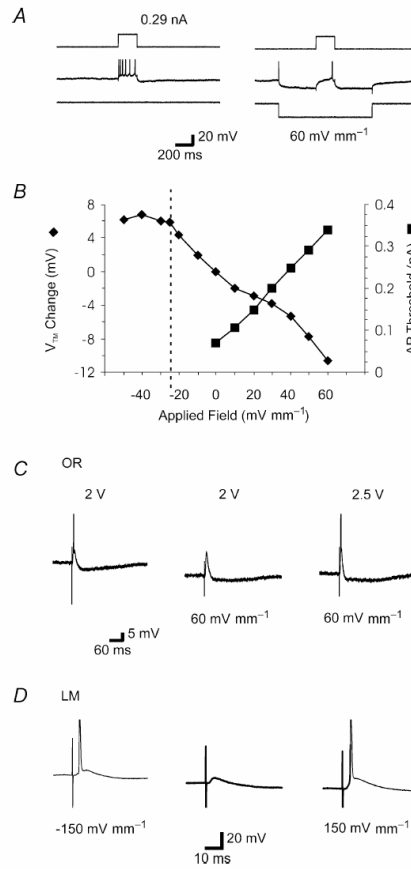
Figure 3.37 – Effect of applied electric fields on single CA1 pyramidal neurons monitored with intracellular sharp microelectrodes. A, left, in the absence of an electric field, intracellular injection of current pulse (200 ms, 0.29 nA) triggered a train of action potentials. A, right, application of +60 mV.mm−1 electric fields induced hyperpolarization. Injection of a current pulse (200 ms, 0.29 nA) during field application triggered only a single action potential. B, effect of applied fields on transmembrane potentials (lozenge symbol) and threshold for triggering a single action potential with an intracellular current pulse (200 ms) during field application (square symbol); summary of single slice. Vertical dashed line indicates the threshold for generation of spontaneous action potential by uniform field application; average transmembrane potential was measured during the interspike interval. C, left, an action potential was evoked by orthodromic stimulation (2 V) in stratum oriens. Middle, during application of +60 mV.mm−1 electric fields the same intensity orthodromic stimulus resulted in an EPSP but failed to trigger an action potential. Right, stronger orthodromic stimulation (2.5 V) triggered an action potential during application of a +60 mV.mm−1 electric field. D, orthodromic stimulation intensity was fixed at a level that failed to trigger an action potential in the absence of an applied field (left), but during application of both −150 mV mm−1 (middle) and 150 mV.mm−1 (right) the same stimulus triggered an action potential. Taken from [Bikson:2004aa]. For this report, permission has not been requested.

between the firing cell and neighbouring neurons. Indeed, due to this sink, a passive current is established inside neurons located in the vicinity of the firing cell. This current is associated with voltage drops along the axial resistance of the dendrite and across the membrane resistance of the soma. Therefore, at the soma, it produces a passive depolarization

transmembrane potential along with an intracellular hyperpolarisation potential (note that the reference electrode is far away from the soma). Figure 3.38 schematically illustrates the mechanism by which neuronal activities are influenced by ephaptic currents.
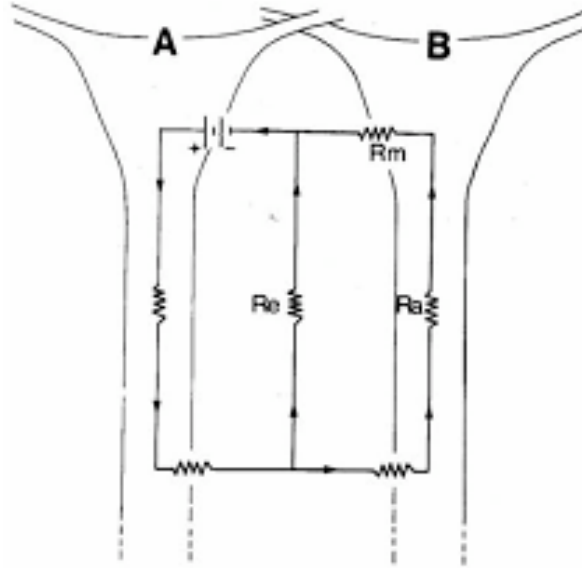
Figure 3.38 – Schematic illustration of hypothesized current flow at the peak of a population spike in CA1. Cell A represents a group of neurons during AP generation and cell B represents neighbouring inactive cells. The battery represents the voltage generated during the AP in cell A, and arrows indicate passive current flow. The generated action potential in cell A produce a current sink in the vicinity of soma, and thereby establishes a passive current flow through the extracellular resistance (Re). The voltage gradient across Re induce a current flow inside dendro-somatic axis (Ra) of cell B. The produced voltage drop on soma membrane resistance (Rm) and dendro-somatic axis (Ra) produce a hyperpolarizing intracellular potential when measured with a somatic ground referenced electrode. However, trans-membrane potentials across soma and dendrites are depolarization and hyperpolarisation potentials, respectively. For this report, permission has not been requested.

It is interesting to know that the same results were also obtained by Taylor and Dudek in the same year [Taylor:1984aa, Taylor:1984ab]. Moreover, they also obtained the laminar profile of extracellular potentials perpendicular to CA1 cell body layer with the use of an array of extracellular recordings. This laminar profile showed that at the peak of the somatic population spike (T_1), there was an extracellular current sink near pyramidal somata and sources in distal dendritic regions that is consistent with Richardson and Turner's hypothesis. After the peak of the somatic population spike (T_2), the sink moves from the soma toward dendrites. Figure 3.39 illustrates CA1 laminar recordings and source-density analysis of electrical field produced by alvear stimulus.

Both abovementioned studies concluded that extracellular field potentials could "ephaptically" discharge CA1 neurons and might play a role in recruitment and synchronization of neuronal activity in the hippocampus. A "qualitative" model, illustrated in Figure 3.40, was reported in [Taylor:1984aa, Taylor:1984ab]. However, to our knowledge, it is still unknown to what extent ephaptic currents are important in modification of brain activities.
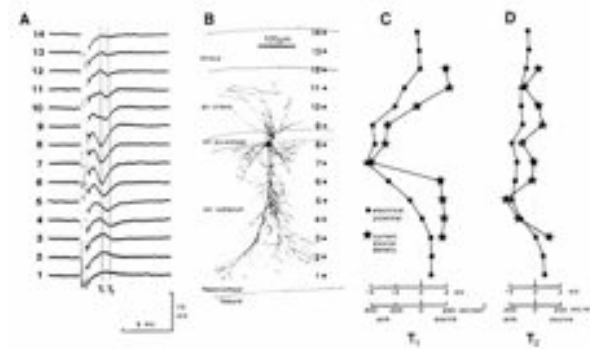
Figure 3.39 – Laminar recording and current source-density analysis of electrical field produced by alvear stimulus with synaptic potentials blocked. (A) Averaged extracellular responses to three alvear stimuli in different laminar positions. (B) Schematic diagram of CA1 pyramidal cell and electrode positions. (C) Potential and source density values at the time of maximum negativity of extracellular potential around the soma (indicated by T1 in A). (D) As in (C) except data are plotted for time T_2. Note dendritic sink instead of somatic sink in C.
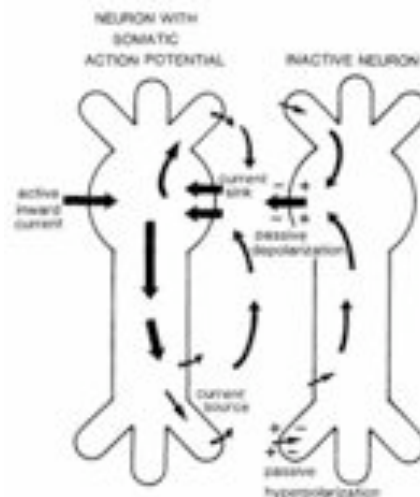
Figure 3.40 – Schematic diagram of current flow proposed to underlie excitatory field effects. Arrows denote current flow of positive charges. The driving force of the ect is the inward action current produced by the synchronous firing of.a population of hippocampal somata (left). Current then flows passively out dendrites of active cells and returns through extracellular space, creating extracellular sink at somata and source in dendrites. Neighboring inactive neuron (center) develops passive current flow across somatic and dendritic membranes, resulting in somatic depolarization and dendritic hyperpolarization. Low-resistance cytoplasmic path between current source and sink facilitates current flow through inactive cell. Adapted from [Taylor:1984aa, Taylor:1984ab]. For this report, permission has not been requested.

3.2.4 Time constant of the membrane polarization due to applied fields

For the first time,[Bikson:2004aa] reported a direct measurement of membrane time constants for polarization by electric fields. Time constants were determined by a single exponential curve fitting to the optical signals 0–20 ms from the onset of the applied field. They showed that the peak amplitude and time constant (15–70 ms) of membrane polarization varied

along the axis of neurons, with the maximal polarization observed at the tips of basal and apical dendrites. While the time constants of basal dendrite, soma and apical dendrite were respectively around 8, 11 and 8 ms in the first initial 20 ms of the polarization responses, the time to 67% peak shifted to 54, 70 and 14 ms. Based on these data, Bikson et al. concluded that the effects of electrical fields on neuronal function are more complex than what was generally believed. The modulation of neuronal excitability is not only a simple function of the orientation of neuronal processes with respect to applied field. Polarization of cell membranes is more complex: the time constant of polarization varies across the cell axis, some parts of the cell have biphasic responses, electric fields can induce transient responses at onset, and fields can polarize afferent axons or change the polarization pattern of dendrites. According to these results, authors also emphasized that neurons should be less sensitive to relatively fast AC electric fields (>15 Hz), whether exogenous or endogenous.

3.2.5 Effects on the spike initiation site

Recently, using laminar electrodes and current source density (CSD) analysis in the hippocampal slice preparation, [Bikson:2004aa] showed that negative fields can move the site of population spike initiation from *stratum radiatum* to *stratum pyramidale*, the mean distance of the shift in spike initiation site being about 125 µm. In contrast, under positive fields, LM stimulation continued to initiate population spikes in *stratum radiatum*, which then propagated to the pyramidal layer (Figure 3.41).

3.2.6 Large versus small electric fields: implications on safety

A number of papers dealing with the effects of electric fields on neuronal networks in slice preparations report that these fields can induce epileptiform activity in 'normal' slices [Jefferys:1981aa, Richardson:1984aa, Bikson:2004aa, Albensi:2007aa] or can alter epileptiform activity generated in 'epileptogenic' slices, whatever the experimental model [Richardson:1995aa, Ghai:2000aa, Bikson:2001aa, Gluckman:2001aa]. Constant DC fields have been shown to suppress epileptiform bursting in high-K+ [Gluckman:1996aa] and low-Ca2+ [Warren:1998aa, Ghai:2000aa] models by directly hyperpolarizing pyramidal neurons. AC fields can also have a similar effect for appropriate setting of the frequency and strength (see section below). For high strength, DC fields have also been shown to induce epileptiform activity as illustrated in Figure 3.42.

3.2.7 Effects of electric fields on non-pyramidal neurons

Although several papers mention the possible effects of applied electrical fields on interneurons and glial cells [Bikson:2001aa, Bikson:2004aa], we were not able to find a quantitative study specifically addressing this issue.

3.2.8 Influence of extracellular AC fields

The influence of extracellular AC fields on excitability in the CA1 cell layer of hippocampal slices was studied by Bawin and collaborators, 25 years ago [Bawin:1984aa]. The authors compared post-tetanic and post-field effects in the same slices in order to confirm preliminary results suggesting that the time courses of the field-induced effects resemble those following repetitive pulse stimulation of afferent hippocampal fibers in the slice and *in vivo*. In this
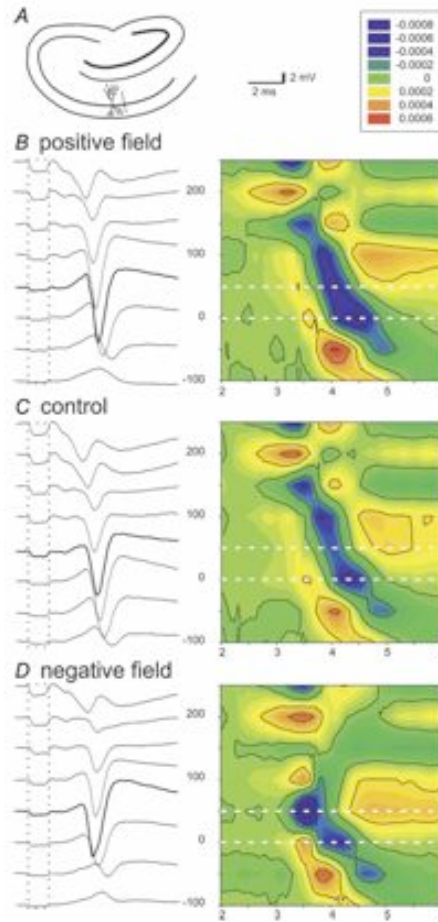
Figure 3.41 – Effect of applied electric fields on population spike initiation zone and population EPSP in response to orthodromic LM stimulation. A, left, supra-threshold activity, evoked by stimulation of stratum lacunosum moleculare, was recorded at a series of sites separated by 50 μm on a line perpendicular to the pyramidal layer (marked by dashed line). B–D, evoked potentials recorded from these sites (left; calibration in A, centre), spatially aligned with a contour plot (right) of the current source densities estimated by the second spatial differences of these potentials (calibration key in mV mm−2 is in A, right; sinks are dark blue, sources are yellow; x-axis is time in ms after the stimulus; y-axis is distance in μm from the border between strata oriens and pyramidale). The location of the pyramidal layer is marked by white dashed lines; on this scale the synaptic sink is just visible at the top of the contour plot. C, responses in the absence of applied fields, showing spike initiation in stratum radiatum and propagating to stratum pyramidale (bold trace). B, responses under +50 mV mm−1 applied DC fields, have a similar pattern to those in C, but are potentiated. D, responses under −50 mV mm−1 applied fields also are potentiated at the pyramidal layer (bold trace), but in this case the population spike initiation site moved into stratum pyramidale. Taken from [Bikson:2004aa]. For this report, permission has not been requested.

study, they stimulated neuronal networks at two different frequencies: 5 Hz and 60 Hz, the former value being intended to approximate the rat hippocampal EEG rhythm (theta band). Field-induced effects were studied in population spikes evoked from independent inputs to the pyramidal neurons and the slices were tested during prolonged fields (3-5 min) to study
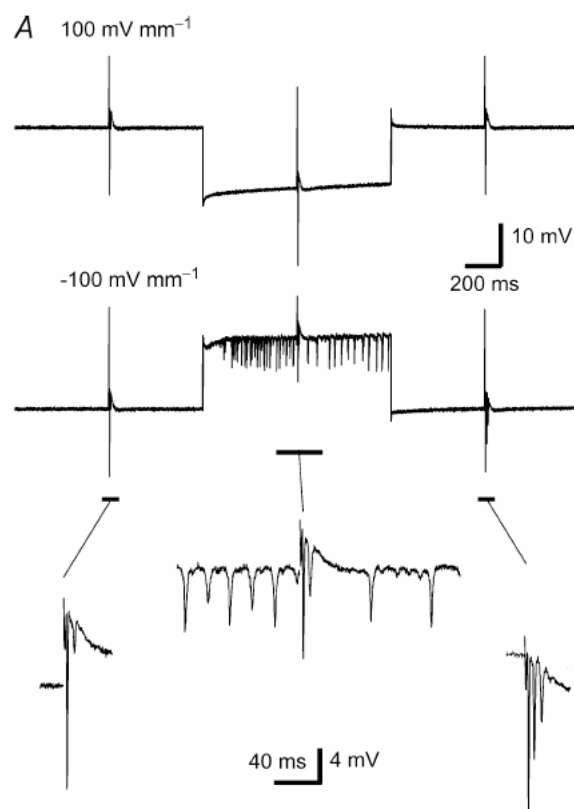
Figure 3.42 – Effect of ±100 mV.mm−1 applied electric fields on evoked population spikes and spontaneous activity A, top, no spontaneous activity was observed in the absence of applied electric fields or after application of +100 mV.mm−1 electric fields. Middle, −100 mV.mm−1 fields (1.0 second) induced spontaneous epileptiform activity. Population spikes were evoked by oriens stimulation continuously at 0.5 Hz. Bottom, expansion of field traces before (left), during (middle), and after (right) application of −100 mV mm−1 electric fields. Note that post-field evoked response (right) did not return to control levels (left). The orthodromic stimulus artefact was removed in the expansion insets. Taken from [Bikson:2001aa]. For this report, permission has not been requested.

frequency dependence during longer stimulation. In addition, the influence of extracellular electric fields was also studied during blockade of chemical synaptic transmission. Results showed that short-duration stimulation (5-30 s) with both 5 and 60 Hz fields (20-70 mV/cm) were able to produce a long-term increase (longer than 10 min) of the population spike. Interestingly, authors found that fields at 60Hz, but not at 5 Hz, induced short-term depression (1-6 min) or transient post-field excitation (15-30 s). Prolonged stimulation (3 min) emphasized this frequency-dependent response: fields at 5 Hz induced long-lasting potentiation while fields at 60 Hz always resulted in progressive depression that persisted for a few minutes after the end of stimulation. Although the physiological significance of the exogenous sine wave fields remained to be understood, the authors suggested that rhythmic extracellular fields, such as the hippocampal rhythmic slow activity, could participate in the regulation of neuronal excitability.

More recently, [Bikson:2001aa] investigated the short and the long term effects of high frequency sinusoidal fields (20-5000 Hz) on spontaneous epileptiform activity. They recorded

extracellular and intracellular potentials, extracellular potassium and optical imaging data in rat hippocampal slices obtained in various experimental models of epilepsy (CA1 and CA3), during field application. Regarding frequency, they did not find a significant difference using 20 Hz and 50Hz in the threshold for suppression of epileptic in the low-Ca^{2+} model. Sinusoidal fields of 500 Hz and 5000 Hz were found to be ineffective at suppressing this activity at any field strength tested. Using ion-sensitive microelectrodes, authors also discovered a large increase in extracellular potassium activity due to suprathreshold stimulation. This increase could be caused by the stimulation of glial cells which further contribute to potassium efflux or by the disruption of glial potassium clearance mechanisms. Overall, this observation led them to propose a possible mechanism of burst blocking: the stimulation engenders a large or very large increase of the extracellular K$^+$ which depolarizes cells and which leads to the disruption of epileptiform activity by depolarization block (block is induced when Na$^+$ channels are inactivated such that action potentials cannot be initiated). A depolarization greater than 20 mV is sufficient to induce depolarization block. It can be induced by large DC depolarising currents or, in the aforementioned study, by increase of extracellular potassium. Interestingly, and conversely to DC fields, the authors discovered an insensitivity of AC field suppression threshold with respect to slice orientation, suggesting that the epileptic activity is not suppressed by direct polarization of pyramidal cell somas. An interpretation could be that all cells exposed to a high frequency field (not just those oriented parallel to the applied field), are affected by stimulation.

3.2.9 A synthetic view on the effects of exogenous and endogenous fields

From the above literature review, we summarized, in Figure 3.43, the effects exogenous and endogenous fields on neurons. By convention, a positive electric field is oriented along decreasing potentials. Along this direction (grey arrow), the exogenous field has minor effects on neuronal activity and excitability is not increased in this case. In the opposite direction (negative field, red arrow), the field will depolarize the soma (close to the anode) and will hyperpolarize the apical dendrite due to induced currents flowing across the transmembrane resistance (see the sense of the transmenbrane voltage VTM). Excitability is increased in this case. In addition, neurons can become active, i.e. can fire action potentials, and therefore, create themselves an endogenous field that will also influence passive neighbouring neurons. This type of influence is called "ephaptic interaction". It is noteworthy that endogenous effects sum up with exogenous ones. This is why ephaptic interactions are supposed to participate in the global increase of the network excitability as well as in the network synchronization.

3.3 Effects on spike timing

Small electric fields have long been recognized to polarize neurons by only a small amount. Therefore, they have been suggested to have no physiologically-relevant effects. The hypothesis that low-amplitude fields can affect brain function has been strengthened by recent experimental and clinical studies. Among these studies, Radman and co-workers reported the first quantitative framework for evaluating the effect of subthreshold fields on neuronal spike timing [Radman:2007aa, Radman:2007ab]. Authors mention that their paper brings a quantitative and experimentally-verified explanation that was previously lacking. They showed that the nonlinear properties of single neurons "amplify" the effect of small electric fields. Indeed, these small electric fields can have significant effects on spike timing when their effects
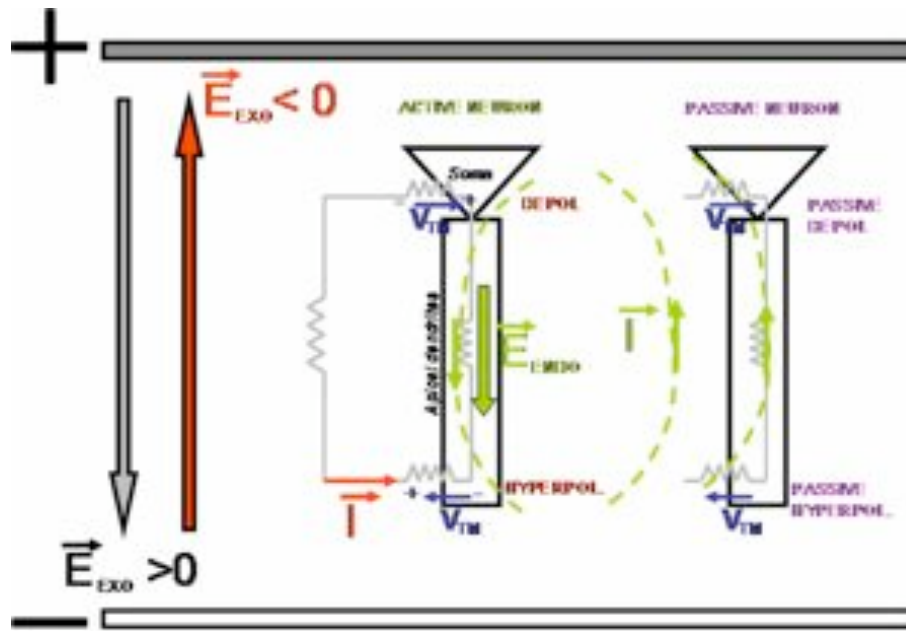
Figure 3.43 – Effects of exogenous and endogenous fields on neurons

occur during suprathreshold synaptic input. For low-frequency fields, the authors discovered a linear dependency of spike timing changes on field strength, as illustrated in Figure 3.44.

Authors also emphasize the functional consequences of this phenomenon at network level. They found that a 1 mV/mm uniform field can induce, on average, a transmembrane potential (TMP) change of 0.1 mV. They demonstrated that these small TMP variations induce changes in spike timing rather than in spike generation. These results also confirm that coherent (synchronous) network activity like, for example, theta-modulated gamma activity in the hippocampus, can have a particularly relevant role in temporal coding.

3.4 Plasticity-related short- and long-term effects

It is now well known that the brain is able to reorganize its functions and structures in response to both physiological experiences (manipulation of sensory input, experience, learning) and pathological events (loss of function due to trauma, stroke). For a review see [Donoghue:1995aa, Sanes:2000aa]. This ability has been termed brain or cortical plasticity.

Cortical plasticity involves several levels of organization and can be applied to cellular as well as to population events. The study of underlying mechanisms of cortical plasticity at cellular level has begun before that at population level. Cortical plasticity primarily emerged from experimental studies on animals that were confined to the synaptic and cellular level. During the last decade, studies of cortical plasticity at population level have been performed by developing non-invasive neuroimaging techniques and transcranial magnetic stimulation (TMS) devices. In this section we focus on brain plasticity at the cellular level.

Cortical plasticity at cellular level mainly takes the form of synaptic plasticity. In neuroscience, synaptic plasticity is the capacity of a synapse to change its strength. The strength of synapses can be increased or decreased for a short or a long period of time. Stimulation of the synapse is one of the ways to modify synaptic strength. Long-term potentiation (LTP)
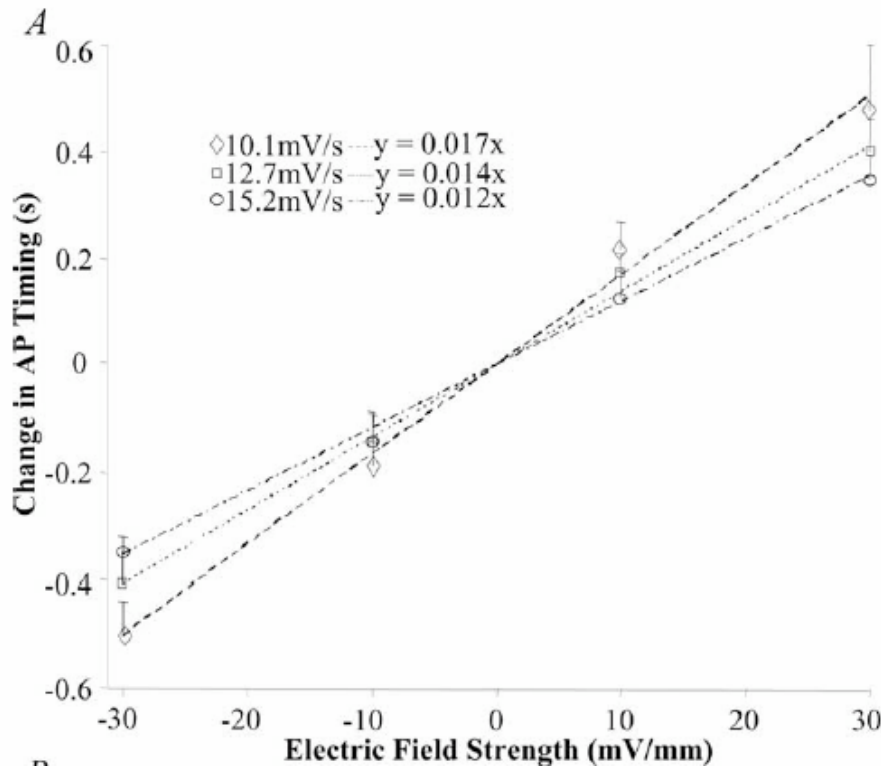
Figure 3.44 – Effects of applied extracellular DC electric fields on CA1 pyramidal neuron firing time in response to intracellular depolarizing ramp slopes. A) Positive (hyperpolarizing) fields delayed action potential initiation, whereas negative (depolarizing) fields expedited AP onset. Note that, for each ramp slope series, the relationship between firing time (t) and applied field amplitude is linear. Moreover, the slope of this relationship varies inversely with the slope of the injected intracellular ramp (i.e., 10.1:12.7:15.2 as 1/.017:1/.015:1/.012). The injected current ramp slope (0.4, 0.5, 0.6 nA/s) translated to voltage slope by cell resistance (25.3 MOhms for this cell). The change in timing for any given field is amplified" as the slope of the ramp is decreased. Reported are the mean_SD (r 2_0.94; p_0.01 for the 3 regressions shown here). Taken from [Radman:2007aa, Radman:2007ab]. For this report, permission has not been requested.

is a persistent increase in synaptic strength (mostly following high frequency stimulation of the synapse) and long-term depression (LTD) is the weakening of neuronal synaptic strength that lasts from hours to months.

It is widely believed that learning and memory are related to modification of cellular firing and synaptic plasticity at the cellular level. In particular, LTP shares many features with memory. For instance, LTP and memory trigger rapidly, they are long-lasting processes, both depend on NMDA receptor activation, each depends upon the synthesis of new proteins, each has properties of associativity, and, the decay of LTP response correlates well with normal forgetting [Otto:1991aa]. In this section, we introduce some common protocols of electrical stimulations that are used experimentally for synaptic stimulations. We also describe the features (sometimes complex) of LTP and LTD responses that are induced by these protocols.

3.4.1 Long term potentiation

For many years it has been and still is a question for neuroscientists to determine stimulating protocols that induce and simulate the physiological conditions that are believed to occur during the formation of new memories. These protocols can be either electrical [Frey:1993aa, Morgan:2001aa, Floel:2007aa] or chemical [Pittenger:2002aa, Fujii:2004aa, Otmakhov:2004aa] protocols for inducing LTP.

To date, electrical stimulations protocols that have gained in popularity can be divided to three categories: tetanic, theta burst and, primed burst stimulations. The tetanic stimulation typically includes a train(s) of 50-100 stimuli (square pulses) at 100 Hz (Figure 3.45). The effectiveness of tetanic stimulations on long-term properties of synapses may vary by the characteristics of the tetanic stimulation. For example, three trains of 100 Hz stimulations (100 pulses for 1 s repeated 3 times with an interval ranging from 0.5 to 10 s) is considered as strong stimulation and produce LTP that lasts 3 h or more and involves protein synthesis [Frey:1993aa] [Matthies:1993aa] [Huang:1994aa], whereas a single 100 Hz train (100 pulses over 1 s) is considered weak stimulation, leads to early LTP (1–3 h), and is protein synthesis independent [Vertes:2005aa].

Although tetanic high frequency stimulations have been shown to induce LTP, their effects appear inherently different than those related to natural firing patterns of neurons. For example, it is not certain that hippocampal neurons in the living animal fire at 100 Hz for one full second. In response to this limitation, other stimulation protocols such as theta burst [Morgan:2001aa] and primed burst [Rose:1986aa] have been developed.

In part, the design of theta burst stimulation is based on the observation that the hippocampal EEG waveform in rats was shown to be dominated by a 5 to 12 Hz (theta, θ) frequency, observed when animals are engaged in learning-related exploratory behaviors. Theta burst stimulation includes a train(s) of bursts each typically including 3-10 pulses at 100 Hz. It has been shown that theta bursts may induce LTP if they are delivered on the positive phase of the theta (measured by EEG) on anesthetized rats. Experimental studies also show that theta bursts may induce LTP. Experiments show that the maximum amplitude of LTP is obtained for 4-pulse, 100 Hz theta burst stimulations if the inter-burst interval is set to 200 ms. It seems that this interval is related to the refractory period for IPSPs that ranges from 200 to 500 ms. At 200 ms interval there is no feed-forward inhibition in the network so repeated theta stimulation allows for more effective temporal summation of excitatory post-synaptic potentials and thus an elevated LTP.

Another experimental paradigm that can induce LTP is the primed burst potentiation. In this protocol, typically five pulses are used where the first pulse precedes the last 4 pulses (at 100 Hz) by 170 ms. It is hypothesized that the LTP is produced in a two-step sequence as follows: the first pulse somehow sensitize the cell and then after a critical period of time, subsequent pulses make persistent changes in the synapse [Rose:1986aa, Diamond:1988aa].

3.4.2 Long term depression

The number of studies related to LTD is limited compared to LTP. Basically, prolonged low frequency stimulations of synapses results in a persistent reduction of synaptic transmission. The number of applied pulses on neurons may change the characteristics of EPSPs. For instance, Figure 3.46 shows the percent change in EPSP slope when synapses were stimulated by 300, 900, 1200 and 1800 pulses at 1 or 3 Hz. This figure shows that both low frequency
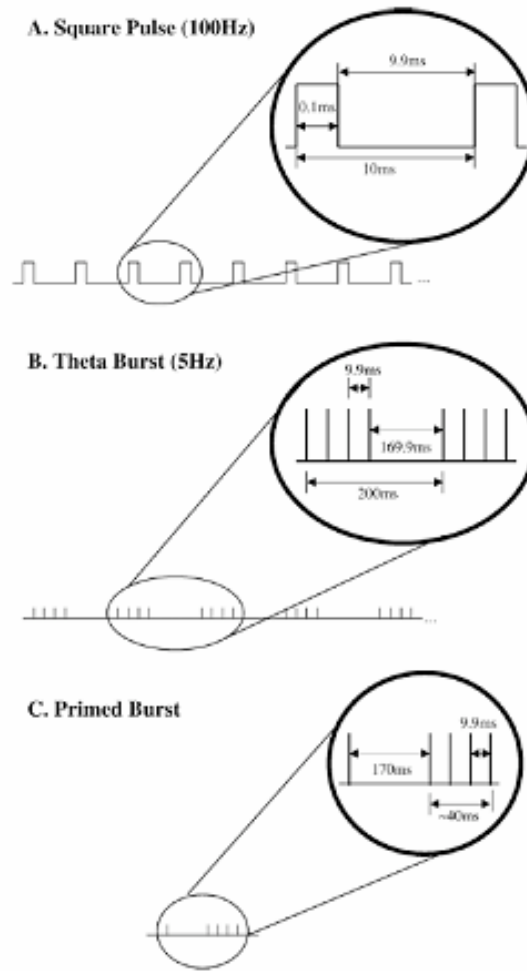
Figure 3.45 – Pulse sequences of three stimulation protocols that are commonly used for LTP induction. (A) Classic high-frequency square waves at 100 Hz entitled as tetanic stimulations. (B) Theta burst stimulation at 5 Hz. Each burst consists of a few pulses at 100 Hz. (C) Primed burst stimulation includes a primary pulse followed by a burst of pulses at 100 Hz. The time delay between the primary pulse and the following burst in this figure is 170ms.

stimulation protocols give more or less the same results, and LTD increases with the total number of applied pulses [Mockett:2002aa]. However, the results for 1200-1800 pulses may be rundown. In other word, the results may have been influenced due to adaptation or exhaustion of the available synaptic vesicles containing neurotransmitter.

By varying the intensity of low frequency stimulations, induced LTDs may have different temporal responses. For example, [Sajikumar:2004aa] showed that a stimulation containing 900 pulses (1 Hz, impulse duration 0.2 ms per half wave) only generates a transient early-LTD, while a strong stimulation containing 900 bursts (1 burst = 3 stimuli at 20 Hz; inter burst interval=1 s; stimulus duration 0.2 ms per half wave) could produce stable late-LTD for 8 h.

It is interesting to notice that stimulations of synapses by low frequency bursts containing high frequency pulses may have different effects on long-term responses of synapses. For example, it was shown that one minute stimulation of subthalamic nucleus by 60 bursts which
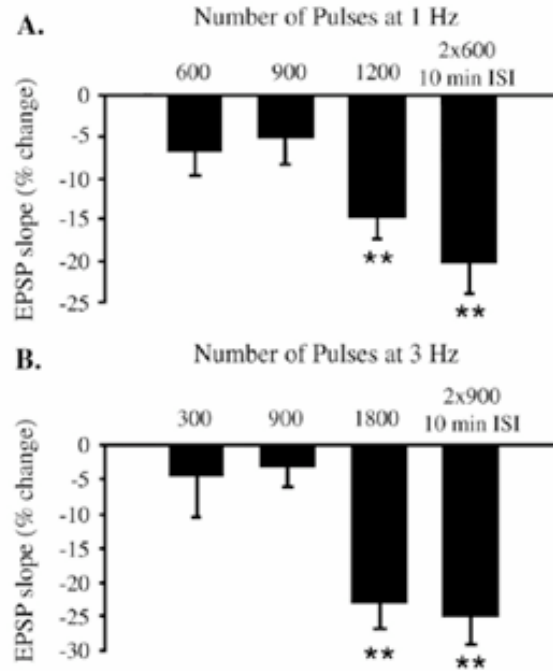
Figure 3.46 – The ability of different low frequencies (1 and 3 Hz) and several pulse sequences (600, 900, 1200 and 1800) to elicit LTD. LTD has been reported by percent change in ESPS slope. Figure from [Mockett:2002aa].

contain 50 pulses at 100 Hz (total: 60 pulses) may induce three types of synaptic plasticity [Shen:2003aa]. In particular, 17 neurons (out of 47 neurons) responded to the stimulation by eliciting LTD, LTP and short-term potentiation (STP). Paired-pulse analysis on these neurons indicated that the site of action for STP and LTD is in the pre-synaptic neuron, while the site of action for LTP is in the post-synaptic neuron.

Although LTP is usually the consequence of tetanic stimulation in hippocampal slices, there are some studies indicating tetanic stimulation may sometimes be followed by LTD. For example tetanic stimulation of corticostriatal fibers (three trains: 3 sec duration, 100 Hz frequency, 20 sec interval) could produce LTD (>2 h) in striatum [Calabresi:1992aa, Calabresi:1992ab]. This LTD response could be observed both in field potentials as well as EPSPs. This study also indicated that some conditions should be fulfilled for inducing LTD. For instance, during the tetanus stimulation, depolarization of membrane potential and discharges of action potentials in the post-synaptic neuron are necessary. In addition, the glutamate metabotropic receptors and D1 and D2 dopamine receptors should be activated (LTD was blocked by AMPA and dopamine antagonists) (see also [Calabresi:1997aa]). [Calabresi:1992aa, Calabresi:1992ab] showed that NMDA and $GABA_A$ receptors antagonists did not affect the expression of LTD so it appeared that they do not participate in underlying mechanism of this LTD response. In another study, they revealed that unblocking of NMDA receptors in the striatum unmasks the LTP responses which could not be obtained in the presence of Mg^{2+} ions [Calabresi:1992aa, Calabresi:1992ab]. They showed tetanic stimulations of corticostriatal fibers induce LTP responses in Mg^{2+}-free medium. This LTP response was not changed by an AMPA antagonist, while it was blocked by an NMDA antagonist.

Together, these data lead authors to deduct that under control conditions, NMDA receptor channels are inactivated and repetitive cortical stimulation induces LTD which does not require activation of NMDA channels. Removal of external Mg^{2+} deinactivates these channels and reveals a component of the EPSP which is potentiated by repetitive activation. This is in accordance with other studies showing that NMDA receptors play a major role in LTP responses [Huang:1993aa].

The influence of the frequency of stimulations (1, 10 and 100 Hz) of corticostriatal fibers on the characteristics of LTD in striatum has also been investigated [Bonsi:2003aa]. This study indicates that a conditioning stimulation at 1 Hz for 5 min does not cause any significant modification either in EPSP or in the membrane potential of the postsynaptic neuron. Accordingly, this stimulation protocol did not change the intracellular Ca^{2+} concentration $[Ca^{2+}]_i$ of the postsynaptic neuron. Stimulation at 10Hz for 1 min depolarized the cell during the stimulation period, but did not induce any LTD or LTP. In addition, this protocol caused a moderate rise in $[Ca^{2+}]_i$ that rapidly returned to baseline after stopping the stimulation. The high-frequency stimulation (tree trains: 3 s duration, at 100 Hz, 20 s intervals) produced LTD of EPSP amplitude. Each high-frequency train strongly depolarized the cell and increased $[Ca^{2+}]_i$. Based on these experiments it can be concluded that another necessary condition for LTD is the large transition in intrecellular calcium concentration of the postsynaptic neuron.

3.4.3   Complexity of LTP and LTD responses

In the two previous subsections we introduced some of the popular protocols that are employed for LTP and LTD inductions. In fact, there are many ways for inducing LTP and LTD responses in neurons, and it seems that our understanding of how electrical stimulation lead to these responses remains very basic. In addition, there is no unique theory that can describe how memory is coded in terms of electrical activities in synapses. As a result, there is no precise answer to describe why, for example, all tetanic, theta burst and prime burst stimulation protocols can produce LTP in hippocampus slices. We also do not know exactly why the high frequency stimulations over 200 Hz, that are used in *in vivo* experiments, induce LTP responses. In fact, this high-frequency stimulation does not have any physiological relation to memory and learning, but it is used for safety reasons to prevent generation of epileptic activities [Namgung:1995aa, Holscher:1997aa, Merrill:2005aa].

Our lack of knowledge becomes more severe if we look at the various responses of different brain regions obtained after quite similar stimulation protocols. For instance, as it was described before, tetanic stimulation can induce LTP and LTD responses in hippocampus and striatum slices, respectively. Similarly, 1 Hz stimulation of the hippocampus slice can generate LTD, while it does not express any significant change in EPSP amplitude in the striatum slice.

Moreover, LTP and LTD responses become more complex when considering that these responses can be modified or even inversed when intra- or extracellular ionic concentrations (e.g. Mg^{2+} and Ca^{2+}) change [Calabresi:1992aa, Calabresi:1992ab, Santschi:2003aa, Lante:2006aa]. Finally, maturation can even change the LTD to LTD response . Together, these data suggest firstly that LTP and LTD responses are very complex and secondly that our understanding about the underlying mechanisms of brain electrical stimulations, LTP/LTD responses, learning and memory still remain rudimentary.

3.5   Conclusions

The level of integration at which electric fields effects are considered is crucial. At cellular level (based on *in vitro* work), some effects of electric fields (DC and AC) are now well described in terms of orientation and polarity, changes of transmembrane potential, modification of firing rates, site of AP initiation. At the level of neuronal networks (based on *in vitro* work), some information is still missing: effects on non-pyramidal neurons (interneurons, glial cells), effects on afferents, effects on LTP/LTD.

4   Effects of TMS and tDCS on the brain: in-vivo findings [FW]

4.1   Effects of TMS

As TMS offers the unique opportunity to interact in a non-invasive and painless way with brain activity, it was first and mostly used for *in vivo* human studies. However, a growing number of studies have been conducted in animals *in vivo* since the early 90s in an attempt to answer questions raised in human studies. Most animal work has aimed at testing a potential therapeutic effect of TMS in animal models. However, a reasonable number of studies also explore the physiological basic mechanisms underlying TMS stimulations, such as its effects on neuronal action potential activity, neuromodulation, neuroprotection, neurogenesis, plasticity or memory and learning behaviours.

The majority of animal TMS studies have been conducted in rodents and cats. Illustrated examples are provided in the Appendix (Section 2). A broad panel of effects is described with, at times, contradictory results. This most likely reflects the diversity in parameters of stimulation used across the studies (coil shape and size, orientation and distance from the scalp, strength of field, stimulation frequency and paradigm). Details are provided in additional material in the Appendix (Section 3).

4.1.1   Effect on neuronal excitability based on electrophysiological data

a) Estimation of induced intracranial voltages

The first and only study providing a quantified measure of the intracerebral voltage induced by TMS was performed a decade ago using intracerebral recordings in monkeys [Lisanby:2001aa]. The authors used a paediatric figure-of-eight TMS coil to stimulate monkeys with repetitive pulses for a short duration and simultaneously recorded potentials induced at ten different contacts of an electrode stereotaxically implanted in the prefrontal cortex (anterior to posterior direction). Their data show that the amplitude of induced voltages was relatively stable across pulses (coefficient of variation = 2.4%), was linearly related to TMS intensity (r^2=0.9), and, as expected, rapidly decreased as the distance from the coil increased. As an example, a single pulse at 70% of maximal output, delivered over the prefrontal region with a "paedratric" figure-of-eight coil generated an induced field of ˜180mV at the most external prefrontal contact (red arrow on Figure 3.47). Unfortunately, in these studies, accurate physical parameters of the stimulation (inner/outer diameter of the figure-of-eight coil, estimated strength of the magnetic field, or estimated distance between the coil and cortex) are not provided.

b) Effect on the neuronal firing rate
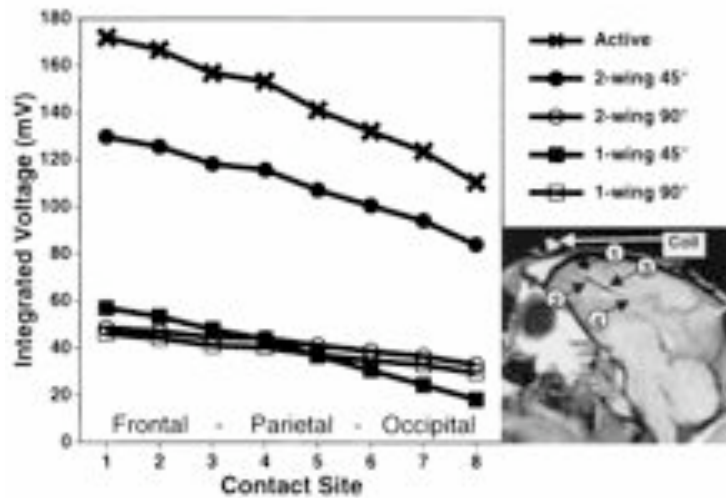
Figure 3.47 – Intracerebral electrode contact sites marked on sagittal view, relative to fiducial marker of coil site.(Left) Intracerebral recordings of voltage induced in the brain in vivo by active and four types of sham transcranial magnetic stimulation. Taken from [Lisanby:2001aa]. For this report, permission has not been requested.

The effects of TMS on spontaneous and evoked neuronal activity have been first explored in cats [Moliadze:2003aa]. Single pulses were delivered every 6s (0.16 Hz) at different field strengths over the primary visual cortex (area 17) and extracellular single-unit recordings were performed at the centre peak of the magnetic field induced by the coil. The authors demonstrated that, compared to baseline, the firing rate of single neurons increased (facilitation) for the first 500 ms following the single TMS pulse, while it decreased (inhibition) from 500 ms to a few seconds post-TMS. The results slightly varied according to the field strength: weak stimuli (20-30% of maximal device output) tent to cause an early facilitation up to 200 ms post-TMS, followed by a late inhibition. Stronger stimuli (40-100% of maximal output) first induced an early suppression of neuronal activity (for 100–200 ms), followed by a delayed facilitation (up to 500 ms) [7] and terminating in the late inhibition (Figure 3.48).

Interestingly they also explored the effect of a single TMS pulse on neuronal activity evoked by a visual stimulus (moving bar). In the protocol they designed, the interval between magnetic and visual stimulation was varying. When the TMS pulse was given close to the response (<100 ms), the visual evoked activity was facilitated. On the contrary, TMS delivered several hundred milliseconds before the visual response had a suppressive effect that could persist for 5–6 s, and could interact with the next evoked response.

Most interestingly, the combination of TMS with a visual stimulation caused a 2–3 times stronger facilitation of neuronal evoked activity than when applied during spontaneous activity (See Figure 3.49).

The main conclusion of this initial study is that the suppression and facilitation of neuronal activity could be related to the stimulation of inhibitory and excitatory interneurons with different thresholds, and that the late, long-lasting suppression would more likely be related to metabolism of vascular responses.

---

[7]In some instances, the authors observed multiple peaks of activity during the facilitating episode, occurring at an alpha-like frequency (100 ms between peak of activity= 10Hz)
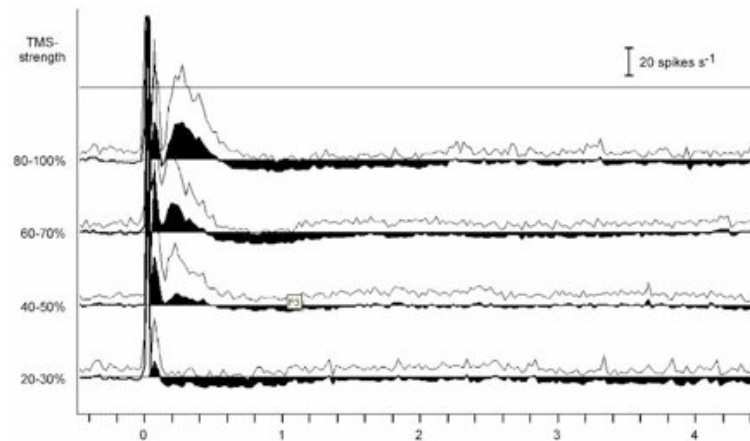
Figure 3.48 – Grand average of records obtained with different TMS strengths during spontaneous activity. The mean level of spontaneous activity prior to TMS was set to zero to emphasise increases and decreases in activity (black filled areas). The thin line depicts the standard deviation. Taken from [Moliadze:2003aa]. For this report, permission has not been requested.

Two years later, the same team reported the effects of another TMS paradigm- called paired pulse TMS (ppTMS) – on the firing rate of neurons in the in cat primary visual cortex [Moliadze:2003aa]. This paradigm, introduced previously in human studies [Kujirai:1993aa], is based on stimulation by a sub-threshold TMS pulse (conditioning stimulus) followed by a supra-threshold TMS pulse (test stimulus). In humans, the effect of the conditioning stimulus depends on the interstimulus interval as well as on the intensity of the conditioning stimulus. An interstimulus interval of 1–4 ms reduces the motor evoked response (MEP) elicited by the test stimulus (intracortical inhibition, ICI) while longer interstimulus intervals of (7– 20 ms) induce a facilitation of the MEP (intracortical facilitation, ICF) [Kujirai:1993aa]. Increasing the strength of the conditioning stimulus leads as well to facilitation even for short interstimulus intervals [Ziemann:1998ac, Chen:2008aa].

Accordingly, in the feline visual cortex, [Moliadze:2005aa] showed that the conditioning stimulus modifies the effect of the supra-threshold test stimulus on visually evoked activity. As in humans, by varying the intensity of the conditioning stimulus, they observed a facilitation of the test stimulus effect (i.e. increased facilitation or strengthened suppression of neuronal activity of visual activity if the test stimulus by itself had a suppressive effect) (Figure 3.50).

Nevertheless this was only the case for conditioning stimulus strenghs 60–130% of test stimulus, whereas weaker conditioning stimuli (15–30% of test stimulus) resulted in reduction of the test stimulus effect (see the slope modification in Figure 3.51). Moreover, contrary to the effects of ppTMS described for the human motor cortex, the authors found that the ppTMS effect was independent of the interstimulus interval.

Physiological differences between visual and motor cortices are possibly one reason for the partly different effects of ppTMS in cat visual cortex and human motor cortex. In human motor cortex, cortical inhibitory and excitatory activity elicited first by the conditioning stimulus and then by the test stimulus interacts at the corticospinal output neurones and determines the amount of population activity. In the visual cortex, this population activity interacts with the sensory input which by itself activates excitatory and inhibitory network activity. Accordingly, in their previous study the facilitation of activity was much stronger when TMS was combined with a visual stimulation than when it was applied alone, which suggests that
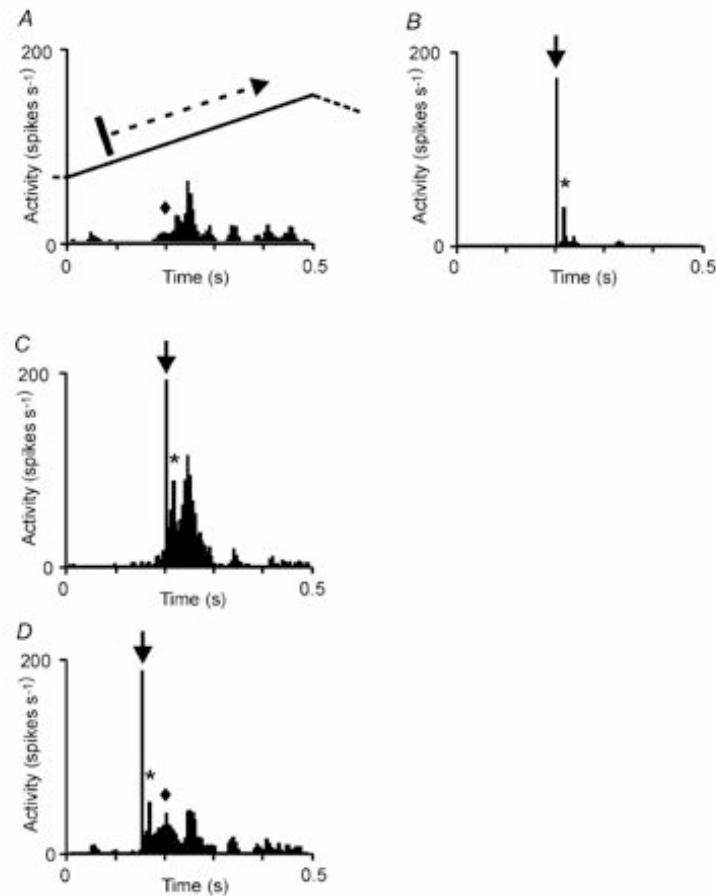
Figure 3.49 – Effect of TMS on visual responses to moving bars. Visual response of a cortical neuron (simple cell) to a bar moving across its receptive field. For simplicity, only the response to one direction of bar motion is shown here (see inset of motion trajectory). A, visual stimulation alone. B, TMS alone. C and D, TMS combined with visual stimulation, with TMS given at two different times. Note that the activity evoked by TMS alone (asterisks) is less than the increase of visual activity during combined TMS and moving bar (see response components labelled with asterisks and diamonds). Arrows indicate the TMS artefact. Taken from [Moliadze:2003aa]. For this report, permission has not been requested.

"the TMS pulse pushes subthreshold, visually pre-activated inputs" [Moliadze:2003aa].

These effects of TMS on action potential activity have recently been confirmed and extended in two reports. In the first one, the authors recorded simultaneously single-unit activities in the cat primary visual cortex and dorsal lateral geniculate nucleus (dLGN) of the thalamus, while applying single pulses or trains of pulses of TMS over area 17 . Their results show that TMS reduced both the cortical and thalamic neuronal response to the visual stimulus and are compatible with the role of a cortical modulation of thalamic activity. Their work also stresses on the different levels of suppression and recovery that can be induced by distinct frequencies of TMS stimulation. Moreover, as in Moliadze et al. study (2003) the suppressive effect of TMS is only obtained when the magnetic stimulation is applied prior to the visual stimulation.

In the second report, [Allen:2007aa] explored the effect of a short (1-4s) TMS trains (1-
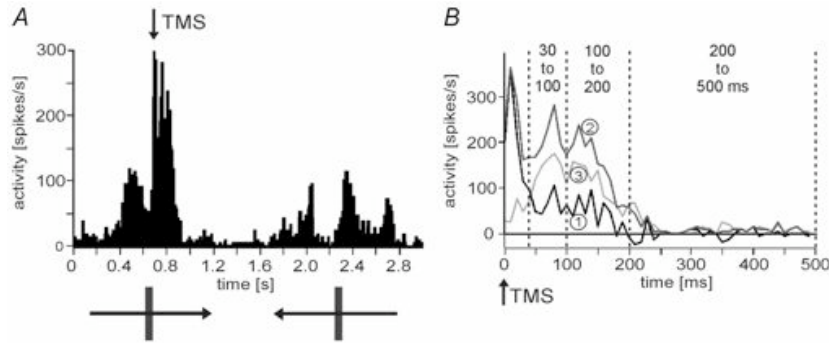
Figure 3.50 – Analysis of paired-pulse transcranial magnetic stimulation (ppTMS) effect on visually evoked activity A, peristimulus time histogram (PSTH) showing single-unit activity evoked by an optimally orientated bright bar moving back and forth across the receptive field of the unit as indicated by the drawing below the diagram. TMS was given close to visually enhanced activity (see arrow). B, mean activity within a time window of 500 ms following TMS (time of suprathreshold test stimulus (TS), the second stimulus in the case of ppTMS). Curves 1–3 are: (1) activity after TS only, (2) activity following ppTMS (in this case a conditioning stimulus (CS) of 60% strength of TS, given 4 ms prior to TS), (3) difference between curves 1 and 2 (2 minus 1). Activity rates were calculated as the mean of 20 identical trials. Three different time windows following TMS were analysed (as indicated by the dashed lines): 30–100 ms, 100–200 ms and 200–500 ms. For further analysis, the activity within these time windows was averaged for each condition. Taken from [Moliadze:2005aa]. For this report, permission has not been requested.
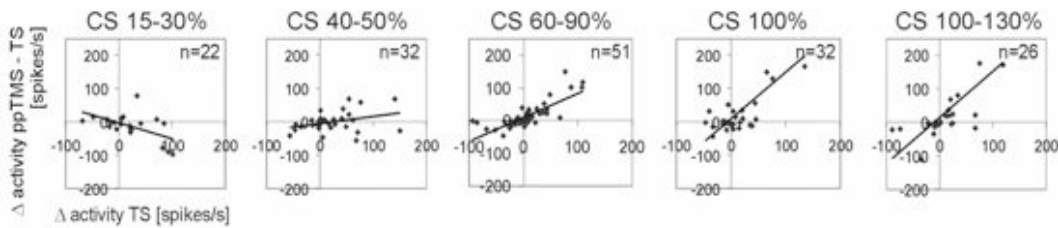
Figure 3.51 – CS Dependent change in correlation between ppTMS effect and TS effect. Scatter plots show the relationship between ppTMS- and TS-induced changes in visual activity. Each of the scatter plots shows data for ppTMS with ISI of 3 ms only, but for 5 different ranges of CS strength. Pearson correlation was significant for CS range 15–30% ($\alpha < 0.01$) and for the range 60–130% ($\alpha < 0.001$). Taken from [Moliadze:2005aa]. For this report, permission has not been requested.

8Hz) over the cat visual cortex on the spontaneous and evoked neuronal spike rate in area 17. Their study shows that TMS applied repetitively (rTMS) induced a substantial frequency-dependant increase of the spontaneous neuronal activity ($\sim 200\%$) persisting for ~ 60s. This increase is interpreted as due to a direct depolarization of neurones from the induced electric field. This depolarization may be amplified via recurrent synaptic excitation to involve a larger population and to give raise to a persisting increase of the firing rate. As earlier studies, they show that unlike spontaneous activity, the neuronal activity evoked by a visual stimulus is reduced ($\sim 50\%$) after rTMS, that this reduction is gradually increasing with the stimulation frequency, and last for more than 5 min suggesting long-term changes after TMS.

c) Effects on field potentials (EEG/EP)
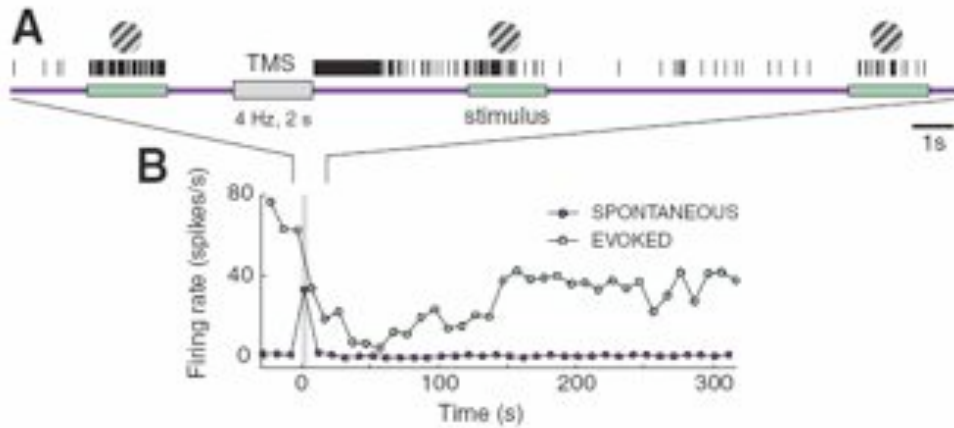
Figure 3.52 – TMS and visual stimulation paradigm. (A) Timeline of a sample trial showing stimulus presentations (green) and interstimulus intervals (ISIs) (purple). The visual stimulus was a high-contrast grating displayed for 2 s at intervals of 8 s. TMS (gray box) was applied during an ISI. TMS pulse trains were varied in frequency and duration on separate trials. Single-unit spikes (black ticks), LFP (not shown), and tissue oxygen (not shown) were recorded continuously; activity during TMS was not analyzed because of artefact contamination (fig. S3A). (B) The full TMS trial. Evoked activity represents neural responses during stimulus presentations, and spontaneous activity represents responses that occurred during ISIs. Taken from [Allen:2007aa]. For this report, permission has not been requested.

At the level of intracranial EEG (or evoked) activity, the effects of TMS are somewhat consistent with works conducted on unitary neuron recordings, although parameters of TMS stimulation is highly variable among studies (details are provided in the Appendix, Section 2) with different stimulation protocols for low and high frequencies as well as for short- and long-lasting applications on different brain areas in the cat, or rat.

In the cat, low frequency stimulation (0.5-3Hz) reduced the amplitude of the visual evoked potential (VEP) N1 (both in the stimulated area of primary visual cortex and in the contralateral occipito-temporal area) only for long duration of stimulation [Aydin-Abidin:2006aa]. Short duration of low frequency rTMS increased the EEG delta power in the cat visual cortex [Aydin-Abidin:2006aa] and decreased the EEG beta and gamma power in the rat motor and sensory cortex [Li:2007aa]. Moderate frequency stimulation (10Hz) applied for short durations (<5min) significantly enhanced early VEP amplitudes in the cat visual cortex, whereas a longer rTMS stimulation (20 min) had no effect [Aydin-Abidin:2006aa]. Finally, in the rat, rTMS stimulation at high frequency (60-70Hz) induced a hypersynchronization of the electrical intracerebral activity recorded in the orbito-frontal area, hippocampus, and stem as well as an increase in interactions (uni- and bilaterally) between these regions [Sharova:2007aa]—see Figure 3.53.

From the single unit or field potential recordings described above, one of the most interesting finding is the late and long-lasting suppression of activity after TMS. These long-term effects are probably related to the fact that, *in vivo*, the synchronous activation of a large number of neurons by TMS leads to a cascade of phenomena in a long-time scale, including vascular, metabolic responses, as well as modification in the neurotransmission systems.
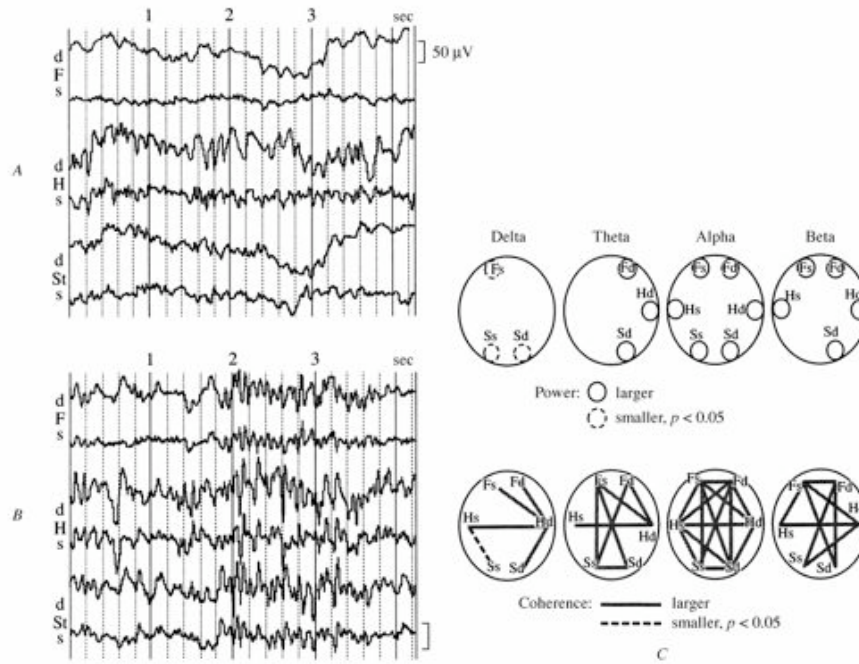
Figure 3.53 – Changes in brain electrical activity (EA) in an intact rat 60 min after the first session of TMS. A) Baseline EA; B) EA 1 h after TEMS at a frequency of 60 Hz; C) spectral (upper plots) and coherence (lower plots) characteristics of EA showing significant ($p < 0.05$) changes from baseline at 1 h. EA recording zones: F is the orbitofrontal cortex, H is the hippocampus, St is the stem at the level of the lateral vestibular nuclei of Deiters. s = left, d = right. Taken from [Sharova:2007aa]. For this report, permission has not been requested.

4.1.2   Vascular and metabolic changes

The study by [Allen:2007aa] quoted earlier shows that neural changes induced by rTMS are similarly reflected in vascular parameters. Indeed, changes in the oxygen tension in brain tissue and in the total level of haemoglobin measured by optical imaging initially increased and subsequently decreased after TMS application. Neural and hemodynamic response components also covaried with stimulation parameters (see Figure 3.54). These data provide an experimental evidence that most of the oxygen response is supported by changes in blood flow and that long-lasting neural and hemodynamic responses to TMS are tighly coupled and co-vary with stimulation duration and frequency.

Interestingly, autoradiography studies in the cat provided supplementary data on the metabolism changes during, just after, and long after rTMS application. During high or low frequency (20Hz vs. 1Hz) rTMS, a selective decrease in glucose consumption appeared in the stimulated area, as well as in distant cortical and subcortical structures receiving strong input from the stimulated brain area citeWagner:2007aa. This decrease persisted shortly after low frequency rTMS but reversed (i.e. increase glucose consumption) after high frequency rTMS [Valero-Cabre:2007aa]. No effect on glucose metabolism was reported 30 min after the stimulation.

Therefore, the paradigm of TMS stimulation seems to influence metabolism parameters along with neuronal activity, field potentials and blood flow.
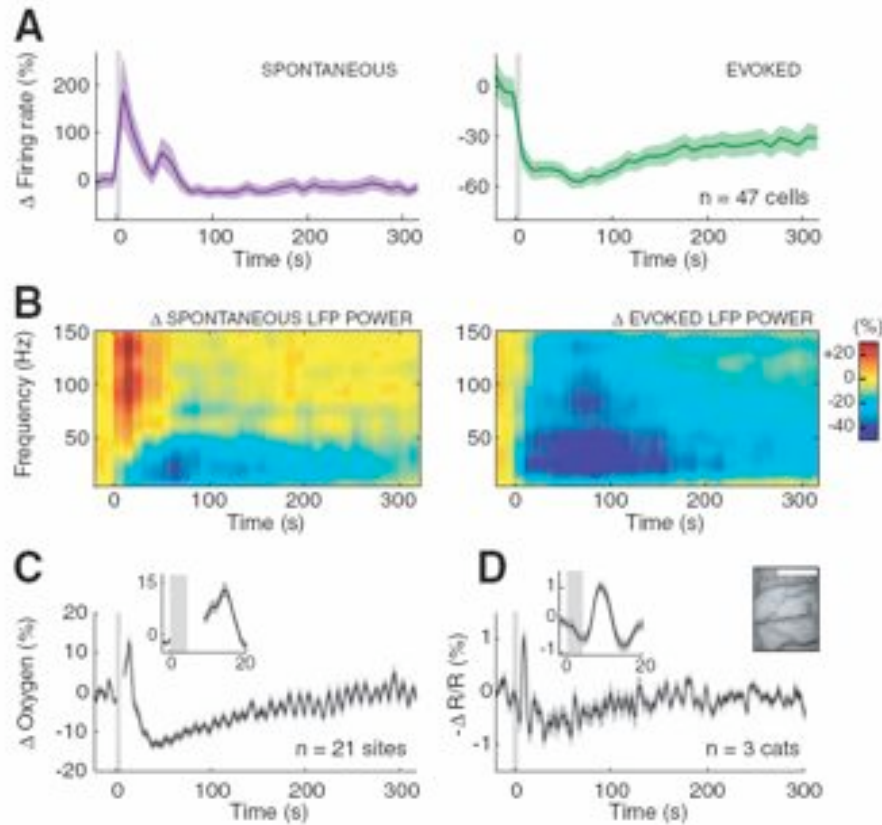
Figure 3.54 – Effects of TMS on neural, oxygen, and optical imaging signals. Shown are average time courses of (A) spiking activity, (B) LFP power, (C) tissue oxygen, and (D) total haemoglobin (Hbt) before and after TMS (gray box). All signals are expressed as a percent change from their pre-TMS baselines. Shaded areas represent ± 1 SEM. (A) Spontaneous (left) and evoked (right) spiking activity (n = 47 cells). (B) Spontaneous (left) and evoked (right) LFP power (n = 42 sites). (C) Tissue oxygen (n = 21 sites). (D) Hbt (n = 3 animals). Insets in (C) and (D) show initial increases. Time periods containing TMS artifacts were removed (fig. S3B). In (D), Hbt was measured by recording the change in 570-nm light reflectance ($\Delta R/R$) from the cortical surface (upper right); scale bar, 1 mm. Taken from[Allen:2007aa]. For this report, permission has not been requested.

4.1.3 Changes in neuromodulation systems

rTMS appears to have numerous effects on neurotransmitter systems. Monoamines have been the most studied probably because of their link with many psychiatric disorder in which rTMS might have therapeutic potential in humans. These effects are usually region-specific and differ whether rTMS is applied once (acute rTMS) or repeated daily for several days (chronic rTMS).

Acute rTMS in rats (usually 20-25 Hz among studies) was shown to decrease the dopamine (DA) concentration in the frontal cortex and increase it in the striatum [Ben-Shachar:1997aa] in the dorsal hippocampus [Keck:2000ab, Keck:2000aa], in the accumbens nucleus and in the dorsal striatum [Keck:2002aa, Kanno:2004aa]. Noticeably, one study showed that the changes in the DA concentration observed in frontal areas were identical for sham and rTMS treated

animals [Kanno:2003ab, Kanno:2003aa]. Acute rTMS also increased the levels of serotonin (5-HT) and its metabolite (5-HIAA) in the hippocampus [Ben-Shachar:1997aa] but not in frontal regions . Interestingly, one study showed that acute rTMS exposure could induce, 24 h after stimulation, an increased binding to 5-HT_{1A} receptors in the frontal and cingulated cortices [Kole:1999aa].

Finally none of these studies reported modifications in norepinephrine (NE) content after acute rTMS.

Amino-acids levels were also modified in the rat paraventricular nucleus after acute rTMS treatment, with a significant increase in aspartate, serine, and taurine (also reported to be increased after antidepressant treatment) [Keck:2000ab, Keck:2000aa]. These authors did not find any significant change in the glutamate, glutamine, arginine, or GABA concentrations after acute rTMS. However, a delayed increased binding to NMDA receptors was detected in the hypothalamus, amygdale, and parietal cortex of rat, 24h after the rTMS acute application [Kole:1999aa].

Unlike in acute rTMS treatment, chronic application of rTMS in rats (15-25Hz repeated daily for 9-20 days) did not induce changes in 5-HT, DA, or NE levels in frontal regions, striatum or hippocampus [Ben-Shachar:1999aa]. However, a 2s-20Hz rTMS stimulation repeated 20 times a day for 20 days in the mouse modulated the expression of monoamine transporters: expression of 5-HT transporters genes were downregulated (i.e. re-uptake inhibition) while expression of DA and NE genes were upregulated [Ogiue-Ikeda:2005aa]. These changes were assessed at a whole-brain level, which possibily might flatten regions-specific modifications.

Additionally, chronic rTMS in rats was reported to downregulate 5-HT_2 receptors in the frontal cortex [Ben-Shachar:1999aa]. β-adrenergic receptors were also downregulated in the striatum [Ben-Shachar:1997aa] and in neocortex [Fleischmann:1996aa].

4.1.4 Neurogenesis: neurotrophic factors, early genes (GFAP, BDNF, cfos, c-jun)

Under a variety of stimuli, such as stress, cytokines, or infections, there is activation of a transcription regulator protein (AP-1 for activation protein 1) composed of proteins belonging to the c-fos, c-jun, families. AP-1 can bind to a specific DNA motif and transactivate the expression of a number of late effector genes to produce neurotrophic factors such as nerve growth factor (NGF), brain-derived neurotrophic factor (BDNF), fibroblast growth factor (FGF). In the adult brain of all mammals, including humans, neuronal and glial trophic factors intervene in the production of new cells from a pool of neural stem cells located mainly in the subventricular zone (SVZ) and in the dentate gyrus subgranular zone (SGZ) of the hippocampus [Arias-Carrion:2006aa]. The expression of transcription factors c-fos, c-jun, or zif268 as well as brain-derived neurotrophic factor (BDNF) or glial fibrillary acidic protein (GFAP) is proposed to be a rapid indicator for neuronal or astroglial activation. Therefore a few recent studies have investigated their expression after TMS.

After acute rTMS (25hz for 10s) in mice, one study reported an increase of glial fibrillary acidic protein (GFAP) in the dentate gyrus and more moderately in the neocortex [Fujiki:2004aa]. Following chronic 20Hz- rTMS in the rat, BDNF was increased in the hippocampal areas CA3, in the parietal and the piriform cortex [Muller:2000aa]. Conversely, in another study in rats, a fairly similar chronic stimulation for a shorter duration (14 days vs. 11 weeks) had no effect on GFAP , BDNF or FGF [Hausmann:2000aa].

Results in relation with c-fos expression are more consistent between studies. In general,

after an acute (20-25Hz) rTMS treatment, c-fos expression was widely increased in rodents cortex [Doi:2001aa, Ogiue-Ikeda:2005aa]. Repeating the stimulation several times on the same day usually strengthened the effect [Ji:1998aa, Doi:2001aa]. Notably, this last study showed that the increased c-fos expression predominated in the paraventricular nucleus of the hypothalamus (PVT) and frontal and cingulated cortices, and could also be found in regions controlling circadian rhythms such as suprachiasmatic nucleus (SCN), subparaventricular zone (SVN) and pineal [Ji:1998aa].

Chronic rTMS seems to have more region-specific effects, with an increase in c-fos expression in the parietal cortex and in the hippocampus [Hausmann:2000aa, Muller:2000aa] or even no effect when considering the entire brain in mice [Ogiue-Ikeda:2005aa].

More recently, [Aydin-Abidin:2008aa] showed that early gene expression can be specifically modulated by acute rTMS depending on the pattern of stimulation applied. In general, zif268 protein was increased only following theta-burst stimulation, whereas c-Fos expression was preferentially increased after 1Hz and 10Hz-rTMS. These results are particularly interesting when confronted to *in vitro* and *in vivo* experimental data obtained in monkeys and rats that indicate that zif268 expression is essential for the induction and persistence of long term potentiation (LTP) [Cole:1989aa, Richardson:1992aa, Abraham:1993aa, Abraham:1994aa] and that associative learning and zif268 expression (but not c-Fos) are correlated [Okuno:1996aa, Guzowski:2001aa].

4.1.5 Effects synaptic plasticity LTP/LTD

LTP is a persistent increase in synaptic efficacy resulting from the stimulation of afferent fibers at high frequency. In the hippocampus, LTP is usually presented as a model of synaptic plasticity in close relationship with learning and memory.

There is growing evidence that the mechanisms underlying long-lasting effects of rTMS on cortical activity as well as on memory or learning behaviours might be related to long-term potentiation (LTP) and long-term depression (LTD) mechanisms. These mechanisms were reported to be highly mediated by NMDA receptors. Accordingly, as described above, a delayed increased binding to NMDA receptors was detected in the hypothalamus, amygdala, and parietal cortex of rats, 24h following a 20Hz-rTMS acute application [Kole:1999aa]. This is consistent with the hypothesis that LTP-like mechanisms may underlie the lasting effects of rTMS.

An early report by [Wang:1996aa] had shown that after a 8 Hz-RTMS application over the auditory cortex of gerbils, the population spike in the temporal neocortex could be either enhanced in a LTP-like manner (1/4 or animals), depressed in a LTD-like manner (1/4 of the animals) or unchanged (1/2 of animals). Such effects were not observed for lower stimulation frequencies (<8Hz).

Another group demonstrated that acute and chronic rTMS enhanced in vivo the reactivity of the rat dentate gyrus to a single stimulation of the perforant path [Levkovitz:1999aa]: at stimulation of the perforant path that yielded 50% of the maximal response in control conditions, the amplitude of the population spike was increased in a dose-dependant way for TMS at 1,10 and 25Hz. This effect seems to be age-dependant as it was not observed in old rats [Levkovitz:2001aa].

In more recent studies, LTP was induced *in vitro* on hippocampal slices just after [Ahmed:2006aa] or 15 hours after animals had been stimulated by rTMS [Ogiue-Ikeda:2005aa, Ogiue-Ikeda:2003ab, Ogiue-Ikeda:2003aa]. The results indicate that LTP can be modulated
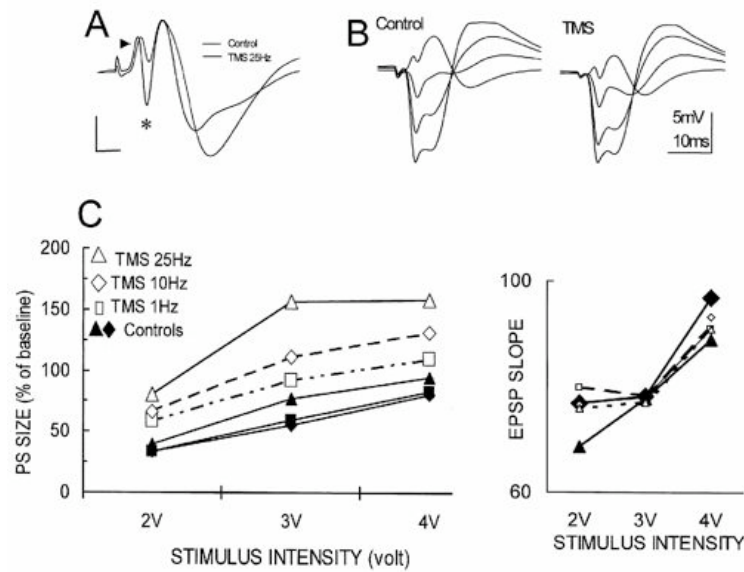
Figure 3.55 – TMS potentiates population spike responses in the rat dentate gyrus. A, A sample record of population response to perforant path stimulation recorded before (thin line) and shortly after (thick line) a 25 Hz, 2 sec train of magnetic stimulation. Note the similar slope of EPSP (arrowhead) and the larger population spike (asterisk) after TMS. Calibration: 5 msec, 5 mV. B, Depth profile produced by stepping the recording pipette into the dentate granular layer. The traces, from bottom to top, are initially negative (down-going) in the molecular layer and reverse to positive EPSPs, with a negative-going population spike, at the granular layer (top traces). Note that after TMS the size of the EPSP is not changed, but the population spike is larger. C, Averages of responses taken before and after acutely applied TMS plotted as a function of stimulation intensity. Left, Magnitude of the population spike. Right, Slopes of EPSP. In both plots, the sizes of responses are expressed as percentage of control values. A TMS dose-dependent increase in population spikes is seen, with no significant differences in population EPSPs (right) to different stimulation intensities. The three control groups (filled symbols) are for each treated group, taken before TMS treatment. SEs are smaller than the symbol sizes. All the treatment groups are different from each other significantly, but the control groups are similar to each other. Taken from [Levkovitz:1999aa]. For this report, permission has not been requested.

by rTMS and that this modulation is intensity- and frequency-dependant. Ogiue-Ikeda et al. found that chronic rTMS at 0.75 T enhanced the *in vitro* induced LTP, while chronic rTMS 1.25 T suppressed it and chronic rTMS at 0.5T and 1T had no effect on LTP.

Using acute rTMS at 15 Hz *in vivo* in mice, [Ahmed:2006aa] enhanced the LTP effect obtained from hippocampal slices *in vitro*, but acute rTMS at 8 Hz reduced it (see Figure 3.56). It is noteworthy that the enhanced potentiation observed after 15Hz-rTMS was decreased by half three days after the stimulation.

Long-term changes in neural function are thought to develop synaptic plasticity. Notably, alterations in synaptic efficacy have been linked to changes in the temporal relationship between action potentials and LFP oscillations [Holscher:1997aa, Wespatat:2004aa]. To examine a link between spike timing and long-term neural changes, [Allen:2007aa] performed analysis of phase relationships between single-unit spikes and LFP oscillations and found that, spontaneous activity showed significant reductions in phase locking within the first 30 s after TMS for all frequency bands (see Figure 3.57 C). One minute after TMS, phase locking index
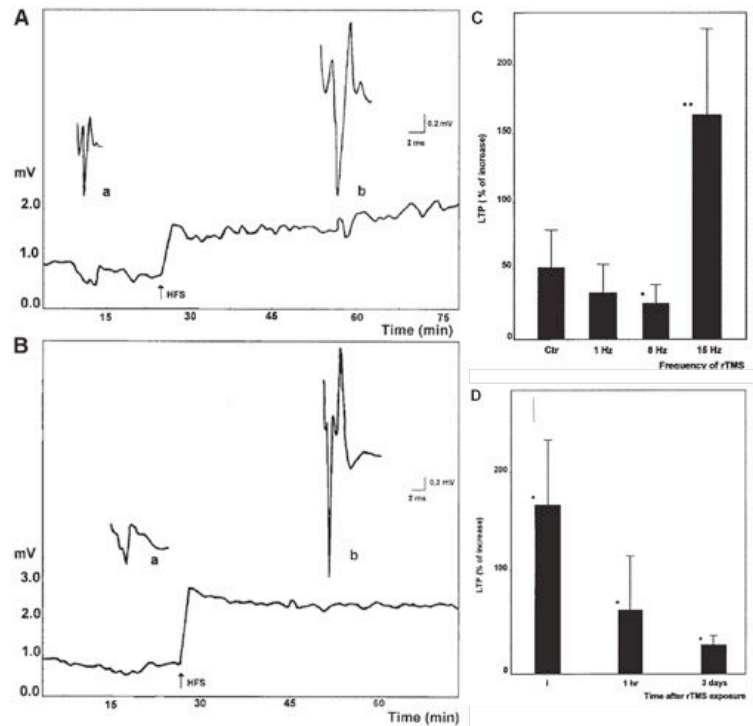
Figure 3.56 – The representative examples of long-term potentiation (LTP) induced in the slices obtained from control animals (A) and from the animals exposed to 15 Hz rTMS (B). The slices from exposed animals were prepared immediately after stimulation with Magnetic fields.The upper part of the figures depicts the average of 10 population spikes recorded just before (a) and 40 min after (b) application of high-frequency stimulation (HFS).The lower part of each figure illustrates the changes in the amplitude of the population spike during the whole experiment. C: The influence of rTMS frequency on LTP. D: The magnitude of LTP recorded from slices prepared at different time intervals (I- immediately,1h and 3days) following the exposure of the animals to 15HzrTMS. Taken from [Ahmed:2006aa]. For this report, permission has not been requested.

returned to baseline, and, in the gamma band, it even exhibited a significant increase. These data are of particular importance as they suggest that TMS can disrupt the precise timing of signals between interconnected neurons and potentially alter brain plasticity.

4.1.6 Effect on normal behavior: memory, learning, visuo-spatial orientation

Short-term or long term cognitive effects of TMS have been explored in a few studies using several types of rTMS protocols to test for potential effects on memory, or learning behaviours in animals.

While the acute or chronic application of either low- or high-frequency rTMS did not show a significant alteration respectively of spatial short-term memory in monkeys [Yamada:1995aa] or olfactory short-term social recognition in rats [Post:1999aa], most of the other studies showed that rTMS under specific stimulation conditions could impair memory. [Kling:1990aa] found that after conditioning rats to a taste aversion, an acute 50 pulses-rTMS treatment impaired retrograde memory but not anterograde memory.

Similarly, rTMS delivered at 1, 8 or 15 Hz substantially decreased the rat performance in differentiating between familiar and unfamiliar objects [Ahmed:2006aa]. Additionally a
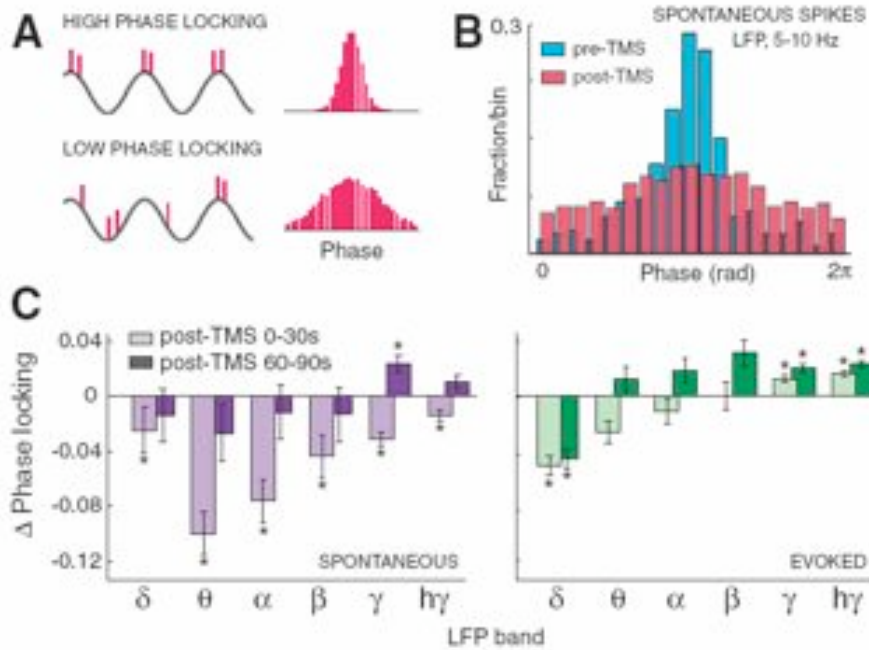
Figure 3.57 – Effects of TMS on spike timing relative to LFP oscillations. (A) Illustration of phase locking between spikes (red) and LFP (black). During periods of high phase locking (top), spikes occur at consistent phases in the LFP (left), and the resulting phase distribution is narrow (right). (B) Example of a TMS-induced change in phase locking. Before TMS (blue), spontaneous spikes occur more frequently at preferred phases of theta-band oscillation. In the first 30 s after TMS (red), the phase distribution broadens, indicating a decrease in phase locking. (C) Changes in phase locking across LFP frequency bands for spontaneous (left) and evoked (right) activity. Change in phase locking was determined by comparing the vector strengths (one minus the circular variance) of phase distributions before and after TMS. Light bars show changes in the first 30 s after TMS; dark bars show changes at 60 to 90 s. Asterisks indicate significance (P < 0.05, randomization test). Source: [Allen:2007aa].

transient impairment of the visuo-spatial orientation in cats was reported 20 min after acute rTMS delivered at 1Hz with a return to baseline 45 after stimulation [Wagner:2007ab]. The number of mistakes as well as the extension of the spatial neglect were positively correlated with the field intensity [Wagner:2007ab].

Interestingly, two recent studies suggest that rTMS might affect differently memory and learning. 5Hz-rTMS was applied over the auditory cortex repeatedly over 5 days between sessions in which gerbils were trained to discriminate frequency-modulated tones [Wang:2006ab]. Results indicated that rTMS affects punctually the short-term consolidation processes without disturbing long-term memory and learning performances at the end of the chronic 5-days treatment [Wang:2006ab]. Most noticeably, rTMS had a detrimental effect on discrimination when it was delivered just after but not just prior to training sessions, suggesting that the consolidation processes but not the tone perception was transiently disrupted. Similarly, at lower frequency (0.5 Hz) Li et al. show that while the retrieval in short term memory is impaired by chronic rTMS, the working memory and learning processes remain unaffected [Li:2007ab].

4.1.7 Effect on animal models of neurological disorders

TMS has been applied to various psychiatric and neurological disorders in humans. Therefore, the use of animal models is essential both to determine the clinical utility of TMS and the physiopathology of the disorders under consideration.

a) TMS and animal models of depression, anxiety and stress

As one of the most studied applications of TMS in humans has been the treatment of psychiatric disorders, many groups have investigated the effect of TMS on rodent behavioural models of depression. Chronic rTMS applied at various frequencies (15-50 Hz among studies) was shown to decrease the immobility time (as an index of depressive state) in the Porsolt swim test [Fleischmann:1995aa, Zyss:1999ab, Zyss:1997aa, Keck:2000aa, Tsutsumi:2002aa, Kim:2006aa, Vieyra-Reyes:2008aa]. Some groups, however, reported that this effect could be mild [Hargreaves:2005aa] or frequency dependant [Loo:2000aa].

On the contrary, acute rTMS seems to give inconsistent results across studies: one group found that acute rTMS (1000 pulses) at either 1, 5, 15, or 25 Hz had a beneficial effect on the depressive behaviour of rats [Loo:2000aa], whereas [Tsutsumi:2002aa] did not show any effect of 3.5s-15Hz-acute rTMS on the Porsolt swim test results.

Likewise, the role of rTMS on stress and anxiety behaviours in animals remains inconclusive to date. On one hand, chronic rTMS at 20Hz was reported to had no effect on anxiety [Keck:2000aa, Hargreaves:2005aa] but to blunt the stress-induced release of ACTH, corticotrophin, corticosterone [Keck:2000aa, Liebetanz:2003aa, Hargreaves:2005aa]. On the other, chronic 15Hz-rTMS for 10 days induced a transient increase of ACTH and CORT [Hedges:2003aa] and an increase of anxiety behaviours [Isogawa:2005aa].

b) TMS and animal models of epilepsy

The application of TMS to animal models of epilepsy followed two main goals. The first one aimed at defining in vivo in animals the threshold for seizure induction, in order to provide safety information for human experiments. After the first study in which [Pascual-Leone:1993aa] reported the induction of a secondarily generalized seizure in a normal subject stimulated at the highest intensity with rTMS [Pascual-Leone:1993aa], one team has currently succeeded in provoking seizures in primates [Lisanby:2001ab]. Later referred as Magnetic Seizure Therapy (MST), this technique induces more focal seizures than electrical convulsive therapy (ECT) and spares cortical regions involved in memory. Therefore, it is currently proposed as an alternative treatment in neuropsychological disorders with no histological effects [Dwork:2004aa] and little cognitive side-effects [Cycowicz:2008aa, Spellman:2008aa].

The other line of research has been the exploration in animals of a possible anticonvulsant effect of TMS. These studies have been conducted mostly in rats. Various frequencies were applied and different models of epilepsy have been used.

Acute rTMS at very high frequency (50 Hz for 5 s) was reported to have no effect on the time to seizure onset following pentylenetetrazol (PTZ) injection [Jennum:1996aa]. Conversely another study showed that a low frequency train (0.5 Hz) decreased the susceptibility of rats to PTZ-induced seizures [Akamatsu:2001aa]. Figure 3.58 illustrates the effect of this stimulation paradigm on the latency of myoclonic seizures after PTZ injection. In kindled rats, the threshold for induction of afterdischarges was increased by 55% in the amygdala up to 14 days after a short 20 Hz-rTMS application [Ebert:1999aa]. Noticeably, these authors reported that the acquisition of kindling starting two weeks after the single train of TMS was not altered.

Finally, in the model of epilepsy induced by intraperitoneal injection of kainic acid (KA),
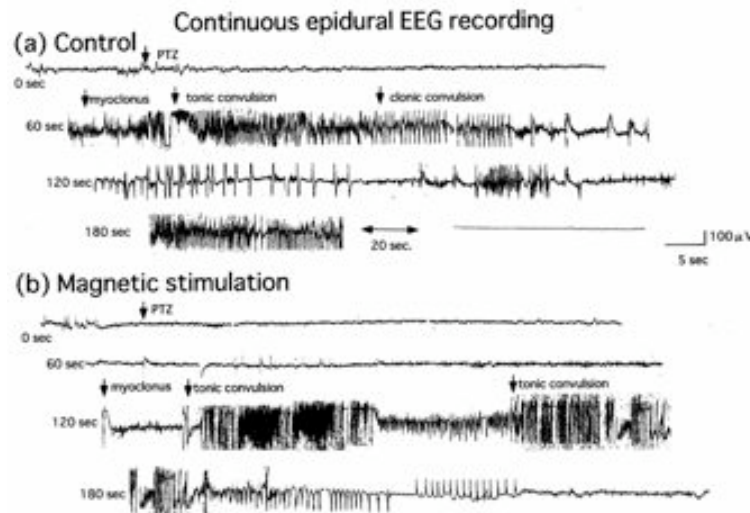
Figure 3.58 – Continuous epidural EEG recordings. (a) A control rat. Fifty seconds after the pentylenetetrazol (PTZ) injection, repetitive spikings appeared with clinical generalized myoclonic jerking. The rat developed generalized tonic-clonic seizure 10 s after the myoclonic seizures. (b) The rat treated with repetitive transcranial magnetic stimulation (rTMS rat). The onset latency of myoclonic seizures after PTZ injection is 110 s. Note the prolonged latency of the seizure onset. After the generalized tonic-clonic seizures, the rat recovered. Taken from [Akamatsu:2001aa] For this report, permission has not been requested.

an acute stimulation at 0.5 and 0.75 Hz applied at the very beginning of the epileptic discharge consistently reduced its duration (Figure 3.59) whereas the stimulation at 0.25Hz had no effect [Rotenberg:2008aa]. A similar result was also reported by [Ives:2006aa] who could stop a KA-induced seizure in a rat after a single pulse TMS (see Figure 3.60).

Like for acute rTMS, the anticonvulsant effect of chronic rTMS depends on the frequency of stimulation. At very high frequency (50Hz-5s for 30 days) the susceptibility of rats to PTZ-induced seizures is increased [Jennum:1996aa]. For medium frequencies of 20-25Hz (7 to 16 days) Fleischmann et al. reported a decreased number of animal seizing after an electric convulsive shock [Fleischmann:1995aa] as well as a shortened duration of seizures [Fleischmann:1999aa]. This effect was reported to be significant just after the TMS treatment but to vanish 5 days later.

Finally in a puzzling study, Pascual Leone's group showed that injecting rats intraventricularly with human CSF from rTMS treated depressive patients seems to be effective on the subsequent induction of myoclonic and generalized tonic seizures by flurothyl [Anschel:2003aa]. According to this study, CSF of 1 Hz-rTMS treated subjects may have an anticonvulsive effect on this animal model of ictogenesis, whereas CSF of the 10Hz-rTMS treated subject tent to lower the seizure threshold Figure 3.61. Wisely the authors acknowledged the need of a bigger number of rats in each group as well as the necessity to better control the study. Since then no such study was reiterated.

c) TMS and other neurological disorders

Recent studies have suggested that rTMS could have a possible impact on Parkinson disease. Using 60 daily rTMS treatments (60 Hz, 0.7 mT) one team recently succeeded in inducing an *in situ* differentiation of precursors of dopamine-producing neurons in rats with

nigro-striatal lesions [Arias-Carrion:2006aa]. Interestingly, the number of new dopaminergic cells was correlated with better locomotor activity and some of the newly differenciated cells showed similar electrophysiological properties than dopaminergic neurons.

Another application of TMS in animals has been dedicated to the study of oxidative stressors. Indeed, amyloid β, glutamate, or 3-nitropropionic acid have a detrimental effect on neurons. Acute or chronic rTMS was reported to either reduced or even abolished the adverse effect of oxidative stressors [Post:1999aa, Tunez:2006ab, Tunez:2006aa]. This is of particular interest when considering that amyloid β is the main constituent of senile plaques and cerebrovascular deposits in Alzheimer's disease [Haass:1993aa, Selkoe:1994aa, Yankner:1996aa] and that its precursor, amyloid precursor protein (APP), may have a neuroprotective role against oxidative stressors. Accordingly, in their study, Post et al. showed that acute as well as chronic rTMS (20 times 2s-trains of 20Hz for one day to 11 weeks) increased the release of APP in the CSF of rats, and in turn, that the CSF from rTMS treated rats protected clonal hippocampal cells in vitro against amyloid β (Figure 3.62).

4.1.8 Technical issues

a) rTMS+EEG simultaneous recordings

As for simultaneous EEG/fMRI acquisitions, recording the EEG during TMS experiments is not an easy issue, as the magnetic stimulation induces currents in the metal electrodes with a risk of skin burning under the electrode [Pascual-Leone:1990aa, Wassermann:1998aa] and can also block or destroy EEG amplifiers. Yet, despite these difficulties, the simultaneous monitoring of brain activity with TMS is of particular help to relate some of the therapeutical,
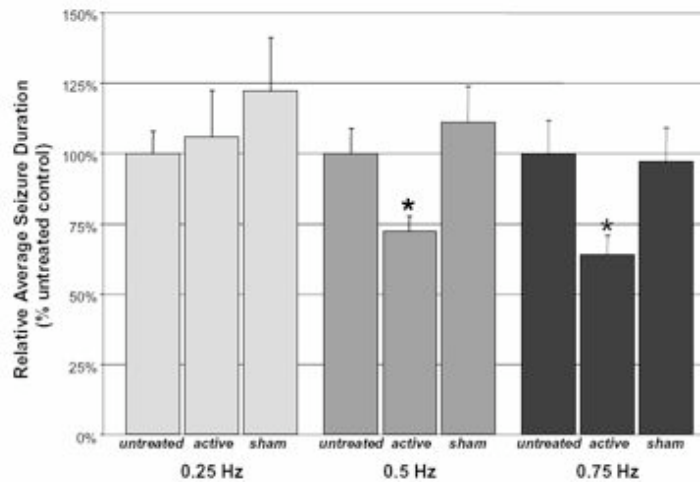
Figure 3.59 – Average seizure duration by rTMS frequency. Values are normalized to average untreated seizure duration in each frequency group. Bar graph illustrates significant suppression of seizures treated with active 0.5 Hz (P = 0.037) or active 0.75 Hz (P = 0.030) EEG-guided rTMS. Average durations (mean % untreated control $\pm$ SEM) for the 0.25 Hz treatment group are active $106 \pm 17\%$, sham $122 \pm 19\%$, untreated $100 \pm 8\%$; for the 0.5 Hz treatment group are active $72 \pm 5\%$, sham $111 \pm 12\%$, untreated $100 \pm 9\%$; for the 0.75 Hz treatment group are active $64 \pm 7\%$, sham $97 \pm 12\%$, and untreated $100 \pm 7\%$. Taken from [Rotenberg:2008aa]. For this report, permission has not been requested.
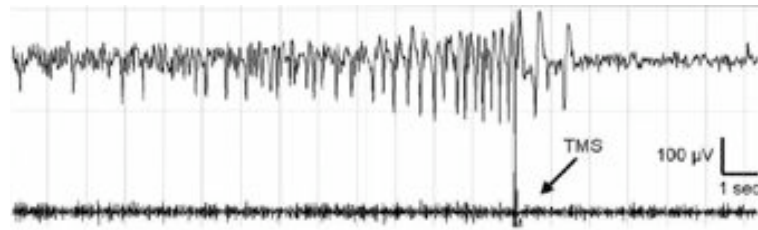
Figure 3.60 – EEG recorded from a rat during a kainate (KA) induced seizure. The bottom tracing is an open channel that is used to detect the TMS artifact (antenna effect). The top tracing shows EEG obtained from two subdermal wire electrodes. Just after the spontaneous seizure discharge starts a single-pulse TMS at 70% is delivered that disrupts both the morphology and the progression of the seizure. The TMS device used was a Cadwell unit (Cadwell Laboratories, Inc., Kennewick, WA). Taken from [Ives:2006aa]. For this report, permission has not been requested.
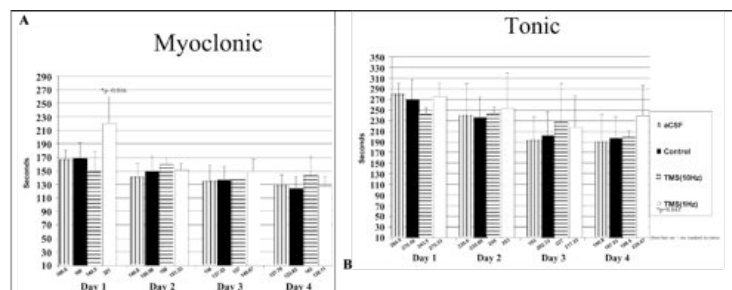
Figure 3.61 – (A) Daily myoclonic seizure onset in response to flurothyl. All groups were compared to the control CSF over all 4 days by ANOVA with repeated measures. The 1 Hz TMS group was significantly different (F = 10.15, P = 0.006). A day-by-day analysis using an unpaired, two-tailed t-test showed a statistically significant difference between control and 1 Hz TMS groups on day 1 (P = 0.016). (B) Daily tonic seizure onset in response to flurothyl. All groups were compared to the control CSF over all 4 days by ANOVA with repeated measures. The 1 Hz TMS group was significantly different from control (F = 4.75, P = 0.045). Taken from [Anschel:2003aa]. For this report, permission has not been requested.

behavioural or cognitive effects of TMS with physiological EEG parameters, but also to make magnetic stimulation safer, and to time TMS pulses with specific EEG events. For example, when the acute effect of the TMS on epileptic seizures is questioned, an accurate recording of the EEG is crucial. A recent paper shows that putting an amplifier/attenuator system between the recording site and the EEG recording device makes the simultaneous recordings of EEG during TMS feasible both in animals and humans [Ives:2006aa]. Their system avoids the blocking of the amplifier and significantly reduces the TMS artefact on EEG. An example of conjoint EEG/TMS recordings is given on Figure 3.60.

b) Sham stimulation

A major methodological concern of TMS experiments is the choice of valid control trials. An ideal sham TMS should not induce any cortical stimulation but should reproduce all the other "side effects" of the stimulation (contention of animals, noise, skin sensation etc. . .). In the animal studies described previously, sham TMS has been applied various ways: the coil can be positioned the same manner as for active stimulation, but stays off, or actual stimuli
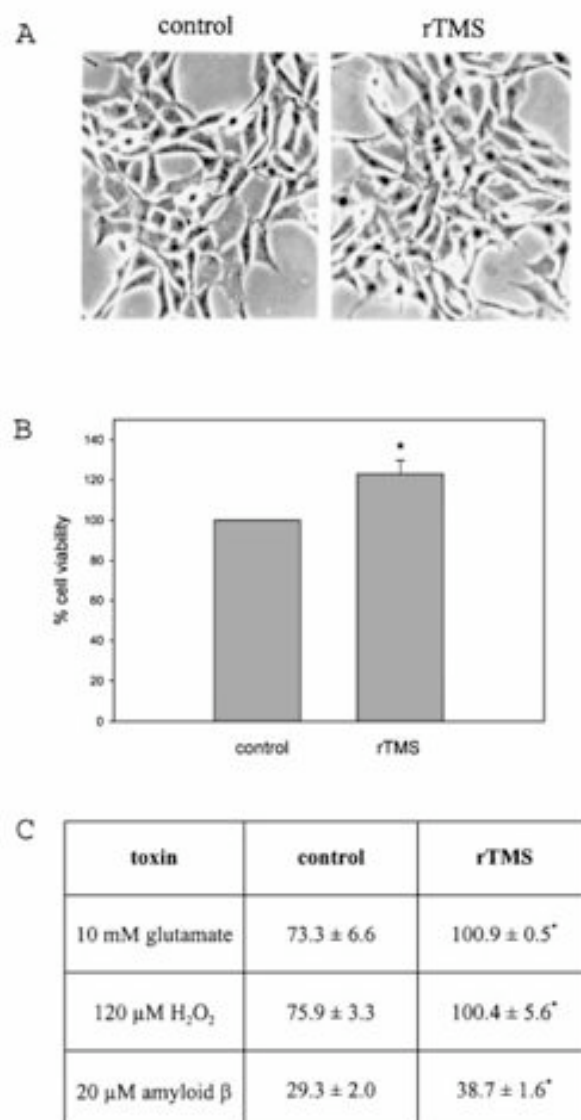
Figure 3.62 – Effects of rTMS treatment (1000 stimuli; 120 A/μs; 20 Hz) on cell survival of HT22 cells. (A) Cell morphology of HT22 cells treated with rTMS compared with controls. Cultures were photographed using phase contrast with magnification of $\times$ 200. (B) HT22 cells were treated with rTMS or left untreated (control). Cell survival, as determined by the MTT assay, is shown. Results are expressed as per cent reduction of MTT relative to untreated controls. The values are expressed as the mean $\pm$ SEM (n = 20) of three independent experiments.*P< 0.001 (Kruskal–Wallis *anova* followed by the Mann–WhitneyU-test). (C) Cytotoxic response of HT22 cells to glutamate, H2O2 and Aβ at the indicated concentrations. Toxins were added to rTMS-pretreated and non-pretreated cells (controls) 8 h after rTMS treatment. Cell viability was determined by the MTT assay after 16 h. Results are expressed as per cent reduction of MTT relative to the non-rTMS-treated control cells. The data are expressed as the mean $\pm$ SEM for quadruplicate cultures. *P < 0.01 (Kruskal–Wallis*anova*followed by the Mann–WhitneyU-test). Taken from [Post:1999aa]. For this report, permission has not been requested.

can also be delivered while the coil is tilted 45° or 90° as compared to active stimulation or positioned farther above the head. To our knowledge, only one study specifically explored the effect of sham TMS on animals [Lisanby:2001aa]. By recording the intracerebral voltage induced by three types of sham TMS in rhesus monkeys, they explicitly show that none of the sham TMS are ineffective. Some sham TMS conditions even produced a non-negligible cortical stimulation (see to Figure 3.47 at the beginning of this section). Similar results have been earlier reported in humans using seven different coil positions for sham stimuli [Loo:2000aa]. In addition, a few animal studies also reported modifications in neurotransmittor levels [Kanno:2003ab, Kanno:2003aa] or early gene expression [Aydin-Abidin:2008aa] after sham stimulation. Altogether, these studies may partly account for the variability TMS effects observed across studies and acknowledge the need of further experiments to minimize as far as possible the biological effects of sham TMS.

4.1.9   Safety

Apart from specific issues related to epileptic seizure induction (described above), safety issues have been addressed in animals to check for potential morphological changes after TMS application. Table 3.2 summarizes theses studies, which have been mainly conducted in rats.

Table 3.2 – Histological, morphological and functional changes induced in animals after rTMS.

Study	Type of stimulation	Stimulation parameters	Modifications		
			Histology	Morphology (MRI)	Other
[Sgro:1991aa]	Acute (rat)	8Hz, 20min, 3.4T	∅		
[Matsumiya:1992aa]	Chronic (rat)	>100 pulses /day, 2.8T (340% motor threshold)	microvascular changes (layer III-IV) up to 30 days after stimulation		
[Ravnborg:1990aa]	Acute (rat)	50 pulses, 15min, 1.9T			∅ blood-brain barrier (BBB)
[Counter:1993aa]	Chronic (rabbit)	100 pulses/week, 12 months, 2T	∅	∅	
[Post:1999aa]	Acute + Chronic (rat)	20 x 20Hz, 2s, 11 weeks, 4T	∅		
[Okada:2002aa]	Chronic (rat)	30Hz, 50s, 200% motor threshold, 7 days			∅ inflammatory mediators, (interleukins, cyclooxygenase, nitric oxide synthetase ∅ seizures
[Liebetanz:2003aa]	Chronic (rat)	1Hz, 200s, 3T, 5 days	∅ (GFAP, OX-6, OX42, ED for microglial and astrocytic activation)		∅ N-acetyl-aspartate creatine, phosphocreatin, myo-inositol, glucose, lactate (MRS in vivo)
[Sauvage:2008aa]	Acute (rat)	10Hz, 10s, 100% maximal output			∅ DNA damage

Except for one study [Matsumiya:1992aa], authors found no histological or morphological changes in the brain after acute [Sgro:1991aa, Post:1999aa] or chronic [Counter:1993aa, Liebetanz:2003aa] application of rTMS delivered at various frequencies. In addition, specific studies also reported no change in the blood-brain barrier permeability [Ravnborg:1990aa], no up-regulation of inflammatory mediators, possibly involved in neurodegenerative disorders, after 7 days of 30Hz-rTMS [Okada:2002aa], no change in cerebral metabolite concentrations or in microglial and astrocytic activation after 1Hz chronic rTMS [Liebetanz:2003aa], and no evidence of DNA damage in rat brain cells following a single 10Hz rTMS pulse [Sauvage:2008aa]. One study noticeably diverges from these data: [Matsumiya:1992aa] indeed reported microvacuolar changes in cortex layers 3 and 4 after when more than 100 single pulses in a day where applied at high intensity (2.8T) to rats. These modifications were seen in half of the rats, up to 30 days after the last stimulation. However, with a lower stimulation intensity (0.8T) or fewer number of pulses (>100 in one day) did not induce such effects.

4.2   Effects of tDCS

The application of direct electric currents to the brain is a much older technique than TMS. It was introduced more than 40 years ago and primarily used in animal research. Despite early promising results, this research field was not extensively explored. However, most recently, the use of DC stimulation of the brain has regained interest as TMS has become a potential non-invasive therapeutic tool. As an alternative to TMS, W. Paulus group at Göttingen University began to test in humans the application of weak direct currents through the skull and referred to it as transcranial direct current stimulation (tDCS). A comprehensive review of the effects of DC stimulation on animals and humans was published in a special number by this group [Nitsche:2003aa]. This review provides a detailed table describing the stimulation protocol, parameters and the effects in 39 animal studies from 1950 to 2003. In the following, we summarize this review and also present recent work conducted in vivo in animals from 2003 to 2009.

4.2.1   Effects on neuronal activity

In an early study in rats, [Bindman:1964aa] showed that brief anodal (positive) currents of 3-25 μA applied on the sensorimotor cortex of rats increased the neuronal firing or even activated neurons that were previously silent whereas cathodal (negative) currents reduced the spontaneous firing or inhibited it Figure 3.63. The authors also noticed that neurons could respond differently according to their depth location in the cortex and suggested that this could be due to different orientation of the pyramidal cells. These data were consistent with the results of previous studies obtained in cat motor and visual cortex using an encephale isol preparation [Creutzfeldt:1962aa] or in the motor cortex of unanaesthetized cats and rabbits ([Morrell:1961aa]. Similar experiments conducted on the cat motor cortex [Purpura:1965aa] or on the guinea-pig olfactory cortex [Scholfield:1990aa] attributed these modifications of firing rate after DC stimulation to an axonal membrane depolarization or hyperpolarization for anodal and cathodal stimulation respectively.

As for TMS, these studies also revealed long-lasting effects of the DC stimulation on the spontaneous neuronal activity. By stimulating for more than 5min at 20 μA, [Bindman:1964aa] observed changes both in the spontaneous and evoked firing rate up to 5h. Similar but shorter after-effects were also noticed by [Purpura:1965aa], but the stimulation was of shorter dura-
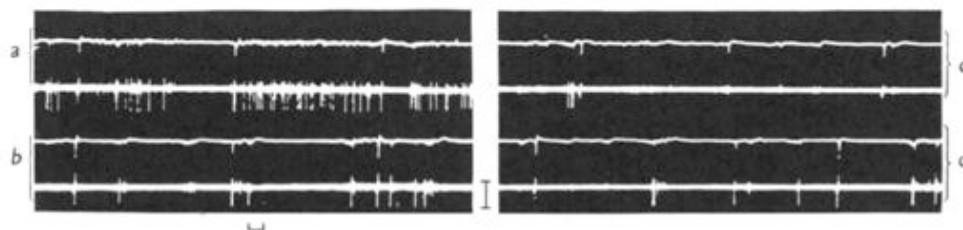
Figure 3.63 – Effect of radially applied polarizing current of 10 μA on unit discharge. Current density across pia approx. 0.5 μA/mm^2. (a) Positive, (b) control, (c) negative and (d) control periods. Voltage 1 mV; Time = 200 msec. Top trace of each pair shows evoked potential at approximately every 2 sec. Bottom trace shows unit firing at 880 μ below pia recorded with micro-electrode filled with 11 % KCl.Taken from [Bindman:1964aa]. For this report, permission has not been requested.

tion (40s). More recently, Weiss et al. also observed effects on neurone excitability in the amygdala, persisting for months after repeated, low frequency (1Hz) and low amplitude (5-15 μA) DC stimulation [Weiss:1998aa].

4.2.2 Mechanisms possibly involved in long-lasting effects of DC stimulation

Probably one of the first reports, exploring the mechanisms by which these long-lasting effects take place, was published in 1968 in Nature. As for the previous studies quoted below, Gartside showed that applying 0.1 to 0.5 mA anodal polarizing currents for 10 min on the cortex of anaesthetized rats increased the firing rate of neurones for at least 30 min. As illustrated on Figure 3.64, this long lasting effect could be transitorily abolished by cooling the body or by application of KCl on the cortex but returned to an elevated level after rewarming or washing, respectively [Gartside:1968ab]. In a following article, the same author showed that the long-lasting effects of the polarizing stimulation were dependant on protein synthesis, as they were prevented when inhibitors of protein synthesis were applied on the cortex before the DC stimulation [Gartside:1968aa].

As a conclusion of these two articles, Gartside writes "the underlying mechanism must involve some type of synaptic modification, the precise nature of which is unknown, but possibilities such as shutting off of synapses of an inhibitory nature, recruitment of previously unused synapses or membrane or enzyme changes exist. The mechanism responsible for this effect may have some relevance to memory storage but the evidence is as yet very weak". This is of particular interest as the author clearly relates his results to synaptic plasticity, a few years before the characterization of LTP/LTD mechanisms [Bliss:1970aa, Bliss:1973aa].

To our knowledge, the LTP/LTD hypothesis as a possible mechanism for sustained changes after tDCS has never been directly tested in animals in vivo in later studies. However the Japanese group of Okayama University Medical School extensively explored some of the molecular changes induced by polarizing currents and known to be in close relation with neuroplastic changes. They showed that anodal polarization with 3μA for 30 min caused an increase in the adenosine-elicited accumulation of cyclic AMP (cAMP) in the polarized cortex while a 0.3 μA decreased it [Hattori:1990aa]. Anodal polarization with 1 μA increased histamine-mediated cAMP in the polarized region while 10 or 30 μA decreased it; in addition, reverse effects (i.e. decrease for 1 μA and increase for 10 μA) were observed in the cortical area contralateral to the polarization [Moriwaki:1994aa]. Autoradiographic studies revealed also an increase of
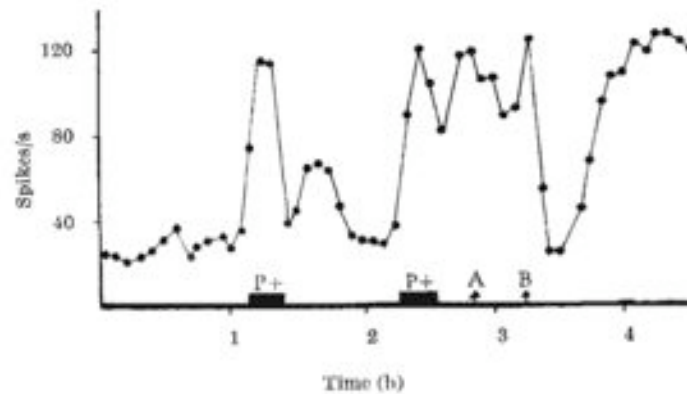
Figure 3.64 – Plot of rate of discharge against time. At P+ surface positive polarization was applied; the first attempt did not produce a sustained after effect, while the second was successful. 2% KCl was applied at A and B and, after B, spreading depression was produced. (The apparent failure of the count rate to reach zero is due to the points being 5 min means of the rate of firing, and because the silence only lasted for a few minutes the zero count was obscured by counts before and after the silence). After the spreading depression was removed, the rate of discharge rose above the control level to the after-effect level. [Taken from [Gartside:1968aa]. For this report, permission has not been requested].

extracellular concentration of Ca2+ after a 30 min anodal stimulation at 3 μA of the rat sensorimotor cortex [Islam:1995aa], both in the stimulated cortex and in subcortical regions (hippocampus and thalamus). This increase persisted for 3 days after the stimulation (Figure 3.65). The same stimulation was also reported to transiently increase early gene expression (c-fos) in the ipsilateral neocortex, cingulated gyrus, hippocampus, and piriform cortex with a maximal expression 1 hour after the stimulation and a return to baseline within 24h [Islam:1995ab]. This findings were shown to depend both on the intensity and duration of the stimulation [Moriwaki:1995aa]. Finally, a 30 min of anodal stimulation at 3 μA also provoked a persisting increase in the cytoplasmic level of protein kinase C [Islam:1995ac, Islam:1997aa].

All these results converge towards a potential LTP-like mechanism after anodal stimulation. On one hand, c-fos expression has been proposed to be associated with the maintenance of LTP [Richardson:1992aa]. On the other, protein kinase C and Ca2+ release are both persistently promoted by the activation neurotransmitter receptors (serotonin5-HT2AB, acetylcholine M1), and involved in learning and memory processes (see [Dash:2007aa] for a recent review).

4.2.3 Effects on behaviour and learning

Concomittantly with the molecular studies, early behavioural studies have been conducted in rabbits and showed that cathodal current (8-10 μA/mm^2) passed respectively through medial cortex or the visual cortex decreased the animal performance in a conditioned avoidance task [Morrell:1962aa, Albert:1966aa]; This effect could persist for 24h. Similarly, Kupfermann showed that a cathodal stimulation of the visual cortex in rats significantly impaired learning processes in a visual categorisation task but that anodal DC stimulation was ineffective [Kupferman:1965aa]. A few year later, by pairing a light flash coupled to a shock with an anodal stimulation (9 μA for 15 min) of the visual cortex in rats, Szeligo et al. found an

Figure 3.65 – Representative autoradiographs of rat brains at the level of the anterior hippocampus. A: sham-operated control rat. No abnormal Ca accumulation is evident. B: polarized rats. Abnormal Ca accumulation is noted in the cerebral cortex, hippocampus, and to a lesser extent in the thalamus following five repeated polarizations with 3.0 μA for 30 min. The degree and extent of Ca accumulation are higher on the polarized (arrow head), than in the contralateral hemisphere. [Taken from [Islam:1995aa]. For this report, permission has not been requested].

increased performance in the conditioned avoidance tasks [Szeligo:1976aa]. In a very recent study, Schweid et al. specifically explored the effect of tDCS on the visuo-spatial orientation behaviour in cats [Schweid:2008aa]. A cathodal (2mA) tDCS over the visuo-parietal cortex in the VP induced significant decreases of the cats performance for visual targets presented in the visual hemifield contralateral to stimulation (see Figure 3.66). The tDCS effect appeared during and just after the stimulation with a return to baseline level performances one hour after stimulation, suggesting a selective and recoverable alteration of the tested behaviour.

4.2.4 Cortical spreading depression

To investigate further the possible mechanisms of action of DC stimulation, a few works examined its relationships to spreading depression (CSD) propagation velocity. Indeed, CSD, first described by Leao (1944) is characterized by wave of neuronal excitation that propagates through the cortex after stimulation of a point in the brain tissue [Leao:1944aa]. This excitation wave is followed by a transient inhibition (referred as suppression on EEG) and associated with major modifications of the ionic concentrations and excitotoxic effects in the cortex. The phenomenon of CDS has been related to migraine aura as well as to neuronal events following ischemia or brain injury. As the susceptibility to CSD is linked to abnormal cortical activity [Maagdenberg:2004aa] it was hypothesized that CSD propagation could be
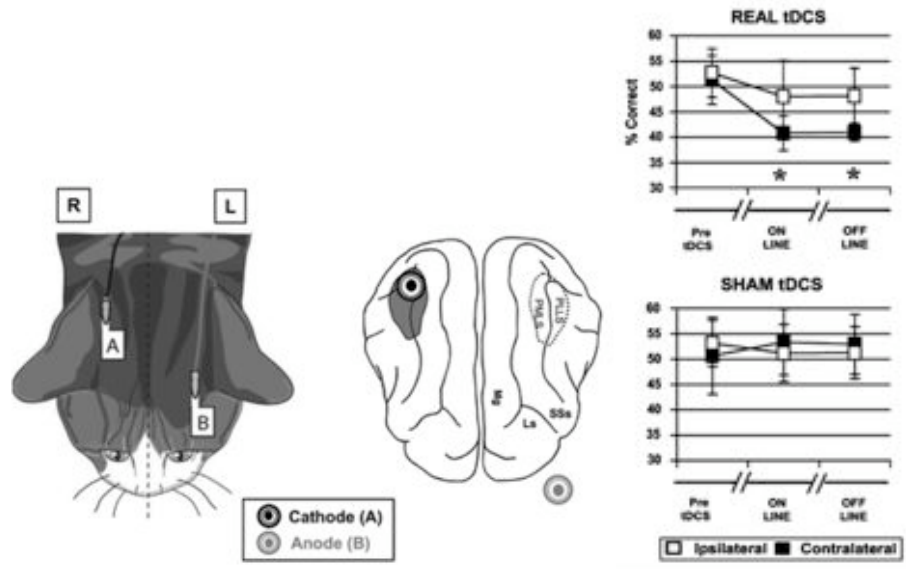
Figure 3.66 – (a) Left: schematic drawings displaying the placement of tDCS electrodes on the cat scalp. The cathode (A) was placed on a right parietal location overlying the VP area. The anode was positioned on a contralateral supraorbital location (B). Each of the subjects underwent a session of 20 min of tDCS and tested before (baseline), during (online), immediately after (offline), and 1 and 24 h thereafter. L left, R right. Right: Enlarged dorsal view of the cats brain. The location of the right visuoparietal (VP) cortex is identified (shaded) as the target area of the cathodal DCS stimulation (dark concentric circles). The medial (PMLS) and lateral (PLLS) banks of the suprasylvian sulcus (SSs), the lateral sulcus (Ls) and the marginal gyrus (Mg) are labelled. (b) Experiment 1: Average percentage correct performance in detection of static targets (LEDs) appearing in the ipsilateral (white squares) or contralateral (black squares) visual hemifield to the tDCS targeted VP cortex. Data are presented for unilateral real tDCS stimulation (upper) and for unilateral sham tDCS stimulation (lower). Data correspond to baseline (pre-tDCS) performance, and performance measured online (during tDCS) and offline (immediately after tDCS). Notice the significant reduction in the percentage of correct orienting responses towards contralateral targets during and immediately after real, but not sham, tDCS. [Taken from [Schweid:2008aa]; For this report, permission has not been requested].

altered by the tDCS-related changes in neuronal excitability. Richter et al., showed that an excitability diminution elicited by cathodal stimulation of brain slices suppressed spreading depression [Richter:1994aa, Richter:1996aa]. Accordingly, recent studies revealed that after 1-Hz and 20-Hz repetitive electrical stimulation (600 μA), the velocity of cortical spreading depression increased in the stimulated hemisphere. This effect was frequency-dependant (the 20 Hz stimulation being more effective than the 1 Hz stimulation) and long-lasting [Fregni:2005aa]. The same group showed similar results using an anodal tDCS stimulation (200 μA for 20 min), while cathodal or sham tDCS did not modify the cortical depression velocity [Liebetanz:2006aa]. These results were interpreted both on a safety point of view, as tDCS might increase the probability of migraine attack, and on a therapeutical point of view to suggest the potential usefulness of tDCS in pathologies characterized by a reduced cortical excitability, such as stroke, Parkinson's disease and major depression. So far, these hypotheses have not been tested on animal models.

4.2.5 Epilepsy

As for TMS, tCDS has been tested as an anticonvulsivant therapeutic tool in animal models of epilepsy, though to a much lesser extent. A prolonged weak anodal DC stimulation at a weak amplitude (20-40 μA) on the motor cortex of rabbits was shown to induce a seizure activity recorded by electrocorticography in the frontal cortex [Hayashi:1988aa]. The authors also reported a decreased threshold for seizure induction if the DC stimulation was repeated. Ten years later, Weiss et al. reported that a 15 minutes low frequency stimulation (1Hz, 0.4mA) was increasing the threshold and decreasing the duration of amygdala-kindled seizures, a phenomenon that they called quenching [Weiss:1995aa]. They further discovered that this phenomenon was not due to the 0.4mA pulses but to a much lower amplitude DC current emitted constantly by their stimulator. In a next study, they reproduced this artefact by applying for 15 min daily a DC stimulation at low intensity (10 μA) and low frequency in the amydgala of kindled rats [Weiss:1998aa]. They observed that the seizure threshold was increased, and the discharges duration reduced, both effects being intensity dependant and remaining stable for weeks or months (see Figure 3.67). However, the polarity of the DC stimulation was not described. The authors obviously concluded to a potential clinical utility of low-level DC treatment for refractory epilepsy but acknowledged the need of further studies to check that the effects could propagate to neighbouring structures without damaging them.

More recently, an anticonvulsive effect of DC stimulation was also reported in a rat electric-ramp model of focal epilepsy in which single trains of bipolar rectangular pulses at 50 Hz with 2 μA–increasing current strength were applied to the frontal cortex to induce seizures [Liebetanz:2006aa]. The authors found that after 1 hour of cathodal tDCS (100 μA) the threshold for localized seizure activity was significantly increased for more than 2 hours. tDCS twice as short showed comparable results when the DC current amplitude was raised to 200 μA (see Figure 3.68), while neither anodal or sham tDCS had an anticonvulsivant effect.

4.3 Conclusions

At the level of large-scale systems, based on in-vivo work in animals, the effects of TMS and tDCS are complex, highly dependant on the stimulation paradigms and parameters. From all the studies aforementioned, it appears clearly that mostly tDCS, but TMS as well, need to be further investigated in animals, in particular regarding their potential effect on EEG rythms.

4.3.1 Neuronal firing

TMS induces a transient increase followed by a long lasting decrease, in parallel with oxygen and haemoglobin rates, as well as glucose metabolism. The effects of tDCS on neuronal activity have not been explored, but early studies using weak amplitudes of DC currents applied intracortically, show that a positive (anodal) polarization increases the neuronal firing rate, while a negative (cathodal) polarization decreases it. Both TMS and tDCS effects are long-lasting effects that seem to imply LTP/LTD mechanisms (which was only indirectly proved for tDCS), modifications in the expression of early genes, and in neurotransmittors release (decreased DA transmission, up-regulation of 5-HT and NMDA receptors).
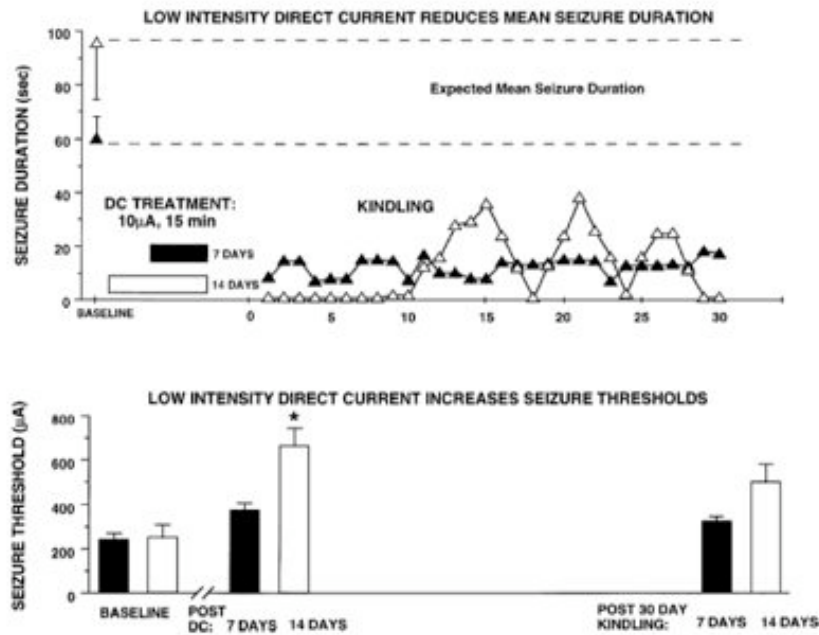
Figure 3.67 – Persistent seizure inhibition produced by prior treatment with low intensity direct current. Group mean seizure duration (top) is plotted during the baseline period (left symbols) and following DC stimulation for 7 (closed symbols) or 14 (open symbols) days (right half). In fully kindled animals, 7 or 14 days of quenching (without concurrent kindling stimulation) suppressed the seizure response to the original kindling stimulation (days 1–30). Accompanying these alterations in seizure response was an increase in the seizure thresholds (bottom; *P <0.01, compared to baseline following 14 days of DC stimulation; P< 0.06 following 7 days of DC). This effect diminished after 30 days of kindling stimulation but approached significance in the group pretreated with 14 days of DC stimulation (P < 0.08 compared to baseline). [Taken from [Weiss:1998aa]. For this report, permission has not been requested].

4.3.2 EEG

Low-frequency rTMS increases δ and decreases γ EEG activity, while high-frequency rTMS shows inverse effects. Interestingly, rTMS seems to transiently disrupt the phase locking between action potentials and EEG oscillations in all frequency bands, but to increase it at a longer term in the γ band. This might have a direct implication for LTP mechanisms that worth further work. We did not find any reports on the effects of tDCS on EEG rythms in animal studies, and this whole field has to be investigated.

4.3.3 Behavior

TMS as well as tDCS appear to modify short-term memory processes, without impairment of long term momory and learning.

4.3.4 Psychiatric/neurological disorders

rTMS seems to have a positive effect on depression behaviors induced in rats, but its effect on anxiety and stress remains controversial to date. We did not find any study exploring the effects of tDCS on animal models of depression, anxiety or stress. TMS and tDCS can induce
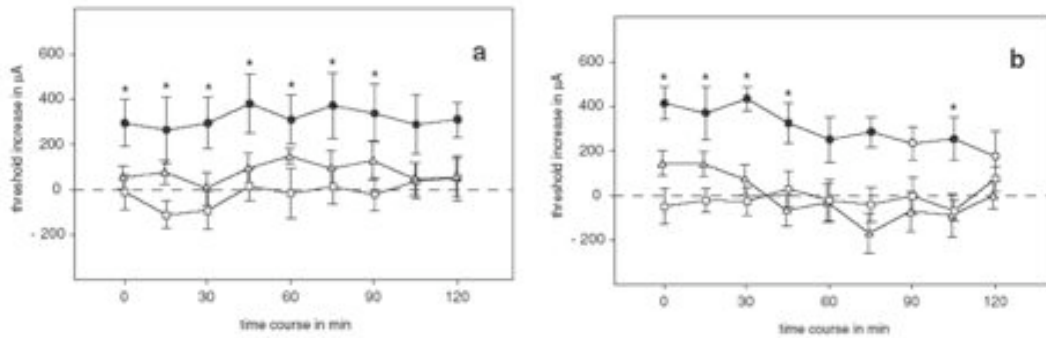
Figure 3.68 – Aftereffects of transcranial direct current stimulation (tDCS) on the threshold for localized seizure activity (TLS). Data are mean deviation from baseline TLS expressed in microamperes. Significant deviations from pre-tDCS baseline values are indicated by solid symbols. a: Time course of the TLS changes induced by tDCS at a current-strength intensity of 100 μA (n = 7). Whereas cathodal tDCS for 30 min (triangles) does not lead to a significant TLS alteration, 60 min of cathodal tDCS (circles) produces a significant TLS elevation that lasts <120 min after the end of tDCS. In contrast, 60 min of anodal tDCS at 100 μA (squares) has no impact on TLS. *Significant deviations between the cathodal and anodal tDCS at 60-min stimulation duration. b: Time course of the TLS changes induced by tDCS at a current strength of 200 μA (n = 8). Fifteen minutes of cathodal tDCS (triangles) leads to only a minor TLS elevation. When tDCS was applied for 30 min (circles), the TLS elevation is increased up to 400 μA and remains elevated for the entire observation period. In contrast, 30 min of anodal tDCS at 200 μA (squares) has no effect on TLS. *Significant deviations between the two polarity conditions (at a stimulation duration of 30 min) for the respective time bins (Fisher's LSD, p ¡ 0.05). Time point 0 is immediately after the end of the tDCS. Taken from [Liebetanz:2006aa]

seizures or have an anticonvulsant effect mostly depending on 1) the frequency and strength of stimulation for TMS and 2) the polarity of direct currents applied in tDCS. Recent work, on animal models of Parkinson or Huntington deseases, suggests that TMS might have a neuroprotective effect that could also be promising for Alzheimer desease.

5 Stimulation and resonance [GR]

It is now thought that the brain is best seen as a system of non-linearly coupled oscillators in which different areas contribute at the same time in different processes, and therefore we have proposed that it can be better stimulated globally using resonance concepts coming from statistical physics [Buzsaki:2006aa].

Here we would like to explore how to exploit the potential freedom in a stimulating system to adjust to specific rhythms and patterns in the oscillating brain, seeking to exploit resonance phenomena to amplify, locally, certain patterns (e.g., alpha).

We can distinguish different *spatial and associated temporal scales* at which resonance can play a role: at the sub-cellular level (e.g., resonance mechanisms at play in ultrasound or electrical stimulation of the neuronal channel), the cellular level (single-neuron), small scale and large scale neuronal circuits.

From the practical point of view, techniques such the ones discussed in [Bartsch:2007aa] and [Moss:2004aa] can be used to measure the degree of entrainment between the stimulating and stimulated systems.

5.1 Resonance and entrainment phenomena

Resonance and entrainment refer to conceptually related phenomena, and both are physiologically relevant.

The term **coherence** refers to the precess whereby two interacting oscillatory systems with initially different periods assume an approximately fixed relative phase relationship (and therefore the same period and frequency) [Buzsaki:2006aa]. By **phase-locking** we refer to a fixed phase reference between two oscillators, and **entrainment** to the same where one of the systems is not purely oscillatory (e.g,. an irregularly spiking neuron may be locked with a period stimulation signal). Entrainment refers therefore to a more general concept.

The term **cross-frequency phase synchrony** can occur between oscillators at different integer frequencies when the oscillators are phase locked at multiple cycles [Buzsaki:2006aa]. It is therefore a cross frequency coherence measure, so to speak. We can measure synchronization or coherence in different ways.

Suppose there is only a small set of frequencies involved (narrow band scenario). An intuitive definition of coherence comes from radio astronomy (see [Thompson:2001aa] and note that this actually used in [Kitajo:2007aa]). The **coherence** function is defined by

$$C(T) = \left| \frac{1}{T} \int_0^T e^{i\phi(t)} \, dt \right|$$

The coherence time may then be defined by the time T it takes for $\langle C^2(T) \rangle$ to drop, say, to 0.5. The phase ϕ can represent the phase difference in the two signals to be compared, $\phi(t) = \phi_1(t) - \phi_2(t)$ (after extraction from the real signals using their analytical versions—from the Hilbert transform), or the generalized phase (see below).

In finite band signals, synchrony may occur only at certain frequencies. One can focus on a particular frequency component of the signals and examine their coherence. More generally, coherence is a measure of the phase covariance, and is quantified by the **cross-spectrum** (the Fourier transform of the cross-correlation function, i.e., the complex product of the spectral amplitudes) of two signals normalized by the product of the two auto-spectra (with sample averaging). The purpose of cross-spectrum analysis is to uncover the correlations between

two series at different frequencies. It is basically obtained treating the spectral amplitudes of the signals at a given frequency computed in temporal blocks as stochastic variables, and the computing their cross-correlation coefficient. That is, if $X_n(t)$ and $Y_n(t)$ are the signals in question, and $X_n(\omega)$, $Y_n(\omega)$ the fourier transforms computed in a time block n, then the **sample coherence function at frequency** ω is defined by

$$C_{xy}(\omega) = \frac{|\langle X_n(\omega) Y_n^*(\omega)\rangle_n|^2}{\langle |X_n(\omega)|^2\rangle_n \langle |Y_n(\omega)|^2\rangle_n},$$

where $\langle \cdots \rangle_n$ stands for block averaging.

Phase synchronization can be defined (classically) by a locking condition

$$|\phi_{nm}(t)| < \text{const, where } \phi_{nm}(t) = n\phi_1(t) - m\phi_2(t)$$

with n, m integers and $\phi_{nm}(t)$ is the **generalized phase difference** (in cycles). In noisy systems, phase synchronization can be defined statistically, as the appearance of peaks in the distribution of the cyclic relative phase $\Psi_{n,m} = \phi_{n,m} \bmod 1$, that enables the detection of preferred values of the phase difference irrespective of the noise-induced phase jumps [Tass:1998aa].

The term **resonance** refers to the phenomenon associated with the forcing of a dynamical system by another one under a preferred set of frequencies in which energy[8] exchange is greatest. At those frequencies, even small periodic driving forces can produce large amplitude vibrations in the forced system.

The role of noise and nonlinearity is emphasized by the concept of **stochastic resonance (SR)**, which is actually a term loosely used to refer to related phenomena.

Dynamical stochastic resonance (the first recognized one) manifests itself by a synchronization of activated hopping events between the potential minima with a weak periodic forcing. Over time, this notion of stochastic resonance has been widened to include a number of different mechanisms. The unifying feature of all these systems is nonlinearity and the increased sensitivity to small perturbations at an optimal noise level. Under this widened notion of stochastic resonance, the first non-bistable systems discussed were excitable systems. These are called "threshold" stochastic resonance systems [Gammaitoni:1998aa, Moss:2004aa].

With **threshold stochastic resonance** [Wiesenfeld:1995aa], the signal-to-noise ratio of a nonlinear system increases for moderate values of noise intensity. The non-linear character of the system is a necessary element. Threshold stochastic resonance results from the concurrence of a threshold, sub-threshold stimulus and noise [Moss:2004aa]. It is common in bistable systems or systems with a sensory threshold and when the input signal to the system is "sub-threshold": for lower noise intensities, the signal does not cause the device to cross threshold, while at large noise intensities the output is dominated by the noise, also leading to a low signal-to-noise ratio. For moderate intensities, the noise allows the signal to reach threshold statistically at the right times, but the noise intensity is not so large as to overcome it. This phenomenon can be described using the concept of Mean Switching Frequency locking [Shulgin:1995aa], which provides a convenient framework for studying resonance in single neurons—although neuron states are not bistable (see below, and [Gammaitoni:1998aa] section V C.3 for further discussion on this point). Thus, a plot of signal-to-noise ratio as a function of noise intensity shows an inverted "U" shape. The occurrence of a maximum in

---

[8]Or more generally, I would propose, information.

the mutual information between the coupled systems at nonzero noise level is a hallmark of this phenomenon [Moss:2004aa]—See Figure 3.69. The role of noise is to sample the stimulus (thus the noise spectrum should be wider than the stimulus).

Strictly speaking, threshold stochastic resonance occurs in bistable systems, when a small periodic (sinusoidal) force is applied together with a large wide band stochastic force (noise). Threshold stochastic resonance may be understood to refer to the coherent addition of the signal to be amplified with the corresponding frequency component in the noise in a nonlinear detection system (the noise should therefore be sufficiently spectrally wide to "hit" the right note—so to speak).

It is now clear that stochastic resonance is a compatible mechanism with neural models and theories of the brain function [Moss:2004aa]. It is important to emphasize that SR can enhance phase locking and coherence and synchronization in neuronal systems (see [Moss:2004aa] and references therein), a fact which ties nicely with EEG/MEG measurement, as these techniques record stimulus-induced or enhanced phase locked synchronization large scale neuronal activity [Cooper:1965aa, Logothetis:2007aa, Ruffini:2008aa]

Finally, I would describe both stochastic resonance phenomena as well as entrainment (dynamic and threshold) in another way: as the enhanced mutual information between systems from nonlinear coupling in the presence of noise. This definition encompasses both the dynamical and threshold resonant processes described, and may generalize it to others.
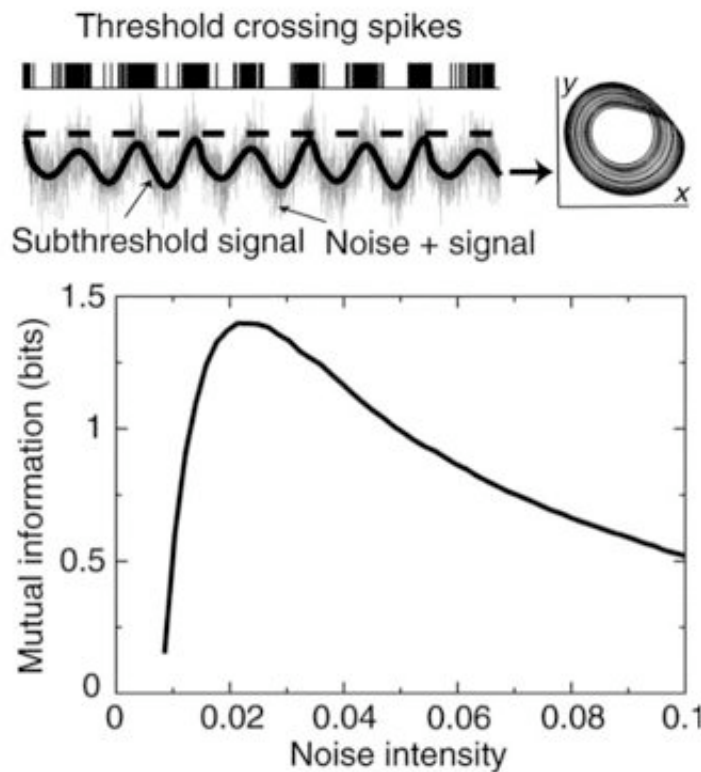
Figure 3.69 – Noise enhanced information transmission in a threshold system (from [Moss:2004aa] Figure 1).

5.2 Experimental evidence for resonance in the brain

5.2.1 Sensorial stimulation

Sensorial stimulation driving effects on EEG (i.e., *entrainment*) were discovered during the beginning of last century, starting with photic stimulation work by [Adrian:1934aa] and auditory driving [Neher:1961aa]—including the detection of harmonics and subharmonics of the stimulating frequency.

In [Longtin:1991aa] the interspike interval histograms associated to repetitive aural sensorial stimulation in the cat and monkey are discussed and explained through the concept of **stochastic resonance**. Interspike interval histogram peaks, at integer multiples of the driving frequency, are characteristic of stochastic driving—see Figure 3.72.

As discussed in [Herrmann:2001aa] and [Silberstein:1995aa], electrophysiological experiments have shown that neurons in human visual cortex synchronize their firing to the frequency of flickering light under **visual stimulation**, leading to EEG responses which show the same frequency as the flickering stimulus—namely SSVEPs (Steady State Visually Evoked Potentials). SSVEPS are a periodic response elicited by the repetitive presentation of a visual stimulus, at a rate of 6–8 Hz or more [Regan:1989aa] (in [Silberstein:1995aa], 13 Hz). This phenomenon is also called *photic driving* (an EEG phenomenon discovered in the 1930s whereby the frequency of the activity recorded over the parieto-occipital regions is time-locked to the flash frequency during photic stimulation) and is routinely used as an activation method in clinical EEG recordings. SSVEPs can be evoked at weak stimulation intensities such as the monitor refresh flicker at frequencies up to at least 75Hz when the flickering is no longer consciously perceived.

Oscillatory phenomena in the brain around ∼**40 Hz seem to play a key role in human perception (gamma) and binding**, and it has been postulated that there is an associated resonance feature in the brain. In [Herrmann:2001aa] ten human subjects were presented flickering light at frequencies from 1 to 100 Hz in 1-Hz steps. The event-related potentials exhibited steady-state oscillations at all frequencies up to at least 90Hz. However, the steady-state potentials exhibited **clear resonance phenomena around 10, 20, 40 and 80Hz**, which is argued could be a potential neural basis for gamma oscillations in binding experiments. The postulated neuroanatomical reasons for the resonance are attributed to to the temporal characteristic of the axonal circuitry. The fact that subharmonic excitation can be produced by the stimulation is attributed to the non-linear character of the oscillating system. The authors also found spectral peaks at 50 Hz (German line frequency) (and 1, 5, 10, 25, 75 and 100).

In [Pastor:2003aa] flicker stimuli of variable frequency (2–90 Hz) confirm the existence of **a peak at 15 Hz, which is shown to be associated to increase synaptic activity in Brodmann's area 17**, and that additionally, visual stimulation at ∼**40 Hz causes selective activation of the macular region of the visual cortex**. An oscillatory EEG response, phase locked to the flash frequency was recorded at 5, 10, 12, 15, 17, 20, 22, 25, 27, 30, 35 40, 47 and 60 Hz (i.e., all the tested frequencies), with **a peak at 15 Hz in the occipital area and at 25 Hz in the frontal areas**. This study also used cerebral blood flow with PET to test for the hypothesis of increased synaptic activity as the cause of the peak (confirmed) as opposed to increase coherence phenomena (phase resetting).

Already in [Makeig:1982aa] (see references therein) it was shown that (**aurally**) attending or discriminating 40 Hz modulated tones induces phase-locked (phase-locked subharmonic)

resonances in EEG, following up earlier work by the authors showing the existence of a resonance at the same frequency.

It is also know that subjects with schizophrenia have lower EEG responses to photic stimulation in alpha frequency [Jin:2000aa]. Using new techniques, the authors show that **alpha photic driving was a well defined resonant system** and suggesting the presence of a peak frequency shift of EEG resonance in schizophrenia.

In [Mori:2002aa] it is pointed out that spatio-temporal entrainment of α, β, γ and δ waves measured on the scalp is associated with perception, cognition, language processing and working memories, and that SR can enhance this entrainment. The present the first observation of **SR in the α range in the human brain's visual processing area**. In their protocol the stimulate the right eye with a sub-threshold periodic optical signal and the left with a noisy one–see Figure 3.70. We note that in this protocol SR cannot occur in the retina itself. It is interesting to note the presence of a peak at the fundamental stimulus frequency (5 Hz) (sensitive to subject conditions, e.g., stress) and another one at twice the fundamental (10 Hz) (rather insensitive to subject condition). The authors found that the stronger the stimulus input, the greater the power spectral response, and that being close to f_α lowers the noise threshold needed. In this particular case we seem to have a case of dynamical resonance.

In the related work by [Kitajo:2007aa] **large-scale phase synchronization (in theta, alpha and gamma bands)** of human brain activity in widely separated areas is increased by the addition of weak visual noise to one eye, **improving a visual detection performance with the other eye**. This work shows that noise can enhance large scale phase synchronization and presumably improve information integration across widespread brain regions and behavioral performance. These results imply that noise-induce large scale neural synchronization via SR may play a significant role in information processing in the brain.

An interesting recent related study to [Mori:2002aa] and [Kitajo:2007aa], [Lugo:2008aa], analyzes the cross-modal (sensorial) effects of stochastic resonance noise in a sensorial modality. More specifically, it is shown that auditory noise can enhance the sensitivity of tactile, visual and proprioceptive system responses to weak signals. The authors conclude that **cross-modal stochastic resonance** is a common phenomenon in humans and can be interpreted in the context of multi-sensory neurons and stochastic resonance, with noise from a sensorial modality acting as amplifier for another. The authors claim that the results strongly support the notion that there is a fundamental stochastic resonance working principle that underlies all sensory processing.

In [Lakatos:2008aa], experiments with monkeys show that when attended stimuli are in a rhythmic stream, delta-band oscillations in the primary visual cortex entrain to the rhythm of the stream, resulting in increased response gain for task-relevant events and decreased reaction times, and that in agreement with hierarchical cross-frequency coupling, delta phase also determines momentary power in higher-frequency activity. Indeed, in both monkeys and humans it is known that neural oscillations in the neurocortex tend to couple hierarchically, with the phases of the low frequencies modulating the power of the higher ones. Excitably is also coupled to phase. **This experiment could be re-examined substituting sensorial stimulation with external electrical stimulation**.

5.2.2 Electrical stimulation

Examples of recent electrical stimulation experimental paradigms include the use of oscillating currents capable of inducing slow cortical oscillations have also been used recently during sleep and shown to improve learning [Marshall:2006aa]. In this paper it is stated that "it is assumed that the oscillating potential fields induced by stimulation through mechanisms of resonance can **potentiate endogenous rhythmic EEG activity** present in these tissues". The experiment relied on slowly varying current stimulation at **0.75 Hz during sleep** seeking to **amplify the effect of natural Delta** for improved declarative memory consolidation. The results from this study suggest that stimulation using such "resonant" protocols can interact and reinforce the effects of natural oscillatory systems in the brain. Stimulation at 5 Hz (a normally predominant band during REM) decreased slow oscillation and left declarative memory unchanged.

In [Antal:2008aa] it is conjectured that "interference with brain rhythms by noninvasive transcranial stimulation that uses **weak transcranial alternating current** may reveal itself to be a new tool for investigating cortical mechanisms currently unresolved". The study aims
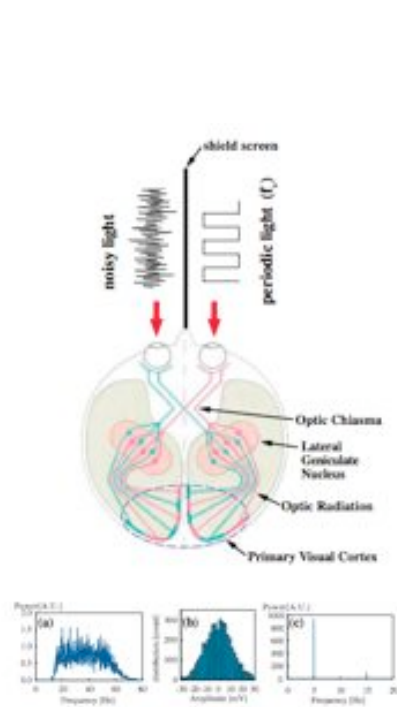
FIG. 1 (color). The experimental protocol and the trajectory of the photic stimulus from the eyes to the primary visual cortex. Visual stimuli from right and left eyes are projected via the optic chiasma onto corresponding hypercolumns (not shown) at the primary visual cortex with a distribution between brain hemispheres that is species dependent. In the human brain, the visual stimulus is equally divided between the left and right hemispheres; i.e., 50% is projected onto the right and 50% onto the left hemisphere of the brain. Characteristics of the photic stimuli. (a) Power spectrum of the noisy stimulus; (b) amplitude distribution of the noisy stimulus, the dotted line indicates a Gaussian distribution; and (c) power spectrum of the periodic stimulus.
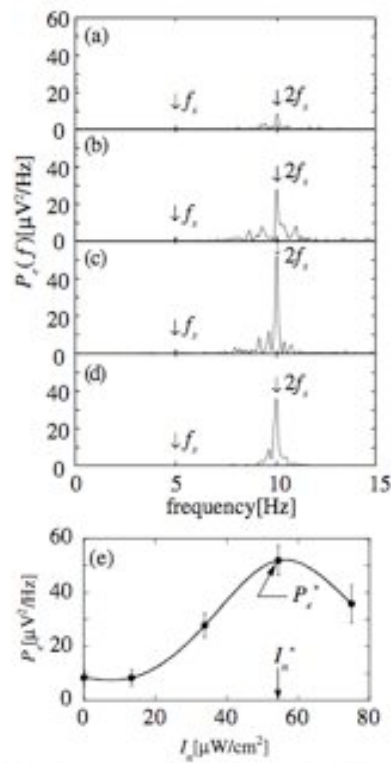
FIG. 4. Power spectrum of the brain wave at O_1, i.e., the left occipital (subject: S). (a) $I_n = 13\ \mu\text{W/cm}^2$, (b) 34 $\mu\text{W/cm}^2$, (c) 54 $\mu\text{W/cm}^2$, (d) 75 $\mu\text{W/cm}^2$. A sharp peak in the power spectrum is observed at the harmonic frequency $2f_s = 10$ Hz of the stimulus ($f_s = 5$ Hz) in (a) to (d). Here f_s is close to $1/2f_\alpha$, that is, the subharmonic frequency of the α wave. (e) The entrainment power density, P_e, shows the bell-shaped dependence as a function of the noise intensity I_n. Here $P_e^* = 51.9\ \mu\text{V}^2/\text{Hz}$ and $I_n^* = 54.5\ \mu\text{W/cm}^2$.

Figure 3.70 – Figures 1 and 3 from [Mori:2002aa] showing the experimental protocol and trajectory of the photic stimulus and noise to the visual cortex. On the right, the power spectrum at O_1 is shown for different noise intensities, displaying the SR characteristic peak.

to extend transcranial direct current stimulation (tDCS) techniques to transcranial alternating current stimulation (tACS). The experimental protocol relied on motor evoked potentials (MEPs) revealed by transcranial magnetic stimulation (TMS), measurement of EEG power as well as reaction times measured in a motor implicit learning task, which were analyzed to detect changes in cortical excitability after 2-10 minutes of AC stimulation and sinusoidal DC stimulation (tSDCS) by using 1, 10, 15, 30, and 45 Hz and sham stimulation over the primary motor cortex in 50 healthy subjects (eight-16 subjects in each study). The results showed a **signicantly improved implicit motor learning after 10 Hz AC stimulation**. However, the stimulation did not modify EEG power when compared with sham. This paper discusses as well the role of the cortex as an "orchestra director", modulating and synchronizing thalamic oscillatory networks through cortico-thalamico-cortico loops. This can provide a possible cellular mechanism to explain the origin of large-scale coherent oscillations in the thalamocortical system.

In [Kanai:2008aa] brain function during eyes open (predominantly beta $\sim$ 14–22 Hz) and closed (predominantly alpha $\sim$ 8–14 Hz) is studied. There appears to be a better efficiency in phosphene generation using tACS (transcranial alternating current stimulation [Antal:2008aa]) **if the stimulation frequency matches the natural spectral peak of each condition (beta and alpha)**. These results could be interpreted from the point of view of resonance. Moderate current intensities were used (5–15 V with peak currents of 1.0–1.5 A mA).

Finally, in [Terney:2008aa] a tDCS variant called tRNS (for **transcranial random noise stimulation**) is presented, with similar effects to tDCS (increase of corticospinal excitability) and it is argued that since no DC component is present there must be a different mechanism at play (since reversing polarity in tDCS also reverses the effects, while this does not appear in tRNS). It is argued that similarly to tACS there may be interference with natural oscillatory activity. It has been suggested that synaptic activity can be boosted by noise, and **stochastic resonance may be associated**. Another mechanism accounting for non-linearity and therefore stochastic resonance in mentioned, "rectification" of high-frequency currents at the membrane. It is stated that "a pure DC stimulus can open the Na$^+$ channels only once, whereas repeated pulses (tRNS) can induce multiple ionic influxes, and achieve substantially heightened effects" (see the discussion on [Schoen:2008aa] for more details on this important point). An important difference with tDCS, it is argued, is that **tRNS is only excitatory** effect (not hyperpolarization, only depolarization). In this paper the random noise was generated at 1280 S/s (white noise). An interesting aspect of this paper relevant to safety aspect of stimulation is its analysis of safety aspects through the measurement of serum neuro-specific enolase (NSE), a sensitive marker of neuronal damage (e.g., in epilepsy).

5.3 Experimental evidence for resonance in-vitro

5.3.1 Electrical stimulation

In [Leung:1998aa] theta-frequency (4-10 Hz) resonance in hippocampal C1 neurons in vitro is demonstrated using sinusoidal current injection in cells in-vitro, and that the resonant peak and its width are dependent on voltage. Slight depolarization was shown to increase the resonance frequency and peak as well as sharpen its bandwidth. Higher amplitude stimulation was shown to give rise to the appearance of higher harmonics. The authors conclude that the theta-frequency resonance in hippocampal C1 neurons in vitro suggests the role of the

same voltage-dependence variable response may be important in enhancing theta frequency response when these neurons are driven by medial septal or other inputs in vivo.

In [Stacey:2000aa] the hypothesis is that **SR plays a role in neural signal detection is in central neurons (hippocampal CA1 cells from rats) tested in silico and in vitro**. The hypothesis that SR plays an important role in the detection of distal synaptic inputs was tested in a computer simulation of a CA1 cell and then veried with in vitro rat hippocampal slices. The results from both tests clearly show that SR can enhance signal detection in CA1 hippocampal cells. The authors also conclude that the levels of noise necessary for SR are within physiological limits and that SR provides a possible explanation for the nding that distal and proximal synapses are detected equally.

In [McIntyre:2002aa] extracelluar stimulation of the CNS in the context of microspinal stimulation with symmetrical charge balanced biphasic stimuli was shown to result in activation of fibers of passage, axon terminals and local cells around the electrode at similar thresholds. **Biphasic stimulation in implants** is mandatory for chronic implant applications if electrode corrosion and tissue damage are to be avoided. A robust technique for selective activation between cells and fibers was seen to be provided by the **waveform shape**. The use of repetitive stimulation for selectivity was also investigated. In the modeling part of this work, it was assumed that the coupling mechanism with the field is through the along-axis gradient factor [Basser:1992aa] and an integrated field-neuron model was developed. The neuron model was developed in 3D using FEM as was the volume conductor model (of the cat spinal cord). The results show that selectivity of target neural populations can be achieved with the **proper choice of waveform and frequency**. In particular, this paper shows that modulation of the stimulus frequency train can enhance selectivity between activation of cells and fibers of passage in the CNS.

In [Jensen:2005aa] it is shown that sinusoidal **high frequency stimulation (HFS) can not only block cellular level firing but also activity in the axons in-vitro**. It discusses the role of inhibition by high frequency stimulation in deep brain stimulation practice as well, highlight the role of 50 Hz sinusoidal HFS.

In relation to the work in [Terney:2008aa] on tRNS, in [Schoen:2008aa] it is demonstrated that **repetitive weak stimulation** is able to elicit action potentials in-vitro, a phenomenon that takes advantage of the "well-known asymmetric voltage dependence of sodium conductances": even for weak capacitive currents, a large depolarization can result from accumulation. This is due to the accumulation of inward Na^+ current pulses during cathodic phases with no compensating currents in the opposite phase. The sum can result in depolarization if the time scale of relaxation is long and the inactivation of sodium channels not too high.

In [Wang:2006aa] **sub-threshold theta-frequency membrane resonance in rat subicular pyramidal neurons is demonstrated** and studied using whole-cell patch-clamp recordings from these neurons in rat horizontal brain slices. Sinusoidal currents with constant amplitudes and linearly increasing frequencies were applied to measure the resonance frequency. The resonance frequencies found were of 2 Hz at room temperature and 4–6 Hz at 32–35 ^{o}C. The resonant frequency increased at hyper-polarized membrane potentials (and vice-versa).

Although not stimulation per se, we highlight here the recent work in [Compte:2008aa] in which it is shown that *the isolated cortical microcircuitry generates β and γ oscillations spontaneously in the absence of externally applied neuromodulators or synaptic agonists* and that *this in a spontaneously active slice preparation that engages in slow oscillatory activity similar to activity during slow-wave sleep. β and γ synchronization appeared during the*

up states of the slow oscillation. From the point of view of future work, these results are interesting: **stimulation in-vitro could seek to amplify these oscillatory states or substitute the underlying slow oscillatory activity (see also [Marshall:2006aa]) to potentiate the phenomenon**. In addition, **synchronous stimulation at β and γ frequencies could also be investigated**. The authors also provide a computer model showing how a synaptic loop between excitatory and inhibitory neurons can explain the emergence of both the slow (<1 Hz) and the β-range oscillations in the neocortical network. This model could provide a natural connection point with single-neuron electric field interaction models and the proposed excitation function [Ruffini:2009aa].
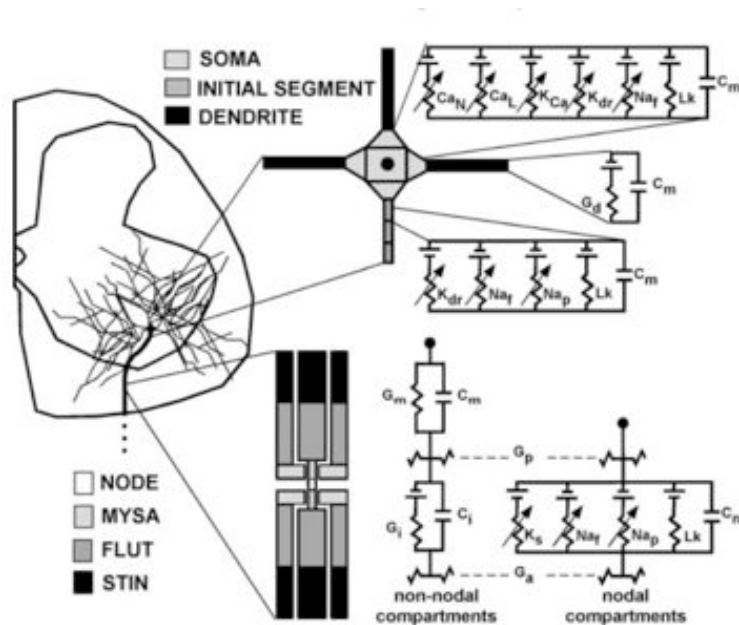
Figure 3.71 – Figure 1 from [McIntyre:2002aa]. *"Multi-compartment cable model of a motoneuron. The model consisted of a 3-dimensional branching dendritic tree, multi-compartment soma and initial segment, and a myelinated axon with explicit representation of the myelin and underlying axolemma (see text for abbreviations). The soma, initial segment, and nodes of Ranvier used nonlinear membrane dynamics derived from voltage- and current-clamp measurements on mammalian neurons. Intracellular resistors, determined by the dimensions of the adjoining compartments, connected the different elements of the model together."*

5.3.2 Ultrasonic stimulation

Although not the focus of the present work (see TN00160 on ultrasound stimulation), we summarize here some work with ultrasounds related to resonance.

Several decades of work show that ultrasound stimulation modulates neuronal activity by enhancing and/or suppressing the amplitude and /or conduction velocities of evoked nerve potentials [Tyler:2008aa] (see also [Fry:1958aa] for earlier work). A potential mechanism for this in neurons is the **modulation of ion channels (i.e., conductances) through ultrasonic mechanical interaction with the membrane**. In [Tyler:2008aa] it is specifically shown that **low frequency low intensity ultrasonic stimulation activates sodium and calcium channels, leading to excitation of neurons**. The mechanisms underlying this activation and hypothesized to rest on the mechanical nature of voltage gated channels. The work is done in-vitro (hippocampal slices) and ex vivo (mouse).

Although this is not mentioned in these papers, the connection with stochastic resonance phenomena is quite clear and similar to electrical stimulation with random noise or AC discussed above.

5.4 Experimental evidence for resonance in-silico

Using the same model as described in [Ruffini:2009aa], it is straightforward to show that resonance in electrical stimulation can play a role at the single neuron level. We have expanded the model (starspikev3.m) to allow for different types of stimulation and different types of post-synaptic excitation: steady, sinusoidal, square repetitive or random. The results from simulations clearly indicate the existence of resonance in the single neuron model, which can be achieved via "natural" post-synaptic potential excitation, or via external stimulation with square pulses (Figure 3.73) or sinusoidal (biphasic) waves (Figure 3.74).

Similar work is reported in [Hutcheon:2000aa], where the origin of the characteristic frequency bands of brain rhythms is questioned: are they arising from connectivity-delay phenomena (re-entrance, feedback) or from single neuron resonance or frequency preferences (or both). Resonances have been shown to exist in a number of excitable cells, including cardiac, hair cells of the inner ear, and various peripheral and central neurons. In particular, **pyramidal neurons in the neocortex have two resonances with different voltage dependence. A 1-2 Hz resonance near the resting potential and a 5-20 Hz (depending on the precise voltage, which must be greater than -55 mV)**. It is also emphasized that the possible functional importance of the resonance and oscillations observed in thalamic and cortical neurons lies in the known participation of these neurons in various brain rhythms, with low frequency resonances in the cortex and thalamus well suited to support the thalamocortical delta-wave oscillations that are particularly prominent during deep sleep, and the higher frequency features in pyramidal and inhibitory neurons of the neocortex having some involvement in the higher frequency rhythms that appear in the cortex during cognition. This paper also explains that resonances arise from the interplay of active and passive membrane properties and associated time constants, which create high and low pass filter behavior (and therefore peaks in the frequency response of the system. So, the approximate frequency of the resonance can be estimated from the values of the activation and passive membrane constants. Furthermore, resonance frequencies are also voltage dependent. **This suggest experiments in-vitro with spontaneous oscillations seeking to demonstrate frequency shifts under DC externally applied fields. Similarly, shifts**

in natural brain frequency band could be observed in vivo.

Although statements on the role of stochastic resonance via rRNS discussed in the previous section may seem a bit fuzzy, using the simulation tool (starspikev3) we can verify the impact of random biphasic noise as a purely excitatory—see Figures 3.76 and 3.77. However, it must be mentioned that the pulse duration times its intensity must be above a certain threshold for this to work. If the pulses are too short, random noise will not initiate action potentials. The mechanism is statistical. If a single positive pulse is sufficient to go over threshold, a following negative pulse will not have an impact, since λ has effectively decreased significantly (see the model description in [Ruffini:2009aa]).

On the other hand, it is clear that weak random noise can bring a neuron membrane over the threshold once it is close to it, and once this happens an action potential will follow. See Figure 3.78 for an example of how random noise can bring a sub-threshold injected current (red) into the firing range. This is essentially stochastic resonance. In [Longtin:1991aa] it is shown in a similar manner that the interaction of noise with external modulation leads to the observed interspike intervals recorded from real systems forced sensorially. Indeed, we can infer from the discussed exercise that some modulation peaks will be missed, and therefore that the interspike histogram will display peaks at integer multiples of the basis system period (see Figure 3.72).

Global stochastic phenomena in bistable coupled extended systems have also been described (see [Inchiosa:1995aa] and [Bulsara:1996aa]) and they may be relevant in large scale phenomena involving populations of large neurons. Essentially, noise can amplify small common signals in the network. In [Inchiosa:1995aa] a network of nonlinear dynamic elements with a nonlinear global coupling, and subject to noise and a time-periodic signal is studied. It is found that cooperative effects arising from noise and coupling lead to an enhancement of the network response over that of a single element.

In [Lindner:1995aa] the behavior of bistable Duffing chain is studied, with a) linear nearest neighbor coupling, b) subjected to white noise indendently at each site, c) with a common subthreshold periodic signal at each site. The ith element has the dynamical equation

$$\dot{x}_i = \alpha x_i - \beta_i^3 + \varepsilon(x_{i-1} - 2x_i + x_{i+1}) + A\sin\omega t + N_n(t)$$

The authors found that the response of a single element can be enhanced by the coupling (as controlled by ε). The maximum response can be achieved by tuning either the noise or coupling parameters. The optimal noise scales as the number of elements N and the optimal coupling as ^{2}. Finally, the global maximum corresponds to noise-induced spatiotemporal synchronization of the array to the external signal frequency ω—see Figure 3.75. The authors conclude that *spatiotemporal order and enhanced stochastic resonance can be induced in a locally and linearly coupled array of overdamped nonlinear oscillators by the optimization of a single adjustable parameter(noise or coupling).* We note in passing the similarities of the above equation system with single neuron compartment models (we don't know if this application has been explored).

In relation to this, in [Melloni:2007aa] it is shown that the transient long distance synchronization of neural activity at gamma frequencies (50–57 and 67–80 Hz) is a good correlate of conscious perception in the human brain. It is not clear that stochastic resonance is playing a role in this phenomenon, but stimulation experiments tuning the driving via tACS at gamma frequencies or the noise level using random noise (tRNS), could explore the threshold of perception. Sensorial stimulation in another modality could be interpreted as the addition of noise as well. In related but earlier work, [Massimini:2005aa], the breakdown of cortical

connectivity during NREM sleep is studied using TMS and EEG. Thus, it is postulated that the fading of consciousness during certain stages of sleep may be related to a breakdown in cortical effective connectivity. This is not the same as synchronization, however: effective connectivity refers to the ability of a set of neuronal groups to causally affect the firing of other neuronal groups within a system. It is related to propagation phenomena in the brain.

Finally, some work has indicated the role of stochastic resonance at the ion channel level. In [Bezrukov:1995aa] the observation of stochastic resonance in a system of voltage-dependent ion channels formed by the peptide alamethicin is reported. A hundred-fold increase in signal transduction induced by external noise is accompanied by a growth in the output signal-to-noise ratio. The system of ion channels considered there represented the simplest biological system yet known to exhibit stochastic resonance. In [Hanggi:2002aa] we find further discussion on this point, and references to more recent work where SR is found at the level of a single channel. As discussed there, an important goal of biological SR-related research has been the validation of the premise that nature has adopted, during evolution, the use of intrinsic ambient noise for the optimization of sensory transduction on its most fundamental level, the ion channels, and, moreover, that the observed SR in biological systems is most likely rooted in a collective property of globally coupled ion channel assemblies.
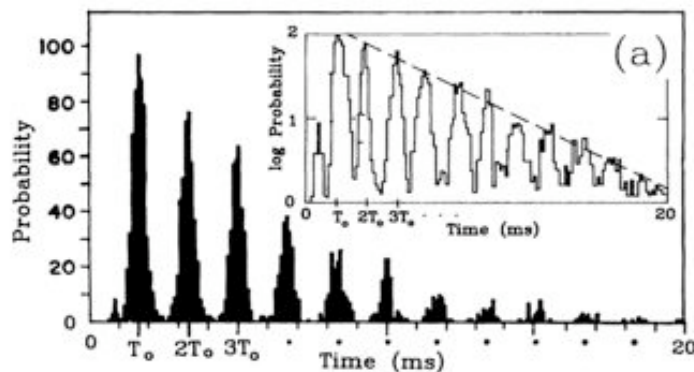
Figure 3.72 – An experimental interspike interval histogram (ISIH) obtained from a a single auditory nerve giver of a squirrel money with a sinusoidal 80-dBsound-presur-level stimulus of period $T_0 = 1.66$ ms applied to the ear. Note the modes at integer multiples of T_0 (from [Longtin:1991aa]).
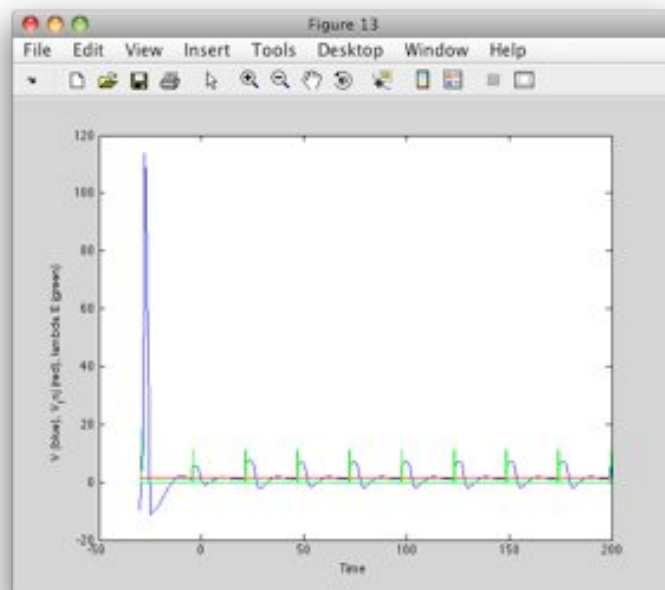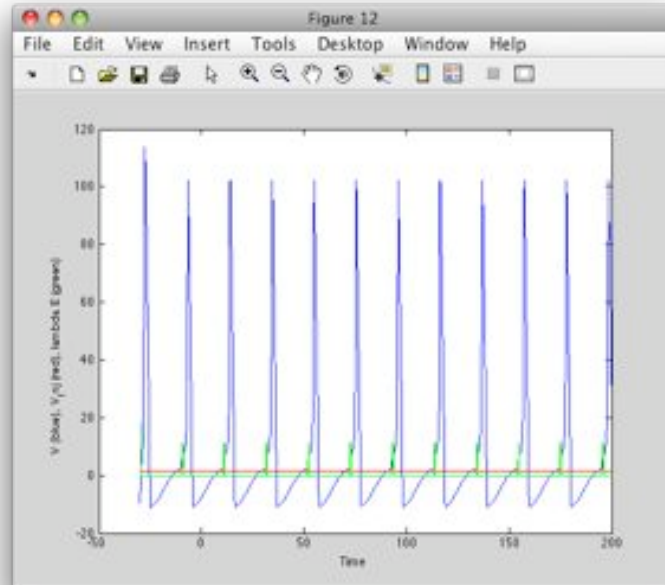
Figure 3.73 – Resonance in-silico: using the right frequency produces firing (top), as opposed to other higher or lower frequencies (bottom). Stimulation is carried out with square pulses (green), while a small excitation is applied (red).
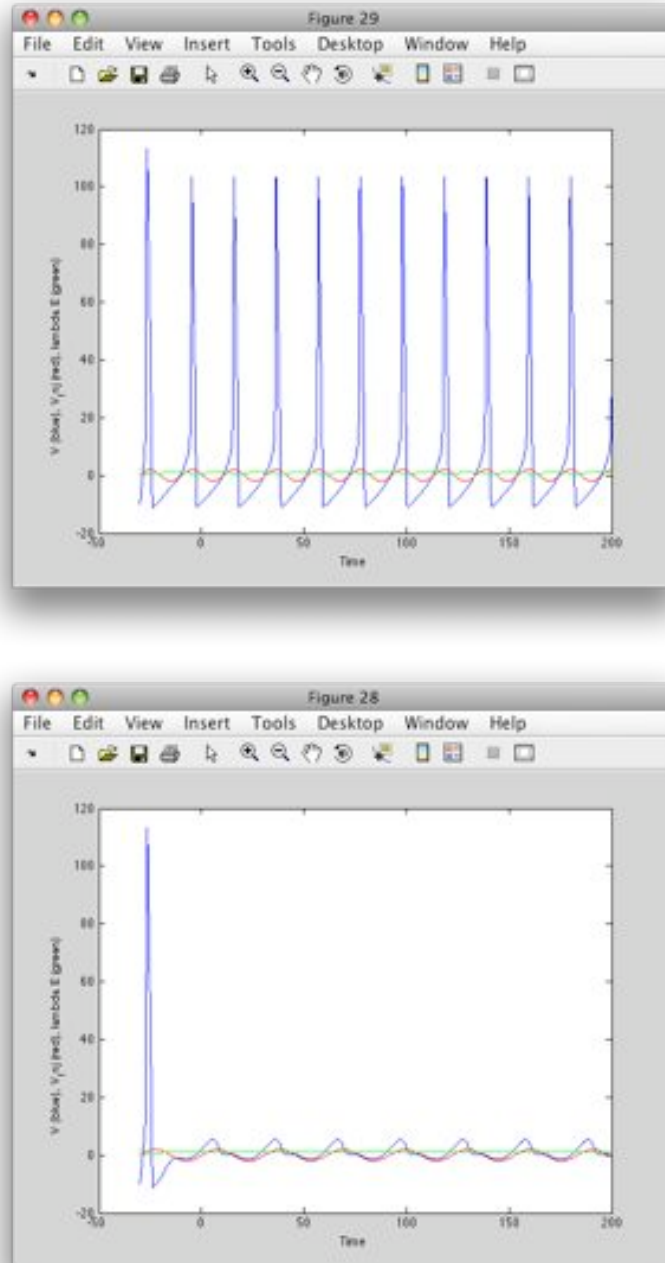
Figure 3.74 – Resonance in-silico: using the right frequency produces firing (top), as opposed to other frequencies (bottom). Stimulation is carried out with sinusoidal waveform (green), while a small excitation is applied (red). A smaller field amplitude is needed than with square pulses.
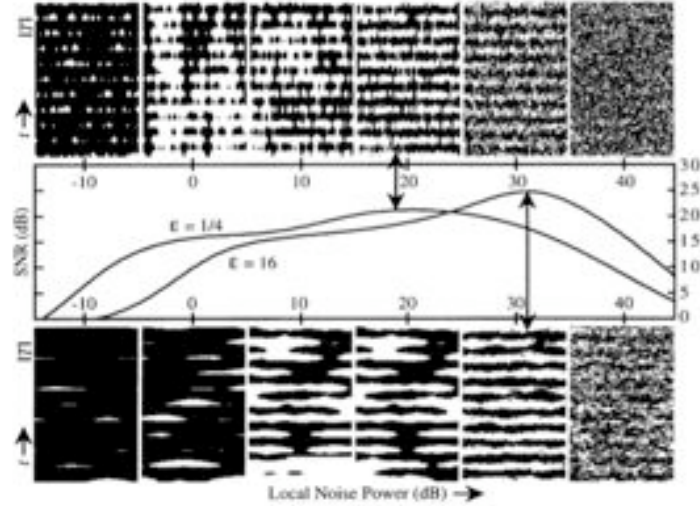
FIG. 3. Sequence of spatiotemporal dynamics of a 101 oscillator array. In each frame, the array is horizontal and time increases upward $(T = 2\pi/\omega)$. One well of the bistable potential is colored black, the other white. Local noise power increases from left (-10 dB) to right (40 dB) in 10 dB steps. Noise-induced synchronization corresponds to maximum SNR: 20 dB at $\varepsilon = 1/4$ (top sequence) and 30 dB at $\varepsilon = 16$ (bottom sequence). Other parameter values are as in Fig. 1.
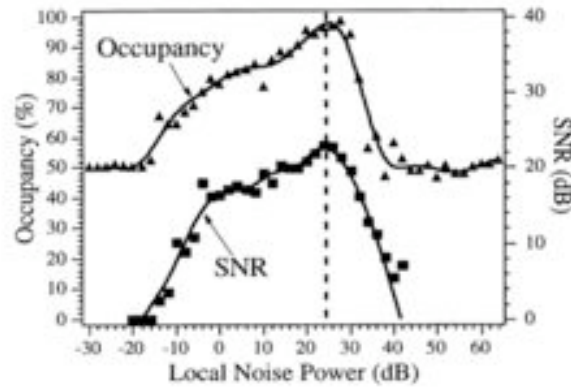
FIG. 4. Occupancy of a chain of 101 oscillators superimposed on the SNR of the middle oscillator of the chain. The (global) average occupancy of the lower well peaks at the same noise power as the (local) SNR of the middle (51st) oscillator. Coupling $\varepsilon = 1$. Other parameter values as in Fig. 1.

Figure 3.75 – Figures 3 and 4 from [Lindner:1995aa] displaying the dynamics of coupled 101 oscillators in different conditions. Occupancy is measure of synchronization which peaks together with individual SNR.
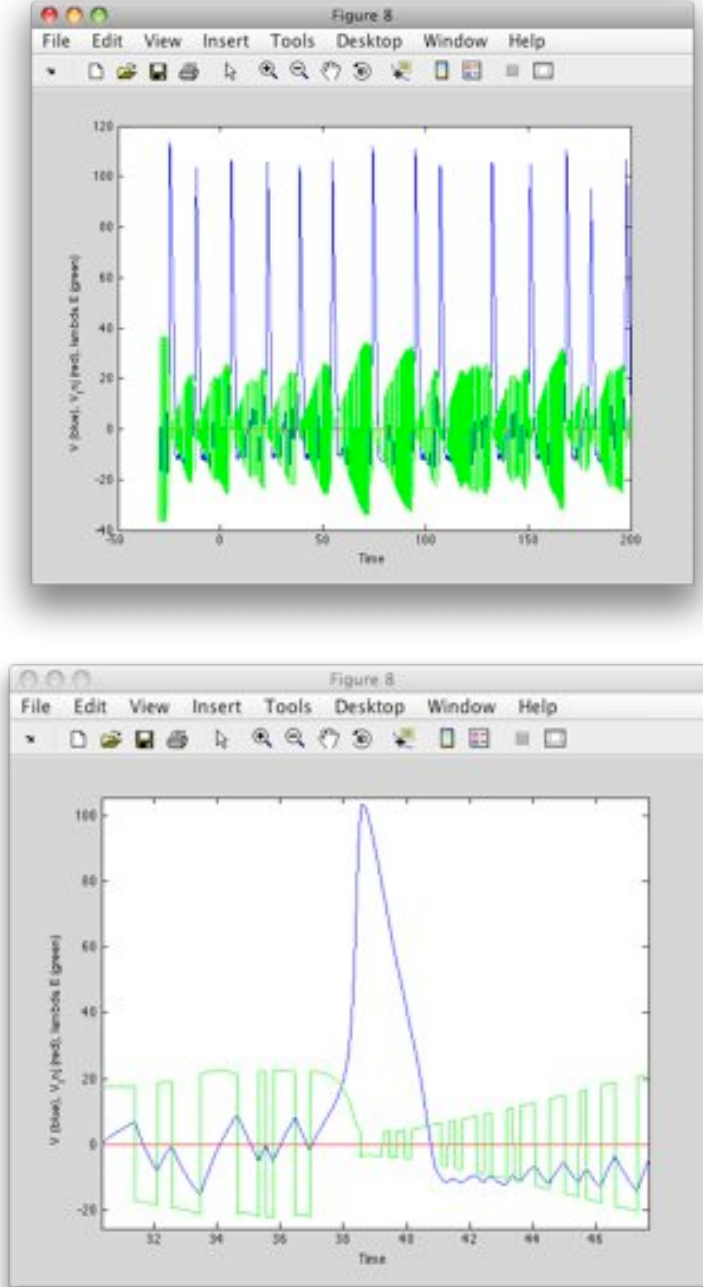
Figure 3.76 – Biphasic stimulation (tRNS) provides an alternative stimulation paradigm (top, with zoom in bottom). Stimulation is carried out with square pulses (with effective perturbation impact $\sim \lambda E$ shown in green), and no injected excitation is applied (red).
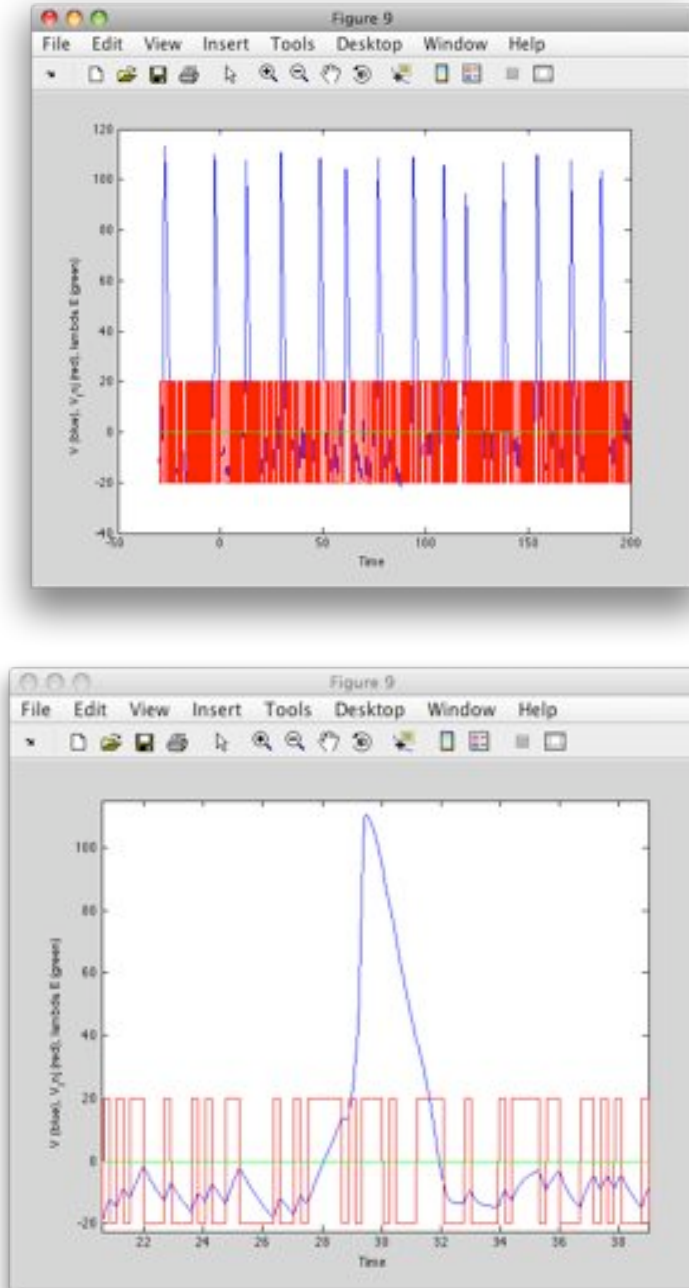
Figure 3.77 – Biphasic current injection provides the same effect as stimulation (top, with zoom in bottom). No external stimulation is applied (green), and RNS injected excitation is applied (red).
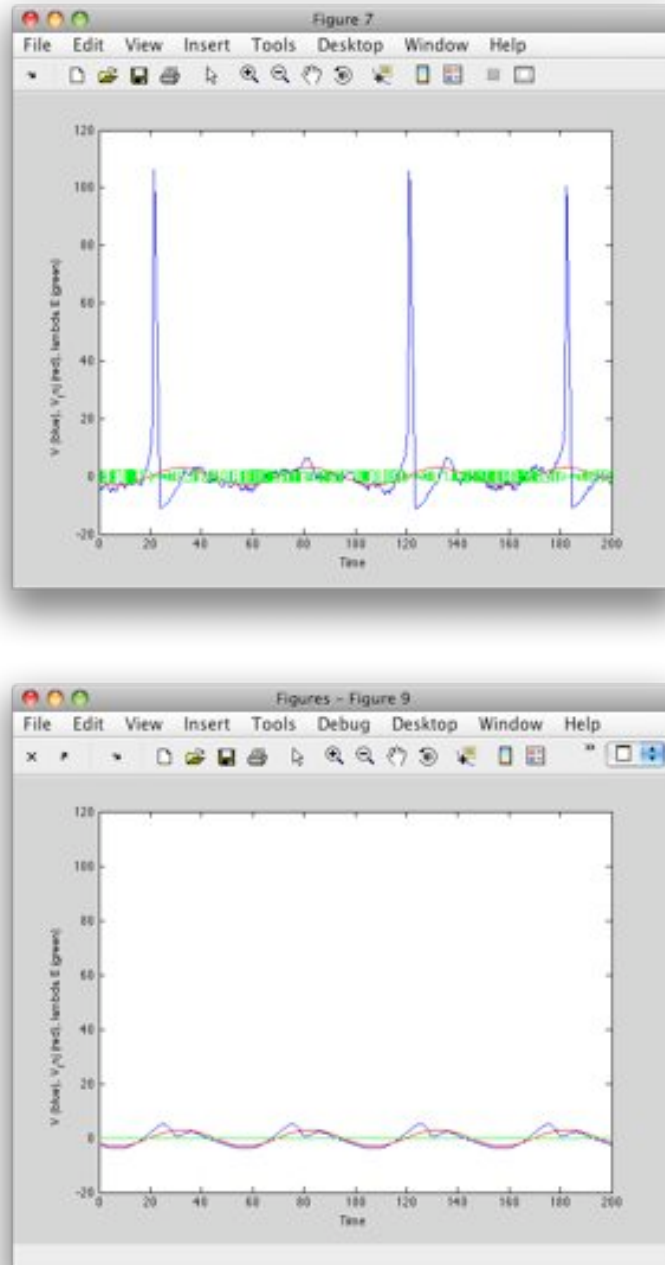
Figure 3.78 – Biphasic stimulation (tRNS) added to a sinusoidal current brings it over the threshold (top, vs. bottom with no stimulation). Stimulation is carried out with square pulses (with effective perturbation impact $\sim \lambda E$ shown in green) of sufficient duration-amplitude. The phenomenon here is dithering or threshold stochastic resonance.

5.5 Conclusions

Resonance/entrainment phenomena are currently best understood at the single neuron level. Some work has been done at the sub-cellular level (ionic channels) and many-cell systems as well, where it appears to be possibly amplified in the case of SR.

Stochastic resonance is a common phenomenon in many systems, and certainly plays a role at the neuron level. The theoretical framework associated to this can help understand phenomena associated to techniques such as tACS, tRNS and probably also ultrasonics. These are mostly excitatory in nature at the neuron level (not necessarily so at higher levels, where they can disrupt function).

There is plenty of evidence for resonance and stochastic resonance in silico at the single neuron or even ion channel level. We have provided a bit of our own evidence using a simple Hodgkin-Huxley model in Matlab that encapsulates the essence of these phenomena.

Theoretical work with simple dynamical models indicates that noise can also act at larger scales, leading to resonant synchronization of coupled oscillators and leading to large scale synchronization. **It would be interesting to test the impact of noise and small driving signals in coupled neural models (in silico).**

It is important to emphasize that SR has been shown to enhance phase-locking and coherence and synchronization in neuronal systems, a fact which ties nicely with EEG/MEG measurement, as these are sensitive to large scale stimulus-induced or enhanced phase-locked synchronization neuronal activity (as discussed in prior TNs).

High frequency stimulation can block firing in neurons in vitro, both from electrical or ultrasound stimulation. There is probably a need for resonance and SR experiments in vitro targeting small neuronal populations. SR has been clearly demonstrated in vitro.

Stimulation in-vitro could also seek to amplify recently observed emerging oscillatory states or substitute the underlying slow oscillatory activity. This is a promising road, since the authors also provide a computer model that can explain the emergence of both the slow (<1 Hz) and the β-range oscillations in the neocortical network and their entrainment. **This model could provide a natural connection point with single-neuron electric field interaction models, and provide a new setting to study resonance and hierarchical resonance in vitro.**

Several large scale resonant frequencies associated to sensorial stimulation have been experimentally observed in the brain. Frequencies include ∼40 Hz and subharmonics and are probably associated to perceptual binding phenomena.

Experiments show that stochastic resonance phenomena can also play a role cross-modally, where noise in one sensorial modality can amplify signals at other sensorial modalities.

Sensorial stimulation which is resonant to neurophysiological rhythms (e.g., delta, alpha) has been shown to potentiate their activity. No experiments have been done with electrical stimulation at 40 Hz so far, and this could be an interesting area to explore, as it seems to play a role in perceptual binding. Generally speaking, gamma frequencies appear to be involved in perceptual binding and perceptual awareness, and provide an interesting arena for stimulation experiments.

In general, electrical stimulation experiments forcing synchronous activity in different brain areas using periodic and random signals could seek to replicate the results of sensorial stimulation experiments.

In particular, hierarchical stimulation schemes could be designed to explore the relationships between oscillatory behavior at different spatial scales—in vivo and in vitro.

Finally, well defined stimulation experiments can provide a very valuable tool to study the postulated hierarchical oscillatory nature of computation in the brain.

Chapter 4

SUMMARY: WHAT WE DO AND DON'T KNOW [GR (Ed.)]

1 Single Neuron-Field interaction

1.1 What we know

- Under electromagnetic stimulation in the quasi-static regime, stimulation affects neuron function through electric field coupling.

- The electric field alters membrane polarization and therefore ion channel function and firing rates. This has been shown theoretically/computationally and experimentally. In particular it has been shown that membrane polarization and action potential threshold vary approximately linearly with field magnitude along axis (i.e., projected). E.g, a field of 1 V/m can lead to 0.1 mV change in membrane polarization.

- While TMS results in both neuro-stimulation and neuro-modulation and can initiate action potentials in axons, tDCS is clearly neuro-modulatory, modifying the level of excitability and the firing rates of individual neurons.

- There are important differences in short and long time scale effects from both tDCS and TMS.

- Short time scale effects are mediated by membrane polarization changes. With regards to long term scales, the effects of tDCS last up to an hour after stimulation, with mechanisms involving an alteration of the membrane function through local changes in ionic concentration, alteration in transmembrane proteins and electrolysis-related charges in hydrogen ion concentration induced by exposure to an electric field. Short applications do not lead to after effects, only excitability shifts during stimulation.

- Membrane time constant values relative to stimulation temporal characteristics are important and independent of fiber geometry. We know that TMS stimulates primarily the axons because of their short time constant and the short pulse nature of the stimulation. Similarly, tDCS stimulates dendrites well because of their long time constant.

- Stimulation pulse waveform is important. Different pulse waveform phases can stimulate differently different areas. In addition, neurons may be less sensitive to AC higher than

15Hz according to some recent work. This is an area to investigate further.

- The field gradient in the orthodromic[1] direction is a factor in field neuron coupling of pyramidal cells, but not the main one in CNS stimulation with TMS or tDCS (as opposed to PNS stimulation, where it is).

- Cable equation boundary conditions are important in CNS stimulation with tDCS and TMS. Neuron termination, bends and inhomogeneities are crucial, and there the strength of the E field along axis (i.e., the orthodromic direction) is most important, not the macroscopic external field gradient.

- Based on these ideas, an excitation function semi-empirical model proportional to the E field strength along a preferred neuron direction (which for pyramidal cells is the orthodromic one, but for others we don't know) has been developed, and is available for work in microscopic, then macroscopic, ensemble models.

- Both pyramidal and interneurons are affected by stimulation. Much less is known about the latter, and we should study it.

1.2   What we don't know

- We need better membrane models, with better knowledge of the relevant bioelectrical parameters.

- We need better neuronal geometric models, especially for inter-neurons. Since detailed simulation of the E-field interaction for each neuron type is beyond the project, some semi-empircal model should be developed for them.

- Effects of tissue anisotropy in the resulting E fields should be better understood.

- The impact of background neuronal activity on neuron function is not understood: how big is it in comparison with other phenomena?

- The impact of glia and other synaptic interaction effects is poorly understood.

- What happens beyond standard stimulation protocols—longer, weaker pulses, etc.? This is uncharted territory, but should be available for study in the projects. In particular, wTMS (weak TMS) is an interesting alternative that so far we have not seen used.

- Can we use frequency dependence for selectivity in stimulation? In other words, the time constants of different neuron types may allow a way to select specific neuronal populations.

- Do we have preferential activation based on activation time or other waveform aspects (shape, pulse length, frequency, resonance)? Is this something we can exploit to improve selectivity?

- We need better models of interneurons, geometric, coupling aspects.

---

[1]Conducting impulses in the normal direction. Used in terms of a nerve cell.

- Preferred orientation maps for different types of neurons should be made available, as they will be relevant to various aspects of the projects. For pyramidal cells, the orthodromic direction is appropriate, but we are uncertain about this direction for other neuron types.

2   Neuron Assembly-Field interaction

2.1   What we know

- Active neurons induce external currents and therefore fields that can affect passive neurons—this is a short-range effect called ephatic coupling. This should be better understood, potentially a paradigm shift. Ephaptic interactions might play a role in recruitment and synchronization of neuronal activity.

- We know that the level of integration at which electric fields are considered is crucial - the further from the cell scale the less sure we can be.

- We also know that the network level is much more sensitive to stimulation than individual neurons. Very weak fields (< 1 V/m) can impact neuronal populations through coherent action on the ensemble. Can we model this? This is clearly an important point given the nature of our projects.

- The origin of LFP[2] is more or less understood— this is dependent on type of synapse and location. This is where the single dipole approximation in forward models comes from - it's an approximation of the LFP valid at (relatively) large distances (sum of al contributions).

- Computer simulations indicate that electrical field effects contribute to the shape of the epileptiform field potential.

- Resonance phenomena, including stochastic resonance, are demonstrated mechanisms at the neuron and assembly levels.

- We have also discussed alternate ways to improve focality in practice, including time and frequency stimulation control to produce local average field extrema. Inter-pulse duration can also be used to tune the response of neurons. Resonance or time-scale properties of neurons or ensembles can also be used to improve focality.

2.2   What we don't know

- All stimulation parameters and combinations of parameters have not been well tested, and more work is needed.

- Non-pyramidal neuron effects on the network are poorly understood (e.g. inter-neurons, glia).

- Many regions of the brain have not been tested.

---

[2]Local Field Potentials

- There is insufficient information on LTP/LTD[3], for instance there are no studies in-vitro for external fields.

- What are the mechanisms for long term effects of TMS and tDCS? Is this an ensemble effect?

- Brain "state" is important to stimulation effects, but not much work done there experimentally.

- What is the relationship of stimulation on neurogenesis and oncogenesis? This is still unclear and care is due.

- What is the appropriate time scale for stimulation (TMS vs. tDCS)?

- Could the time constant of the Ag/AgCl - Cl redox reaction have an impact in in-vitro stimulation studies? This is an important engineering aspect : especially in the near-DC regime.

- Can the COMPTE model explain slowing of frequencies in degenerative diseases? Does this depend on connectivity?

- Can we reproduce experimental work in models showing the sensitivity of populations to very weak fields?

- Can we model/verify resonance phenomena properly in silico?

- What is the role of signal propagation delay on network oscillations? Should this be better modelled?

- We don't understand network/global effects such as inhibition. In-vivo experiments could help.

3   3D models of conduction

3.1   What we know

- The quasistatic/steady state regime in which tDCS and TMS work simplifies 4D modeling into 3Dx1D (i.e., solve for static fields, then modulate using temporal variation of stimulation parameters).

- Fundamental modeling aspects of tDCS and TMS

- In TMS the impact of coil shape is now well understood and modelled.

- Grey matter is resistive and fairly steady up to 1 kHz: this is good news, as it facilitates modeling.

- Grey matter is isotropic, white matter is anisotropic.

---

[3]Long term potentiation/Long term depression

- Electrodes are traditionally large but because of a clinical misconception that this is safer in terms of the induced current densities. Current densities are not a linear function of electrode size

- In the electrode scalp interface, highest current densities occur at the edges and especially corners. Circular electrodes should reduce edge affects somewhat

- Edge effects are much less on cortex surface because of the "blurring" effect of the skull, skull resistance drops as area

- Current density distributions are very different in TMS and tDCS, almost 2 orders of magnitude in amplitude, as well as direction (more tangential for TMS) and extent

- In TMS, there is almost no radial component of the E field

- Current densities in tDCS are much smaller than in TMS (factor of $\sim$100)

- General properties of fields in TMS and tDCS are understood

- Geometry of the conductor at 1mm resolution geometry of the volume

- Max. and min. of electric field only occur at boundaries, but our media is non-uniform so we can take advantage of inhomogeneities.

- Max of stimulation locus for pyramidal cells in the cortex can be computed using the proposed excitation function if an orthodromic map is available.

3.2 What we don't know

- The dielectric properties (conductivity values) of tissues are not well known, particularly for AC

- Accuracy of our current propagation/E field models is unknown, how can we validate this? Can we improve this with animal work in HIVE?

4 In-vitro and in-vivo experiments

4.1 What we know

- Both stimulation with local or global (uniform) fields are interesting.

- Hippocampus has been used until now because of its nice layered structure, etc.

- Cortex on the other hand is not very laminated, and much less studied in stimulation work. Yet, we are mostly concerned about cortical effects of stimulation

- Propagation speed depends heavily on length of connections in-vitro. These must be short in a small slice: a) Item In-vitro 10 mm/s wave propagation, b) In-vivo 100 mm/s wave propagation.

- Results show spontaneous oscillations in cortex when the medium is adjusted.

4.2   What we don't know

- Where are rhythms generated? In-vivo we can't say, it's just cortex so role of hippocampus, for example, is unknown.

- What is the role of extra-cellular ephatic currents?

- How does the localization actually work in in-vivo tests? Seems like it could validate to some extent the excitation function model proposed. What does it tell us about NAFI (Neuron/Assembly-stimulation Field Interaction)? Can we fine-tune these experiments to maximize return?

- No work in-vitro in **cerebral cortex** (a more relevant aspect in view of transcranial applications). See next points:

- In-vitro evoked responses effects, inhibition effects. Effects/coupling to network rhythms (slow wave sleep, beta, gamma).

- In-vitro LTD, LTP or short term plasticity

- Potential for local controlled activation of areas in network (in slices).

- Potential for in-vitro manipulation of epilepsy

- Stochastic resonance in-vitro in cortex, relation to Ultra Sound SR effects.

- Electrochemical impact of DC stimulation with different types of electrodes

5   Clinical aspects and safety

5.1   What we know

- rTMS can induce some very long term effects weeks. What are the mechanisms?

- Glucose consumption is altered by TMS

- Neurogenesis can be affected by TMS

- TMS can alter plasticity as well

- In MCS and PVS we know that DBS of thalamus and brain stem helps

- Extra-cranial reference has been used with no problems in some studies

- Current densities are very non-uniform: instrumental given values are pretty meaningless

- Using resonant frequencies is an interesting possibility for selective stimulation on a particular clinical aspect

5.2 What we don't know

- We don't know what the real current density is inside the brain (as it is model based)

- What frequency should we use for clinical stimulation?

- How do we replicate DBS results with tDCS?

- Where should we place anodal/cathodal electrodes?

- What is the max. current density?

- What happens in the other areas?

- How do we replicate TMS and/or tACS with tDCS?

6 Conclusions and Questions

Finally, we can provide the following recommendations for further research in the project.

An overall recommendation is for all experimental groups in the project to review this document and update the experimental plans accordingly to focus on the key questions:

1. Validation of current propagation models

2. Validation of single neuron excitation function models

3. Development and validation of microscopic and macroscopic models of stimulation coupling

Chapter 5

APPENDICES

1   Hippocampus: anatomy and connections
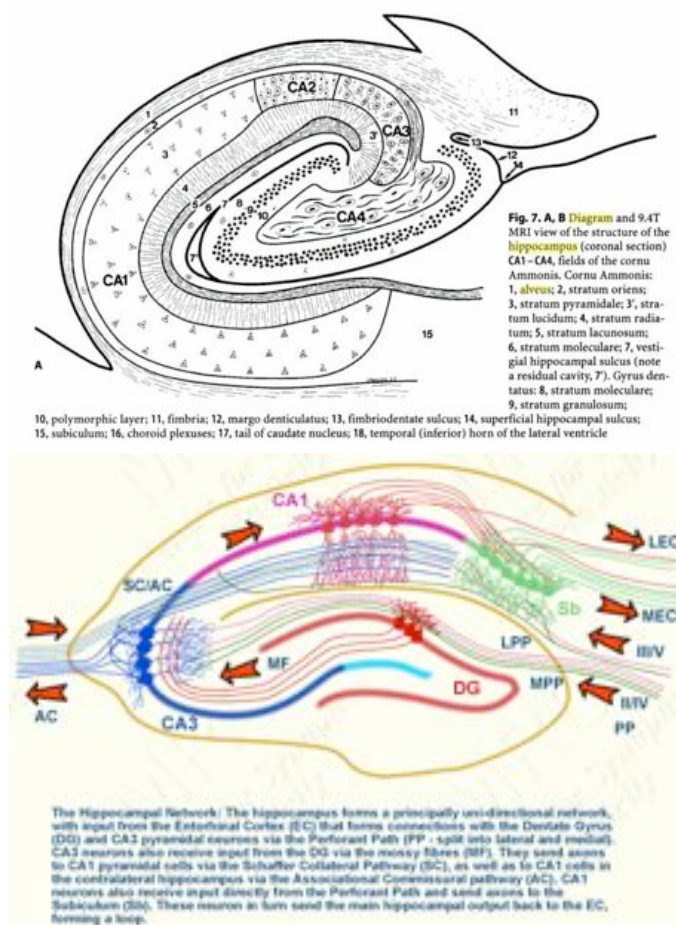
Figure 5.1 – Hippocampus anatomy (top) and connections (bottom)

2 TMS in animals [FW]

Paper	animal	TMS device	Stim	Measure	Recording	Mag	f	Num. pulses	effect
[Lisanby:1998aa] [Lisanby:1998ab] **Induced voltage**	Rhesus monkey	paediatric FOE coil	single pulses	induced V	SEEG prefrontal 10 contacts 0.5 mm length, 6 mm apart	50% of max	1hz	5	V ↓ with distance / ΔV small (2,4%) / V =140mV at prefrontal contact
[Lisanby:2001aa] **Induced voltage**	macaca	paediatric FOE coil	single pulses	induced V + V induced by Sham	SEEG prefrontal 10 contacts 0.5 mm length, 6 mm apart	70% of max	1hz	5	V =180mV at prefrontal contact / Sham 2 wings 45° = 130mV / Sham 90° = 60 mV
[Moliadze:2003aa] **Action potentials**	cat (area 17)	FOE 2*70mm Coil/cortical surf=10mm	single pulses	Neuronal activity in area 17	extracellular single-unit recordings	20-30% 40-100%	0,16Hz (1/6s)		0-100 ms = ↑PA (facilitation) / 100-1000ms = ↓ PA (suppression) / 100-200 ms = ↓ PA (suppression) / 200-500 ms ↑ PA / 500-up to 5s = ↓ PA
[Moliadze:2005aa] **Action potentials**	cat (area 17)	FOE 2*70mm	ppTMS	Neuronal activity in area 17	extracellular single-unit recordings	CS=15-30% of TS CS=60-130% TS	At ISI 3ms Varying ISI		Effect of TS on visual activity is ↓ (facilitation or suppression) / Effect of TS on visual activity is ↑ (facilitation or suppression) / No clear change.
[Labra:2007aa] **Action potentials**	Cat level of area 17	FOE (2 x 25 mm).	rTMS	cortical +dLGN single units extracellular recordings	low-impedance implanted in the deep layers of V1 tungsten microelectrodes	50% (1.5 T, E=220 V/m)	1 Hz 1min 6-Hz pulses of 1s every 10s	60	TMS at 1 Hz reduced PA by 24 ± 8% for 500 ms and recovery / TMS at 6@0.1 Hz reduced PA 33 ± 6 + long time to recover / Only when TMS applied before the visual stimulation / →rTMS strongly and reversibly suppressed cortical feedback to the dLGN
[Allen:2007aa] **Action potentials+ metabolism**	cat (area 17)	FOE 2*70mm	rTMS	Tissue oxygen single-cell neural activity (visually evoked + spontaneous) changes in total hemoglobin (Hbt) within the cortical vasculature	Oxygen microelectrode adjacent platinum microelectrode 570-nm optical imaging	100% Induced E field = 100-200 V/m	(1,4,8 Hz) and duration (1,2,4 s)	1,2,4,8, 16,32	↑ 10 to 15 s after TMS and ↓ for over 2 min / ↑ spontaneous spike rate (200%) for 60 s / ↓evoked firing rate (50%) for more than 5 min / ↑ 10 s and ↓ for over 1 min / These effects (↑ or ↓) were enhanced as the frequency of stimulation increased
[Valero-Cabre:2005aa] **Metabolism**	cat	50 mm circular coil VP cortex +sensori-motor (SM) cortex	rTMS	Glucose metabolism	^{14}C-2DG during TMS	55% MO 135% MT	56 trains of 20 Hz for 2 s with 28 s inter-train intervals	2240	↓uptake of ^{14}C-2DG the medial (VPm) and lateral (VPl) banks of the VP cortex as compared to the homologue areas in the unstimulated hemisphere / ^{14}C-2DG uptake was maximally suppressed at the site of stimulation ↑ towards normal values with distance from the site of rTMS application / ↓uptake of ^{14}C-2DG in specific distant cortical and subcortical structures that receive substantial projections from VP cortex / ↓ uptake ^{14}C-2DG in specific subcortical structures compared with homologous structures in the contralateral unstimulated hemisphere

Paper	animal	TMS device	Stim	Measure	Recording	Mag	f	Num. pulses	effect
[Wagner:2007ab] **Metabolism**	cat	50 mm circular coil VP cortex		Glucose metabolism	^{14}C-2DG during TMS - during rTMS - just after rTMS - 30min after	55% MO 135% MT	HF=56 trains of 20 Hz for 2 s with 28 s intertrain intervals LF=1Hz continuous	2240 1800	During rTMS : LF+HF= ↓^{14}C-2DG uptake in the stimulated VP cortex and tightly linked cortical and subcortical structures (superficial superior colliculus, pulvinar, e LPI nucleus) % homologue areas in the unstimulated hemisphere Just after rTMS HF= ↑^{14}C-2DG uptake in the targeted VP cortex LF= ↓^{4}C-2DG uptake in the targeted VP cortex + mild effect on network 30 min post-rTMS No effect → opposite modulation of rTMS on local and distant metabolism along a specific network, depending on the pattern of stimulation
[Ben-Shachar:1997aa] **Neurotransmitters**	Rat (model of depression)	50mm coil	rTMS	Concentration of monoamine	HPLC	100% (2.3T)	25Hz 2s	50	10 s post stim :changes in brain monoamine levels and turnover rates DA ↓ in the frontal cortex ↑ in the striatum and hippocampus DA turnover rates ↑ in the frontal cortex and ↓ in the striatum and hippocampus ↑ 5-HT 5HIAA only in the hippocampus no change in serotonin turnover rate. Norepinephrine not affected.
[Ben-Shachar:1999aa] **Neurotransmittors**	Rat	7 cm circular stimulation coil	rTMS	Receptor density	Bmax Kd [3H]DHA	peak magnetic field 2 T (76% of maximum intensity)	15 Hz for 3.5s daily for 10 days (duration?)	500	no effect on monoamine concentrations in Frontal striatum and hippocampus β-adrenergic receptors up regulated in the frontal cortex, down regulated in the striatum and were unchanged in the hippocampus. 5-HT$_2$ receptors down regulated in the frontal cortex and not changed in the other brain areas. No change in benzodiazepine receptors in the frontal cortex and cerebellum
[Fleischmann:1996aa] **Neurotransmittors**	Rat	9 cm circular stimulation coil	rTMS	Receptor density β-adrenergic	Bmax Kd [3H]CGP-12177		25 Hz for 2 sec daily for 9 days	450	downregulated β-adrenergic receptors in the cortex, but not the hippocampus ↓ cortical cAMP generation
[Kole:1999aa] **Neurotransmittors +LTP/LTD**	rat	Circular coil (diameter 12.5 cm)	rTMS	Receptor density NMDA 5-HT	125 I-MK-801 for NMDA 3H-8-OH-DPAT for 5-HT1A		20Hz for 3s	60	24h after : ↑ 5-HT 1A in the frontal cortex, the cingulated cortex, and the anterior olfactory nucleus ↑ NMDA sites in the ventromedial hypothalamus, the basolateral amygdala and layers 5–6 of the parietal cortex.
[Gur:2000aa] **Neurotransmittors**	rat		Chronic rTMS	5-HT levels in the prefrontal cortex	microdialysis + with or without 8-OH-DPAT (5-HT1A) and GR 127935 (5-HT1B) treatment				reduced sensitivity of presynaptic 5-HT1A autoreceptors and postsynaptic 5-HT1B heteroreceptors →Like with some antidepressant treatment
[Fujiki:2004aa] **Early genes**	mouse	Circular coil 5cm diameter	Acute rTMS	GFAP	situ hybridization for GFAP mRNA.	70% (1.63T)	25Hz for 10s Tains, 1,2,4,6,8, 10,30 times (3-5min between trains		↑↑ in the levels of GFAP mRNA in dentate gyrus; more modest ↑ in the cerebral cortex. Glial gene expression like after injury

Paper	animal	TMS device	Stim	Measure	Recording	Mag	f	Num. pulses	effect
[Ji:1998aa] **Early genes**	rat	Circular coil (diameter 5 cm) site of stimulation at the orbit level	Acute rTMS	c-fos mRNA expression.	*In Situ* Hybridization : c-*fos* specific antisense oligonucleotide labelled with α-[35S]thio-dATP + incubation anti-c-Fos and anti-c-Jun serum + Western Blotting. Coronal brain slices 400 mm thick cut at the level of the paraventricular nucleus of the thalamus (PVT)	100% (2T)	25Hz for 2s 3x 25Hz for 2s (5-min inter-train intervals)	50 150	↑↑ the level of c-Fos and c-Jun proteins in the PVT , moderate ↑ in cingulate, primary, and secondary motor cortex + paraventricular nucleus of the hypothalamus (PVN) subparaventricular zone, the suprachiasmatic nucleus (SCN), and the retina (=regions controlling circadian rhythm + having strong connections with PVT) → stronger ↑ of c-Fos in the same brain regions + moderate ↑ c-Fos in additional regions (habenular nucleus and hippocampus)
[Hausmann:2000aa] **Early genes**	rat	FOE coil (diameter 2,3 cm) without touching the skull	Chronic rTMS	c-fos mRNA expression. With or without MK-801 15min before stimulation	*In Situ* Hybridization : Anti- sense oligonucleotides (labelled with [α-35S]dATP) against cFos, brain-derived neurotrophic factor (BDNF), fibroblast growth factor-2 (FGF-2), glial fibrillary acidic protein (GFAP)	75%	20Hz * 10s	200 * 14jours	↑↑ neuronal c-fos mRNA expression in layers I–IV and VI of the parietal cortex ↑ c-fos expression only in scattered neurons in the hippocampus No change c-fos mRNA expression in layer V No change in BDNF, GFAP, FGF-2 Pre-treatment with MK-801 did not block the rTMS-enhanced c-fos expression in the parietal cortex. → chronic rTMS effects are not mediated by glutamate acting on NMDA receptors, but rather rTMS treatment directly activates a specific pattern of intrinsic or corticofugal neurons.
[Muller:2000aa] **Early genes / neuroprotection**	conscious rats	prototype coil 21 windings (6mm diameter) at the left frontal cortex.	Chronic rTMS	brain-derived neurotrophic factor (BDNF), cholecystokinin (CCK), and neuropeptide tyrosine (NPY) mRNA	In situ Hybridization with oligonucleotide DNA probes (labelled with [α-35S]dATP)	130% of rats' motor threshold	20 Hz for 2.5 s 5-day series separated by 2-day intervals for 11 weeks	150 stimuli/day	↑ BDNF mRNA in the hippocampal areas CA3 and CA3c, the granule cell layer, parietal and the piriform cortex (→contribute to the neuroprotective effects) ↑CCK mRNA all brain resions explored(like with antidepressant drug treatment) No change in NPY mRNA
[Doi:2001aa] **Early genes**	Rat						6 sessions of rTMS ?		↑ c-Fos-like immunoreactivity in frontal cortex, lateral orbital cortex, striatum, lateral septal nucleus, piriform cortex, dentate gyrus, Ammon's horn, cingulate cortex, parietal cortex, thalamus, occipital cortex, and amygdala

Paper	animal	TMS device	Stim	Measure	Recording	Mag	f	Num. pulses	effect
[Aydin-Abidin:2008aa] **Early genes**	rat	FOE coil, diameter 7cm centred at the inter-hemispheric cleft 8 mm above the occipital cortex	Acute rTMS + iTBS	c-fos zif268	Immunohistochemistry of c-fos zif268 + neuronal marker NeuN as a control of neuronal cell loss	1Hz rTMS =30–33% MO 10Hz rTMS = 29–32% MO iTBS = 25–30% MO Sham = like test but stimulation coil positioned 8 cm above the rat's head.	1 Hz rTMS, we applied pulses within 70 min 3xx 20 min -1 Hz train (inter-train 5min) 10 Hz rTMS 4 blocks of 5 x 12 1s-trains (10 Hz) with 5s inter-train. (10 min pause between blocks iTBS 5 blocks of 10 trains 3 -50 Hz every 200 ms (5 Hz), repeated 20 times every 10 s.	3600 2400 3000	1 + 10 Hz rTMS ↑ c-Fos protein expression in all cortical areas tested iTBS ↑ c-Fos only in limbic areas. 1 Hz rTMS = no effect on zif268 10 Hz rTMS= ↑ zif268 only in the primary motor and sensory cortices iTBS=↑ zif268 in almost all cortical areas sham-rTMS =↑ c-Fos in limbic cortices (no effect on zif268 expression)
[Ogiue-Ikeda:2005aa] **Neurotransmitters early genes**	mouse	(7.5 cm outer diameter)	Acute + chronic rTMS	mRNA expression of monoamine transporter genes	real-time RT-PCR (probes)+ 3H-labeled autoradiography.	30% (0.75 T)	20 Hz for 2 s, 20 times/day inter-train interval 1 min	1 day Or 20 days	Chronic : ↓ mRNA levels of serotonin transporter (SERT) mRNA + subsequent decrease in serotonin uptake + binding ↑ mRNA levels of dopamine transporter (DAT) and norepinephrine transporter (NET) ↓5HT, ↑DA, NE ↓ mRNA levels of c-fos + cjun genes after chronic rTMS Acute : ↑ mRNA levels of c-fos + cjun genes at 1 h after acute rTMS,

Paper	animal	TMS device	Stim	Measure	Recording	Mag	f	Num. pulses	effect
[Keck:2000aa] [Keck:2000ab] **Neurotransmitters (AA)**	rat	prototype coil 21 windings (6mm diameter) Frontal brain regions	Acute rTMS	Release of Neuropeptid arginin vasopressin (AVP) + AA (GLU, GLN, SER, ARG, GABA, Taurine) in PVN + Monoamines in Hippocampus	microdialysis	130% motor threshold (4T)	20Hz for 2,5s 20 times (every 2min)	1000	↓AVP (High in depressive patients and decreased after fluoxetine treatment) ↑ taurine in PVN (inhibitory AA, might participate to the ↓AVP) ↑ASP, SER in PVN (AA reported to be depressed in depressive patients ans increased after antidepressive treatment) No change in GLU, GLN, ARG, GABA ↑ DA in dorsal hipp (see psychratric syndroms associates with depleted DA transmission) No change in NE, 5-HT, DA, 5-HIAA, DOPAC levels in the hippocampus.
[Keck:2002aa] **Neurotransmitters**	Rat urethane-anesthetized and conscious	prototype coil 21 windings (6mm diameter) frontal brain regions	Acute rTMS	Release of DA and its metabolites (homovanillic acid, 3,4-dihydroxy phenylacetic acid)	Microdialysis probes stereotaxically implanted in right dorsal hippocampus right shell of the nucleus accumbens and the dorsal striatum	130% motor threshold (4T)	20Hz for 2,5s 20 times (every 2min)	1000	↑ extracellular DA in dorsal hippocampus, shell of the nucleus accumbens and dorsal striatum No change in HVA or DOPAC during or after rTMS → modulatory effect on both the mesolimbic and the mesostriatal dopaminergic systems
[Kanno:2003aa] [Kanno:2003ab] **Neurotransmitters**	rat	FOE (70mm 7 windings)	Acute rTMS	Extracellular 5HT +DA in PFC	microdialysis	110% motor threshold (sham + 60% machine output + coil 90°)	20 trains at 25 Hz for 1s	500	Transient (1h) ↑DA concentrations(Sham + test vs non treated) No difference in DA between rTMS-treated and sham treated groups Sham treatment ↑ the extracellular 5-HT levels No difference in 5HT between rTMS and non treated.
[Kanno:2004aa] **Neurotransmitters**	rat	FOE (70mm 7 windings)	Acute rTMS	Extracellular DA in dorsolateral striatum + 5HT in right PFC	microdialysis	20,60,80% (0.2, 0.6 and 0.8 T)	20 trains at 25 Hz for 1s	500	↑ Extracellular DA concentrations in the rat dorsolateral striatum in the 60% rTMS-treated group (compared to sham and non treated, + compared to stim 20% and 80%) No change in 5HT
[Keck:2003aa] **Neurotransmitters**	Review of previous studies.								
[Wang:1996aa] **LTP/LTD**	Rat **No pdf**		LF rTMS				1 to 10Hz		frequency dependant ↑ spike rate repeated rTMS → long-term potentiation (LTP)-like, and more durable long-term depression (LTD)-like changes in evoked spike rate

Paper	animal	TMS device	Stim	Measure	Recording	Mag	f	Num. pulses	effect
[Levkovitz:1999aa] **LTP/LTD**	rat	5 cm coil	Acute RTMS + Choinic rTMS	Response to paired pulse stim of PP in the DG	stimulating electrode in the perforant path (PP) twin pulse PP with interpulse intervals (15, 30, and 60 msec),	100% (2.2T)	1, 10, and 25 Hz for 2s Chronic = 25Hz for 2s / day for 7 days		Chronic stim = long-lasting effect on neuronal excitability in the hippocampus Does not affect basal conduction in the PP to th DG, ↓ paired-pulse and frequency-dependent inhibition, → ↓ local circuit inhibition in the DG ↑ the expression of LTP in the PP synapse in the dentate gyrus. ↓ serotonin-dependent potentiating action of fenfluramine on population spike in the dentate gyrus. (common mechanisms as antidepressant drugs and effect is erased with aging
[Ahmed:2006aa] **LTP + memory**	mouse	5 cm coil	Acute rTMS	Response to LTP in vitro on hippocampal slices Memory test in vivo	LTP : stimulating on Schaffer Collateralsand recording in the pyramidal cell layer,. LTP induced by high-frequency stimulation (3 times 100 Hz for 1 s every 10 s). LTP considered successful if the population spike was enhanced by at least 20% for no less than 30 min	50% (1.8T)	15Hz : 6 trains of 5 s every 15 s 8 Hz: 6 trains of 9.5 s every 17 s 1 Hz: continuously for 7.5 min		rTMS at 15 Hz improved animals' performance in novel object recognition test (NOR) but 1 h and 3 days after 15 Hz stimulation worse than controls. rTMS at 1 and 8 Hz impaired the memory. + enhancement of the synaptic efficiency expressed as of the long-term potentiation (LTP) recorded from hippocampal slices 1 and 8 Hz had no influence on the magnitude of LTP.
[Ogiue-Ikeda:2005aa] **LTP/LTD**	rat	Circular coil (inner diameter = 15 mm, outer diameter = 75 mm)	chronic	Response to LTP in vitro on hippocampal slices 15 h after the chronic treatment.		0.75 T (<MT) or 1T (>MT)	10 1-s trains of 25 Hz with a 1-s intertrain interval four times per day for 7 days	1000/ day	LTP is enhanced in the 0.75T group but not in th 1T group. Effect of amplitude.
[Sgro:1991aa] **LTP/LTD**	Rat **No pdf**	Circular coil (inner diameter = 15 mm, outer diameter = 75 mm)	chronic	Response to LTP in vitro on hippocampal slices 15 h after the chronic treatment.	LTP : stimulating on Schaffer Collateralsand recording in the pyramidal cell layer,. LTP induced by high-frequency stimulation (3 times 100 Hz for 1 s every 10 s).	0.50 (>MT) or 1.25T (>MT)	10 1-s trains of 25 Hz with a 1-s intertrain interval four times per day for 7 days	1000/ day	No change on LTP in the 0.5T group, but suppression of LTP in the 1.25T group
[Sgro:1991aa] **Structural modifications**	rat	round-coil 5.5 inch diameter		histology	light microscopy with hematoxylin and eosin staining, or electron microscopy	3,4T	8Hz for 20 min	10000	No change in neocortex, hippocampus, basal ganglia, and cerebellum
[Ravnborg:1990aa] **Structural modifications**	Rat **No pdf**	Circular coil 14 cm	Single pulse		permeability to the tracers [^{3}H]sucrose, [^{14}C]urea, and ^{36}Cl$^-$	1.9T		50-60 during 15 min	No change in permeability of blood brain barrier

Paper	animal	TMS device	Stim	Measure	Recording	Mag	f	Num. pulses	effect
[Matsumiya:1992aa] Structural modifications No pdf	Rat No pdf	Circular coil 7.5 cm				100-340% motor threshold(0.8-2.8T)		50-100 stim/day	High stimulus intensity (2.8 T) and nb stim >100 = 50% animals : microvacuolar changes in cortex layers 3 and 4 (seen up to 30 days after last stim) Lower stim intensity or fewer nb of stim = no change.
Structural modifications [Counter:1993aa] No pdf	Rabbit No pdf	round-coil (5 cm	Single pulse			100% (2T)	100 stim /week (1̃2month)	1000	No MRI structural change No microscopic histological change
[Post:1999aa] Structural modifications + memory + neuroprotection	rats	prototype coil 21 windings (6mm diameter) at the left frontal cortex.	Acute + chronic rTMS	Memory test oxidative stressors (amyloid beta (Aβ) and glutamate.	social discrimination paradigm (recall olfactory-cued short-term memory information) amyloid precursor protein (sAPP) release in CSF Immunohistochemistry Histopathological examination	130% motor threshold (4T)	20 Hz for 2 s, 20 times/ 3 trains of 20 Hz for 2.5 s separated by 2 min	1000 150/day in 5-day series separated by 2-day pauses for 11 weeks,	rTMS has no deleterious effects on learning and memory functions in rats rTMS does not induce structural brain alterations in rats rTMS increases the cell viability of HT22 cells (in vitro) acute+ chronic rTMS : ↑ (x2) release of sAPP into the CSF ↑ the cell viability following the Aβ challenge HT22 cells preincubated with CSF from rTMS-treated rats → protected against Aβ →neurochemical effects induced by rTMS do not lead to reduced neuronal viability, and may even reduce the detrimental effects of oxidative stress in neurons
[Liebetanz:2003aa] Structural modifications	rat	Coil inner 7 mm and an outer diameter of 32 mm	Chronic rTMS	quantitative evaluations of cerebral metabolite concentrations microglial/ astrocytic activation (48h post rTMS)	in vivo localized proton magnetic resonance spectroscopy (MRS) and post mortem histological analysis (antibodies against OX-6, OX-42, ED, and GFAP)	115% of motor threshold	1 Hz.	1000 stimuli 5 consecutive days	proton MRS : no significant alterations of N-acetyl-aspartate, creatine and phosphocreatine, choline-containing compounds, myo-inositol, glucose and lactate post mortem histology : no changes in microglial and astrocytic activation after rTMS
[Sauvage:2008aa] Structural modifications	rat	flat copper coil (inner/outer diameter = 15/64 mm, thickness = 4 mm)	Acute rTMS	Genotoxicity +MT+current density evaluated by a model in motor area.	alkaline comet assay on rat brain cells, measuring Olive moment and %DNA in the tail	100%	20 trains 10Hz for 10s (50s intertrain)	2000	No toxicity
[Okada:2002aa] Structural modifications	rat	8-cm round coil	Chronic rTMS + acute electrical stim	inflammatory mediators	mRNA levels of interleukin (IL)-1b, IL-6, cyclooxygenase (COX)-2 and inducible nitric oxide synthetase (iNOS) in the brain	200% MT	30 Hz 50s 100 Hz, 1 s, 50 mA	1500/day 7 days	rTMS = No seizure mRNA IL-1b, IL-6 and COX-2 , iNOS not induced in hippocampus and Pa cx ES = seizure mRNA of IL-1b, IL-6 and COX-2 is induced in Pa cx

Paper	animal	TMS device	Stim	Measure	Recording	Mag	f	Num. pulses	effect
[Tunez:2006aa] **Neuroprotection**	rat	Coil 7 cm diameter contained in plastic boxes (10.5 · 10.5 · 3.5 cm)	rTMS	oxidative and nitrosative stress, neuronal death, anatomic and neurochemical changes = similar to those occurring in Huntington's disease	3-nitropropionic acid	0.7 mT	60 Hz for 2h (morning) + 2h (afternoon)	8 days 4 days before and continued for 4 days after the first injection	TMS decreases oxidative damage TMS partially prevents the reduction of SDH activity induced by 3-nitropropionic acid in cortical synaptosomes
[Tunez:2006ab] **Neuroprotection**	rat	7 cm diameter) contained in plastic boxes (10.5 · 10.5 · 3.5 cm)	rTMS	anatomic and neurochemical changes = similar to those occurring in Huntington's disease (LDH) levels in plasma and striatum, and nitric oxide concentration in striatum	3-nitropropionic Acid 1) effect of TMS on total radical-trapping antioxidant potential (TRAP) and hydroperoxides formation in the 3-nitropropionic acid model 2) effect of TMS on oxidative stress and changes in SDH activity induced by 3-nitropropionic acid in the striatal synaptosomes 3) histological injury triggered by 3-nitropropionic acid in the striatum and the effect of TMS administration 4) lactate dehydrogenase (LDH) levels in plasma and striatum, and nitric oxide concentration in striatum	0.7 mT	60 Hz for 2h (morning) + 2h (afternoon)		3-nitropropionic acid induces oxidative and nitrosative stress in the striatum, + cell loss TMS prevents the effects induced by the acid
[Fleischmann:1995aa] **Depression model + seizure threshold**	rat	Circular coil (5cm)	Chronic rTMS SHAM = coil OFF	Depression behaviour + seiz thresh using electroconvulsive shock (ECS)	apormorphine-induced stereotypy Porsolt swim test	100% (2.3T)	25Hz for 2s 1/day for 7 days	500	enhancement of apormorphine-induced stereotypy reduction of immobility in the Porsolt swim test increase in seizure threshold for subsequent stimulation : single TMS treatment↓ the % of rats seizing in response to a ECS-like electrical stimulus to the brain 10 s later. Seizure duration in rats who do seize to electrical stimulus 10 s after TMS is also reduced and the effect of TMS is related to dose of TMS in seconds of stimuli

Paper	animal	TMS device	Stim	Measure	Recording	Mag	f	Num. pulses	effect
[Zyss:1997aa] **Depression model**	Rat	?	Chronic rTMS SHAM = coil OFF + click	anhedonia	tail-flick test Porsolt swim test Cyclic AMP	0.1 T	50 Hz for 5 min	2x 5-day series, sepa-rated by a 2-day break.	no significant effect on tail-flick test ↓ immobility time in the forced swimming test. Insignificant ↓ cyclic AMP generation (13%)
[Zyss:1999aa] **Depression model** **No pdf**	Rat	?	Chronic rTMS No SHAM (com-par-ison with ECS)	Depression behavior	Porsolt swim test	1.6 T	20 Hz for 5 min or 30 Hz for 5 min	9 or 18 days	↓ immobility time (20-30%) for 20Hz @18 days or 30Hz @9 days
[Zyss:1999ab] **Depression model** **No pdf**	Rat	?		responsive-ness to DA stimulation (locomotion)	Apomorphine injected after TMS treatement	1.6T	20Hz for 5 min (18 days)	54,000 108,000	↑ hyperactivity induced by apomorphine → increasing the total number of pulses during the rTMS may increase the responsiveness of rats to dopaminergic stimulation to the level comparable with that induced by ECS.
[Keck:2001aa] **Depression model**	high (HAB) and low (LAB) anxiety-related behav-ior and stress-coping behav-ior	prototype coil 21 wind-ings (6mm diameter)	Acute rTMS SHAM = coil 90° ON + click	neuroen-docrine and behavioral effects	blood samples from rTMS-treated and control HAB and LAB rats, (5, 15, 60 min after stress) Forced swimm test !!! = (1) time spent strug-gling, defined as strongly moving all four limbs, with the front paws breaking the water surface; (2) time spent swim-ming, defined as mov-ing all four limbs, swimming around in the tank or actively diving; (3) time spent floating, defined as re-maining immobile with only occasional slight movements to keep the body bal-anced and the nose above water; and (4) latency until the first floating reaction	130% mo-tor thresh-old (4T)	20Hz for 2,5s 20 times (every 2min)	1,000 stim-uli/day	*forced swim test: HAB rat ↑ coping strategy (*=struggled significantly more than the controls, floated less and took longer to show the first floating reaction.) *time spent struggling; 332% vs. controls),* *→ reach the performance of LAB rats.* . *LAB rat : no change in swimming behavior* basal plasma levels of ACTH and corticosterone almost identical in all groups, forced swimming induced a neuroendocrine response → was blunted in HAB rats. But not in LAB animals. ↓ *stress-induced elevation of plasma corticotropin and cor-ticosterone concentrationsin HAB*

Paper	animal	TMS device	Stim	Measure	Recording	Mag	f	Num. pulses	effect
[Kim:2006aa] Depression model	rat	FOE (7cm)	Chronic rTMS SHAM = click	synaptic plasticity LTP	1) forced swim test for 15 min → baseline immobility time 2) LTP induction Stim Electrode perforant path (PP)+ recording electrode in the gyrus dentate Test pulses (1 ms, 200–500 μA) were delivered at every 15 s → baseline response Tetanisation Test puslses again Magnitude of potentiation (% change in fEPSP slope% baseline)	1.4 T	20* 10 Hz for 5s 25-sec intertrain	1000 7 days	↓ immobility time only after 7 days rTMS ↑ in field EPSP after LTP → mediated by a cellular process that can reverse the impaired synaptic efficacy caused by the forced swim procedure
[Loo:2000aa] Depression model	rat	FOE (7cm)	Acute + chronic rTMS	Depression behavior	Porsolt swim test	70% max output (2.3T)	1,5,15,25 Hz	1000 over 16 min 1 5 or 7 days	↓ immobility times (no diff between frcy) After 5days : only group 15-25Hz After 7 days : only group 25 Hz Sustained effect → high frequency
[Tsutsumi:2002ab] Depression model	rat	round coil (4-cm diameter) center of the coil above the vertex	Acute + chronic rTMS	Depression behavior	Porsolt swim test		15 Hz for 3.5s	52 pulses/ train (nb trains?) 1 or 10 days	immobility time not affected after acute rTMS ↓ immobility times after 10days-rTMS
[Vieyra-Reyes:2008aa] Depression model	Rat (olfactory bulbectomy model of depression)	Double coil Each coil =1000 turns of enamelled copper wire (7 cm diameter) in plastic boxes (10.5 cm × 10.5 cm × 3.5 cm).	chronic rTMS + injection of nicotine	Depression behavior	Porsolt swim test	0.7 T	60 Hz for 2 h in the morning and 2 h in the afternoon during 14 days		↓ immobility times but less than nicotinic injection
[Keck:2000aa] [Keck:2000ab] Model of stress	conscious rats	prototype coil 21 windings (6mm diameter) at the left frontal cortex.	Chronic rTMS SHAM = coil stimulation at low lumbar spine	Anxiety Stress hormons	Elevated plus-maze test (reduced openarm exploration serves as a measure of increased anxiety) social interaction paradigm(validated for the detection of emotional responses to anxiogenic and anxiolytic substances (File, 1980). Forced swim test	130% motor threshold (4T, 120 A/ms)	three trains of 20 Hz; 2.5 s for 8 weeks	150 stim / day	↑struggling+ swimming, ↓ floating ↑active stress coping strategy % control rats ↓ stress-induced elevation of plasma ACTH concentrations. Pituitary changes accounting for the attenuation were ruled out by the corticotropinreleasing hormone test. Baseline concentrations of and corticosterone =similar in the two group No change in the anxiety-related behavior on the elevated plus-maze or in behavior during the social interaction test. Same binding characteristics of the benzodiazepine agonist [3H]flunitrazepamat GABAa receptors → attenuated neuroendocrine response to stress but no change in anxiety parameters.

Paper	animal	TMS device	Stim	Measure	Recording	Mag	f	Num. pulses	effect
[Liebetanz:2003aa] Model of stress	rats submitted to daily psychosocial stress	prototype coil 21 windings (6mm diameter) Left frontal brain region	Chronic rTMS SHAM = coil OFF	Plasma ACTH + corticosterone hippocampal neurogenesis	Immunohistochemistry : quantification of BrdU-labeled cells with peroxydase	130% motor threshold (4T)	20Hz for 2,5s 6 trains (every 2 min) for 18 jours	300 stimuli/day	Basal plasma ACTH and cort levels were comparable in the control and control + rTMS rats chronic psychosocial stress ↑ plasma ACTH (+94%) and corticosterone (+97%) Stress-induced elevation of ACTH and corticosterone is normalized by rTMS treatment the decrement of hippocampal cell proliferation only mildly attenuated by repetitive transcranial magnetic stimulation, + survival rate of BrdU-labeled cells was further suppressed by rTMS in hippocampal DG
[Kanno:2003aa] [Kanno:2003ab] Model of anxiety	Rats Model of anxiety	70 mm; 7 windings Tangential to sagittal axis on the head surface of the frontal brain	Acute +Chronic rTMS	Anxiety-related behavior Extracellular concentration of 5HT+ DA	plus-maze test (open and close arms) microdialisis electrode stereotaxically implanted into the PFC	20%, 40%, 60% and 80% of Max output (0.2, 0.4, 0.6 and 0.8 T)	5 trains of 25 Hz for 1 s with 2 min intervals between trains 1,2,or 3 days	375 (3 days)	Only 3 day rtMS (not acute) = Suppression of 5-HT levels increase induced by the plus-maze test no change on DA levels. → anxiolytic effet of chronic rTMS
[Hedges:2003aa] Model of anxiety	Rats	FOE 5-cm	Chronic rTMS SHAM = click only	hypothalamic–pituitary–adrenal (HPA) function depression behavior	serum ACTH, CORT, testosterone, and luteinizing hormone (LH) concentrations immediately and 1, 3, 5, 7, and 14 days post rTMS Forced swim test	80% MO	15 Hz for 3 s	Once per day for 10 days	↓ immobility times just after TMS but not at day 1,3,5,7,14 ↑ ACTH and CORT concentrations immediatelyafter TMS but not at day1,3,5,7 and 14 no change in testosterone and LH levels → HPA stress axis significantly altered + depression behaviour improved but short term.
[Hedges:2005aa] Model of anxiety + memory No pdf.	Rats			Memory Anxiety behavoir	one-time learning paradigm elevated-plus maze task plus-maze tes	?	?		No memory impairment anxiety-like behavior
[Hargreaves:2005aa] Model of anxiety	Rats Model of anxiety	focal butterfly coil (5-cm inner coil, 7-cm outer winding)	SHAM = coil OFF	anxiety + depression behavior	social interaction, emergence, elevated plus-maze, and predator odor avoidance forced swim test.	130% of MT, 74% of the machine's maximal intensity	4 x 20-Hz for 4 s inter-train interval of 30 s	320 Daily 18 days	No effect on anxiety Mild effect on the immobility (depression)
[Isogawa:2005aa] Model of anxiety	Rat	round coil (4 cm in diameter)	Chronic rTMS SHAM = coil ON + 15cm above head	Anxiety behavior	Elevated plus-maze test + locomotor activity	1.5 times motor thresholds (52-67% MO)	15 Hz for 3.5 s (52 pulses)	10 days	↑ anxiety after rTMS anxiety suppressed by acute treatment with diazepam, alprazolam, or buspirone → chronic rTMS treatment provides a good animal model for anxiety
[Nielsen:2007aa] Motor function	rat	Circular coil 4 cmt		MEP Motoneurons lesions	Latency of motor response + EPSP in motor neurons	?	? single pulse?		MEP responses depend strongly on the coil position and the stimulation intensity EPSPs and MEPs evoked by TMS not mediated by the corticospinal tract, but by other descending motor pathways

Paper	animal	TMS device	Stim	Measure	Recording	Mag	f	Num. pulses	effect
[Kling:1990aa] Memory Structural modifications	Rat No pdf	?	Single pulses	Memory of aversion		?	50 pulse / session		retrograde memory disruption but no effect on anterograd memory. No change in histo
[Li:2007aa] [Li:2007ab] Memory	rat	Circular coil 55 mm diameter, 15 windings	Acute +Chronic rTMS	memory	Morris water maze test	1.0 T	6 trains at 0.5 Hz	300/day 1 day or 10 days	chronic 0.5 Hz rTMS = disrupts spatial short- and long-term reference memory function acute low-frequency rTMS =no deficits in acquisition or short-term spatial reference memory as well as working memory but impaired long-term reference memory. → special care in human studies. . .
[Yamada:1995aa] Memory	monkey	small round S70, large round S100 and FOE butterflyB55	Acute +Chronic rTMS	Memory 30 min after acute rTMS And memory 10 days after chronic 30days rTMS	Monkeys trained in a delayed response task which required spatial short-term memory.	100% MO = 3.3/ 1.9 / 2.4 T	0.2 Hz 0.2Hz daily for 30 days.	100 100/day = 3000	No effect of any of the coils and paradigms on short term memory.
[Wang:1999aa] Memory	Gerbils No pdf								
[Wang:2006aa] [Wang:2006ab] Memory	Gerbils	concentric coil (cone-shaped magnetic field) centred alternately over the left and the right auditory cortex	Acute +Chronic rTMS	Short term and long term memory	Discrimination task = discriminate between upward and downward frequency modulated tones.	3̃ tesla within 4 mm2	5min of 5Hz for 1s, 5s intertrain	1 day of 5 days	strong ↓ short-term memory during days 2–5. (impairs early consolidation) Only if rTMS given just after the learning session but not before. However, performance at the end of the 5 days was the same as controls : learning or long-term memory unchanged
[Wagner:2007ab] Behaviour	cat	50 mm circular coil on VP cortex	Acute rTMS	Effect on visuospatial orientation	simple spatial visual detection task	40% of the MO Ĩ20 - 125% of the cats MT	1Hz for 20 min	1200	↑ mistakes detecting and orienting to contralateral visual targets during the 15–20 min immediately following rTMS Return to baseline 45min after. Still on the baseline level after 24h. → rTMS disrupts a behavioral task, known to depend on VP cortex, for the far periphery of the visual field, but not for more central targets
[Wagner:2007ab] Behaviour			Acute rTMS/ Cumulative sessions of rTMS	Effect on visuospatial orientation	simple spatial visual detection task after each session	40% of the MO Ĩ20 - 125% of the cats MT	1Hz for 20 min	1200	↑ visuospatial neglect-like effect (progressive ↑ 5-10% to 40-50% error levels) and progressive ↑ spatial extent (from 90-75 degrees to 45-30 degrees eccentricity locations) of neglect Return to baseline after each rTMS session

Paper	animal	TMS device	Stim	Measure	Recording	Mag	f	Num. pulses	effect
[Aydin-Abidin:2006aa] **EEG/EP**	cat (area 17)	FOE 2*70mm	rTMS	VEP (1) N1P1amp (2) P1N2 ampl	EcOG on area 17 + electrode on contralateral Occ-Te region	30%	1 Hz 1 min 1 Hz 5 min 1 Hz 20 min 3 Hz 1 min 3 Hz 5 min 3 Hz 20 min 10 Hz 1 min 10 Hz 5 min 10 Hz 20 min	60 300 1200 180 900 1200 120 600	VEP Ø EEG delta power↑ VEP Ø EEG delta power↑ VEP(1) ↓ for 0-5min VEP Ø EEG delta power↑ VEP(1,2) ↓ for 0–10 min VEP(1,2) ↓ for 5–15 min VEP(2) ↑ 0–5 min VEP(2) ↑0–5 min VEP Ø
[Li:2007aa] **EEG/EP**	rat	FOE 2*5 cm	Low frequency rTMS	EEG	ECoG right and left primary motor cortex +primary somatosensory cortex -before rTMS -immediately after sham -immediately rTMS	110% % motor threshold (4T)	100 stimulations at 0.5 Hz	100	↓EEG correlation dimension(D2) ↓absolute power of the gamma band and relative power of the beta and gamma bands
[Sharova:2007aa] **EEG/EP**	rat	?		Electric activity	SEEG in orbitofrontal CA1, and stem at the level of the lateral vestibular nucleus of Deiters	100-200 V/m	3-min /day for 7 days	60–70 Hz	significant increase in the power of biopotentials in most of the brain areas recorded with synchronization of the major baseline EA rhythms – to the extent that bursts of exalted epileptiform activity appeared, maximally in the hippocampus →significant increase in interactions between the cerebral areas studied (coherence) of both symmetrical (stem, hippocampus, and cortex) and unilateral (stem-hippocampal) areas of the brain → Hypersynchronization, identified as a major element in the reactivity to this type of stimulation, may be of the greatest value in the recovery of patients with cerebral pathology in cases with initially reduced levels of intercenter interactions in the absence of pathologically increased functional connections in the brain
[Luft:2001aa] **Motor function**	rat	FOE 5 cm	Single pulses	MEP to TMS (MEPTMS) MEP by electrical stimulation of cervical spinal cord (MEPCES)	subcutaneous electrodes implanted bilaterally over the calf	130% MT 150% MT + 15 different intensities Start 36% below MT, + steps of 7%	ISI = 30 s	20 20	MEPTMS =onset latencies of 6.7±1.3 ms ↓Latency with higher stimulation intensity MEPCES showed a significantly shorter latency 5.29±0.24 →supraspinal origin of the MEPTMS

Paper	animal	TMS device	Stim	Measure	Recording	Mag	f	Num. pulses	effect
[Jenrow:1998aa] EP + motor integrity	Rat + myelin deficient mice	5 cm diameter coil	Single pulses	Electrically + MSEP M-SEP obtained 1 week after lacerating the spinal cord MEP in mice H-reflex with coil placed over the sacrum with the edge at the L4-5 vertebra	ECoG on sensory cortices of rats	M-SSEP 50% maximum intensity in rats MEP at 100% in mice	Not specified		electrically induced SSEP latencies were minimally shorter than those of the M-SSEP Peak-to-peak amplitudes were also similar M-SSEP in which the MS was increased from 10% to 60% intensity showed a decrease in latency and an increase in amplitude M-SSEPs eliminated after selective dorsal column lacerations of the spinal cord → transmitted via this tract M-MEPs on myelin deficient mice = longer onset latencies and smaller amplitudes than in normal mice
[Fleischmann:1999aa] Epilepsy	rat	5 cm diameter coil SHAM = coil off + click	Chronic rTMS	ECS to test seizure parameters at day 11, 17, 21		2,5T	20Hz for 4s 2xday For 16 days	160/day For 16 days	Day 10, Low energy ECS ↓ % rats convulsing vs. Sham but not difference at medium ECS level. Day 17 rTMS-treated animals convulsed significantly less (both at presence/absence of seizures, and at seizure length) Day 21, anticonvulsant effect disappear.
[Ebert:1999aa] Epilepsy	Rat	12.5 cm-diameter circular coil Over Fr. PA region SHAM = coil on tilted 90° + 20 cm distance from the skull	Acute rTMS	recording/stimulation electrode stereotaxically positioned in the right basolateral amygdale for kindling		120 A/μs = > MT	20 Hz for 3s		single rTMS train has a long-term effect on seizure susceptibility in the amygdale significant ↓ of limbic seizure susceptibility 14 days after rTMS. But no influence of rTMS on kindling acquisition starting two weeks after the magnetic stimulation
[Jennum:1996aa] Epilepsy	rat	13-cm coil	Acute + chronic	pentylenetrazole (PTZ)-induced clonic seizures		90 and 150% MT 90% MT	50 Hz for 5 s 50 Hz for 1 or 5s	30 days	Acute : No differences were observed in time to onset of clonic seizures after PTZ injection compared to control rats chronic : ↓ Time to onset of PTZ clonic seizures with a stimulus duration of 1s and 5s → daily stimulations have a facilitatory effect on seizure induction.
[Akamatsu:2001aa] Epilepsy	rat	8-cm round coil 1cm above Pa bone SHAM = coil on 20cm above head	acute	pentylenetrazole (PTZ)-induced clonic seizures		200% MT	0.5 Hz 33 min	1000	long train of 0.5 Hz-rTMS significantly decrease seizure susceptibility in PTZ-induced myoclonic and tonic-clonic convulsive seizures in rats. Evidence of the decreased susceptibility to the PTZ-induced seizures are based on the prolonged seizure latencies and decreased rate of developing convulsive status epilepticus
[Lisanby:2001ab] Epilepsy	No pdf access								

Paper	animal	TMS device	Stim	Measure	Recording	Mag	f	Num. pulses	effect
[Anschel:2003aa] Epilepsy	rat		chronic	Electrode stereo-taxically positioned ventricule for CSF injection - artificial CSF - Human CSF	Human CSF obtained from 2 patients with medication-resistant depression +left or right pre-frontal rTMS at a stimulation frequency of 1 or 10 Hz.	90% of the patient's motor threshold	1) CSF from a man treated daily with 1 Hz-rTMS contin-uous train for 26.6 min duration 2) CSF from a man treated daily with 20 trains of 10 Hz rTMS for 8 s inter-train interval 22 s	1600 Stimuli / day for 8 days	CSF 10Hz : trend toward an increased kindling rate. CSF 1 Hz : significant ↓ kindling rate (but at day 1 not later)
[Rotenberg:2008aa] Epilepsy	rat	8 cm hand-held figure-8 coil centered overhead - sham rTMS =tail at 70% MO - untreated			intraperitoneal kainic acid for seizure induction After KA injection, baseline EEG col-lected for 60 min . At 60 min following KA injection, EEG-guided rTMS is initiated	(1) active rTMS 90% MO (2) sham rTMS =tail at 70% MO	seizures treated per either 0.25Hz, 0.5Hz or 0.75Hz	vari-able	KA-induced seizures were abbreviated by 0.75 Hz (P = 0.019) and 0.5 Hz (P = 0.033) active EEG guided rTMS. Neither active 0.25 Hz rTMS nor the control conditions affected seizure duration (P > 0.2)

Table 5.1 – TMS in animals—literature summary.

3   Stimulation coils in animals: examples [FW]

	[Liebetanz:2003aa]
	[Sauvage:2008aa]
	[Valero-Cabre:2005aa] *Coil unilaterally targeting the parietal cortex*
	[Ogiue-Ikeda:2003ab]
	[Rotenberg:2008aa] *"Rat with torso restraint. Torso restraint permits clinical observation of seizures and full access of head to the TMS coil. Access to the rat's tails for sham TMS is also available. Subdermal wire EEG electrodes (arrows) were placed after restraint. In our experience, unanesthetized rats tolerate the restraint and electrode placement with minimal discomfort"*

4   The Poisson equation: toy models [GR]

4.0.1   Toy model 1: a 1D circuit

Consider a toy example with a simple circuit in 1D (see Figure 5.2). A battery provides a driving voltage V, and there is a single wire connecting the two battery electrodes. This wire has a variable resistivity $r(s)$ (Ohms/m), where s is the path length. The current is everywhere I. We now show that the established current I leads to a nonzero charge density.

At any point in the wire, $\vec{E} = E\hat{s}$ only (we use here arrows to make directions explicit, the hat denoting a unit vector pointing along the wire). If this was not the case, charges would continuously accumulate at the wire boundaries—which is not the case in steady state. At any given point in the wire, we have the potential drop

$$dV = -I\,rds, \tag{5.1}$$

and the E field is simply

$$\vec{E} = -\frac{dV}{ds}\hat{s} = I\,r\hat{s}. \tag{5.2}$$

Hence

$$\nabla \cdot E = \partial_s E = I\,r'(s) = 4\pi\rho\epsilon, \tag{5.3}$$
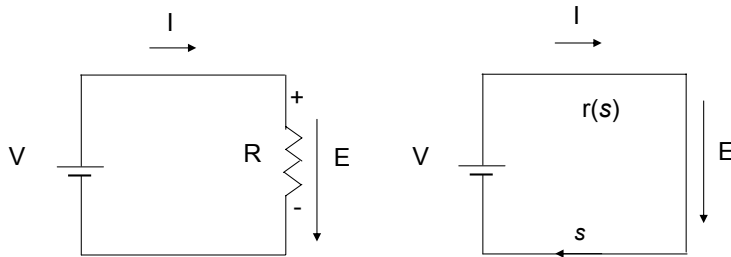
Figure 5.2 – Toy models to illustrate that variations in conductivity lead to charge accumulations. On the left a typical circuit is shown. There is a conductivity discontinuity at the wire-resistor boundary, where charges will accumulate.
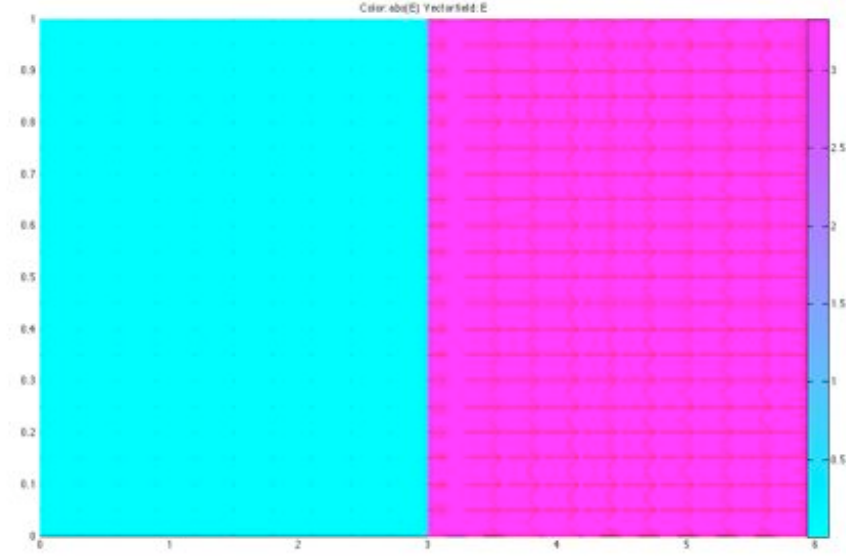
Figure 5.3 – Simple interface with two different media and conductivities differing by a factor of 1000. There is a conductivity discontinuity at the boundary of the two media, where charges will accumulate under an electric field. The arrows and color show the electric field.

and

$$\rho = \frac{\epsilon}{4\pi} I\, r'(s). \tag{5.4}$$

Using

$$V = IR, \quad R = \int_0^L ds\, r, \tag{5.5}$$

we can write

$$\rho = \frac{\epsilon}{4\pi} \frac{V}{R}\, r'(s). \tag{5.6}$$

Summary: *under steady state, spatial conductivity variations lead to charge accumulations, which then lead to E fields and potentials. When the resistivity increases along the current, positive charge density appears (and viceversa).* Note here that the resistivity derivative can be both positive or negative, leading to positive or negative charge density.

4.0.2 Toy model 2: 2D conductive media interface

Consider next the analogous 2D situation in which again there are no impressed currents. Two large parallel conductive plates are set at 10 and 0 V, and the current normal to the surface is set to zero in the top and bottom sides (Newmann boundary conditions). Between them we have conductive media with different conductivities (one 1000 larger than the other). As can be seen in Figure 5.3, the electric field rises sharply at the interface. Since the only component of the field is in the horizontal direction, the divergence of the field is directly the derivative of the field, and this is the charge density, which is therefore seen to be positive at the junction.
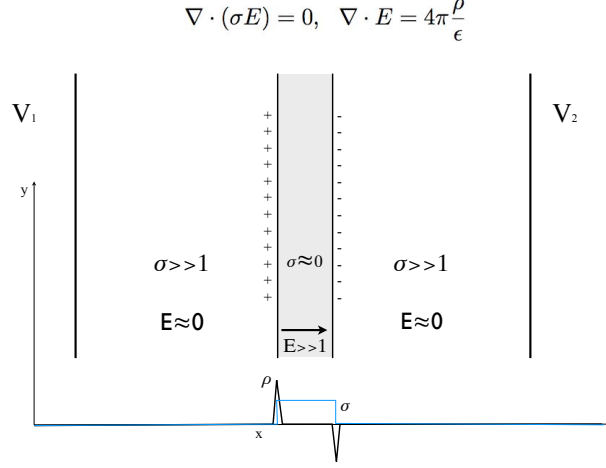
Figure 5.4 – Simple interface with three different media and conductivities differing by a large factor in the middle layer (the others being equal). There is a conductivity discontinuity at the media boundaries, where charges will accumulate under an electric field—first positive, then negative. Charge density and conductivity schematic plots are provided in the bottom.

4.0.3   Toy model 3: 2D double junction

A slightly more interesting example is provided by a double junction—as in a membrane—because the electric field x-component first rises (positive horizontal derivative, then falls (negative)—see Figure 5.4 and Figure 5.5. Thus, we have positive then negative charge densities. The two equations that govern the situation are again

$$\nabla \cdot (\sigma E) = 0, \quad \nabla \cdot E = 4\pi \frac{\rho}{\epsilon} \tag{5.7}$$

The first is a consequence of current conservation under steady state and Ohm's law and the second is Coulomb's law in differential form. In the 2D situation we are considering, the field has only an x-component ($E_y = 0$). Therefore, we can rewrite the first equation as

$$\frac{\partial \sigma}{\partial x} E_x + \sigma \frac{\partial E_x}{\partial x} = 0 \tag{5.8}$$

which we can easily solve to

$$E_x = A \frac{1}{\sigma} = Ar \tag{5.9}$$

with A a constant to be fixed by the boundary conditions (by requiring that the integral of the field in the middle layer be the specified potential difference ΔV), and therefore

$$\rho = \frac{A\epsilon}{4\pi} \frac{\partial r}{\partial x} \tag{5.10}$$
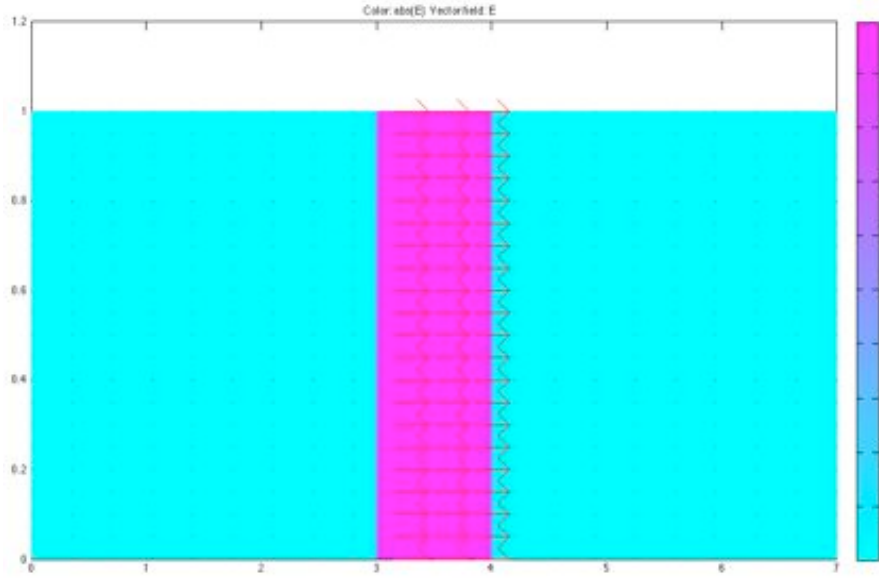
Figure 5.5 – Simple interface with three different media and conductivities differing by a factor of 1000 in the middle layer (the others being equal). There is a conductivity discontinuity at the media boundaries, where charges will accumulate under an electric field—first positive, then negative. The arrows and color show the electric field.

Suppose that the resistivity is a square function (first zero, then 1, then 0 again). The charge density is concentrated at the boundaries in the form of two Dirac delta functions (the first positive, the second negative). The electric field is constant inside the membrane—see Figure 5.5 and Figure 5.7. More generally, let the membrane's thickness be δ. Then $A = \Delta V / \int_0^\delta r dx$ and

$$\rho = r'(x) \frac{\Delta V}{\int_0^\delta r dx} \frac{\epsilon}{4\pi}, \quad E = \Delta V \frac{r(x)}{\int_0^\delta r(x) dx}$$

to ensure that the voltage drop across the membrane is as it should.

If the conductivity is constant in the membrane we can write

$$\rho \approx r'(x) \frac{\Delta V}{\delta} \frac{\epsilon}{4\pi}, \quad E \approx \frac{\Delta V}{\delta}$$

4.0.4 Toy model 4: 2D neuron in conductive medium

Finally, a simplified model of a neuron of diameter $2R$ in a bath and under a constant external field is depicted in Figure 5.7. Half of the potential drop is carried by each of the two membranes (equally, by symmetry). Firs we note that since the total field inside the fiber is approximately zero (no current flows in the sealed neuron), the secondary field induced inside and associated to charge in the membranes must equal the primary external field with a sign change (so that the total field inside is zero). If we imagine going around the fiber (outside) from one side to the other, we will experience a potential drop of about $\Delta V \approx 2RE_{\text{ext}}$. The same drop has to result if we take another path through the fiber (the electric field is locally conservative on these scales, even if it is the result a magnetic induction this is a good approximation). Since the field inside the fiber is null, each crossing in the membrane must produce potential change of $\Phi_m \approx RE_{\text{ext}}$.
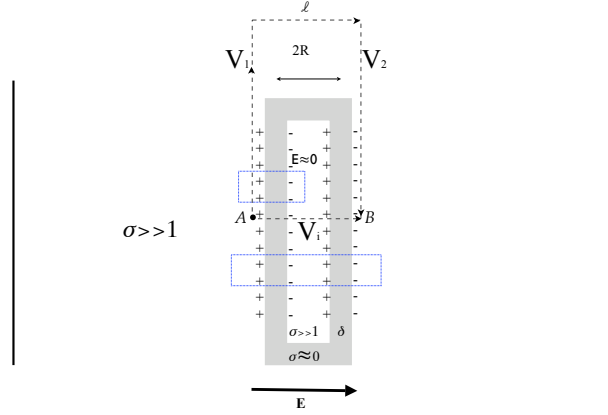
Figure 5.6 – Simplified model of a neuron in a bath and under a constant external field. Half of the potential drop is carried by each membrane portion. Blue pillboxes are shown which can be used to see that the total charge in the membrane is not zero (the field is zero inside but non-zero outside, top pillbox), or that the charges are equal and opposite in each side (bottom pillbox). Also, a conservative path is shown (l) to illustrate the potential drop experienced crossing the fiber from side to side, from point A to point B, which must equal $V_2 - V_1 \approx 2RE$, roughly the isopotentials on each side of the fiber.

We also observe that there is an overall excess of charge on each side, which cancel each other.

This is an important example, as it shows the importance of terminations and spatial scales.

4.0.5 Toy model 4: Stimulating a brain slice

In this last example we consider a situation close to that in an in-vitro experiment. We have a surface with constant conductivity and where we can independently control the currents between 2 pairs of opposite plates. As can be observed, this allows for the creation of a uniform field with arbitrary orientation.
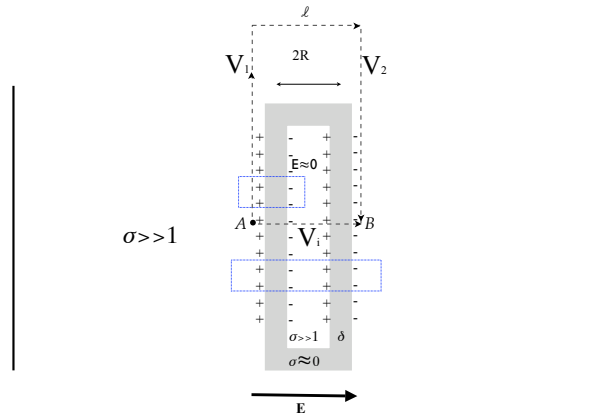
Figure 5.7 – In this figure we show the field (arbitrary units) for a slice 2x4 mm where there are two sets of current sources/drains (top/bottom and left/right) tuned to give an inclined field. The use of independent current bipolar setups allows for easy orientation of the field, as explained in Starlab TN00162.

5   The quasi-static approximation in more detail [GR]

To further understand the quasi-stationary assumption, we follow [Plonsey:1969aa] and write a Fourier decomposition of the impressed currents in time. That is, consider the impressed current frequency component $J_\omega^I(x)$—we compute this Fourier transform point by point in space. The we have the Helmolz equations for the scalar and vector potentials,

$$A_\omega = \frac{\mu}{4\pi} \int_V dV \, \frac{J_\omega^I}{R} \, e^{i\kappa R}, \tag{5.11}$$

and

$$\Phi_\omega = \frac{1}{4\pi(\sigma + i\omega\epsilon)} \int_V dV \, \frac{-\nabla \cdot J_\omega^I}{R} \, e^{i\kappa R}, \tag{5.12}$$

with, $\kappa^2 = -i\omega\mu\sigma_c$ and $\sigma_c = \sigma(1 + i\omega\epsilon/\sigma)$, leading to the usual

$$E_\omega = -\nabla\Phi_\omega + i\omega A_\omega. \tag{5.13}$$

We see that we have used the expression for the charge density derived above in the potential integral expression.

Given the properties of living tissues, some approximations can be made to previous equations. Given the equation $\sigma_c = \sigma(1 + i\omega\epsilon/\sigma)$, where the complex part is the capacitive factor. To avoid capacitive effects this quantity has to be essentially real, that is:

$$\omega\epsilon/\sigma << 1. \tag{5.14}$$

Table 2.1 gives de value of this factor for different living tissues. At physiological frequency range (less than 1000 Hz), condition (5.14) is followed. *The values of this ratio at 10 Hz, which do not appear to be completely negligible, are reported to be conservative, and the conclusion of Schwan and Kay is that the medium can be considered to be resistive* (literally from [Plonsey:1969aa]).Within this, capacitive effects can be ignored.

On the other hand, propagation effects can be negligible if the exponential in 5.12 can be approximated to the unit. The Taylor expression of this exponential is:

$$e^{-i\kappa R} = 1 - i\kappa R - \frac{(\kappa R)^2}{2!} - i\frac{(\kappa R)^3}{3!} \tag{5.15}$$

Therefore exponential could be close to unity if $\kappa R_{max} << 1$. This assumption is true for typical physiological problems. Typical frequencies we are concerned about are less than 1 kHz. The relative permittivity of the brain is 50 times the one in the vacuum, therefore the light speed in brain is $\sim$7 times less. The typical wavelengths will be in the order of 40 km.

Finally we need to study inductive effect, that is, those related with $i\omega A_\omega$ term in (5.13).We could neglect inductive effects if $|\omega A_\omega| << |\nabla\Phi_\omega|$. It can be shown that [Plonsey:1969aa]

$$\left| \frac{\omega A}{\nabla\Phi_\omega} \right| = |\kappa R|^2 \tag{5.16}$$

and, as justified before, this value is more less than the unity (0.0032 for some typical applications). Therefore inductive effects can be neglect. A summary of those conditions is summarized in Table 2 [Plonsey:1969aa].

Condition	Criteria
Neglect propagation effects	$\kappa R_{max} << 1$
Neglect capacitance effects	$\omega \epsilon / \sigma << 1$
Neglect inductive effects	$(\kappa R_{max})^2 << 1$

Table 5.3 – Criteria for simplifications (from [Plonsey:1969aa])

These equations basically mean that we assume we have long wavelengths (low frequencies) and the sources are in the brain (which they are in EEG) and hence very close measured in wavelengths. Then we can write

$$A_\omega \approx \frac{\mu}{4\pi} \int_V dV \, \frac{J_\omega^I}{R}, \tag{5.17}$$

$$\Phi_\omega \approx \frac{1}{4\pi\sigma} \int_V dV \, \frac{-\nabla \cdot J_\omega^I}{R}, \tag{5.18}$$

and (see [Plonsey:1969aa] for experimental justification)

$$E_\omega \approx -\nabla \Phi_\omega. \tag{5.19}$$

Note that there is no ω dependence left in the potential and field.

6 Equations and boundary conditions on E [GR]

We work here under the quasi-stationary conditions.

6.1 The equations

We write here Maxwell's equations and others relevant to the problem.

Ohm's law

This is relationship for an isotropic medium, stating that

$$J = \sigma E, \tag{5.20}$$

where σ is the conductivity.

Maxwell's equations

Here they are (using Jackson units [Jackson:1962aa], see section I.4)

$$\nabla \cdot B = 0, \quad \nabla \cdot E = 4\pi \frac{\rho}{\epsilon},$$

$$\nabla \times B = \frac{\epsilon}{c\mu} \frac{\partial E}{\partial t} + \frac{4\pi}{c\mu} J, \quad \nabla \times E = -\frac{1}{c} \frac{\partial B}{\partial t}. \tag{5.21}$$

I: Using Ohm's law in the third equation we can write

$$\nabla \times B = \frac{\epsilon}{c\mu\sigma} \frac{\partial J}{\partial t} + \frac{4\pi}{c\mu} J, \tag{5.22}$$

and if we write $J = J(x) \exp i\omega t$, we have

$$\nabla \times B = \frac{\epsilon\omega}{c\mu\sigma} J(x) + \frac{4\pi}{c\mu} J(x). \tag{5.23}$$

II: If $\epsilon\omega/\sigma << 1$, we can drop the displacement current term, and use

$$\nabla \times B \approx \frac{4\pi}{c\mu} J \tag{5.24}$$

in general, which allows us to state that $\nabla \cdot J \approx 0$. Thus, ignoring the displacement current term implies that $\dot{\rho} = 0$ (known as steady-state condition). This is a valid approximation if the current time scales (spectrum) are reasonably bounded. In fact, to get a better physical feeling about the implications of this assumption, as described in [Heller:1992aa], we can use $J = \sigma E$ and the continuity equation to write

$$4\pi\sigma\rho/\epsilon + \frac{\partial \rho}{\partial t} = 0$$

in a region of constant conductivity. Thus, we see that $\sigma/\epsilon = \tau$ is a "relaxation" or diffusion time scale. As discussed in [Heller:1992aa], this time scale is of the order of a nano second. Therefore, for the frequencies of interest in bioelectric phenomena or stimulation under slow changing fields, we can drop the displacement current term and assume steady-state.

III: We can now us the vector identity

$$\nabla \times \nabla \times A = \nabla(\nabla \cdot A) - \nabla^2 A$$

and take the curl of the last of Maxwell's equations above,

$$\nabla \times E = -\frac{1}{c}\frac{\partial B}{\partial t}$$

to write

$$\nabla(\nabla \cdot E) - \nabla^2 E = -\frac{1}{c}\frac{\partial \nabla \times B}{\partial t}$$

or

$$\frac{4\pi}{\epsilon}\nabla\rho - \nabla^2 E = -\frac{\epsilon}{c^2\mu}\frac{\partial^2 E}{\partial t^2} - \frac{4\pi}{c^2\mu}\frac{\partial J}{\partial t}$$

Now, the first term in the RHS has to do with propagation. If the spatial scales are small compared to the wavelengths involved, we can ignore it (and we do). The second term is part of the aforementioned diffusion process (see [Jackson:1962aa] section 5.18, p 219). Moreover, since we are mostly concerned here with focusing of impressed fields, we can assume we are creating these fields in the vacuum. It is clear than in the vacuum we can approximate

$$\nabla^2 E \approx 0$$

i.e., harmonicity. Note that the total field satisfies

$$\frac{4\pi}{\epsilon}\nabla\rho - \nabla^2 E \approx 0$$

Indeed, when the conductivity is not constant, we have charge densities and local maxima of the total field are indeed possible.

The current continuity equation

The current continuity condition is expressed by

$$\nabla \cdot J + \frac{\partial \rho}{\partial t} = 0. \tag{5.25}$$

and is a consequence of Maxwell's equations [Jackson:1962aa].

The solenoidal condition

As mentioned, this states that the current is basically the curl of a field (B), and hence its divergence is null.

$$\nabla \cdot J = 0. \tag{5.26}$$

By the continuity equation, it also implies that $\partial_t\rho = 0$.

6.2 BC: The potential Φ must be continuous

We want to have finite electric fields. Therefore the potential field needs to be continuous.

6.3   BC: The normal component of the E field is discontinuous

Using

$$\nabla \cdot E = 4\pi\rho/\epsilon \tag{5.27}$$

in integral form, with Q the charge,

$$4\pi Q/\epsilon = \int_V dV \, \nabla \cdot E = \oint_S E \cdot dS = \Delta E_n \, S, \tag{5.28}$$

leading to

$$\Delta E_n = \frac{4\pi}{\epsilon} \frac{Q}{S}. \tag{5.29}$$

6.4   BC: The tangential component of the E must be continuous

Using

$$\nabla \times E = 0 \tag{5.30}$$

in integral form,

$$\oint E \cdot dl = 0 \tag{5.31}$$

and using the usual loop argument with very short sides, we reach the conclusion that the tangential component of the electric field must be continuous.

6.5   BC: The normal component of J must be continuous

We use here the (approximate) equation

$$\nabla \cdot J = 0 \tag{5.32}$$
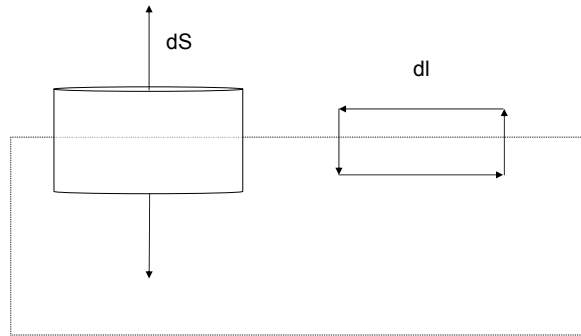
Figure 5.8 – Geometry for "pillbox" discussion on boundary conditions.

in integral form

$$\oint_S J \cdot dS = 0 \tag{5.33}$$

to reach the conclusion that the normal component of the current must be continuous. This implies that $J_z = 0$ at a boundary with zero conductivity, for instance.

6.6   On the terms irrotational and solenoidal

Again, referring to Jackson [Jackson:1962aa], any vector field can be written as the sum of two terms,

$$J = J_l + J_t, \tag{5.34}$$

where $\nabla \times J_l = 0$ and $\nabla \cdot J_t = 0$. The first term is called *longitudinal/irrotational*, while the second is called *solenoidal*.

7   Harmonic fields [GR]

7.1   Uniform conductivity media

We note here the important result that at the low frequencies considered here it is not possible to focalize the electric field in a **constant conductivity medium** so that a local maximum or minimum is attained [Heller:1992aa]. This follows from the fact that inside a constant conductivity region the electric field components are harmonic ($\nabla^2 E_i \approx 0$, see the Annex). The limitation of constant conductivity is rather unrealistic, so we will revisit this point.

Suppose $f(x)$ and $g(x)$ are harmonic functions in 2D, that is, $\nabla^2 f(x) = \nabla^2 g(x) = 0$. Clearly, any linear combination of these functions will also be harmonic.

It may be useful to remember here that **the Laplacian of the function is the trace of the Hessian of the function**[1] Also, since we are looking for maxima, we recall that If the Hessian is negative definite at x, then f attains a local maximum at x.

What can we say about $w(x) = f(x)^2$?

$$\nabla^2 w(x) = \nabla \cdot \nabla \, w(x) = \nabla \cdot (2f(x)\nabla f(x))$$

We now use the identity

$$\nabla(\psi E) = E \cdot \nabla \psi + \psi \nabla \cdot E$$

to write

$$\nabla^2 w(x) = \nabla \cdot (\nabla f(x)^2) = \nabla \cdot (2f(x)\nabla f(x))$$
$$= 2(\nabla f \cdot \nabla f + f \nabla^2 f) = 2||\nabla f||^2 \geq 0$$

So we see that if f is harmonic, f^2 will not be, in general. In fact we see that the Hessian of f^2 has a positive trace.

In fact, the first derivative of $w(x) = f(x)^2$ is

$$\nabla w(x) = 2f(x)\nabla f(x)$$

This will be zero if either f or ∇f are zero. So although f does not have an extremum, f^2 may at $f = 0$. Moreover, at that point the laplacian is positive (assuming $\nabla f \neq 0$), and therefore the locus is not a maximum. It could be a minimum or saddle point.

To summarize: let $f(x)$ be a harmonic function and therefore with no maxima or minima except at the boundaries. The function $w(x) = f(x)^2$ is in general not harmonic, and $\lambda_1 + \lambda_2 \geq 0$, that is, the trace of the Hessian is greater or equal to zero.

What about $u(x) = f(x)^2 + g(x)^2$? The first derivative is

$$\nabla u(x)^2 = 2f(x)\nabla f(x) + 2g(x)\nabla g(x)$$

and setting it to zero implies

$$\frac{f(x)}{g(x)} = -\frac{\nabla g(x)}{\nabla f(x)}$$

which a priori seems to have interesting solutions. The second derivative is

$$\nabla^2 u^2 = 2||\nabla f||^2 + 2||\nabla g||^2 \geq 0$$

---

[1]The Hessian of a function is the matrix $\partial_i \partial_j f(x)$.

For an extremum to be a minimum we need its Hessian to be positive definite (all eigenvalues positive). What the previous equation tells us is the trace of the Hessian is greater or equal to zero. This does not imply positivity of the Hessian. But clearly the sum $u(x)$ cannot have a maximum either—this would imply $\nabla^2 u^2 = 2||\nabla f||^2 + 2||\nabla g||^2 < 0$ (if the Hessian is negative definite its trace will be negative).

Thus, neither the sum of harmonic functions, nor the sum of squares of harmonic functions can attain local maxima outside their boundaries.

Despite the strong nature of this conclusion, there is an important caveat in our problem, and that is the fact that we are dealing with non-uniform conductive media.

7.2 Non-uniform conductivity media

The brain conductivity field is definitely non-uniform, and therefore the electric field is not really harmonic. In [Ferdjallah:1996aa] (see Figure 5.9) several values for the conductivity are provided for the different layers in the brain, and it is generally assumed that the conductivity is constant in each region. Of course, the brain is not spherical, and each layer has its geometry. Of special interest is the cortex, with a complex geometry (sulci and gyri).

What this means is that, since the electric field is harmonic within each region of constant conductivity, that as far as the cortical region is concerned, the maxima will occur on the outer part of the cortex. In principle, it should be possible to modulate where the maxima occur, but **maxima will reside in the outer layer of the cortex.**

In order to exploit this, E field simulations carried out within HIVE could also use MRI data to define the $n(x)$ field in the cortex, and using that to create and excitation map for different stimulation set ups.

7.3 Conclusions on the relevance of harmonic functions properties on stimulation

With regards to the issue of relevance of harmonic conditions on stimulation we can conclude:
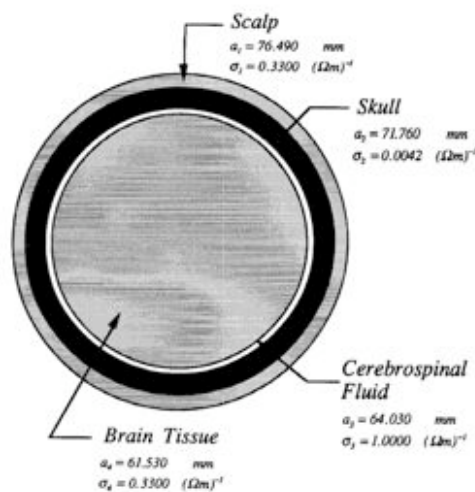
Figure 5.9 – Conductivities in different brain regions (from [Ferdjallah:1996aa] Fig 1).

- The electric field in uniform conductivity media is harmonic (in the quasi-static approximation).

- Harmonic functions can only attain maxima or minima at their boundaries.

- Monotonic functions of harmonic functions can only attain maxima or minima at their boundaries.

- Sums of monotonic functions of harmonic functions can only attain maxima at their boundaries.

- In particular, neither the sum of fields nor the sum of their squares can produce local maxima inside regions of constant conductivity.

- In the brain, maximal of field strength in the cortex will occur at the cortex outer boundary. The same can be said of excitation, assuming that the excitation function is a monotonic function of the field vector. This may not be the case (e.g., as excitation depends also on the orientation of the target neurons).

- In general, however, excitation will be a function of field and neuron orientation, and this function may have many local maxima, as it will not be in general monotonic.

Bibliography

[Abdeen:1994aa] Mohammed A. Abdeen and Maria A. Stuchly. Modeling of magnetic field stimulation of bent neurons. *IEEE Transactions on Biomedical Engineering*, 41(11):1092–1095, 1994.

> **Abstract:** We consider a simple model of magnetic stimulation of a long bent neuron located in a semi-infinite volume conductor with a planar interface. It is shown that the stimulating coil characteristics (size, shape and location) and the neuron shape affect the location of the stimulation. The activating function, defined as the electric field derivative along the neuron, has two components. One component depends on the derivative of the electric field along the straight section of the neuron, and the other on the field magnitude. The maximal stimulation point is at the bent part of the nerve and its position depends on the nerve shape and coil parameters. The analysis also has shown a better performance (a stronger stimulus) for a double-circular (figure eight) coil than for a double-square coil.

35, 41, 54, 61

[Abraham:1993aa] W. C. Abraham, S. E. Mason, J. Demmer, J. M. Williams, C. L. Richardson, W. P. Tate, P. A. Lawlor, and M. Dragunow. Correlations between immediate early gene induction and the persistence of long-term potentiation. *Neuroscience*, 56(3):717–27, 1993.

> **Abstract:** The duration of long-term potentiation in the dentate gyrus of awake rats was examined following systematic manipulation of the number of stimulus trains delivered. This was correlated with the induction of immediate early genes in separate groups of animals given identical stimulus regimes. Following 10 trains of stimulation, long-term potentiation decayed with a time constant of up to several days (long-term potentiation 2), and this correlated with the appearance of an increase in the messenger RNA and protein levels of zif/268. Increasing the number of stimulus trains resulted in a greater probability of eliciting long-term potentiation with a time constant of several weeks (long-term potentiation 3), as well as increasing the induction of zif/268, c-Jun, Jun-B, Jun-D and Fos-related proteins. When 10 trains were delivered repeatedly on up to five consecutive days, only the zif/268 protein levels showed associated changes. These data provide support for the hypothesis that long-term potentiation 3 involves mechanisms additional to those for long-term potentiation 2. One possible mechanism is altered gene expression, initiated by immediate early gene transcription factors such as zif/268 and possibly homo- or heterodimers of Fos and Jun family members, that then contributes to the stabilization or maintenance of long-term potentiation 3.

114

[Abraham:1994aa] W. C. Abraham, B. R. Christie, B. Logan, P. Lawlor, and M. Dragunow. Immediate early gene expression associated with the persistence of heterosynaptic long-term depression in the hippocampus. *Proc Natl Acad Sci U S A*, 91(21):10049–53, 1994.

> **Abstract:** Long-term depression (LTD) of synaptic efficacy is likely to be as important in memory processing as the more well-known long-term potentiation (LTP). The case for LTD serving as a memory mechanism, however, requires that it be shown to persist across days or weeks at least. Here we examined the persistence of heterosynaptic LTD in the medial and lateral perforant path inputs

to the dentate gyrus in awake rats and correlated this persistence with the degree of immediate early gene expression as assessed immunohistochemically. Rats were chronically implanted with separate stimulating electrodes in the medial and lateral perforant paths and an extracellular field potential recording electrode in the dentate hilus. After recovery from surgery, either the medial or the lateral perforant path was tetanized with 400-Hz trains, and homosynaptic LTP and heterosynaptic LTD were followed across time. Heterosynaptic LTD was shown to occur readily in awake animals and to persist across days or weeks, depending on the stimulation protocol. The persistence of LTD and LTP was highly correlated within animals. Additional animals, given the same tetanization protocols, showed that the greatest immediate early gene expression occurred following that protocol which consistently gave the longest-lasting LTP and LTD. These data support the proposed role of LTD in memory processing but question whether immediate early genes are important for the persistence of LTP, LTD, or both.

114

[Adrian:1934aa] E. D. Adrian and B.H.C. Matthews. The berger rhythm: potential changes from the occipital lobes in man. *Brain*, 57:355–384, 1934. 136

[Ahmed:2006aa] Z. Ahmed and A. Wieraszko. Modulation of learning and hippocampal, neuronal plasticity by repetitive transcranial magnetic stimulation (rtms). *Bioelectromagnetics*, 27(4):288–94, 2006.

Abstract: The influence of high-frequency repetitive transcranial magnetic stimulation (rTMS) on learning process in mice and on neuronal excitability of the hippocampal tissue obtained from stimulated animals were investigated. While the stimulation with rTMS at higher frequency (15 Hz) improved animals' performance in novel object recognition test (NOR), lower frequency (1 and 8 Hz) impaired the memory. The effect was observed when evaluated immediately after rTMS exposure and declined with time. In parallel to the results of behavioral test, there was a significant enhancement of the synaptic efficiency expressed as of the long-term potentiation (LTP) recorded from hippocampal slices prepared from the animals exposed to 15 Hz rTMS. The stimulation with 1 and 8 Hz had no influence on the magnitude of LTP. Our results demonstrate that rTMS modifies mechanisms involved in memory formation. The effects of rTMS in vivo are preserved and expressed in the hippocampus tested in vitro.

114, 115, 116, 168, 341

[Akamatsu:2001aa] N. Akamatsu, Y. Fueta, Y. Endo, K. Matsunaga, T. Uozumi, and S. Tsuji. Decreased susceptibility to pentylenetetrazol-induced seizures after low-frequency transcranial magnetic stimulation in rats. *Neurosci Lett*, 310(2-3):153–6, 2001.

Abstract: We studied the effects of low-frequency repetitive transcranial magnetic stimulation (rTMS) on seizure susceptibility in rats. rTMS of 1000 pulses at 0.5 Hz led to a prolonged latency for seizure development after an intraperitoneal injection of pentylenetetrazol. The rTMS effectively prevented the development of status epilepticus of pentylenetetrazol-induced convulsions. These findings indicate that low-frequency rTMS affects the neural excitability, in the direction of anticonvulsive, and therefore, suggest the possibility of therapeutic use of rTMS in epilepsy.

118, 119, 176, 341

[Akhtari:2002aa] M. Akhtari, H. C. Bryant, A. N. Mamelak, E. R. Flynn, L. Heller, J. J. Shih, M. Mandelkern, A. Matlachov, D. M. Ranken, E. D. Best, M. A. DiMauro, R. R. Lee, and W. W. Sutherling. Conductivities of three-layer live human skull. *Brain Topogr*, 14(3):151–67, 2002.

Abstract: Electrical conductivities of compact, spongiosum, and bulk layers of the live human skull were determined at varying frequencies and electric fields at room temperature using the four-electrode method. Current, at higher densities that occur in human cranium, was applied and withdrawn over the top and bottom surfaces of each sample and potential drop across different layers was measured.

We used a model that considers variations in skull thicknesses to determine the conductivity of the tri-layer skull and its individual anatomical structures. The results indicate that the conductivities of the spongiform (16.2-41.1 milliS/m), the top compact (5.4-7.2 milliS/m) and lower compact (2.8-10.2 milliS/m) layers of the skull have significantly different and inhomogeneous conductivities. The conductivities of the skull layers are frequency dependent in the 10-90 Hz region and are non-ohmic in the 0.45-2.07 A/m2 region. These current densities are much higher than those occurring in human brain.

18

[Akhtari:2006aa] M. Akhtari, N. Salamon, R. Duncan, I. Fried, and G. W. Mathern. Electrical conductivities of the freshly excised cerebral cortex in epilepsy surgery patients; correlation with pathology, seizure duration, and diffusion tensor imaging. *Brain Topogr*, 18(4):281–90, 2006.

Abstract: The electrical conductivities (sigma) of freshly excised neocortex and subcortical white matter were studied in the frequency range of physiological relevance for EEG (5-1005 Hz) in 21 patients (ages 0.67 to 55 years) undergoing epilepsy neurosurgery. Surgical patients were classified as having cortical dysplasia (CD) or non-CD pathologies. Diffusion tensor imaging (DTI) for apparent diffusion coefficient (ADC) and fractional anisotropy (FA) was obtained in 9 patients. Results found that electrical conductivities in freshly excised neocortex vary significantly from patient to patient (sigma = 0.0660-0.156 S/m). Cerebral cortex from CD patients had increased conductivities compared with non-CD cases. In addition, longer seizure durations positively correlated with conductivities for CD tissue, while they negatively correlated for non-CD tissue. DTI ADC eigenvalues inversely correlated with electrical conductivity in CD and non-CD tissue. These results in a small initial cohort indicate that electrical conductivity of freshly excised neocortex from epilepsy surgery patients varies as a consequence of clinical variables, such as underlying pathology and seizure duration, and inversely correlates with DTI ADC values. Understanding how disease affects cortical electrical conductivity and ways to non-invasively measure it, perhaps through DTI, could enhance the ability to localize EEG dipoles and other relevant information in the treatment of epilepsy surgery patients.

17

[Albensi:2007aa] B. C. Albensi, D. R. Oliver, J. Toupin, and G. Odero. Electrical stimulation protocols for hippocampal synaptic plasticity and neuronal hyper-excitability: are they effective or relevant? *Exp Neurol*, 204(1):1–13, 2007.

Abstract: Long-term potentiation (LTP) of synaptic transmission is a widely accepted model that attempts to link synaptic plasticity with memory. LTP models are also now used in order to test how a variety of neurological disorders might affect synaptic plasticity. Interestingly, electrical stimulation protocols that induce LTP appear to display different efficiencies and importantly, some may not be as physiologically relevant as others. In spite of advancements in our understanding of these differences, many types of LTP inducing protocols are still widely used. In addition, in some cases electrical stimulation leads to normal biological phenomena, such as putative memory encoding and in other cases electrical stimulation triggers pathological phenomena, such as epileptic seizures. Kindling, a model of epileptogenesis involving repeated electrical stimulation, leads to seizure activity and has also been thought of, and studied as, a form of long-term neural plasticity and memory. Furthermore, some investigators now use electrical stimulation in order to reduce aspects of seizure activity. In this review, we compare in vitro and in vivo electrical stimulation protocols employed in the hippocampal formation that are utilized in models of synaptic plasticity or neuronal hyperexcitability. Here the effectiveness and physiological relevance of these electrical stimulation protocols are examined in situations involving memory encoding (e.g., LTP/LTD) and epileptiform activity.

95

[Albert:1966aa] D. J. Albert. The effect of spreading depression on the consolidation of learning. *Neuropsychologia*, 4(1):49–64, 1966.

> **Abstract:** The consolidation of an interhemispherically transferred avoidance response was studied using spreading depression to control transfer and consolidation times. Transmission of the learning required 3 min. The length of time following transfer when consolidation could be disturbed varied with the duration of spreading depression, from 3 min to 2 hr. The effect appears not to be due to disruption of neural firing, but to the cortical potential change caused by spreading depression since a pulsating cathodal current (8.5 [mu]A/mm2) passed through medial (but not anterior, lateral, or posterior) cortex can abolish retention. It is suggested that the consolidation process may require electrical potential gradients in the cortex and that it is disturbed by agents which decrease or reverse them.

127

[Allen:2007aa] E. A. Allen, B. N. Pasley, T. Duong, and R. D. Freeman. Transcranial magnetic stimulation elicits coupled neural and hemodynamic consequences. *Science*, 317(5846):1918–21, 2007.

> **Abstract:** Transcranial magnetic stimulation (TMS) is an increasingly common technique used to selectively modify neural processing. However, application of TMS is limited by uncertainty concerning its physiological effects. We applied TMS to the cat visual cortex and evaluated the neural and hemodynamic consequences. Short TMS pulse trains elicited initial activation (approximately 1 minute) and prolonged suppression (5 to 10 minutes) of neural responses. Furthermore, TMS disrupted the temporal structure of activity by altering phase relationships between neural signals. Despite the complexity of this response, neural changes were faithfully reflected in hemodynamic signals; quantitative coupling was present over a range of stimulation parameters. These results demonstrate long-lasting neural responses to TMS and support the use of hemodynamic-based neuroimaging to effectively monitor these changes over time.

108, 110, 111, 112, 115, 117, 163, 340, 341

[Amassian:1992aa] V. E. Amassian, L. Eberle, P. J. Maccabee, and R. Q. Cracco. Modelling magnetic coil excitation of human cerebral cortex with a peripheral nerve immersed in a brain-shaped volume conductor: the significance of fiber bending in excitation. *Electroencephalogr Clin Neurophysiol*, 85(5):291–301, 1992.

> **Abstract:** To help elucidate some basic principles of magnetic coil (MC) excitation of cerebral cortex, a model system was devised in which mammalian phrenic nerve, or amphibian sciatic nerve with its branches was suspended in appropriate Ringer's solution in a human brain-shaped volume conductor, an inverted plastic skull. The nerve was recorded monophasically out of the volume conductor. The site of nerve excitation by the MC was identified by finding where along the nerve a bipolar electrical stimulus yielded a similar action potential latency. MC excitation of hand-related corticospinal (CT) neurons was modelled by giving the distal end of nerve attached to the lateral skull an initial radial (perpendicular) trajectory, with subsequent bends towards the base and posterior part of the skull; this nerve was optimally excited by a laterally placed figure 8 or round MC when the induced electric field led to outward membrane current at the initial bend. By contrast, nerve given a trajectory modelling CT neurons related to the foot was optimally excited when the coil windings were across the midline, but again when membrane current flowed outward at the first bend. Corticocortical fibers were modelled by placing the nerve in the anteroposterior axis lateral to the midline; with the round MC vertex-tangentially orientated, optimal excitation occurred at the bend nearest the interaural line, i.e., near the peak electric field. The findings emphasize the importance of orientation and direction of current in the MC and fiber bends in determining nerve excitation. The findings in the peripheral nerve-skull model help explain (1) why lateral and vertex-tangentially orientated

MCs preferentially excite arm-related CT neurons directly and indirectly (through corticocortical fibers), respectively, and (2) why the MC orientations for optimally exciting directly arm and leg-related CT neurons differ.

35

[Anderson:2007aa] W. S. Anderson, P. Kudela, J. Cho, G. K. Bergey, and P. J. Franaszczuk. Studies of stimulus parameters for seizure disruption using neural network simulations. *Biol Cybern*, 97(2):173–94, 2007.

> **Abstract:** A large scale neural network simulation with realistic cortical architecture has been undertaken to investigate the effects of external electrical stimulation on the propagation and evolution of ongoing seizure activity. This is an effort to explore the parameter space of stimulation variables to uncover promising avenues of research for this therapeutic modality. The model consists of an approximately 800 mum x 800 mum region of simulated cortex, and includes seven neuron classes organized by cortical layer, inhibitory or excitatory properties, and electrophysiological characteristics. The cell dynamics are governed by a modified version of the Hodgkin-Huxley equations in single compartment format. Axonal connections are patterned after histological data and published models of local cortical wiring. Stimulation induced action potentials take place at the axon initial segments, according to threshold requirements on the applied electric field distribution. Stimulation induced action potentials in horizontal axonal branches are also separately simulated. The calculations are performed on a 16 node distributed 32-bit processor system. Clear differences in seizure evolution are presented for stimulated versus the undisturbed rhythmic activity. Data is provided for frequency dependent stimulation effects demonstrating a plateau effect of stimulation efficacy as the applied frequency is increased from 60 to 200 Hz. Timing of the stimulation with respect to the underlying rhythmic activity demonstrates a phase dependent sensitivity. Electrode height and position effects are also presented. Using a dipole stimulation electrode arrangement, clear orientation effects of the dipole with respect to the model connectivity is also demonstrated. A sensitivity analysis of these results as a function of the stimulation threshold is also provided.

60, 62, 63, 64, 336

[Anschel:2003aa] D. J. Anschel, A. Pascual-Leone, and G. L. Holmes. Anti-kindling effect of slow repetitive transcranial magnetic stimulation in rats. *Neurosci Lett*, 351(1):9–12, 2003.

> **Abstract:** The cerebrospinal fluid (CSF) of animals exposed to electroconvulsive shock (ECS) has anticonvulsant properties when injected into naive animals. The present study investigated whether the CSF of humans exposed to 1 or 10 Hz repetitive transcranial magnetic stimulation (rTMS) has similar properties. Using a 4 day rat flurothyl kindling seizure model we found that the kindling rate was significantly decreased by intraventricular injection of CSF from depressed patients exposed to 1 Hz rTMS. The CSF from patients that underwent 10 Hz rTMS showed a trend toward an increased kindling rate. These results support the similarity of ECS and rTMS and suggest that 1 Hz and 10 Hz rTMS produce distinct physiologic changes.

119, 121, 177, 342

[Antal:2008aa] Andrea Antal and et al. Comparatively weak after-effects of transcranial alternating current stimulation (tacs) on cortical excitability in humans. *Brain Stimulation*, 1:97–105, 2008.

> **Abstract:** Objective Interference with brain rhythms by noninvasive transcranial stimulation that uses weak transcranial alternating current may reveal itself to be a new tool for investigating cortical mechanisms currently unresolved. Here, we aim to extend transcranial direct current stimulation (tDCS) techniques to transcranial alternating current stimulation (tACS). Background Parameters such as electrode size and position were taken from those used in previous tDCS studies. Methods Motor evoked potentials (MEPs) revealed by transcranial magnetic

stimulation (TMS), electroenceph- alogram (EEG)-power, and reaction times measured in a motor implicit learning task, were analyzed to detect changes in cortical excitability after 2-10 minutes of AC stimulation and sinusoidal DC stimulation (tSDCS) by using 1, 10, 15, 30, and 45 Hz and sham stimulation over the primary motor cortex in 50 healthy subjects (eight-16 subjects in each study). Results A significantly improved implicit motor learning was observed after 10 Hz AC stimulation only. No significant changes were observed in any of the analyzed frequency bands of EEG and with regard to the MEP amplitudes after AC or tSDCS stimulation. Similarly, if the anodal or cathodal DC stimulation was superimposed on 5, 10, and 15 Hz AC stimulation, the MEP amplitudes did not change significantly. Conclusions Transcranial application of weak AC current may appear to be a tool for basic and clinical research in diseases with altered EEG activity. However, its effect seems to be weaker than tDCS stimulation, at least in the present context of stimulus intensity and duration. Further studies are required to extend cautiously the safety range and uncover its influence on neuronal circuitries.

45, 138, 139

[Ardolino:2005aa] G. Ardolino and et al. Non-synaptic mechanisms underlie the after-effects of cathodal transcutaneous direct current stimulation of the human brain. *J. Physiol*, 568.2:563–663, 2005.

> **Abstract:** Although cathodal transcranial direct current stimulation (tDCS) decreases cortical excitability, the mechanisms underlying DC-induced changes remain largely unclear. In this study we investigated the effect of cathodal DC stimulation on spontaneous neural activity and on motor responses evoked by stimulation of the central and peripheral nervous system. We studied 17 healthy volunteers. Transcranial magnetic stimulation (TMS) and transcranial electrical stimulation (TES) of the motor area were used to study the effects of cathodal tDCS (1.5 mA, 10 min) on resting motor threshold and motor evoked potentials (MEPs) recorded from the contralateral first dorsal interosseous muscle (FDI). The electroencephalographic (EEG) activity in response to cathodal tDCS was analysed by power spectral density (PSD). Motor axonal excitability changes in response to transcutaneous DC stimulation of the ulnar nerve (0.3 mA, 10 min) were assessed by testing changes in the size of the compound muscle action potential (CMAP) elicited by submaximal nerve stimulation. Cathodal tDCS over the motor area for 10 min increased the motor threshold and decreased the size of MEPs evoked by TMS for at least 60 min after current offset. The tDCS also significantly decreased the size of MEPs elicited by TES. At the same time in the EEG the power of delta (2–4 Hz) and theta (4–7 Hz) rhythms increased. At the peripheral level cathodal DC stimulation increased the size of the ulnar nerve CMAP. Our findings demonstrate that the after-effects of tDCS have a non-synaptic mechanism of action based upon changes in neural membrane function. These changes apart from reflecting local changes in ionic concentrations, could arise from alterations in transmembrane proteins and from electrolysis-related changes in [H+] induced by exposure to constant electric field.

34, 45

[Arias-Carrion:2006aa] O. Arias-Carrion, S. Hernandez-Lopez, O. Ibanez-Sandoval, J. Bargas, A. Hernandez-Cruz, and R. Drucker-Colin. Neuronal precursors within the adult rat subventricular zone differentiate into dopaminergic neurons after substantia nigra lesion and chromaffin cell transplant. *J Neurosci Res*, 84(7):1425–37, 2006.

> **Abstract:** Neurogenesis in the adult mammalian brain continues in the subventricular zone (SVZ). Neuronal precursors from the SVZ migrate along the rostral migratory stream to replace olfactory bulb interneurons. After the destruction of the nigro-striatal pathway (SN-lesion), some SVZ precursors begin to express tyrosine hydroxylase (TH) and neuronal markers (NeuN). Grafting of chromaffin cells (CCs) into the denervated striatum increases the number of TH+ cells (SVZ

TH+ cells; Arias-Carrion et al., 2004). This study examines the functional properties of these newly differentiating TH+ cells. Under whole-cell patch-clamp, most SVZ cells recorded from lesioned and grafted animals (either TH+ or TH-) were non-excitable. Nevertheless, a small percentage of SVZ TH+ cells had the electrophysiologic phenotype of mature dopaminergic neurons and showed spontaneous postsynaptic potentials. Dopamine (DA) release was measured in SVZ and striatum from both control and SN-lesioned rats. As expected, 12 weeks after SN lesion, DA release decreased drastically. Nevertheless, 8 weeks after CCs graft, release from the SVZ of SN-lesioned rats recovered, and even surpassed that from control SVZ, suggesting that newly formed SVZ TH+ cells release DA. This study shows for the first time that in response to SN-lesions and CC grafts neural precursors within the SVZ change their developmental program, by not only expressing TH, but more importantly by acquiring excitable properties of mature dopaminergic neurons. Additionally, the release of DA in a Ca(2+)-dependent manner and the attraction of synaptic afferents from neighboring neuronal networks gives further significance to the overall findings, whose potential importance is discussed.

113, 120

[Awiszus:1999aa] F. Awiszus, H. Feistner, D. Urbach, and H. Bostock. Characterisation of paired-pulse transcranial magnetic stimulation conditions yielding intracortical inhibition or i-wave facilitation using a threshold-hunting paradigm. *Exp Brain Res*, 129(2):317–24, 1999.

Abstract: Short-interval, paired-pulse transcranial magnetic stimulation (TMS) is usually used to demonstrate intracortical inhibition. It was shown recently that with short-interval, paired-pulse TMS a facilitation - called intracortical I-wave facilitation - can also be demonstrated. It was the aim of this study to investigate which stimulus conditions lead to intracortical inhibition and what conditions yield an intracortical I-wave facilitation in a hand muscle of normal subjects. Paired-pulse TMS responses with an interstimulus interval of 1.2 ms were obtained from the abductor digiti minimi muscle of four normal subjects. A threshold-hunting paradigm with hunting through first or second stimulus variation was used to obtain a curve of threshold-pair strengths. All subjects showed two branches of stimulus interaction on this diagram. If the first stimulus of a threshold pair was below approximately 65motor threshold it modified the response primarily due to the second stimulus through intracortical inhibition. However, if the first stimulus of a threshold pair exceeded approximately 65became responsible for the spinal action-potential initiation. The subsequent second stimulus served as a "booster" for the ongoing intracortical I-wave activity, making it impossible to observe the intracortical inhibition evoked by the first stimulus.

24

[Aydin-Abidin:2006aa] S. Aydin-Abidin, V. Moliadze, U. T. Eysel, and K. Funke. Effects of repetitive tms on visually evoked potentials and eeg in the anaesthetized cat: dependence on stimulus frequency and train duration. *J Physiol*, 574(Pt 2):443–55, 2006.

Abstract: Repetitive transcranial magnetic stimulation (rTMS) has been shown to alter cortical excitability that lasts beyond the duration of rTMS application itself. High-frequency rTMS leads primarily to facilitation, whereas low-frequency rTMS leads to inhibition of the treated cortex. However, the contribution of rTMS train duration is less clear. In this study, we investigated the effects of nine different rTMS protocols, including low and high frequencies, as well as short and long applications (1, 3 and 10 Hz applied for 1, 5 and 20 min), on visual cortex excitability in anaesthetized and paralysed cats by means of visual evoked potential (VEP) and electroencephalography (EEG) recordings. Our results show that 10 Hz rTMS applied for 1 and 5 min significantly enhanced early VEP amplitudes, while 1 and 3 Hz rTMS applied for 5 and 20 min significantly reduced them. No significant changes were found after 1 and 3 Hz rTMS applied for only 1 min, and 10 Hz rTMS applied for 20 min. EEG activity was only transiently (¡20 s) affected, with increased delta activity after 1 and 3 Hz rTMS applied for 1 or 5 min.

These findings indicate that the effects of rTMS on cortical excitability depend on the combination of stimulus frequency and duration (or total number of stimuli): short high-frequency trains seem to be more effective than longer trains, and low-frequency rTMS requires longer applications. Changes in the spectral composition of the EEG were not correlated to changes in VEP size.

110, 175

[Aydin-Abidin:2008aa] S. Aydin-Abidin, J. Trippe, K. Funke, U. T. Eysel, and A. Benali. High- and low-frequency repetitive transcranial magnetic stimulation differentially activates c-fos and zif268 protein expression in the rat brain. *Exp Brain Res*, 188(2):249–61, 2008.

Abstract: Repetitive transcranial magnetic stimulation (rTMS) has been shown to alter cortical excitability depending on the stimulus-frequency used, with high frequency (5 Hz and higher) increasing it but low frequency (usually 1 Hz or lower) reducing it. To determine the efficiency of different rTMS protocols in inducing cortical network activity, we tested the acute effect of one low-frequency rTMS protocol (1 Hz) and two different high-frequency protocols (10 Hz and intermittent theta-burst stimulation, iTBS) on the expression of the two immediate early gene (IEG) proteins c-Fos and zif268 in the rat brain. The cortical expression of both IEGs was specifically changed in an rTMS-dependent manner. One and 10 Hz rTMS enhanced c-Fos protein expression in all cortical areas tested, while iTBS was effective only in limbic cortices. Zif268 expression was increased in almost all cortical areas after iTBS, while 10 Hz rTMS was effective only in the primary motor and sensory cortices. One Hertz rTMS had no effect on cortical zif268 expression. Furthermore, sham-rTMS had no effect on zif268 expression but increased c-Fos in limbic cortices. This is the first study demonstrating that cortical zif268 and c-Fos expression can be specifically modulated by acute rTMS depending on the pattern of stimulation applied.

114, 123, 166

[Banks:2000aa] M. I. Banks, J. A. White, and R. A. Pearce. Interactions between distinct gaba(a) circuits in hippocampus. *Neuron*, 25(2):449–57, 2000. 68

[Bannister:2005aa] A. P. Bannister. Inter- and intra-laminar connections of pyramidal cells in the neocortex. *Neurosci Res*, 53(2):95–103, 2005.

Abstract: The flow of excitation through cortical columns has long since been predicted by studying the axonal projection patterns of excitatory neurones situated within different laminae. In grossly simplified terms and assuming random connectivity, such studies predict that input from the thalamus terminates primarily in layer 4, is relayed 'forward' to layer 3, then to layers 5 and 6 from where the modified signal may exit the cortex. Projection patterns also indicate 'back' projections from layer 5 to 3 and layer 6 to 4. More recently it has become clear that the interconnections between these layers are not random; forward projections primarily contact specific pyramidal subclasses and intracortical back projections innervate interneurones. This indicates that presynaptic axons or postsynaptic dendrites are capable of selecting their synaptic partners and that this selectivity is layer dependent. For the past decade, we and others have studied pyramidal cell targeting in circuits both within, and between laminae using paired intracellular recordings with biocytin filling and have begun to identify further levels of selectivity through the preferential targeting of electrophysiologically and/or morphologically distinct pyramidal subtypes. Presented here, therefore, is a brief overview of current thinking on the layer and subclass specific connectivity of neocortical principle excitatory cells.

60

[Barker:1985aa] A. T. Barker, R. Jalinous, and I. L. Freeston. Non-invasive magnetic stimulation of human motor cortex. *Lancet*, 1(8437):1106–7, 1985. 23

[Bartsch:2007aa] Ronny Bartsch and et al. Experimental evidence for phase synchronization transitions in the human cardiorespiratory system. *Physical Review Letters*, 98(5), February 2007.

Abstract: Transitions in the dynamics of complex systems can be characterized by changes in the synchronization behavior of their components. Taking the human cardiorespiratory system as an example and using an automated procedure for screening the synchrograms of 112 healthy subjects we study the frequency and the distribution of synchronization episodes under different physiological conditions that occur during sleep. We find that phase synchronization between heartbeat and breathing is significantly enhanced during non-rapid-eye-movement (non-REM) sleep (deep sleep and light sleep) and reduced during REM sleep. Our results suggest that the synchronization is mainly due to a weak influence of the breathing oscillator upon the heartbeat oscillator, which is disturbed in the presence of long-term correlated noise, superimposed by the activity of higher brain regions during REM sleep.

133

[Basser:1992aa] Peter J. Basser and et al. The activating function for magnetic stimulation derived from a three-dimensional volume conductor model. *IEEE Transactions on Biomedical Engineering*, 39(11):1207–1210, 1992.

Abstract: A three-dimensional volume conductor model of magnetic stimulation is proposed that relates transmembrane potential of an axon to the induced electric field in a uniform volume conductor. This model validates assumptions used to derive a one-dimensional cable model of magnetic stimulation (Roth and Basser, IEEE Trans. Biomed. Eng., vol. 37, pp. 588-597, 1990) of unmyelinated axons. The three-dimensional volume conductor model reduces to this one-dimensional cable equation forced by the activating function, -delta EzA/delta z.

40, 41, 54, 140

[Basser:1993aa] P. J. Basser. Cable equation for a myelinated axon derived from its microstructure. *Med Biol Eng Comput*, 31 Suppl:S87–92, 1993.

Abstract: A simplified cable equation that describes the subthreshold behaviour of a myelinated axon is derived from its microstructure. Specifically, a micro-continuum cable model of a composite axon is homogenised, yielding a familiar macrocontinuum cable equation of electrotonus, for which the space and time constants depend on microstructural electrical parameters. Activating functions for magnetic and electrical stimulation can be incorporated into this homogenised cable equation as sources or sinks of transmembrane potential. An integral solution to the forced cable equation is also presented for the subthreshold regime. Errors are introduced when myelin membrane resistance is assumed to be infinite.

34

[Basser:2000aa] P. J. Basser and B. J. Roth. New currents in electrical stimulation of excitable tissues. *Annu Rev Biomed Eng*, 2:377–397, 2000.

Abstract: Electric fields can stimulate excitable tissue by a number of mechanisms. A uniform long, straight peripheral axon is activated by the gradient of the electric field that is oriented parallel to the fiber axis. Cortical neurons in the brain are excited when the electric field, which is applied along the axon-dendrite axis, reaches a particular threshold value. Cardiac tissue is thought to be depolarized in a uniform electric field by the curved trajectories of its fiber tracts. The bidomain model provides a coherent conceptual framework for analyzing and understanding these apparently disparate phenomena. Concepts such as the activating function and virtual anode and cathode, as well as anode and cathode break and make stimulation, are presented to help explain these excitation events in a unified manner. This modeling approach can also be used to describe the response of excitable tissues to electric fields that arise from charge redistribution (electrical stimulation) and from time-varying magnetic fields (magnetic stimulation) in a self-consistent manner. It has also proved useful to predict the behavior of excitable tissues, to test hypotheses about possible excitation mechanisms, to design novel electrophysiological experiments, and to interpret their findings.

33

[Baumann:1997aa] S. B. Baumann, D. R. Wozny, S. K. Kelly, and F. M. Meno. The electrical conductivity of human cerebrospinal fluid at body temperature. *IEEE Trans Biomed Eng*, 44(3):220–3, 1997.

> **Abstract:** The electrical conductivity of human cerebrospinal fluid (CSF) from seven patients was measured at both room temperature (25 degrees C) and body temperature (37 degrees C). Across the frequency range of 10 Hz-10 kHz, room temperature conductivity was 1.45 S/m, but body temperature conductivity was 1.79 S/m, approximately 23Modelers of electrical sources in the human brain have underestimated human CSF conductivity by as much as 44corrected to increase the accuracy of source localization models.

18

[Bawin:1984aa] S. M. Bawin, A. R. Sheppard, M. D. Mahoney, and W. R. Adey. Influences of sinusoidal electric fields on excitability in the rat hippocampal slice. *Brain Res*, 323(2):227–37, 1984.

> **Abstract:** The influence of extracellular sinusoidal electric fields on the amplitude of population spikes evoked by single test pulses in excitatory pathways to CA1 pyramidal neurons was studied in rat hippocampal slices. The fields in the tissue were of the order of EEG gradients. Stimulation at 5 Hz, a frequency representative of hippocampal theta activity, was compared with 60 Hz, which is often used in kindling procedures. Brief stimulation (5-30 s) with both 5 and 60 Hz fields (20-70 mV/cmp-p in the perfusing solution) often produced a long-term increase (longer than 10 min) of the population spike. Fields at 60 Hz, but not at 5 Hz, also induced short-term depression (1-6 min) or transient post-field excitation (15-30 s). Prolonged stimulation (3 min) emphasized this frequency dependent response: fields at 5 Hz induced long-lasting potentiation while fields at 60 Hz always resulted in progressive depression persisting for a few minutes after the end of stimulation. These effects appeared as a global response of CA1 neurons. Antidromic responses studied during blockade of synaptic transmission (0.2 mM Ca2+, 4 mM Mg2+) were depressed during and following 3 min field stimulation at either frequency, which could reflect failing calcium mechanisms in the tissue. The field influence on the potential evoked by synaptic or antidromic stimulation was independent of the phase of the sine wave at which the test pulse was delivered, arguing against a direct polarization of the cell membrane by the fields. The experimental evidence suggests a functional role for EEG-like fields in hippocampal excitability.

85, 95

[Been:2007aa] Gregory Been and et al. The use of tdcs and cvs as methods of non-invasive brain stimulaion. *Brain Research Reviews*, 56:346–361, 2007.

> **Abstract:** Transcranial direct current stimulation (tDCS) and caloric vestibular stimulation (CVS) are safe methods for selectively modulating cortical excitability and activation, respectively, which have recently received increased interest regarding possible clinical applications. tDCS involves the application of low currents to the scalp via cathodal and anodal electrodes and has been shown to affect a range of motor, somatosensory, visual, affective and cognitive functions. Therapeutic effects have been demonstrated in clinical trials of tDCS for a variety of conditions including tinnitus, post-stroke motor deficits, fibromyalgia, depression, epilepsy and Parkinson's disease. Its effects can be modulated by combination with pharmacological treatment and it may influence the efficacy of other neurostimulatory techniques such as transcranial magnetic stimulation. CVS involves irrigating the auditory canal with cold water which induces a temperature gradient across the semicircular canals of the vestibular apparatus. This has been shown in functional brain-imaging studies to result in activation in several contralateral cortical and subcortical brain regions. CVS has also been shown to have effects on a wide range of visual and cognitive phenomena, as well as on post-stroke conditions, mania and chronic pain states. Both these techniques have been shown to modulate a range of brain functions, and display potential as clinical treatments. Importantly,

they are both inexpensive relative to other brain stimulation techniques such as electroconvulsive therapy (ECT) and transcranial magnetic stimulation (TMS).

45

[Ben-Shachar:1997aa] D. Ben-Shachar, R. H. Belmaker, N. Grisaru, and E. Klein. Transcranial magnetic stimulation induces alterations in brain monoamines. *J Neural Transm*, 104(2-3):191–7, 1997.

> **Abstract:** Transcranial magnetic stimulation has been suggested as a possible therapeutic tool in depression. In behavioral models of depression, magnetic stimulation induced similar effects to those of electroconvulsive shock. This study demonstrates the effect of a single session of rapid TMS on tissue monoamines in rat brain. Alterations in monoamines were selective and specific in relation to brain areas and type of monoamine. The results imply on a biochemical basis to the suggested ECT-like treatment potential of TMS.

112, 113, 164

[Ben-Shachar:1999aa] D. Ben-Shachar, H. Gazawi, J. Riboyad-Levin, and E. Klein. Chronic repetitive transcranial magnetic stimulation alters beta-adrenergic and 5-ht2 receptor characteristics in rat brain. *Brain Res*, 816(1):78–83, 1999.

> **Abstract:** Repetitive transcranial magnetic stimulation (rTMS) has been shown to affect mood in health and disease. Evidence to date has demonstrated an antidepressant potential for low- and high-frequency rTMS treatment. In animal behavioral models of depression magnetic stimulation of the brain induced similar effects to those of electroconvulsive shock (ECS). In this study the effects of repeated rTMS on rat brain noradrenaline, dopamine, serotonin and their metabolites levels, as well as on beta-adrenergic and 5-HT2 receptor characteristics were studied. After 10 days of treatment, beta-adrenergic receptors were significantly up regulated in the frontal cortex, down regulated in the striatum and were unchanged in the hippocampus. 5-HT2 receptors were down regulated in the frontal cortex and were not changed in the other brain areas. No change in benzodiazepine receptors in the frontal cortex and cerebellum were demonstrated. These findings demonstrate specific and selective alterations induced by repeated rTMS, which are distinct from those induced by other antidepressant treatments. TMS therapeutic effects in humans and behavioral and biochemical effects in animal, suggest that TMS has a unique mechanism of action which requires further investigation.

113, 164

[Benuskova2008] Lubica Benuskova and Nikola Kasabov. Modeling brain dynamics using computational neurogenetic approach. *Cognitive Neurodynamics*, 2(4):319–334, December 2008. 72, 76, 77, 78, 79, 80, 81, 337

[Bezrukov:1995aa] Sergey M. Bezrukov and Igor Vodyanoy. Noise-induced enhancement of signal transduction across voltage-dependent ion channels. *Nature*, 378:362–364, 1995.

> **Abstract:** THE presence of noise in a signal transduction system usually interferes with its ability to transfer information reliably. But many nonlinear systems can use noise to enhance performance1, and this phenomenon, called stochastic resonance, may underlie the extraordinary ability of some biological systems to detect and amplify small signals in noisy environments2–5. Previous work has demonstrated the occurrence of stochastic resonance in a complex system of biological transducers and neural signal pathways6, but the possibility that it could occur at the sub-cellular level has remained open. Here we report the observation of stochastic resonance in a system of voltage-dependent ion channels formed by the peptide alamethicin. A hundred-fold increase in signal transduction induced by external noise is accompanied by a growth in the output signal-to-noise ratio. The system of ion channels considered here represents the simplest biological system yet known to exhibit stochastic resonance.

144

[Bikson:2001aa] M. Bikson, J. Lian, P. J. Hahn, W. C. Stacey, C. Sciortino, and D. M. Durand. Suppression of epileptiform activity by high frequency sinusoidal fields in rat hippocampal slices. *J Physiol*, 531(Pt 1):181–91, 2001.

> **Abstract:** 1. Sinusoidal high frequency (20-50 Hz) electric fields induced across rat hippocampal slices were found to suppress zero-Ca2+, low-Ca2+, picrotoxin, and high-K+ epileptiform activity for the duration of the stimulus and for up to several minutes following the stimulus. 2. Suppression of spontaneous activity by high frequency stimulation was found to be frequency (¡ 500 Hz) but not orientation or waveform dependent. 3. Potassium-sensitive microelectrodes showed that block of epileptiform activity was always coincident with a stimulus-induced rise in extracellular potassium concentration during stimulation. Post-stimulus inhibition was always associated with a decrease in extracellular potassium activity below baseline levels. 4. Intracellular recordings and optical imaging with voltage-sensitive dyes showed that during suppression neurons were depolarized yet did not fire action potentials. 5. Direct injection of sinusoidal current into individual pyramidal cells did not result in a tonic depolarization. Injection of large direct current (DC) depolarized neurons and suppressed action potential generation. 6. These findings suggest that high frequency stimulation suppresses epileptiform activity by inducing potassium efflux and depolarization block.

85, 95, 97, 339

[Bikson:2004aa] M. Bikson, M. Inoue, H. Akiyama, J. K. Deans, J. E. Fox, H. Miyakawa, and J. G. Jefferys. Effects of uniform extracellular dc electric fields on excitability in rat hippocampal slices in vitro. *J Physiol*, 557(Pt 1):175–90, 2004.

> **Abstract:** The effects of uniform steady state (DC) extracellular electric fields on neuronal excitability were characterized in rat hippocampal slices using field, intracellular and voltage-sensitive dye recordings. Small electric fields ($< 40/$ mV mm(-1)), applied parallel to the somato-dendritic axis, induced polarization of CA1 pyramidal cells; the relationship between applied field and induced polarization was linear (0.12 +/- 0.05 mV per mV mm(-1) average sensitivity at the soma). The peak amplitude and time constant (15-70 ms) of membrane polarization varied along the axis of neurons with the maximal polarization observed at the tips of basal and apical dendrites. The polarization was biphasic in the mid-apical dendrites; there was a time-dependent shift in the polarity reversal site. DC fields altered the thresholds of action potentials evoked by orthodromic stimulation, and shifted their initiation site along the apical dendrites. Large electric fields could trigger neuronal firing and epileptiform activity, and induce long-term (>1 s) changes in neuronal excitability. Electric fields perpendicular to the apical-dendritic axis did not induce somatic polarization, but did modulate orthodromic responses, indicating an effect on afferents. These results demonstrate that DC fields can modulate neuronal excitability in a time-dependent manner, with no clear threshold, as a result of interactions between neuronal compartments, the non-linear properties of the cell membrane, and effects on afferents.

84, 86, 88, 90, 91, 92, 94, 95, 96, 337, 338, 339

[Bindman:1964aa] Lynn J. Bindman and et al. The action of brief polarizing currents on the cerebral cortex of the rat (i) during current flow and (ii) in the production of long-lasting effects. *J. Physiol*, 172:369–382, 1964. 45, 87, 88, 125, 126, 337, 342

[Bliss:1970aa] T. V. Bliss and T. Lomo. Plasticity in a monosynaptic cortical pathway. *J Physiol*, 207(2), 1970. 126

[Bliss:1973aa] T. V. Bliss and T. Lomo. Long-lasting potentiation of synaptic transmission in the dentate area of the anaesthetized rabbit following stimulation of the perforant path. *J Physiol*, 232(2):331–56, 1973. 126

[Bonsi:2003aa] P. Bonsi, A. Pisani, G. Bernardi, and P. Calabresi. Stimulus frequency, calcium levels and striatal synaptic plasticity. *Neuroreport*, 14(3):419–22, 2003.

Abstract: Electrophysiological and microfluorimetric measurements were combined to correlate the changes in intracellular calcium concentration to synaptic plasticity in striatal medium spiny projection neurons, during three different protocols of synaptic stimulation (1, 10, and 100 Hz). The 1 Hz stimulation protocol did not cause significant changes either in excitatory postsynaptic potential amplitude or in intracellular calcium concentration. The 10 Hz stimulation protocol induced a moderate increase of intracellular calcium without significantly affecting the excitatory postsynaptic potential amplitude. During the high frequency stimulation large, transient intracellular calcium elevations were recorded, and a significant long-term depression of excitatory postsynaptic potential was achieved. These results suggest that the induction of long-term depression required large, transient increases in intracellular calcium concentration.

104

[Bower:1998aa] J. M. Bower and D. Beeman. *The book of GENESIS: exploring realistic neural models with the GEneral NEural SImulation System*. Springer-Verlag, New York, 1998. 38

[Bower:2003aa] James M. Bower and David Beeman. *The book of GENESIS: exploring realistic neural models with the GEneral NEural SImulation System*. Internet Edition, 2003. 38, 40, 41, 52, 57, 58, 335

[Bower:2007aa] J. M. Bower and D. Beeman. Constructing realistic neural simulations with genesis. *Methods Mol Biol*, 401:103–25, 2007.

Abstract: The GEneral NEural SImulation System (GENESIS) is an open source simulation platform for realistic modeling of systems ranging from subcellular components and biochemical reactions to detailed models of single neurons, simulations of large networks of realistic neurons, and systems-level models. The graphical interface XODUS permits the construction of a wide variety of interfaces for the control and visualization of simulations. The object-oriented scripting language allows one to easily construct and modify simulations built from the GENESIS libraries of simulation components. Here, we present procedures for installing GENESIS and its supplementary tutorials, running GENESIS simulations, and creating new neural simulations.

38

[Bulsara:1996aa] Adi R. Bulsara and Luca Gammaitoni. Tuninig in to noise. *Physics Today*, pages 39–45, March 1996. 143

[Burger:1961aa] H. C. Burger and R. van Dongen. Specific electric resistivity of body tissues. *Phys Med Biol*, 5(4):431–47, 1961. 17

[Buzsaki:2006aa] G. Buzsaki. *Rhythms of the Brain*. Oxford University Press Press, 2006. 133

[Calabresi:1992aa] P. Calabresi, R. Maj, A. Pisani, N. B. Mercuri, and G. Bernardi. Long-term synaptic depression in the striatum: physiological and pharmacological characterization. *J Neurosci*, 12(11):4224–33, 1992.

Abstract: The effect of tetanic activation of corticostriatal glutamatergic fibers was studied in striatal slices by utilizing extracellular and intracellular recording techniques. Tetanic stimulation produced a long-term synaptic depression (LTD) (¿ 2 h) of both extracellularly recorded field potentials and intracellularly recorded EPSPs. LTD was not coupled with changes of intrinsic membrane properties of the recorded neurons. In some neurons, repetitive cortical activation produced a short-term posttetanic potentiation (1-3 min). Subthreshold tetanic stimulation, which under control condition did not cause LTD, induced LTD when associated with membrane depolarization. Moreover, LTD was not expressed in cells in which the conditioning tetanus was coupled with hyperpolarization of the membrane. Bath application of aminophosphonovalerate (30-50 microM), an antagonist of NMDA receptors, did not affect the amplitude of the synaptic potentials and the expression of LTD. Striatal LTD was significantly reduced by the pretreatment of the

slices with 30 microM 2-amino-3-phosphonopropionic acid, an antagonist of glutamate metabotropic receptors. LTD was not blocked by bicuculline (30 microM), a GABA(A) receptor antagonist. Scopolamine (3 microM), an antagonist of muscarinic receptors, induced a slight, but significant, increase of the amplitude of LTD. Both SCH 23390 (3 microM), an antagonist of D1 dopamine (DA) receptors, and I-sulpiride (1 microM), an antagonist of D2 DA receptors, blocked LTD. LTD was also absent in slices obtained from rats in which the nigrostriatal DA system was lesioned by unilateral nigral injection of 6-hydroxydopamine. In DA-depleted slices, LTD could be restored by applying exogenous DA (30 microM) before the conditioning tetanus. In DA-depleted slices, LTD could also be restored by coadministration of SKF 38393 (3-10 microM), a D1 receptor agonist, and of LY 171555 (1-3 microM), a D2 receptor agonist. Application of a single class of DA receptor agonists failed to restore LTD. These data show that striatal LTD requires three main physiological and pharmacological conditions: (1) membrane depolarization and action potential discharge of the postsynaptic cell during the conditioning tetanus, (2) activation of glutamate metabotropic receptors, and (3) coactivation of D1 and D2 DA receptors. Striatal LTD may alter the output signals from the striatum to the other structures of the basal ganglia. This form of synaptic plasticity can influence the striatal control of motor activity.

103, 104

[Calabresi:1992ab] P. Calabresi, A. Pisani, N. B. Mercuri, and G. Bernardi. Long-term potentiation in the striatum is unmasked by removing the voltage-dependent magnesium block of nmda receptor channels. *Eur J Neurosci*, 4(10):929–935, 1992.

Abstract: We have studied the effects of tetanic stimulation of the corticostriatal pathway on the amplitude of striatal excitatory synaptic potentials. Recordings were obtained from a corticostriatal slice preparation by utilizing both extracellular and intracellular techniques. Under the control condition (1.2 mM external Mg2+), excitatory postsynaptic potentials (EPSPs) evoked by cortical stimulation were reversibly blocked by 10 microM 6-cyano-7-nitroquinoxaline-2,3-dione (CNQX), an antagonist of dl-alpha-amino-3-hydroxy-5-methyl-4-isoxazole propionic acid (AMPA) ionotropic glutamate receptors, while they were not affected by 30 - 50 microM 2-amino-5-phosphonovalerate (APV), an antagonist of N-methyl-d-aspartate (NMDA) glutamate receptors. In the presence of 1.2 mM external Mg2+, tetanic activation of cortical inputs produced long-term depression (LTD) of both extracellularly and intracellularly recorded synaptic potentials. When Mg2+ was removed from the external medium, EPSP amplitude and duration increased. In Mg2+-free medium, cortically evoked EPSPs revealed an APV-sensitive component; in this condition tetanic stimulation produced long-term potentiation (LTP) of synaptic transmission. Incubation of the slices in 30 - 50 microM APV blocked striatal LTP, while it did not affect LTD. In Mg2+-free medium, incubation of the slices in 10 microM CNQX did not block the expression of striatal LTP. Intrinsic membrane properties (membrane potential, input resistance and firing pattern) of striatal neurons were altered neither by tetanic stimuli inducing LTD and LTP, nor by removal of Mg2+ from the external medium. These findings show that repetitive activation of cortical inputs can induce long-term changes of synaptic transmission in the striatum. Under control conditions NMDA receptor channels are inactivated by the voltage-dependent Mg2+ block and repetitive cortical stimulation induces LTD which does not require activation of NMDA channels. Removal of external Mg2+ deinactivates these channels and reveals a component of the EPSP which is potentiated by repetitive activation. Since the striatum has been involved in memory and in the storage of motor skills, LTD and LTP of synaptic transmission in this structure may provide the cellular substrate for motor learning and underlie the physiopathology of some movement disorders.

103, 104

[Calabresi:1997aa] P. Calabresi, A. Pisani, D. Centonze, and G. Bernardi. Role of dopamine receptors in the short- and long-term regulation of corticostriatal transmission. *Nihon Shinkei Seishin Yakurigaku Zasshi*, 17(2):101–4, 1997.

> **Abstract:** Several studies have tried to clarify the role of different dopamine (DA) receptors in the control of membrane excitability of striatal neurons. Activation of DA receptors influences both synaptic and intrinsic membrane properties of striatal neurons. More recently it has been reported that endogenous DA plays an important role in the expression of striatal synaptic plasticity. In this review we will try to summarize and discuss the available data concerning the possible impact of the functional role of D1 and D2 receptor activation on the short- and long-term modulation of the excitatory glutamatergic corticostriatal transmission. Moreover, we will also describe the function of the striatum in the integration of glutamatergic and DAergic inputs to produce long-term changes of synaptic efficacy: long-term depression (LTD) and long-term potentiation (LTP).

103

[Carbunaru:2001aa] R. Carbunaru and D. M. Durand. Toroidal coil models for transcutaneous magnetic stimulation of nerves. *IEEE Trans Biomed Eng*, 48(4):434–41, 2001.

> **Abstract:** A novel design of coils for transcutaneous magnetic stimulation of nerves is presented. These coils consist of a toroidal winding around a high-permeability material (Supermendur) core embedded in a conducting medium. Theoretical numerical calculations are used to analyze the effect of the design parameters of these coils, such as coil width, toroidal radius, conducting layer thickness and core transversal shape on the induced electric fields in terms of the electric field strength and distribution. Results indicate that stimulation of nerves with these coils has some of the advantages of both electrical and magnetic stimulation. These coils can produce localized and efficient stimulation of nerves with induced electric fields parallel and perpendicular to the skin similar to surface electrical stimulation. However, they retain some of the advantages of magnetic stimulation such as no risk of tissue damage due to electrochemical reactions at the electrode interface and less uncomfortable sensations or pain. The driving current is reduced by over three orders of magnitude compared to traditional magnetic stimulation, eliminating the problem of coil heating and allowing for long duration and high-frequency magnetic stimulation with inexpensive stimulators.

27

[Cartee:1992aa] Lianne A. Cartee and Robert Plonsey. The transient subthreshold response of spherical and cylindrical cell models to extracellular stimulation. *IEEE Transactions on Biomedical Engineering*, 39(1):76–85, 1992.

> **Abstract:** The effect of extracellular stimulation on excitable tissue is evaluated using analytical models. Primary emphasis is placed on the determination of the rate of rise of the membrane potential in response to subthreshold stimulation. Three models are studied: 1) a spherical cell in a uniform electric field, 2) an infinite cylindrical fiber with a point source stimulus, and 3) a finite length cable with sealed ends and a stimulus electrode at each end.

41

[Chen:1997ab] R. Chen, C. Gerloff, J. Classen, E. M. Wassermann, M. Hallett, and L. G. Cohen. Safety of different inter-train intervals for repetitive transcranial magnetic stimulation and recommendations for safe ranges of stimulation parameters. *Electroencephalogr Clin Neurophysiol*, 105(6):415–21, 1997.

> **Abstract:** Induction of a seizure in a normal subject with trains of repetitive transcranial magnetic stimulation (rTMS) applied in close succession suggested that short inter-train intervals, a parameter not considered in our previous safety studies, may not be safe. Here, we evaluate the safety of different inter-train intervals for rTMS in 10 healthy volunteers. Ten rTMS trains at 20 Hz for 1.6 s and

a stimulus intensity of 110train interval of 5 s. However, inter-train intervals of 1 s or less were unsafe for trains of 20 Hz for 1.6 s and stimulus intensities higher than 100inter-train intervals at different stimulus intensities. We also analyzed the stimulus parameters, used in 3 studies, that led to seizures in normal subjects. One seizure was due to short inter- train intervals, one was likely related to intense individual rTMS trains close to the limit of our previous safety recommendations, and one was likely due to a combination of these two factors. To provide an additional safety margin, we suggest reducing the duration for individual rTMS trains by 25Updated safety tables currently in use at our institution are provided.

31

[Chen:2007aa]   Ming Chen and D.J. Mogul. A structurally-detailed finite element human head model for brain-electromagnetic field simulations. In *3rd International IEEE/EMBS Conference on Neural Engineering*, pages 291–293, 2007.

> **Abstract:** Early studies on the modeling of electromagnetic (EM) field interactions with the human head have shown that induced current densities in the brain depend on both tissue geometry and its conductive properties. However, no head model of sufficient complexity for studying the physics of induced brain activation has been developed which provides well-defined smooth boundaries between tissues of different conductivities and orientations. In our study, we generated a detailed finite element model of the head that includes structural details to the level of cerebral gyri and sulci as well as axonal fiber tracts by combining different imaging modalities, namely computed tomography, magnetic resonance and diffusion tensor imaging. The anisotropic properties of brain tissues accompanying these details have also been included

31

[Chen:2008aa]   R. Chen, D. Cros, A. Curra, V. Di Lazzaro, J. P. Lefaucheur, M. R. Magistris, K. Mills, K. M. Rosler, W. J. Triggs, Y. Ugawa, and U. Ziemann. The clinical diagnostic utility of transcranial magnetic stimulation: report of an ifcn committee. *Clin Neurophysiol*, 119(3):504–32, 2008.

> **Abstract:** The review focuses on the clinical diagnostic utility of transcranial magnetic stimulation (TMS). The central motor conduction time (CMCT) is a sensitive method to detect myelopathy and abnormalities may be detected in the absence of radiological changes. CMCT may also detect upper motor neuron involvement in amyotrophic lateral sclerosis. The diagnostic sensitivity may be increased by using the triple stimulation technique (TST), by combining several parameters such as CMCT, motor threshold and silent period, or by studying multiple muscles. In peripheral facial nerve palsies, TMS may be used to localize the site of nerve dysfunction and clarify the etiology. TMS measures also have high sensitivity in detecting lesions in multiple sclerosis and abnormalities in CMCT or TST may correlate with motor impairment and disability. Cerebellar stimulation may detect lesions in the cerebellum or the cerebellar output pathway. TMS may detect upper motor neuron involvement in patients with atypical parkinsonism and equivocal signs. The ipsilateral silent period that measures transcallosal inhibition is a potential method to distinguish between different parkinsonian syndromes. Short latency afferent inhibition (SAI), which is related to central cholinergic transmission, is reduced in Alzheimer's disease. Changes in SAI following administration of cholinesterase inhibitor may be related to the long-term efficacy of this treatment. The results of MEP measurement in the first week after stroke correlate with functional outcome. We conclude that TMS measures have demonstrated diagnostic utility in myelopathy, amyotrophic lateral sclerosis and multiple sclerosis. TMS measures have potential clinical utility in cerebellar disease, dementia, facial nerve disorders, movement disorders, stroke, epilepsy, migraine and chronic pain.

107

[Chokroverty:1990aa]   S. Chokroverty. *Magnetic stimulation in clinical neurophysiology*. Butterworths, Boston, 1990. 23

[Coburn:1989aa] B. Coburn. Neural modeling in electrical stimulation. *Crit Rev Biomed Eng*, 17(2):133–78, 1989.

Abstract: In general, complete mathematical modeling of electrical neurostimulation encompasses two separate problems; clear delineation of this article becomes important. Solutions are required for the time-varying macroscopic fields generated by the stimulating electrodes, and only then can biophysical analysis be brought to bear on neural structures within those fields. This article is focused on the second of these aspects, and provides a survey of mathematical representations including nerve cell bodies, myelinated and unmyelinated fibers of passage, branched systems, fiber terminals and composite neurons. Effects on nerve cells of fields generated by remote electrodes are given primary attention, although methods for obtaining field solutions in biological media are discussed in detail only where the issue is inextricably linked to the use of a particular neural model, or relates crucially to experimental validation. Within these guidelines, it is intended to show the significant role that current nerve cell models may play in attempts to understand mechanisms of neural stimulation, and in the development of more advanced strategies for electronic intervention and control of neural function.

33

[Cohen:1990aa] L. G. Cohen, B. J. Roth, J. Nilsson, N. Dang, M. Panizza, S. Bandinelli, W. Friauf, and M. Hallett. Effects of coil design on delivery of focal magnetic stimulation. technical considerations. *Electroencephalogr Clin Neurophysiol*, 75(4):350–7., 1990.

Abstract: The localization of effects from magnetic coil stimulation is not immediately obvious. We measured the magnetic fields produced by several different coils and compared the results with theoretical calculations. Magnetic stimuli were delivered from a Cadwell MES-10 magnetic stimulator using 3 circular coils (one 9 cm in diameter; two with an angulated extension, 5 and 9 cm in diameter) and twin oval coils arranged in a butterfly shape (each coil approximately 4 cm in diameter) and from a Novametrix Magstim 200 using two circular flat- spiral coils (6.7 and 14 cm in diameter). Peak-induced strength of the magnetic field was recorded with a measuring loop (1 cm in diameter) at different distances from the center of the coil. When the measuring loop was moved in the same plane laterally from the center of the coil, for all coils except the butterfly-shaped coil, the field was highest in the center and fell off near the circumference of the coil. The field dropped progressively when measurements were made more distant from the plane of the coils. The electric field induced from the magnetic coil could be calculated from the coil geometry. For all coils except the butterfly-shaped coil, the largest electric field was at the circumference of the coils. The 6.7 cm flat-spiral coil induced currents similar to those induced by the larger coils but more focally. The butterfly-shaped coil induced the largest currents under its center, where the circumferences of the two component coils come together. The component of the electric field parallel to the wire in the center of this coil was the largest and most localized.

25, 27

[Cohen:1991aa] D. Cohen and B. N. Cuffin. Developing a more focal magnetic stimulator. part i: Some basic principles. *J Clin Neurophysiol*, 8(1):102–11, 1991.

Abstract: Some general properties of currents induced by magnetic stimulators in volume conductors of any shape are first reviewed. Then, the property of focality (concentration at some internal point) of the current induced in a spherical model of the head is discussed, due to coils of various orientations and configurations. It is shown that one important property for focality is the complete absence of the radial component of current, regardless of the coil used. The theoretically computed current distributions in the sphere produced by three different coils are illustrated. These are (1) a circular coil parallel to the head (very nonfocal). (2) a circular coil erect on the head (more focal), and (3) a figure-eight coil parallel to the head (most focal). A computational search for yet more focal coil configurations

shows that the figure-eight focality can only be altered somewhat, but basically not improved. A plot of focality of the figure-eight coil versus the diameter of its coils shows an improvement in focality with decreasing diameter down to one cm. At this diameter, the induced current at a level 2 cm below the coil is concentrated in a band 1.5 cm wide (half- maximum points). Finally, it is noted that as the diameter of the figure-eight coil is decreased, the current in the coil necessary for stimulation increases rapidly, with increasing engineering problems.

26

[Cohen:1991ab] L. G. Cohen, S. Bandinelli, H. R. Topka, P. Fuhr, B. J. Roth, and M. Hallett. Topographic maps of human motor cortex in normal and pathological conditions: mirror movements, amputations and spinal cord injuries. *Electroencephalogr Clin Neurophysiol Suppl*, 43:36–50, 1991.

Abstract: We studied motor evoked potentials to transcranial magnetic stimulation in patients with unilateral upper limb amputations, complete T10-T12 spinal cord transection, and congenital mirror movements and in controls. Different muscles in the trunk and upper and lower extremities were evaluated at rest. In controls, muscles could be activated with stimulation of regions several centimeters wide. These areas overlapped extensively when muscles studied were from the same limb and shifted positions abruptly when muscles were from different limbs. Distal muscles were easier to activate than proximal muscles and normally evidenced exclusively a contralateral representation. Congenital defects in motor control in patients with mirror movements resulted in marked derangement of the map of outputs of distal hand muscles with enlarged and ipsilateral representations. Peripheral lesions, either acquired (amputations) or congenital (congenital absence of a limb), resulted in plastic reorganization of motor outputs targeting muscles immediately proximal to the stump. Central nervous system lesions (i.e., spinal cord injury producing paraplegia) also resulted in enlargement of the map of outputs targeting muscles proximal to the lesion. These results indicate that magnetic stimulation is a useful non-invasive tool for exploring plastic changes in human motor pathways following different types of injury.

24

[Cole:1989aa] A. J. Cole, D. W. Saffen, J. M. Baraban, and P. F. Worley. Rapid increase of an immediate early gene messenger rna in hippocampal neurons by synaptic nmda receptor activation. *Nature*, 340(6233):474–6, 1989.

Abstract: Recent studies in invertebrates indicate that a rapid genomic response to neuronal stimulation has a critical role in long-term changes in synaptic efficacy. Because several of the genes (immediately early genes; IEGs) that respond rapidly to growth factor stimulation of vertebrate cells in vitro are also activated by neuronal stimulation in vivo, attention has focused on the possibility that they play a part in synaptic plasticity in vertebrate nervous systems. Four IEGs thought to encode transcription factors, zif/268 (also termed Egr-1, NGFI-A, Krox 24), c-fos, c-jun, and jun-B are rapidly induced in the brain by seizure activity, and we have now studied the induction of these genes in a well-characterized model of synaptic plasticity in the vertebrate brain–long-term potentiation (LTP) of the perforant pathgranule cell (pp-gc) synapse in vivo. We found that high-frequency (but not low-frequency) stimulation of the pp-gc synapse markedly increases zif/268 messenger RNA (mRNA) levels in the ipsilateral granule cell neurons; mRNA of c-fos, c-jun and jun-B is less consistently increased. The stimulus frequency and intensity required to increase zif/268 mRNA levels are similar to those required to induce LTP, which is also seen only ipsilaterally, and both responses are blocked by NMDA-receptor antagonists as well as by convergent synaptic inhibitory inputs already known to block LTP. Accordingly, zif/268 mRNA levels and LTP seem to be regulated by similar synaptic mechanisms.

114

[Compte:2008aa] Albert Compte and et al. Spontaneous high-frequency (10 – 80 hz) oscillations during up states in the cerebral cortex in vitro. *The Journal of Neuroscience*, 28(51):13828–13844, 2008.

Abstract: High-frequency oscillations in cortical networks have been linked to a variety of cognitive and perceptual processes. They have also been recorded in small cortical slices in vitro, indicating that neuronal synchronization at these frequencies is generated in the local cortical circuit. However, in vitro experiments have hitherto necessitated exogenous pharmacological or electrical stimulation to generate robust synchronized activity in the β/γ range. Here, we demonstrate that the isolated cortical microcircuitry generates β and γ oscillations spontaneously in the absence of externally applied neuromodulators or synaptic agonists. We show this in a spontaneously active slice preparation that engages in slow oscillatory activity similar to activity during slow-wave sleep. β and γ synchronization appeared during the up states of the slow oscillation. Simultaneous intracellular and extracellular recordings revealed synchronization between the timing of incoming synaptic events and population activity. This rhythm was mechanistically similar to pharmacologically induced γ rhythms, as it also included sparse, irregular firing of neurons within the population oscillation, predominant involvement of inhibitory neurons, and a decrease of oscillation frequency after barbiturate application. Finally, we show in a computer model how a synaptic loop between excitatory and inhibitory neurons can explain the emergence of both the slow (<1 Hz) and the β-range oscillations in the neocortical network. We therefore conclude that oscillations in the β/γ range that share mechanisms with activity reported in vivo or in pharmaco- logically activated in vitro preparations can be generated during slow oscillatory activity in the local cortical circuit, even without exogenous pharmacological or electrical stimulation.

140

[Cooley:1966aa] J. W. Cooley and Jr. Dodge, F. A. Digital computer solutions for excitation and propagation of the nerve impulse. *Biophys J*, 6(5):583–99, 1966. 38

[Cooper:1965aa] R. Cooper. Comparison of subcortical, cortical and scalp activity using chronically indwelling electrodes in man. *Electroencephalography and Clinical Neurophysiology*, 18:217–228, 1965.

Abstract: 1. Intracerebral recordings show that there is little field spread (volume conduction) in brain tissue and that cerebral models with dipoles deep within the brain are not satisfactory. 2. Comparison of subdural and scalp recordings shows that only widely synchronised components of the cortical activity are observed on the scalp. 3. For strictly localised activity the attenuation from cortex to scalp can be as high as 5000:1, but for coherent activity over a wide area it may be only 2:1 4. Model experiments indicate that cortical areas of at least 6 sq cm must be involved in synchronous or near synchronous activity before the scalp EEG is observed, using standard working gains. 5. A plea is made for higher working gains for part of routine EEG recordings.

135

[Corthout:2001aa] E. Corthout, A. T. Barker, and A. Cowey. Transcranial magnetic stimulation. which part of the current waveform causes the stimulation? *Exp Brain Res*, 141(1):128–32, 2001.

Abstract: To investigate the mechanism of transcranial magnetic stimulation (TMS), we compared the directional effects of two stimulators (Magstim 200 and Magstim Super Rapid). First, stimulating visual cortex and facial nerve with occipital mid-line TMS, we found that, for a particular coil orientation, these two stimulators affected a particular neural structure in opposite hemispheres and that, to affect a particular neural structure in a particular hemisphere, these two stimulators required opposite coil orientations. Second, stimulating a membrane-simulating circuit, we found that, for a particular coil orientation, these two stimulators resulted in a peak induced current of the same polarity but in a peak induced charge accumulation of opposite polarity. We suggest that the critical parameter in TMS is the amplitude of the induced charge accumulation rather than the amplitude

of the induced current. Accordingly, TMS would be elicited just before the end of the first (Magstim 200) and second (Magstim Super Rapid) phase of the induced current rather than just after the start of the first phase of the induced current.

27, 28

[Cosandier2007] D. Cosandier-Rimele, J. M. Badier, P. Chauvel, and F. Wendling. A physiologically plausible spatio-temporal model for eeg signals recorded with intracerebral electrodes in human partial epilepsy. *Biomedical Engineering, IEEE Transactions on*, 54(3):380–388, 2007. 68, 69, 70, 71, 337

[Cosandier2008] D. Cosandier-Rimele, I. Merlet, J. Badier, P. Chauvel, and F. Wendling. The neuronal sources of eeg: Modeling of simultaneous scalp and intracerebral recordings in epilepsy. *NeuroImage*, 42(1):135–146, August 2008. 68, 69, 70, 72

[Cossart:2001aa] R. Cossart, C. Dinocourt, J. C. Hirsch, A. Merchan-Perez, J. De Felipe, Y. Ben-Ari, M. Esclapez, and C. Bernard. Dendritic but not somatic gabaergic inhibition is decreased in experimental epilepsy. *Nat Neurosci*, 4(1):52–62, 2001. 68

[Counter:1993aa] S. A. Counter. Neurobiological effects of extensive transcranial electromagnetic stimulation in an animal model. *Electroencephalogr Clin Neurophysiol*, 89(5):341–8, 1993.

Abstract: The effects of transcranial electromagnetic stimulation (TEMS) on the cellular morphology of the cortex, cerebellum, and brain-stem were systematically investigated in rabbits exposed to 1000 pulsed stimuli at 100at the skull) over a 12 month period with a 5 cm circular magnetic coil positioned over the cranium. Also, the acute effects of TEMS on heart rate and respiration were examined. (1) T1 and T2 weighted magnetic resonance images (MRI) of 1-3 mm sections in both sagittal and axial planes revealed no evidence of gross morphological changes or subtler tissue damage to the cerebrum, cerebellum, or brain-stem. (2) Light microscopic examination of 60 microns hematoxylin-eosin/Cresyl Violet Luxol Fast Blue stained sections of the brain-stem, cerebellum, and cerebral cortex showed no TEMS-related changes in cellular organization or histological damage. (3) Autonomic activity as reflected by heart rate was also unaffected by high intensity TEMS. Normal heart rate was maintained during repeated TEMS at 100maximum. (4) Respiration rate was briefly altered at the time of the stimulus, but returned to normal immediately after the stimulus. These findings in experimental animals revealed no biohazardous effects on the brain following extensive exposure to high intensity, low frequency time-varying magnetic field stimulation from the coil of a clinical instrument.

124, 125, 169

[Creutzfeldt:1962aa] O. D. Creutzfeldt, G. H. Fromm, and H. Kapp. Influence of transcortical d-c currents on cortical neuronal activity. *Exp Neurol*, 5:436–52, 1962. 125

[Crile:1922aa] G. W. Crile, H. R. Hosmer, and A. F. Rowland. The electrical conductivity of animal tissues under normal and pathological conditions. *Am J Physiol*, 60:59–106, 1922. 17, 18, 19

[Cycowicz:2008aa] Y. M. Cycowicz, B. Luber, T. Spellman, and S. H. Lisanby. Differential neurophysiological effects of magnetic seizure therapy (mst) and electroconvulsive shock (ecs) in non-human primates. *Clin EEG Neurosci*, 39(3):144–9, 2008.

Abstract: Magnetic seizure therapy (MST) is under development as a means of reducing the side effects of electroconvulsive therapy (ECT) through enhanced control over patterns of seizure induction and spread. We previously reported that chronic treatment with MST resulted in less impairment in cognitive function than electroconvulsive shock (ECS) in a non-human primate model of convulsive therapy. Here we present quantitative analyses of ictal expression and post-ictal suppression following ECS, MST, and anesthesia-alone sham in the same model to test whether differential neurophysiological characteristics of the seizures could be identified. Rhesus monkeys received 4 weeks of daily treatment with ECS, MST, and anesthesia-alone sham in a counterbalanced order separated by a recovery

period. Both ECS and MST were given bilaterally at 2.5 x seizure threshold. Neurophysiological characteristics were derived from two scalp EEG electrode recording sites during and immediately following the ictal period, and were compared to sham treatment. EEG power within four frequencies (delta, theta, alpha and beta) was calculated. Our results support earlier findings from intracerebral electrode recordings demonstrating that MST- and ECS- induced seizures elicit differential patterns of EEG activation. Specifically, we found that ECS shows significantly more marked ictal expression, and more intense post-ictal suppression than MST in the theta, alpha, and beta frequency bands (Ps ¡ .05). However, the ECS and MST were indistinguishable in the delta frequency band during both ictal and post-ictal periods. These results demonstrate that magnetic seizure induction can result in seizures that differ in some neurophysiological respects compared with ECS, but that these modalities share some aspects of seizure expression. The clinical significance of these similarities and differences awaits clinical correlation.

118

[Dash:2007aa]   P.K. Dash, A.N. Moore, and et al. Molecular activity underlying working memory. *Learn Mem*, 14(8):554–63, 2007.

Abstract: The prefrontal cortex is necessary for directing thought and planning action. Working memory, the active, transient maintenance of information in mind for subsequent monitoring and manipulation, lies at the core of many simple, as well as high-level, cognitive functions. Working memory has been shown to be compromised in a number of neurological and psychiatric conditions and may contribute to the behavioral and cognitive deficits associated with these disorders. It has been theorized that working memory depends upon reverberating circuits within the prefrontal cortex and other cortical areas. However, recent work indicates that intracellular signals and protein dephosphorylation are critical for working memory. The present article will review recent research into the involvement of the modulatory neurotransmitters and their receptors in working memory. The intracellular signaling pathways activated by these receptors and evidence that indicates a role for Gq-initiated PI-PLC and calcium-dependent protein phosphatase calcineurin activity in working memory will be discussed. Additionally, the negative influence of calcium- and cAMP-dependent protein kinase (i.e., calcium/calmodulin-dependent protein kinase II (CaMKII), calcium/diacylglycerol-activated protein kinase C (PKC), and cAMP-dependent protein kinase A (PKA)) activities on working memory will be reviewed. The implications of these experimental findings on the observed inverted-U relationship between D1 receptor stimulation and working memory, as well as age-associated working memory dysfunction, will be presented. Finally, we will discuss considerations for the development of clinical treatments for working memory disorders.

127

[Datta:2008aa]   A. Datta, M. Elwassif, F. Battaglia, and M. Bikson. Transcranial current stimulation focality using disc and ring electrode configurations: Fem analysis. *J Neural Eng*, 5(2):163–74, 2008.

Abstract: We calculated the electric fields induced in the brain during transcranial current stimulation (TCS) using a finite-element concentric spheres human head model. A range of disc electrode configurations were simulated: (1) distant-bipolar; (2) adjacent-bipolar; (3) tripolar; and three ring designs, (4) belt, (5) concentric ring, and (6) double concentric ring. We compared the focality of each configuration targeting cortical structures oriented normal to the surface ('surface-radial' and 'cross-section radial'), cortical structures oriented along the brain surface ('surface-tangential' and 'cross-section tangential') and non-oriented cortical surface structures ('surface-magnitude' and 'cross-section magnitude'). For surface-radial fields, we further considered the 'polarity' of modulation (e.g. superficial cortical neuron soma hyper/depolarizing). The distant-bipolar configuration, which is comparable with commonly used TCS protocols, resulted in diffuse (unfocal) modulation with bi-directional radial modulation under each electrode and

tangential modulation between electrodes. Increasing the proximity of the two electrodes (adjacent-bipolar electrode configuration) increased focality, at the cost of more surface current. At similar electrode distances, the tripolar-electrodes configuration produced comparable peak focality, but reduced radial bi-directionality. The concentric-ring configuration resulted in the highest spatial focality and uni-directional radial modulation, at the expense of increased total surface current. Changing ring dimensions, or use of two concentric rings, allow titration of this balance. The concentric-ring design may thus provide an optimized configuration for targeted modulation of superficial cortical neurons.

21, 23

[Davey:2000aa] K. Davey and C. M. Epstein. Magnetic stimulation coil and circuit design. *IEEE Trans Biomed Eng*, 47(11):1493–9, 2000.

Abstract: A detailed analysis of the membrane voltage rise commensurate with the electrical charging circuit of a typical magnetic stimulator is presented. The analysis shows how the membrane voltage is linked to the energy, reluctance, and resonant frequency of the electrical charging circuit. There is an optimum resonant frequency for any nerve membrane depending on its capacitive time constant. The analysis also shows why a larger membrane voltage will be registered on the second phase of a biphasic pulse excitation [1]. Typical constraints on three key quantities voltage, current, and silicone controlled rectifier (SCR) switching time dictate key components such as capacitance, inductance, and choice of turns.

28

[Davey:2005aa] Kent Davey. Designing transcranial magnetic stimulation systems. *IEEE Transactions on Biomedical Engineering*, 41(3):1142–1148, 2005.

Abstract: We explain the process of designing optimized tran- scranial magnetic stimulation systems and outline a method for identifying optimal system parameters such as the number of turns, the capacitor size, the working voltage, and the size of the stimulation coil. The method combines field analysis, linear and nonlinear circuit analysis, and neural strength–duration response parameters. The method uses boundary-element analysis to predict the electric field as a function of depth, frequency, current, and excitation coil size. It then uses the field analysis to determine the inductance as a function of size and, in general, current when a saturable core is used. Circuit analysis allows these electric field computations to be indexed against system parameters, and optimized for total system energy and stimula- tion coil size. System optimizations depend on desired stimulation depth. A distinguishing feature of the method is that it inherently treats excitation frequency as an unknown to be determined from optimization.

27

[Davey:2006aa] K.R. Davey and M. Riehl. Suppressing the surface field during transcranial magnetic stimulation. *IEEE Trans Biomed Eng*, 53(2):190–194, 2006. 27

[David:2003aa] O. David and K. J. Friston. A neural mass model for meg/eeg: coupling and neuronal dynamics. *Neuroimage*, 20(3):1743–55, 2003.

Abstract: Although MEG/EEG signals are highly variable, systematic changes in distinct frequency bands are commonly encountered. These frequency-specific changes represent robust neural correlates of cognitive or perceptual processes (for example, alpha rhythms emerge on closing the eyes). However, their functional significance remains a matter of debate. Some of the mechanisms that generate these signals are known at the cellular level and rest on a balance of excitatory and inhibitory interactions within and between populations of neurons. The kinetics of the ensuing population dynamics determine the frequency of oscillations. In this work we extended the classical nonlinear lumped-parameter model of alpha rhythms, initially developed by Lopes da Silva and colleagues [Kybernetik 15

(1974) 27], to generate more complex dynamics. We show that the whole spectrum of MEG/EEG signals can be reproduced within the oscillatory regime of this model by simply changing the population kinetics. We used the model to examine the influence of coupling strength and propagation delay on the rhythms generated by coupled cortical areas. The main findings were that (1) coupling induces phase-locked activity, with a phase shift of 0 or pi when the coupling is bidirectional, and (2) both coupling and propagation delay are critical determinants of the MEG/EEG spectrum. In forthcoming articles, we will use this model to (1) estimate how neuronal interactions are expressed in MEG/EEG oscillations and establish the construct validity of various indices of nonlinear coupling, and (2) generate event-related transients to derive physiologically informed basis functions for statistical modelling of average evoked responses.

66

[David:2004aa] O. David, D. Cosmelli, and K. J. Friston. Evaluation of different measures of functional connectivity using a neural mass model. *Neuroimage*, 21(2):659–73, 2004. 66

[Dayan:2001aa] Peter Dayan and L.F. Abbott. *Theoretical Neuroscience. Computational and Mathematical Modeling of Neural systems.* MIT Press, 2001. 52

[De-Lucia:2007aa] M. De Lucia, G.J.M. Parker, K. Embleton, J.M. Newton, and V. Walsh. Diffusion tensor mri-based estimation of the influence of brain tissue anisotropy on the effects of transcranial magnetic stimulation. *NeuroImage*, 36(4):1159–1170, 2007.

Abstract: We evaluate and discuss the relevance of fiber anisotropy in estimating the effect of transcranial magnetic stimulation (TMS) on the human brain. Finite element simulations were carried out on a three-dimensional model of the head that included anisotropic conductivity information derived from diffusion tensor imaging (DTI). The results show that anisotropy has minor effects both on the position of the main locus of activation and on its intensity. It has considerably more effect on the spatial distribution of the induced electric field, yielding differences of the order of 10area affected by magnetic stimulation is slightly larger when we include fiber anisotropy in the calculations than in an isotropic model. We also show that the induced field observed in the anisotropic model does not always align with the local fiber orientation but rather follows specific patterns of parallelity. These findings will help to improve the estimation of the areas involved in magnetic stimulation.

30, 31

[De-Schutter:1992aa] E. De Schutter. A consumer guide to neuronal modeling software. *Trends Neurosci.*, 15:462–464, 1992. 39

[Deans:2007aa] J. K. Deans, A. D. Powell, and J. G. Jefferys. Sensitivity of coherent oscillations in rat hippocampus to ac electric fields. *J Physiol*, 583(Pt 2):555–65, 2007.

Abstract: The sensitivity of brain tissue to weak extracellular electric fields is important in assessing potential public health risks of extremely low frequency (ELF) fields, and potential roles of endogenous fields in brain function. Here we determine the effect of applied electric fields on membrane potentials and coherent network oscillations. Applied DC electric fields change transmembrane potentials in CA3 pyramidal cell somata by 0.18 mV per V m(-1) applied. AC sinusoidal electric fields have smaller effects on transmembrane potentials: sensitivity drops as an exponential decay function of frequency. At 50 and 60 Hz it is approximately 0.4 that for DC fields. Effects of fields of ¡ or = 16 V m(-1) peak-to-peak (p-p) did not outlast application. Kainic acid (100 nm) induced coherent network oscillations in the beta and gamma bands (15-100 Hz). Applied fields of ¿ or = 6 V m(-1) p-p (2.1 V m(-1) r.m.s.) shifted the gamma peak in the power spectrum to centre on the applied field frequency or a subharmonic. Statistically significant effects on the timing of pyramidal cell firing within the oscillation appeared at distinct thresholds: at 50 Hz, 1 V m(-1) p-p (354 mV m(-1) r.m.s.) had statistically significant effects in 71slices, and 0.5 V m(-1) p-p (177 mV m(-1) r.m.s.) in 20fields

are consistent with current environmental guidelines. They correspond to changes in somatic potential of approximately 70 microV, below membrane potential noise levels for neurons, demonstrating the emergent properties of neuronal networks can be more sensitive than measurable effects in single neurons.

84, 86

[Di-Lazzaro:1998aa] V. Di Lazzaro, D. Restuccia, A. Oliviero, P. Profice, L. Ferrara, A. Insola, P. Mazzone, P. Tonali, and J. C. Rothwell. Magnetic transcranial stimulation at intensities below active motor threshold activates intracortical inhibitory circuits. *Exp Brain Res*, 119(2):265–8, 1998.

Abstract: A magnetic transcranial conditioning stimulus given over the motor cortex at intensities below threshold for obtaining electromyographical (EMG) responses in active hand muscles can suppress responses evoked in the same muscles at rest by a suprathreshold magnetic test stimulus given 1-5 ms later. In order to define the mechanism of this inhibitory effect, we recorded descending volleys produced by single and paired magnetic transcranial stimulation of motor cortex through high cervical, epidural electrodes implanted for pain relief in two conscious subjects with no abnormality of the central nervous system. The conditioning stimulus evoked no recognisable descending activity in the spinal cord, whilst the test stimulus evoked 3-4 waves of activity (I-waves). Conditioning stimulation suppressed the size of both the descending spinal cord volleys and the EMG responses evoked by the test stimulus. Inhibition of the descending spinal volleys was most pronounced at ISI 1 ms and had disappeared by ISI 5 ms. It was evident for all components following the I1-wave, while the I1-wave itself was not inhibited at all. We conclude that a small conditioning magnetic stimulus can suppress the excitability of human motor cortex, probably by activating local corticocortical inhibitory circuits.

62

[Di-Lazzaro:2001aa] V. Di Lazzaro, A. Oliviero, P. Mazzone, A. Insola, F. Pilato, E. Saturno, A. Accurso, P. Tonali, and J. C. Rothwell. Comparison of descending volleys evoked by monophasic and biphasic magnetic stimulation of the motor cortex in conscious humans. *Exp Brain Res*, 141(1):121–7, 2001.

Abstract: The descending spinal volleys evoked by monophasic and biphasic magnetic stimulation of the motor cortex were recorded from a bipolar electrode inserted into the cervical epidural space of four conscious human subjects. The results suggest that both phases of the biphasic pulse are capable of activating descending motor output. The pattern of recruitment of descending activity depends on the intensity of the stimulus and the relative threshold of each volley to each direction of current flow.

62

[Diamond:1988aa] D. M. Diamond, T. V. Dunwiddie, and G. M. Rose. Characteristics of hippocampal primed burst potentiation in vitro and in the awake rat. *J Neurosci*, 8(11):4079–88, 1988.

Abstract: A pattern of electrical stimulation based on 2 prominent physiological features of the hippocampus, complex spike discharge and theta rhythm, was used to induce lasting increases in responses recorded in area CA1 of hippocampal slices maintained in vitro and from the hippocampus of behaving rats. This effect, termed primed burst (PB) potentiation, was elicited by as few as 3 stimuli delivered to the commissural/associational afferents to CA1. The patterns of stimulus presentation consisted of a single priming pulse followed either 140 or 170 msec later by a high-frequency burst of 2-10 pulses; control stimulation composed of unprimed high-frequency trains of up to 10 pulses had no enduring effect. Of all intervals tested, only 140 and 170 msec delays between the priming and burst stimuli were effective. PB potentiation could be induced both homo- and heterosynaptically. In the latter case, the priming pulse and burst stimuli were delivered to different dendritic fields; under these conditions, the PB effect was confined to the "burst"

pathway. PB potentiation is not dependent on somal spiking; dendritic activation appears to be both necessary and sufficient for lasting changes to occur. Two findings indicate that PB potentiation and LTP have common mechanisms: (1) The effects of PB stimulation and LTP were not additive, in that saturation of the enhancement by PB stimulation eliminated any further increases in response with LTP stimulation; and (2) both PB potentiation and LTP were prevented if the N-methyl-D-aspartate antagonists 2-amino-5-phosphonovaleric acid or phencyclidine were added to the in vitro perfusion medium. Recordings from the hippocampus of awake rats demonstrated that PB potentiation of the CA1 population spike and slope of the EPSP are reliably induced under physiological conditions. This extensive characterization of PB stimulation provides novel information regarding the physiological and pharmacological basis of a possible role of endogenous rhythms in the processing and storage of information.

101

[Dodge:1973aa] F. A. Dodge and J. W. Cooley. Action potential of the motorneuron. *IBM Journal of Research and Development*, 17:219–229, 1973. 65

[Dodge:1979aa] F. A. Dodge. The nonuniform excitability of central neurons as exemplified by a model of the spinal motoneuron. In F. O. Schmidt and F. G. Worden, editors, *The neurosciences: fourth study program*, pages 439–455. MIT Press, Cambridge, 1979. 65

[Doi:2001aa] W. Doi, D. Sato, H. Fukuzako, and M. Takigawa. c-fos expression in rat brain after repetitive transcranial magnetic stimulation. *Neuroreport*, 12(6):1307–10, 2001.

Abstract: We investigated neuronal response to repetitive transcranial magnetic stimulation (rTMS) and electroconvulsive shock (ECS) in terms of c-Fos expression. In rats at postnatal day 49, six rTMS sessions induced widespread nuclear c-Fos-like immunoreactivity in frontal cortex, lateral orbital cortex, striatum, lateral septal nucleus, piriform cortex, dentate gyrus, Ammon's horn, cingulate cortex, parietal cortex, thalamus, occipital cortex, and amygdala; this reactivity was greater than with two sessions of rTMS or sham rTMS. ECS produced even stronger c-Fos expression than six sessions of rTMS in all regions except thalamus (no difference) and striatum (stronger with rTMS). Thus, functional modification of neuroanatomic substrates as demonstrated by c-Fos expression may partially differ between rTMS and ECS.

114, 165

[Donoghue:1995aa] J. P. Donoghue. Plasticity of adult sensorimotor representations. *Curr Opin Neurobiol*, 5(6):749–54, 1995.

Abstract: Plasticity of sensory and motor cortical and subcortical representations in the adult brain appears to be a general phenomenon in animals that has now been extended to humans. There is a growing understanding of the mechanisms and rules that regulate the form and extent of reorganization; these appear to include activity-dependent control of synaptic efficacy, details of circuit arrangements, and growth of new axonal arbors. Of particular relevance to plasticity of cerebral cortical sensorimotor representations is recent evidence for the participation of intracortical horizontal pathways. These fibers provide a substrate for reorganization and contain mechanisms for increases or decreases in synaptic efficacy that depend on particular spatiotemporal activation patterns.

99

[Duck:1990aa] FA Duck. *Physical properties of tissues. A comprehensive reference book*. London: Academic Press, 1990. 16

[Dwork:2004aa] A. J. Dwork, V. Arango, M. Underwood, B. Ilievski, G. Rosoklija, H. A. Sackeim, and S. H. Lisanby. Absence of histological lesions in primate models of ect and magnetic seizure therapy. *Am J Psychiatry*, 161(3):576–8, 2004.

Abstract: OBJECTIVE: The authors present preliminary findings from the first nonhuman primate neuropathological study of ECT to use perfusion fixation and adequate controls and the first to compare ECT with magnetic seizure therapy, to their knowledge. METHOD: Twelve Macaca mullata received 6 weeks of daily ECT, magnetic seizure therapy, or anesthesia alone. After perfusion fixation, their brains were examined while masked to intervention. RESULTS: No identified lesions were attributable to the interventions. Cortical and hippocampal immunoreactivity for glial fibrillary acidic protein (an astrocytic marker) was most intense in the group that received ECT. CONCLUSIONS: This small but rigorous primate study supports the view that ECT does not produce histological lesions in the brain and provides the first comparable safety data on magnetic seizure therapy.

118

[Dymond:1975aa] A. M. Dymond, R. W. Coger, and E. A. Serafetinides. Intracerebral current levels in man during electrosleep therapy. *Biol Psychiatry*, 10(1):101–4, 1975. 22

[Eaton:1992aa] H. Eaton. Electric field induced in a spherical volume conductor from arbitrary coils: application to magnetic stimulation and meg. *Med Biol Eng Comput*, 30(4):433–40, 1992.

Abstract: A mathematical method is presented that allows fast and simple computation of the electric field and current density induced inside a homogeneous spherical volume conductor by current flowing in a coil. The total electric field inside the sphere is computed entirely from a set of line integrals performed along the coil current path. Coils of any closed shape are easily accommodated by the method. The technique can be applied to magnetic brain stimulation and to magnetoencephalography. For magnetic brain stimulation, the total electric field anywhere inside the head can be easily computed for any coil shape and placement. The reciprocity theorem may be applied so that the electric field represents the lead field of a magnetometer. The finite coil area and gradiometer loop spacing can be precisely accounted for without any surface integration by using this method. The theory shows that the steady-state, radially oriented induced electric field is zero everywhere inside the sphere for ramping coil current and highly attenuated for sinusoidal coil current. This allows the model to be extended to concentric spheres which have different electrical properties.

26

[Ebert:1999aa] U. Ebert and U. Ziemann. Altered seizure susceptibility after high-frequency transcranial magnetic stimulation in rats. *Neurosci Lett*, 273(3):155–8, 1999.

Abstract: The long-term effect of repetitive transcranial magnetic stimulation (rTMS) on the susceptibility of amygdala kindling was studied. Two weeks after a single high-frequency rTMS train (120 A/micros, 20 Hz for 3 s), the rats had a 55of epileptic afterdischarges compared with sham-treated or control rats. However, subsequent kindling revealed no difference between rTMS-treated and control rats. Our data suggest that a single rTMS train has long-term effects on the neuronal excitability. These effects may be anticonvulsant and therefore support the safety of rTMS in clinical use.

118, 176

[Epstein:1983aa] B. R. Epstein and K. R. Foster. Anisotropy in the dielectric properties of skeletal muscle. *Med Biol Eng Comput*, 21(1):51–5, 1983. 17

[Epstein:1990aa] C. M. Epstein, D. G. Schwartzberg, K. R. Davey, and D. B. Sudderth. Localizing the site of magnetic brain stimulation in humans. *Neurology*, 40(4):666–70, 1990.

Abstract: Magnetic stimulation of the human brain is performed in clinical and research settings, but the site of activation has not been clearly localized in humans or other species. We used a set of magnetic stimulus coils with different field profiles to isolate movement of single digits at motor threshold and to calculate corresponding electric field strengths at various distances beneath the scalp. Two coils could produce the same electric field intensity at only 1 point. Thus, we could

estimate the depth of stimulation by finding the intersection of the electric field plots, which were then superimposed on MRIs of the underlying brain. In each of 3 subjects the field plots intersected at the crown of a gyrus, in the region of the central sulcus, an near the level of the gray-white junction. This position and the electric field orientation support localization to layer VI of cerebral cortex.

29

[Esselle:1992aa] K. P. Esselle and M. A. Stuchly. Neural stimulation with magnetic fields: analysis of induced electric fields. *IEEE Trans Biomed Eng*, 39(7):693–700, 1992.

> **Abstract:** Spatial distributions of the derivative of the electric field induced in a planar semi-infinite tissue model by various current-carrying coils and their utility in neural stimulation are evaluated. Analytical expressions are obtained for the electric field and its spatial derivatives produced by an infinitely short current element. Fields and their derivatives for an arbitrarily shaped coil are then obtained by numerical summation of contributions from all the elements forming the coil. The simplicity of the solution and a very short computation time make this method particularly attractive for gaining a physical insight into the spatial behavior of the stimulating parameter and for the optimization of coils. Such analysis is useful as the first step before undertaking a more complex numerical analysis of a model more closely representing the tissue geometry and heterogeneity.

25, 27

[Esselle:1994aa] K. P. Esselle and M. A. Stuchly. Quasi-static electric field in a cylindrical volume conductor induced by external coils. *IEEE Trans Biomed Eng*, 41(2):151–8, 1994.

> **Abstract:** An expansion technique based on modified Bessel functions is used to obtain an analytical solution for the electric field induced in a homogeneous cylindrical volume conductor by an external coil. The current in the coil is assumed to be changing slowly so that quasi- static conditions can be justified. Valid for any coil type, this solution is ideal for fast computation of the induced electric field at a large number of points. Efficient implementation of this method in a computer code is described and numerical results are presented for a perpendicular circular coil and a tangential double-square coil.

26, 27

[Esser:2005aa] S. K. Esser, S. L. Hill, and G. Tononi. Modeling the effects of transcranial magnetic stimulation on cortical circuits. *J Neurophysiol*, 94(1):622–39, 2005.

> **Abstract:** Transcranial magnetic stimulation (TMS) is commonly used to activate or inactivate specific cortical areas in a noninvasive manner. Because of technical constraints, the precise effects of TMS on cortical circuits are difficult to assess experimentally. Here, this issue is investigated by constructing a detailed model of a portion of the thalamocortical system and examining the effects of the simulated delivery of a TMS pulse. The model, which incorporates a large number of physiological and anatomical constraints, includes 33,000 spiking neurons arranged in a 3-layered motor cortex and over 5 million intra- and interlayer synaptic connections. The model was validated by reproducing several results from the experimental literature. These include the frequency, timing, dose response, and pharmacological modulation of epidurally recorded responses to TMS (the so-called I-waves), as well as paired-pulse response curves consistent with data from several experimental studies. The modeled responses to simulated TMS pulses in different experimental paradigms provide a detailed, self-consistent account of the neural and synaptic activities evoked by TMS within prototypical cortical circuits.

60, 61, 62, 63, 336

[Faes:1999aa] T. J. Faes, H. A. van der Meij, J. C. de Munck, and R. M. Heethaar. The electric resistivity of human tissues (100 hz-10 mhz): a meta- analysis of review studies. *Physiol Meas*, 20(4):R1–10, 1999.

Abstract: The electric resistivity of various human tissues has been reported in many studies, but on comparison large differences appear between these studies. The aim of this study was to investigate systematically the resistivities of human tissues as published in review studies (100 Hz- 10 MHz). A data set of 103 resistivities for 21 different human tissues was compiled from six review studies. For each kind of tissue the mean and its 95an analysis of covariance showed that the calculated means were not statistically different for most tissues, namely skeletal (171 omega cm) and cardiac (175 omega cm) muscle, kidney (211 omega cm), liver (342 omega cm), lung (157 omega cm) and spleen (405 omega cm), with bone (¿ 17,583 omega cm), fat (3,850 omega cm) and, most likely, the stratum corneum of the skin having higher resistivities. The insignificance of differences between various tissue means could imply an equality of their resistivities, or, alternatively, could be the result of the large confidence intervals which obscured real existing differences. In either case, however, the large 95confidence intervals reflected large uncertainties in our knowledge of resistivities of human tissues. Applications based on these resistivities in bioimpedance methods, EEG and EKG, should be developed and evaluated with these uncertainties in mind.

16, 17

[Ferdjallah:1996aa] Mohammed Ferdjallah and et al. Potential and current density distributions of cranial electrotherapy stimulation (ces) in a four-concentric-spheres model. *IEEE Transactions on Biomedical Engineering*, 43(9):939–943, 1996.

Abstract: Cranial electrotherapy stimulation (CES) has been successfully used for treatment of many psychiatric diseases. Its noninvasive nature is its major advantage over other forms of treatments such as drugs. It is postulated that the low electric current of CES causes the release of neurotransmitters. However, the current pathways have not been extensively investigated. In this paper, analytical and numerical methods are used to determine the distribution of potential and current density in a four zone concentric spheres model of the human head when excited by two electrodes diametrically opposite to each other. Because of the azimuthal symmetry, which is assumed in this study, a two-dimensional (2-D) finite difference approximation is derived in the spherical grid. The current density distribution is projected around the center of the model, where the thalamus is modeled as a concentric sphere. All dimensions and electrical properties of the model are adapted from clinical data. Results of this simulation indicate that, in contrast to previous beliefs, a small fraction of the CES current does reach the thalamic area and may facilitate the release of neurotransmitters.

20, 192, 344

[Fleischmann:1995aa] A. Fleischmann, K. Prolov, J. Abarbanel, and R. H. Belmaker. The effect of transcranial magnetic stimulation of rat brain on behavioral models of depression. *Brain Res*, 699(1):130–2, 1995.

Abstract: Magnetic stimulation of the brain in unanesthetized humans and animals can painlessly induce motor movements and has recently been reported to have antidepressant properties. In behavioral models of depression and electroconvulsive therapy including enhancement of apormorphine-induced stereotypy, reduction of immobility in the Porsolt swim test and increases in seizure threshold for subsequent stimulation, magnetic stimulation of rat brain had effects similar to those of electroconvulsive shock.

118, 119, 170

[Fleischmann:1996aa] A. Fleischmann, A. Sternheim, A. M. Etgen, C. Li, N. Grisaru, and R. H. Belmaker. Transcranial magnetic stimulation downregulates beta-adrenoreceptors in rat cortex. *J Neural Transm*, 103(11):1361–6, 1996.

Abstract: Recently, a method for transcranial magnetic stimulation (TMS) of the brain has been developed. Thus, it is possible to explore neurochemical and

behavioral effects of TMS in rats. Repeated TMS (9 days) reduced beta-adrenergic receptor binding in cortex, as does electroconvulsive shock (ECS) and other antidepressant treatments. Thus TMS appears to be a potential antidepressive treatment.

113, 164

[Fleischmann:1999aa] A. Fleischmann, S. Hirschmann, O. T. Dolberg, P. N. Dannon, and L. Grunhaus. Chronic treatment with repetitive transcranial magnetic stimulation inhibits seizure induction by electroconvulsive shock in rats. *Biol Psychiatry*, 45(6):759–63, 1999.

Abstract: BACKGROUND: Studies in laboratory animals suggest that repetitive transcranial magnetic stimulation (rTMS) and electroconvulsive shock (ECS) increase seizure inhibition acutely. This study was designed to explore whether chronic rTMS would also have seizure inhibition properties. METHODS: To this purpose we administered rTMS (Magstim Rapid) and sham rTMS twice daily (2.5 T, 4-sec train duration, 20 Hz) to two groups of 10 rats for 16 days. The rTMS coil was a 50-mm figure-8 coil held directly over the rat's head. Raters were blind to experimental groups. On days 11, 17, and 21 (5 days after the last rTMS) ECS was administered with a Siemens convulsator using three electrical charge levels. Variables examined were the presence or absence of seizures and seizure length (measured from the initiation of the tonic contraction until the end of the limb movement). RESULTS: At day 11 rTMS had no effect on seizures, and both rTMS and sham rTMS animals convulsed equally. At day 17, however, rTMS-treated animals convulsed significantly less (both at presence/absence of seizures, and at seizure length) than sham rTMS animals. At day 21 the effects of rTMS had disappeared. CONCLUSIONS: These findings suggest that rTMS administered chronically leads to changes in seizure threshold similar to those reported for ECS and ECT; however, these effects were short-lived.

119, 176

[Floel:2007aa] A. Floel and L. G. Cohen. Contribution of noninvasive cortical stimulation to the study of memory functions. *Brain Res Rev*, 53(2):250–9, 2007.

Abstract: In the memory domain, a large body of experimental evidence about subsystems of memory has been collected from classic lesion studies and functional brain imaging. Animal studies have provided information on molecular mechanisms of memory formation. Compared to this work, transcranial magnetic stimulation and transcranial direct current stimulation have made their own unique contribution. Here, we describe how noninvasive brain stimulation has been used to study the functional contribution of specific cortical areas during a given memory task, how these techniques can be used to assess LTP- and LTD-like plasticity in the living human brain, and how they can be employed to modulate memory formation in humans, suggesting an adjuvant role in neurorehabilitative treatments following brain injury.

101

[Foster:1979aa] K. R. Foster, J. L. Schepps, R. D. Stoy, and H. P. Schwan. Dielectric properties of brain tissue between 0.01 and 10 ghz. *Phys Med Biol*, 24(6):1177–87, 1979.

Abstract: Dielectric permittivity and conductivity are reported for grey and white matter from dog brain tissue between 0.01 and 10 GHz. Between 0.01 and approximately 1 GHz, the permittivity decreases and conductivity increases as a power law of frequency. Above 1 GHz, the conductivity increases quadratically with frequency due to dipolar reorientation of free water molecules in tissue; the apparent rotational relaxation frequency at 37 degrees C is 21–25 GHz, slightly below the 25 GHz characteristic frequency of pure water at that temperature. The microwave data are analysed using the Maxwell mixture theory applicable for a suspension of nonconducting, low permittivity spheres in bulk water. From the increase in conductivity above 1 GHz, and the tissue permittivity at 2–4 GHz, the apparent volume fraction of water is approximately 0.70 and 0.55 for grey

and white matter, respectively, about 10–15apparently due to a small fraction of water which does not contribute to the tissue permittivity above 1 GHz. Empirical equations are given to summarise the dielectric properties of 'average' brain tissue at 37 degrees C for future theoretical studies of microwave absorption in the head.

16

[Francis:2003aa] J. T. Francis, B. J. Gluckman, and S. J. Schiff. Sensitivity of neurons to weak electric fields. *J Neurosci*, 23(19):7255–61, 2003.

> **Abstract:** Weak electric fields modulate neuronal activity, and knowledge of the interaction threshold is important in the understanding of neuronal synchronization, in neural prosthetic design, and in the public health assessment of environmental extremely low frequency fields. Previous experimental measurements have placed the threshold between 1 and 5 mV/mm, although theory predicts that elongated neurons should have submillivolt per millimeter sensitivity near 100 microV/mm. We here provide the first experimental confirmation that neuronal networks are detectably sensitive to submillivolt per millimeter electrical fields [Gaussian pulses 26 msec full width at half-maximal, 140 microV/mm root mean square (rms), 295 microV/mm peak amplitude], an order of magnitude below previous findings, and further demonstrate that these networks are more sensitive than the average single neuron threshold (185 microV/mm rms, 394 microV/mm peak amplitude) to field modulation.

89

[Freeman:1963aa] W. J. Freeman. The electrical activity of a primary sensory cortex: Analysis of eeg waves. *Int Rev Neurobiol*, 5:53–119, 1963. 66

[Freeman:1968aa] W. J. Freeman. Patterns of variation in waveform of averaged evoked potentials from prepyriform cortex of cats. *J Neurophysiol*, 31(1):1–13, 1968. 66

[Freeman:1973aa] W. J. Freeman. *Neural modeling*, chapter A model of the olfactory system, pages 41–62. U. of California, Los Angeles, 1973. 66

[Freeman:1987aa] W. J. Freeman. Simulation of chaotic eeg patterns with a dynamic model of the olfactory system. *Biol Cybern*, 56(2-3):139–50, 1987. 67

[Freeman:1992aa] WJ Freeman. Tutorial on neurobiology: from single neurons to brain chaos. *Int J Bifurcation and Chaos*, 2(3):451–482, 1992. 66

[Fregni:2005aa] F. Fregni, P. S. Boggio, M. Nitsche, F. Bermpohl, A. Antal, E. Feredoes, M. A. Marcolin, S. P. Rigonatti, M. T. Silva, W. Paulus, and A. Pascual-Leone. Anodal transcranial direct current stimulation of prefrontal cortex enhances working memory. *Exp Brain Res*, 166(1):23–30, 2005.

> **Abstract:** Previous studies have claimed that weak transcranial direct current stimulation (tDCS) induces persisting excitability changes in the human motor cortex that can be more pronounced than cortical modulation induced by transcranial magnetic stimulation, but there are no studies that have evaluated the effects of tDCS on working memory. Our aim was to determine whether anodal transcranial direct current stimulation, which enhances brain cortical excitability and activity, would modify performance in a sequential-letter working memory task when administered to the dorsolateral prefrontal cortex (DLPFC). Fifteen subjects underwent a three-back working memory task based on letters. This task was performed during sham and anodal stimulation applied over the left DLPFC. Moreover seven of these subjects performed the same task, but with inverse polarity (cathodal stimulation of the left DLPFC) and anodal stimulation of the primary motor cortex (M1). Our results indicate that only anodal stimulation of the left prefrontal cortex, but not cathodal stimulation of left DLPFC or anodal stimulation of M1, increases the accuracy of the task performance when compared to sham stimulation of the same area. This accuracy enhancement during active stimulation cannot be accounted for by slowed responses, as response times were not changed by stimulation. Our results indicate that left prefrontal anodal stimulation leads to an enhancement of working memory performance. Furthermore,

this effect depends on the stimulation polarity and is specific to the site of stimulation. This result may be helpful to develop future interventions aiming at clinical benefits.

21, 129

[Frey:1993aa] U. Frey, Y. Y. Huang, and E. R. Kandel. Effects of camp simulate a late stage of ltp in hippocampal ca1 neurons. *Science*, 260(5114):1661–4, 1993.

> **Abstract:** Hippocampal long-term potentiation (LTP) is thought to serve as an elementary mechanism for the establishment of certain forms of explicit memory in the mammalian brain. As is the case with behavioral memory, LTP in the CA1 region has stages: a short-term early potentiation lasting 1 to 3 hours, which is independent of protein synthesis, precedes a later, longer lasting stage (L-LTP), which requires protein synthesis. Inhibitors of cyclic adenosine monophosphate (cAMP)-dependent protein kinase (PKA) blocked L-LTP, and analogs of cAMP induced a potentiation that blocked naturally induced L-LTP. The action of the cAMP analog was blocked by inhibitors of protein synthesis. Thus, activation of PKA may be a component of the mechanism that generates L-LTP.

101

[Freygang:1955aa] Jr. Freygang, W. H. and W. M. Landau. Some relations between resistivity and electrical activity in the cerebral cortex of the cat. *J Cell Comp Physiol*, 45:377–92, 1955. 18, 19

[Fry:1958aa] F.J. Fry and et al. Production of reversible changes in the central nervous system by ultrasound. *Science*, 127:83–84, 1958. 142

[Fujii:2004aa] S. Fujii, H. Sasaki, K. Mikoshiba, Y. Kuroda, Y. Yamazaki, A. Mostafa Taufiq, and H. Kato. A chemical ltp induced by co-activation of metabotropic and n-methyl-d-aspartate glutamate receptors in hippocampal ca1 neurons. *Brain Res*, 999(1):20–8, 2004.

> **Abstract:** In CA1 neurons of guinea pig hippocampal slices, long-term depression (LTD) was induced in the field EPSP response in the absence of test synaptic inputs (one stimulus every 20 s) by application of the metabotropic glutamate receptor (mGluR) agonist, aminocyclopentane-1S, 3R-dicarboxylic acid (ACPD). This effect was blocked and long-term potentiation (LTP) was induced by co-application of N-methyl-D-aspartate (NMDA) during ACPD perfusion (ACPD/NMDA-induced LTD). These results indicate that the state of NMDA receptor activation during ACPD perfusion determines whether LTP or LTD is induced in hippocampal CA1 neurons. Co-application of an inositol 1, 4, 5-trisphosphate (IP3) receptor inhibitor, 2-aminotheoxydiphenyl borate, during ACPD application had no effect on the ACPD/NMDA-induced LTP, but increased the magnitude of the ACPD-induced LTD, suggesting that the ACPD/NMDA-induced LTP involves NMDA receptors, but not IP3 receptors, whereas the converse applies to the ACPD-induced LTD.

101

[Fujiki:2004aa] M. Fujiki, H. Kobayashi, R. Inoue, and K. Ishii. Immediate plasticity in the motor pathways after spinal cord hemisection: implications for transcranial magnetic motor-evoked potentials. *Exp Neurol*, 187(2):468–77, 2004.

> **Abstract:** The present study evaluates motor functional recovery after C2 spinal cord hemisection with or without contralateral brachial root transection, which causes a condition that is similar to the crossed phrenic phenomenon on rats. Descending motor pathways, including the reticulospinal extrapyramidal tract and corticospinal pyramidal tracts, were evaluated by transcranial magnetic motor-evoked potentials (mMEPs) and direct cortical electrical motor-evoked potentials (eMEP), respectively. All MEPs recorded from the left forelimb were abolished immediately after the left C2 hemisection. Left mMEPs recovered dramatically immediately after contralateral right brachial root transection. Corticospinal eMEPs never recovered, regardless of transection. The facilitation of mMEPs in animals that had undergone combined contralateral root transection was well correlated

with open-field behavioral motor performance. Both electrophysiological and neurological facilitations were significantly attenuated by the selective serotonin synthesis inhibitor para-chlorophenylalanine (p-CPA). These results suggest that serotonergic reticulospinal fibers located contralateral to hemisection contribute to the behavioral and electrophysiological improvement that immediately follows spinal cord injury (SCI).

113, 164

[Fuortes1962]   M. G. Fuortes and F. Mantegazzini. Interpretation of the repetitive firing of nerve cells. *The Journal of general physiology*, 45:1163–1179, July 1962. 76

[Gabriel:1996aa] C. Gabriel, S. Gabriel, and E. Corthout. The dielectric properties of biological tissues: I. literature survey. *Phys Med Biol*, 41(11):2231–49, 1996.

> **Abstract:** The dielectric properties of tissues have been extracted from the literature of the past five decades and presented in a graphical format. The purpose is to assess the current state of knowledge, expose the gaps there are and provide a basis for the evaluation and analysis of corresponding data from an on-going measurement programme.

16, 18

[Gabriel:1996ab] S. Gabriel, R. W. Lau, and C. Gabriel. The dielectric properties of biological tissues: Iii. parametric models for the dielectric spectrum of tissues. *Phys Med Biol*, 41(11):2271–93, 1996.

> **Abstract:** A parametric model was developed to describe the variation of dielectric properties of tissues as a function of frequency. The experimental spectrum from 10 Hz to 100 GHz was modelled with four dispersion regions. The development of the model was based on recently acquired data, complemented by data surveyed from the literature. The purpose is to enable the prediction of dielectric data that are in line with those contained in the vast body of literature on the subject. The analysis was carried out on a Microsoft Excel spreadsheet. Parameters are given for 17 tissue types.

16, 18, 19

[Gabriel:1996ac] S. Gabriel, R. W. Lau, and C. Gabriel. The dielectric properties of biological tissues: Ii. measurements in the frequency range 10 hz to 20 ghz. *Phys Med Biol*, 41(11):2251–69, 1996.

> **Abstract:** Three experimental techniques based on automatic swept-frequency network and impedance analysers were used to measure the dielectric properties of tissue in the frequency range 10 Hz to 20 GHz. The technique used in conjunction with the impedance analyser is described. Results are given for a number of human and animal tissues, at body temperature, across the frequency range, demonstrating that good agreement was achieved between measurements using the three pieces of equipment. Moreover, the measured values fall well within the body of corresponding literature data.

16, 17, 18

[Gammaitoni:1998aa] Luca Gammaitoni and et al. Stochastic resonance. *Reviews of Modern Physics*, 70(1):223–287, 1998.

> **Abstract:** Over the last two decades, stochastic resonance has continuously attracted considerable attention. The term is given to a phenomenon that is manifest in nonlinear systems whereby generally feeble input information (such as a weak signal) can be be amplified and optimized by the assistance of noise. The effect requires three basic ingredients: (i) an energetic activation barrier or, more generally, a form of threshold; (ii) a weak coherent input (such as a periodic signal); (iii) a source of noise that is inherent in the system, or that adds to the coherent input. Given these features, the response of the system undergoes resonance-like behavior as a function of the noise level; hence the name stochastic resonance. The underlying mechanism is fairly simple and robust. As a consequence, stochastic resonance

has been observed in a large variety of systems, including bistable ring lasers, semiconductor devices, chemical reactions, and mechanoreceptor cells in the tail fan of a crayfish. In this paper, the authors report, interpret, and extend much of the current understanding of the theory and physics of stochastic resonance. They introduce the readers to the basic features of stochastic resonance and its recent history. Definitions of the characteristic quantities that are important to quantify stochastic resonance, together with the most important tools necessary to actually compute those quantities, are presented. The essence of classical stochastic resonance theory is presented, and important applications of stochastic resonance in nonlinear optics, solid state devices, and neurophysiology are described and put into context with stochastic resonance theory. More elaborate and recent developments of stochastic resonance theory are discussed, ranging from fundamental quantum properties—being important at low temperatures—over spatiotemporal aspects in spatially distributed systems, to realizations in chaotic maps. In conclusion the authors summarize the achievements and attempt to indicate the most promising areas for future research in theory and experiment.

134

[Gartside:1968aa] Ivor B. Gartside. Mechanisms of sustained increases of firing rate of neurones in the rat cerebral cortex after polarization: Role of protein synthesis. *Nature*, 220:383–384, October 1968.

> **Abstract:** THERE is increasing evidence that some long-term changes in the functioning of the central nervous system, for example, learning and memory, are dependent on protein synthesis1,2. The functioning of individual elements, however, is unaffected for long periods of time (24 h) using actinomycin D (ref. 3), which prevents RNA synthesis and for 7–12 h after puromycin has been given4, which blocks protein synthesis. It has been shown that sustained elevations of neuronal firing rate in the cortex following a 10 min period of polarization are not dependent on the activity of reverberating circuits, but more probably on changes in synaptic conduction (see preceding communication), and so it was decided to investigate the effects of inhibitors of protein synthesis on the establishment of these sustained changes.

45, 126, 127, 342

[Gartside:1968ab] Ivor B. Gartside. Mechanisms of sustained increases of firing rate of neurons in the rat cerebral cortex after polarization: reverberating circuits or modification of synaptic conductance? *Nature*, 220:382–383, October 1968.

> **Abstract:** THERE is increasing evidence that some long-term changes in the functioning of the central nervous system, for example, learning and memory, are dependent on protein synthesis1,2. The functioning of individual elements, however, is unaffected for long periods of time (24 h) using actinomycin D (ref. 3), which prevents RNA synthesis and for 7–12 h after puromycin has been given4, which blocks protein synthesis. It has been shown that sustained elevations of neuronal firing rate in the cortex following a 10 min period of polarization are not dependent on the activity of reverberating circuits, but more probably on changes in synaptic conduction (see preceding communication), and so it was decided to investigate the effects of inhibitors of protein synthesis on the establishment of these sustained changes.

126

[Geddes:1967aa] L. A. Geddes and L. E. Baker. The specific resistance of biological material–a compendium of data for the biomedical engineer and physiologist. *Med Biol Eng*, 5(3):271–93, 1967. 16, 17

[Geddes:1989aa] L.A. Geddes and L.E. Baker. *Principles of applied biomedical instrumentation*. J. Wiley & Sons, 1989. 16

[George:2000aa] M.S. George. *Transcranial magnetic stimulation in neuropsychiatry*. American Pscychiatric Press, 2000. 23

[Gerstner2002] Wulfram Gerstner and Werner M. Kistler. *Spiking Neuron Models*. Cambridge University Press, August 2002. 72, 73, 74, 75, 76, 337

[Ghai:2000aa] R. S. Ghai, M. Bikson, and D. M. Durand. Effects of applied electric fields on low-calcium epileptiform activity in the ca1 region of rat hippocampal slices. *J Neurophysiol*, 84(1):274–80, 2000.

> **Abstract:** It is well established that exogenous electric fields can suppress activity obtained in different models of epileptiform discharge such as penicillin and high potassium. In the low-calcium model of epilepsy, spontaneous epileptiform bursting is generated in the absence of synaptic transmission. It has been suggested that ephaptic interactions play a critical role in neuronal synchronization and burst propagation in this nonsynaptic model. We, therefore, tested the hypothesis that low-calcium bursting induced in the CA1 region of transverse and longitudinal hippocampal slices should be highly sensitive to exogenous electric fields. Uniform, low amplitude DC electric fields were applied during spontaneous low-calcium epileptiform activity. Modulation and full suppression of epileptiform activity was observed at field strengths between 1 and 5 mV/mm, a value significantly lower than in other in vitro models of epilepsy. We further investigated the hypothesis that the efficacy of electrical fields was related to changes in the extracellular space. Our results suggest that the osmolality of the perfusate can modulate the efficacy of electric fields. It was also observed that the ability of a field to suppress or modulate low-calcium activity was highly dependent on its orientation, polarity, as well as magnitude. Finally, it was observed that the extracellular potassium "waves" that normally accompany individual epileptiform events was abolished when the individual events were suppressed. These results suggest that DC fields modulate and suppress low-calcium activity by directly polarizing CA1 pyramidal cells.

85, 95

[Gielen:1984aa] F. L. Gielen, W. Wallinga-de Jonge, and K. L. Boon. Electrical conductivity of skeletal muscle tissue: experimental results from different muscles in vivo. *Med Biol Eng Comput*, 22(6):569–77, 1984. 17

[Gielen:1986aa] F. L. Gielen, H. E. Cruts, B. A. Albers, K. L. Boon, W. Wallinga-de Jonge, and H. B. Boom. Model of electrical conductivity of skeletal muscle based on tissue structure. *Med Biol Eng Comput*, 24(1):34–40, 1986. 17

[Gleeson:2007aa] P. Gleeson, V. Steuber, and R. A. Silver. neuroconstruct: a tool for modeling networks of neurons in 3d space. *Neuron*, 54(2):219–35, 2007.

> **Abstract:** Conductance-based neuronal network models can help us understand how synaptic and cellular mechanisms underlie brain function. However, these complex models are difficult to develop and are inaccessible to most neuroscientists. Moreover, even the most biologically realistic network models disregard many 3D anatomical features of the brain. Here, we describe a new software application, neuroConstruct, that facilitates the creation, visualization, and analysis of networks of multicompartmental neurons in 3D space. A graphical user interface allows model generation and modification without programming. Models within neuroConstruct are based on new simulator-independent NeuroML standards, allowing automatic generation of code for NEURON or GENESIS simulators. neuroConstruct was tested by reproducing published models and its simulator independence verified by comparing the same model on two simulators. We show how more anatomically realistic network models can be created and their properties compared with experimental measurements by extending a published 1D cerebellar granule cell layer model to 3D.

39

[Gluckman:1996aa] B. J. Gluckman, E. J. Neel, T. I. Netoff, W. L. Ditto, M. L. Spano, and S. J. Schiff. Electric field suppression of epileptiform activity in hippocampal slices. *J Neurophysiol*, 76(6):4202–5, 1996.

Abstract: 1. The effects of relatively small external DC electric fields on synchronous activity in CA1 and CA3 from transverse and longitudinal type hippocampal slices were studied. 2. To record neuronal activity during significant field changes, differential DC amplification was employed with a reference electrode aligned along an isopotential with the recording electrode. 3. Suppression of epileptiform activity was observed in 31 of 33 slices independent of region studied and type of slice but was highly dependent on field orientation with respect to the apical dendritic-somatic axis. 4. Modulation of neuronal activity in these experiments was readily observed at field strengths < or = 5-10 mV/mm. Suppression was seen with the field oriented (positive to negative potential) from the soma to the apical dentrites. 5. In vivo application of these results may be feasible.

95

[Gluckman:2001aa] B. J. Gluckman, H. Nguyen, S. L. Weinstein, and S. J. Schiff. Adaptive electric field control of epileptic seizures. *J Neurosci*, 21(2):590–600, 2001.

Abstract: We describe a novel method of adaptively controlling epileptic seizure-like events in hippocampal brain slices using electric fields. Extracellular neuronal activity is continuously recorded during field application through differential extracellular recording techniques, and the applied electric field strength is continuously updated using a computer-controlled proportional feedback algorithm. This approach appears capable of sustained amelioration of seizure events in this preparation when used with negative feedback. Seizures can be induced or enhanced by using fields of opposite polarity through positive feedback. In negative feedback mode, such findings may offer a novel technology for seizure control. In positive feedback mode, adaptively applied electric fields may offer a more physiological means of neural modulation for prosthetic purposes than previously possible.

85, 95

[Gnatkovsky:2008aa] V. Gnatkovsky, L. Librizzi, F. Trombin, and M. de Curtis. Fast activity at seizure onset is mediated by inhibitory circuits in the entorhinal cortex in vitro. *Ann Neurol*, 64(6):674–86, 2008.

Abstract: OBJECTIVE: Network mechanisms responsible for focal seizure initiation are still largely unknown. One of the prevalent seizure patterns observed during diagnostic intracranial recordings performed in patients with mesial temporal lobe epilepsy is characterized by fast activity at 20 to 30 Hz. We reproduced 20 to 30 Hz oscillations at seizure onset in the temporal lobe of the in vitro isolated guinea pig brain to study cellular and network mechanisms involved in its generation. METHODS: Seizure-like activity was induced in the isolated brain by 3-minute arterial perfusion of 50 microM bicuculline. Intracellular, extracellular, and ion-selective electrophysiological recordings were performed simultaneously in the entorhinal cortex (EC) during interictal-ictal transition. RESULTS: Principal neurons in deep and superficial layers of the EC did not generate action potentials during fast activity at ictal onset, whereas sustained firing was observed in putative interneurons. Within 5 to 10 seconds from seizure initiation, principal neurons generated a prominent firing that correlated with the appearance of extracellular hypersynchronous bursting discharges. In superficial neurons, fast activity correlated with rhythmic IPSPs that progressively decreased in amplitude during the development of a slow depolarization associated with an increase in extracellular potassium. INTERPRETATION: We conclude that in an acute model of temporal lobe ictogenesis, sustained inhibition without firing of EC principal neurons correlates with the onset of a focal seizure. The progression of the ictal discharge is contributed by a potassium-dependent change in reversal potential of inhibitory postsynaptic potentials. These findings demonstrate a prominent role of inhibitory networks during the transition to seizure in the EC.

68

[Goldberg1989] David E. Goldberg. *Genetic Algorithms in Search, Optimization, and Machine Learning.* Addison-Wesley Professional, January 1989. 79, 80

[Goncalves:2003aa] S. I. Goncalves, J. C. de Munck, J. P. Verbunt, F. Bijma, R. M. Heethaar, and F. H. Lopes da Silva. In vivo measurement of the brain and skull resistivities using an eit-based method and realistic models for the head. *IEEE Trans Biomed Eng*, 50(6):754–67, 2003.

Abstract: In vivo measurements of equivalent resistivities of skull (rho(skull)) and brain (rho(brain)) are performed for six subjects using an electric impedance tomography (EIT)-based method and realistic models for the head. The classical boundary element method (BEM) formulation for EIT is very time consuming. However, the application of the Sherman-Morrison formula reduces the computation time by a factor of 5. Using an optimal point distribution in the BEM model to optimize its accuracy, decreasing systematic errors of numerical origin, is important because cost functions are shallow. Results demonstrate that rho(skull)/rho(brain) is more likely to be within 20 and 50 rather than equal to the commonly accepted value of 80. The variation in rho(brain)(average = 301 omega x cm, SD = 13and rho(skull)(average = 12230 omega x cm, SD = 18when compared with the results using the sphere model, showing that the correction for geometry errors is essential to obtain realistic estimations. However, a factor of 2.4 may still exist between values of rho(skull)/rho(brain) corresponding to different subjects. Earlier results show the necessity of calibrating rho(brain) and rho(skull) by measuring them in vivo for each subject, in order to decrease errors associated with the electroencephalogram inverse problem. We show that the proposed method is suited to this goal.

17, 18, 19

[Grandori:1991aa] F. Grandori and P. Ravazzani. Magnetic stimulation of the motor cortex–theoretical considerations. *IEEE Trans Biomed Eng*, 38(2):180–91, 1991.

Abstract: The aim of this paper is to present a first approximation model for the computation of the electric fields produced in the brain tissues by magnetic stimulation. Results are given in terms of induced electric field and current density caused by coils of different radii and locations. Nontraditional coil locations and assemblies are also considered (multicoil arrangements). Model simulations show that a good control of the excitation spread can be achieved by proper positioning of the coil. It is also predicted that one of the major drawbacks of the technique, i.e., the poor ability to concentrate the current spread into a small brain area can be partially overcome by more effective coil positioning and/or assembly. Finally, some comparisons are made among the results obtained from electric and magnetic stimulation. This is thought to be of great help in the design of experiments aimed to understand the relative role of the different brain structures responsible for the motor response.

25, 27

[Griffiths:1999aa] D.J. Griffiths. *Introduction to electrodynamics*. Prentice Hall, 1999. 25

[Gur:2000aa] E. Gur, B. Lerer, E. Dremencov, and M. E. Newman. Chronic repetitive transcranial magnetic stimulation induces subsensitivity of presynaptic serotonergic autoreceptor activity in rat brain. *Neuroreport*, 11(13):2925–9, 2000.

Abstract: Repetitive transcranial magnetic stimulation (rTMS) is a novel procedure which has proven effective in the treatment of major depression. We administered rTMS chronically to rats in order to determine whether this procedure affected serotonergic neurotransmission in the prefrontal cortex. Basal 5-HT levels, and the effects of challenges with the 5-HT1A receptor agonist 8-OH-DPAT and the 5-HT1B antagonist GR 127935 on 5-HT levels were determined using in vivo microdialysis. Rats which had undergone chronic rTMS showed reduced responses to both challenges, indicating subsensitivity of both the presynaptic 5-HT1A autoreceptors situated somatodendritically in the raphe nuclei and the

5-HT1B autoreceptors situated on nerve terminals. Since such subsensitivity has been demonstrated after other antidepressant treatments, our results indicate that these treatments and rTMS may have a common mechanism of action.

164

[Guzowski:2001aa] J. F. Guzowski, B. Setlow, E. K. Wagner, and J. L. McGaugh. Experience-dependent gene expression in the rat hippocampus after spatial learning: a comparison of the immediate-early genes arc, c-fos, and zif268. *J Neurosci*, 21(14):5089–98, 2001.

Abstract: Neuronal immediate-early gene (IEG) expression is regulated by synaptic activity and plays an important role in the neuroplastic mechanisms critical to memory consolidation. IEGs can be divided into two functional classes: (1) regulatory transcription factors (RTFs), which can broadly influence cell function depending on the "downstream" genes they regulate, and (2) "effector" proteins, which may directly modulate specific cellular functions. The objective of the current study was to determine whether the expression of an effector IEG (Arc) was similar to, or different from, that of two well characterized RTF IEGs (c-fos and zif268) after learning. IEG RNA levels from rats trained in spatial and nonspatial water tasks were determined using RNase protection assays and in situ hybridization. Overall, the regulation of the three IEGs was similar in the hippocampus and the entorhinal and primary visual cortices. Consequently, IEG RNA levels were positively correlated within a structure. By contrast, Arc and zif268 RNA levels were not correlated or only weakly correlated across structures, although c-fos RNA levels were moderately correlated across structures. Arc RNA expression differed from that of zif268 and c-fos in two regards: (1) hippocampal Arc RNA levels were correlated with learning of the hippocampal-dependent spatial, but not hippocampal-independent cued response, water task, and (2) Arc RNA levels in the hippocampus and entorhinal cortex increased after spatial reversal learning relative to an asymptotic performance group. Thus, although the expression of Arc, zif268, and c-fos exhibited many similarities, Arc was most responsive to differences in behavioral task demands.

114

[Haass:1993aa] C. Haass and D. J. Selkoe. Cellular processing of beta-amyloid precursor protein and the genesis of amyloid beta-peptide. *Cell*, 75(6):1039–42, 1993. 120

[Hallet:2005aa] M Hallet and S. Chokroverty. *Magnetic stimulation in clinical neurophysiology*. Butterworth-Heinemann, 2005. 23

[Hallett:2007aa] M. Hallett. Transcranial magnetic stimulation: a primer. *Neuron*, 55(2):187–99, 2007.

Abstract: Transcranial magnetic stimulation (TMS) is a technique for noninvasive stimulation of the human brain. Stimulation is produced by generating a brief, high-intensity magnetic field by passing a brief electric current through a magnetic coil. The field can excite or inhibit a small area of brain below the coil. All parts of the brain just beneath the skull can be influenced, but most studies have been of the motor cortex where a focal muscle twitch can be produced, called the motor-evoked potential. The technique can be used to map brain function and explore the excitability of different regions. Brief interference has allowed mapping of many sensory, motor, and cognitive functions. TMS has some clinical utility, and, because it can influence brain function if delivered repetitively, it is being developed for various therapeutic purposes.

24

[Hamalainen:1989aa] M. S. Hamalainen and J. Sarvas. Realistic conductivity geometry model of the human head for interpretation of neuromagnetic data. *IEEE Trans Biomed Eng*, 36(2):165–71, 1989.

Abstract: In this paper, the computational and practical aspects of a realistically-shaped multilayer model for the conductivity geometry of the human head are discussed. A novel way to handle the numerical difficulties caused by the presence

of the poorly conducting skull is presented. Using our method, both the potential on the surface of the head and the magnetic field outside the head can be computed accurately. The procedure was tested with the multilayer sphere model, for which analytical expressions are available. The method is then applied to a realistically-shaped head model, and it is numerically shown that for the computation of B, produced by cerebral current sources, it is sufficient to consider a brain-shaped homogeneous conductor only since the secondary currents on the outer interfaces give only a negligible contribution to the magnetic field outside the head. Comparisons with the sphere model are also included to pinpoint areas where the homogeneous conductor model provides essential improvements in the calculation of the magnetic field outside the head.

30

[Hanggi:2002aa] Peter Hänggi. Stochastic resonance in biology. *ChemPhysChem*, 3:285–290, 2002.

Abstract: Noise is usually thought of as the enemy of order rather than as a constructive influence. In nonlinear systems that possess some sort of threshold, random noise plays a beneficial role in enhancing the detection of weak information-carrying signals. This phenomenon, termed stochastic resonance, does find useful applications in physical, biological, and biomedical contexts. Certain biological systems may even use this effect for optimizing function and behavior.

144

[Hargreaves:2005aa] G. A. Hargreaves, I. S. McGregor, and P. S. Sachdev. Chronic repetitive transcranial magnetic stimulation is antidepressant but not anxiolytic in rat models of anxiety and depression. *Psychiatry Res*, 137(1-2):113–21, 2005.

Abstract: Transcranial magnetic stimulation (TMS) has been proposed as a treatment for depression and anxiety disorders. While the antidepressant effect has been modelled in animals, there have been few attempts to examine a possible anxiolytic effect of repetitive TMS (rTMS) in animal models. We administered 18 days of rTMS to male Sprague-Dawley rats. On days 10 through 18, rats were tested in several anxiety models (social interaction, emergence, elevated plus-maze, and predator odor avoidance) and in the forced swim test. No group differences were apparent on any of the anxiety models, while TMS produced an antidepressant effect in the forced swim test. Interestingly, on day 1 of the forced swim test, the home cage control group displayed increased swimming behaviour compared with sham-treated animals, suggesting an observable level of stress may have accompanied sham treatment. The results from the forced swim test suggested that TMS had modest antidepressant properties, but it did not show anxiolytic properties in the models examined. The study also suggested that stress associated with handling should be taken into account in the interpretation of TMS studies in animals.

118, 173

[Hattori:1990aa] A. Hattori, Y. and et al. Biphasic effects of polarizing current on adenosine-sensitive generation of cyclic amp in rat cerebral cortex. *Neurosci Lett*, 116(3):320–4, 1990. 126

[Haueisen:1997aa] J. Haueisen, C. Ramon, M. Eiselt, H. Brauer, and H. Nowak. Influence of tissue resistivities on neuromagnetic fields and electric potentials studied with a finite element model of the head. *IEEE Trans Biomed Eng*, 44(8):727–35, 1997.

Abstract: Modeling in magnetoencephalography (MEG) and electroencephalography (EEG) requires knowledge of the in vivo tissue resistivities of the head. The aim of this paper is to examine the influence of tissue resistivity changes on the neuromagnetic field and the electric scalp potential. A high-resolution finite element method (FEM) model (452,162 elements, 2-mm resolution) of the human head with 13 different tissue types is employed for this purpose. Our main finding was that the magnetic fields are sensitive to changes in the tissue resistivity in the vicinity of the source. In comparison, the electric surface potentials are sensitive

to changes in the tissue resistivity in the vicinity of the source and in the vicinity of the position of the electrodes. The magnitude (strength) of magnetic fields and electric surface potentials is strongly influenced by tissue resistivity changes, while the topography is not as strongly influenced. Therefore, an accurate modeling of magnetic field and electric potential strength requires accurate knowledge of tissue resistivities, while for source localization procedures this knowledge might not be a necessity.

30

[Hausmann:2000aa] A. Hausmann, C. Weis, J. Marksteiner, H. Hinterhuber, and C. Humpel. Chronic repetitive transcranial magnetic stimulation enhances c-fos in the parietal cortex and hippocampus. *Brain Res Mol Brain Res*, 76(2):355–62, 2000.

Abstract: Repetitive transcranial magnetic stimulation (rTMS) is a novel non-invasive method with anti-depressant properties. However, the mechanism of activation on the cellular level is unknown. Twelve hours after the last chronic rTMS treatment (14 days, once per day, 20 Hz, 10 s, 75markedly increased in neurons in layers I-IV and VI of the parietal cortex and in few scattered neurons in the hippocampus of Sprague-Dawley rats. The cortical activation was not blocked by the NMDA antagonist MK-801. The increase of c-fos was not paralleled by an increased glial response and activation of cortical growth factors. Thus, it is concluded that chronic rTMS differentially activates parietal cortical layers and this might be involved in mediating anti-depressant activity in other brain areas.

113, 114, 165

[Hayashi:1988aa] Y. Hayashi, Y. Hattori, A. Moriwaki, H. Asaki, and Y. Hori. Effects of prolonged weak anodal direct current on electrocorticogram in awake rabbit. *Acta Med Okayama*, 42(5):293–6, 1988.

Abstract: The effects of prolonged weak anodal direct current (DC) on the electrocorticogram (ECoG) were investigated in awake rabbits. When the current (20-40 microA) was applied to the motor region of the cerebral cortex, seizure activity in the ECoG appeared from the frontal cortex. Repeated application of the DC decreased the threshold current for producing the seizure activity. Diazepam significantly elevated the threshold of the seizure activity. In contrast to the marked changes in the ECoG, no behavioral changes were observed during or after the application of weak anodal DC. The changes in the ECoG are discussed in relation to the intensity and duration of the DC.

130

[Hayward:2007aa] G. Hayward, M. A. Mehta, C. Harmer, T. J. Spinks, P. M. Grasby, and G. M. Goodwin. Exploring the physiological effects of double-cone coil tms over the medial frontal cortex on the anterior cingulate cortex: an h2(15)o pet study. *Eur J Neurosci*, 25(7):2224–33, 2007.

Abstract: Transcranial magnetic stimulation (TMS) using a double-cone coil over the medial frontal cortex has the potential to clarify the function of the anterior cingulate cortex (ACC) in cognition, emotion and mood disorders. Following demonstration of disruption of performance on psychological tasks closely linked to cingulate function using this TMS technique, the current study aimed to directly measure the regional distribution of physiological effects of stimulation in the brain with H2(15)O PET. Experiment 1 assessed the effect of increasing numbers of pulse trains of TMS on regional cerebral blood flow (rCBF). Experiment 2 assessed the capacity of medial frontal TMS to modulate brain activity associated with the Stroop task using medial parietal TMS as a control site of stimulation. SPM99 analyses, using the ACC as a region of interest, revealed clusters of increased rCBF during medial frontal TMS in Brodmann area 24 and reduced rCBF in more ventral ACC, the latter occurring in both experiments. In a whole-brain analysis, striking changes in rCBF were observed distal to the ACC following medial frontal TMS. Although TMS reliably affected Stroop task performance in early

trials, there was no interaction between TMS and Stroop condition in rCBF. Our results suggest that medial frontal TMS using the double-cone coil can affect ACC activity. However, a number of more distal cortical areas were also affected in these experiments. These additional changes may reflect either 'downstream' effects of altered cingulate cortex activity or direct effects of the coil.

29

[Hedges:2003aa] D. W. Hedges, C. Massari, D. L. Salyer, T. D. Lund, J. L. Hellewell, A. C. Johnson, and E. D. Lephart. Duration of transcranial magnetic stimulation effects on the neuroendocrine stress response and coping behavior of adult male rats. *Prog Neuropsychopharmacol Biol Psychiatry*, 27(4):633–8, 2003.

Abstract: BACKGROUND: Transcranial magnetic stimulation (TMS) is a relatively novel, noninvasive method of altering cerebral electrophysiological activity that produces localized and reversible changes in brain tissue. TMS has been shown to have antidepressant properties in both human trials and animal models. Additionally, TMS may alter hypothalamic-pituitary-adrenal (HPA) function resulting in a normalized dexamethasone suppression test in some depressed subjects and an attenuated stress-induced increase in adrenocorticotropic hormone (ACTH) and a possibly lowered basal corticosterone (CORT) concentration in rats. This research was undertaken to investigate the duration of these behavioral and neuroendocrine effects of TMS in rats. METHODS: In this study, serum ACTH, CORT, testosterone, and luteinizing hormone (LH) concentrations following and immobility parameters during a forced-swim test in adult male rats were evaluated immediately and 1, 3, 5, 7, and 14 days subsequent to a 10-day course of once-daily TMS or sham application. RESULTS: TMS animals had significantly higher ACTH and CORT concentrations immediately following the 10-day course of TMS compared to sham controls. Higher CORT concentrations (numerically but not statistically) were displayed by TMS-treated animals 1 and 3 days after the 10-day application course, although there were no significant differences between TMS and sham groups for ACTH or CORT levels 1, 3, 5, 7, and 14 days following application of sham or TMS. No significant differences were found between groups for serum testosterone and LH levels at any given collection time point. Immobility time, a measure of coping ability that is predictive of human antidepressant response, was significantly decreased (i.e., time spent actively swimming was significantly increased) immediately after the 10-day course of TMS. Thereafter, a nonsignificant numerical trend at 1 and 3 days after TMS application for immobility times between the TMS and control groups was observed (TMS¡control values). No significant differences in immobility between TMS and control animals were found at subsequent time points. CONCLUSIONS: The present findings suggest that the HPA stress axis is significantly altered immediately following a 10-day course of TMS in that a significant increase in ACTH and CORT levels in TMS-treated animals corresponded to a significant decrease in immobility times in the forced-swim test compared to control values. Finally, based upon the obtained results, the TMS effects in rats appear to be of relatively short duration.

118, 173

[Hedges:2005aa] D. W. Hedges, B. J. Higginbotham, D. L. Salyer, and T. D. Lund. Transcranial magnetic stimulation effects on one-trial learning and response to anxiogenic stimuli in adult male rats. *J Ect*, 21(1):25–30, 2005.

Abstract: Transcranial magnetic stimulation (TMS) is a relatively new technique for inducing small, localized, and reversible changes in living brain tissue and has been suggested to have antidepressant properties in humans and animal models of depression. Memory function generally has been found to be unaffected by TMS, although some studies have raised the possibility of memory interference from TMS. Additionally, there have been indirect indications that TMS may possess anxiolytic features. This study examines the effects of TMS in animal models of one-trial learning and anxiety. In this study, short-term treatment with TMS

compared with identically handled animals not given TMS in adult rats resulted in no significant differences in memory as assessed both by a one-time learning paradigm and by components of an elevated-plus maze task, that TMS does not impair memory as assessed by these tasks. In addition, no changes were found in anxiety-like behavior on the elevated plus maze task. In summary, these findings support previous reports that TMS does not interfere with memory function. There was no evidence of an anxiolytic response from TMS in rats as assessed by the elevated plus maze test.

173

[Heller:1992aa] Leon Heller and David B. van Hulsteyn. Brain stimulation using electromagnetic sources: theoretical aspects. *Biophys. J.*, 63:129–138, 1992.

> **Abstract:** ABSTRACT We prove that, at the frequencies generally proposed for extracranial stimulation of the brain, it is not possible, using any superposition of external current sources, to produce a three-dimensional local maximum of the electric field strength inside the brain. The maximum always occurs on a boundary where the conductivity jumps in value. Nevertheless, it may be possible to achieve greater two-dimensional focusing and shaping of the electric field than is currently available. Towards this goal we have used the reciprocity theorem to present a uniform treatment of the electric field inside a conducting medium produced by a variety of sources: an external magnetic dipole (current loop), an external electric dipole (linear antenna), and surface and depth electrodes. This formulation makes use of the lead fields from magneto- and electroencephalography. For the special case of a system with spherically symmetric conductiv- ity, we derive a simple analytic formula for the electric field due to an external magnetic dipole. This formula is independent of the conductivity profile and therefore embraces spherical models with any number of shells. This explains the "insensitivity" to the skull's conductivity that has been described in numerical studies. We also present analytic formulas for the electric field due to an electric dipole, and also surface and depth electrodes, for the case of a sphere of constant conductivity.

16, 26, 187, 191

[Hemingway:1932aa] A. Hemingway and J. F. McClendon. The high frequency resistance of human tissue. *Am J Physiol*, 102:56–9, 1932. 17

[Herrmann:2001aa] Christoph S. Herrmann. Human eeg responses to 1–100hz flicker: resonance phenomena in visual cortex and their potential correlation to cognitive phenomena. *Exp Brain Res*, 137:346–353, 2001.

> **Abstract:** The individual properties of visual objects, like form or color, are represented in different areas in our visual cortex. In order to perceive one coherent ob- ject, its features have to be bound together. This was found to be achieved in cat and monkey brains by tem- poral correlation of the firing rates of neurons which code the same object. This firing rate is predominantly observed in the gamma frequency range (approx. 30–80Hz, mainly around 40Hz). In addition, it has been shown in humans that stimuli which flicker at gamma frequencies are processed faster by our brains than when they flicker at different frequencies. These effects could be due to neural oscillators, which preferably oscillate at certain frequencies, so-called resonance frequencies. It is also known that neurons in visual cortex respond to flickering stimuli at the frequency of the flickering light. If neural oscillators exist with resonance frequencies, they should respond more strongly to stimulation with their resonance frequency. We performed an experiment, where ten human subjects were presented flickering light at frequencies from 1 to 100 Hz in 1-Hz steps. The event-related potentials exhibited steady-state oscilla- tions at all frequencies up to at least 90Hz. Interestingly, the steady-state potentials exhibited clear resonance phe- nomena around 10, 20, 40 and 80Hz. This could be a potential neural basis for gamma oscillations in binding experiments. The pattern of results resembles that of multiunit activity and local field potentials in cat visual cortex.

136

[Hines:1984aa] M. Hines. Efficient computation of branched nerve equations. *Int J Biomed Comput*, 15(1):69–76, 1984.

> **Abstract:** Three simple improvements are presented which, for a given accuracy, result in a 10-20-fold decrease in computation time for simulation of arbitrarily branched active cables with Hodgkin Huxley (HH) kinetics. The first improvement takes advantage of the essentially tridiagonal character of the matrix equation for each branch of a 'tree' network and solves the equations as efficiently as for an unbranched cable. The second improvement evaluates the HH membrane conductances at the midpoint of a time step, delta t, to maintain full second order accuracy, 0(delta t2), with no increase in the number of computational steps. The third improvement makes use of 'premultiplied' HH rate function tables for very efficient second order correct integration of HH membrane conductance.

38, 39

[Hines:2001aa] M. L. Hines and N. T. Carnevale. Neuron: a tool for neuroscientists. *Neuroscientist*, 7(2):123–35, 2001.

> **Abstract:** NEURON is a simulation environment for models of individual neurons and networks of neurons that are closely linked to experimental data. NEURON provides tools for conveniently constructing, exercising, and managing models, so that special expertise in numerical methods or programming is not required for its productive use. This article describes two tools that address the problem of how to achieve computational efficiency and accuracy.

38

[Hines:2003aa] M. L. Hines and N. T. Carnevale. The neuron simulation environment. In M. A. Arbib, editor, *The Handbook of Brain Theory and Neural Networks*. MIT Press, Cambridge, 2nd edition, 2003. 38

[Hines:2007aa] M. L. Hines, T. M. Morse, and N. T. Carnevale. Model structure analysis in neuron : toward interoperability among neural simulators. *Methods Mol Biol*, 401:91–102, 2007.

> **Abstract:** One of the more important recent additions to the NEURON simulation environment is a tool called ModelView, which simplifies the task of understanding exactly what biological attributes are represented in a computational model. Here, we illustrate how ModelView contributes to the understanding of models and discuss its utility as a neuroinformatics tool for analyzing models in online databases and as a means for facilitating interoperability among simulators in computational neuroscience.

38

[Hodgkin:1952aa] A. L. Hodgkin and A. F. Huxley. Currents carried by sodium and potassium ions through the membrane of the giant axon of loligo. *J Physiol*, 116(4):449–72, 1952. 37

[Hoekema:2004aa] R. Hoekema and et al. Measurement of the conductivity of skull, temporarily removed during epilepsy surgery. *Brain Topography*, 16(1):29–38, 2004.

> **Abstract:** Abstract The conductivity of the human skull plays an important role in source localization of brain activity, because it is low as compared to other tissues in the head. The value usually taken for the conductivity of skull is questionable. In a carefully chosen procedure, in which sterility, a stable temperature, and relative humidity were guaranteed, we measured the (lumped, homogeneous) conductivity of the skull in five patients undergoing epilepsy surgery, using an extended four-point method. Twenty-eight current configurations were used, in each of which the potential due to an applied current was measured. A finite difference model, incorporating the geometry of the skull and the electrode locations, derived from CT data, was used to mimic the measurements. The conductivity values found were ranging from 32 mS/m to 80 mS/m, which is much higher than the values reported in other studies. Causes for these higher conductivity values are discussed.

18

[Hoeltzell:1979aa] P. B. Hoeltzell and R. W. Dykes. Conductivity in the somatosensory cortex of the cat –
evidence for cortical anisotropy. *Brain Res*, 177(1):61–82, 1979.

Abstract: Orthogonal conductivity components were determined for 3 depths in
the somatosensory cortex of cats and relative vertical conductivities were deter-
mined for all depths. (2) For cortical layers II–III, the conductivity was nearly
twice as large (1.7 times) in the anteroposterior direction as it was in the medio-
lateral direction, whereas in layer IV the conductivity in the mediolateral direction
was about 1.4 times greater than it was in the anteroposterior direction. (3) With
the exception of the anteroposterior direction of layers II–III and the mediolateral
direction of layer IV, the vertical conductivity of the cortex was always greater
than either of the horizontal conductivities. (4) Vertical conductivities varied with
cortical depth. The lowest vertical conductivity occurred in layer I. It increased in
layers II–III, dropped in layer IV, and increased again in layer VI to a value com-
parable to layers II–III. (5) Adjacent determinations of conductivity indicated that
over short distances (1–2 mm) the cortex was electrically homogeneous. (6) These
data suggest that the cellular organization of the somatosensory cortex changes
markedly and abruptly with cortical depth. Furthermore, they suggest that a sig-
nificant portion of the coritcal neuropile in layers II–III and in layer IV is highly
polarized. The possible anatomical basis for this polarization is discussed as are
the effects of cortical anisotropy upon conductivity measurements.

18

[Holdefer:2006aa] R. N. Holdefer, R. Sadleir, and M. J. Russell. Predicted current densities in the brain during
transcranial electrical stimulation. *Clin Neurophysiol*, 117(6):1388–97, 2006.

Abstract: OBJECTIVE: We sought an electrical modeling approach to evalu-
ate the potential application of finite element method (FEM) modeling to predict
current pathways and intensities in the brain after transcranial electrical stim-
ulation. METHODS: A single coronal MRI section through the head, including
motor cortex, was modeled using FEM. White matter compartments with both
anatomically realistic anisotropies in resistivity and with a homogeneous resistivity
were modeled. Current densities in the brain were predicted for electrode sites on
the scalp and after theoretical application of a conductive head restraint device.
RESULTS: Localized current densities were predicted for the model with white
matter anisotropies. Differences in predicted peak current densities were related
to location of stimulation sites relative to deep sulci in the brain and scalp shunt-
ing that was predicted to increase with inter-electrode proximity. A conductive
head restraint device was predicted to shunt current away from the brain when
a constant current source was used. CONCLUSIONS: The complex geometry of
different tissue compartments in the head and their contrasting resistivities may
jointly determine the strength and location of current densities in the brain af-
ter transcranial stimulation. This might be predictable with FEM incorporating
white matter anisotropies. Conductive head restraint devices during surgery may
be contraindicated with constant current stimulation. SIGNIFICANCE: Individu-
ally optimized tcMEP monitoring and localized transcranial activation in the brain
might be possible through FEM modeling.

30

[Holscher:1997aa] C. Holscher, R. Anwyl, and M. J. Rowan. Stimulation on the positive phase of hippocampal
theta rhythm induces long-term potentiation that can be depotentiated by stimulation on the
negative phase in area ca1 in vivo. *J Neurosci*, 17(16):6470–7, 1997.

Abstract: Long-term potentiation (LTP) of synaptic transmission induced by
high-frequency stimulation (HFS) is considered to be a model for learning pro-
cesses; however, standard HFS protocols consisting of long trains of HFS are very
different from the patterns of spike firing in freely behaving animals. We have

investigated the ability of brief bursts of HFS triggered at different phases of background theta rhythm to mimic more natural activity patterns. We show that a single burst of five pulses at 200 Hz given on the positive phase of tail pinch-triggered theta rhythm reliably induced LTP in the stratum radiatum of the hippocampus of urethane-anesthetized rats. Three of these bursts saturated LTP, and 10 bursts occluded the induction of LTP by long trains of HFS. Burst stimulation on the negative phase or at zero phase of theta did not induce LTP or long-term depression. In addition, stimulation with 10 bursts on the negative phase of theta reversed previously established LTP. The results show that the phase of sensory-evoked theta rhythm powerfully regulates the ability of brief HFS bursts to elicit either LTP or depotentiation of synaptic transmission. Furthermore, because complex spike activity of approximately five pulses on the positive phase of theta rhythm can be observed in freely moving rats, LTP induced by the present theta-triggered stimulation protocol might model putative synaptic plastic changes during learning more closely than standard HFS-induced LTP.

104, 115

[Hsu:2000aa] K. H. Hsu and D. M. Durand. Prediction of neural excitation during magnetic stimulation using passive cable models. *IEEE Trans Biomed Eng*, 47(4):463–71, 2000.

Abstract: A method for predicting neural excitation during magnetic stimulation using passive cable models has been developed. This method uses the information of the threshold capacitor voltage for magnetic stimulation coils to determine the equivalent excitation thresholds for the passive transient (PT) and passive steady-state (PSS) cable models as well as for the activating function. The threshold values for the PT, PSS models, and the activating function vary only with the pulsewidth of the stimulus for a variety of coils at different locations and orientations. Furthermore, the excitation threshold for the PSS model is also independent of axon diameter and best fitted to a simple mathematical function. By comparing the transmembrane potential of the PSS model with the corresponding threshold, the prediction of excitation during magnetic stimulation can be made. Similarly, it is also possible to predict excitation using the PT model and the activating function with the corresponding thresholds provided. By taking advantage of the weighted pulsewidth, this method can even predict the excitation for stimuli with various waveforms, greatly simplifying the determination of neural excitation for magnetic stimulation.

60

[Hsu:2001aa] K. H. Hsu and D. M. Durand. A 3-d differential coil design for localized magnetic stimulation. *IEEE Trans Biomed Eng*, 48(10):1162–8, 2001.

Abstract: A novel three-dimensional (3-D) differential coil has been designed for improving the localization of magnetic stimulation. This new coil design consists of a butterfly coil with two additional wing units and an extra bottom unit, both perpendicular to the plane of the butterfly coil. The wing units produce opposite fields to restrict the spread of induced fields while the bottom unit enhances the induced fields at the excitation site. The peak induced field generated by this new design is located at the center of the coil, providing an easy identification of the excitation site. The field localization of the new coil is comparable with that of much smaller coils but with an inductance compatible to current magnetic stimulators. Numerical computations based on the principles of electromagnetic induction and using a human nerve model were performed to analyze the induced fields and the stimulation thresholds of new coil designs. The localization of the coil design was assessed by a half power region (HPR), within which the magnitude of the normalized induced field is greater than 1/square root of 2. The HPR for a 3-D differential coil built is improved (decreased) by a factor of three compared with a standard butterfly coil. Induced fields by this new coil were measured and in agreement with theoretical calculations.

27

[Hsu:2003aa] Kai-Hsiung Hsu and et al. Analysis of efficiency of magnetic stimulation. *IEEE Transactions on Biomedical Engineering*, 50(11):1276–1285, 2003.

Abstract: Magnetic stimulation can activate excitable tissues noninvasively. However, this method requires high energy to operate and can produce equipment heat that leads to inefficient stimulation. In this study, a comprehensive optimization of efficiency for magnetic stimulation has been conducted. A total of 16 781 coil designs were tested in order to determine the optimal coil geometry and inductance for neural excitation. Induced electric fields were calculated to find the optimal stimulation site (OSS) of a given coil. The threshold energy of a magnetic pulse for neural excitation was then calculated based on the transmem- brane responses of a nerve model. Simulation results show that there exists an optimal inductance, as a consequence of an optimal pulse duration, corresponding to a minimum threshold energy. A longer pulse width is required to obtain the maximum efficiency for axons with slower membrane dynamics, a longer coil-to-fiber distance, and greater values of resistance (R) and capacitance (C) of the resistance–inductance–capacitance circuit. The optimal geometry features a minimum coil height, suggesting a flat coil design for optimal efficiency. The dimension of the optimal coil design increases with the coil-to-fiber distance. Moreover, the cloverleaf design achieves the highest efficiency for infinitely long fibers whereas the butterfly design is optimal for terminating or bending fibers.

42, 60

[Huang:1993aa] Y. Y. Huang and R. C. Malenka. Examination of tea-induced synaptic enhancement in area ca1 of the hippocampus: the role of voltage-dependent ca2+ channels in the induction of ltp. *J Neurosci*, 13(2):568–76, 1993.

Abstract: The role of voltage-dependent Ca2+ channels (VDCCs) in the induction of long-term potentiation (LTP) in the CA1 region of rat hippocampus was determined by examining the relationship between LTP and the long-lasting synaptic enhancement induced by extracellular application of tetraethylammonium (TEA). Consistent with previous findings (Aniksztejn and Ben-Ari, 1991), the TEA-induced synaptic enhancement did not require NMDA receptor activation. It was blocked by the L-type VDCC antagonist nifedipine or by intracellular injection of the Ca2+ chelator 1,2-bis(2-amino-phenoxy)ethane N,N,N',N'-tetra-acetic acid (BAPTA) and could be mimicked by direct activation of VDCCs with repetitive depolarizing current pulses. In contrast to its effect on TEA-induced synaptic enhancement, nifedipine had no effect on the magnitude or duration of NMDA receptor-dependent LTP. Saturation of NMDA receptor-dependent LTP reduced the magnitude of the TEA-induced synaptic enhancement. Similarly, increasing synaptic strength by initial application of TEA reduced the magnitude of the subsequent tetanus-induced LTP. Like LTP, the TEA-induced synaptic enhancement did not significantly affect paired-pulse facilitation. These results suggest that dihydropyridine-sensitive VDCCs do not normally contribute to the induction of NMDA receptor-dependent LTP even though their repetitive activation can generate an increase in synaptic strength. The mutual occlusion of LTP and TEA-induced synaptic enhancement suggests that they share a common expression mechanism and perhaps are generated by activation of common Ca(2+)-dependent intracellular processes.(ABSTRACT TRUNCATED AT 250 WORDS)

104

[Huang:1994aa] Y. Y. Huang and E. R. Kandel. Recruitment of long-lasting and protein kinase a-dependent long-term potentiation in the ca1 region of hippocampus requires repeated tetanization. *Learn Mem*, 1(1):74–82, 1994.

Abstract: To study how the late phase of long-term potentiation (LTP) in hippocampus arises, we examined the resulting LTP for its time course and its dependence on protein synthesis and different second-messenger kinases by applying various conditioning tetani. We find that one high-frequency train (100 Hz) produces

a form of LTP that lasts longer than 1 hr but less than 3 hr (the early phase of LTP, or E-LTP). It is blocked by inhibitors of calcium/calmodulin kinase II (Cam kinase II) but is not affected by an inhibitor of cAMP-dependent protein kinase [protein kinase A (PKA) and the protein synthesis inhibitor anisomycin] nor is it occluded by the cAMP activator forskolin. In contrast, when three high-frequency trains are used, the resulting potentiation persists for at least 6-10 hr. The L-LTP induced by three trains differs from the E-LTP in that it requires new protein synthesis, is blocked by an inhibitor of cAMP-dependent protein kinase, and is occluded by forskolin. These results indicate that the two mechanistically distinctive forms of LTP, a transient, early component (E-LTP) and a more enduring form (L-LTP), can be recruited selectively by changing the number of conditioning tetanic trains. Repeated tetani induce a PKA and protein synthesis-dependent late component that adds to the amplitude and duration of the potentiation induced by a single tetanus.

101

[Huang:2005aa] Y. Z. Huang, M. J. Edwards, E. Rounis, K. P. Bhatia, and J. C. Rothwell. Theta burst stimulation of the human motor cortex. *Neuron*, 45(2):201–6, 2005.

Abstract: It has been 30 years since the discovery that repeated electrical stimulation of neural pathways can lead to long-term potentiation in hippocampal slices. With its relevance to processes such as learning and memory, the technique has produced a vast literature on mechanisms of synaptic plasticity in animal models. To date, the most promising method for transferring these methods to humans is repetitive transcranial magnetic stimulation (rTMS), a noninvasive method of stimulating neural pathways in the brain of conscious subjects through the intact scalp. However, effects on synaptic plasticity reported are often weak, highly variable between individuals, and rarely last longer than 30 min. Here we describe a very rapid method of conditioning the human motor cortex using rTMS that produces a controllable, consistent, long-lasting, and powerful effect on motor cortex physiology and behavior after an application period of only 20-190 s.

24

[Hubel:1963aa] D. H. Hubel and T. N. Wiesel. Shape and arrangement of columns in cat's striate cortex. *J Physiol*, 165:559–68, 1963. 65

[Hubel:1965aa] D. H. Hubel and T. N. Wiesel. Receptive fields and functional architecture in two nonstriate visual areas (18 and 19) of the cat. *J Neurophysiol*, 28:229–89, 1965. 65

[Hutcheon:2000aa] Bruce Hutcheon and Yosef Yarom. Resonance,oscillation and the intrinsic frequency preferences of neurons. *Trends Neurosci.*, 23:216–222, 2000.

Abstract: The realization that different behavioural and perceptual states of the brain are associated with different brain rhythms has sparked growing interest in the oscillatory behaviours of neurons. Recent research has uncovered a close association between electrical oscillations and resonance in neurons. Resonance is an easily measurable property that describes the ability of neurons to respond selectively to inputs at preferred frequencies. A variety of ionic mechanisms support resonance and oscillation in neurons. Understanding the basic principles involved in the production of resonance allows for a simplified classification of these mechanisms.The characterization of resonance and frequency preference captures those essential properties of neurons that can serve as a substrate for coordinating network activity around a particular frequency in the brain.

142

[Inchiosa:1995aa] M. E. Inchiosa and A. R. Bulsara. Nonlinear dynamic elements with noisy sinusoidal forcing: enhancing response via nonlinear coupling. *Phys. Rev. E*, 52(1):327–339, 1995.

Abstract: We consider a network of nonlinear dynamic elements with nonlinear, global coupling, subject to noise and a time-periodic signal. The system response, characterized by its signal-to-noise ratio, is computed via approximate analytic

techniques and precise numerical simulations. We find that cooperative effects arising from the noise and coupling lead to an enhancement of the response of the network over that of a single element.

143

[Islam:1995aa] N. Islam and et al. Increase in the calcium level following anodal polarization in the rat brain. *Brain Res*, 648(2):206–8, 1995.

Abstract: The accumulation of calcium ions (Ca) was examined in the rat brain by means of 45Ca autoradiography following the application of a weak anodal direct current to the surface of the sensorimotor cortex. Repetition of the anodal polarization with 3.0 A for 30 min caused more Ca to accumulate in the cerebral cortex. The degree and extent of accumulation was greater in the hemisphere ipsilateral to the polarization than in the other. Accumulation was also noted in the hippocampus and thalamus. Ca accumulation was detected after 24 h and it remained virtually constant up to 72 h after the last polarization. The results suggest that a long-lasting disturbance of Ca homeostasis is involved in the cortical plastic changes seen following anodal polarization.

127, 128, 342

[Islam:1995ab] N. Islam and et al. c-fos expression mediated by n-methyl-d-aspartate receptors following anodal polarization in the rat brain. *Exp Neurol*, 133(1):25–31, 1995. 127

[Islam:1995ac] N. Islam and et al. Co-localization of c-fos protein and protein kinase c gamma in the rat brain following anodal polarization. *Indian J Physiol Pharmacol*, 39(3):209–15, 1995.

Abstract: The expression of protein kinase c gamma (PKC gamma) and c-fos protein was examined by means of double labeling in the rat brain in relation to the molecular mechanism of central plastic changes associated with anodal polarization. Under normal, non-polarized condition, approximately 75% of all fos positive neurons in the neocortex were immunopositive for PKC gamma. Conversely, nearly all PKC gamma positive neurons were fos immunopositive. Although both pyramidal and non-pyramidal neurons express both types of protein, the pyramidal cell type represents the vast majority. An anodal direct current of 3.0 microA for 30 min to the surface of the left sensorimotor cortex resulted in a pronounced increase in the intensity of immunoreactivity for both PKC gamma and c-fos protein ipsilateral to the polarization. Approximately, 91% of fos positive neurons in the polarized neocortex was also intensely immunoreactive for PKY gamma. The high degree of codistribution of both transduction proteins in specific neurons following anodal polarization suggests the functional connection between PKY gamma activation and c-fos expression in polarization phenomenon.

127

[Islam:1997aa] N. Islam and et. Effects of anodal polarization on protein kinase cgamma (pkcgamma) in the rat brain. *Indian J Physiol Pharmacol*, 41(3):204–10, 1997.

Abstract: An anodal direct current of 0.3 microA or 30.0 microA was unilaterally applied for 30 min or 3 hr to the surface of the sensorimotor cortex of rats, and the effects of anodal polarization on protein kinase C (PKCgamma) activity were examined. The brains were processed by means of immunocytochemistry using the monoclonal antibody 36G9 raised against purified PKCgamma. In sham-operated animals, PKCgamma-like-immunoreactivity (PKCgamma LI) was noted in neuronal cytoplasm, as well as in processes in the cerebral cortex and in the hippocampus. Anodal polarization with 3.0 miroA for 30 min resulted in a pronounced increase in the number of PKCgamma-like-positive neurons in accordance with the intensity of immunostaining in the cerebral cortex, and an increase in the polarized hemispheres was highlighted by repeated applications of the currents. Polarization with 0.3 microA for 3 hr also increased the PKCgamma LI, but 0.3 microA for 30 min or 30.0 microA for any duration had no effects. The effect of polarization on PKCgamma activity, as evaluated by the intensity of immunostaining

and the number of neurons, began to increase 1 h after polarization, peaked at 3 hr and thereafter decreased to the control levels by 72 hr. These results indicated the involvement of the gamma-isoform of PKC in the neurochemical mechanism of long-standing central and behavioral changes induced by anodal polarization.

127

[Isogawa:2005aa] K. Isogawa, M. Fujiki, J. Akiyoshi, T. Tsutsumi, K. Kodama, H. Matsushita, Y. Tanaka, and H. Kobayashi. Anxiolytic suppression of repetitive transcranial magnetic stimulation-induced anxiety in the rats. *Prog Neuropsychopharmacol Biol Psychiatry*, 29(5):664–8, 2005.

Abstract: Repetitive transcranial magnetic stimulation (rTMS) is effective for treatment of several psychiatric disorders such as depression and anxiety disorder. However, some reports suggest that rTMS induced anxiety in normal volunteers. Consistent with this observation, we have reported that chronic rTMS induces anxiety in normal rats which was suppressed by chronic treatment, but not acute paroxetine treatment. The current study evaluates rTMS as animal model of anxiety by investigating the effect of rTMS on anxiety behaviors and the ability of standard anxiolytics to block expression of these behaviors. We found that 10-day rTMS induced anxiety in normal rats, as evidenced by expression of anxiety behaviors in the elevated plus-maze. This anxiety was suppressed by acute treatment with diazepam, alprazolam, or buspirone suggesting that chronic rTMS treatment provides a good animal model for anxiety.

118, 173

[Ives:2006aa] J. R. Ives, A. Rotenberg, R. Poma, G. Thut, and A. Pascual-Leone. Electroencephalographic recording during transcranial magnetic stimulation in humans and animals. *Clin Neurophysiol*, 117(8):1870–5, 2006.

Abstract: OBJECTIVE: We report on the development of an EEG recording system, comprised of electrodes and amplifiers that are compatible with TMS (single and rapid-rate) in both human and animal studies. METHODS: We assembled a versatile multi-channel EEG recording system consisting of: (1) two types of electrodes that are safe during TMS or rTMS. (2) Low slew-rate EEG amplifiers that recover within a few milliseconds after the application of TMS pulses. RESULTS: The two electrode types: (a) a conductive-plastic surface electrode with a conductive-silver epoxy coat and (b) a subdermal silver wire electrode (SWE) are compatible to TMS pulses. The amplifiers recover within 30 ms, so that the EEG can be viewed online, essentially without interruption and/or blocking or excessive artifact. CONCLUSIONS: Our TMS compatible electrode and EEG recording system allows safe and online viewing/recording of the subject's (human or animal) EEG/EP during experiments or studies involving TMS or rTMS applications. The TMS compatible electrode/amplifier system can be used with any EEG recording instrument. SIGNIFICANCE: A simple recording technique coupled with new electrodes permit safe and readable EEG records during TMS in humans and animals. Such online monitoring of the EEG would allow control of TMS/rTMS parameters based on EEG activity.

119, 121, 342

[Iyer:2005aa] M. B. Iyer, U. Mattu, J. Grafman, M. Lomarev, S. Sato, and E. M. Wassermann. Safety and cognitive effect of frontal dc brain polarization in healthy individuals. *Neurology*, 64(5):872–5, 2005.

Abstract: BACKGROUND: Data from the human motor cortex suggest that, depending on polarity, direct current (DC) brain polarization can depress or activate cortical neurons. Activating effects on the frontal lobe might be beneficial for patients with frontal lobe disorders. This phase 1 study tested the safety of frontal DC, including its effects on frontal and other brain functions. METHODS: The authors applied 20 minutes of anodal, cathodal, or sham DC to the left prefrontal cortex in three groups of right-handed subjects and looked for effects on global

measures of processing and psychomotor speed, emotion, and verbal fluency, a measure of local cortical function. In one experiment (n = 30), the authors tested before and after 1 mA DC and monitored EEG in 9 subjects. In two other experiments using 1 mA (n = 43) and 2 mA (n = 30), the authors tested before and then starting 5 minutes after the onset of DC. RESULTS: All subjects tolerated DC well. There were no significant effects on performance with 1 mA DC. At 2 mA, verbal fluency improved significantly with anodal and decreased mildly with cathodal DC. There were no clinically significant effects on the other measures. CONCLUSIONS: Limited exposure to direct current polarization of the prefrontal cortex is safe and can enhance verbal fluency selectively in healthy subjects. As such, it deserves consideration as a procedure to improve frontal lobe function in patients.

21, 32

[Izhikevich2003] E. M. Izhikevich. Simple model of spiking neurons. *Neural Networks, IEEE Transactions on*, 14(6):1569–1572, 2003. 72

[Jackson:1962aa] J. D. Jackson. *Classical Electrodynamics*. J. Wiley & Sons, 1962. 25, 187, 188, 190

[Jansen:1993aa] B. H. Jansen, G. Zouridakis, and M. E. Brandt. A neurophysiologically-based mathematical model of flash visual evoked potentials. *Biol Cybern*, 68(3):275–83, 1993. 66

[Jansen:1995aa] B. H. Jansen and V. G. Rit. Electroencephalogram and visual evoked potential generation in a mathematical model of coupled cortical columns. *Biol Cybern*, 73(4):357–66, 1995. 66

[Jefferys:1981aa] J. G. Jefferys. Influence of electric fields on the excitability of granule cells in guinea-pig hippocampal slices. *J Physiol*, 319:143–52, 1981. 85, 87, 89, 90, 95

[Jefferys:1995aa] J. G. Jefferys. Nonsynaptic modulation of neuronal activity in the brain: electric currents and extracellular ions. *Physiol Rev*, 75(4):689–723, 1995.

> **Abstract:** Nonsynaptic interactions between neurons have been eclipsed by our increasingly detailed understanding of chemical synapses, but they do play significant roles in the nervous system. This review considers four classes of nonsynaptic interaction, mainly in mammalian brain. 1) Electrotonic (and chemical) coupling through gap junctions has effects during development and under some, often pathological, conditions in the mature brain. 2) Ephaptic transmission is mediated by electrical coupling between specific neuronal elements in the absence of specialized contacts, notably in the cerebellum, and in axon tracts affected by demyelination. 3) Field effect interactions are mediated by large extracellular currents and potential fields generated by the hippocampus and other cortical structures. Both endogenous and applied electric fields alter neuronal excitability at field strengths over a few millivolts per millimeter. Weaker fields have more subtle effects, for instance, on axonal growth during development and repair and, more controversially, in behavioral responses to environmental fields. 4) There are fluctuations in extracellular ions such as K+, which are released during neuronal activity and which alter neuronal excitability. Field effects and ion fluctuations probably have modest effects during physiological activity but have a significant impact on epileptic seizures, and can sustain them in the absence of synaptic transmission.

33

[Jefferys:1996aa] J. G. Jefferys, R. D. Traub, and M. A. Whittington. Neuronal networks for induced '40 hz' rhythms. *Trends Neurosci*, 19(5):202–8, 1996. 68

[Jennum:1996aa] P. Jennum and H. Klitgaard. Repetitive transcranial magnetic stimulations of the rat. effect of acute and chronic stimulations on pentylenetetrazole-induced clonic seizures. *Epilepsy Res*, 23(2):115–22, 1996.

> **Abstract:** Repetitive transcranial magnetic stimulation (RTMS) has been reported to induce epileptic seizures in normal control and in epileptic patients. Therefore we characterized the effect of acute or chronic stimulations with RTMS on the induction of pentylenetetrazole (PTZ)-induced clonic seizures in the rat. Male Wistar rats were stimulated with a 13-cm coil with a stimulus frequency of

50 Hz. The motor threshold (Tm) was determined by a single transcranial stimulus. Acute stimulation was performed with a stimulus intensity of 0.9 x Tm and 1.5 x Tm using a duration of the train of stimuli of five seconds. Chronic stimulation was performed with a duration of the train of stimuli of one and five seconds using a stimulus intensity of 1.8 x Tm, every day for 30 days. Time to onset of PTZ-induced clonic seizure was determined after the acute stimulation or the last stimulation in chronic RTMS. In the groups of rats receiving acute RTMS (0.9 and 1.5 x Tm) no seizures developed. No differences were observed in time to onset of clonic seizures after PTZ injection compared to control rats. In the group of rats receiving chronic RTMS some rats showed facial contractions, chewing or head movements during or immediately after the stimulations. None of the rats developed tonic or clonic seizures in relation to RTMS. Time to onset of PTZ clonic seizures was reduced in both groups receiving RTMS with a stimulus duration of one (P ¡ 0.01) and five (P ¡ 0.05) seconds compared to control rats. The results from this study suggest that acute suprathreshold stimulation with a stimulus frequency of 50 Hz does not affect the induction of clonic PTZ seizures, whereas chronic (daily) stimulations have a facilitatory effect. This indicates that chronic stimulation with RTMS may induce a kindling process in the rat. Chronic RTMS stimulation may therefore represent an interesting alternative non-invasively kindling model to chemical and electrical stimulations.

118, 119, 176

[Jenrow:1998aa] K. A. Jenrow, X. Zhang, W. E. Renehan, and A. R. Liboff. Weak elf magnetic field effects on hippocampal rhythmic slow activity. *Exp Neurol*, 153(2):328–34, 1998.

Abstract: Several investigations have revealed that electrical activity within the central nervous system (CNS) can be affected by exposure to weak extremely-low-frequency (ELF) magnetic fields. Many of these studies have implicated CNS structures exhibiting endogenous oscillation and synchrony as optimal sites for field coupling. A particularly well characterized structure in this regard is the rat hippocampus. Under urethane anesthesia, synchronous bursting among hippocampal pyramidal neurons produces a large-amplitude quasi-sinusoidal field potential oscillation, termed "rhythmic slow activity" (RSA) or "theta." Using this in vivo model, we investigated the effect of exposure to an externally applied sinusoidal magnetic field (16.0 Hz; 28.9 microT(rms)) on RSA. During a 60-min exposure interval, the probability of RSA decaying to a less coherent mode of oscillation, termed "large irregular-amplitude activity" (LIA), was increased significantly. Moreover, this instability persisted for up to 90 min postexposure. These results are consistent with the hypothesis that endogenous CNS oscillators are uniquely susceptible to field-mediated perturbation and suggest that the sensitivity of these networks to such fields may be far greater than had previously been assumed. This sensitivity may reflect nonlinearities inherent to these networks which permit amplification of endogenous fields mediating the initiation and propagation of neuronal synchrony.

176

[Jensen:2005aa] Alicia L. Jensen and D. M. Durand. High frequency stimulation suppresses compound action potentials in vitro. In *Proceedings of the 2nd International IEEE EMBS Conference on neural engineering, Arlington, Virginia, March 16-19, 2005*, pages 70–73. IEEE EMBS, March 2005.

Abstract: Summary:Deep brain stimulation (DBS), also known as high frequency stimulation (HFS), is a promising method for the therapeutic control of epilepsy; although, the way DBS affects neural elements close to the stimulating electrode remains an important question. Sinusoidal HFS (50 Hz) suppresses synaptic and non-synaptic cellular neural activity in several in vitro epilepsy models. Although, the effects of HFS on axonal conduction are not known. In the present study, we tested the hypothesis that HFS suppresses local axonal conduction in vitro. HFS was locally applied to either the CA1 pyramidale cell layer or the alvear axon field of rat hippocampal slices. Complete suppression was indicated by a 100reduction in amplitude of the field potential for the duration of the HFS. The results show

that sinusoidal HFS suppresses the alvear compound action potential (CAP) as well as the CA1 antidromic evoked potential (AEP). Suppression was dependent on HFS amplitude, while HFS frequency was found not to be statistically significant. HFS applied to the alveus was more effective in suppressing the CAP than HFS applied to the CA1 pyramidale cell layer. These data suggest that HFS can block not only cellular neural firing but also activity in the axons of these cells or axons of passage

140

[Ji:1998aa] R. R. Ji, T. E. Schlaepfer, C. D. Aizenman, C. M. Epstein, D. Qiu, J. C. Huang, and F. Rupp. Repetitive transcranial magnetic stimulation activates specific regions in rat brain. *Proc Natl Acad Sci U S A*, 95(26):15635–40, 1998.

> **Abstract:** Repetitive transcranial magnetic stimulation (rTMS) is a noninvasive technique to induce electric currents in the brain. Although rTMS is being evaluated as a possible alternative to electroconvulsive therapy for the treatment of refractory depression, little is known about the pattern of activation induced in the brain by rTMS. We have compared immediate early gene expression in rat brain after rTMS and electroconvulsive stimulation, a well-established animal model for electroconvulsive therapy. Our result shows that rTMS applied in conditions effective in animal models of depression induces different patterns of immediate-early gene expression than does electroconvulsive stimulation. In particular, rTMS evokes strong neural responses in the paraventricular nucleus of the thalamus (PVT) and in other regions involved in the regulation of circadian rhythms. The response in PVT is independent of the orientation of the stimulation probe relative to the head. Part of this response is likely because of direct activation, as repetitive magnetic stimulation also activates PVT neurons in brain slices.

114, 165

[Jin:2000aa] Y. Jin and et al. Eeg resonant responses in schizophrenia: a photic driving study with improved harmonic resolution. *Schizophrenia Research*, 44(3):213–220, 2000.

> **Abstract:** Twenty seven drug-free schizophrenic patients and 25 normal controls were studied in an EEG photic driving paradigm with an improved harmonic resolution. Consistent with previous results, the present data show that schizophrenics have lower EEG responses to photic stimulation in alpha frequency. The differences between normal and schizophrenic subjects were distributed across major brain areas except centro-temporal regions. It also demonstrated that 1-Hz narrow-pulsed stimulation was feasible in EEG photic driving studies. The enhanced harmonic resolution produced significantly more information in the frequency domain about EEG oscillatory responses to visual stimulus. Using this new technique, the authors showed for the first time that alpha photic driving was a well defined resonant system and that the group differences in harmonic responses were primarily confined in the high frequency portion of alpha band, suggesting a peak frequency shift of EEG resonance in schizophrenia.

137

[Johnson:1997aa] C. R. Johnson. Computational and numerical methods for bioelectric field problems. *Crit Rev Biomed Eng*, 25(1):1–81, 1997.

> **Abstract:** Fundamental problems in electrophysiology can be studied by computationally modeling and simulating the associated microscopic and macroscopic bioelectric fields. To study such fields computationally, researchers have developed a variety of numerical and computational techniques. Advances in computer architectures have allowed researchers to model increasingly complex biophysical systems. Modeling such systems requires a researcher to apply a wide variety of computational and numerical methods to describe the underlying physics and physiology of the associated three-dimensional geometries. Issues naturally arise as

to the accuracy and efficiency of such methods. In this paper we review computational and numerical methods of solving bioelectric field problems. The motivating applications represent a class of bioelectric field problems that arise in electrocardiography and electroencephalography.

30

[Jurcak:2007aa] V. Jurcak, D. Tsuzuki, and I. Dan. 10/20, 10/10, and 10/5 systems revisited: their validity as relative head-surface-based positioning systems. *NeuroImage*, 34(4):1600–11, 2007.

Abstract: With the advent of multi-channel EEG hardware systems and the concurrent development of topographic and tomographic signal source localization methods, the international 10/20 system, a standard system for electrode positioning with 21 electrodes, was extended to higher density electrode settings such as 10/10 and 10/5 systems, allowing more than 300 electrode positions. However, their effectiveness as relative head-surface-based positioning systems has not been examined. We previously developed a virtual 10/20 measurement algorithm that can analyze any structural MR head and brain image. Extending this method to the virtual 10/10 and 10/5 measurement algorithms, we analyzed the MR images of 17 healthy subjects. The acquired scalp positions of the 10/10 and 10/5 systems were normalized to the Montreal Neurological Institute (MNI) stereotactic coordinates and their spatial variability was assessed. We described and examined the effects of spatial variability due to the selection of positioning systems and landmark placement strategies. As long as a detailed rule for a particular system was provided, it yielded precise landmark positions on the scalp. Moreover, we evaluated the effective spatial resolution of 329 scalp landmark positions of the 10/5 system for multi-subject studies. As long as a detailed rule for landmark setting was provided, 241 scalp positions could be set effectively when there was no overlapping of two neighboring positions. Importantly, 10/10 positions could be well separated on a scalp without overlapping. This study presents a referential framework for establishing the effective spatial resolutions of 10/20, 10/10, and 10/5 systems as relative head-surface-based positioning systems.

22

[Kammer:2001aa] T. Kammer, S. Beck, A. Thielscher, U. Laubis-Herrmann, and H. Topka. Motor thresholds in humans: a transcranial magnetic stimulation study comparing different pulse waveforms, current directions and stimulator types. *Clin Neurophysiol*, 112(2):250–8, 2001.

Abstract: OBJECTIVES: To evaluate the stimulation effectiveness of different magnetic stimulator devices with respect to pulse waveform and current direction in the motor cortex. METHODS: In 8 normal subjects we determined motor thresholds of transcranial magnetic stimulation in a small hand muscle. We used focal figure-of-eight coils of 3 common stimulators (Dantec Magpro, Magstim 200 and Magstim Rapid) and systematically varied current direction (postero-anterior versus antero- posterior, perpendicular to the central sulcus) as well as pulse waveform (monophasic versus biphasic). The coil position was kept constant with a stereotactic positioning device. RESULTS: Motor thresholds varied consistently with changing stimulus parameters, despite substantial interindividual variability. By normalizing the values with respect to the square root of the energy of the capacitors in the different stimulators, we found a homogeneous pattern of threshold variations. The normalized Magstim threshold values were consistently higher than the normalized Dantec thresholds by a factor of 1.3. For both stimulator types the monophasic pulse was more effective if the current passed the motor cortex in a postero-anterior direction rather than antero-posterior. In contrast, the biphasic pulse was weaker with the first upstroke in the postero-anterior direction. We calculated mean factors for transforming the intensity values of a particular configuration into that of another configuration by normalizing the different threshold values of each individual subject to his lowest threshold value. CONCLUSIONS: Our transformation factors allow us to compare stimulation intensities from studies

using different devices and pulse forms. The effectiveness of stimulation as a function of waveform and current direction follows the same pattern as in a peripheral nerve preparation (J Physiol (Lond) 513 (1998) 571).

15, 27, 28, 29, 335

[Kanai:2008aa] R. Kanai, L. Chaieb, A. Antal, V. Walsh, and W. Paulus. Frequency-dependent electrical stimulation of the visual cortex. *Curr Biol*, 18(23):1839–43, 2008.

Abstract: Noninvasive cortical stimulation techniques, such as transcranial magnetic stimulation (TMS) and transcranial direct current stimulation (tDCS), have proved to be powerful tools for establishing causal relationships between brain regions and their functions. In the present study, we demonstrate that a new technique called transcranial alternating current stimulation (tACS) can interact with ongoing rhythmic activities in the visual cortex in a frequency-specific fashion and induce visual experiences (phosphenes). We delivered an oscillatory current over the occipital cortex with tACS. In order to observe interactions with ongoing cortical rhythms, we compared the effects of delivering tACS under conditions of light ("Light" condition) or darkness ("Dark" condition). Stimulation over the occipital cortex induced perception of continuously flickering light most effectively when the beta frequency range was applied in an illuminated room, whereas the most effective stimulation frequency shifted to the alpha frequency range during testing in darkness. Stimulation with theta or gamma frequencies did not produce any visual phenomena. The shift of the effective stimulation frequency indicates that the frequency dependency is caused by interactions with ongoing oscillatory activity in the stimulated cortex. Our results suggest that tACS can be used as a noninvasive tool for establishing a causal link between rhythmic cortical activities and their functions.

22, 139

[Kandel2000] Eric R. Kandel, James H. Schwartz, and Thomas M. Jessell. *Principles of Neural Science*. McGraw-Hill Medical, January 2000. 74

[Kandel2001] Eric R. Kandel. The molecular biology of memory storage: A dialogue between genes and synapses. *Science*, 294(5544):1030–1038, November 2001. 78, 79

[Kaneko:1996aa] K. Kaneko, S. Kawai, Y. Fuchigami, H. Morita, and A. Ofuji. The effect of current direction induced by transcranial magnetic stimulation on the corticospinal excitability in human brain. *Electroencephalogr Clin Neurophysiol*, 101(6):478–82, 1996.

Abstract: Evoked spinal cord potentials (ESCPs) from the cervical epidural space and motor evoked potentials (MEPs) from the hand muscles were recorded simultaneously in 6 subjects following transcranial magnetic stimulation in two different coil orientations on motor cortex. The onset latency of the MEPs was approximately 1 ms shorter when the induced current flowed in a latero-medial direction (L-M stimulation) on the motor cortex as compared to a postero-anterior direction (P-A stimulation). Hence, L-M stimulation elicited an earlier component of the ESCPs than that induced by P-A stimulation. During general anesthesia with Sevoflurane, only the first component of the ESCPs could be elicited routinely following L-M stimulation. In contrast, all components of the ESCPs were dramatically attenuated following P-A stimulation. Moreover, first component latency of the ESCPs induced by L-M stimulation was almost the same as that induced by transcranial anodal electrical stimulation. These results suggest that if the induced current following transcranial magnetic stimulation flows in a latero-medial direction on motor cortex, it preferentially stimulates the corticospinal tract non-synaptically (producing a D-wave). However, if the induced current flows in a postero-anterior direction, it preferentially stimulates the corticospinal tract trans-synaptically (producing I-waves). Therefore, the direction of magnetically induced current is crucial in determining corticospinal excitability in the human brain.

27

[Kaneko:2000aa] T. Kaneko, R. Cho, Y. Li, S. Nomura, and N. Mizuno. Predominant information transfer from layer iii pyramidal neurons to corticospinal neurons. *J Comp Neurol*, 423(1):52–65, 2000.

Abstract: Connections of layer III pyramidal neurons to corticospinal neurons of layer V and corticothalamic neurons of layer VI in the rat primary motor cortex were examined in brain slices by combining intracellular staining with Golgi-like retrograde labeling of corticofugal neurons. Forty layer III pyramidal neurons stained intracellularly were of the regular-spiking type, showed immunoreactivity for glutaminase, and emitted axon collaterals arborizing locally in layers II/III and/or V. Nine of them were reconstructed for morphologic analysis; 15.23.8apposed to dendrites of corticospinal or corticothalamic neurons, respectively. By confocal laser scanning and electron microscopy, some of these appositions were revealed to make synapses. These findings suggest that corticospinal neurons receive information from the superficial cortical layers four times more frequently than corticothalamic neurons. The connections were further examined by intracellular recording of excitatory postsynaptic potential (EPSP) that were evoked in layer V and layer VI pyramidal neurons by stimulation of layer II/III. EPSPs evoked in layer V pyramidal neurons showed short and constant onset latencies, suggesting their monosynaptic nature. In contrast, most EPSPs evoked in layer VI pyramidal neurons had long onset latencies, showed double-shock facilitation of onset latency, and were largely suppressed by an N-methyl-D-aspartic acid receptor blocker, suggesting that they were polysynaptic. The results suggest that information from the superficial cortical layers is transferred directly and efficiently to corticospinal neurons in layer V and thereby exerts an important influence on cortical motor output. Corticothalamic neurons are, in contrast, considered relatively independent of, or indirectly related to, information processing of the superficial cortical layers.

60

[Kang:1994aa] Y. Kang, T. Kaneko, H. Ohishi, K. Endo, and T. Araki. Spatiotemporally differential inhibition of pyramidal cells in the cat motor cortex. *J Neurophysiol*, 71(1):280–93, 1994.

Abstract: 1. The spatiotemporal pattern of inhibition in the cat motor cortex was studied in in vitro slice preparations in the presence of 6-cyano-7-nitroquinoxaline-2,3-dione (CNQX) and 2-amino-5-phosphonovaleric acid (APV). 2. After intracortical microstimulation (0.5-6 microA), fast and slow inhibitory postsynaptic potentials (IPSPs) were produced in layers II-VI pyramidal cells and selectively reduced with bicuculline methiodide and phaclofen, respectively. 3. Fast IPSPs were maximally produced by stimulation of the same layer where their cell bodies were located, and they decreased in amplitude as the more superficial layer was stimulated. In contrast, slow IPSPs were maximally produced by stimulation of layer II regardless of the location of the recorded pyramidal cell and decreased in amplitude as the deeper layer was stimulated. 4. The reduction of amplitude of fast IPSPs, in response to a vertical shift of the stimulation site toward more superficial layers, was always correlated with an increase in rise time and with a shift of the reversal potential to a more hyperpolarized level. 5. When the stimulation site was moved horizontally to the more lateral site, fast IPSPs increased in latency and decreased in amplitude gradually without appreciable changes in rise time. Fast IPSPs could be evoked from horizontally remote sites of up to 800-1,200 microns. 6. Inhibitory interneurons, which are responsible for evoking fast IPSPs, appear to be distributed through almost all layers to send horizontally spreading parallel axons making synaptic contacts at different electrotonic distances along apical dendrites of single pyramidal cells. 7. Horizontal spreads were much less in slow IPSPs (¡ 340-680 microns). The time-to-peak of slow IPSPs produced in layer V pyramidal cells (159.5 +/- 6.8 ms, mean +/- SD, n = 10) was significantly (P ¡ 0.0001) longer than that in layers II and III pyramidal cells (128.5 +/- 7.5 ms, n = 7). Asymmetric reversal properties of slow IPSPs were seen, suggesting the spatial dispersion of synaptic inputs along apical dendrites of pyramidal cells. 8.

In layer V pyramidal cells, the time-to-peak of slow IPSPs decreased with increasing membrane hyperpolarization, indicating that the later portion of slow IPSPs was more sensitive to the membrane-potential change than the early portion. This further indicates that the late portion of slow IPSPs is generated at synapses on the more proximal dendrite of pyramidal cells than the early portion, contrary to that expected from the Rall's model of passive dendrite under the condition of synchronous inputs.(ABSTRACT TRUNCATED AT 400 WORDS)

60

[Kanno:2003aa] M. Kanno, M. Matsumoto, H. Togashi, M. Yoshioka, and Y. Mano. Effects of acute repetitive transcranial magnetic stimulation on extracellular serotonin concentration in the rat prefrontal cortex. *J Pharmacol Sci*, 93(4):451–7, 2003.

Abstract: Repetitive transcranial magnetic stimulation (rTMS) changes the function of the cortex. This study clarified the effects of acute rTMS treatment on extracellular serotonin (5-HT) concentrations in the rat prefrontal cortex (PFC) by using in vivo microdialysis methods. Each rat received acute rTMS treatment of the frontal brain at 500 stimuli from twenty trains applied at 25 Hz for 1 s at 1-min intervals between trains. Sham-treated rats received the same handling procedure and sound of the stimulator. Sham treatment increased the extracellular 5-HT levels compared with the non-treated group. However, rTMS treatment using the stimulation intensity of 110the increase in 5-HT levels induced by the sham treatment. Acute rTMS treatment of the frontal brain is related to the serotonergic neuronal system in the rat PFC, and it may have therapeutic implications for emotional disorders.

113, 123, 167, 173

[Kanno:2003ab] M. Kanno, M. Matsumoto, H. Togashi, M. Yoshioka, and Y. Mano. Effects of repetitive transcranial magnetic stimulation on behavioral and neurochemical changes in rats during an elevated plus-maze test. *J Neurol Sci*, 211(1-2):5–14, 2003.

Abstract: In transcranial magnetic stimulation (TMS) the regional electrical activity in the brain is influenced by a pulsed magnetic field. The rapidly changed magnetic field produces electrical currents that activate neurons. Repetitive TMS (rTMS) treatment can cause functional changes in the cortex. The present study clarified the effects of rTMS treatment on behavioral changes in rats, focusing on anxiety by using an elevated plus-maze (plus-maze) test. The effects of rTMS treatment on neurochemical changes during the plus-maze test were investigated by determining the extracellular levels of serotonin (5-HT) and dopamine (DA) in the prefrontal cortex by using in vivo microdialysis. Each rat received rTMS of the frontal brain for 3 days, during which 125 stimuli from five trains in a day were applied at 25 Hz for 1 s with 2-min intervals between trains. Three-day series of (chronic) rTMS treatment caused significant increases in the time spent in open arms and the number of entries into open arms of the plus-maze compared with non-treated and sham-treated rats, which were not observed in 1-day series of (acute) rTMS treatment. Chronic rTMS treatment suppressed the increases in 5-HT levels induced by the plus-maze test, but did not influence the elicited DA levels. These data suggest that chronic rTMS treatment of the frontal brain has anxiolytic effects in rats, which are related to the 5-HTergic neuronal system.

113, 123, 167, 173

[Kanno:2004aa] M. Kanno, M. Matsumoto, H. Togashi, M. Yoshioka, and Y. Mano. Effects of acute repetitive transcranial magnetic stimulation on dopamine release in the rat dorsolateral striatum. *J Neurol Sci*, 217(1):73–81, 2004.

Abstract: Animal studies have shown that descending pathways from the frontal cortex modulate dopamine (DA) release in the striatum. This modulation is thought to be relevant to the pathophysiology of Parkinson's disease. In human, repetitive transcranial magnetic stimulation (rTMS) can result in functional

changes in the cortex. The present study intended to clarify the effects of acute rTMS treatment using various stimulation intensities on the extracellular DA concentrations in the rat dorsolateral striatum. The frontal brain of each rat received acute rTMS treatment, which consisted of 500 stimuli from 20 trains in a day. Each train was applied at 25 Hz for 1 s with 1-min intervals between trains. The neurochemical effects of acute rTMS treatment were investigated by determining the extracellular concentrations of DA in the rat dorsolateral striatum using in vivo microdialysis. Acute rTMS treatment of the frontal brain using the stimulation intensity of almost 110markedly and continuously increased the extracellular DA concentrations in the rat dorsolateral striatum. The present study demonstrates that acute rTMS treatment of the frontal brain affects the DAergic neuronal system in the rat dorsolateral striatum, and may have therapeutic implications for Parkinson's disease.

112, 167

[Kasabov2008] N. Kasabov. Evolving intelligence in humans and machines: Integrative evolving connectionist systems approach. *Computational Intelligence Magazine, IEEE*, 3(3):23–37, 2008. 68, 72, 78, 79, 80, 81

[Keck:2000aa] M. E. Keck, M. Engelmann, M. B. Muller, M. S. Henniger, B. Hermann, R. Rupprecht, I. D. Neumann, N. Toschi, R. Landgraf, and A. Post. Repetitive transcranial magnetic stimulation induces active coping strategies and attenuates the neuroendocrine stress response in rats. *J Psychiatr Res*, 34(4-5):265–76, 2000.

> **Abstract:** The effects of repetitive transcranial magnetic stimulation (rTMS) on various brain functions were investigated in adult male Wistar rats. The stimulation parameters were adjusted according to the results of accurate computer-assisted, magnetic resonance imaging-based reconstructions of the current density distributions induced by rTMS in the rat and human brain, ensuring comparable stimulation patterns in both cases. The animals were subjected to daily rTMS-treatment (three trains of 20 Hz; 2.5 s) for 8 weeks from the age of 4 weeks on. In the forced swim test these rats showed a more active stress coping strategy than the control rats. This was accompanied by a significantly attenuated stress-induced elevation of plasma ACTH concentrations. Pituitary changes accounting for the attenuation were ruled out bymore active stress coping strategy than the control rats the corticotropin-releasing hormone test. Baseline concentrations of ACTH and corticosterone were indistinguishable in the two groups. No changes were found in the anxiety-related behavior of the rats on the elevated plus-maze or in behavior during the social interaction test. Accordingly, the binding characteristics of the benzodiazepine agonist [(3)H]flunitrazepam at the benzodiazepine/gamma-aminobutyric acid type A receptor complex were similar in the rTMS and control groups. In summary, chronic rTMS treatment of frontal brain regions in rats resulted in a change in coping strategy that was accompanied by an attenuated neuroendocrine response to stress, thus revealing parallels to the effects of antidepressant drug treatment.

112, 113, 118, 167, 172

[Keck:2000ab] M. E. Keck, I. Sillaber, K. Ebner, T. Welt, N. Toschi, S. T. Kaehler, N. Singewald, A. Philippu, G. K. Elbel, C. T. Wotjak, F. Holsboer, R. Landgraf, and M. Engelmann. Acute transcranial magnetic stimulation of frontal brain regions selectively modulates the release of vasopressin, biogenic amines and amino acids in the rat brain. *Eur J Neurosci*, 12(10):3713–20, 2000.

> **Abstract:** Using intracerebral microdialysis in urethane-anaesthetized adult male Wistar rats, we monitored the effects of acute repetitive transcranial magnetic stimulation (rTMS; 20 trains of 20 Hz, 2.5 s) on the intrahypothalamic release of arginine vasopressin (AVP) and selected amino acids (glutamate, glutamine, aspartate, serine, arginine, taurine, gamma-aminobutyric acid) and the intrahippocampal release of monoamines (dopamine, noradrenaline, serotonin) and their metabolites (homovanillic acid, 3,4-dihydroxyphenylacetic acid, 5-hydroxyindoleacetic

acid). The stimulation parameters were adjusted according to the results of accurate computer reconstructions of the current density distributions induced by rTMS in the rat and human brains, ensuring similar stimulation patterns in both cases. There was a continuous reduction in AVP release of up to 50In contrast, the release of taurine, aspartate and serine was selectively stimulated within this nucleus by rTMS. Furthermore, in the dorsal hippocampus the extracellular concentration of dopamine was elevated in response to rTMS. Taken together, these data provide the first in vivo evidence that acute rTMS of frontal brain regions has a differentiated modulatory effect on selected neurotransmitter/neuromodulator systems in distinct brain areas.

112, 113, 167, 172

[Keck:2001aa]   M. E. Keck, T. Welt, A. Post, M. B. Muller, N. Toschi, A. Wigger, R. Landgraf, F. Holsboer, and M. Engelmann. Neuroendocrine and behavioral effects of repetitive transcranial magnetic stimulation in a psychopathological animal model are suggestive of antidepressant-like effects. *Neuropsychopharmacology*, 24(4):337–49, 2001.

Abstract: The neuroendocrine and behavioral effects of repetitive transcranial magnetic stimulation (rTMS) were investigated in two rat lines selectively bred for high and low anxiety-related behavior. The stimulation parameters were adjusted according to the results of accurate computer-assisted and magnetic resonance imaging-based reconstructions of the current density distributions induced by rTMS in the rat and human brain, ensuring comparable stimulation patterns in both cases. Adult male rats were treated in two 3-day series under halothane anesthesia. In the forced swim test, rTMS-treatment induced a more active coping strategy in the high anxiety-related behavior rats only (time spent struggling; 332performance of low anxiety-related behavior rats. In contrast, rTMS-treated low anxiety-related behavior rats did not change their swimming behavior. The development of active coping strategies in high anxiety-related behavior rats was accompanied by a significantly attenuated stress-induced elevation of plasma corticotropin and corticosterone concentrations. In summary, the behavioral and neuroendocrine effects of rTMS of frontal brain regions in high anxiety-related behavior rats are comparable to the effects of antidepressant drug treatment. Interestingly, in the psychopathological animal model repetitive transcranial magnetic stimulation induced changes in stress coping abilities in the high-anxiety line only.

171

[Keck:2002aa]   M. E. Keck, T. Welt, M. B. Muller, A. Erhardt, F. Ohl, N. Toschi, F. Holsboer, and I. Sillaber. Repetitive transcranial magnetic stimulation increases the release of dopamine in the mesolimbic and mesostriatal system. *Neuropharmacology*, 43(1):101–9, 2002.

Abstract: Repetitive transcranial magnetic stimulation (rTMS) is suggested to be a potentially useful treatment in major depression. In order to optimize rTMS for therapeutic use, it is necessary to understand the neurobiological mechanisms involved, particularly the nature of the neurochemical changes induced. Using intracerebral microdialysis in urethane-anesthetized and conscious adult male Wistar rats, we monitored the effects of acute rTMS (20 Hz) on the intrahippocampal, intraaccumbal and intrastriatal release patterns of dopamine and its metabolites (homovanillic acid, 3,4-dihydroxyphenylacetic acid). The stimulation parameters were adjusted according to the results of accurate MRI-based computer-assisted reconstructions of the current density distributions induced by rTMS in the rat brain, ensuring stimulation of frontal brain regions. In the dorsal hippocampus, the shell of the nucleus accumbens and the dorsal striatum the extracellular concentration of dopamine was significantly elevated in response to rTMS. Taken together, these data provide the first in vivo evidence that acute rTMS of frontal brain regions has a modulatory effect on both the mesolimbic and the mesostriatal dopaminergic systems. This increase in dopaminergic neurotransmission may contribute to the beneficial effects of rTMS in the treatment of affective disorders and Parkinson's disease.

112, 167

[Keck:2003aa]   M. E. Keck. rtms as treatment strategy in psychiatric disorders–neurobiological concepts. *Suppl Clin Neurophysiol*, 56:100–16, 2003. 167

[Kim:2006aa]   E. J. Kim, W. R. Kim, S. E. Chi, K. H. Lee, E. H. Park, J. H. Chae, S. K. Park, H. T. Kim, and J. S. Choi. Repetitive transcranial magnetic stimulation protects hippocampal plasticity in an animal model of depression. *Neurosci Lett*, 405(1-2):79–83, 2006.

Abstract: Despite its therapeutic success in treating mood-related disorders, little is known about the mechanism by which repetitive transcranial magnetic stimulation (rTMS) alters physiological responses of neurons. Using the forced swim test (FST) in rats as a model of depression, we tested the protective effect of rTMS on synaptic plasticity, specifically, on the induction of hippocampal long-term potentiation (LTP). Male Sprague-Dawley rats were subjected to FST to induce immobility, a behavioral symptom of depression. They were subsequently treated with one of the three conditions: rTMS (rTMS: 1000 stimuli at 10Hz), sham rTMS (SHAM: acoustic stimulation only), or an antidepressant drug, fluoxetine (FLX: 10mg/kg, i.p.) for 7 days. There was a significant difference in immobility time between rTMS and SHAM groups after 7 days of treatment, but not after a single day. Following the second swim test on day 7, they were anesthetized and LTP was induced in vivo in the perforant path-dentate gyrus synapses. Another group (NAIVE) that had received no prior treatment was used as a control for LTP. The SHAM or FLX group exhibited little signs of LTP induction. On the contrary, the rTMS and NAIVE group showed a significant increase in field excitatory postsynaptic potentials after LTP induction. These results show that rTMS has an antidepressant-like effect after a relatively short period of treatment, and this effect might be mediated by a cellular process that can potentially reverse the impaired synaptic efficacy caused by the forced swim procedure.

118, 172

[Kitajo:2007aa]   K. Kitajo and et al. Noise-induced large-scale phase synchronization of human-brain activity with behavioural stochastic resonance. *Europhysics Letters*, 80(40009), 2007.

Abstract: We demonstrate that both detection of weak visual signals to the right eye and phase synchronization of electro-encephalogram (EEG) signals from widely separated areas of the human brain are increased by addition of weak visual noise to the left eye. We found a close relationship between the resulting noise-induced changes in behavioural performance and the similarly resulting changes in phase synchronization between widely separated brain areas. These results imply that noise-induced large-scale neural synchronization may play a significant role in information transmission in the brain.

133, 137

[Kling:1990aa]   J. W. Kling, M. Yarita, T. Yamamoto, and Y. Matsumiya. Memory for conditioned taste aversions is diminished by transcranial magnetic stimulation. *Physiol Behav*, 48(5):713–7, 1990.

Abstract: Rats were allowed to drink distinctively flavored water and later received an IP injection of LiCl. In Phase I, between drinking and the onset of the mild malaise, Experimental Group rats received stimulations of the head and Controls received equivalent stimulations of the back. Later, when the flavor was again presented. Experimentals drank 10-15extent that the flavor was associated with illness. In Phase II, the procedure was repeated with a different distinctive flavor. Again, the Experimentals drank more on the test day. In Phase III, all rats received stimulations of the back between tasting and illness. Experimentals and Controls were not different on the test day, indicating that 100 prior head stimulations did not interfere with the establishment of a new taste aversion. Histological examinations revealed no gross morphopathology. We conclude that 50 brief pulse transcranial magnetic stimulations may cause a retrograde memory disruption, but we find no evidence for an anterograde memory effect or for structural changes.

116, 174

[Kole:1999aa] M. H. Kole, E. Fuchs, U. Ziemann, W. Paulus, and U. Ebert. Changes in 5-ht1a and nmda binding sites by a single rapid transcranial magnetic stimulation procedure in rats. *Brain Res*, 826(2):309–12, 1999.

> **Abstract:** The effects of a single rapid-rate transcranial magnetic stimulation (rTMS) exposure on neurotransmitter binding sites in the rat brain 24 h after the stimulation were examined. Quantification by in vitro-autoradiography showed no differences for 3H-paroxetine binding (5-HT uptake sites) between rTMS-treated, sham and control animals. In contrast, the number of 5-HT1A binding sites (labeled with 3H-8-OH-DPAT) were selectively increased in the rTMS-group with significantly higher BMAX values in the frontal cortex, the cingulate cortex, and the anterior olfactory nucleus. A non-specific increase in NMDA binding sites (labeled with 125I-MK-801) in rTMS and sham animals was observed in the hippocampal formation. A selective increase of these binding sites after rTMS was detected in the ventromedial hypothalamus, the basolateral amygdala and layers 5-6 of the parietal cortex. These findings imply that a single rTMS exposure can result in persistent effects on NMDA and 5-HT1A binding sites even 24 h after stimulation and therefore may be of relevance with respect to the therapeutic action of rTMS reported from clinical studies.

113, 114, 164

[Kowalski:2002aa] T. Kowalski, J. Silny, and H. Buchner. Current density threshold for the stimulation of neurons in the motor cortex area. *Bioelectromagnetics*, 23(6):421–8, 2002.

> **Abstract:** The aim of this study was to determine a current density threshold for exciting the motor cortex area of the brain. The current density threshold for excitation of nerve fibres (20 microm in diameter) found in the literature is approximately 1 A/m(2) at frequencies lower than 1 kHz. In consideration of a safety factor of 100, the International Commission on Non-Ionizing Radiation Protection (ICNIRP) recommends to restrict the exposure to 0.01 A/m(2). The electromagnetic stimulation of neurons in the motor cortex is used in the clinical diagnosis of nerve lesions and neuropathy by means of magnetic or electrical transcranial stimulation. Combining medical data from clinical studies and technical specifications of the Magstim Model 200 stimulator, we were able to compute the current density threshold for the excitation of the human motor cortex by means of the finite element method (FEM). A 3D-CAD head model was built on the basis of magnetic resonance imaging (MRI) slices and segmented into four anatomical structures (scalp, skull, brain, and ventricular system) with different conductivities. A current density threshold for the stimulation of the motor cortex area of the upper limbs of 6 and 2.5 A/m(2) at 2.44 kHz and 50 Hz, respectively, was calculated. As these values lie above the recommended ICNIRP values by two orders of magnitude there is no need for lower safety standards with regard to stimulation of the brain.

28

[Kujirai:1993aa] T. Kujirai, M. D. Caramia, J. C. Rothwell, B. L. Day, P. D. Thompson, A. Ferbert, S. Wroe, P. Asselman, and C. D. Marsden. Corticocortical inhibition in human motor cortex. *J Physiol*, 471:501–19, 1993.

> **Abstract:** 1. In ten normal volunteers, a transcranial magnetic or electric stimulus that was subthreshold for evoking an EMG response in relaxed muscles was used to condition responses evoked by a later, suprathreshold magnetic or electric test shock. In most experiments the test stimulus was given to the lateral part of the motor strip in order to evoke EMG responses in the first dorsal interosseous muscle (FDI). 2. A magnetic conditioning stimulus over the hand area of cortex could suppress responses produced in the relaxed FDI by a suprathreshold magnetic test stimulus at interstimulus intervals of 1-6 ms. At interstimulus intervals

of 10 and 15 ms, the test response was facilitated. 3. Using a focal magnetic stimulus we explored the effects of moving the conditioning stimulus to different scalp locations while maintaining the magnetic test coil at one site. If the conditioning coil was moved anterior or posterior to the motor strip there was less suppression of test responses in the FDI. In contrast, stimulation at the vertex could suppress FDI responses by an amount comparable to that seen with stimulation over the hand area. With the positions of the two coils reversed, conditioning stimuli over the hand area suppressed responses evoked in leg muscles by vertex test shocks. 4. The intensity of both conditioning and test shocks influenced the amount of suppression. Small test responses were more readily suppressed than large responses. The best suppression was seen with small conditioning stimuli (0.7-0.9 times motor threshold in relaxed muscle); increasing the intensity to motor threshold or above resulted in less suppression or even facilitation. 5. Two experiments suggested that the suppression was produced by an action on cortical, rather than spinal excitability. First, a magnetic conditioning stimulus over the hand area failed to produce any suppression of responses evoked in active hand muscles by a small (approximately 200 V, 50 microsecond time constant) anodal electric test shock. Second, a vertex conditioning shock had no effect on forearm flexor H reflexes even though responses in the same muscles produced by magnetic cortical test shocks were readily suppressed at appropriate interstimulus intervals. 6. Small anodal electric conditioning stimuli were much less effective in suppressing magnetic test responses than either magnetic or cathodal electric conditioning shocks.(ABSTRACT TRUNCATED AT 400 WORDS)

107

[Kupferman:1965aa] I. Kupferman. Effects of cortical polarization on visual discriminations. *Exp Neurol*, 12(2):179–189, 1965.

> **Abstract:** The performance of rats on various visual tasks was studied while the normal d-c fields of their cerebral cortex were altered by means of external polarizing currents. The experimental groups, when compared to nonpolarized controls, were not significantly impaired in the acquisition of either a brightness or a pattern discrimination. An analysis of variance on the scores of a pattern-reversal problem fell just short of statistical significance (p ¡ 0.06). A closer analysis of the reversal scores showed that only the group that was cathodally polarized on visual cortex was significantly different from the controls (p ¡ 0.002, two-tailed Mann Whitney U-test).

127

[Labra:2007aa] C. de Labra, C. Rivadulla, K. Grieve, J. Marino, N. Espinosa, and J. Cudeiro. Changes in visual responses in the feline dlgn: selective thalamic suppression induced by transcranial magnetic stimulation of v1. *Cereb Cortex*, 17(6):1376–85, 2007.

> **Abstract:** Transcranial magnetic stimulation (TMS) of the cortex can modify activity noninvasively and produce either excitatory or inhibitory effects, depending on stimulus parameters. Here we demonstrate controlled inhibitory effects on the large corticogeniculate feedback pathway from primary visual cortex to cells of the dorsal lateral geniculate nucleus (dLGN) that are focal and reversible-induced by either single pulses or trains of pulses of TMS. These effects selectively suppress the sustained component of responses to flashed spots or moving grating stimuli and are the result of loss of spikes fired in tonic mode, whereas the number of spikes fired in bursts remain the same. We conclude that acute inactivation of the corticogeniculate downflow selectively affects the tonic mode. We found no evidence to suggest that cortical inactivation increased burst frequency.

163

[Lakatos:2008aa] Peter Lakatos and et al. Entrainment of neuronal oscillations as a mechanism of attentional selection. *Science*, 320:110–113, April 2008.

Abstract: Whereas gamma-band neuronal oscillations clearly appear integral to visual attention, the role of lower-frequency oscillations is still being debated. Mounting evidence indicates that a key functional property of these oscillations is the rhythmic shifting of excitability in local neuronal ensembles. Here, we show that when attended stimuli are in a rhythmic stream, delta-band oscillations in the primary visual cortex entrain to the rhythm of the stream, resulting in increased response gain for task-relevant events and decreased reaction times. Because of hierarchical cross-frequency coupling, delta phase also determines momentary power in higher-frequency activity. These instrumental functions of low-frequency oscillations support a conceptual framework that integrates numerous earlier findings.

137

[Lante:2006aa] F. Lante, M. Cavalier, C. Cohen-Solal, J. Guiramand, and M. Vignes. Developmental switch from ltd to ltp in low frequency-induced plasticity. *Hippocampus*, 16(11):981–9, 2006.

Abstract: The stimulation of the Schaffer collateral/commissural fibers at low frequency (1 Hz) for 3-5 min can trigger a slow-onset form of low-frequency stimulation (LFS)-long-term potentiation (LTP) (LFS-LTP) in the CA1 area of the adult rat hippocampus. Here we have examined the developmental profile of this plasticity. In 9-15 day-old rats, the application of 1 Hz for 5 min induced long-term depression (LFS-LTD). In 17-21 day-old rats, 1 Hz stimulation had no effect when applied for 5 min but mediated LTD when stimulus duration was increased to 15 min. Over 25 day-old, 1 Hz stimulation mediated LFS-LTP. LFS-LTD was dependent on both N-methyl-D-aspartate (NMDA) and mGlu5 receptor activation. Antagonists of mGlu1alpha and cannabinoid type 1 receptor were ineffective to block LTD induction. LFS-LTD was not associated with a change in paired-pulse facilitation ratio, suggesting a postsynaptic locus of expression of this plasticity. Next, we examined whether LFS-LTD was related to 'chemical' LTDs obtained by the direct stimulation of mGlu5 and NMDA receptors. The saturation of LFS-LTD completely occluded NMDA- and (RS)-2-Chloro-5-hydroxyphenylglycine (CHPG)-induced LTD. CHPG-LTD and NMDA-LTD occluded each other. In addition, we observed that NMDA-LTD was dependent on mGlu5 receptor activation in 9-12 day old rats while it was not in animals older than 15 day-old. Therefore we postulate that during LFS application, NMDA and mGlu5 receptor could interact to trigger LTD. Low-frequency-mediated synaptic plasticity is subject to a developmental switch from NMDA- and mGlu5 receptor-dependent LTD to mGlu5 receptor-dependent LTP with a transient period (17-21 day-old) during which LFS is ineffective.

104

[Law:1993aa] S. K. Law. Thickness and resistivity variations over the upper surface of the human skull. *Brain Topogr*, 6(2):99–109, 1993.

Abstract: A study of skull thickness and resistivity variations over the upper surface was made for an adult human skull. Physical measurements of thickness and qualitative analysis of photographs and CT scans of the skull were performed to determine internal and external features of the skull. Resistivity measurements were made using the four-electrode method and ranged from 1360 to 21400 Ohm-cm with an overall mean of 7560 +/- 4130 Ohm-cm. The presence of sutures was found to decrease resistivity substantially. The absence of cancellous bone was found to increase resistivity, particularly for samples from the temporal bone. An inverse relationship between skull thickness and resistivity was determined for trilayer bone (n = 12, p 0.001). The results suggest that the skull cannot be considered a uniform layer and that local resistivity variations should be incorporated into realistic geometric and resistive head models to improve resolution in EEG. Influences of these variations on head models, methods for determining these variations, and incorporation into realistic head models, are discussed.

18, 31

[Le:1993aa]   J. Le and A. Gevins. Method to reduce blur distortion from eeg's using a realistic head model. *IEEE Trans Biomed Eng*, 40(6):517–28, 1993.

> **Abstract:** A mathematical procedure, which we call "Deblurring," was developed to reduce spatial blur distortion of scalp-recorded brain potentials due to transmission through the skull and other tissues. Deblurring estimates potentials at the superficial cerebral cortical surface from EEG's recorded at the scalp using a finite element model of each subject's scalp, skull and cortical surface constructed from their magnetic resonance images (MRI's). Simulations indicate that Deblurring is numerically stable, while a comparison of deblurred data with a direct cortical recording from a neurosurgery patient suggests that the procedure is valid. Application of Deblurring to somatosensory evoked potential data recorded at 124 scalp sites suggests that the method produces a dramatic improvement in spatial detail, and merits further development.

> 30

[Leao:1944aa]   A.A.P. Leao. Spreading depression of activity in the crebral cortex. *J. Neurophysiol.*, 7:359–390., 1944. 128

[Lefaucheur:2006aa]   J. P. Lefaucheur. The use of repetitive transcranial magnetic stimulation (rtms) in chronic neuropathic pain. *Neurophysiol Clin*, 36(3):117–24, 2006.

> **Abstract:** Chronic motor cortex stimulation using implanted epidural stimulation was proposed to treat chronic, drug-resistant neuropathic pain. Various studies showed that repetitive transcranial magnetic stimulation (rTMS) applied over the motor cortex could also relieve neuropathic pain, at least partially and transiently. Controlled rTMS studies with other cortical targets, such as the dorsolateral prefrontal cortex, are in waiting. The mechanisms of action of rTMS on chronic pain are mostly unknown. The changes induced by rTMS in neural activities may occur at the stimulated cortical site as well as in remote structures along functional anatomical connections. Compared to chronic implanted procedure, the main limitation of rTMS application is the short duration of clinical effects. Repeated daily rTMS sessions have proved some efficacy to induce long-lasting pain relief that could have therapeutic potential. However, rTMS-induced analgesia varies with the site and parameters of stimulation, in particular the stimulus rate. The efficacious rTMS parameters could differ from those used in chronic epidural stimulation. Differences in the pattern of the current fields respectively induced in the brain by these two techniques might explain this finding. Actually, stimulation parameters remain to be optimised and clinical efficacy to be confirmed by multi-centre randomised trials, before considering rTMS as therapeutic tool for patients with chronic pain in neurological practice.

> 24

[Leung:1998aa] L. Stan Leung and Hui-Wen Yu. Theta-frequency resonance in hippocampal ca1 neurons in vitro demonstrated by sinusoidal current injection. *J. Neurophysiol*, 79:1592–1596, 1998.

> **Abstract:** Sinusoidal currents of various frequencies were injected into hippocampal CA1 neurons in vitro, and the membrane potential responses were analyzed by cross power spectral analysis. Sinusoidal currents induced a maximal (resonant) response at a theta frequency (3-10 Hz) in slightly depolarized neurons. As predicted by linear systems theory, the resonant frequency was about the same as the natural (spontaneous) oscillation frequency. However, in some cases, the resonant frequency was higher than the spontaneous oscillation frequency, or resonance was found in the absence of spontaneous oscillations. The sharpness of the resonance (Q), measured by the peak frequency divided by the half-peak power bandwidth, increased from a mean of 0.44 at rest to 0.83 during a mean depolarization of 6.5 mV. The phase of the driven oscillations changed most rapidly near the resonant frequency, and it shifted about 90° over the half-peak bandwidth of 8.4 Hz. Similar results were found using a sinusoidal function of slowly changing frequency as the input. Sinusoidal currents of peak-to-peak intensity of ¿100 pA

may evoke nonlinear responses characterized by second and higher harmonics. The theta-frequency resonance in hippocampal neurons in vitro suggests that the same voltage-dependent phenomenon may be important in enhancing a theta-frequency response when hippocampal neurons are driven by medial septal or other inputs in vivo.

139

[Levkovitz:1999aa] Y. Levkovitz, J. Marx, N. Grisaru, and M. Segal. Long-term effects of transcranial magnetic stimulation on hippocampal reactivity to afferent stimulation. *J Neurosci*, 19(8):3198–203, 1999.

> **Abstract:** Transcranial magnetic stimulation (TMS) has become a promising treatment of affective disorders in humans, yet the neuronal basis of its long-lasting effects in the brain is still unknown. We studied acute and lasting effects of TMS on reactivity of the rat hippocampus to stimulation of the perforant path. Application of TMS to the brain of the anesthetized rat caused a dose-dependent transient increase in population spike (PS) response of the dentate gyrus to perforant path stimulation. In addition, TMS caused a marked decrease in inhibition and an increase in paired-pulse potentiation of reactivity to stimulation of the perforant path. Also, TMS suppressed the ability of fenfluramine (FFA), a serotonin releaser, to potentiate PS response to perforant path stimulation. Chronic TMS did not affect single population spikes but caused an increase in paired-pulse potentiation, which was still evident 3 weeks after the last of seven daily TMS treatments. After chronic TMS, FFA was ineffective in enhancing reactivity to perforant path stimulation, probably because it lost the ability to release serotonin. In addition, the beta adrenergic receptor agonist isoproterenol, which caused an increase in PS in the control rats, failed to do so in the TMS-treated rats. These results indicate that TMS produces a long-term reduction in efficacy of central modulatory systems.

114, 115, 168, 341

[Levkovitz:2001aa] Y. Levkovitz and M. Segal. Aging affects transcranial magnetic modulation of hippocampal evoked potentials. *Neurobiol Aging*, 22(2):255–63, 2001. 114

[Levkovitz:2007aa] Y. Levkovitz, Y. Roth, E. V. Harel, Y. Braw, A. Sheer, and A. Zangen. A randomized controlled feasibility and safety study of deep transcranial magnetic stimulation. *Clin Neurophysiol*, 118(12):2730–44, 2007.

> **Abstract:** OBJECTIVE: The H-coils are a new development in transcranial magnetic stimulation (TMS) research, allowing direct stimulation of deeper neuronal pathways than does standard TMS. This study assessed possible health risks, and some cognitive and emotional effects, of two H-coil versions designed to stimulate deep portions of the prefrontal cortex, using several stimulation frequencies. METHODS: Healthy volunteers (n=32) were randomly assigned to one of four groups: each of two H-coil designs (H1/H2), standard figure-8 coil, and sham-coil control. Subjects were tested in a pre-post design, during three increasing (single pulses, 10Hz, and 20Hz) stimulation sessions, as well as 24-36h after the last stimulation. RESULTS: The major finding of the present study is that stimulation with the novel H-coils was well tolerated, with no adverse physical or neurological outcomes. Computerized cognitive tests found no deterioration in cognitive functions, except for a transient short-term effect of the H1-coil on spatial recognition memory on the first day of rTMS (but not in the following treatment days). On the other hand, spatial working memory was transiently improved by the H2-coil treatment. Finally, the questionnaires showed no significant emotional or mood alterations, except for reports on 'detachment' experienced by subjects treated with the H1-coil. CONCLUSIONS: This study provides additional evidence for the feasibility and safety of the two H-coil designs (H1/H2). SIGNIFICANCE: The H-coils offer a safe new tool with potential for both research and clinical applications for psychiatric and neurological disorders associated with dysfunctions of deep brain regions.

27

[Li:2007aa] L. Li, Z. Yin, and X. Huo. The influence of low-frequency rtms on eeg of rats. *Neurosci Lett*, 412(2):143–7, 2007.

Abstract: This study aimed to determine the effect of low-frequency repetitive transcranial magnetic stimulation (rTMS) on electroencephalograms (EEGs) of rats. Fifteen Sprague-Dawley rats were subject to 100 pulses of 0.5 Hz rTMS, or sham stimulation. EEGs were recorded before stimulation and within 1 min after rTMS or sham stimulation. Estimates of the EEG correlation dimension (D(2)) and power spectra were calculated. Results show that the D(2) reduced significantly after low-frequency rTMS, but not after sham stimulation. Mean absolute power (MAP) of the gamma band and relative power (RP) of the beta and gamma bands reduce markedly after low-frequency rTMS, but there are no changes with sham stimulation. These results indicate that low-frequency rTMS could affect cortical activities significantly, but effects were markedly different from those of high-frequency rTMS.

110, 174, 175

[Li:2007ab] W. Li, Y. Yang, Q. Ye, B. Yang, and Z. Wang. Effect of chronic and acute low-frequency repetitive transcranial magnetic stimulation on spatial memory in rats. *Brain Res Bull*, 71(5):493–500, 2007.

Abstract: Repetitive transcranial magnetic stimulation (rTMS) is a novel, non-invasive neurological and psychiatric tool. The low-frequency (1 Hz or less) rTMS is likely to play a particular role in its mechanism of action with different effects in comparison with high-frequency (¿1 Hz) rTMS. There is limited information regarding the effect of low-frequency rTMS on spatial memory. In our study, each male Wistar rat was daily given 300 stimuli (1.0 T, 200 micros) at a rate of 0.5 Hz or sham stimulation. We investigated the effects of chronic and acute rTMS on reference/working memory process in Morris water maze test with the hypothesis that the effect would differ by chronic or acute condition. Chronic low-frequency rTMS impaired the retrieval of spatial short- and long-term spatial reference memory but not acquisition process and working memory, whereas acute low-frequency rTMS predominantly induced no deficits in acquisition or short-term spatial reference memory as well as working memory except for long-term reference memory. In summary, chronic 0.5 Hz rTMS disrupts spatial short- and long-term reference memory function, but acute rTMS differently affects reference memory. Chronic low-frequency rTMS may be used to modulate reference memory. Treatment protocols using low-frequency rTMS in neurological and psychiatric disorders need to take into account the potential effect of chronic low-frequency rTMS on memory and other cognitive functions.

117, 174

[Liebetanz:2003aa] D. Liebetanz, S. Fauser, T. Michaelis, B. Czeh, T. Watanabe, W. Paulus, J. Frahm, and E. Fuchs. Safety aspects of chronic low-frequency transcranial magnetic stimulation based on localized proton magnetic resonance spectroscopy and histology of the rat brain. *J Psychiatr Res*, 37(4):277–86, 2003.

Abstract: Because repetitive transcranial magnetic stimulation (rTMS) is capable of inducing lasting alterations of cortical excitability, it represents a promising therapeutic tool in several neuropsychiatric disorders. However, rTMS, especially when applied chronically, may cause harmful effects in the stimulated tissue. To study the safety of chronic rTMS we used a novel small stimulation coil, which was specially designed to treat rats, and investigated brain tissue using in vivo localized proton magnetic resonance spectroscopy (MRS) and post mortem histological analysis. Histology was based on a modified stereology method in combination with immunohistochemistry applying antibodies against OX-6, OX-42, ED, and GFAP to detect any microglial and/or astrocytic activation 48 h after the last

TMS session. Conscious rats were treated with a daily suprathreshold rTMS regimen of 1000 stimuli applied on 5 consecutive days at a frequency of 1 Hz. In comparison with control animals receiving magnetic stimulation over the lumbar spine, quantitative evaluations of cerebral metabolite concentrations by proton MRS revealed no significant alterations of N-acetyl-aspartate, creatine and phosphocreatine, choline-containing compounds, myo-inositol, glucose and lactate after chronic rTMS. Similarly to the in vivo results, post mortem histology revealed no changes in microglial and astrocytic activation after rTMS. In conclusion, these data provide support for the safety of chronic rTMS. However, they do not exclude acute changes on neurotransmitters systems or other physiologic responses during or directly after the rTMS treatment.

118, 124, 125, 169, 173, 178

[Liebetanz:2006aa] D. Liebetanz, F. Fregni, K. K. Monte-Silva, M. B. Oliveira, A. Amancio-dos Santos, M. A. Nitsche, and R. C. Guedes. After-effects of transcranial direct current stimulation (tdcs) on cortical spreading depression. *Neurosci Lett*, 398(1-2):85–90, 2006.

Abstract: Abnormal cortical excitability influences susceptibility to cortical spreading depression (CSD) in migraine. Because transcranial direct current stimulation (tDCS) is capable of inducing lasting changes of cortical excitability, we investigated the after-effects of tDCS on the propagation velocity of CSD in the rat. Twenty-five anesthetised rats received either anodal, cathodal or sham tDCS. The stimulation was applied for 20 min at a current strength of 200 microA after the recording of three baseline CSD measurements. Starting 5 min after tDCS, a further three CSDs were elicited and CSD velocity recorded at intervals of 20 min. tDCS and CSD recording was performed under anaesthesia with chloralose and urethane. As compared to the baseline velocity of 3.14 mm/min, anodal tDCS induced a significant increase of propagation velocity during the first post-tDCS recording (3.49 mm/min). In contrast to anodal tDCS, neither cathodal tDCS nor sham tDCS, which consisted of an initial ramped DC stimulation lasting only 20 s, showed a significant effect on CSD propagation velocity. As anodal tDCS is known to induce a lasting increase of cortical excitability in the clinical setting, our results support the notion that CSD propagation velocity reflects cortical excitability. Since cortical excitability and susceptibility to CSD is elevated in migraine patients, anodal tDCS - by increasing cortical excitability - might increase the probability of migraine attack in these patients, even beyond the end of its application.

129, 130, 132, 343

[Lindner:1995aa] John F. Lindner and et al. Array enhanced stochastic resonance and spatiotemporal synchronization. *Physical Review Letters*, 75(1):3–6, 1995.

Abstract: We enhance the response of a "stochastic resonator" by coupling it into a chain of identical resonators. Specifically, we show via numerical simulation that local linear coupling of overdamped nonlinear oscillators significantly enhances the signal-to-noise ratio of the response of a single oscillator to a time-periodic signal and noise. We relate this array enhanced stochastic resonance to the global spatiotemporal dynamics of the array and show how noise, coupling, and bistable potential cooperate to organize spatial order, temporal periodicity, and peak signal-to-noise ratio.

143, 147, 344

[Lisanby:1998aa] S. H. Lisanby, B.L. Luber, C. Schroeder, M. Osman, D. Finck, VE Amassian, J. Arezzo, and H.A. Sackheim. rtms in primates: intracerebral measurement of rtms ans ecs induced voltages in vivo. *Electroencephalogr Clin Neurophysiol*, 107(3):79p, 1998. 163

[Lisanby:1998ab] S. H. Lisanby, B.L. Luber, C. Schroeder, M. Osman, D. Finck, R. Jalinous, VE Amassian, J. Arezzo, and H.A. Sackheim. Intracerebral measurement of rtms and ecs induced voltage in vivo. *Biological Psychiatry*, 43(8 (suppl1)):S100, 1998. 163

[Lisanby:2001aa] S. H. Lisanby, D. Gutman, B. Luber, C. Schroeder, and H. A. Sackeim. Sham tms: intracerebral measurement of the induced electrical field and the induction of motor-evoked potentials. *Biol Psychiatry*, 49(5):460–3, 2001.

Abstract: Testing the therapeutic potential of transcranial magnetic stimulation (TMS) in controlled trials requires a valid sham condition. Sham TMS is typically administered by tilting the coil 45–90 degrees off the scalp, with one or two wings of the coil touching the scalp. Lack of cortical effects has not been verified. We compared sham manipulations in their thresholds for eliciting motor-evoked potentials (MEPs) in human volunteers and in intracerebral measurements of voltage induced in the prefrontal cortex of a rhesus monkey. Three types of sham (one-wing 45 degrees and 90 degrees and two-wing 90 degrees tilt) induced much lower voltage in the brain than active TMS (67–73However, the two-wing 45 degrees sham induced values just 24TMS. This sham was about half as potent in inducing MEPs over the motor cortex as active TMS. Some sham TMS conditions produce substantial cortical stimulation, making it critical to carefully select the sham manipulation for clinical trials.

105, 106, 123, 163, 339

[Lisanby:2001ab] S. H. Lisanby, B. Luber, A. D. Finck, C. Schroeder, and H. A. Sackeim. Deliberate seizure induction with repetitive transcranial magnetic stimulation in nonhuman primates. *Arch Gen Psychiatry*, 58(2):199–200, 2001. 118, 176

[Liu:2000aa] R. Liu and S. Ueno. Calculating the activation function of nerve excitation in inhomogeneous volume conductor during magnetic stimulation using the finite element method. *IEEE Trans Magn*, 36(4):1796–9, 2000. 26

[Lo:2007aa] Y. L. Lo and S. Fook-Chong. Magnetic brainstem stimulation of the facial nerve. *J Clin Neurophysiol*, 24(1):44–7, 2007.

Abstract: Electrophysiological evaluation of cranial nerves provides information on its functional aspects and may be a valuable adjunct to imaging. In 10 normal subjects, we used transcranial magnetic stimulation with a double cone coil at the posterior head region to obtain orbicularis oris motor evoked potentials. Our findings suggest activation of descending facial fibers proximal to brainstem motoneurons. This method is advocated as an adjunct in the electrodiagnostic workup of facial nerve dysfunction.

29

[Logothetis:2007aa] Nikos K. Logothetis and et al. In vivo measurement of cortical impedance spectrum in monkeys: implications for signal propagation. *Neuron*, 55:809–823, 2007.

Abstract: To combine insights obtained from electric field potentials (LFPs) and neuronal spiking activity (MUA) we need a better understanding of the relative spatial summation of these indices of neuronal activity. Compared to MUA, the LFP has greater spatial coherence, resulting in lower spatial specificity and lower stimulus selectiv- ity. A differential propagation of low- and high- frequency electric signals supposedly underlies this phenomenon, which could result from cor- tical tissue specifically attenuating higher frequencies, i.e., from a frequency-dependent impedance spectrum. Here we directly mea- sure the cortical impedance spectrum in vivo in monkey primary visual cortex. Our results show that impedance is independent of fre- quency, is homogeneous and tangentially isotropic within gray matter, and can be theo- retically predicted assuming a pure-resistive conductor. We propose that the spatial summa- tion of LFP and MUA is determined by the size of these signals' generators and the nature of neural events underlying them, rather than by biophysical properties of gray matter.

18, 135

[Longtin:1991aa] A. Longtin and et al. Time-interval sequences in bistable systems and the noise-induced transmission of information by sensory neurons. *Physical Review Letters*, 67(5):656–659, 1991.

Abstract: We discuss the two time-interval sequences which play a crucial role in studies of escape times in bistable systems driven by periodic functions embedded in noise. We demonstrate that the probability density of escape times for one of the sequences exhibits all the substantive features of experimental interspike interval histograms recorded from real, periodically forced sensory neurons. Our analysis relies on linking this interval sequence to the firing-reset mechanism of real neurons, and illustrates the importance of the noise, without which the substantive features cannot exist, for the transmission of sensory information.

136, 143, 144, 343

[Loo:2000aa] C. K. Loo, J. L. Taylor, S. C. Gandevia, B. N. McDarmont, P. B. Mitchell, and P. S. Sachdev. Transcranial magnetic stimulation (tms) in controlled treatment studies: are some "sham" forms active? *Biol Psychiatry*, 47(4):325–31, 2000.

Abstract: BACKGROUND: Carefully designed controlled studies are essential in further evaluating the therapeutic efficacy of transcranial magnetic stimulation (TMS) in psychiatric disorders. A major methodological concern is the design of the "sham" control for TMS. An ideal sham would produce negligible cortical stimulation in conjunction with a scalp sensation akin to real treatment. Strategies employed so far include alterations in the position of the stimulating coil, but there has been little systematic study of their validity. In this study, we investigated the effects of different coil positions on cortical activation and scalp sensation. METHODS: In nine normal subjects, single TMS pulses were administered at a range of intensities with a "figure eight" coil held in various positions over the left primary motor cortex. Responses were measured as motor-evoked potentials in the right first dorsal interosseus muscle. Scalp sensation to TMS with the coil in various positions over the prefrontal area was also assessed. RESULTS: None of the coil positions studied met the criteria for an ideal sham. Arrangements associated with a higher likelihood of scalp sensation were also more likely to stimulate the cortex. CONCLUSIONS: The choice of a sham for TMS involves a trade-off between effective blinding and truly inactive "stimulation." Further research is needed to develop the best sham condition for a range of applications.

118, 123, 172

[Lu:2007aa] M. Lu, T. Thorlin, S. Ueno, and M. Persson. Comparison of maximum induced current and electric field from transcranial direct current and magnetic stimulations of a human head model. *PIERS 2007 Beijing: Progress in Electromagnetics Research Symposium, Pts I and II, Proceedings*, pages 178–83, 2007.

Abstract: As important non-invasive techniques in brain stimulation, transcranial direct current stimulation (tDCS) and transcranial magnetic stimulation (TMS) have been studied and compared in this paper by employing impedance method and a 3D human head model. The quantitative analysis of distributions of current density and electric field by tDCS and TMS have been presented. Results are compared and potential applications are discussed.

21

[Luft:2001aa] A. R. Luft, A. Kaelin-Lang, T. K. Hauser, L. G. Cohen, N. V. Thakor, and D. F. Hanley. Transcranial magnetic stimulation in the rat. *Exp Brain Res*, 140(1):112–21, 2001.

Abstract: Transcranial magnetic stimulation (TMS) allows for quantification of motor system excitability. While routinely used in humans, application in other species is rare and little is known about the characteristics of animal TMS. The unique features of TMS, i.e., predominantly interneuronal stimulation at low intensity and non-invasiveness, are particularly useful in evaluating injury and recovery in animal models. This study was conducted to characterize the rodent motor evoked potential to TMS (MEPTMS) and to develop a methodology for reproducible assessment of motor excitability in the rat. MEPTMS were compared with responses evoked by electrical stimulation of cervical spinal cord (MEPCES) and

peripheral nerve. MEP were recorded by subcutaneous electrodes implanted bilaterally over the calf. Animals remained under propofol infusion and restrained in a stereotactic frame while TMS followed by CES measurements were obtained before and after 2 h of idle time. TMS was applied using a 5-cm-diameter figure-of-eight coil. MEPTMS had onset latencies of 6.7+/-1.3 ms. Latencies decreased with higher stimulation intensity (r=-0.7, P¡0.05). Two morphologies, MEPTMS, 1 and MEPTMS, 2, were distinguished by latency of the first negative peak (N1), overall shape, and amplitude. MEPTMS, 2 were more frequent at higher stimulation intensity. While recruitment curves for MEPTMS, 1 followed a sigmoid course, no supramaximal response was reached for MEPTMS, 2. Mid-cervical spinal transection completely abolished any response to TMS. MEPCES showed a significantly shorter latency (5.29+/-0.24, P¡0.0001). Two types of MEPCES resembling MEPTMS, 1 and 2 were observed. Neither MEPTMS nor MEPCES changed on repeat assessment after 2 h. This study demonstrates the feasibility and reproducibility of TMS in the rat. Sigmoid recruitment curves for MEPTMS, 1 suggest input-output properties similar to those of the human corticospinal system. Latency differences between CES and TMS point to a supraspinal origin of the MEPTMS. The two morphologies likely reflect different cortical or subcortical origins of MEPTMS.

175

[Lugo:2008aa] Eduardo Lugo and et al. Ubiquitous crossmodal stochastic resonance in humans: auditory noise facilitates tactile, visual and proprioceptive sensations. *Plos One*, 3(8), 2008.

Abstract: Abstract Background:Stochastic resonance is a nonlinear phenomenon whereby the addition of noise can improve the detection of weak stimuli. An optimal amount of added noise results in the maximum enhancement, whereas further increases in noise intensity only degrade detection or information content. The phenomenon does not occur in linear systems, where the addition of noise to either the system or the stimulus only degrades the signal quality. Stochastic Resonance (SR) has been extensively studied in different physical systems. It has been extended to human sensory systems where it can be classified as unimodal, central, behavioral and recently crossmodal. However what has not been explored is the extension of this crossmodal SR in humans. For instance, if under the same auditory noise conditions the crossmodal SR persists among different sensory systems. Methodology/Principal Findings: Using physiological and psychophysical techniques we demonstrate that the same auditory noise can enhance the sensitivity of tactile, visual and proprioceptive system responses to weak signals. Specifically, we show that the effective auditory noise significantly increased tactile sensations of the finger, decreased luminance and contrast visual thresholds and significantly changed EMG recordings of the leg muscles during posture maintenance. Conclusions/Significance:We conclude that crossmodal SR is a ubiquitous phenomenon in humans that can be interpreted within an energy and frequency model of multisensory neurons spontaneous activity. Initially the energy and frequency content of the multisensory neurons' activity (supplied by the weak signals) is not enough to be detected but when the auditory noise enters the brain, it generates a general activation among multisensory neurons of different regions, modifying their original activity. The result is an integrated activation that promotes sensitivity transitions and the signals are then perceived. A physiologically plausible model for crossmodal stochastic resonance is presented.

137

[Maagdenberg:2004aa] A. M. van den Maagdenberg, D. Pietrobon, T. Pizzorusso, S. Kaja, L. A. Broos, T. Cesetti, R. C. van de Ven, A. Tottene, J. van der Kaa, J. J. Plomp, R. R. Frants, and M. D. Ferrari. A cacna1a knockin migraine mouse model with increased susceptibility to cortical spreading depression. *Neuron*, 41(5):701–10, 2004.

Abstract: Migraine is a common, disabling, multifactorial, episodic neurovascular disorder of unknown etiology. Familial hemiplegic migraine type 1 (FHM-1) is

a Mendelian subtype of migraine with aura that is caused by missense mutations in the CACNA1A gene that encodes the alpha(1) subunit of neuronal Ca(v)2.1 Ca(2+) channels. We generated a knockin mouse model carrying the human pure FHM-1 R192Q mutation and found multiple gain-of-function effects. These include increased Ca(v)2.1 current density in cerebellar neurons, enhanced neurotransmission at the neuromuscular junction, and, in the intact animal, a reduced threshold and increased velocity of cortical spreading depression (CSD; the likely mechanism for the migraine aura). Our data show that the increased susceptibility for CSD and aura in migraine may be due to cortical hyperexcitability. The R192Q FHM-1 mouse is a promising animal model to study migraine mechanisms and treatments.

128

[Maccabee:1993aa] P. J. Maccabee, V. E. Amassian, L. P. Eberle, and R. Q. Cracco. Magnetic coil stimulation of straight and bent amphibian and mammalian peripheral nerve in vitro: locus of excitation. *J Physiol*, 460:201–19, 1993.

Abstract: 1. According to classical cable theory, a magnetic coil (MC) should excite a linear nerve fibre in a homogeneous medium at the negative- going first spatial derivative of the induced electric field. This prediction was tested by MC stimulation of mammalian phrenic and amphibian sciatic nerve and branches in vitro, immersed in Ringer solution within a trough, and identifying the sites of excitation by recording responses of similar latency to local electrical stimulation. Subsequently, the identified sites of excitation were compared with measurements of the induced electric field and its calculated first spatial derivative. A special hardware device was used to selectively reverse MC current direction and to generate predominantly monophasic- or polyphasic-induced pulse profiles whose initial phases were identical in polarity, shape and amplitude. When using the amphibian nerve preparation, a complication was excitation at low threshold points related to cut branches. 2. Reversal of monophasic current resulted in latency shifts corresponding approximately to the distance between induced cathode and anode. The location of each site of excitation was at, or very near, the negative-going first spatial derivative peaks of the induced electric field measured parallel to the straight nerve. Significantly, excitation of the nerve did not occur at the peak of the induced electric field above the centre of the 'figure of eight' MC junction. 3. A polyphasic pulse excited the nerve at both sites, by the negative-going first phase at one location, and approximately 150 microseconds later, by the reversed negative-going second phase at the other location. Polyphasic and monophasic pulses elicited responses with similar latency when the induced current flowed towards the recording electrode. 4. Straddling a nerve with non-coding solid lucite cylinders created a localized spatial narrowing and increase in the induced electric field, resulting in a lowered threshold of excitation. The corresponding closer spacing between first spatial derivative peaks was exhibited by a significant reduction in latency shift when MC current direction was reversed. 5. When a nerve is bent and the induced current is directed along the nerve towards the bend, the threshold of excitation is reduced there. Increasing the angle of the bend from 0 deg to more than 90 deg graded the decrease in threshold. 6. In a straight nerve the threshold was lowest when current was directed towards the cut end.(ABSTRACT TRUNCATED AT 400 WORDS)

35, 61

[Maccabee:1998aa] P. J. Maccabee, S. S. Nagarajan, V. E. Amassian, D. M. Durand, A. Z. Szabo, A. B. Ahad, R. Q. Cracco, K. S. Lai, and L. P. Eberle. Influence of pulse sequence, polarity and amplitude on magnetic stimulation of human and porcine peripheral nerve. *J Physiol*, 513(Pt 2):571–85., 1998.

Abstract: 1. Mammalian phrenic nerve, in a trough filled with saline, was excited by magnetic coil (MC)-induced stimuli at defined stimulation sites, including the negative-going first spatial derivative of the induced electric field along a straight nerve, at a bend in the nerve, and at a cut nerve ending. At all such sites, the largest

amplitude response for a given stimulator output setting was elicited by an induced damped polyphasic pulse consisting of an initial quarter-cycle hyperpolarization followed by a half-cycle depolarization compared with a predominantly 'monophasic' quarter-cycle depolarization. 2. Simulation studies demonstrated that the increased efficacy of the induced quarter-cycle hyperpolarizing-half-cycle depolarizing polyphasic pulse was mainly attributed to the greater duration of the outward membrane current phase, resulting in a greater outward charge transfer afforded by the half-cycle (i.e. quarter-cycles 2 and 3). The advantage of a fast rising initial quarter-cycle depolarization was more than offset by the slower rising, but longer duration depolarizing half-cycle. 3. Simulation further revealed that the quarter-cycle hyperpolarization-half-cycle depolarization showed only a 2.6 transfer at threshold, compared with a half-cycle depolarization alone. Presumably, this slight increase in efficacy reflects modest reversal of Na+ inactivation by the very brief initial hyperpolarization. 4. In vitro, at low bath temperature, the nerve response to an initial quarter-cycle depolarization declined in amplitude as the second hyperpolarizing phase progressively increased in amplitude and duration. This 'pull-down' phenomenon nearly disappeared as the bath temperature approached 37 C. Possibly, at the reduced temperature, delay in generation of the action potential permitted the hyperpolarization phase to reduce excitation. 5. Pull-down was not observed in the thenar muscle responses to median nerve stimulation in a normal human at normal temperature. However, pull-down emerged when the median nerve was cooled by placing ice over the forearm. 6. In a nerve at subnormal temperature straddled with non-conducting inhomogeneities, polyphasic pulses of either polarity elicited the largest responses. This was also seen when stimulating distal median nerve at normal temperature. These results imply excitation by hyperpolarizing-depolarizing pulse sequences at two separate sites. Similarly, polyphasic pulses elicited the largest responses from nerve roots and motor cortex. 7. The pull-down phenomenon has a possible clinical application in detecting pathologically slowed activation of Na+ channels. The current direction of the polyphasic waveform may become a significant factor with the increasing use of repetitive magnetic stimulators which, for technical reasons, induce a cosine-shaped half-cycle, preceded and followed by quarter-cycles of opposite polarity.

28

[Makeig:1982aa] Scott Makeig and et al. Attending or discriminating 40 hz modulated tones induces phase-locked subharmonic resonances in eeg. *Psychopharmacology Bulletin*, 18(3):55–58, 1982. 136

[Manola:2005aa] L. Manola, B. H. Roelofsen, J. Holsheimer, E. Marani, and J. Geelen. Modelling motor cortex stimulation for chronic pain control: electrical potential field, activating functions and responses of simple nerve fibre models. *Med Biol Eng Comput*, 43(3):335–43, 2005.

Abstract: This computer modelling study on motor cortex stimulation (MCS) introduced a motor cortex model, developed to calculate the imposed electrical potential field characteristics and the initial response of simple fibre models to stimulation of the precentral gyrus by an epidural electrode, as applied in the treatment of chronic, intractable pain. The model consisted of two parts: a three-dimensional volume conductor based on tissue conductivities and human anatomical data, in which the stimulation-induced potential field was computed, and myelinated nerve fibre models allowing the calculation of their response to this field. A simple afferent fibre branch and three simple efferent fibres leaving the cortex at different positions in the precentral gyrus were implemented. It was shown that the thickness of the cerebrospinal fluid (CSF) layer between the dura mater and the cortex below the stimulating electrode substantially affected the distribution of the electrical potential field in the precentral gyrus and thus the threshold stimulus for motor responses and the therapeutic stimulation amplitude. When the CSF thickness was increased from 0 to 2.5 mm, the load impedance decreased by 28by 6.6 V for each millimetre of CSF. Owing to the large anode-cathode distance (10 mm centre-to-centre) in MCS, the cathodal fields in mono- and bipolar stimulation were almost identical. Calculation of activating functions and fibre responses showed that only

nerve fibres with a directional component parallel to the electrode surface were excitable by a cathode, whereas fibres perpendicular to the electrode surface were excitable under an anode.

60

[Manola:2007aa] L. Manola, J. Holsheimer, P. Veltink, and J. R. Buitenweg. Anodal vs cathodal stimulation of motor cortex: a modeling study. *Clin Neurophysiol*, 118(2):464–74, 2007.

Abstract: OBJECTIVE: To explore the effects of electrical stimulation performed by an anode, a cathode or a bipole positioned over the motor cortex for chronic pain management. METHODS: A realistic 3D volume conductor model of the human precentral gyrus (motor cortex) was used to calculate the stimulus-induced electrical field. The subsequent response of neural elements in the precentral gyrus and in the anterior wall and lip of the central sulcus was simulated using compartmental neuron models including the axon, soma and dendritic trunk. RESULTS: While neural elements perpendicular to the electrode surface are preferentially excited by anodal stimulation, cathodal stimulation excites those with a direction component parallel to its surface. When stimulating bipolarly, the excitation of neural elements parallel to the bipole axis is additionally facilitated. The polarity of the contact over the precentral gyrus determines the predominant response. Inclusion of the soma-dendritic model generally reduces the excitation threshold as compared to simple axon model. CONCLUSIONS: Electrode polarity and electrode position over the precentral gyrus and central sulcus have a large and distinct influence on the response of cortical neural elements to stimuli. SIGNIFICANCE: Modeling studies like this can help to identify the effects of electrical stimulation on cortical neural tissue, elucidate mechanisms of action and ultimately to optimize the therapy.

36, 42, 43, 44, 60, 335, 347

[Marin:1998aa] G. Marin, C. Guerin, S. Baillet, L. Garnero, and G. Meunier. Influence of skull anisotropy for the forward and inverse problem in eeg: simulation studies using fem on realistic head models. *Hum Brain Mapp*, 6(4):250–69, 1998.

Abstract: For the sake of realism in the description of conduction from primary neural currents to scalp potentials, we investigated the influence of skull anisotropy on the forward and inverse problems in brain functional imaging with EEG. At present, all methods available for cortical imaging assume a spherical geometry, or when using realistic head shapes do not consider the anisotropy of head tissues. However, to our knowledge, no study relates the implication of this simplifying hypothesis on the spatial resolution of EEG for source imaging. In this paper, a method using finite elements in a realistic head geometry is implemented and validated. The influence of erroneous conductivity values for the head tissues is presented, and results show that the conductivities of the brain and the skull in the radial orientation are the most critical ones. In the inverse problem, this influence has been evaluated with simulations using a distributed source model with a comparison of two regularization techniques, with the isotropic model working on data sets produced by a nonisotropic model. Regularization with minimum norm priors produces source images with spurious activity, meaning that the errors in the head model totally annihilate any localization ability. But nonlinear regularization allows the accurate recovery of simultaneous spots of activity, while the restoration of very close active regions is profoundly disabled by errors in the head model. We conclude that for robust cortical source imaging with EEG, a realistic head model taking anisotropy of tissues into account should be used.

30

[Marshall:2006aa] Lisa Marshall and et al. Boosting slow oscillations during sleep potentiates memory. *Nature*, 444:610–613, 2006.

Abstract: There is compelling evidence that sleep contributes to the long- term consolidation of new memories1. This function of sleep has been linked to slow

(<1 Hz) potential oscillations, which pre- dominantly arise from the prefrontal neocortex and characterize slow wave sleep. However, oscillations in brain potentials are commonly considered to be mere epiphenomena that reflect syn- chronized activity arising from neuronal networks, which links the membrane and synaptic processes of these neurons in time. Whether brain potentials and their extracellular equivalent have any physiological meaning per se is unclear, but can easily be investigated by inducing the extracellular oscillating potential fields of interest. Here we show that inducing slow oscillation- like potential fields by transcranial application of oscillating potentials (0.75 Hz) during early nocturnal non-rapid-eye-move- ment sleep, that is, a period of emerging slow wave sleep, enhances the retention of hippocampus-dependent declarative memories in healthy humans. The slowly oscillating potential stimulation induced an immediate increase in slow wave sleep, endogenous cortical slow oscillations and slow spindle activity in the frontal cortex. Brain stimulation with oscillations at 5 Hz—another fre- quency band that normally predominates during rapid-eye-move- ment sleep—decreased slow oscillations and left declarative memory unchanged. Our findings indicate that endogenous slow potential oscillations have a causal role in the sleep-associated consolidation of memory, and that this role is enhanced by field effects in cortical extracellular space.

22, 138, 141

[Mascagni:1998aa] MV Mascagni and et al. *Methods in Neuronal Modeling*, chapter Numerical methods for neuronal modeling. MIT Press, 1998. 38

[Massimini:2005aa] Marcello Massimini and et al. Breakdown of cortical effective connectivity during sleep. *Science*, 309:2228–2232, 2005.

Abstract: When we fall asleep, consciousness fades yet the brain remains active. Why is this so? To investigate whether changes in cortical information transmission play a role, we used transcranial magnetic stimulation together with high-density electroencephalography and asked how the activation of one cortical area (the premotor area) is transmitted to the rest of the brain. During quiet wakefulness, an initial response (È15 milliseconds) at the stimulation site was followed by a sequence of waves that moved to connected cortical areas several centimeters away. During non–rapid eye movement sleep, the initial response was stronger but was rapidly extinguished and did not propagate beyond the stimulation site. Thus, the fading of consciousness during certain stages of sleep may be related to a breakdown in cortical effective connectivity.

143

[Matsumiya:1992aa] Y. Matsumiya, T. Yamamoto, M. Yarita, S. Miyauchi, and J. W. Kling. Physical and physiological specification of magnetic pulse stimuli that produce cortical damage in rats. *J Clin Neurophysiol*, 9(2):278–87, 1992.

Abstract: The effects of transcranial magnetic pulse stimuli on the brain tissue of rats were examined. In Experiment I, 52 male albino rats received pulsed magnetic stimulation of the head. Stimulus intensity, number of stimulations, stimulated sites, and interval between last stimulation and sacrifice for neuropathological examination were varied. High stimulus intensity (2.8 T) and 100 or more stimulations produced clearly defined microvacuolar changes in the neuropil portion of cortical layers 2-6 (especially layers 3 and 4) in 12 of 24 animals. Fewer stimulations and lower intensities produced no such effects in 28 rats given that stimulation. Midline stimulation and stimulation over the left hemisphere produced similar results. No other brain, ocular, or spinal structures manifested such changes. Lesions were present in animals that had intervals up to 30 days between the last stimulation and perfusion. In Experiment II with 18 animals, compound motor action potentials (CMAPs) evoked by magnetic stimulation of the cortical motor area and recorded from the right lower extremity were examined. The electromyographic threshold was 0.83 T. Further increases in stimulus intensity produced

increases in CMAP amplitude, up to approximately 1.9 T. It was noted that the lesion-producing intensity (2.8 T) was 0.9 T greater than the intensity needed for near-asymptotic reactions and was 3.4 times the CMAP threshold value.

124, 125, 169

[Matthies:1993aa] H. Matthies and K. G. Reymann. Protein kinase a inhibitors prevent the maintenance of hippocampal long-term potentiation. *Neuroreport*, 4(6):712–4, 1993.

Abstract: The possible involvement of cAMP-dependent protein kinase A (PKA) in mechanisms of long-term potentiation of the Schaffer collateral-commissural input of rat CA1 neurones was investigated using several inhibitors in vitro. If 10 microM H-8, 100 nM KT5720 or 50 microM Rp-cAMPs was applied to the bath before a triple 100 Hz/0.5 s tetanization, post-tetanic and short-term potentiation developed almost normally. However, from about 3 h after tetanization the long-term potentiation (LTP) of the field-EPSP declined with respect to the control in an irreversible manner. These data suggest that besides protein kinase C the synergistic activation of PKA is necessary for the maintenance of LTP.

101

[McIntyre:1999aa] C. C. McIntyre and W. M. Grill. Excitation of central nervous system neurons by nonuniform electric fields. *Biophys J*, 76(2):878–88, 1999.

Abstract: The goal of this study was to determine which neural elements are excited by microstimulation of the central nervous system. A cable model of a neuron including an axon, initial segment, axon hillock, soma, and simplified dendritic tree was used to study excitation with an extracellular point source electrode. The model reproduced a wide range of experimentally documented extracellular excitation patterns. The site of action potential initiation (API) was a function of the electrode position, stimulus duration, and stimulus polarity. The axon or initial segment was always the site of API at threshold. When the electrode was positioned near the cell body, the site of excitation was dependent on the stimulus amplitude. With the electrode in close proximity to the neuron, short-duration cathodic pulses produced lower thresholds with the electrode positioned over the axon than over the cell body, and long-duration stimuli produced opposite relative thresholds. This result was robust to alterations in either the maximum conductances or the intracellular resistivities of the model. The site of maximum depolarization was not always an accurate predictor of the site of API, and the temporal evolution of the changes in membrane potential played a strong role in determining the site of excitation.

60, 61

[McIntyre:2002aa] Cameron C. McIntyre and et al. Extracellular stimulation of central neurons: Influence of stimulus waveform and frequency on neuronal output. *J. Neurophysiol*, 88:1592–1604, 2002.

Abstract: The objective of this project was to examine the influence of stimulus waveform and frequency on extracellular stimulation of neurons with their cell bodies near the electrode (local cells) and fibers of passage in the CNS. Detailed computer-based models of CNS cells and axons were developed that accurately reproduced the dynamic firing properties of mammalian motoneurons including afterpotential shape, spike-frequency adaptation, and firing frequency as a function of stimulus amplitude. The neuron models were coupled to a three-dimensional finite element model of the spinal cord that solved for the potentials generated in the tissue medium by an extracellular electrode. Extracellular stimulation of the CNS with symmetrical charge balanced biphasic stimuli resulted in activation of fibers of passage, axon terminals, and local cells around the electrode at similar thresholds. While high stimulus frequencies enhanced ac- tivation of fibers of passage, a much more robust technique to achieve selective activation of targeted neuronal populations was via alter- ations in the stimulus waveform. Asymmetrical charge-balanced bi- phasic stimuli, consisting of a long-duration low-amplitude

cathodic prepulse phase followed by a short-duration high-amplitude anodic stimulus phase, enabled selective activation of local cells. Conversely, an anodic prepulse phase followed by a cathodic stimulus phase enabled selective activation of fibers of passage. The threshold for activation of axon terminals in the vicinity of the electrode was lower than the threshold for direct activation of local cells, independent of the stimulus waveform. As a result, stimulation induced trans-synap- tic influences (indirect depolarization/hyperpolarization) on local cells altered their neural output, and this indirect effect was dependent on stimulus frequency. If the indirect activation of local cells was inhib- itory, there was little effect on the stimulation induced neural output of the local cells. However, if the indirect activation of the local cells was excitatory, attempts to activate selectively fibers of passage over local cells was limited. These outcomes provide a biophysical basis for understanding frequency-dependent outputs during CNS stimula- tion and provide useful tools for selective stimulation of the CNS.

140, 141, 343

[McIntyre:2004aa] C. C. McIntyre, W. M. Grill, D. L. Sherman, and N. V. Thakor. Cellular effects of deep brain stimulation: model-based analysis of activation and inhibition. *J Neurophysiol*, 91(4):1457–69, 2004.

> **Abstract:** Deep brain stimulation (DBS) is an effective therapy for medically refractory movement disorders. However, fundamental questions remain about the effects of DBS on neurons surrounding the electrode. Experimental studies have produced apparently contradictory results showing suppression of activity in the stimulated nucleus, but increased inputs to projection nuclei. We hypothesized that cell body firing does not accurately reflect the efferent output of neurons stimulated with high-frequency extracellular pulses, and that this decoupling of somatic and axonal activity explains the paradoxical experimental results. We studied stimulation using the combination of a finite-element model of the clinical DBS electrode and a multicompartment cable model of a thalamocortical (TC) relay neuron. Both the electric potentials generated by the electrode and a distribution of excitatory and inhibitory trans-synaptic inputs induced by stimulation of presynaptic terminals were applied to the TC relay neuron. The response of the neuron to DBS was primarily dependent on the position and orientation of the axon with respect to the electrode and the stimulation parameters. Stimulation subthreshold for direct activation of TC relay neurons caused suppression of intrinsic firing (tonic or burst) activity during the stimulus train mediated by activation of presynaptic terminals. Suprathreshold stimulation caused suppression of intrinsic firing in the soma, but generated efferent output at the stimulus frequency in the axon. This independence of firing in the cell body and axon resolves the apparently contradictory experimental results on the effects of DBS. In turn, the results of this study support the hypothesis of stimulation-induced modulation of pathological network activity as a therapeutic mechanism of DBS.

61

[McNeal:1976aa] Donald R. McNeal. Analysis of model for excitation of myelinated nerve. *IEEE Transactions on Biomedical Engineering*, BM-23(4), July 1976.

> **Abstract:** Excellent models have been presented in the literature which relate membrane potential to transverse membrane current and which describe the propagation of action potentials along the axon, for both myelinated and nonmyelinated fibers. There is not, however, an adequate model for nerve excitation which allows one to compute the threshold of a nerve fiber for pulses of finite duration using electrodes that are not in direct contact with the fiber. This paper considers this problem and presents a model of the electrical properties of myelinated nerve which describes the time course of events following stimulus application up to the initiation of the action potential. The time-varying current and potential at all nodes can be computed from the model, and the strength-duration curve can be determined for arbitrary electrode geometries, although only the case of a

monopolar electrode is considered in this paper. It is shown that even when the stimulus is a constant-current pulse, the membrane current at the nodes varies considerably with time. The strength-duration curve calculated from the model is consistent with previously published experimental data, and the model provides a quantitative relationship between threshold and fiber diameter which shows there is less selectivity among fibers of large diameter than those of small diameter.

36, 39

[McRobbie:1984aa] D. McRobbie and M. A. Foster. Thresholds for biological effects of time-varying magnetic fields. *Clin Phys Physiol Meas*, 5(2):67–78, 1984.

Abstract: Investigations of the biological effects of time-varying magnetic fields in the extremely low frequency range have been carried out with particular reference to NMR imaging. One effect encountered is the stimulation of nerves and muscles by induced eddy currents. The nature of this effect has been studied in rats exposed to whole body homogeneous fields and in the human forearm with local exposures. Electromyography was used to provide quantitative measurements of thresholds and responses for human exposures. The field exposures required to produce a detectable response are dependent upon the pulse period, pulse waveform and the current path in tissue. For the rat experiments the lowest threshold occurred for a damped sinusoidal pulse of period 0.33 ms with a maximum rate of change of field of 2400 T s-1. The lowest threshold for sensation in the human experiments was 2100 T s-1 for a similar type of field. Simple theory for conduction is considered and current densities induced are estimated as 5 A m-2.

28

[Melloni:2007aa] Lucia Melloni and et al. Synchronization of neural activity across cortical areas correlates with conscious perception. *The Journal of Neuroscience*, 27(11):2858–2865, 2007.

Abstract: Subliminal stimuli can be deeply processed and activate similar brain areas as consciously perceived stimuli. This raises the question which signatures of neural activity critically differentiate conscious from unconscious processing. Transient synchronization of neural activity has been proposed as a neural correlate of conscious perception. Here we test this proposal by comparing the electrophysiological responses related to the processing of visible and invisible words in a delayed matching to sample task. Both perceived and nonperceived words caused a similar increase of local (gamma) oscillations in the EEG, but only perceived words induced a transient long-distance synchronization of gamma oscillations across widely separated regions of the brain. After this transient period of temporal coordination, the electrographic signatures of conscious and unconscious processes continue to diverge. Only words reported as perceived induced (1) enhanced theta oscillations over frontal regions during the maintenance interval, (2) an increase of the P300 component of the event- related potential, and (3) an increase in power and phase synchrony of gamma oscillations before the anticipated presentation of the test word. We propose that the critical process mediating the access to conscious perception is the early transient global increase of phase synchrony of oscillatory activity in the gamma frequency range.

143

[Merrill:2005aa] D. R. Merrill, M. Bikson, and J. G. Jefferys. Electrical stimulation of excitable tissue: design of efficacious and safe protocols. *J Neurosci Methods*, 141(2):171–98, 2005.

Abstract: The physical basis for electrical stimulation of excitable tissue, as used by electrophysiological researchers and clinicians in functional electrical stimulation, is presented with emphasis on the fundamental mechanisms of charge injection at the electrode/tissue interface. Faradaic and non-Faradaic charge transfer mechanisms are presented and contrasted. An electrical model of the electrode/tissue interface is given. The physical basis for the origin of electrode potentials is given. Various methods of controlling charge delivery during pulsing

are presented. Electrochemical reversibility is discussed. Commonly used electrode materials and stimulation protocols are reviewed in terms of stimulation efficacy and safety. Principles of stimulation of excitable tissue are reviewed with emphasis on efficacy and safety. Mechanisms of damage to tissue and the electrode are reviewed.

104

[Mills:1992aa] K. R. Mills, S. J. Boniface, and M. Schubert. Magnetic brain stimulation with a double coil: the importance of coil orientation. *Electroencephalogr Clin Neurophysiol*, 85(1):17–21., 1992.

Abstract: The human motor cortex can be excited by currents induced by a transient magnetic field generated in a coil over the scalp. A 9 cm mean diameter circular coil centered at the vertex is optimally placed for exciting the hand area. Anticlockwise current flow in the coil preferentially excites the left hemisphere and vice versa. A double coil has been used to investigate the orientation of inducing currents at which activation of cortical neural elements is maximal. The inducing current flowed in the same direction in the central segment of the coil and followed a monophasic wave form. The coil was rotated through 360 degrees over the motor area in increments of 45 degrees and compound muscle action potentials from the first dorsal interosseous muscle were recorded. The largest responses were obtained with the coil at about 50 degrees to the parasagittal plane with a backward flowing inducing current. The optimal angle did not depend on stimulus intensity or background voluntary contraction. This orientation corresponds to an maximal induced current flowing forwards approximately at right angles to the central sulcus. It is postulated that horizontal neural elements are aligned in this direction and are preferentially excited by these monophasic magnetic stimuli. The results have important implications for mapping the motor areas with magnetic stimulators.

27

[Mills:1999aa] K.R. Mills. *Magnetic stimulation of the human nervous system*. Oxford University Press, 1999.
23

[Miranda:2003aa] P. C. Miranda, M. Hallett, and P. J. Basser. The electric field induced in the brain by magnetic stimulation: a 3-d finite-element analysis of the effect of tissue heterogeneity and anisotropy. *IEEE Trans Biomed Eng*, 50(9):1074–85, 2003.

Abstract: We investigate the effect of tissue heterogeneity and anisotropy on the electric field and current density distribution induced in the brain during magnetic stimulation. Validation of the finite-element (FE) calculations in a homogeneous isotropic sphere showed that the magnitude of the total electric field can be calculated to within an error of approximately 5a significant surface charge contribution. We used a high conductivity inclusion within a sphere of lower conductivity to simulate a lesion due to an infarct. Its effect is to increase the electric field induced in the surrounding low conductivity region. This boost is greatest in the vicinity of interfaces that lie perpendicular to the current flow. For physiological values of the conductivity distribution, it can reach a factor of 1.6 and extend many millimeters from the interface. We also show that anisotropy can significantly alter the electric field and current density distributions. Either heterogeneity or anisotropy can introduce a radial electric field component, not present in a homogeneous isotropic conductor. Heterogeneity and anisotropy are predicted to significantly affect the distribution of the electric field induced in the brain. It is, therefore, expected that anatomically faithful FE models of individual brains which incorporate conductivity tensor data derived from diffusion tensor measurements, will provide a better understanding of the location of possible stimulation sites in the brain.

26, 30, 60

[Miranda:2006aa] Pedro Cavaleiro Miranda and et al. Modeling the current distribution during transcranial direct current stimulation. *Clinical Neurophysiology*, 117:1623–1629, 2006.

Abstract: OBJECTIVE: To investigate the spatial distribution of the magnitude and direction of the current density in the human head during transcranial direct current stimulation (tDCS). METHODS: The current density distribution was calculated using a numerical method to implement a standard spherical head model into which current was injected by means of large electrodes. The model was positioned in 'MNI space' to facilitate the interpretation of spatial coordinates. RESULTS: The magnitude and direction of the current density vector are illustrated in selected brain slices for four different electrode montages. Approximately half of the current injected during tDCS is shunted through the scalp, depending on electrode dimension and position. Using stimulating currents of 2.0 mA, the magnitude of the current density in relevant regions of the brain is of the order of 0.1 A/m2, corresponding to an electric field of 0.22 V/m. CONCLUSIONS: Calculations based on a spherical model of the head can provide useful information about the magnitude and direction of the current density vector in the brain during tDCS, taking into account the geometry and position of the electrodes. Despite the inherent limitations of the spherical head model, the calculated values are comparable to those used in the most recent in vitro studies on modulation of neuronal activity. SIGNIFICANCE: The methodology presented in this paper may be used to assess the current distribution during tDCS using new electrode montages, to help optimize montages that target a specific region of the brain or to preliminarily investigate compliance with safety guidelines.

20, 22, 42

[Miranda:2007aa] Pedro Cavaleiro Miranda and et al. Tissue heterogeneity as a mechanism for localized neural stimulation by applied electric fields. *Physics in Medicine and Biology*, 52:5603–5617, 2007.

Abstract: We investigate the heterogeneity of electrical conductivity as a new mechanism to stimulate excitable tissues via applied electric fields. In particular, we show that stimulation of axons crossing internal boundaries can occur at boundaries where the electric conductivity of the volume conductor changes abruptly. The effectiveness of this and other stimulation mechanisms was compared by means of models and computer simulations in the context of transcranial magnetic stimulation. While, for a given stimulation intensity, the largest membrane depolarization occurred where an axon terminates or bends sharply in a high electric field region, a slightly smaller membrane depolarization, still sufficient to generate action potentials, also occurred at an internal boundary where the conductivity jumped from 0.143 S m1 to 0.333 S m1, simulating a white-matter-grey-matter interface. Tissue heterogeneity can also give rise to local electric field gradients that are considerably stronger and more focal than those impressed by the stimulation coil and that can affect the membrane potential, albeit to a lesser extent than the two mechanisms mentioned above. Tissue heterogeneity may play an important role in electric and magnetic 'far-field' stimulation.

35, 42

[Mitchell1998] Melanie Mitchell. *An Introduction to Genetic Algorithms (Complex Adaptive Systems)*. The MIT Press, February 1998. 80

[Mockett:2002aa] B. Mockett, C. Coussens, and W. C. Abraham. Nmda receptor-mediated metaplasticity during the induction of long-term depression by low-frequency stimulation. *Eur J Neurosci*, 15(11):1819–26, 2002.

Abstract: Metaplasticity refers to the activity-dependent modification of the ability of synapses to undergo subsequent synaptic plasticity. Here, we have addressed the question of whether metaplasticity contributes to the induction of long-term depression (LTD) by low-frequency stimulation (LFS). The experiments were conducted using standard extracellular recording techniques in stratum radiatum of area CA1 in hippocampal slices made from adult Sprague-Dawley rats. The degree of LTD induction was found to be a nonlinear function of the number of pulses during a 1-Hz LFS. Little LTD was observed following 600 or 900 pulses, but a

significant LTD occurred following 1200 pulses of LFS, whether delivered in one episode, or in two bouts of 600 pulses given 10 min apart. A similar pattern was observed for 3 Hz LFS. The data support the suggestion that pulses occurring early in the LFS train prime synapses for LTD induction, as triggered by later occurring stimuli. The priming effect lasted at least 120 min, when tested by giving two bouts of 1 Hz LFS (600 pulses each) at different intervals. Neither heterosynaptic nor homosynaptic stimulation by itself was sufficient to prime LTD. However, a combination of the stimuli, induced by increased stimulus strength during the LFS, appeared necessary for inducing the effect. An N-methyl-d-aspartate (NMDA) receptor antagonist markedly reduced total LTD induction, regardless of whether it was administered during the first or second LFS in a protocol employing two bouts of 600 pulse LFS, 30 min apart. These findings strongly support the hypothesis that NMDA receptor-dependent metaplasticity processes contribute to the induction of LTD during standard LFS protocols.

102, 103, 339

[Moliadze:2003aa] V. Moliadze, Y. Zhao, U. Eysel, and K. Funke. Effect of transcranial magnetic stimulation on single-unit activity in the cat primary visual cortex. *J Physiol*, 553(Pt 2):665–79, 2003.

Abstract: Transcranial magnetic stimulation (TMS) has become a well established procedure for testing and modulating the neuronal excitability of human brain areas, but relatively little is known about the cellular processes induced by this rather coarse stimulus. In a first attempt, we performed extracellular single-unit recordings in the primary visual cortex (area 17) of the anaesthetised and paralysed cat, with the stimulating magnetic field centred at the recording site (2 x 70 mm figure-of-eight coil). The effect of single biphasic TMS pulses, which induce a lateral-to-medial electric current within the occipital pole of the right hemisphere, was tested for spontaneous as well as visually evoked activity. For cat visual cortex we found that a single TMS pulse elicited distinct episodes of enhanced and suppressed activity: in general, a facilitation of activity was found during the first 500 ms, followed thereafter by a suppression of activity lasting up to a few seconds. Strong stimuli exceeding 50 activity during the first 100-200 ms, followed by stronger (rebound) facilitation. Early suppression and facilitation of activity may be related to a more or less direct stimulation of inhibitory and excitatory interneurons, probably with different thresholds. The late, long-lasting suppression is more likely to be related to metabotropic or metabolic processes, or even vascular responses. The time course of facilitation/inhibition may provide clues regarding the action of repetitive TMS application.

106, 107, 108, 163, 339, 340

[Moliadze:2005aa] V. Moliadze, D. Giannikopoulos, U. T. Eysel, and K. Funke. Paired-pulse transcranial magnetic stimulation protocol applied to visual cortex of anaesthetized cat: effects on visually evoked single-unit activity. *J Physiol*, 566(Pt 3):955–65, 2005.

Abstract: In this study, we tested the paired-pulse transcranial magnetic stimulation (ppTMS) protocol - a conditioning stimulus (CS) given at variable intervals prior to a test stimulus (TS) - for visually evoked single-unit activity in cat primary visual cortex. We defined the TS as being supra-threshold when it caused a significant increase or decrease in the visually evoked activity. By systematically varying the interstimulus interval (ISI) between 2 and 30 ms and the strength of CS within the range 15-130dependence of the ppTMS effect on CS strength but little relation to ISI. The CS effect was strongest with an ISI of 3 ms and steadily declined for longer ISIs. A switch from enhancement of intracortical inhibition at short ISIs (2-5 ms, SICI) to intracortical facilitation (ICF) at longer ISIs (7-30 ms), as demonstrated for human motor cortex, was not evident. Whether the CS caused facilitation or suppression of the TS effect mainly depended on the strength of CS and the polarity of the TS effect: within a range of 60-130positive correlation between ppTMS and TS effect was evident, resulting in a stronger facilitation if the TS caused facilitation of visual activity, and more suppression if the TS was

suppressive by itself. The correlation inverted when CS was reduced to 15-30sum of the CS and TS effect, it was much smaller at weak CS strength (15-50but stronger than the sum of CS and TS effects at CS strength 60-100Differences in the physiological state between sensory and motor cortices and the interactions of paired synaptic inputs are discussed as possible reasons for the partly different effects of ppTMS in cat visual cortex and human motor cortex.

107, 109, 163, 340

[Morgan:2001aa] S. L. Morgan and T. J. Teyler. Electrical stimuli patterned after the theta-rhythm induce multiple forms of ltp. *J Neurophysiol*, 86(3):1289–96, 2001.

Abstract: The induction of long-term potentiation (LTP) by high-frequency stimulation is considered an acceptable model for the study of learning and memory. In area CA1 calcium influx through N-methyl-D-aspartate receptors (NMDARs; nmdaLTP) and/or L-type voltage-dependent calcium channels (vdccLTP) results in distinct forms of LTP. In the light of significant accumulation of knowledge about patterns of naturally occurring activity in the intact animal, we examined whether the application of stimuli patterned after natural activity induced nmdaLTP and/or vdccLTP. In rat hippocampal slices we examined LTP induced by three types of patterned stimulation short (S-TBS), long (L-TBS), and high-intensity long theta-patterned stimulation (HL-TBS). The patterns of stimulation were applied in control, nifedipine (blocks vdccLTP), D,L-2-amino-5-phosphonovaleric acid (APV; blocks nmdaLTP), or APV and nifedipine containing media. We found that S-TBS resulted in LTP that was completely attenuated in the presence of APV but was unaffected by nifedipine. Thus S-TBS results in the selective induction of nmdaLTP. L-TBS resulted in LTP that was completely blocked by APV and only partially blocked by nifedipine. Therefore L-TBS results in a compoundLTP consisting of both nmdaLTP and vdccLTP components. In the presence of APV, HL-TBS resulted in vdccLTP, and when APV and nifedipine were both present, LTP was completely blocked. Thus HL-TBS results in a vdccLTP in isolation when APV is present. We also examined saturation of S-TBS-induced LTP (nmdaLTP) by applying S-TBS at short intervals. When nifedipine was present, multiple S-TBS trains resulted in a substantially smaller final LTP as compared with controls. We conclude that multiple bursts of S-TBS eventually summate to result in compoundLTP. Stimuli patterned after innate rhythms in the hippocampus effectively induce nmdaLTP (S-TBS), compoundLTP (L-TBS), or vdccLTP (HL-TBS).

101

[Mori:2002aa] Toshio Mori and Shoichi Kai. Noise-induced entrainment and stochastic resonance in human brain waves. *Physical Review Letters*, 88(21), 2002.

Abstract: We present the first observation of stochastic resonance (SR) in the human brain's visual processing area. The novel experimental protocol is to stimulate the right eye with a subthreshold periodic optical signal and the left eye with a noisy one. The stimuli bypass sensory organs and are mixed in the visual cortex. With many noise sources present in the brain, higher brain functions, e.g., perception and cognition, may exploit SR.

137, 138, 343

[Moriwaki:1994aa] A. Moriwaki and et al. Repeated application of anodal direct current produces regional dominance in histamine-elicited cyclic amp accumulation in rabbit cerebral cortex. *Acta Med Okayama*, 48(6):323–6, 1994. 126

[Moriwaki:1995aa] A. Moriwaki and N. Islam. Induction of fos expression following anodal polarization in rat brain. *Psychiatry Clin Neurosci*, 49(6):323–6, 1995.

Abstract: Expression of c-fos immunoreactivity was investigated in rat brain after unilateral application of a weak anodal direct current (anodal polarization) to the sensorimotor cortex of rats. Increases in Fosimmunopositive neurons were observed

transiently in the neocortex, cingulate cortex, piriform cortex, and hippocampal formation, which were ipsilateral to the polarization, as a function of the duration and intensity of the currrent applied. It is likely that anodal polarization enhances the neuronal activities in the cortex dependent on polarization paradigms.

127

[Morrell:1961aa] F. Morrell. Effect of anodal polarization on the firing pattern of single cortical cells. *Ann N Y Acad Sci*, 92:860–876, 1961. 125

[Morrell:1962aa] Frank Morrell and Paul Naitoh. Effect of cortical polarization on a conditioned avoidance response. *Experimental Neurology*, 6(6):507–523, 1962.

Abstract: A conditioned forelimb flexion response was established in twelve rabbits using a flickering light as the conditional signal and an electric shock to the limb as the unconditional stimulus. Transcortical potential gradients (current density, 10 [mu]a per mm2) were imposed upon the visual receiving area, or upon the relevant portion of motor cortex bilaterally. Surface cathodal polarization of visual cortex produced a striking decrement in performance of the conditioned avoidance response in trials carried out during the period of current flow, and also on the subsequent day of training. No definite change in performance was seen during surface cathodal polarization of motor cortex, or during passage of surface anodal current through either motor or visual cortex. There was suggestive evidence of an improvement in performance on the day following application of surface anodal current to the visual cortex.

127

[Moss:2004aa] Frank Moss and et al. Stochastic resonance and sensory information processing: a tutorial and review of application. *Clinical Neurophysiology*, 115:267–281, 2004.

Abstract: Objective: To review the stochastic resonance phenomena observed in sensory systems and to describe how a random process ('noise') added to a subthreshold stimulus can enhance sensory information processing and perception. Results: Nonlinear systems need a threshold, subthreshold information bearing stimulus and 'noise' for stochastic resonance phenomena to occur. These three ingredients are ubiquitous in nature and man-made systems, which accounts for the observation of stochastic resonance in fields and conditions ranging from physics and engineering to biology and medicine. The stochastic resonance paradigm is compatible with single-neuron models or synaptic and channels properties and applies to neuronal assemblies activated by sensory inputs and perceptual processes as well. Here we review a few of the landmark experiments (including psychophysics, electrophysiology, fMRI, human vision, hearing and tactile functions, animal behavior, single/multiunit activity recordings). Models and experiments show a peculiar consistency with known neuronal and brain physiology. A number of naturally occurring 'noise' sources in the brain (e.g. synaptic transmission, channel gating, ion concentrations, membrane conductance) possibly accounting for stochastic resonance phenomena are also reviewed. Evidence is given suggesting a possible role of stochastic resonance in brain function, including detection of weak signals, synchronization and coherence among neuronal assemblies, phase resetting, 'carrier' signals, animal avoidance and feeding behaviors. Conclusions: Stochastic resonance is a ubiquitous and conspicuous phenomenon compatible with neural models and theories of brain function. The available evidence suggests cautious interpretation, but justifies research and should encourage neuroscientists and clinical neurophysiologists to explore stochastic resonance in biology and medical science.

133, 134, 135, 343

[Mountcastle:1997aa] V. B. Mountcastle. The columnar organization of the neocortex. *Brain*, 120 (Pt 4):701–22, 1997. 65

[Muller:2000aa] M. B. Muller, N. Toschi, A. E. Kresse, A. Post, and M. E. Keck. Long-term repetitive transcranial magnetic stimulation increases the expression of brain-derived neurotrophic factor and cholecystokinin mrna, but not neuropeptide tyrosine mrna in specific areas of rat brain. *Neuropsychopharmacology*, 23(2):205–15, 2000.

> **Abstract:** Repetitive transcranial magnetic stimulation (rTMS) is increasingly used as a therapeutic tool in various neurological and psychiatric disorders, and we recently found that it has a neuroprotective effect both in vitro and in vivo. However, the neurochemical mechanisms underlying the therapeutic effects are still unknown. We investigated the effects of long-term rTMS on the expression of brain-derived neurotrophic factor (BDNF), cholecystokinin (CCK), and neuropeptide tyrosine (NPY) mRNA in rat brain. In situ hybridization revealed a significant increase in BDNF mRNA in the hippocampal areas CA3 and CA3c, the granule cell layer, as well as in the parietal and the piriform cortex after rTMS. BDNF-like immunoreactivity was markedly increased in the same areas. A significant increase in CCK mRNA was observed in all brain regions examined. NPY mRNA expression, in contrast, was not altered. The present results suggest that BDNF may contribute to the neuroprotective effects of rTMS. Furthermore, the rTMS-induced changes in BDNF and CCK expression are similar to those reported after antidepressant drug treatment and electroconvulsive seizures, suggesting that a common molecular mechanism may underlie different antidepressant treatment strategies.

113, 114, 165

[Nadeem:2003aa] M. Nadeem, T. Thorlin, O. P. Gandhi, and M. Persson. Computation of electric and magnetic stimulation in human head using the 3-d impedance method. *IEEE Trans Biomed Eng*, 50(7):900–7, 2003.

> **Abstract:** A comparative, computational study of the modeling of transcranial magnetic stimulation (TMS) and electroconvulsive therapy (ECT) is presented using a human head model. The magnetic fields from a typical TMS coil of figure-eight type is modeled using the Biot-Savart law. The TMS coil is placed in a position used clinically for treatment of depression. Induced current densities and electric field distributions are calculated in the model using the impedance method. The calculations are made using driving currents and wave forms typical in the clinical setting. The obtained results are compared and contrasted with the corresponding ECT results. In the ECT case, a uniform current density is injected on one side of the head and extracted from the equal area on the opposite side of the head. The area of the injected currents corresponds to the electrode placement used in the clinic. The currents and electric fields, thus, produced within the model are computed using the same three-dimensional impedance method as used for the TMS case. The ECT calculations are made using currents and wave forms typical in the clinic. The electrical tissue properties are obtained from a 4-Cole-Cole model. The numerical results obtained are shown on a two-dimenaional cross section of the model. In this study, we find that the current densities and electric fields in the ECT case are stronger and deeper penetrating than the corresponding TMS quantities but both methods show biologically interesting current levels deep inside the brain.

60

[Nagarajan:1993aa] Srikantan S. Nagarajan and et al. Effects of induced electric fields on finite neuronal structures: a simulation study. *IEEE Transactions on Biomedical Engineering*, 40(11):1175–1188, 1993.

> **Abstract:** An analysis is presented of magnetic stimulation of finite length neuronal structures using computer simulations. Models of finite neuronal structures in the presence of extrinsically applied electric fields indicate that excitation can be characterized by two driving functions: one due to field gradients and the other due to fields at the boundaries of neuronal structures. It is found that boundary

field driving functions play an important role in governing excitation characteristics during magnetic stimulation. Simulations indicate that axons whose lengths are short compared to the spatial extent of the induced field are easier to excite than longer axons of the same diameter. Simulations also indicate that independent cellular dendritic processes are probably not excited during magnetic stimulation. Analysis of the temporal distribution of induced fields indicates that the temporal shape of the stimulus waveform modulates excitation thresholds and propagation of action potentials.

36, 41, 42, 60

[Nagarajan:1995aa] Srikantan S. Nagarajan. Analysis of magnetic stimulation of a concentric axon in a nerve bundle. *IEEE Transactions on Biomedical Engineering*, 42(9):926–933, 1995.

Abstract: The authors present an analysis of magnetic stimulation of an axon located at the center of a nerve bundle. A three-dimensional axisymmetric volume conductor model is used to determine the transmembrane potential response along an axon due to induced electric fields produced by a toroidal coil. The authors evaluate four such models of an axon located in: (1) an isotropic nerve bundle with no perineurium, (2) an anisotropic nerve bundle without a perineurium, (3) an isotropic nerve bundle surrounded by a perineurium, and (4) an anisotropic nerve bundle surrounded by a perineurium. The transmembrane polarization computed along an axon for the above four models is compared to that for an axon located in an infinite homogenous medium. These calculations indicate that a nerve bundle with no sheath has little effect on the transmembrane potential. However, the presence of a perineurium around the nerve bundle and anisotropy in the bundle significantly affects the shape of the transmembrane response. Therefore, during magnetic stimulation, nerve bundle anisotropy and the presence of perineurium must be taken into account for calculation of stimulus intensities for threshold excitation.

41

[Nagarajan:1996aa] Srikantan S. Nagarajan. A generalized cable equation for magnetic stimulation of axons. *IEEE Transactions on Biomedical Engineering*, 43(3):304–312, 1996 1996.

Abstract: During magnetic stimulation, electric fields are induced both on the inside (intracellular region) and the outside (extracellular region) of nerve fibers. The induced electric fields in each region can be expressed as the sum of a primary and a secondary component. The primary component arises due to an applied time varying magnetic field and is the time derivative of a vector potential. The secondary component of the induced field arises due to charge separation in the volume conductor surrounding the nerve fiber and is the gradient of a scalar potential. The question, "What components of intracellular fields and extracellular induced electric fields contribute to excitation?" has, so far, not been clearly addressed. Here, the authors address this question while deriving a generalized cable equation for magnetic stimulation and explicitly identify the different components of applied fields that contribute to excitation. In the course of this derivation, the authors review several assumptions of the core-conductor cable model in the context of magnetic stimulation. It is shown that out of the possible 4 components, only the first spatial derivative of the intracellular primary component and the extracellular secondary component of the fields contribute to excitation of a nerve fiber. An earlier form of the cable equation for magnetic stimulation has been shown to result in solutions identical to three-dimensional (3D) volume-conductor model for the specific configuration of an isolated axon in a located in an infinite homogenous conducting medium. The authors extend and generalize this result by demonstrating that their generalized cable equation results in solutions identical to 3D volume conductor models even for complex geometries of volume conductors surrounding axons such as a nerve bundle of different conductivity surrounding axons. This equivalence in the solutions is valid for several representations of a nerve bundle such as anisotropic monodomain and bidom- - ain models.

55

[Namgung:1995aa] U. Namgung, E. Valcourt, and A. Routtenberg. Long-term potentiation in vivo in the intact mouse hippocampus. *Brain Res*, 689(1):85–92, 1995.

> **Abstract:** We describe the characteristics of long-term potentiation (LTP) in the intact mouse. Perforant path stimulation evokes both a population excitatory postsynaptic potential (pop-EPSP) and a population spike potential (pop-spike) from the hippocampal dentate gyrus in urethane anesthetized animals. LTP, as measured by increased pop-spike amplitude and pop-EPSP slope, was successfully induced and reliably maintained at a stable level for at least 12 h, the longest time tested. The LTP-inducing stimulus (3 trains of 400 Hz, 8 0.4 ms pulses/train) used in two strains of mice was less by half than that used in rat. These parameters for inducing LTP were also successfully applied to obtain LTP in two different transgenic mouse strains: one bearing a F1/Gap-43 promoter-lacZ fusion gene and another which overexpresses the S100 beta gene. We also examined the effects of protein synthesis inhibitors, cycloheximide (CXM) and anisomycin (ANI). When CXM or ANI was given 30 min before LTP induction, there was no persistent loss of LTP at the 4 h time point. However, if CXM was given 4 h before LTP induction, significant decay of the potentiated responses occurred 90 min after induction. Half of the animals receiving CXM but not ANI showed a complete and sudden elimination of the entire response after the LTP-inducing stimulus. It was speculated that loss of a constitutively-expressed housekeeping protein, for example a calcium buffering protein, with an estimated half-life of 2 h would lead to an inability to buffer LTP-induced alterations, such as intracellular calcium elevation, increasing intracellular calcium to toxic levels.(ABSTRACT TRUNCATED AT 250 WORDS)

104

[Neher:1961aa] A. Neher. Auditory driving observed with scalp electrodes in normal subjects. *Journal of Electroencephalography and Clinical Neurophysiology*, 13:449–451, 1961. 136

[Nicholls:1992aa] JG Nicholls and et al. *From neuron to brain : a cellular and molecular approach to the function of the nervous system*. Sunderland, Mass.: Sinauer Associates, 1992. 34

[Nicholson:1965aa] P. W. Nicholson. Specific impedance of cerebral white matter. *Exp Neurol*, 13(4):386–401, 1965. 19

[Nicholson:1975aa] C. Nicholson and J. A. Freeman. Theory of current source-density analysis and determination of conductivity tensor for anuran cerebellum. *J Neurophysiol*, 38(2):356–68, 1975.

> **Abstract:** The theoretical basis of current source-density (CSD) analysis in the central nervous system is described. Equations relating CSD, the current flow vector, and the extracellular field potential are given. It is shown that the CSD provides superior resolution of neuronal events when compared to conventional field-potential analysis. Expressions for the CSD in rectangular Cartesian coordinates are derived, including the general case of anisotropic, inhomogeneous conductive tissue, and a coordinate system rotated with respect to the principal axes (APPENDIX). The minimum number of spatial dimensions for accurate CSD analysis is discussed. The conductivity tensor was experimentally measured in frog and toad cerebella. All three principal components of the tensor were evaluated and their spatial gradients determined to be negligible. It was also shown that the conductivity was independent of potential. Thus the anuran cerebellum is anisotropic, homogeneous, and ohmic. On the basis of these results the appropriate mathematical expression for the CSD was selected.

18

[Niehaus:2000aa] L. Niehaus, B. U. Meyer, and T. Weyh. Influence of pulse configuration and direction of coil current on excitatory effects of magnetic motor cortex and nerve stimulation. *Clin Neurophysiol*, 111(1):75–80, 2000.

Abstract: This paper describes the influence of pulse configuration and current direction on the excitation of the hand-associated motor cortex and the median nerve by magnetic stimulation. Monophasic and biphasic current pulses with the same peak rise time of 80 micros and a maximum rate of current change (dI/dt) were discharged through an eight-shaped coil of the stimulator used (Dantec Mag-Pro). Two current directions with opposite orientation in the coil axis were studied. FINDINGS: (1) for both, cortex and nerve stimulation, biphasic stimuli were more effective and elicited compound muscle action potentials (CMAPs) with lower thresholds and larger amplitudes. (2) Using biphasic pulses the direction of the currents in the first phase of the pulse did not influence the CMAP amplitude. (3) Using monophasic pulses induced currents oriented postero-anteriorly in the motor cortex or orthodromically along the nerve axis elicited larger CMAPs than currents in the opposite orientation. (4) Pulse configuration did not influence the CMAP-latencies and by this the stimulation site (cortex, nerve). CONCLUSION: Monophasic stimuli are useful to investigate excitation effects which are dependent on the current direction. The application of biphasic stimuli with their stronger excitation effects might be advantageous when patients with high cortical thresholds or deep lying nerves shall be investigated.

27

[Nielsen:2007aa] J. B. Nielsen, M. A. Perez, M. Oudega, M. Enriquez-Denton, and J. M. Aimonetti. Evaluation of transcranial magnetic stimulation for investigating transmission in descending motor tracts in the rat. *Eur J Neurosci*, 25(3):805–14, 2007.

Abstract: In the rat, non-invasive transcranial magnetic stimulation (TMS) has shown promise for evaluation of transmission through the spinal cord before and after repair strategies, but it is still unclear which pathways are activated by TMS. The aim of the present study was therefore to identify these pathways and to analyse the effect of TMS on spinal neurons. In 19 rats, TMS evoked responses bilaterally in forelimb (biceps brachii; BB) and hindlimb muscles (tibialis anterior). The latency and amplitude of these motor-evoked responses (MEPs) were highly variable and depended strongly on the coil position and the stimulation intensity. The most frequently observed latencies for the BB MEPs could be divided into three groups: 3-6 ms, 8-12 ms and 14-18 ms. Lesions in the dorsal columns, which destroyed the corticospinal tract at C2 and C5, significantly depressed MEPs in the mid- and high-latency ranges, but not those in the low-latency range. Lesions in the dorsolateral funiculus, which interrupted the rubrospinal tract, had no effect on MEPs in any of the latency ranges. By contrast, bilateral lesion of the reticulospinal tract and other ventro-laterally located descending pathways abolished all responses. Intracellular recordings from 54 cervical motoneurons in five rats revealed that TMS evoked excitatory postsynaptic potentials (EPSPs) at latencies that corresponded well with those of the BB MEPs. The short-latency EPSPs had rise times of around 1 ms, suggesting that they were mediated by a monosynaptic pathway. EPSPs with longer latencies had considerably longer rise times, which indicated conduction through polysynaptic pathways. Selective electrical stimulation of the pyramidal tract in the brainstem was performed in seven rats, where intracellular recordings from 70 motoneurons revealed that the earliest EPSPs and MEPs evoked by TMS were not mediated by the corticospinal tract, but by other descending motor pathways. Together, these results showed that in the rat TMS activates several descending pathways that converge on common spinal interneurons and motoneurons. Our observations confirm that the corticospinal tract has weak (and indirect) projections to cervical spinal motoneurons.

173

[Nilsson:1992aa] J. Nilsson, M. Panizza, B. J. Roth, P. J. Basser, L. G. Cohen, G. Caruso, and M. Hallett. Determining the site of stimulation during magnetic stimulation of a peripheral nerve. *Electroencephalogr Clin Neurophysiol*, 85(4):253–64, 1992.

Abstract: Magnetic stimulation has not been routinely used for studies of peripheral nerve conduction primarily because of uncertainty about the location of the stimulation site. We performed several experiments to locate the site of nerve stimulation. Uniform latency shifts, similar to those that can be obtained during electrical stimulation, were observed when a magnetic coil was moved along the median nerve in the region of the elbow, thereby ensuring that the properties of the nerve and surrounding volume conductor were uniform. By evoking muscle responses both electrically and magnetically and matching their latencies, amplitudes and shapes, the site of stimulation was determined to be 3.0 +/- 0.5 cm from the center of an 8-shaped coil toward the coil handle. When the polarity of the current was reversed by rotating the coil, the latency of the evoked response shifted by 0.65 +/- 0.05 msec, which implies that the site of stimulation was displaced 4.1 +/- 0.5 cm. Additional evidence of cathode- and anode- like behavior during magnetic stimulation comes from observations of preferential activation of motor responses over H-reflexes with stimulation of a distal site, and of preferential activation of H- reflexes over motor responses with stimulation of a proximal site. Analogous behavior is observed with electrical stimulation. These experiments were motivated by, and are qualitatively consistent with, a mathematical model of magnetic stimulation of an axon.

35

[Nitsche:2000aa] M. A. Nitsche and W. Paulus. Excitability changes induced in the human motor cortex by weak transcranial direct current stimulation. *J Physiol*, 527 Pt 3:633–9, 2000.

Abstract: In this paper we demonstrate in the intact human the possibility of a non-invasive modulation of motor cortex excitability by the application of weak direct current through the scalp. Excitability changes of up to 40 stimulation, were accomplished and lasted for several minutes after the end of current stimulation. Excitation could be achieved selectively by anodal stimulation, and inhibition by cathodal stimulation. By varying the current intensity and duration, the strength and duration of the after-effects could be controlled. The effects were probably induced by modification of membrane polarisation. Functional alterations related to post-tetanic potentiation, short-term potentiation and processes similar to postexcitatory central inhibition are the likely candidates for the excitability changes after the end of stimulation. Transcranial electrical stimulation using weak current may thus be a promising tool to modulate cerebral excitability in a non-invasive, painless, reversible, selective and focal way.

20, 21, 22

[Nitsche:2001aa] M. A. Nitsche and W. Paulus. Sustained excitability elevations induced by transcranial dc motor cortex stimulation in humans. *Neurology*, 57(10):1899–901, 2001.

Abstract: The authors show that in the human transcranial direct current stimulation is able to induce sustained cortical excitability elevations. As revealed by transcranial magnetic stimulation, motor cortical excitability increased approximately 150up to 90 minutes after the end of stimulation. The feasibility of inducing long-lasting excitability modulations in a noninvasive, painless, and reversible way makes this technique a potentially valuable tool in neuroplasticity modulation.

20

[Nitsche:2003aa] M. A. Nitsche, D. Liebetanz, A. Antal, N. Lang, F. Tergau, and W. Paulus. Modulation of cortical excitability by weak direct current stimulation–technical, safety and functional aspects. *Suppl Clin Neurophysiol*, 56:255–76, 2003. 125

[Nitsche:2003ab] M. A. Nitsche, D. Liebetanz, N. Lang, A. Antal, F. Tergau, and W. Paulus. Safety criteria for transcranial direct current stimulation (tdcs) in humans. *Clin Neurophysiol*, 114(11):2220–2; author reply 2222–3, 2003. 32

[Nitsche:2007aa] M. A. Nitsche and et al. Shaping the effects of transcranial direct current stimulation of the human motor cortex. *J. Neurophysiol*, 97:3109–3117, January 2007.

Abstract: Transcranial DC stimulation (tDCS) induces stimulation polarity-dependent neuroplastic excitability shifts in the human brain. Because it accomplishes long-lasting effects and its application is simple, it is used increasingly. However, one drawback is its low focality, caused by 1) the large stimulation electrode and 2) the functionally effective reference electrode, which is also situated on the scalp. We aimed to increase the focality of tDCS, which might improve the interpretation of the functional effects of stimulation because it will restrict its effects to more clearly defined cortical areas. Moreover, it will avoid unwanted reversed effects of tDCS under the reference electrode, which is of special importance in clinical settings, when a homogeneous shift of cortical excitability is needed. Because current density (current strength/electrode size) determines the efficacy of tDCS, increased focality should be accomplished by 1) reducing stimulation electrode size, but keeping current density con- stant; or 2) increasing reference electrode size under constant current strength. We tested these hypotheses for motor cortex tDCS. The results show that reducing the size of the motor cortex DC-stimulation electrode focalized the respective tDCS-induced excitability changes. Increasing the size of the frontopolar reference electrode rendered stimulation over this cortex functionally inefficient, but did not com- promise the tDCS-generated motor cortical excitability shifts. Thus tDCS-generated modulations of cortical excitability can be focused by reducing the size of the stimulation electrode and by increasing the size of the reference electrode. For future applications of tDCS, such paradigms may help to achieve more selective tDCS effects.

21

[Nitsche:2008aa] Michael A. Nitsche and et al. Transcranial direct current stimulation: State of the art 2008. *Brain Stimulation*, 1:206–223, 2008.

Abstract: Effects of weak electrical currents on brain and neuronal function were first described decades ago. Recently, DC polarization of the brain was reintroduced as a noninvasive technique to alter cortical activity in humans. Beyond this, transcranial direct current stimulation (tDCS) of different cortical areas has been shown, in various studies, to result in modifications of perceptual, cognitive, and behavioral functions. Moreover, preliminary data suggest that it can induce beneficial effects in brain disorders. Brain stimulation with weak direct currents is a promising tool in human neuroscience and neurobehavioral research. To facilitate and standardize future tDCS studies, we offer this overview of the state of the art for tDCS.

20, 21, 22, 23, 33, 45

[OKeefe:2006aa] O'Keefe. *The hippocampus book*. Oxford University Press, 2006. 83

[OReardon:2007aa] J. P. O'Reardon, H. B. Solvason, P. G. Janicak, S. Sampson, K. E. Isenberg, Z. Nahas, W. M. McDonald, D. Avery, P. B. Fitzgerald, C. Loo, M. A. Demitrack, M. S. George, and H. A. Sackeim. Efficacy and safety of transcranial magnetic stimulation in the acute treatment of major depression: a multisite randomized controlled trial. *Biol Psychiatry*, 62(11):1208–16, 2007.

Abstract: BACKGROUND: We tested whether transcranial magnetic stimulation (TMS) over the left dorsolateral prefrontal cortex (DLPFC) is effective and safe in the acute treatment of major depression. METHODS: In a double-blind, multisite study, 301 medication-free patients with major depression who had not benefited from prior treatment were randomized to active (n = 155) or sham TMS (n = 146) conditions. Sessions were conducted five times per week with TMS at 10 pulses/sec, 120of motor threshold, 3000 pulses/session, for 4-6 weeks. Primary outcome was the symptom score change as assessed at week 4 with the Montgomery-Asberg Depression Rating Scale (MADRS). Secondary outcomes included changes on the 17- and 24-item Hamilton Depression Rating Scale (HAMD) and response and remission rates with the MADRS and HAMD. RESULTS: Active TMS was significantly superior to sham TMS on the MADRS at week 4 (with a post hoc

correction for inequality in symptom severity between groups at baseline), as well as on the HAMD17 and HAMD24 scales at weeks 4 and 6. Response rates were significantly higher with active TMS on all three scales at weeks 4 and 6. Remission rates were approximately twofold higher with active TMS at week 6 and significant on the MADRS and HAMD24 scales (but not the HAMD17 scale). Active TMS was well tolerated with a low dropout rate for adverse events (4.5pain. CONCLUSIONS: Transcranial magnetic stimulation was effective in treating major depression with minimal side effects reported. It offers clinicians a novel alternative for the treatment of this disorder.

27

[Ogiue-Ikeda:2003aa] M. Ogiue-Ikeda, S. Kawato, and S. Ueno. The effect of repetitive transcranial magnetic stimulation on long-term potentiation in rat hippocampus depends on stimulus intensity. *Brain Res*, 993(1-2):222–6, 2003.

Abstract: We investigated the effect of repetitive transcranial magnetic stimulation (rTMS) on long-term potentiation (LTP) in the rat hippocampus. Rats were magnetically stimulated at a rate of 1000 pulses/day for 7 days by a round coil, in which the peak magnetic fields at the center of the coil were 0.75 and 1.00 T. LTP enhancement was observed only in the 0.75-T rTMS group, while no change was observed in the 1.00-T rTMS group. These results suggest that the effect of rTMS on LTP depends on the stimulus intensity.

114

[Ogiue-Ikeda:2003ab] M. Ogiue-Ikeda, S. Kawato, and S. Ueno. The effect of transcranial magnetic stimulation on long-term potentiation in rat hippocampus. *Magnetics, IEEE Transactions on*, 39(5):3390–3392, 2003.

Abstract: We investigated the effect of transcranial magnetic stimulation (TMS) on the brain by focusing on long-term potentiation (LTP) in the rat hippocampus. Male Wistar rats were magnetically stimulated by a round coil positioned over the rat's head. The stimulator delivered biphasic cosine current pulses 238 us in duration. The peak magnetic fields were set to 0.50 T (<motor threshold) and 1.25 T (>motor threshold) at the center of the coil. Rats received 10 1 s trains of 25 pulses/s with a 1 s intertrain interval 4 times per day for 7 days. There was no significant difference between the LTP of the 0.50 T stimulated and sham control groups. The LTP of the 1.25 T stimulated group, however, was inhibited compared with the LTP of the sham control group, suggesting that the synaptic plasticity in the hippocampus was impaired by strong TMS. It is necessary to control the intensity of TMS for maximizing treatment efficacy and safety.

114, 178

[Ogiue-Ikeda:2005aa] M. Ogiue-Ikeda, S. Kawato, and S. Ueno. Acquisition of ischemic tolerance by repetitive transcranial magnetic stimulation in the rat hippocampus. *Brain Res*, 1037(1-2):7–11, 2005.

Abstract: We investigated the acquisition of ischemic tolerance in the rat hippocampus using repetitive transcranial magnetic stimulation (rTMS). Rats received 1000 pulses/day for 7 days, and the field excitatory postsynaptic potentials were measured in the hippocampal CA1. After slices were exposed to ischemic conditions, long-term potentiation (LTP) was induced. The LTP of the stimulated group was enhanced compared with the LTP of the sham control group in each ischemic condition, suggesting that rTMS has the potential to protect hippocampal function from ischemia.

113, 114, 166, 168

[Okada:1994aa] Y. C. Okada, J. C. Huang, M. E. Rice, D. Tranchina, and C. Nicholson. Origin of the apparent tissue conductivity in the molecular and granular layers of the in vitro turtle cerebellum and the interpretation of current source-density analysis. *J Neurophysiol*, 72(2):742–53, 1994.

Abstract: 1. We determined the origin of the apparent tissue conductivity (sigma 2) of the turtle cerebellum in vitro. 2. Application of a current with a known current density (J) along the longitudinal axis of a conductivity cell produced an electric field in the cerebellum suspended in the cell. The measured electric field (E) perpendicular to the cerebellar surface indicated a significant inhomogeneity in sigma a (= J/E) with a major discontinuity between the molecular layer (0.25 +/- 0.05 S/m, mean +/- SD) and granular layers (0.15 +/- 0.03 S/m) (n = 39). 3. This inhomogeneity was more pronounced after anoxic depolarization. The value of sigma a decreased to 0.11 +/- 0.03 and 0.040 +/- 0.008 S/m in the molecular and granular layers, respectively. The ratio of sigma a S in the two layers increased from 1.67 in the normoxic condition to 2.75 after anoxic depolarization. 4. This difference in sigma a across the two layers was present within the range of frequencies (DC to 10 kHz) studied where the phase of sigma a was small (less than +/- 2 degrees) and therefore sigma a was ohmic. 5. The inhomogeneity in sigma a was in part due to an inhomogeneity in the extracellular conductivity (sigma e) as determined from the extracellular diffusion of ionophoresed tetramethylammonium. Like sigma a, the value of sigma e was also higher in the molecular layer (0.165 S/m) than in the granular layer (0.097 S/m). The inhomogeneity in sigma e was due to a smaller tortuosity and a larger extracellular volume fraction in the molecular layer compared with the granular layer. 6. sigma a was, however, consistently higher, by approximately 50model of the cerebellum indicated that these discrepancies between sigma a and sigma e were attributable to additional conductivity produced by a passage of the longitudinal applied current through the intracellular space of Purkinje cells and ependymal glial cells, with the glial compartment playing the dominant role. Cells with a long process and a short space constant such as the ependymal glia evidently enhance the effective "extracellular" conductivity by serving as intracellular conduits for the applied current. The result implies that the effective sigma e may be larger than sigma e for neuronally generated currents in the turtle cerebellum because the space constant for Purkinje cells is several times greater than that for the ependymal glia and consequently Purkinje cell-generated currents travel over a long distance relative to the space constant of glial cells.(ABSTRACT TRUNCATED AT 400 WORDS)

18

[Okada:2002aa] K. Okada, K. Matsunaga, T. Yuhi, E. Kuroda, U. Yamashita, and S. Tsuji. The long-term high-frequency repetitive transcranial magnetic stimulation does not induce mrna expression of inflammatory mediators in the rat central nervous system. *Brain Res*, 957(1):37–41, 2002.

Abstract: Repetitive transcranial magnetic stimulation (rTMS) has been applied for treatment of several diseases such as depression. However, the safety and biological effects of rTMS have not been fully elucidated. In this study, the effects of rTMS on the levels of inflammatory mediators in the central nervous system (CNS), which may be involved in neurodegenerative disorders, were investigated in comparison with the electric convulsive model. Long-term rTMS (1500 pulses at 30 Hz/day for series of 7 days) stimulation, which did not elicit convulsion, was given to rats (rTMS rats). Single high-frequency electrical stimulation (100 Hz, 0.5-ms pulse width, 1 s duration, 50 mA), which induced convulsion, was given to rats (ES rats). mRNA levels of interleukin (IL)-1beta, IL-6, cyclooxygenase (COX)-2 and inducible nitric oxide synthetase (iNOS) in the brain were evaluated by reverse transcription-polymerase chain reaction before and after these stimulations. mRNA of IL-1beta, IL-6 and COX-2 was induced in the brains of ES rats but not in the brains of long-term rTMS rats. mRNA of iNOS was not induced in the brain of long-term rTMS rats. These results suggest that long-term rTMS may safe and modulate neural function without up-regulation of inflammatory mediators, which may be involved in neurodegenerative disorders.

124, 125, 169

[Okhotin:2002aa] V. E. Okhotin and S. G. Kalinichenko. The histophysiology of neocortical basket cells. *Neurosci Behav Physiol*, 32(5):455–70, 2002. 60

[Okuno:1996aa] H. Okuno and Y. Miyashita. Expression of the transcription factor zif268 in the temporal cortex of monkeys during visual paired associate learning. *Eur J Neurosci*, 8(10):2118–28, 1996. 114

[Oostendorp:2000aa] T. F. Oostendorp, J. Delbeke, and D. F. Stegeman. The conductivity of the human skull: results of in vivo and in vitro measurements. *IEEE Trans Biomed Eng*, 47(11):1487–92, 2000.

Abstract: The conductivity of the human skull was measured both in vitro and in vivo. The in vitro measurement was performed on a sample of fresh skull placed within a saline environment. For the in vivo measurement a small current was passed through the head by means of two electrodes placed on the scalp. The potential distribution thus generated on the scalp was measured in two subjects for two locations of the current injecting electrodes. Both methods revealed a skull conductivity of about 0.015 [symbol: see text]/m. For the conductivities of the brain, the skull and the scalp a ratio of 1:1/15:1 was found. This is consistent with some of the reports on conductivities found in the literature, but differs considerably from the ratio 1:1/80:1 commonly used in neural source localization. An explanation is provided for this discrepancy, indicating that the correct ratio is 1:1/15:1.

18

[Otmakhov:2004aa] N. Otmakhov, L. Khibnik, N. Otmakhova, S. Carpenter, S. Riahi, B. Asrican, and J. Lisman. Forskolin-induced ltp in the ca1 hippocampal region is nmda receptor dependent. *J Neurophysiol*, 91(5):1955–62, 2004.

Abstract: Chemically induced long-term potentiation (cLTP) could potentially work by directly stimulating the biochemical machinery that underlies synaptic plasticity, bypassing the need for synaptic activation. Previous reports suggested that agents that raise cAMP concentration might have this capability. We examined the cLTP induced in acute slices by application of Sp-cAMPS or a combination of the adenylyl cyclase activator, forskolin, and the phosphodiesterase inhibitor, rolipram. Under our conditions, cLTP was induced but only if inhibition was reduced. We found that this form of cLTP was blocked by a N-methyl-d-aspartate receptor (NMDAR) antagonist and required the low-frequency test stimulation typically used to monitor the strength of synapses. Interestingly, similar LTP could be induced by lowering the Mg(2+) concentration of the ACSF during forskolin/rolipram or Sp-cAMPS application or even by just lowering Mg(2+) concentration alone. This LTP was also NMDAR dependent and required only a few (approximately 5) low-frequency stimuli for its induction. The finding that even low-frequency synaptic stimulation was sufficient for LTP induction indicates that a highly sensitized plasticity state was generated. The fact that some stimulation was required means that potentiation is probably restricted to the stimulated axons, limiting the usefulness of this form of cLTP. However, when similar experiments were conducted using slice cultures, potentiation occurred without test stimuli, probably because the CA3-CA1 connections are extensive and because presynaptic spontaneous activity is sufficient to fulfill the activity requirement. As in acute slices, the potentiation was blocked by an NMDAR antagonist. Our general conclusion is that the induction of LTP caused by elevating cAMP requires presynaptic activity and NMDA channel opening. The method of inducing cLTP in slice cultures will be useful when it is desirable to produce NMDAR-dependent LTP in a large fraction of synapses.

101

[Otto:1991aa] T. Otto, H. Eichenbaum, S. I. Wiener, and C. G. Wible. Learning-related patterns of ca1 spike trains parallel stimulation parameters optimal for inducing hippocampal long-term potentiation. *Hippocampus*, 1(2):181–92, 1991.

Abstract: Recent studies have revealed 3 stimulation parameters that together comprise the temporal pattern of neuronal activation optimal for the induction of hippocampal LTP: high-frequency bursts, activity 100-200 ms prior to a burst,

and burst delivery in phase with the ongoing hippocampal theta rhythm. The present paper reports that these 3 aspects of patterned neural activity, collectively referred to as "theta-bursting," are characteristic of the spike trains of CA1 pyramidal cells in rats during the sampling and analysis of learning cues in an odor discrimination task and during performances of a spatial memory task. In contrast, theta-bursting occurs relatively infrequently during behavioral events less directly related to task-relevant mnemonic processing. These findings suggest that the optimal conditions for the induction of LTP occur naturally in behaving animals, time-locked to behavioral events critical to learning.

100

[Pajevic:2002aa] S. Pajevic, A. Aldroubi, and P. J. Basser. A continuous tensor field approximation of discrete dt-mri data for extracting microstructural and architectural features of tissue. *J Magn Reson*, 154(1):85–100, 2002.

> **Abstract:** The effective diffusion tensor of water, D, measured by diffusion tensor MRI (DT-MRI), is inherently a discrete, noisy, voxel-averaged sample of an underlying macroscopic effective diffusion tensor field, D(x). Within fibrous tissues this field is presumed to be continuous and smooth at a gross anatomical length scale. Here a new, general mathematical framework is proposed that uses measured DT-MRI data to produce a continuous approximation to D(x). One essential finding is that the continuous tensor field representation can be constructed by repeatedly performing one-dimensional B-spline transforms of the DT-MRI data. The fidelity and noise-immunity of this approximation are tested using a set of synthetically generated tensor fields to which background noise is added via Monte Carlo methods. Generally, these tensor field templates are reproduced faithfully except at boundaries where diffusion properties change discontinuously or where the tensor field is not microscopically homogeneous. Away from such regions, the tensor field approximation does not introduce bias in useful DT-MRI parameters, such as Trace(D(x)). It also facilitates the calculation of several new parameters, particularly differential quantities obtained from the tensor of spatial gradients of D(x). As an example, we show that they can identify tissue boundaries across which diffusion properties change rapidly using in vivo human brain data. One important application of this methodology is to improve the reliability and robustness of DT-MRI fiber tractography.

31

[Pascual-Leone:1990aa] A. Pascual-Leone, A. Dhuna, B. J. Roth, L. Cohen, and M. Hallett. Risk of burns during rapid-rate magnetic stimulation in presence of electrodes. *Lancet*, 336(8724):1195–6, 1990. 120

[Pascual-Leone:1993aa] A. Pascual-Leone, C. M. Houser, K. Reese, L. I. Shotland, J. Grafman, S. Sato, J. Valls-Sole, J. P. Brasil-Neto, E. M. Wassermann, L. G. Cohen, and et al. Safety of rapid-rate transcranial magnetic stimulation in normal volunteers. *Electroencephalogr Clin Neurophysiol*, 89(2):120–30, 1993.

> **Abstract:** In 9 normal volunteers, we studied the safety of rapid-rate transcranial magnetic stimulation (rTMS) applied to different scalp positions at various frequencies and intensities. Pure tone threshold audiometry showed temporary threshold shifts in 3 subjects. In the subject stimulated at the highest intensity, rTMS induced a focal, secondarily generalized seizure despite the absence of definite risk factors for seizures. Rapid-rate TMS did not result in any important changes in the neurological examination findings, cognitive performance, electroencephalogram, electrocardiogram, and hormone levels (prolactin, adrenocorticotropic hormone, thyroid-stimulating hormone, luteinizing hormone, and follicle-stimulating hormone). In 10 additional subjects, the electromyographic activity in several contralateral muscles showed that trains of rTMS applied to the motor cortex induced a spread of cortical excitability. The spread of excitability depended on the intensity and frequency of the stimuli and probably constituted an early

epileptogenic effect of rTMS. Guidelines for preventing the undesirable side effects of rTMS are offered.

118

[Pascual-Leone:1994aa] A. Pascual-Leone, L. G. Cohen, J. P. Brasil-Neto, and M. Hallett. Non-invasive differentiation of motor cortical representation of hand muscles by mapping of optimal current directions. *Electroencephalogr Clin Neurophysiol*, 93(1):42–8, 1994.

Abstract: Non-invasive mapping of human motor cortex by stimulating different scalp positions with a magnetic coil held at a constant orientation allows differentiation of proximal and distal arm muscles. This study describes a technique for more precise mapping of closely represented muscles using different orientations of a coil that delivers nearly monopolar current pulses. EMG was recorded from abductor pollicis brevis (APB), first dorsal interosseous (FDI), abductor digiti minimi (ADM), and flexor carpi radialis (FCR) of 9 normal volunteers. Stimuli were delivered from a Dantec stimulator through an 8-shaped coil. The center of the coil was kept flat on the scalp on a given position, and the coil rotated at different angles. The amplitudes of the motor evoked potentials were used for calculation of optimal current directions in the brain for activation of each muscle in each position. The optimal current direction for FCR activation pointed antero-medially. ADM, FDI and APB mapped progressively more antero-laterally. The relationship between current directions was constant across subjects and did not change in different scalp positions. This technique improves the spatial resolution of non-invasive cortical mapping and may express the differences in orientations of interneuronal nets in the precentral gyrus.

27

[Pascual-Leone:1994ab] A. Pascual-Leone, L. G. Cohen, J. P. Brasil-Neto, J. Valls-Sole, and M. Hallett. Differentiation of sensorimotor neuronal structures responsible for induction of motor evoked potentials, attenuation in detection of somatosensory stimuli, and induction of sensation of movement by mapping of optimal current directions. *Electroencephalogr Clin Neurophysiol*, 93(3):230–6., 1994.

Abstract: Transcranial magnetic stimulation (TMS) of the sensorimotor cortex can evoke motor evoked potentials (MEPs), attenuation in detection of somatosensory stimuli (ADSS), and sensation of movement (SOM) referred to the same body part. In this study we tried to differentiate the substrates responsible for these effects. In 6 normal volunteers, TMS was applied with a nearly monopolar Dantec stimulator and a butterfly coil. Optimal scalp location and current direction were determined for induction of MEPs in abductor pollicis brevis (APB), first dorsal interosseous (FDI), and adductor digiti minimi (ADM); SOM in digits 2 and 5 in an ischemically paralyzed hand; and ADSS applied to digits 2 and 5. All 3 muscles' MEPs and SOM and ADSS in both digits were optimally activated from a single scalp position. In all subjects, optimal current directions for MEPs pointed anteriorly; those for ADSS and SOM pointed posteriorly. Optimal current directions showed the same progression in all subjects for MEPs (ADM, FDI, and APB from antero- lateral to antero-medial), ADSS (digit 5 postero-medial, 2 postero- lateral), and SOM (digit 1 through 5 postero-lateral to postero- medial). We conclude that neuronal networks targeting corticospinal neurons responsible for MEPs are different from those leading to SOM and ADSS (which could not be differentiated).

27

[Pascual-Leone:1999ab] Alvaro Pascual-Leone. Transcranial magnetic stimulation: studying the brain-behaviour relationship by induction of 'virtual lesions'. *Phil. Trans. R. Soc. Lond. B*, 354:1229–1238, 1999.

Abstract: Transcranial magnetic stimulation (TMS) provides a non-invasive method of induction of a focal current in the brain and transient modulation

of the function of the targeted cortex. Despite limited understanding about focality and mechanisms of action, TMS provides a unique opportunity of studying brain-behaviour relations in normal humans. TMS can enhance the results of other neuroimaging techniques by establishing the causal link between brain activity and task performance, and by exploring functional brain connectivity.

24

[Pascual-Leone:2002aa] Alvaro Pascual-Leone. *Handbook of transcranial magnetic stimulation*. A Hodder Arnold Publication, 2002. 23

[Pastor:2003aa] Maria A. Pastor and et al. Human cerebral activation during steady-state visual-evoked responses. *The Journal of Neuroscience*, 23(37):11621–11627, 2003.

Abstract: Flicker stimuli of variable frequency (2–90 Hz) elicit a steady-state visual-evoked response (SSVER) in the electroencephalogram (EEG) with the same frequency as the stimulus. In humans, the amplitude of this response peaks at ∼15 Hz, decreasing at higher stimulation frequencies. It was not known whether this peak response corresponds to increased synaptic activity in the visual cortex or to other mechanisms [for instance, the temporal coherence (phase summation) of evoked responses]. We studied the SSVER in 16 normal volunteers by means of visual stimulation at 14 different frequencies (from 5 to 60 Hz) while recording the EEG. In nine subjects of the group, we measured regional cerebral blood flow (rCBF) with positron emission tomography (PET)-H2 15O at rest and during visual stimulation at five different frequencies: 5, 10, 15, 25, and 40 Hz. We confirmed that the amplitude of the SSVER in occipital regions peaks at 15 Hz stimulation. Applying to the PET rCBF data a contrast weighted by the amplitude of the SSVER, we determined that the primary visual cortex rCBF follows an activation pattern similar to the SSVER. This finding suggests that the amplitude of the SSVER corresponds to increased synaptic activity, specifically in Brodmann's area 17. Additionally, this study showed that visual stimulation at 40 Hz causes selective activation of the macular region of the visual cortex, and that a region in the dorsal aspect of the Crus I lobule of the left cerebellar hemisphere is activated during repetitive visual stimulation.

136

[Pinsky:1994aa] P. F. Pinsky and J. Rinzel. Intrinsic and network rhythmogenesis in a reduced traub model for ca3 neurons. *J Comput Neurosci*, 1(1-2):39–60, 1994.

Abstract: We have developed a two-compartment, eight-variable model of a CA3 pyramidal cell as a reduction of a complex 19-compartment cable model [Traub et al, 1991]. Our reduced model segregates the fast currents for sodium spiking into a proximal, soma-like, compartment and the slower calcium and calcium-mediated currents into a dendrite-like compartment. In each model periodic bursting gives way to repetitive soma spiking as somatic injected current increases. Steady dendritic stimulation can produce periodic bursting of significantly higher frequency (8-20 Hz) than can steady somatic input (¡ 8 Hz). Bursting in our model occurs only for an intermediate range of electronic coupling conductance. It depends on the segregation of channel types and on the coupling current that flows back-and-forth between compartments. When the soma and dendrite are tightly coupled electrically, our model reduces to a single compartment and does not burst. Network simulations with our model using excitatory AMPA and NMDA synapses (without inhibition) give results similar to those obtained with the complex cable model [Traub et al, 1991; Traub et al, 1992]. Brief stimulation of a single cell in a resting network produces multiple synchronized population bursts, with fast AMPA synapses providing the dominant synchronizing mechanism. The number of bursts increases with the level of maximal NMDA conductance. For high enough maximal NMDA conductance synchronized bursting repeats indefinitely. We find that two factors can cause the cells to desynchronize when AMPA synapses are blocked: heterogeneity of properties amongst cells and intrinsically chaotic burst dynamics.

But even when cells are identical, they may synchronize only approximately rather than exactly. Since our model has a limited number of parameters and variables, we have studied its cellular and network dynamics computationally with relative ease and over wide parameter ranges. Thereby, we identify some qualitative features that parallel or are distinguished from those of other neuronal systems; e.g., we discuss how bursting here differs from that in some classical models.

39

[Pittenger:2002aa] C. Pittenger, Y. Y. Huang, R. F. Paletzki, R. Bourtchouladze, H. Scanlin, S. Vronskaya, and E. R. Kandel. Reversible inhibition of creb/atf transcription factors in region ca1 of the dorsal hippocampus disrupts hippocampus-dependent spatial memory. *Neuron*, 34(3):447–62, 2002.

Abstract: CREB is critical for long-lasting synaptic and behavioral plasticity in invertebrates. Its role in the mammalian hippocampus is less clear. We have interfered with CREB family transcription factors in region CA1 of the dorsal hippocampus. This impairs learning in the Morris water maze, which specifically requires the dorsal hippocampus, but not context conditioning, which does not. The deficit is specific to long-term memory, as shown in an object recognition task. Several forms of late-phase LTP are normal, but forskolin-induced and dopamine-regulated potentiation are disrupted. These experiments represent the first targeting of the dorsal hippocampus in genetically modified mice and confirm a role for CREB in hippocampus-dependent learning. Nevertheless, they suggest that some experimental forms of plasticity bypass the requirement for CREB.

101

[Plonsey:1967aa] R. Plonsey and D. B. Heppner. Considerations of quasi-stationarity in electrophysiological systems. *Bull Math Biophys*, 29(4):657–64, 1967. 16

[Plonsey:1969aa] R. Plonsey. *Bioelectric phenomena*. McGraw-Hill, 1969. 15, 185, 186, 345

[Plonsey:1988aa] R. Plonsey and K. W. Altman. Electrical-stimulation of excitable cells - a model approach. *Proceedings of the IEEE*, 76(9):1122–1129, 1988. 35

[Plonsey:1995aa] R. Plonsey and R. C. Barr. Electric field stimulation of excitable tissue. *IEEE Trans Biomed Eng*, 42(4):329–36, 1995.

Abstract: This paper examines the transmembrane voltage response of an un-myelinated fiber to a stimulating electric field from a point current source. For subthreshold conditions, analytic expressions for the transmembrane potential, vm, are developed that include the specific effects of fiber-source distance, h, and time from the onset of the stimulus, T. Suprathreshold effects are determined for two examples by extending the analytical results with a numerical model. The vm response is a complex evolution in time, especially for small h, that differs markedly from the ”activating function.” In general, the subthreshold response is a good predictor of the wave shape of the suprathreshold vm, but a poor predictor of its magnitude. The subthreshold response also is a good (but not a precise) predictor of the region where excitation begins.

34

[Plonsey:2007aa] Robert Plonsey and Roger C. Barr. *Bioelectricity*. Springer, 2007. 40

[Polk:1996aa] C Polk and E Postow. *CRC handbook of biological effects of electromagnetic fields, 2nd Ed.* CRC Press, 1996. 16

[Poreisz:2007aa] Csaba Poreisz and et al. Safety aspects of transcranial direct current stimulation concerning healthy subjects and patients. *Brain Research Bulletin*, 72:2008–214, 2007.

Abstract: Cortical excitability changes induced by tDCS and revealed by TMS, are increasingly being used as an index of neuronal plasticity in the human cortex. The aim of this paper is to summarize the partially adverse effects of 567 tDCS sessions over motor and non-motor cortical areas (occipital, temporal, parietal) from the last 2 years, on work performed in our laboratories. One-hundred

and two of our subjects who participated in our tDCS studies completed a questionnaire. The questionnaire contained rating scales regarding the presence and severity of headache, difficulties in concentrating, acute mood changes, visual perceptual changes and any discomforting sensation like pain, tingling, itching or burning under the electrodes, during and after tDCS. Participants were healthy subjects (75.5%), migraine patients (8.8%), post-stroke patients (5.9sensation was the most common reported adverse effect (70.6fatigue was felt by 35.3% of the subjects, whereas a light itching sensation under the stimulation electrodes occurred in 30.4% of cases. After tDCS headache (11.8%), nausea (2.9%) and insomnia (0.98fairly infrequently. In addition, the incidence of the itching sensation (p=0.02) and the intensity of tingling sensation (p=0.02) were significantly higher during tDCS in the group of the healthy subjects, in comparison to patients; whereas the occurrence of headache was significantly higher in the patient group (p=0.03) after the stimulation. Our results suggest that tDCS applied to motor and non-motor areas according to the present tDCS safety guidelines, is associated with relatively minor adverse effects in healthy humans and patients with varying neurological disorders.

32

[Post:1999aa]   A. Post, M. B. Muller, M. Engelmann, and M. E. Keck. Repetitive transcranial magnetic stimulation in rats: evidence for a neuroprotective effect in vitro and in vivo. *Eur J Neurosci*, 11(9):3247–54, 1999.

Abstract: In recent years, repetitive transcranial magnetic stimulation (rTMS) of the human brain has been used as a therapeutic tool in a variety of psychiatric and neurological disorders. However, to understand the mechanisms underlying any potential therapeutic effects, and possible adverse effects, studies are necessary on how magnetic stimuli induced by rTMS interact with central nervous system (CNS) regulation. In the current study, we failed to find cognitive impairments or structural alterations in rat brains after 11 weeks of long-term treatment with rTMS, which if present would indicate neuronal damage. In contrast, our in vitro studies showed that magnetic stimulation analogous to rTMS increased the overall viability of mouse monoclonal hippocampal HT22 cells and had a neuroprotective effect against oxidative stressors, e.g. amyloid beta (Abeta) and glutamate. The treatment increased the release of secreted amyloid precursor protein (sAPP) into the supernatant of HT22 cells and into cerebrospinal fluid from rats. HT22 cells preincubated with cerebrospinal fluid from rTMS-treated rats were found to be protected against Abeta. These findings suggest that neurochemical effects induced by rTMS do not lead to reduced neuronal viability, and may even reduce the detrimental effects of oxidative stress in neurons.

116, 120, 122, 124, 125, 169, 342

[Priori:1998aa]   A. Priori, A. Berardelli, S. Rona, N. Accornero, and M. Manfredi. Polarization of the human motor cortex through the scalp. *Neuroreport*, 9(10):2257–60, 1998.

Abstract: Direct currents (DC) applied directly to central nervous system structures produce substantial and long-lasting effects in animal experiments. We tested the functional effects of very weak scalp DC (¡ 0.5 mA, 7 s) on the human motor cortex by assessing the changes in motor potentials evoked by transcranial magnetic brain stimulation. We performed four different experiments in 15 healthy volunteers. Our findings led to the conclusion that such weak (¡ 0.5 mA) anodal scalp DC, alternated with a cathodal DC, significantly depresses the excitability of the human motor cortex, providing evidence that a small electric field crosses the skull and influences the brain. A possible mechanism of action of scalp DC is the hyperpolarization of the superficial excitatory interneurones in the human motor cortex.

20

[Purpura:1965aa] D. P. Purpura and J. G. McMurtry. Intracellular activities and evoked potential changes during polarization of motor cortex. *J Neurophysiol*, 28:166–85, 1965. 125

[Radman:2007aa] T. Radman, A. Datta, and A. V. Peterchev. In vitro modulation of endogenous rhythms by ac electric fields: Syncing with clinical brain stimulation. *J Physiol*, 584(Pt 2):369–70, 2007. 86, 89, 98, 100, 339

[Radman:2007ab] T. Radman, Y. Su, J. H. An, L. C. Parra, and M. Bikson. Spike timing amplifies the effect of electric fields on neurons: implications for endogenous field effects. *J Neurosci*, 27(11):3030–6, 2007.

> **Abstract:** Despite compelling phenomenological evidence that small electric fields (¡5 mV/mm) can affect brain function, a quantitative and experimentally verified theory is currently lacking. Here we demonstrate a novel mechanism by which the nonlinear properties of single neurons "amplify" the effect of small electric fields: when concurrent to suprathreshold synaptic input, small electric fields can have significant effects on spike timing. For low-frequency fields, our theory predicts a linear dependency of spike timing changes on field strength. For high-frequency fields (relative to the synaptic input), the theory predicts coherent firing, with mean firing phase and coherence each increasing monotonically with field strength. Importantly, in both cases, the effects of fields on spike timing are amplified with decreasing synaptic input slope and increased cell susceptibility (millivolt membrane polarization per field amplitude). We confirmed these predictions experimentally using CA1 hippocampal neurons in vitro exposed to static (direct current) and oscillating (alternating current) uniform electric fields. In addition, we develop a robust method to quantify cell susceptibility using spike timing. Our results provide a precise mechanism for a functional role of endogenous field oscillations (e.g., gamma) in brain function and introduce a framework for considering the effects of environmental fields and design of low-intensity therapeutic neurostimulation technologies.

98, 100, 339

[Radvan-Ziemnowicz:1964aa] S. A. Radvan-Ziemnowicz, J. C. McWilliams, and W. E. Kucharski. Conductivity versus frequency in human and feline cerebrospinal fluid. In *Proc. 17th Ann. Conf. Eng. Med., Biol*, volume 6, page 108, 1964. 18

[Rall:1968aa] W. Rall and G. M. Shepherd. Theoretical reconstruction of field potentials and dendrodendritic synaptic interactions in olfactory bulb. *J Neurophysiol*, 31(6):884–915, 1968. 65

[Ranck:1963aa] Jr. Ranck, J. B. Specific impedance of rabbit cerebral cortex. *Exp Neurol*, 7:144–52, 1963. 18

[Ranck:1965aa] Jr. Ranck, J. B. and S. L. BeMent. The specific impedance of the dorsal columns of cat: an anisotropic medium. *Exp Neurol*, 11:451–63, 1965. 19

[Ranck:1966aa] Jr. Ranck, J. B. Electrical impedance in the subicular area of rats during paradoxical sleep. *Exp Neurol*, 16(4):416–37, 1966. 18

[Ranck:1975aa] J.B. Ranck. Which elements are excited in electrical stimulation of the mammalian central nervous system: a review. *Brain Res*, 98:417–440, 1975. 33, 36

[Rattay:1986aa] Frank Rattay. Analysis of models for external stimulation of axons. *IEEE Transactions on Biomedical Engineering*, 33(10):974–977, 1986. 34, 36, 39

[Rattay:1989aa] Frank Rattay. Analysis of models for extracellular fiber stimulation. *IEEE Transactions on Biomedical Engineering*, 36(7):676–682, 1989.

> **Abstract:** The mathematical basis for analysis as well as for the computer simulation of the stimulus-response characteristics of nerve or muscle fibers is presented. The results follow from the extracellular potential along the fiber as a function of electrode geometry. The theory is of a general nature, but special investigations are made on monopolar, bipolar, and ring electrodes. Stimulation with monopolar electrodes shows better recruitment characteristics than with ring electrodes.

39

[Rattay:1998aa] F. Rattay. Analysis of the electrical excitation of cns neurons. *IEEE Trans Biomed Eng*, 45(6):766–72, 1998.

> **Abstract:** The artificial excitation process of neurons of the central nervous system depends on the applied extracellular field, on the geometry of the neuron and on the electrical properties of the neural subunits. Results of computer simulations are based on a compartment model of the neuron and its equivalent electrical network. Furthermore, a theory is presented which generalizes the activating function concept known from peripheral nerve stimulation. The theory predicts the influence of electrical and geometrical parameters on the excitation threshold. Generally, the myelinated axon is the part of a neuron which is most excitable to a given applied field. An example demonstrates that for a target neuron the quotient (anodic threshold current)/(cathodic threshold current) essentially depends on the position and orientation of the neuron relative to the electrode.

39, 60

[Ravazzani:1996ab] P. Ravazzani, J. Ruohonen, F. Grandori, and G. Tognola. Magnetic stimulation of the nervous system: induced electric field in unbounded, semi-infinite, spherical, and cylindrical media. *Ann Biomed Eng*, 24(5):606–16, 1996.

> **Abstract:** Knowledge of the electric field that is induced in the brain or the limbs is of importance in magnetic stimulation of the nervous system. Here, an analytical model based on the reciprocity theorem is used to compare the induced electric field in unbounded, semi-infinite, spherical, and cylinder-like volume conductors. Typical stimulation coil arrangements are considered, including the double coil and various orientations of the single coil. The results can be used to determine when the influence of the boundaries is negligible enough to allow the use of more simplified geometries.

26, 27, 60

[Ravnborg:1990aa] M. Ravnborg, G. M. Knudsen, and M. Blinkenberg. No effect of pulsed magnetic stimulation on the blood-brain barrier in rats. *Neuroscience*, 38(1):277–80, 1990.

> **Abstract:** The impact of transcranial pulsed magnetic stimulation on blood-brain barrier permeability was studied in rats. An integral uptake technique was used to asses the blood-brain barrier permeability to the tracers [3H]sucrose, [14C]urea, and 36Cl-. From the arterial plasma concentration-time curve-integral the permeability surface-area products were calculated. A Dantec magnetic stimulator delivering a peak magnetic field of 1.9 T with a rise-time of 160 microseconds was used for transcranial stimulation of the rats. One group of rats had about 50-60 stimulations during the 15-min infusion of the tracers while another group was exposed to 50 magnetic stimulations a day for one week. A third group comprised the controls. No differences in permeability surface-area product were found for any of the three tracers in the rats exposed to magnetic stimulation as compared with the controls. It is concluded that with regard to blood-barrier integrity, pulsed magnetic stimulation of the brain can be regarded as safe.

124, 125, 168

[Regan:1989aa] D. Regan. *Human Brain Electrophysiology: Evoked Potentials and Evoked Magnetic Fields in Science and Medicine*. Elsevier, 1989. 136

[Reilly:1998aa] JP Reilly. *Applied bioelectricity: from electrical stimulation to electropathology*. Springer, 1998.

> **Abstract:** This book discusses short-term biological responses to electric currents and electromagnetic fields. It examines electricity as used for medical purposes, covers fundamental physical and engineering principles of responses to short-term electrical exposure, and emphasizes human reactions as well as animal responses to electricity.This work discusses biological responses to electric currents and electromagnetic fields, including medical applications and shock hazards. It covers basic physical and engineering principles of responses to short-term exposure, from the just-detectable to the clearly detrimental.

17, 19, 335

[Ren:1995aa]   C. Ren, P. P. Tarjan, and D. B. Popovic.   A novel electric design for electromagnetic stimulation–the slinky coil. *IEEE Trans Biomed Eng*, 42(9):918–25, 1995.

> **Abstract:** A novel coil design for inductive electromagnetic stimulation of neural cells has been simulated and experimentally tested. This coil improves the focal effect of a magnetic stimulator, and it reduces its inductance, hence the efficiency of the system is improved. The basic structure of the device is derived from the popular "Slinky" toy. The actual device is formed by winding different numbers of loops forming a helical coil on a half torus. The loops are bunched at the axis of the torus. The coil, due to its geometry, generates a unique distribution of eddy currents in nearby tissues which is favorable compared to a solenoid type stimulator. This renders the Slinky coil more selective than conventional coils used for magnetic stimulation. The distribution of eddy currents was analyzed using Matlab, following Faraday's Law of Induction. Improved focality permits the current through the coil to be reduced for the same effect. In addition, the reduced inductance of the Slinky coil decreases the power requirement; thus, the improved efficiency of the system may allow the generation of bursts of pulses, and expand the utilization of the system to possible functional activation of certain neuro-muscular structures when peripheral nerves are stimulated.

27

[Richardson:1984aa] T. L. Richardson, R. W. Turner, and J. J. Miller. Extracellular fields influence transmembrane potentials and synchronization of hippocampal neuronal activity. *Brain Res*, 294(2):255–62, 1984.

> **Abstract:** The influence of extracellular fields on the transmembrane potential (TMP) of CA1 pyramidal neurons was investigated following both ortho- and antidromic stimulation in the in vitro hippocampal slice preparation. A short latency negative deflection on the intracellular potential coincided with the falling phase of the extracellular population spike. Subtraction of extracellular field potentials from ground referenced intracellular records revealed a sharp depolarizing wave of the TMP superimposed upon the underlying synaptic potential. This graded depolarization was capable of discharging CA1 cells and displayed a parallel shift in latency and amplitude with the extracellular population spike. A similar depolarizing wave was associated with the antidromically evoked population spike which persisted following blockade of synaptic activity. Finally, multiple population spike activity similar to that observed during epileptiform discharge was associated with repetitive depolarizing waves of the TMP. These data suggest that extracellular field potentials can ephaptically discharge CA1 neurons and may play a role in recruitment and synchronization of neuronal activity in the hippocampus.

85, 90, 95

[Richardson:1992aa] C. L. Richardson, W. P. Tate, S. E. Mason, P. A. Lawlor, M. Dragunow, and W. C. Abraham. Correlation between the induction of an immediate early gene, zif/268, and long-term potentiation in the dentate gyrus. *Brain Res*, 580(1-2):147–54, 1992. 114, 127

[Richardson:1995aa] T. L. Richardson and C. N. O'Reilly. Epileptiform activity in the dentate gyrus during low-calcium perfusion and exposure to transient electric fields. *J Neurophysiol*, 74(1):388–99, 1995.

> **Abstract:** 1. The dentate gyrus fails to develop epileptiform activity in many experimental models of epilepsy, including the in vitro low-Ca2+ model. Although manipulating the K+ concentration or osmolality of normal low-Ca2+ perfusion mediums can enhance the propensity of the dentate gyrus to develop seizure activity, the specific mechanisms contributing to this change are still under investigation. Identification of these mechanisms should improve our understanding of epileptogenesis and of the factors contributing to the propensity for seizure discharge in other tissues. 2. In the present experiments we used externally generated

electric fields to depolarize the somata of large populations of dentate granule cells during exposure to a perfusion medium with no added Ca2+ (low-Ca2+ medium). Uniform electric fields were generated across an individual slice by passing current between two parallel AgCl-coated silver wires placed on the surface of the artificial cerebral spinal fluid. The wires were positioned to straddle the slice such that the current flow was parallel to the dendrosomatic axis of the cell population under investigation. 3. Under control conditions (low-Ca2+ medium, no applied field), stimulation of the dentate hilus evoked a single antidromic population spike in 89slices studied (n = 27). During application of electric fields the same stimulus evoked epileptiform activity in all trials. Well-formed bursts first occurred at an average field intensity of +22.9 +/- 2.5 (SE) mV/mm (n = 24). The amplitude of individual spikes and the total number of spikes, within a burst increased in a graded fashion as the magnitude of the applied field was increased. 4. High field intensities evoked epileptiform activity in the absence of a synchronizing antidromic stimulus. These field-induced bursts occurred after a progressive buildup of rhythmic activity recorded in the extrasomatic space and could persist for the entire duration of an applied field, lasting for several seconds. The average field intensity required to produce a threshold burst was +84.6 +/- 3.6 mV/mm (n = 24). 5. In 11trials (3 of 27) the dentate gyrus exhibited poorly developed antidromic bursting without the application of depolarizing electric fields. These bursts were completely suppressed by hyperpolarizing fields in the range of -10 to -20 mV/mm. 6. The results of this investigation support the hypothesis that granule cell sensitivity to nonsynaptic interactions is adequate to support bursting in a normal low-Ca2+ medium, but bursting fails to occur because these cells are normally too hyperpolarized relative to their action potential threshold.(ABSTRACT TRUNCATED AT 400 WORDS)

95

[Richter:1994aa] F. Richter, R. Fechner, W. Haschke, and V. V. Fanardijan. Transcortical polarization in rat inhibits spreading depression. *Int J Neurosci*, 75(3-4):145–51, 1994.

> **Abstract:** In cerebral cortex of rats single spreading depressions (SD) were elicited by a slight needle prick. SDs were monitored by recording changes of direct current (DC) potential via an array of four glass microelectrodes providing a simultaneous depth profile. Using an epicortical Ag-AgCl wire electrode surrounding the recording site and a contralateral Ag-AgCl electrode penetrating the whole grey matter, a polarization current was applied starting 5 min before and ending 3 min after eliciting a SD. By anodic polarization of the cortical surface with intensities of 10 to 20 microA the SD was blocked in the whole grey matter. Restitution of SD in course and amplitudes was found only 45 min to 60 min after ending the polarization. Cathodic polarization of the cortical surface resulted in similar effects. Both polarizing and restitution effects were replicable in the same animal. The results are relevant for further investigations to discover the particular role of glial cells in regulation of extracellular potassium concentration during SD.

129

[Richter:1996aa] F. Richter, R. Fechner, and W. Haschke. Initiation of spreading depression can be blocked by transcortical polarization of rat cerebral cortex. *Int J Neurosci*, 86(1-2):111–8, 1996.

> **Abstract:** Spreading depression (SD) was elicited in urethane anesthetized rats by pricking the cortical gray matter with a needle. The SDs were monitored by recording changes of direct current (DC) potentials and changes of extracellular potassium concentrations ([K+]e). Simultaneous recordings were made at cortical depths of 400 microns and 1200 microns by an array of two double-barrelled electrodes, one served to measure DC the other contained an ion-sensitive resin. An additional DC microelectrode was inserted in the gray matter near the point of SD elicitation at a depth of about 400 microns. An epicortical Ag-AgCl wire electrode surrounding the recording site and a remote Ag-AgCl electrode penetrating the cortex in the contralateral hemisphere were used for polarizing DC currents. These

currents were applied 5 min before elicitation of SD by a needle prick and were sustained for a period ending 3 min after SD. Cathodic polarization of cortical surface with intensities of 30 microA and higher blocked the SD completely. Lower intensities of polarizing currents (10 or 20 microA) had no effect. After ending polarizations normal SDs could be elicited. The polarizing and restitution effects were replicable in the same animal. The results suggest that longer lasting DC polarization of the cortex blocks initiation of SD but not propagation.

129

[Rigaud:1994aa] B. Rigaud, L. Hamzaoui, N. Chauveau, M. Granie, J. P. Scotto Di Rinaldi, and J. P. Morucci. Tissue characterization by impedance: a multifrequency approach. *Physiol Meas*, 15 Suppl 2a:A13–20, 1994.

> **Abstract:** Two experimental set-ups for in vitro characterization of electrical bio-impedance are described. The first one, based on a commercially available instrument, operates in the frequency range 1 Hz-10 MHz. The second one uses an identification process and operates in the frequency range 1 Hz-1 MHz. Some results are presented and discussed in the context of multifrequency electrical impedance tomography.

17

[Robillard:1977aa] P. N. Robillard and Y. Poussart. Specific-impedance measurements of brain tissues. *Med Biol Eng Comput*, 15(4):438–45, 1977. 18, 19

[Rose:1986aa] G. M. Rose and T. V. Dunwiddie. Induction of hippocampal long-term potentiation using physiologically patterned stimulation. *Neurosci Lett*, 69(3):244–8, 1986.

> **Abstract:** Lasting increases in the population spike recorded in area CA1 of hippocampal slices may be evoked by the patterned presentation of as few as 5 stimulus pulses delivered to the commissural/associational afferents. The most effective pattern of stimulus presentation was a single priming pulse followed 170 ms later by 4 pulses at 100 Hz; control trains of 5 pulses at 100 Hz had no significant enduring effect. This pattern-dependent phenomenon, termed primed burst potentiation, is of lesser magnitude than is the long-term potentiation induced by 100 Hz/l s stimulation, but appears to show a similar time course and duration. In addition, the two phenomena are not additive, suggesting that they may share a common mechanism.

101

[Rossini:1994aa] P. M. Rossini, A. T. Barker, A. Berardelli, M. D. Caramia, G. Caruso, R. Q. Cracco, M. R. Dimitrijevic, M. Hallett, Y. Katayama, C. H. Lucking, and et al. Non-invasive electrical and magnetic stimulation of the brain, spinal cord and roots: basic principles and procedures for routine clinical application. report of an ifcn committee. *Electroencephalogr Clin Neurophysiol*, 91(2):79–92, 1994. 24

[Rotenberg:2008aa] A. Rotenberg, P. Muller, D. Birnbaum, M. Harrington, J. J. Riviello, A. Pascual-Leone, and F. E. Jensen. Seizure suppression by eeg-guided repetitive transcranial magnetic stimulation in the rat. *Clin Neurophysiol*, 119(12):2697–702, 2008.

> **Abstract:** OBJECTIVE: To test the anticonvulsive potential of a range of repetitive transcranial magnetic stimulation (rTMS) frequencies by novel methods for simultaneous EEG and rTMS in a rat seizure model. METHODS: Seizures were triggered by intraperitoneal kainic acid (KA; 10mg/kg). Rats (n=21) were divided into three groups in which individual seizures were treated with rTMS trains at one of three frequencies: 0.25, 0.5 or 0.75 Hz. EEG was continuously viewed by an operator who identified each seizure onset. Consecutive seizures in each animal were (1) treated with active rTMS, (2) treated with sham rTMS, or (3) were untreated. EEG was re-analyzed post hoc by visual inspection, and seizure durations were compared within and between treatment groups. RESULTS: KA-induced seizures were abbreviated by 0.75 Hz (P=0.019) and 0.5 Hz (P=0.033) active

EEG-guided rTMS. In contrast, neither active 0.25 Hz rTMS nor the control conditions affected seizure duration (P¿0.2). CONCLUSIONS: We demonstrate that EEG-guided rTMS can suppress seizures in the rat KA epilepsy model, and that the effect is frequency dependent, with 0.75 and 0.5 Hz rTMS being superior to 0.25 Hz rTMS. SIGNIFICANCE: These data support the use of rat seizure models in translational research aimed at evaluation and development of effective rTMS anticonvulsive protocols. We also offer a proof of principle that real-time analysis of EEG can be used to guide rTMS to suppress individual seizures.

119, 120, 177, 178, 341

[Roth:1990aa] Bratley J. Roth and Peter J. Basser. A model of the stimulation of a nerve fiber by electromagnetic induction. *IEEE Transactions on Biomedical Engineering*, 37(6):588–597, 1990.

Abstract: A model is presented to explain the physics of nerve stimulations by electromagnetic induction. Maxwell's equations predict the induced electric field distribution that is produced when a capacitor is discharged through a stimulating coil. A nonlinear Hodgkin-Huxley cable model describes the response of the nerve fiber to this induced electric field. Once the coil's position, orientation, and shape are given and the resistance, capacitance, and initial voltage of the stimulating circuit are specified, this model predicts the resulting transmembrane potential of the fiber as a function of distance and time. It is shown that the nerve fiber is stimulated by the gradient of the component of the induced electric field that is parallel to the fiber, which hyperpolarizes or depolarizes the membrane and may stimulate an action potential. The model predicts complicated dynamics such as action potential annihilation and dispersion.

26, 27, 34, 39, 40, 52, 56

[Roth:1990ab] B. J. Roth, L. G. Cohen, M. Hallett, W. Friauf, and P. J. Basser. A theoretical calculation of the electric field induced by magnetic stimulation of a peripheral nerve. *Muscle Nerve*, 13(8):734–41., 1990.

Abstract: A mathematical model is presented that predicts the electric field induced in the arm during magnetic stimulation of a peripheral nerve. The arm is represented as a homogeneous, cylindrical volume conductor. The electric field arises from two sources: the time-varying magnetic field and the accumulation of charge on the arm surface. In magnetic stimulation both of these contributions are significant. The magnitude of the electric field is greatest near the surface of the arm, and is well localized. Various coil orientations are examined; the smallest electric fields are induced when the coil is perpendicular to the arm surface, the largest when the coil is parallel. These results are consistent with many experimental observations in the literature, and aid in the basic understanding of magnetic stimulation of the peripheral nervous system.

26, 27

[Roth:1991aa] B. J. Roth, L. G. Cohen, and M. Hallett. The electric field induced during magnetic stimulation. *Electroencephalogr Clin Neurophysiol Suppl*, 43:268–78, 1991.

Abstract: The electric field induced in tissue during magnetic stimulation is calculated. There are two sources of the electric field: charge and a time-dependent magnetic field: both sources are important in magnetic stimulation. Charge accumulation on the tissue surface tends to shield the nerve from the stimulus. The induced electric field is generally parallel to the tissue surface. Simulations of both peripheral and central nervous system stimulation are presented.

16, 26, 27

[Roth:1991ab] B. J. Roth, J. M. Saypol, M. Hallett, and L. G. Cohen. A theoretical calculation of the electric field induced in the cortex during magnetic stimulation. *Electroencephalogr Clin Neurophysiol*, 81(1):47–56, 1991.

Abstract: We present a mathematical model for calculating the electric field induced in the head during magnetic stimulation of the cortex. The electric field arises from 2 sources: (1) the changing magnetic field creates an electric field in the tissue by electromagnetic induction, and (2) a charge distribution arises on the surface of the head and produces its own electrostatic field. A 3-sphere model is used to represent the brain, skull and scalp. The electric field as a function of the coil position, shape and orientation is computed numerically. The charge distribution partially shields the brain from the stimulus. The electric field is insensitive to the skull conductivity, in contrast with electrical stimulation using surface electrodes. Different coil shapes and orientations are considered, and a figure-of- eight coil is shown to deliver the largest and most focal stimulus.

26

[Roth:1994aa] B. J. Roth. Mechanisms for electrical stimulation of excitable tissue. *Crit Rev Biomed Eng*, 22(3-4):253–305, 1994.

Abstract: Electric fields excite electrically active tissue by several mechanisms. A long, straight, uniform fiber is polarized by an activating function, proportional to the axial gradient of the axial electric field. During unipolar anodal stimulation, the activating function results in two areas of depolarization (virtual cathodes) that are responsible for anode-make stimulation. During unipolar cathodal stimulation, the virtual anodes can be exploited to produce unidirectional propagation and physiological recruitment of axons. Anode-break stimulation of nerves arises from the intrinsic properties of the sodium channel kinetics; cathode-break stimulation in nerves is anode-break stimulation at a virtual anode. The activating function applies to magnetic stimulation as well as to electric stimulation. Other important mechanisms of stimulation arise if the fiber is terminated, nonuniform, or curved. In the brain, cortical neurons are excited when the electric field is directed from the dendrites toward the axon. Possible mechanisms for cortical excitation are the impedance mismatch between the axon and dendritic tree, and the axon bending as it enters the white matter. Transcranial magnetic stimulation differs from transcranial electric stimulation because during magnetic stimulation the electric field is parallel to the brain surface, whereas during electric stimulation the electric field has components both parallel and perpendicular to the brain surface. Cardiac tissue can be represented by use of the bidomain model. This model predicts that a point-source stimulus results in adjacent areas of depolarized and hyperpolarized tissue. The presence of virtual anodes during cathodal stimulation is analogous to the creation of virtual anodes along a one-dimensional fiber by the activating function. Anode- and cathode-break stimulation both occur in cardiac tissue, but the mechanism may be different than for nerve and may depend on diffusion of depolarization into a previously hyperpolarized region. Electrical stimulation of cardiac tissue can cause reentry through a critical point mechanism. Two mechanisms for defibrillation have been hypothesized: (1) the relatively high junctional resistance between cardiac cells causes each cell to be depolarized on one side and hyperpolarized on the other; and (2) the fiber tracts within the heart behave like individual fibers, with fiber curvature providing a mechanism for polarization. Similarities among nerve, brain, and cardiac stimulation are emphasized.

33, 35

[Roth:1994ab] B. J. Roth, P. J. Maccabee, L. P. Eberle, V. E. Amassian, M. Hallett, J. Cadwell, G. D. Anselmi, and G. T. Tatarian. In vitro evaluation of a 4-leaf coil design for magnetic stimulation of peripheral nerve. *Electroencephalogr Clin Neurophysiol*, 93(1):68–74, 1994.

Abstract: The performance of a 4-leaf magnetic coil was evaluated during magnetic stimulation of a peripheral nerve in vitro. The site of stimulation was below the coil center, and a 90 degrees rotation of the coil was equivalent to a change in current polarity. A hyperpolarizing magnetic stimulus failed to slow or block a propagating action potential.

27

[Roth:1997aa] B. J. Roth, D. Ko, I. R. von Albertini-Carletti, D. Scaffidi, and S. Sato. Dipole localization in patients with epilepsy using the realistically shaped head model. *Electroencephalogr Clin Neurophysiol*, 102(3):159–66., 1997.

Abstract: Dipole sources were localized in 3 patients with epilepsy using both the realistically shaped head model and the 3-sphere model. Interictal spikes were recorded from 63 closely spaced scalp electrodes. The scalp, skull, and brain surfaces were digitized from a MRI of each patient's head, and each surface was tessellated by 1600 triangles. Single dipole fits to the EEG were performed using both the realistically shaped head model and the 3-sphere model. The 2 models localized dipoles to positions that differed from one another by 1-3 cm. For dipoles localized to the temporal lobe, the most important difference between models was that the realistically shaped head model localized the dipole lower in the brain than the 3-sphere model. The realistically shaped head model was more in accordance with the ECoG findings than the 3-sphere model.

30

[Roth:2002aa] Y. Roth, A. Zangen, and M. Hallett. A coil design for transcranial magnetic stimulation of deep brain regions. *J Clin Neurophysiol*, 19(4):361–70, 2002.

Abstract: Noninvasive magnetic stimulation of the human central nervous system has been used in research and the clinic for several years. However, the coils used previously stimulated mainly the cortical brain regions but could not stimulate deeper brain regions directly. The purpose of the current study was to develop a coil to stimulate deep brain regions. Stimulation of the nucleus accumbens and the nerve fibers connecting the prefrontal cortex with the nucleus accumbens was one major target of the authors' coil design. Numeric simulations of the electrical field induced by several types of coils were performed and accordingly an optimized coil for deep brain stimulation was designed. The electrical field induced by the new coil design was measured in a phantom brain and compared with the double-cone coil. The numeric simulations show that the electrical fields induced by various types of coils are always greater in cortical regions (closer to the coil placement); however, the decrease in electrical field within the brain (as a function of the distance from the coil) is markedly slower for the new coil design. The phantom brain measurements basically confirmed the numeric simulations. The suggested coil is likely to have the ability of deep brain stimulation without the need to increase the intensity to levels that stimulate cortical regions to a much higher extent and possibly cause undesirable side effects.

27

[Roth:2007aa] Y. Roth, A. Amir, Y. Levkovitz, and A. Zangen. Three-dimensional distribution of the electric field induced in the brain by transcranial magnetic stimulation using figure-8 and deep h-coils. *J Clin Neurophysiol*, 24(1):31–8, 2007.

Abstract: The H-coils are a novel development in transcranial magnetic stimulation (TMS), designed to achieve effective stimulation of deep neuronal regions without inducing unbearable fields cortically, thus broadly expanding the potential feasibility of TMS for research and for treating various neurologic disorders. This study compared the field distribution of two H-coil versions, termed H1 and H2, and of a standard figure-of-eight coil. Three-dimensional electrical field distributions of the H1 and H2-coils, designed for effective stimulation of prefrontal regions, and of a standard figure-8 coil, were measured in a head model filled with physiologic saline solution. With stimulator output at 120of the hand motor threshold, suprathreshold field is induced by the H1-coil at lateral and medial frontal regions at depths of up to 4 to 5 cm, and by the H2-coil at medial prefrontal regions up to 2 to 3 cm, and at lateral frontal regions up to 5 to 6 cm. The figure-8 coil induced suprathreshold field focally under the coil's central segment, at depths of up to 1.5 cm. The ability of the H-coils to stimulate effectively deeper neuronal structures is

obtained at the cost of a wider electrical field distribution in the brain. However, the H-coils enable simultaneous stimulation of several brain regions, whereas the depth penetration in each region can be controlled either by adjusting the stimulator output, and/or by varying the distance between various coil elements and the skull.

27

[Rudiak:1994aa] D. Rudiak and E. Marg. Finding the depth of magnetic brain stimulation: a re-evaluation. *Electroencephalogr Clin Neurophysiol*, 93(5):358–71, 1994.

Abstract: The depth of threshold magnetic nerve stimulation can be estimated by using thresholds from two different-sized stimulus coils and plotting their induced electric field vs. depth profiles. Stimulation is presumed to take place where the two field profiles are equal. If the two coils have unequal inductances, however, there is a relative shift in threshold between coils that alters the intersection point and the apparent stimulus depth. This systematic error arises from two sources: (1) there is a difference in the fraction of stimulator energy reaching each coil, and (2) pulse durations are different, causing threshold shifts governed by the nerve strength-duration curve. Both sources of error are additive. If the larger coil has the lesser inductance, stimulus depth is underestimated; if it has the greater inductance, it is overestimated. This can lead to large disparities in the measured depth, depending on the sets of coils used. In this paper, we show how to correct for errors introduced by unequal inductance and how this resolves discrepancies in depth measurement. Our own depth measurements in the motor area for threshold finger movements, and recalculated depths from Epstein et al., indicate that stimulation is slightly deeper (18-21 mm, average 19+ mm) than previously thought. This suggests that threshold magnetic stimulation in the motor area may arise from large, tangentially oriented fibers in the superficial white matter, or in the gray matter at the upper sulcus or lip of the gyrus.

29

[Ruffini:2008aa] Giulio Ruffini. The interaction of slowly varying electric fields with single neurons. Starlab Technical Note TN00162, Starlab Barcelona S.L., December 2008.

Abstract: This note aims to clarify several aspects of bioelectric phenomena with a focus on stimulation of a single neuron. When an electromagnetic field is coupled to a neuron, whether TMS or tDCS, the interaction is through the induced electric field and the neuron and surrounding conductive medium. We will elucidate the mechanisms for interaction and salient points to guide further work, including theoretical/numerical work with neuronal ensembles, experimental work and system design. Here we will provide:

1. A brief review of the origin of bioelectric potentials (mostly based on TN00011)
2. The derivation of the cable equation for a generic bent neuron
3. A discussion of termination boundary conditions
4. Analysis of the interaction of external fields with single neurons in steady state
5. 2D simulations in steady state
6. An analytic 1D solution with many key elements
7. An overview of neuron modeling and compartment models and how to include stimulation in them
8. A review of the state of the art in neuron electro-magnetic stimulation
9. A review of EM boundary conditions

We provide a set of conclusions for discussion.

135, 298

[Ruffini:2009aa] Giulio Ruffini. Improving focality in electromagnetic stimulation. Starlab Technical Note TN00163, Starlab Barcelona S.L., January 2009.

Abstract: As part of discussions on how to improve transcranial stimulation focality, the possibility of using bipolar configurations has been discussed, or, more generally, the use of different current or voltage sources, such as different batteries. Here we show that the combination of different current or voltage sources is a boundary value problem in conductive media, and that it therefore cannot be used to bypass the limitations associated to focality using harmonic fields. In fact, superposition of bipolar fields can be used to calculate multipolar setups as long as there are no electrode overlaps. We describe in depth the concept of harmonic fields and their relevance to electric fields in uniformly conductive media. We show that neither the sum of harmonic functions, nor the sum of squares of harmonic functions can attain local maxima outside their boundaries. Although the relevance of this to the stimulation problem is not direct, since in the brain we deal with non-conductive media, we conclude that electric field maxima will reside on the outer cortical layer. Stimulation patterns can be designed to target specific cortical regions, but with the caveat that the field maximum will occur on the cortical surface. However, the effect of stimulation at the neuron level is not simply proportional to field strength, since neuron characteristics also play an important role in the coupling. We define the concept of "single-neuron excitation function" and provide a model for this reflecting the results of TN00162 ([Ruffini:2008aa]), namely the dependence of excitation on field intensity and relative orientation. This model can be used to couple electric field models to neuronal ensembles. We implement this excitation function into a simple single neuron model, showing it can alter the firing rate of the neuron in the expected manner. In addition, we discuss how we may target specific sets of neurons by tuning the stimulus pulse duration, since the excitation function for a given type of neuron will have a characteristic time constant. Shorter pulses than a given constant will generate limited stimulation. We discuss alternative ways to improve focality, including time and frequency stimulation control to control stimulation maps over the cortex, and also the possibility of using resonance phenomena (to be discussed in TN00164).

141, 142, 143

[Ruohonen:1995aa] Jarmo Ruohonen and et al. An analytical model to predict the electric field and excitation zones due to magnetic stimulation of peripheral nerves. *IEEE Transactions on Biomedical Engineering*, 42(2):158–161, 1995.

Abstract: The main unknown factor in understanding magnetic stimulation of peripheral nerves is the distribution of the induced electric field. The authors have applied the so-called reciprocity theorem and developed an analytical model to compute the electric field and its spatial derivatives inside pseudocylindrical structures. The results can be used to predict the site of excitation in magnetic stimulation of peripheral nerves.

26, 27, 41

[Ruohonen:1996aa] Jarmo Ruohonen and et al. A volume-conduction analysis of magnetic stimulation of peripheral nerves. *IEEE Transactions on Biomedical Engineering*, 43(7):669–678, 1996.

Abstract: Magnetic stimulation is a method to study several nervous disorders as well as the intact nervous system in humans. Interest in magnetic stimulation of peripheral nerves has grown rapidly, but difficulties in locating the site of excitation have prevented it from becoming a routine clinical tool. It has been reasoned that the activating function of long and straight nerves is the first spatial derivative of the electric field component parallel to the nerves. Therefore, to predict the site of activation, one has to compute this field feature. We describe here an analytical mathematical model and investigate the influence of volume-conductor shape on the induced field, predictions of the site of activation are given for typical stimulation coil arrangements and these results are compared with experimental

and literature data. Comparisons suggest that the activating function is not simply the spatial gradient of the induced electric field, but that other mechanisms are also involved. The model can be easily utilized in the search for more efficient coil constructions and improved placements with respect to the target nerves.

41

[Ruohonen:1996ab] J. Ruohonen, P. Ravazzani, J. Nilsson, M. Panizza, F. Grandori, and G. Tognola. A volume-conduction analysis of magnetic stimulation of peripheral nerves. *IEEE Trans Biomed Eng*, 43(7):669–78, 1996.

Abstract: Magnetic stimulation is a method to study several nervous disorders as well as the intact nervous system in humans. Interest in magnetic stimulation of peripheral nerves has grown rapidly, but difficulties in locating the site of excitation have prevented it from becoming a routine clinical tool. It has been reasoned that the activating function of long and straight nerves is the first spatial derivative of the electric field component parallel to the nerves. Therefore, to predict the site of activation, one has to compute this field feature. We describe here an analytical mathematical model and investigate the influence of volume-conductor shape on the induced field. Predictions of the site of activation are given for typical stimulation coil arrangements and these results are compared with experimental and literature data. Comparisons suggest that the activating function is not simply the spatial gradient of the induced electric field, but that other mechanisms are also involved. The model can be easily utilized in the search for more efficient coil constructions and improved placements with respect to the target nerves.

60, 61

[Ruohonen:1998aa] J. Ruohonen and R. J. Ilmoniemi. Focusing and targeting of magnetic brain stimulation using multiple coils. *Med Biol Eng Comput*, 36(3):297–301, 1998.

Abstract: Neurones can be excited by an externally applied time-varying electromagnetic field. Focused magnetic brain stimulation is attained using multiple small coils instead of one large coil, the resultant induced electric field being a superposition of the fields from each coil. In multichannel magnetic brain stimulation, partial cancellation of fields from individual coils provides a significant improvement in the focusing of the stimulating field, and independent coil channels allow targeting of the stimuli on a given spot without moving the coils. The problem of shaping the stimulating field in multichannel stimulation is analysed, and a method is derived that yields the driving currents required to induce a field with a user-defined shape. The formulation makes use of lead fields and minimum-norm estimation from magneto-encephalography. Using these methods, some properties of multichannel coil arrays are examined. Computer-assisted multichannel stimulation of the cortex will enable several new studies, including quick determination of the cortical regions, the stimulation of which disrupts cortical processing required by a task.

28, 41, 42, 335

[Ruohonen:1999aa] J. Ruohonen, P. Ravazzani, F. Grandori, and R. J. Ilmoniemi. Theory of multichannel magnetic stimulation: toward functional neuromuscular rehabilitation. *IEEE Trans Biomed Eng*, 46(6):646–51, 1999.

Abstract: Human excitable cells can be stimulated noninvasively with externally applied time-varying electromagnetic fields. The stimulation can be achieved either by directly driving current into the tissue (electrical stimulation) or by means of electro-magnetic induction (magnetic stimulation). While the electrical stimulation of the peripheral neuromuscular system has many beneficial applications, peripheral magnetic stimulation has so far only a few. This paper analyzes theoretically the use of multiple magnetic stimulation coils to better control the excitation and also to eventually mimic electrical stimulation. Multiple coils allow electronic spatial adjustment of the shape and location of the stimulus without moving the

coils. The new properties may enable unforeseen uses for peripheral magnetic stimulation, e.g., in rehabilitation of patients with neuromuscular impairment.

28

[Rush:1963aa] S. Rush, J. A. Abildskov, and R. McFee. Resistivity of body tissues at low frequencies. *Circ Res*, 12:40–50, 1963. 17

[Rush:1968aa] S. Rush and D. A. Driscoll. Current distribution in the brain from surface electrodes. *Anesth Analg*, 47(6):717–23, 1968. 17, 18, 20

[Rush:1969aa] Stanley Rush and et al. Eeg electrode sensitivity—an application of reciprocity. *IEEE Transactions on Biomedical Engineering*, 16(1):15–22, 1969. 20, 26

[Rushton:1927aa] W. A. H. Rushton. The effect upon the threshold for nervous excitation of the length of nerve exposed, and the angle between current and nerve. *J Physiol*, 63:357–77, 1927. 33

[Sajikumar:2004aa] S. Sajikumar and J. U. Frey. Late-associativity, synaptic tagging, and the role of dopamine during ltp and ltd. *Neurobiol Learn Mem*, 82(1):12–25, 2004.

Abstract: Protein synthesis-dependent, synapse input-specific late phases of long-term potentiation (LTP) and depression (LTD) may underlie memory formation at the cellular level. Recently, it was described that the induction of LTP can mark a specifically activated synapse by a synaptic tag to capture synapse non-specific plasticity-related proteins (PRPs) and thus maintaining input-specific LTP for prolonged periods. Here we show in rat hippocampal slices in vitro, that the induction of protein synthesis-dependent late-LTD is also characterized by synaptic tagging and that heterosynaptic induction of either LTD or LTP on two sets of independent synaptic inputs S1 and S2 can lead to late-associative interactions: early-LTD in S2 was transformed into a late-LTD, if late-LTP was induced in S1. The synthesis of process-independent PRPs by late-LTP in S1 was sufficient to transform early- into late-LTD in S2 when process-specific synaptic tags were set. We name this new associative property of cellular information processing 'cross-tagging.'

102

[Sakai:1997aa] K. Sakai, Y. Ugawa, Y. Terao, R. Hanajima, T. Furubayashi, and I. Kanazawa. Preferential activation of different i waves by transcranial magnetic stimulation with a figure-of-eight-shaped coil. *Exp Brain Res*, 113(1):24–32, 1997.

Abstract: Transcranial magnetic stimulation (TMS) over the human primary motor cortex (MI) evokes motor responses in the contralateral limb muscles. The latencies and amplitudes of those responses depend on the direction of induced current in the brain by the stimuli (Mills et al. 1992, Werhahn et al. 1994). This observation suggests that different neural elements might be activated by the differently directed induced currents. Using a figure-of-eight-shaped coil, which induces current with a certain direction, we analyzed the effect of direction of stimulating current on the latencies of responses to TMS in normal subjects. The latencies were measured from surface electromyographic responses of the first dorsal interosseous muscles and the peaks in the peristimulus time histograms (PSTHs) of single motor units from the same muscles. The coil was placed over the MI, with eight different directions each separated by 45 degrees. Stimulus intensity was adjusted just above the motor threshold while subjects made a weak tonic voluntary contraction, so that we can analyse the most readily elicited descending volley in the pyramidal tracts. In most subjects, TMS with medially and anteriorly directed current in the brain produced responses or a peak that occurred some 1.5 ms later than those to anodal electrical stimulation. In contrast, TMS with laterally and posteriorly directed current produced responses or a peak that occurred about 4.5 ms later. There was a single peak in most of PSTHs under the above stimulation condition, whereas there were occasionally two peaks under the transitional current directions between the above two groups. These results suggest that TMS with medially and anteriorly directed current in the brain readily elicits I1 waves, whereas that with

laterally and posteriorly directed current preferentially elicits I3 waves. Functional magnetic resonance imaging studies indicated that this direction was related to the course of the central sulcus. TMS with induced current flowing forward relative to the central sulcus preferentially elicited I1 waves and that flowing backward elicited I3 waves. Our finding of the dependence of preferentially activated I waves on the current direction in the brain suggests that different sets of cortical neurons are responsible for different I waves, and are contrarily oriented. The present method using a figure-of-eight-shaped coil must enable us to study physiological characteristics of each I wave separately and, possibly, analyse different neural elements in MI, since it activates a certain I wave selectively without D waves or other I waves.

62

[Sanes:2000aa] J. N. Sanes and J. P. Donoghue. Plasticity and primary motor cortex. *Annu Rev Neurosci*, 23:393–415, 2000.

Abstract: One fundamental function of primary motor cortex (MI) is to control voluntary movements. Recent evidence suggests that this role emerges from distributed networks rather than discrete representations and that in adult mammals these networks are capable of modification. Neuronal recordings and activation patterns revealed with neuroimaging methods have shown considerable plasticity of MI representations and cell properties following pathological or traumatic changes and in relation to everyday experience, including motor-skill learning and cognitive motor actions. The intrinsic horizontal neuronal connections in MI are a strong candidate substrate for map reorganization: They interconnect large regions of MI, they show activity-dependent plasticity, and they modify in association with skill learning. These findings suggest that MI cortex is not simply a static motor control structure. It also contains a dynamic substrate that participates in motor learning and possibly in cognitive events as well.

99

[Santschi:2003aa] L. A. Santschi and P. K. Stanton. A paired-pulse facilitation analysis of long-term synaptic depression at excitatory synapses in rat hippocampal ca1 and ca3 regions. *Brain Res*, 962(1-2):78–91, 2003.

Abstract: Paired-pulse facilitation (PPF) is a form of short-term, activity-dependent synaptic plasticity common to most chemically transmitting synapses, manifested as an enhancement in the amplitude of the second of two rapidly evoked excitatory postsynaptic potentials (EPSPs). The generally accepted explanation of PPF posits that residual intraterminal free $[Ca(2+)]$ from the first action potential facilitates the probability of transmitter release evoked by the second stimulus. A common extension of this hypothesis postulates that any plastic change which alters the probability of transmitter release, should also alter the magnitude of PPF. In the present study, we examined the relationship between PPF and both stimulus- and chemically-evoked long-term depression of synaptic strength (LTD) at Schaffer collateral-CA1, commissural/associational-CA3 and mossy fiber-CA3 synapses in rat hippocampal slices. We observed no significant change in mean PPF associated with either electrically- or chemically-induced LTD at any of these synapses. However, a correlation analysis revealed a complex pattern of PPF changes with LTD, such that low initial PPF was correlated with increases in PPF, while high initial PPF was associated with decreases. Combined with previous findings supporting a presynaptic site for chemical and stimulus-evoked LTD, our current data suggests a complex set of neurosecretory modifications downstream of presynaptic $Ca(2+)$ influx, may, at least in part, underlie the expression of LTD.

104

[Sarvas:1987aa] J. Sarvas. Basic mathematical and electromagnetic concepts of the biomagnetic inverse problem. *Phys Med Biol*, 32(1):11–22, 1987.

Abstract: In this paper basic mathematical and physical concepts of the biomagnetic inverse problem are reviewed with some new approaches. The forward problem is discussed for both homogeneous and inhomogeneous media. Geselowitz' formulae and a surface integral equation are presented to handle a piecewise homogeneous conductor. The special cases of a spherically symmetric conductor and a horizontally layered medium are discussed in detail. The non-uniqueness of the solution of the magnetic inverse problem is discussed and the difficulty caused by the contribution of the electric potential to the magnetic field outside the conductor is studied. As practical methods of solving the inverse problem, a weighted least-squares search with confidence limits and the method of minimum norm estimate are discussed.

16

[Sauvage:2008aa] R. C. de Sauvage, I. Lagroye, B. Billaudel, and B. Veyret. Evaluation of the potential genotoxic effects of rtms on the rat brain and current density mapping. *Clin Neurophysiol*, 119(2):482–91, 2008.

Abstract: OBJECTIVE: The objectives of this work were: (i) to evaluate the relevance for clinical studies of repetitive transcranial magnetic stimulation (rTMS) investigations on rats, (ii) to investigate the occurrence of DNA damage in rat brain cells following rTMS under conditions similar to those used in clinical treatment of depression. METHODS: Rats were exposed to 2000 magnetic pulses at 100(MT). Software, written to take detailed anatomical and conductivity data into account, was used to map current density in the rat brain. A method was developed for standardizing magnetic pulse efficacy to facilitate comparison with other rTMS studies. Genotoxicity was explored using the alkaline comet assay on rat brain cells, measuring Olive moment and RESULTS: The current density was ca. 6.6 A/m2 in the motor cortex at MT (Motor Cortex Threshold Densities: MCTDs), 5.2 A/m2 in the brain (range 0-17 A/m2), and 2.0 A/m2 at prefrontal cortex. Similar standard MCTDs were found in rats and humans. Concerning the comet assay, both Olive moment and the tail, there was no statistically-significant difference between rTMS-exposed and sham-exposed brain cell samples. In contrast, significant increases in both parameters were detected in positive controls. CONCLUSIONS: Under the assumptions developed in the discussion, these data showed no evidence that the standard current density at motor threshold in human motor cortex would differ from that in rats. Furthermore, there was no evidence of DNA damage in rat brain cells following a single scheme of rTMS, under conditions similar to the clinical treatment of depression. SIGNIFICANCE: This study supports the use of rats as a model for studying the bioeffects of rTMS (molecular targets, action mechanisms, toxicology, etc.) and suggests that a single rTMS scheme, similar to that used daily in the treatment of depression, is not genotoxic.

124, 125, 169, 178

[Saypol:1991aa] J. M. Saypol, B. J. Roth, L. G. Cohen, and M. Hallett. A theoretical comparison of electric and magnetic stimulation of the brain. *Ann Biomed Eng*, 19(3):317–28, 1991.

Abstract: We present a theoretical comparison of the electric field produced in the brain by three modalities of transcranial stimulation of the cortex: magnetic stimulation, bifocal electric stimulation, and unifocal electric stimulation. The primary focus of this comparison is the focality and direction of the electric fields produced. A three- sphere model is used to represent the scalp, skull, and brain. All electric fields are calculated numerically. For magnetic stimulation we consider only a figure-of-eight coil. We find that magnetic stimulation produces the most focal field, while unifocal electric produces the least. Fields produced during magnetic stimulation are parallel to the head surface, while fields produced during electric stimulation have components both parallel and perpendicular to the head surface. The electric field produced by magnetic stimulation is shown to be insensitive to the skull conductivity, while that produced by electric stimulation is very sensitive to it.

20, 33

[Schoen:2008aa] Ingmar Schoen and Peter Fromherz. Extracellular stimulation of mammalian neurons through repetitive activation of Na$^+$ channels by weak capacitive currents on a silicon chip. *J. Neurophysiol*, 100:346–357, 2008.

> **Abstract:** Reliable extracellular stimulation of neuronal activity is the prerequisite for electrical interfacing of cultured networks and brain slices, as well as for neural implants. Safe stimulation must be achieved without damage to the cells. With respect to a future application of highly integrated semiconductor chips, we present an electrophysiological study of capacitive stimulation of mammalian cells in the geometry of adhesion on an insulated titanium dioxide/silicon electrode. We used HEK293 cells with overexpressed NaV1.4 channels and neurons from rat hippocampus. Weak biphasic stimuli of falling and rising voltage ramps were applied in the absence of Faradaic current and electropo- ration. We recorded the response of the intra- and extracellular voltage and evaluated the concomitant polarization of the attached and free cell membranes. Falling ramps efficiently depolarized the central area of the attached membrane. A transient sodium inward current was activated that gave rise to a weak depolarization of the cell on the order of 1 mV. The depolarization could be enhanced step by step by a train of biphasic stimuli until self-excitation of sodium channels set in. We applied the same protocol to cultured rat neurons and found that pulse trains of weak capacitive stimuli were able to elicit action potentials. Our results provide a basis for safe extracellular stimula- tion not only for cultured neurons on insulated semiconductor elec- trodes, but also more generally for metal electrodes in cell culture and brain tissue.

139, 140

[Scholfield:1990aa] C. N. Scholfield. Properties of k-currents in unmyelinated presynaptic axons of brain revealed revealed by extracellular polarisation. *Brain Res*, 507(1):121–8, 1990.

> **Abstract:** Thin pial surface slices of guinea-pig olfactory cortex contain unmyelinated axons derived from the lateral olfactory tract (LOT). The severed ends of the groups of these axons were drawn into a suction electrode to record the currents resulting from propagated action potentials. On stimulating these unmyelinated axons, a tetrodotoxin-sensitive positive current of 22.5 +/- 3.0 nA was recorded by the suction electrode. The positive current was often followed by a small negative current. A 100 mV positive polarisation applied to the suction electrode revealed a large negative after-current (25.8 +/- 3.5 nA). In contrast, the positive current was slightly reduced by the polarisation. The early phases of the negative after-current induced by the electrode polarisation were blocked by 3,4-diaminopyridine, 4-aminopyridine or 2,3-diaminopyridine (in order of potency). The entire negative after-current was blocked by prolonged (3 h) equilibration in a medium containing 3.5 mmol/l Cs and 1.5 mmol/l K. Tetraethylammonium (TEA) or Ba2+ by themselves had little effect. In aminopyridine, the residual negative after-current was blocked by TEA (10 mmol/l) or 1 mmol/l Ba2+. Muscarinic agonists had no effect on these currents. These experiments show that some axonal currents can be revealed by extracellular polarisation and that these axons rely on an 'A' type of current for the rapid repolarisation of the membrane although slower K-channels are present.

125

[Schwan:1956aa] H. P. Schwan and C. F. Kay. Specific resistance of body tissues. *Circ Res*, 4:664–70, 1956.
17

[Schweid:2008aa] L. Schweid, R. J. Rushmore, and A. Valero-Cabre. Cathodal transcranial direct current stimulation on posterior parietal cortex disrupts visuo-spatial processing in the contralateral visual field. *Exp Brain Res*, 186(3):409–17, 2008.

> **Abstract:** Transcranial direct current stimulation (tDCS) has recently undergone a resurgence in popularity as a powerful tool to non-invasively manipulate brain

activity. While tDCS has been used to alter functions tied to primary motor and visual cortices, its impact on extrastriate visual areas involved in visuo-spatial processing has not yet been examined. In the current study, we applied tDCS to the cat visuoparietal (VP) cortex and assayed performance in a paradigm designed to assess the capacity to detect, localize and orient to static targets appearing at different spatial eccentricities within the visual field. Real or sham cathodal tDCS was unilaterally applied to the VP cortex, and orienting performance was assessed during (online), immediately after (offline; Experiments 1 and 2), and 1 or 24 h after the end of the tDCS stimulation (Experiment 2). Performance was compared to baseline data collected immediately prior to stimulation. Real, but not sham, tDCS induced significant decreases in performance for static visual targets presented in the contrastimulated visual hemifield. The behavioral impact of tDCS was most apparent during the online and immediate offline periods. The tDCS effect decayed progressively over time and performance returned to baseline levels approximately 60 min after stimulation. These results are consistent with the effects of both invasive and non-invasive deactivation methods applied to the same brain region, and indicate that tDCS has the potential to modify neuronal activity in extrastriate visual regions and to sculpt brain activity and behavior in normal and neurologically impaired subjects.

128, 129, 343

[Segev:1999aa] Idan Segev and Rober E. Burke. *Methods in Neuronal Modeling*, chapter 3, pages 93–136. MIT Press, 1999. 41

[Selkoe:1994aa] D. J. Selkoe. Cell biology of the amyloid beta-protein precursor and the mechanism of alzheimer's disease. *Annu Rev Cell Biol*, 10:373–403, 1994. 120

[Sgro:1991aa] J. A. Sgro, N. R. Ghatak, P. C. Stanton, R. G. Emerson, and R. Blair. Repetitive high magnetic field stimulation: the effect upon rat brain. *Electroencephalogr Clin Neurophysiol Suppl*, 43:180–5, 1991.

Abstract: The effect on rat brain of a large number of stimulations with a high strength pulsed magnetic field was investigated in 31 rats: 10 naive controls, 10 anesthetized controls, and 11 stimulated and anesthetized rats. An investigational magnetic stimulating device with a circular 5.5 inch diameter stimulating head was used. The stimulating coil was energized by 1000 V, 8000A, 200 microseconds half sine pulses at a rate of 8 Hz. The peak field strength was 3.4 T, and the peak field flux was approximately 53,000 T/sec. Stimulation was performed for 20 min at a rate of 8/stimuli per second, for a total of at least 10,000 stimulations. The rats were sacrificed after 8 days, and their brains were examined using light microscopy with hematoxylin and eosin staining, or electron microscopy. Histological samples were taken from the neocortex, the hippocampus, the basal ganglia, and the cerebellum. No significant changes were seen.

124, 125, 168

[Sharova:2007aa] E. V. Sharova, A. V. Mel'nikov, M. R. Novikova, M. A. Kulikov, T. N. Grechenko, E. D. Shekhter, and A. Y. Zaslavskii. Changes in spontaneous brain bioelectrical activity during transcranial electrical and electromagnetic stimulation. *Neurosci Behav Physiol*, 37(5):451–7, 2007.

Abstract: The systems responses of the brain to therapeutic transcranial electrical and electromagnetic stimulation were studied and the neurophysiological criteria for assessing the efficacy of this treatment were identified using comparative clinical and experimental studies with analysis of spontaneous bioelectrical activity, along with assessment of behavioral and clinical measures. Study groups consisted of six patients with chronic post-traumatic unconscious states during courses of transcranial electrical stimulation and 17 intact Wistar rats subjected to transcranial electromagnetic stimulation. A relationship was found between the effects of transcranial stimulation and the initial level of intercenter interactions of brain bioelectrical activity assessed in terms of coherence. Hypersynchronization

of biopotentials, identified as a major element in the reactivity to this type of stimulation, may be of the greatest value in the recovery of patients with cerebral pathology in cases with initially reduced levels of intercenter interactions in the absence of pathologically increased functional connections in the brain.

110, 111, 175, 340

[Shen:2003aa] K. Z. Shen, Z. T. Zhu, A. Munhall, and S. W. Johnson. Synaptic plasticity in rat subthalamic nucleus induced by high-frequency stimulation. *Synapse*, 50(4):314–9, 2003.

Abstract: The technique of deep brain stimulation (DBS) has become a preferred surgical choice for the treatment of advanced Parkinson's disease. The subthalamic nucleus (STN) is presently the most promising target for such DBS. In this study, whole-cell patch-clamp recordings were made from 46 STN neurons in rat brain slices to examine the effect of high-frequency stimulation (HFS) of the STN on glutamatergic synaptic transmission in STN neurons. HFS, consisting of trains of stimuli at a frequency of 100 Hz for 1 min, produced three types of synaptic plasticity in 17 STN neurons. First, HFS of the STN induced short-term potentiation (STP) of evoked postsynaptic current (EPSC) amplitude in four neurons. STP was associated with a reduction in the EPSC paired-pulse ratio, suggesting a presynaptic site of action. Second, HFS of the STN generated long-term potentiation (LTP) of EPSC amplitude in eight neurons. Although the EPSC paired-pulse ratio was reduced transiently in the first 2 min following HFS, ratios measured 6-20 min after HFS were unchanged from control. This suggests that LTP is maintained by a postsynaptic mechanism. Third, HFS produced long-term depression (LTD) of EPSC amplitude in five STN neurons. LTD was associated with a significant increase in EPSC paired-pulse ratios, indicating a presynaptic site of action. These results suggest that HFS can produce long-term changes in the efficacy of synaptic transmission in the STN. HFS-induced synaptic plasticity might be one mechanism underlying the effectiveness of DBS in the STN as a treatment of advanced Parkinson's disease.

103

[Shulgin:1995aa] Boris Shulgin and et al. Mean switching frequency locking in stochastic bistable systems driven by a periodic force. *Physical Review Letters*, 75(23):4157–4160, 1995.

Abstract: The nonlinear response of noisy bistable systems driven by a strong amplitude-periodic force is investigated by physical experiment. The new phenomenon of locking of the mean switching frequency between states of a bistable system is found. It is shown that there is an interval of noise intensities in which the mean switching frequency remains constant and coincides with the frequency of the external periodic force. The region on the parameter plane "noise intensity-amplitude of periodic excitation" which corresponds to this phenomenon is similar to the synchronization (phase locking) region (Arnold's tongue) in classical oscillatory systems

134

[Silberstein:1995aa] R.B. Silberstein and et al. Steady-state visually evoked potential topography during the wisconsin card sorting task. *Electroencephalography and Clinical Neurophysiology*, 96:24–35, 1995.

Abstract: This paper describes, for the first time, changes in steady-state visually evoked potential (SSVEP) topography associated with the performance of a computerised version of the Wisconsin card sort test (WCS). The SSVEP was recorded from 64 scalp sites and was elicited by a 13 Hz spatially uniform visual flicker presented continuously while 16 subjects performed the WCS. In the WCS, the sort criterion was automatically changed after subjects had sorted 10 cards correctly. Feedback on the 11th card always constituted a cue for a change in the sort criterion. It was found that in the l-2 set interval after the occurrence of the cue to change sort criterion, the prefrontal, central and right parieto-temporal regions showed a pronounced attenuation in SSVEP amplitude and an increase in

phase lag. These changes, interpreted as an increase in regional cortical activity, are not apparent in the equivalent portions of the WCS when the sort criterion does not need to be changed. These results indicate that the levels of prefrontal and right parieto-temporal activity varied during the performance of the WCS, peaking at the times a change in sort criterion was required.

136

[Smythe:1989aa] W.R. Smythe. *Static and dynamic electricity*. Taylor & Francis, 1989. 25

[Somogyi:1998aa] P. Somogyi, G. Tamas, R. Lujan, and E. H. Buhl. Salient features of synaptic organisation in the cerebral cortex. *Brain Res Brain Res Rev*, 26(2-3):113–35, 1998.

Abstract: The neuronal and synaptic organisation of the cerebral cortex appears exceedingly complex, and the definition of a basic cortical circuit in terms of defined classes of cells and connections is necessary to facilitate progress of its analysis. During the last two decades quantitative studies of the synaptic connectivity of identified cortical neurones and their molecular dissection revealed a number of general rules that apply to all areas of cortex. In this review, first the precise location of postsynaptic GABA and glutamate receptors is examined at cortical synapses, in order to define the site of synaptic interactions. It is argued that, due to the exclusion of G protein-coupled receptors from the postsynaptic density, the presence of extrasynaptic receptors and the molecular compartmentalisation of the postsynaptic membrane, the synapse should include membrane areas beyond the membrane specialisation. Subsequently, the following organisational principles are examined: 1. The cerebral cortex consists of: (i) a large population of principal neurones reciprocally connected to the thalamus and to each other via axon collaterals releasing excitatory amino acids, and, (ii) a smaller population of mainly local circuit GABAergic neurones. 2. Differential reciprocal connections are also formed amongst GABAergic neurones. 3. All extrinsic and intracortical glutamatergic pathways terminate on both the principal and the GABAergic neurones, differentially weighted according to the pathway. 4. Synapses of multiple sets of glutamatergic and GABAergic afferents subdivide the surface of cortical neurones and are often co-aligned on the dendritic domain. 5. A unique feature of the cortex is the GABAergic axo-axonic cell, influencing principal cells through GABAA receptors at synapses located exclusively on the axon initial segment. The analysis of these salient features of connectivity has revealed a remarkably selective array of connections, yet a highly adaptable design of the basic circuit emerges when comparisons are made between cortical areas or layers. The basic circuit is most obvious in the hippocampus where a relatively homogeneous set of spatially aligned principal cells allows an easy visualization of the organisational rules. Those principles which have been examined in the isocortex proved to be identical or very similar. In the isocortex, the basic circuit, scaled to specific requirements, is repeated in each layer. As multiple sets of output neurones evolved, requiring subtly different needs for their inputs, the basic circuit may be superimposed several times in the same layer. Tangential intralaminar connections in both the hippocampus and isocortex also connect output neurones with similar properties, as best seen in the patchy connections in the isocortex. The additional radial superposition of several laminae of distinct sets of output neurones, each representing and supported by its basic circuit, requires a co-ordination of their activity that is mediated by highly selective interlaminar connections, involving both the GABAergic and the excitatory amino acid releasing neurones. The remarkable specificity in the geometry of cells and the selectivity in placement of neurotransmitter receptors and synapses on their surface, strongly suggest a predominant role for time in the coding of information, but this does not exclude an important role also for the rate of action potential discharge in cortical representation of information.

60

[Spellman:2008aa] T. Spellman, S. M. McClintock, H. Terrace, B. Luber, M. M. Husain, and S. H. Lisanby. Differential effects of high-dose magnetic seizure therapy and electroconvulsive shock on cognitive function. *Biol Psychiatry*, 63(12):1163–70, 2008.

Abstract: BACKGROUND: Magnetic seizure therapy (MST) is under investigation as an alternative form of convulsive therapy that induces more focal seizures and spares cortical regions involved in memory. With a newly expanded version of the Columbia University Primate Cognitive Profile, we compared the cognitive effects of high-dose MST delivered at 100 Hz (6 x seizure threshold) with electroconvulsive shock (ECS) delivered at 2.5 x seizure threshold. METHODS: Daily high-dose MST, ECS, and sham (anesthesia-only) were administered for 4 weeks each in a within-subject crossover design. Rhesus macaques (n = 3) were trained on five cognitive tasks assessing automatic memory, anterograde learning and memory, combined anterograde and retrograde simultaneous chaining, and spatial and serial working memory. Acutely after each intervention, monkeys were tested on the cognitive battery twice daily, separated by a 3-hour retention interval. RESULTS: Subjects were slower to complete criterion tasks (p values ¡ .0001) after ECS, compared with sham and high-dose MST. Moreover, time to task-completion after high-dose MST did not differ from sham. Of six measures of accuracy, treatment effects were found in four; in all of these, ECS but not MST fared worse than sham. On all accuracy and time to completion measurements, subjects performed as well after high-dose MST as subjects from a previous study on moderate-dose MST. CONCLUSIONS: These findings provide evidence that high-dose MST results in benign acute cognitive side-effect profile relative to ECS and are in line with our previous studies.

118

[Stacey:2000aa] William C. Stacey and Dominique M. Durand. Stochastic resonance improves signal detection in hippocampal ca1 neurons. *J. Neurophysiol*, 83:1394–1402, 2000.

Abstract: Stochastic resonance (SR) is a tems whereby the introduction of noise enhances the detection of a subthreshold signal for a certain range of noise intensity. The nonlinear threshold detection mechanism that neurons employ and the noisy environment in which they reside makes it likely that SR plays a role in neural signal detection. Although the role of SR in sensory neural systems has been studied extensively, its role in central neurons is unknown. In many central neurons, such as the hippocampal CA1 cell, very large dendritic trees are responsible for detecting neural input in a noisy environment. Attenuation due to the electrotonic length of these trees is significant, suggesting that a method other than passive summation is necessary if signals at the distal ends of the tree are to be detected. The hypothesis that SR plays an important role in the detection of distal synaptic inputs first was tested in a computer simulation of a CA1 cell and then verified with in vitro rat hippocampal slices. The results clearly showed that SR can enhance signal detection in CA1 hippocampal cells. Moreover, high levels of noise were found to equalize detection of synaptic signals received at varying positions on the dendritic tree. The amount of noise needed to evoke the effect is compared with physiological noise in slices and in vivo.

140

[Stecker:2005aa] M. M. Stecker. Transcranial electric stimulation of motor pathways: a theoretical analysis. *Comput Biol Med*, 35(2):133–55, 2005.

Abstract: The response to transcranial electrical stimulation of the brain is an important means of assessing motor pathways in the anesthetized patient. The purposes of this study were to elucidate the pattern of axonal excitation produced by transcranial stimulation and to demonstrate how this pattern is affected by changes in the conductivity or geometry of the skull-CSF-brain complex. To this end, analytic solutions to the problem of electrodes placed on a three shell spherical model were obtained under constant current conditions. The potentials, currents and fields generated were computed and the "activating function" was computed for an idealized set of radially organized axons in order to estimate the degree of membrane depolarization produced by stimulation. The degree to which electromagnetic/radiation effects change these solutions was also estimated. The

pattern of stimulation was only slightly dependent on the conductivity and the thickness of the CSF layer. Axons very close to the anode were stimulated with lowest threshold at the brain surface. Axons further away were stimulated with higher thresholds and the point of maximum stimulation moved nearer the center of the sphere. Near the cathode, stimulation was maximal about 5-7 degrees away from the edge of the electrode but the peak magnitude of the activating function was generally 20 times lower than over the anode.

20

[Stefan:2000aa] K. Stefan, E. Kunesch, L. G. Cohen, R. Benecke, and J. Classen. Induction of plasticity in the human motor cortex by paired associative stimulation. *Brain*, 123(3):572–84, 2000.

Abstract: Current models of motor cortical plasticity, developed in studies on experimental animals, emphasize the importance of the conjoint activity of somatosensory afferents and intrinsic motor cortical circuits. The hypothesis that an enduring change in excitability in the cortical output circuitry can be induced in the human motor cortex by a paired- stimulation protocol was tested. Low-frequency median nerve stimulation was paired with transcranial magnetic stimulation (TMS) over the optimal cranial site for stimulating the abductor pollicis brevis muscle (APB). This protocol induced an increase in the amplitudes of the motor evoked potentials (MEPs) in the resting APB as well as a prolongation of the silent period measured in the precontracted APB following TMS; amplitudes of MEPs measured in voluntary contraction remained unchanged. Experiments testing the excitability of spinal motoneurons using F-wave studies and electrical stimulation of the brainstem suggested that the site of the plastic changes was within the motor cortex. The increases in resting amplitudes and silent period duration were conditionally dependent on the timing between the afferent and the magnetic stimulation in that they were present when events elicited by afferent and magnetic stimulation were synchronous at the level of the motor cortex. Plasticity induced by paired stimulation evolved rapidly (within 30 min), was persistent (minimum duration 30-60 min) yet reversible, and was topographically specific. This combination of features and the similarity to properties of induced enduring changes in synaptic efficacy, as elucidated in animal studies, leads us to propose that the induced plasticity may represent a signature of associative long-term potentiation of cortical synapses or closely related neuronal mechanisms in the human cortex.

24

[Stuchly:1980aa] M. A. Stuchly and S. S. Stuchly. Dielectric properties of biological substances - tabulated. *J Microwave Power*, 15(1):19–26, 1980. 16

[Suffczynski:2001aa] P. Suffczynski, S. Kalitzin, G. Pfurtscheller, and F. H. Lopes da Silva. Computational model of thalamo-cortical networks: dynamical control of alpha rhythms in relation to focal attention. *Int J Psychophysiol*, 43(1):25–40, 2001.

Abstract: EEG/MEG rhythmic activities such as alpha rhythms, of the visual or of the somato-sensory cortex, are commonly modulated as subjects perform certain tasks or react to specific stimuli. In general, these activities change depending on extrinsic or intrinsic events. A decrease of the amplitude of alpha rhythmic activity occurring after a given event, which manifests as a decrease of a spectral peak, is called event-related desynchronization (ERD), whereas the inverse is called event-related synchronization (ERS), since it is assumed that the power of a spectral peak is related to the degree of synchrony of the underlying oscillating neuronal populations. An intriguing observation in this respect [Pfurtscheller and Neuper, Neurosci. Lett. 174 (1994) 93-96] was that ERD of alpha rhythms recorded over the central areas was accompanied by ERS, within the same frequency band, recorded over neighboring areas. In case the event was a hand movement, ERD was recorded over the scalp overlying the hand cortical area, whereas ERS was concomitantly recorded over the midline, whereas if the movement was of the foot the opposite

was found. We called this phenomenon 'focal ERD/surround ERS'. The question of how this phenomenon may be generated was approached by means of a computational model of thalamo-cortical networks, that incorporates basic properties of neurons and synaptic interactions. These simulation studies revealed that this antagonistic ERD/ERS phenomenon depends on the functional interaction between the populations of thalamo-cortical cells (TCR) and reticular nucleus cells (RE) and on how this interaction is modulated by cholinergic inputs. An essential feature of this interaction is the existence of cross-talk between different sectors of RE that correspond to distinct sensory modules (e.g. hand, foot). These observations led us to formulate the hypothesis that this basic neurophysiological mechanism can account for the general observation that enhanced attention given to a certain stimulus (the focus) is coupled to inhibition of attention to other stimuli (the surround).

66, 67

[Suffczynski:2006aa] P. Suffczynski, F. H. Lopes da Silva, J. Parra, D. N. Velis, B. M. Bouwman, C. M. van Rijn, P. van Hese, P. Boon, H. Khosravani, M. Derchansky, P. Carlen, and S. Kalitzin. Dynamics of epileptic phenomena determined from statistics of ictal transitions. *IEEE Trans Biomed Eng*, 53(3):524–32, 2006. 66, 67

[Suffczynski:2008aa] P. Suffczynski, S. Kalitzin, F. L. da Silva, J. Parra, D. Velis, and F. Wendling. Active paradigms of seizure anticipation: computer model evidence for necessity of stimulation. *Phys Rev E Stat Nonlin Soft Matter Phys*, 78(5 Pt 1):051917, 2008.

Abstract: It has been shown that the analysis of electroencephalographic (EEG) signals submitted to an appropriate external stimulation (active paradigm) is efficient with respect to anticipating epileptic seizures [S. Kalitzin, Clin. Neurophysiol. 116, 718 (2005)]. To better understand how an active paradigm is able to detect properties of EEG signals by means of which proictal states can be identified, we performed a simulation study using a computational model of seizure generation of a hippocampal network. Applying the active stimulation methodology, we investigated (i) how changes in model parameters that lead to a transition from the normal ongoing EEG to an ictal pattern are reflected in the properties of the simulated EEG output signals and (ii) how the evolution of neuronal excitability towards seizures can be reconstructed from EEG data using an active paradigm, rather than passively, using only ongoing EEG signals. The simulations indicate that a stimulation paradigm combined with appropriate analytical tools, as proposed here, may yield information about the change in excitability that precedes the transition to a seizure. Such information is apparently not fully reflected in the ongoing EEG activity. These findings give strong support to the development and application of active paradigms with the aim of predicting the occurrence of a transition to an epileptic seizure.

68

[Svirskis:1997aa] G. Svirskis, A. Baginskas, J. Hounsgaard, and A. Gutman. Electrotonic measurements by electric field-induced polarization in neurons: theory and experimental estimation. *Biophys J*, 73(6):3004–15, 1997.

Abstract: We present a theory for estimation of the dendritic electrotonic length constant and the membrane time constant from the transmembrane potential (TMP) induced by an applied electric field. The theory is adapted to morphologically defined neurons with homogeneous passive electric properties. Frequency characteristics and transients at the onset and offset of the DC field are considered. Two relations are useful for estimating the electrotonic parameters: 1) steady-state polarization versus the dendritic electrotonic length constant; 2) membrane time constant versus length constant. These relations are monotonic and may provide a unique estimate of the electrotonic parameters for 3D-reconstructed neurons. Equivalent tip-to-tip electrotonic length of the dendritic tree was estimated by measuring the equalization time of the field-induced TMP. For 11 turtle spinal motoneurons, the electrotonic length from tip to tip of the dendrites was in the range

of 1-2.5 lambda, whereas classical estimation using injection of current pulses gave an average dendrite length of 0.9-1.1 lambda. For seven ventral horn interneurons, the estimates were 0.7-2.6 lambda and 0.6-0.9 lambda, respectively. The measurements of the field-induced polarization promise to be a useful addition to the conventional methods using microelectrode stimulation.

60

[Szeligo:1976aa] F. Szeligo. Electrophysiological and behavioral effects of transcortical polarizing current: comparison with the behaviorally determined characteristics of learning. *Brain Res*, 103(3):463–75, 1976.

Abstract: Passage of polarizing current through the cerebral cortex, with the anode at the surface (Anp), produces neurophysiological changes which may be related to those which occur during learning. This relationship was evaluated at the visual cortex of unanesthetized, Sprague-Dawley rats, under a number of experimental conditions, with chronic light flash (LF)-evoked electrocortical response recording and LF-shock avoidance. During experimental treatments electrophysiologically studied animals received either 30 paired presentations of Anp and LF or parametrically equal, unpaired presentations; behaviorally studied animals received either these treatments or 30 presentations of LF alone. Each LF presentation contained 15 LF at the rate of one/sec. Anp presentations consisted of a 15-sec rise of current from 0 to 9 muA/sq.mm, 15 sec of steady 9 muA/sq.mm, and a 15-sec period of current decrease from 9 back to 0 muA/sq.mm. Each presentation was separated from the next by a randomized interval of 45-120 sec. Paired Anp and LF produced large waves (50 muV or greater) in the late negative phase of the evoked response. These waves appeared towards the end of pairings, were evident in recordings made 48 h after pairings and again diminished, but rapidly reappeared when pairings were reintroduced. Anpp and LF pairings also produced a 55in the number of trials needed to reach criterion on the LF-shock avoidance task as compared to the performance of the group treated with LF alone. Unpaired Anp and LF had no discernable electrophysiological or behavioral effects.

128

[Tass:1998aa] P. Tass and et al. Detection of $n{:}m$ phase locking from noisy data: Application to magnetoencephalography. *Physical Review Letters*, 81(15):3291–3294, 1998.

Abstract: We use the concept of phase synchronization for the analysis of noisy nonstationary bivariate data. Phase synchronization is understood in a statistical sense as an existence of preferred values of the phase difference, and two techniques are proposed for a reliable detection of synchronous epochs. These methods are applied to magnetoencephalograms and records of muscle activity of a Parkinsonian patient. We reveal that the temporal evolution of the peripheral tremor rhythms directly reflects the time course of the synchronization of abnormal activity between cortical motor areas.

134

[Taylor:1984aa] C. P. Taylor and F. E. Dudek. Excitation of hippocampal pyramidal cells by an electrical field effect. *J Neurophysiol*, 52(1):126–42, 1984.

Abstract: The effects of electrical fields from antidromic stimulation of CA1 pyramidal cells were studied in slices of rat hippocampus in which chemical synaptic transmission had been blocked by superfusion with physiological solution containing Mn2+ and lowered concentration of Ca2+. Differential voltage recordings were made between two microelectrode positions, on intracellular to a pyramidal cell and the other in the adjacent extracellular space. This technique revealed brief transmembrane depolarizations that occurred synchronously with negative-going extracellular population spikes in the adjacent cell body layer. Glial cells in this region did not exhibit these depolarizations. In some pyramidal cells, alvear stimulation that was too weak to excite the axon of the impaled cell elicited action

potentials, which appeared to arise from transmembrane depolarizations at the soma. When subthreshold transmembrane depolarizations were superimposed on subthreshold depolarizing current pulses, somatic action potentials were generated synchronously with the antidromic population spikes. The depolarizations of pyramidal somata were finely graded with stimulus intensity, were unaffected by polarization of the membrane, and were not occluded by preceding action potentials. The laminar profile of extracellular field potentials perpendicular to the cell body layer was obtained with an array of extracellular recording locations. Numerical techniques of current source-density analysis indicated that at the peak of the somatic population spike, there was an extracellular current sink near pyramidal somata and sources in distal dendritic regions. It is concluded that during population spikes an extracellular electrical field causes currents to flow passively across inactive pyramidal cell membranes, thus depolarizing their somata. The transmembrane depolarizations associated with population spikes would tend to excite and synchronize the population of pyramidal cells.

85, 93, 94, 338

[Taylor:1984ab] C. P. Taylor, K. Krnjevic, and N. Ropert. Facilitation of hippocampal ca3 pyramidal cell firing by electrical fields generated antidromically. *Neuroscience*, 11(1):101–9, 1984.

Abstract: In experiments on rats under urethane anaesthesia–in which the fimbria and hippocampal commissure had been cut previously to eliminate orthodromic inputs–the negative antidromic population spike evoked in CA3 by fimbrial stimulation was measured inside and outside 73 neurons in the stratum pyramidale. Subtraction of the extracellular from the intracellular records showed that on the average 39.2(S.E. 1.93) of the extracellular population spikes appeared as a positive, depolarizing transmembrane potential. Similar measurements in the dendritic zone of CA3, where the extracellular antidromic population spike is positive, revealed a smaller and hyperpolarizing transmembrane potential, whereas presumed neuroglia showed no consistent transmembrane potential in either direction. Further tests demonstrated clear facilitation of individual pyramidal cell firing, synchronous with the antidromic population spike. These observations are consistent with the possibility that, owing to the unusually close packing and regular alignment of the pyramidal neurons, electrical field interactions in CA3 tend to promote synchronized mass discharges.

85, 93, 94, 338

[Terao:2000aa] Y. Terao, Y. Ugawa, R. Hanajima, K. Machii, T. Furubayashi, H. Mochizuki, H. Enomoto, Y. Shiio, H. Uesugi, N. K. Iwata, and I. Kanazawa. Predominant activation of i1-waves from the leg motor area by transcranial magnetic stimulation. *Brain Res*, 859(1):137–46, 2000.

Abstract: We performed transcranial magnetic stimulation (TMS) to elucidate the D- and I-wave components comprising the motor evoked potentials (MEPs) elicited from the leg motor area, especially at near-threshold intensity. Recordings were made from the tibialis anterior muscle using needle electrodes. A figure-of-eight coil was placed so as to induce current in the brain in eight different directions, starting from the posterior-to-anterior direction and rotating it in 45 degrees steps. The latencies were compared with those evoked by transcranial electrical stimulation (TES) and TMS using a double cone coil. Although the latencies of MEPs ranged from D to I3 waves, the most prominent component evoked by TMS at near-threshold intensity represented the I1 wave. With the double cone coil, the elicited peaks always represented I1 waves, and D waves were evoked only at very high stimulus intensities, suggesting a high effectiveness of this coil in inducing I1 waves. Using the figure-of-eight coil, current flowing anteriorly or toward the hemisphere contralateral to the recorded muscle was more effective in eliciting large responses than current flowing posteriorly or toward the ipsilateral hemisphere. The effective directions induced I1 waves with the lowest threshold, whereas the less effective directions elicited I1 and I2 waves with a similar frequency. Higher stimulus intensities resulted in concomitant activation of

D through I3 waves with increasing amount of D waves, but still the predominance of I1 waves was apparent. The amount of I waves, especially of I1 waves, was greater than predicted by the hypothesis that TMS over the leg motor area activates the output cells directly, but rather suggests predominant transsynaptic activation. The results accord with those of recent human epidural recordings.

62

[Terney:2008aa] Daniellla Terney and et al. Increasing human brain excitability by transcranial high-frequency random noise stimulation. *The Journal of Neuroscience*, 28(52):14147–14155, 2008.

Abstract: For >20 years, noninvasive transcranial stimulation techniques like repetitive transcranial magnetic stimulation (rTMS) and direct current stimulation (tDCS) have been used to induce neuroplastic-like effects in the human cortex, leading to the activity-dependent modification of synaptic transmission. Here, we introduce a novel method of electrical stimulation: transcranial random noise stimula- tion (tRNS), whereby a random electrical oscillation spectrum is applied over the motor cortex. tRNS induces consistent excitability increases lasting 60 min after stimulation. These effects have been observed in 80 subjects through both physiological measures and behavioral tasks. Higher frequencies (100 − 640 Hz) appear to be responsible for generating this excitability increase, an effect that may be attributed to the repeated opening of Na^+ channels. In terms of efficacy tRNS appears to possess at least the same therapeutic potential as rTMS/tDCS in diseases such as depression, while furthermore avoiding the constraint of current flow direction sensitivity characteristic of tDCS.

22, 45, 139, 140

[Terzuolo:1956aa] C. A. Terzuolo and T. H. Bullock. Measurement of imposed voltage gradient adequate to modulate neuronal firing. *Proc Natl Acad Sci U S A*, 42(9):687–94, 1956. 87

[Thielscher:2002aa] A Thielscher and T Kammer. Linking physics with physiology in tms: a sphere field model to determine the cortical stimulation site in tms. *Neuroimage*, 17(3):1117–30, 2002.

Abstract: A fundamental problem of transcranial magnetic stimulation (TMS) is determining the site and size of the stimulated cortical area. In the motor system, the most common procedure for this is motor mapping. The obtained two-dimensional distribution of coil positions with associated muscle responses is used to calculate a center of gravity on the skull. However, even in motor mapping the exact stimulation site on the cortex is not known and only rough estimates of its size are possible. We report a new method which combines physiological measurements with a physical model used to predict the electric field induced by the TMS coil. In four subjects motor responses in a small hand muscle were mapped with 9-13 stimulation sites at the head perpendicular to the central sulcus in order to keep the induced current direction constant in a given cortical region of interest. Input-output functions from these head locations were used to determine stimulator intensities that elicit half-maximal muscle responses. Based on these stimulator intensities the field distribution on the individual cortical surface was calculated as rendered from anatomical MR data. The region on the cortical surface in which the different stimulation sites produced the same electric field strength (minimal variance, 4.2 +/- 0.8all subjects, it was located at the lateral part of the hand knob in the motor cortex. Comparisons of model calculations with the solutions obtained in this manner reveal that the stimulated cortex area innervating the target muscle is substantially smaller than the size of the electric field induced by the coil. Our results help to resolve fundamental questions raised by motor mapping studies as well as motor threshold measurements.

26, 28

[Thielscher:2004aa] A. Thielscher and T. Kammer. Electric field properties of two commercial figure-8 coils in tms: calculation of focality and efficiency. *Clin Neurophysiol*, 115(7):1697–708, 2004.

Abstract: Objective: To compare two commonly used TMS coils, namely the Medtronic MC-B70 double coil and the Magstim 70 mm double coil, with respect to their electric field distributions induced on the cortex. Methods: Electric field properties are calculated on a hemisphere representing the cortex using a spherical head model. The coil designs are characterised using several parameters, such as focality, efficiency and stimulation depth. Results: Medtronic and Magstim coils exhibit similar focality values and stimulation depths, despite very different coil designs. However, the Medtronic coil is about 1.2 times more efficient compared to the Magstim coil. This difference corresponds to different motor and visual phosphene thresholds obtained in previous physiological studies, thereby validating the chosen coil modelling approach. Focality of the Medtronic coil changed less with varying coil-cortex distance compared to the Magstim coil, whereas both coils exhibited similar dependencies on changes in cortex radius. Conclusions: The similar values for focality and stimulation depth indicate that both coil types should evoke similar physiological effects when adjusting for the different efficiencies. The different physiological thresholds of the two coils can be traced back to differences in coil design. Ideally, focality should depend neither on coil-cortex distance nor on cortex radius in order to allow for an inter-subject comparability. In particular, in motor mapping experiments the size of the resulting maps is affected by these two parameters. Consequently, they are at least partially the cause of the variability across subjects seen in these experiments.

27

[Thompson:2001aa] A. Richard Thompson and et al. *Interferometry and synthesis in radio astronomy*. Wiley-Interscience, May 2, 2001 2001. 133

[Thomson:1997aa] A. M. Thomson and J. Deuchars. Synaptic interactions in neocortical local circuits: dual intracellular recordings in vitro. *Cereb Cortex*, 7(6):510–22, 1997.

Abstract: Properties of local synaptic connections in neocortex, studied with dual intracellular recordings in vitro and correlated with cell and synaptic morphology are summarized. The different durations and sensitivities to somatic membrane potential of pyramid-pyramid excitatory postsynaptic potentials (EPSPs) apparently reflect the positions of the synapses on the postsynaptic dendrites. Their time-, frequency- and voltage-dependent properties enable supra-linear summation of several low-frequency inputs arising in the same dendritic region, even if only loosely coincident, but they depress during repetitive firing in any one input. Pyramidal input to classical fast spiking and low threshold spiking interneurones are strikingly different. Here low presynaptic firing rates results in many transmission failures. EPSPs are brief and inputs must be near coincident for summation. However, these synapses display pronounced. frequency-dependent, incrementing facilitation at higher presynaptic frequencies. Once initiated by a brief high-frequency burst, this facilitation is maintained at lower frequencies. GABAA receptor-mediated inhibitory postsynaptic potentials (IPSPs) arising proximally are of very different durations depending on the type of interneurone activated and can prevent and subsequently synchronize firing in their many postsynaptic partners with very different delays (eg. 10-100 ms). Low threshold spiking interneurones, in contrast, generate brief IPSPs only in more distal dendritic regions and have little effect on somatic excitability acting to shunt input distally.

60

[Thomson:2003aa] A. M. Thomson and A. P. Bannister. Interlaminar connections in the neocortex. *Cereb Cortex*, 13(1):5–14, 2003.

Abstract: This review summarizes the local circuit, interlaminar connections in adult mammalian neocortex. These were first demonstrated with anatomical techniques, which indicate some of the exquisite spatial precision present in the circuitry. Details, such as the class(es) of neurons targeted by some of these projections, have begun to be added in studies that combine paired/triple intracellular

recordings with dye-filling of connected neurons. Clear patterns are emerging from these studies, with 'forward' projections from layer 4 to 3 and from 3 to 5 targeting both selected pyramidal cells and interneurons, while 'back' projections from layer 5 to 3 and from 3 to 4 target only interneurons. To place these data in a wider context, the major afferent inputs to and efferent outputs from each of the layers are discussed first.

60

[Tofts:1990aa]   P. S. Tofts. The distribution of induced currents in magnetic stimulation of the nervous system. *Phys Med Biol*, 35(8):1119–28., 1990.

Abstract: Magnetic stimulation of the nervous system is being used as an alternative to electrical stimulation, principally because it is painless. The spatial distribution of induced currents from the stimulating coil is calculated from a computer model with graphical output. Two configurations of a plane circular coil are considered: parallel to the tissue surface and perpendicular to the surface. The surface is assumed planar and infinite in extent. The tissue is modelled as a uniform, isotropic volume conductor. A quasi-static approximation is made in calculating the electric field. Maps of current density, J, as a function of position, including depth, are shown. In both configurations, J is always parallel to the surface, and is maximum at the surface. There is no perpendicular (vertical) current. For a one-turn 10 cm diameter coil, spaced 1 cm from conducting tissue and parallel to it, with rate of change of current 10(8) A s(-1), Jmax = 6.8 A m(-2) (assuming conductivity 0.2 omega -1 m(-1)). In the perpendicular configuration Jmax = 4.1 A m(-2). These results suggest that nerve fibres running parallel to the skin surface are more likely to be stimulated than those running obliquely; and that it is extremely difficult to stimulate nerve fibres running perpendicularly. This model can be used to characterise the performance of other shapes of stimulating coils and the dependence on fibre orientation.

26

[Tranchina:1986aa] D. Tranchina and C. Nicholson. A model for the polarization of neurons by extrinsically applied electric fields. *Biophys J*, 50(6):1139–56, 1986.

Abstract: A model is presented for the subthreshold polarization of a neuron by an applied electric field. It gives insight into how morphological features of a neuron affect its polarizability. The neuronal model consists of one or more extensively branched dendritic trees, a lumped somatic impedance, and a myelinated axon with nodes of Ranvier. The dendritic trees branch according to the 3/2-power rule of Rall, so that each tree has an equivalent cylinder representation. Equations for the membrane potential at the soma and at the nodes of Ranvier, given an arbitrary specified external potential, are derived. The solutions determine the contributions made by the dendritic tree and the axon to the net polarization at the soma. In the case of a spatially constant electric field, both the magnitude and sign of the polarization depend on simple combinations of parameters describing the neuron. One important combination is given by the ratio of internal resistances for longitudinal current spread along the dendritic tree trunk and along the axon. A second is given by the ratio between the DC space constant for the dendritic tree trunk and the distance between nodes of Ranvier in the axon. A third is given by the product of the electric field and the space constant for the trunk of the dendritic tree. When a neuron with a straight axon is subjected to a constant field, the membrane potential decays exponentially with distance from the soma. Thus, the soma seems to be a likely site for action potential initiation when the field is strong enough to elicit suprathreshold polarization. In a simple example, the way in which orientation of the various parts of the neuron affects its polarization is examined. When an axon with a bend is subjected to a spatially constant field, polarization is focused at the bend, and this is another likely site for action potential initiation.

35

[Trappenberg:2002aa] Thomas P. Trappenberg. *Fundamentals of Computational Neuroscience.* Oxford University Press, 2002. 52

[Traub:1979aa] R. D. Traub. Neocortical pyramidal cells: a model with dendritic calcium conductance reproduces repetitive firing and epileptic behavior. *Brain Res*, 173(2):243–57, 1979. 65

[Traub:1979ab] R. D. Traub and R. Llinas. Hippocampal pyramidal cells: significance of dendritic ionic conductances for neuronal function and epileptogenesis. *J Neurophysiol*, 42(2):476–96, 1979.

> **Abstract:** 1. Starting with published data derived mainly from hippocampal slice preparations, we have used computer-modeling techniques to study hippocampal pyramidal cells (HPCs). 2. The dendrites of the HPC apparently have a short electrotonic length. Calcium spikes are apparently generated by a voltage-dependent mechanism whose kinetics are slow in comparison with those generating sodium spikes of the soma. Inward calcium currents are assumed to trigger a long-lasting potassium conductance. This slow calcium-potassium system, which in our model is located predominantly on the dendrites, provides a heuristic model to describe the mechanism for a) the after-depolarization following an HPC soma (sodium) spike, b) the long afterhyperpolarization following repetitive firing, c) bursts of spikes that sometimes occur after orthodromic or antidromic stimulation, and d) the buildup of the "depolarizing shift" during the strong synaptic input presumed to occur during seizures. 3. Fast prepotentials or d-spikes are shown to arise most probably from dendritic "hot spots" of sodium-regenerative membrane. The limited amplitude and short duration of these prepotentials imply that the hot spots are located on small dendrites. 4. Dendritic electroresponsiveness, first postulated for the HPC by Spencer and Kandel (52), is analyzed quantitatively here and is shown to provide rich integrative possibilities for this cell. Our model suggests that, for these nerve cells, alterations in specific membrane properties, particularly calcium electroresponsiveness, can lead to bursting behavior that resembles epileptogenic neuronal responses.

65

[Traub:1982aa] R. D. Traub. Simulation of intrinsic bursting in ca3 hippocampal neurons. *Neuroscience*, 7(5):1233–42, 1982. 65

[Tsutsumi:2002aa] T. Tsutsumi, M. Fujiki, J. Akiyoshi, Y. Horinouchi, K. Isogawa, S. Hori, and H. Nagayama. Effect of repetitive transcranial magnetic stimulation on forced swimming test. *Prog Neuropsychopharmacol Biol Psychiatry*, 26(1):107–11, 2002.

> **Abstract:** Repetitive transcranial magnetic stimulation (rTMS) and electroconvulsive shock (ECS) have been shown to affect mood in health and disease. Evidence to date has demonstrated an antidepressant potential for rTMS and electroconvulsive therapy (ECT). The present experiment, aimed at comparing the effects of ECS and rTMS in rats, employed one test used for screening of antidepressant activity: the forced swimming test (FST). In this study, the authors investigated whether chronic rTMS influenced active behavior in the rat FST, similar to ECS. Male Wistar rats received rTMS treatment daily, for 10 days as is commonly used for ECT treatment. Control rats received sham treatment by placing the stimulation coil in a perpendicular position to the rat's head. Passing a current through earclip electrodes for 1 s induced ECS. The control animals were treated identically, but current was not applied. The FST was carried out 24 h after the last rTMS or ECS. The immobility time in the FST was not significantly affected by rTMS and ECS for 1 day. The immobility time in the FST was significantly shortened at rTMS and ECS for 10 days. Chronic treatment with rTMS, similar to chronic treatment with ECS, decreased the immobility time in the FST. These results indicate that chronic treatment with rTMS might have antidepressant effect similar to chronic treatment with ECS.

118

[Tsutsumi:2002ab] T. Tsutsumi and et al. Effect of repetitive transcranial magnetic stimulation on forced swimming test. *Prog Neuropsychopharmacol Biol Psychiatry*, 26(1):107–11, 2002.

Abstract: Repetitive transcranial magnetic stimulation (rTMS) and electroconvulsive shock (ECS) have been shown to affect mood in health and disease. Evidence to date has demonstrated an antidepressant potential for rTMS and electroconvulsive therapy (ECT). The present experiment, aimed at comparing the effects of ECS and rTMS in rats, employed one test used for screening of antidepressant activity: the forced swimming test (FST). In this study, the authors investigated whether chronic rTMS influenced active behavior in the rat FST, similar to ECS. Male Wistar rats received rTMS treatment daily, for 10 days as is commonly used for ECT treatment. Control rats received sham treatment by placing the stimulation coil in a perpendicular position to the rat's head. Passing a current through earclip electrodes for 1 s induced ECS. The control animals were treated identically, but current was not applied. The FST was carried out 24 h after the last rTMS or ECS. The immobility time in the FST was not significantly affected by rTMS and ECS for 1 day. The immobility time in the FST was significantly shortened at rTMS and ECS for 10 days. Chronic treatment with rTMS, similar to chronic treatment with ECS, decreased the immobility time in the FST. These results indicate that chronic treatment with rTMS might have antidepressant effect similar to chronic treatment with ECS.

172

[Tuch:2001aa] D. S. Tuch, V. J. Wedeen, A. M. Dale, J. S. George, and J. W. Belliveau. Conductivity tensor mapping of the human brain using diffusion tensor mri. *Proc Natl Acad Sci U S A*, 98(20):11697–11701, 2001.

Abstract: Knowledge of the electrical conductivity properties of excitable tissues is essential for relating the electromagnetic fields generated by the tissue to the underlying electrophysiological currents. Efforts to characterize these endogenous currents from measurements of the associated electromagnetic fields would significantly benefit from the ability to measure the electrical conductivity properties of the tissue noninvasively. Here, using an effective medium approach, we show how the electrical conductivity tensor of tissue can be quantitatively inferred from the water self-diffusion tensor as measured by diffusion tensor magnetic resonance imaging. The effective medium model indicates a strong linear relationship between the conductivity and diffusion tensor eigenvalues (respectively, final sigma and d) in agreement with theoretical bounds and experimental measurements presented here (final sigma/d approximately 0.844 +/- 0.0545 S small middle dots/mm(3), r(2) = 0.945). The extension to other biological transport phenomena is also discussed.

17

[Tunez:2006aa] I. Tunez, R. Drucker-Colin, I. Jimena, F. J. Medina, C. Munoz Mdel, J. Pena, and P. Montilla. Transcranial magnetic stimulation attenuates cell loss and oxidative damage in the striatum induced in the 3-nitropropionic model of huntington's disease. *J Neurochem*, 97(3):619–30, 2006.

Abstract: An investigation was conducted on the effect of transcranial magnetic field stimulation (TMS) on the free radical production and neuronal cell loss produced by 3-nitropropionic acid in rats. The effects of 3-nitropropionic acid were evaluated by examining the following changes in: the quantity of hydroperoxides and total radical-trapping antioxidant potential (TRAP), lipid peroxidation products, protein carbonyl groups, reduced glutathione (GSH) content, glutathione peroxidase (GSH-Px), catalase and succinate dehydrogenase (SDH) activities; total nitrite and cell death [morphological changes, quantification of neuronal loss and lactate dehydrogenase (LDH) levels]. Our results reveal that 3-nitropropionic acid induces oxidative and nitrosative stress in the striatum, prompts cell loss and also shows that TMS prevents the harmful effects induced by the acid. In conclusion, the results show the ability of TMS to modify neuronal response to 3-nitropropionic acid.

120, 170

[Tunez:2006ab] I. Tunez, P. Montilla, M. del Carmen Munoz, F. J. Medina, and R. Drucker-Colin. Effect of transcranial magnetic stimulation on oxidative stress induced by 3-nitropropionic acid in cortical synaptosomes. *Neurosci Res*, 56(1):91–5, 2006.

> **Abstract:** This study evaluates the effect of transcranial magnetic stimulation (TMS; 60 Hz and 0.7 mT) treatment on 3-nitropropionic acid (20 mg/kg i.p./day for 4 days)-induced oxidative stress in cortical synaptosomes of Wistar rats. The oxidative derangement was confirmed by a high level of lipid peroxidation products and protein carbonyls, together with a decreased in reduced glutathione (GSH) content, catalase and GSH-peroxidase (GSH-Px) activities. Additionally, it was observed a reduction in succinate dehydrogenase (SDH) activity. All changes were partially prevented or reversed by administration of TMS. These results show that TMS reduces oxidative stress in cortical synaptosomes, and suggest that TMS may protect neuronal and maintain synaptic integrity.

120, 170

[Tyler:2008aa] William J. Tyler and et al. Remote excitation of neuronal circuits using low-intensity, low-frequency ultrasound. *Plos One*, 3(10), 2008.

> **Abstract:** Possessing the ability to noninvasively elicit brain circuit activity yields immense experimental and therapeutic power. Most currently employed neurostimulation methods rely on the somewhat invasive use of stimulating electrodes or photon- emitting devices. Due to its ability to noninvasively propagate through bone and other tissues in a focused manner, the implementation of ultrasound (US) represents a compelling alternative approach to current neuromodulation strategies. Here, we investigated the influence of low-intensity, low-frequency ultrasound (LILFU) on neuronal activity. By transmitting US waveforms through hippocampal slice cultures and ex vivo mouse brains, we determined LILFU is capable of remotely and noninvasively exciting neurons and network activity. Our results illustrate that LILFU can stimulate electrical activity in neurons by activating voltage-gated sodium channels, as well as voltage-gated calcium channels. The LILFU-induced changes in neuronal activity were sufficient to trigger SNARE-mediated exocytosis and synaptic transmission in hippocampal circuits. Because LILFU can stimulate electrical activity and calcium signaling in neurons as well as central synaptic transmission we conclude US provides a powerful tool for remotely modulating brain circuit activity.

142

[Valero-Cabre:2005aa] A. Valero-Cabre, B. R. Payne, J. Rushmore, S. G. Lomber, and A. Pascual-Leone. Impact of repetitive transcranial magnetic stimulation of the parietal cortex on metabolic brain activity: a 14c-2dg tracing study in the cat. *Exp Brain Res*, 163(1):1–12, 2005.

> **Abstract:** Transcranial magnetic stimulation (TMS) is increasingly utilized in clinical neurology and neuroscience. However, detailed knowledge of the impact and specificity of the effects of TMS on brain activity remains unresolved. We have used 14C-labeled deoxyglucose (14C-2DG) mapping during repetitive TMS (rTMS) of the posterior and inferior parietal cortex in anesthetized cats to study, with exquisite spatial resolution, the local and distant effects of rTMS on brain activity. High-frequency rTMS decreases metabolic activity at the primary site of stimulation with respect to homologue areas in the unstimulated hemisphere. In addition, rTMS induces specific distant effects on cortical and subcortical regions known to receive substantial efferent projections from the stimulated cortex. The magnitude of this distal impact is correlated with the strength of the anatomical projections. Thus, in the anesthetized animal, the impact of rTMS is upon a distributed network of structures connected to the primary site of application.

163, 178

[Valero-Cabre:2007aa] A. Valero-Cabre, B. R. Payne, and A. Pascual-Leone. Opposite impact on 14c-2-deoxyglucose brain metabolism following patterns of high and low frequency repetitive transcranial magnetic stimulation in the posterior parietal cortex. *Exp Brain Res*, 176(4):603–15, 2007.

Abstract: Repetitive transcranial magnetic stimulation (rTMS) appears capable of modulating human cortical excitability beyond the duration of the stimulation train. However, the basis and extent of this "off-line" modulation remains unknown. In a group of anesthetized cats, we applied patterns of real or sham focal rTMS to the visuo-parietal cortex (VP) at high (HF) or low (LF) frequency and recorded brain glucose uptake during (on-line), immediately after (off-line), or 1 h after (late) stimulation. During the on-line period LF and HF rTMS induced a significant relative reduction of (14)C-2DG uptake in the stimulated VP cortex and tightly linked cortical and subcortical structures (e.g. the superficial superior colliculus, the pulvinar, and the LPl nucleus) with respect to homologue areas in the unstimulated hemisphere. During the off-line period HF rTMS induced a significant relative increase in (14)C-2DG uptake in the targeted VP cortex, whereas LF rTMS generated the opposite effect, with only mild network impact. Moderate distributed effects were only recorded after LF rTMS in the posterior thalamic structures. No long lasting cortical or subcortical effects were detected during the late period. Our findings demonstrate opposite modulation of rTMS on local and distant effects along a specific network, depending on the pattern of stimulation. Such effects are demonstrated in the anesthetized animal, ruling out behavioral and non-specific reasons for the differential impact of the stimulation. The findings are consistent with previous differential electrophysiological and behavioral effects of low and high frequency rTMS patterns and provide support to uses of rTMS in neuromodulation.

111

[Van-Harreveld:1963aa] A. Van Harreveld, T. Murphy, and K. W. Nobel. Specific impedance of rabbit's cortical tissue. *Am J Physiol*, 205:203–7, 1963. 18, 19

[Van-Uitert:2003aa] R. Van Uitert, D. Weinstein, and C. Johnson. Volume currents in forward and inverse magnetoencephalographic simulations using realistic head models. *Ann Biomed Eng*, 31(1):21–31, 2003.

Abstract: Volume currents are important for the accurate calculation of magnetoencephalographic (MEG) forward or inverse simulations in realistic head models. We verify the accuracy of our finite element method implementation for MEG simulations by comparing its results for spheres containing dipoles to those obtained from the analytic solution. We then use this finite element method to show that, in an inhomogeneous, nonspherical realistic head model, the magnetic field normal to the MEG detector due to volume currents often has a magnitude on the same order or greater than the magnitude of the normal component of the primary magnetic field from the dipole. We also demonstrate the disparity in forward solutions between a model that employs spheres, one that uses the realistic head and primary currents alone, and a realistic head model that incorporates both primary and volume currents. In forward and inverse MEG simulations using the inhomogeneous realistic model, the results obtained from calculations containing volume currents are more accurate than those derived without considering volume currents.

30

[Vertes:2005aa] R. P. Vertes. Hippocampal theta rhythm: a tag for short-term memory. *Hippocampus*, 15(7):923–35, 2005.

Abstract: The theta rhythm is the largest extracellular synchronous signal that can be recorded from the mammalian brain, and has been strongly implicated in mnemonic functions of the hippocampus. We advance the proposal that the theta rhythm represents a "tag" for short-term memory processing in the hippocampus.

We propose that the hippocampus receives two main types of input, theta from ascending brainstem-diencephalo-septal systems and "information bearing" mainly from thalamocortical and cortical systems. The temporal convergence of activity of these two systems results in the encoding of information in the hippocampus, primarily reaching it via cortical routes. By analogy to processes associated with long-term potentiation (LTP), we suggest that theta represents a strong depolarizing influence on NMDA receptor-containing cells of the hippocampus. The temporal coupling of a theta-induced depolarization and the release of glutamate to these cells from intra- and extrahippocampal sources activates them. This, in turn, initiates processes leading to a (short-term) strengthening of connections between presynaptic ("information bearing") and postsynaptic neurons of the hippocampus. Theta is selectively present in the rat during active exploratory movements. During exploration, a rat continually gathers and updates information about its environment. If this information is temporally coupled to theta (as with the case of locomotion), it becomes temporarily stored in the hippocampus by mechanisms similar to the early phase of LTP (E-LTP). If the exploratory behavior of the rat goes unreinforced, these relatively short-lasting traces (1-3 h) gradually weaken and eventually fade-to be reupdated. On the other hand, if the explorations of the rat lead to rewards (or punishments), additional modulatory inputs to the hippocampus become activated and convert the short-term, theta-dependent memory, into long-term stores.

101

[Vieyra-Reyes:2008aa] P. Vieyra-Reyes, Y. S. Mineur, M. R. Picciotto, I. Tunez, R. Vidaltamayo, and R. Drucker-Colin. Antidepressant-like effects of nicotine and transcranial magnetic stimulation in the olfactory bulbectomy rat model of depression. *Brain Res Bull*, 77(1):13–8, 2008.

Abstract: In this study, we compared the depression-like symptoms induced by olfactory bulbectomy (OBX) in the two inbred Wistar and Long Evans rat strains. We also analyzed the self-regulated oral intake of nicotine in these strains and the effect of nicotine on the depression-like symptoms of olfactory bulbectomy. Furthermore, we compared the antidepressant-like effects of nicotine on Wistar rats to those of transcranial magnetic stimulation (TMS), which has emerged as a therapeutic alternative for depression management. Our results show that Wistar rats develop depression-like symptoms, demonstrated by the forced swim test (FST), 4 weeks after OBX. However, in bulbectomized Long Evans rats these symptoms cannot be assessed due to a higher degree of variability of the swimming behavior of this strain. These results suggest that there are some innate differences in susceptibility to stress between these two rat strains. In Wistar rats, voluntary oral nicotine intake (1.2 mg/(kg day) for 14 days) as well as nicotine administered as a single daily i.p. injection (1.5 mg/(kg day) for 14 days) decrease the depression-like symptoms of OBX. Daily transcranial magnetic stimulation (60 Hz and 0.7 mT for 2h/day for 14 days) also decreases depression-like symptoms but is less effective than nicotine. In conclusion, our results support the idea that there are possible innate differences for depression susceptibility and that nicotine and TMS may be useful in the treatment of this syndrome.

118, 172

[Wagner:2004aa] T. Wagner, M. Gangitano, R. Romero, H. Theoret, M. Kobayashi, D. Anschel, J. Ives, N. Cuffin, D. Schomer, and A. Pascual-Leone. Intracranial measurement of current densities induced by transcranial magnetic stimulation in the human brain. *Neurosci Lett*, 354(2):91–4, 2004.

Abstract: Transcranial magnetic stimulation (TMS) is a non-invasive technique that uses the principle of electromagnetic induction to generate currents in the brain via pulsed magnetic fields. The magnitude of such induced currents is unknown. In this study we measured the TMS induced current densities in a patient with implanted depth electrodes for epilepsy monitoring. A maximum current density of 12 microA/cm(2) was recorded at a depth of 1 cm from scalp surface with the

optimum stimulation orientation used in the experiment and an intensity of 7stim-ulator output. During TMS we recorded relative current variations under different stimulating coil orientations and at different points in the subject's brain. The results were in accordance with current theoretical models. The induced currents decayed with distance form the coil and varied with alterations in coil orienta-tions. These results provide novel insight into the physical and neurophysiological processes of TMS.

28

[Wagner:2004ab] T. A. Wagner, M. Zahn, A. J. Grodzinsky, and A. Pascual-Leone. Three-dimensional head model simulation of transcranial magnetic stimulation. *IEEE Trans Biomed Eng*, 51(9):1586–98, 2004.

Abstract: This paper presents a finite element method used to evaluate the induced current density in a realistic model of the human head exposed to a time varying magnetic field. The tissue electric properties were varied to ascertain their influence on the induced currents. Current density magnitude and vector plots were generated throughout the tissue layers to determine the effects of tissue boundaries on the field. The current density magnitude correlated to the conductivity of the tissue in all the cases tested except where the tissue permittivity was raised to a level to allow for displacement currents. In this case, the permittivity of the tissue was the dominant factor. Current density components normal to the tissue interface were shown to exist in all solutions within the cortex contrary to the predictions of present models that rely on symmetrical geometries. Additionally, modifications in the cortical geometry were shown to perturb the field so that the site of activation could be altered in diseased patient populations. Finally, by varying the tissue permittivity values and the source frequency, we tested the effects of alpha dispersion theories on transcranial magnetic stimulation.

30, 60

[Wagner:2007aa] T. Wagner, F. Fregni, S. Fecteau, A. Grodzinsky, M. Zahn, and A. Pascual-Leone. Tran-scranial direct current stimulation: a computer-based human model study. *Neuroimage*, 35(3):1113–24, 2007.

Abstract: OBJECTIVES: Interest in transcranial direct current stimulation (tDCS) in clinical practice has been growing, however, the knowledge about its efficacy and mechanisms of action remains limited. This paper presents a realis-tic magnetic resonance imaging (MRI)-derived finite element model of currents applied to the human brain during tDCS. EXPERIMENTAL DESIGN: Current density distributions were analyzed in a healthy human head model with varied electrode montages. For each configuration, we calculated the cortical current den-sity distributions. Analogous studies were completed for three pathological models of cortical infarcts. PRINCIPAL OBSERVATIONS: The current density magni-tude maxima injected in the cortex by 1 mA tDCS ranged from 0.77 to 2.00 mA/cm(2). The pathological models revealed that cortical strokes, relative to the non-pathological solutions, can elevate current density maxima and alter their lo-cation. CONCLUSIONS: These results may guide optimized tDCS for application in normal subjects and patients with focal brain lesions.

21, 30, 41, 42, 44, 52, 60

[Wagner:2007ab] Tim Wagner and et al. Noninvasive human brain stimulation. *Annu. Rev. Biomed. Eng.*, 9(19):1–39, 2007.

Abstract: Noninvasive brain stimulation with transcranial magnetic stimulation (TMS) or transcranial direct current stimulation (tDCS) is valuable in research and has potential therapeutic applications in cognitive neuroscience, neurophysiology, psychiatry, and neurology. TMS allows neurostimulation and neuromodulation, while tDCS is a purely neuromodulatory application. TMS and tDCS allow di-

agnostic and interventional neurophysiology applications, and fo- cal neurophar-macology delivery. However, the physics and basic mechanisms of action remain in-completely explored. Following an overview of the history and current applications of noninvasive brain stimulation, we review stimulation device design principles, the electromagnetic and physical foundations of the techniques, and the current knowledge about the electrophysiologic basis of the effects. Finally, we discuss po-tential biomedical and electrical engineering developments that could lead to more effective stimulation devices, better suited for the specific applications.

117, 164, 174

[Walsh:2003aa] V Walsh and Alvaro Pascual-Leone. *Transcranial magnetic stimulation: a neurochronometrics of mind.* MIT Press, 2003. 23

[Wang:1994aa] W. Wang and S. R. Eisenberg. A three-dimensional finite element method for computing magnetically induced currents in tissues. *IEEE Trans Magn*, 30(6):5015–23, 1994. 26

[Wang:1996aa] H. Wang, X. Wang, and H. Scheich. Ltd and ltp induced by transcranial magnetic stimulation in auditory cortex. *Neuroreport*, 7(2):521–5, 1996.

> **Abstract:** Using a system capable of relatively localized and rapidrate transcra-nial magnetic stimulation (rTMS), evoked trains of complex spikes were studied in rodent auditory cortex. Low rate rTMS from 1 to 10Hz produced a frequency-dependent increase in spike rate. Iterations of rTMS resulted in long-term po-tentiation (LTP)-like, and more durable long-term depression (LTD)-like changes in evoked spike rate. These observations generate new perspectives for studying mechanisms of learning and memory non-invasively as well as introducing some caveats for use of rTMS in humans.

114, 167

[Wang:1999aa] H. Wang, X. Wang, W. Wetzel, and H. Scheich. Rapid-rate transcranial magnetic stimula-tion in auditory cortex induces ltp and ltd and impairs discrimination learning of frequency-modulated tones. *Electroencephalogr Clin Neurophysiol Suppl*, 51:361–7, 1999. 174

[Wang:2006aa] W.-T. Wang and et al. Theta-frequency membrane resonance and its ionic mechanisms in rat subicular pyramidal neurons. *Neuroscience*, 140:45–55, 2006.

> **Abstract:** Abstract—The neuron population of the hippocampal forma- tion exhibits oscillatory activity within the theta frequency band (4 –10 Hz), and the intrinsic resonance properties of individual hippocampal neurons contribute to this network oscillation. The subiculum is the pivotal output region of the hippocampal formation and it is involved in many of the physiological and pathological functions of the limbic sys- tem. To study the characteristics and underlying mecha- nisms of resonance activity in subicular pyramidal neurons, we performed whole-cell patch-clamp recordings from these neurons in rat horizontal brain slices. We applied sinusoidal currents with constant amplitudes and linearly increasing frequencies to measure the resonance frequency of subicular pyramidal neurons. We found that the resonance frequency of subicular pyramidal neurons was about 2 Hz at room temperature and 4 – 6 Hz at 32–35 °C. The resonance fre- quency increased at hyperpolarized membrane potentials and decreased at depolarized membrane potentials. We also investigated three sub-threshold currents involved in the res-onance: a slow hyperpolarization-activated cation current; an instantaneously ac-tivating, inwardly rectifying potassium current; and an inwardly persistent sodium current. The ap- plication of ZD7288 abolished the resonance hump, indicat- ing that hyperpolarization-activated cation current generated resonance. The appli-cation of Ba2+ enlarged the resonance hump at hyperpolarized potentials below -80 mV, indicating that inwardly rectifying potassium current attenuated reso-nance. The application of TTX suppressed the resonance at depolarized poten-tials, indicating that persistent sodium cur- rent amplified resonance when neu-rons were depolarized. Thus, there is a theta-frequency resonance mediated by hyper- polarization-activated cation current in subicular pyramidal neurons. This

theta-frequency resonance of individual subicular pyramidal neurons may participate in the population's theta os- cillation and contribute to the functions of the subiculum.

140, 174

[Wang:2006ab] H. Wang, X. Wang, W. Wetzel, and H. Scheich. Rapid-rate transcranial magnetic stimulation of animal auditory cortex impairs short-term but not long-term memory formation. *Eur J Neurosci*, 23(8):2176–84, 2006.

Abstract: Bilateral rapid-rate transcranial magnetic stimulation (rTMS) of gerbil auditory cortex with a miniature coil device was used to study short-term and long-term effects on discrimination learning of frequency-modulated tones. We found previously that directional discrimination of frequency modulation (rising vs. falling) relies on auditory cortex processing and that formation of its memory depends on local protein synthesis. Here we show that, during training over 5 days, certain rTMS regimes contingent on training had differential effects on the time course of learning. When rTMS was applied several times per day, i.e. four blocks of 5 min rTMS each followed 5 min later by a 3-min training block and 15-min intervals between these blocks (experiment A), animals reached a high discrimination performance more slowly over 5 days than did controls. When rTMS preceded only the first two of four training blocks (experiment B), or when prolonged rTMS (20 min) preceded only the first block, or when blocks of experiment A had longer intervals (experiments C and D), no significant day-to-day effects were found. However, in experiment A, and to some extent in experiment B, rTMS reduced the within-session discrimination performance. Nevertheless the animals learned, as demonstrated by a higher performance the next day. Thus, our results indicate that rTMS treatments accumulate over a day but not strongly over successive days. We suggest that rTMS of sensory cortex, as used in our study, affects short-term memory but not long-term memory formation.

117, 174

[Warren:1998aa] R. J. Warren and D. M. Durand. Effects of applied currents on spontaneous epileptiform activity induced by low calcium in the rat hippocampus. *Brain Res*, 806(2):186–95, 1998.

Abstract: It is known that both applied and endogenous electrical fields can modulate neuronal activity. In this study, we have demonstrated that anodic current injections can inhibit spontaneous epileptiform events in the absence of synaptic transmission. Activity was induced with low-Ca2+ (0.2 mM) artificial cerebrospinal fluid (ACSF) and detected with a voltage threshold detector. At the onset of an event, a current was injected into the stratum pyramidale via a tungsten electrode positioned within 150 micron of the recording site. Data was recorded with a glass pipette electrode. The results show that spontaneous epileptiform activity can be fully suppressed by subthreshold anodic currents with an average amplitude of 3.9 microA and a minimum amplitude of 1 microA. In addition, we observed that some events could be blocked by current pulses with shorter durations than the duration of the event itself. The possibility that increased tissue resistance could contribute to the efficacy of the currents was tested by measuring the step-potential increase evoked by anodic current injections. The data show a significant increase in the amplitude of the evoked potential after introduction of a low-Ca2+ medium, suggesting that tissue resistance is increasing. These results indicate that low-amplitude, subthreshold current pulses are sufficient to block epileptiform activity in a low-Ca2+ environment. The increased tissue resistance induced by sustained exposure to a low-Ca2+ medium could contribute to the low current amplitudes required to block the epileptiform events.

95

[Wasserman:2008aa] E Wasserman, CM Epstein, and U Ziemann. *The Oxford handbook of transcranial stimulation*. Oxford University Press, 2008. 23

[Wassermann:1998aa] E. M. Wassermann. Risk and safety of repetitive transcranial magnetic stimulation: report and suggested guidelines from the international workshop on the safety of repetitive transcranial magnetic stimulation, june 5-7, 1996. *Electroencephalogr Clin Neurophysiol*, 108(1):1–16, 1998.

> **Abstract:** Single-pulse transcranial magnetic stimulation (TMS) is a safe and useful tool for investigating various aspects of human neurophysiology, particularly corticospinal function, in health and disease. Repetitive TMS (rTMS), however, is a more powerful and potentially dangerous modality, capable of regionally blocking or facilitating cortical processes. Although there is evidence that rTMS is useful for treating clinical depression, and possibly other brain disorders, it had caused 7 known seizures by 1996 and could have other undesirable effects. In June 1996 a workshop was organized to review the available data on the safety of rTMS and to develop guidelines for its safe use. This article summarizes the workshop's deliberations. In addition to issues of risk and safety, it also addresses the principles and applications of rTMS, nomenclature, and potential therapeutic effects of rTMS. The guidelines for the use of rTMS, which are summarized in an appendix, cover the ethical issues, recommended limits on stimulation parameters, monitoring of subjects (both physiologically and neuropsychologically), expertise and function of the rTMS team, medical and psychosocial management of induced seizures, and contra-indications to rTMS.

31, 120

[Watts:2005aa] J. Watts and A. M. Thomson. Excitatory and inhibitory connections show selectivity in the neocortex. *J Physiol*, 562(Pt 1):89–97, 2005.

> **Abstract:** The cerebral cortex is pivotal in information processing and higher brain function and its laminar structure of six distinct layers, each in receipt of a different constellation of inputs, makes it important to identify connectivity patterns and distinctions between excitatory and inhibitory pathways. The 'feed-forward' projections from layer 4-3 and from 3-5 target pyramidal cells and to lesser degrees interneurones. 'Feedback' projections from layer 5-3 and from 3-4, on the other hand, mainly target interneurones. Understanding the microcircuitry may give some insight into the computation and information processing performed in this brain region.

60

[Weiss:1995aa] S. R. Weiss, X. L. Li, J. B. Rosen, H. Li, T. Heynen, and R. M. Post. Quenching: inhibition of development and expression of amygdala kindled seizures with low frequency stimulation. *Neuroreport*, 6(16):2171–6, 1995.

> **Abstract:** Using low frequency (quenching) stimulation parameters (1 Hz for 15 min), similar to those that induce long-term depression (LTD) in vitro, we attempted to alter amygdala kindling in vivo in rats. Quenching completely blocked the development and progression of after-discharges and seizures in seven of eight animals. In fully kindled animals, once-daily quenching stimulation for one week (without concurrent kindling) suppressed the seizures when kindling stimulation was resumed. These effects of quenching probably resulted from the marked and long-lasting increases in the afterdischarge and seizure thresholds that were observed in these animals. These data indicate that quenching with low frequency electrical stimulation (which does not disrupt ongoing behavior) can have profound and long-lasting effects on seizure development, expression, and thresholds. The ultimate clinical applicability of low frequency stimulation in the treatment of seizures and related neuropsychiatric disorders remains to be explored.

130

[Weiss:1998aa] S. R. Weiss. Quenching revisited: low level direct current inhibits amygdala-kindled seizures. *Exp Neurol*, 154(1):185–92, 1998.

Abstract: We have reported that low frequency stimulation (1 Hz for 15 min), applied after kindling stimulation of the amygdala, inhibited the development and expression of amygdala-kindled seizures, an effect we termed quenching. Subsequently, we discovered that this effect could only be achieved when certain stimulators were used that also emitted a low-level direct current (DC). The studies reported here indicate that DC, applied once daily for 15 min at intensities of 5–15 μA, produced an intensity-related attenuation of kindling development and an increase in the afterdischarge threshold. This effect persisted in some animals for at least 1 month after discontinuation of the DC. In fully kindled animals, a robust increase in seizure threshold and persistent seizure inhibition were also observed using 10 μA of DC administered for 14 days. These results clarify and extend our original findings of a quenching effect; however, the mechanisms by which low level DC induces quenching require further elucidation.

126, 130, 131, 343

[Weitzenfeld:2002aa] A. Weitzenfeld, M. Arbib, and A. Alexander. *The Neural Simulation Language: A System for Brain Modeling.* MIT Press, Cambridge, 2002. 39

[Wendling:2000aa] F. Wendling, J. J. Bellanger, F. Bartolomei, and P. Chauvel. Relevance of nonlinear lumped-parameter models in the analysis of depth-eeg epileptic signals. *Biol Cybern*, 83(4):367–78, 2000.

Abstract: In the field of epilepsy, the analysis of stereoelectroencephalographic (SEEG, intra-cerebral recording) signals with signal processing methods can help to better identify the epileptogenic zone, the area of the brain responsible for triggering seizures, and to better understand its organization. In order to evaluate these methods and to physiologically interpret the results they provide, we developed a model able to produce EEG signals from "organized" networks of neural populations. Starting from a neurophysiologically relevant model initially proposed by Lopes Da Silva et al. [Lopes da Silva FH, Hoek A, Smith H, Zetterberg LH (1974) Kybernetic 15: 27-37] and recently re-designed by Jansen et al. [Jansen BH, Zouridakis G, Brandt ME (1993) Biol Cybern 68: 275 283] the present study demonstrates that this model can be extended to generate spontaneous EEG signals from multiple coupled neural populations. Model parameters related to excitation, inhibition and coupling are then altered to produce epileptiform EEG signals. Results show that the qualitative behavior of the model is realistic; simulated signals resemble those recorded from different brain structures for both inter-ictal and ictal activities. Possible exploitation of simulations in signal processing is illustrated through one example; statistical couplings between both simulated signals and real SEEG signals are estimated using nonlinear regression. Results are compared and show that, through the model, real SEEG signals can be interpreted with the aid of signal processing methods.

66, 67, 70

[Wendling:2002aa] F. Wendling, F. Bartolomei, J. J. Bellanger, and P. Chauvel. Epileptic fast activity can be explained by a model of impaired gabaergic dendritic inhibition. *Eur J Neurosci*, 15(9):1499–508, 2002.

Abstract: This paper focuses on high-frequency (gamma band) EEG activity, the most characteristic electrophysiological pattern in focal seizures of human epilepsy. It starts with recent hypotheses about: (i) the behaviour of inhibitory interneurons in hippocampal or neocortical networks in the generation of gamma frequency oscillations; (ii) the nonuniform alteration of GABAergic inhibition in experimental epilepsy (reduced dendritic inhibition and increased somatic inhibition); and (iii) the possible depression of GABA(A,fast) circuit activity by GABA(A,slow) inhibitory postsynaptic currents. In particular, these hypotheses are introduced in a new computational macroscopic model of EEG activity that includes a physiologically relevant fast inhibitory feedback loop. Results show that strikingly realistic activity is produced by the model when compared to real EEG signals recorded

with intracerebral electrodes. They show that, in the model, the transition from interictal to fast ictal activity is explained by the impairment of dendritic inhibition.

66, 67

[Wendling:2005aa] F. Wendling, A. Hernandez, J. J. Bellanger, P. Chauvel, and F. Bartolomei. Interictal to ictal transition in human temporal lobe epilepsy: insights from a computational model of intracerebral eeg. *J Clin Neurophysiol*, 22(5):343–56, 2005.

> **Abstract:** In human partial epilepsies and in experimental models of chronic and/or acute epilepsy, the role of inhibition and the relationship between the inhibition and excitation and epileptogenesis has long been questioned. Besides experimental methods carried out either in vitro (human or animal tissue) or in vivo (animals), pathophysiologic mechanisms can be approached by direct recording of brain electrical activity in human epilepsy. Indeed, in some clinical presurgical investigation methods like stereoelectroencephalography, intracerebral electrodes are used in patients suffering from drug resistant epilepsy to directly record paroxysmal activities with excellent temporal resolution (in the order of 1 millisecond). The study of neurophysiologic mechanisms underlying such depth-EEG activities is crucial to progress in the understanding of the interictal to ictal transition. In this study, the authors relate electrophysiologic patterns typically observed during the transition from interictal to ictal activity in human mesial temporal lobe epilepsy (MTLE) to mechanisms (at a neuronal population level) involved in seizure generation through a computational model of EEG activity. Intracerebral EEG signals recorded from hippocampus in five patients with MTLE during four periods (during interictal activity, just before seizure onset, during seizure onset, and during ictal activity) were used to identify the three main parameters of a model of hippocampus EEG activity (related to excitation, slow dendritic inhibition and fast somatic inhibition). The identification procedure used optimization algorithms to minimize a spectral distance between real and simulated signals. Results demonstrated that the model generates very realistic signals for automatically identified parameters. They also showed that the transition from interictal to ictal activity cannot be simply explained by an increase in excitation and a decrease in inhibition but rather by time-varying ensemble interactions between pyramidal cells and local interneurons projecting to either their dendritic or perisomatic region (with slow and fast GABAA kinetics). Particularly, during preonset activity, an increasing dendritic GABAergic inhibition compensates a gradually increasing excitation up to a brutal drop at seizure onset when faster oscillations (beta and low gamma band, 15 to 40 Hz) are observed. These faster oscillations are then explained by the model feedback loop between pyramidal cells and interneurons targeting their perisomatic region. These findings obtained from model identification in human temporal lobe epilepsy are in agreement with some results obtained experimentally, either on animal models of epilepsy or on the human epileptic tissue.

66

[Wendling:2008aa] F Wendling and P Chauvel. *Transition to ictal activity in Temporal Lobe Epilepsy: insights from macroscopic models.* in Computational Neuroscience in Epilepsy, Ivan Soltesz and Kevin Staley Eds. Elsevier, 2008.

> **Abstract:** Temporal lobe epilepsy (TLE) is one of the most common forms of partial epilepsy. It is characterized by recurrent seizures originating from one or several areas of the temporal cortex and propagating through interconnected neuronal networks within and outside the temporal lobe. Although there is current evidence that seizures are related to abnormal excessive firing and synchronization of neurons, little is known about the precise basic mechanisms underlying human epileptic seizures and mecha- nisms of transitions from normal to paroxysmal activity. This chapter presents some insights into transition mechanisms to ictal activity in human TLE that can be drawn from a macroscopic modeling approach that developed over the three past decades. The term 'macroscopic' relates to the modeling

level. Indeed, relevant variables in considered models describe the average activity of interconnected subpopulations of principal neurons and interneurons without explicit representation of mechanisms lying at the level of single cells, conversely to biologically-inspired detailed models. Although macroscopic, these models rely on neurophysiological data and have two essential features. First, their parameters relate to excitatory and inhibitory processes taking place in the considered neuronal tissue. Second, the temporal dynamics of their output is analogous to a field activity, allowing for direct comparison with real electroencephalographic signals recorded with intracerebral electrodes (depth-EEG, stereotaxic method) during presurgical evaluation of patients candidate to epilepsy surgery. The chapter provides a historical perspective about macroscopic models and describes their theoretical bases. A model-based interpretation of depth-EEG signals recorded during the transition to ictal activity is illustrated and discussed.

67, 336

[Werhahn:1994aa] K. J. Werhahn, J. K. Fong, B. U. Meyer, A. Priori, J. C. Rothwell, B. L. Day, and P. D. Thompson. The effect of magnetic coil orientation on the latency of surface emg and single motor unit responses in the first dorsal interosseous muscle. *Electroencephalogr Clin Neurophysiol*, 93(2):138–46, 1994.

> **Abstract:** We examined the effect of the orientation of a figure-of-eight coil on the latency of surface electromyographic (EMG) responses and the firing pattern of single motor units evoked in the first dorsal interosseous muscle by transcranial magnetic brain stimulation. Two coil positions were used: the coil held on a parasagittal line either with the induced current in the brain flowing in a postero-anterior direction (PA) or with the current flowing latero-medially (LM). The results were compared with those observed after anodal electrical stimulation. LM stimulation produced surface and single unit responses which occurred 0- 3 msec earlier than PA stimulation. In many cases responses to LM stimulation had the same latency as those produced by anodal electrical stimulation. Responses evoked by LM stimulation were less affected by changes in motor cortical excitability (cortico-cortical inhibition and transcallosal inhibition) than those to PA stimulation. We suggest that LM stimulation can sometimes stimulate corticospinal fibres directly, at or near the same site as anodal stimulation. In contrast, PA stimulation tends to activate corticospinal fibres trans-synaptically. The difference in stimulation sites may make a comparison of PA and LM stimulation a useful method of localising changes in corticospinal excitability to a cortical level.

27

[Wespatat:2004aa] V. Wespatat, F. Tennigkeit, and W. Singer. Phase sensitivity of synaptic modifications in oscillating cells of rat visual cortex. *J Neurosci*, 24(41):9067–75, 2004.

> **Abstract:** Synaptic modifications depend on the amplitude and temporal relations of presynaptic and postsynaptic activation. The interactions among these variables are complex and hard to predict when neurons engage in synchronized high-frequency oscillations in the beta and gamma frequency range, as is often observed during signal processing in the cerebral cortex. Here we investigate in layer II/III pyramidal cells of rat visual cortex slices how synapses change when synchronized, oscillatory multifiber activity impinges on postsynaptic neurons during membrane potential (V(m)) oscillations at 20 and 40 Hz. Synapses underwent long-term potentiation (LTP) when EPSPs coincided with the peaks of the V(m) oscillations but exhibited long-term depression (LTD) when EPSPs coincided with the troughs. The induction of LTP but not of LTD was NMDA receptor dependent, required additional activation of muscarinic receptors in older animals, and persisted in a kainate-driven increased conductance state. Thus, even when neuronal networks engage in high-frequency oscillations, synaptic plasticity remains exquisitely sensitive to the timing of discharges. This is an essential prerequisite for theories which assume that precise synchronization of discharges serves as signature of relatedness in distributed processing.

115

[Wesselink:1999aa] W. A. Wesselink, J. Holsheimer, and H. B. Boom. A model of the electrical behaviour of myelinated sensory nerve fibres based on human data. *Med Biol Eng Comput*, 37(2):228–35, 1999.

> **Abstract:** Calculation of the response of human myelinated sensory nerve fibres to spinal cord stimulation initiated the development of a fibre model based on electrophysiological and morphometric data for human sensory nerve fibres. The model encompasses a mathematical description of the kinetics of the nodal membrane, and a non-linear fibre geometry. Fine tuning of only a few, not well-established parameters was performed by fitting the shape of a propagating action potential and its diameter-dependent propagation velocity. The quantitative behaviour of this model corresponds better to experimentally determined human fibre properties than other mammalian, nonhuman models do. Typical characteristics, such as the shape of the action potential, the propagation velocity and the strength-duration behaviour show a good fit with experimental data. The introduced diameter-dependent parameters did not result in a noticeable diameter dependency of action potential duration and refractory period. The presented model provides an improved tool to analyse the electrical behaviour of human myelinated sensory nerve fibres.

37

[Whittington:2000aa] M. A. Whittington, R. D. Traub, N. Kopell, B. Ermentrout, and E. H. Buhl. Inhibition-based rhythms: experimental and mathematical observations on network dynamics. *Int J Psychophysiol*, 38(3):315–36, 2000. 68

[Wiesenfeld:1995aa] Kurt Wiesenfeld and Frank Moss. Stochastic resonance and the benefits of noise: from ice ages to crayfish and squids. *Nature*, 373:33–36, 1995.

> **Abstract:** Noise in dynamical systems is usually considered a nuisance. But in certain nonlinear systems, including electronic circuits and biological sensory apparatus, the presence of noise can in fact enhance the detection of weak signals. This phenomenon, called stochastic resonance, may find useful application in physical, technological and biomedical contexts.

134

[Wilson:1972aa] H. R. Wilson and J. D. Cowan. Excitatory and inhibitory interactions in localized populations of model neurons. *Biophys J*, 12(1):1–24, 1972. 65

[Wolters:1999aa] C. H. Wolters, R. F. Beckmann, A. Rienacker, and H. Buchner. Comparing regularized and non-regularized nonlinear dipole fit methods: a study in a simulated sulcus structure. *Brain Topogr*, 12(1):3–18, 1999.

> **Abstract:** The inverse problem arising from EEG and MEG is largely under-determined. One strategy to alleviate this problem is the restriction to a limited number of point-like sources, the focal source model. Although the singular value decomposition of the spatio-temporal data gives an estimate of the minimal number of dipoles contributing to the measurement, the exact number is unknown in advance and noise complicates the reconstruction. Classical non-regularized nonlinear dipole fit algorithms do not give an estimate for the correct number because they are not stable with regard to an overestimation of this parameter. Too many sources may only describe noise but can still attain a large magnitude during the inverse procedure and may be indiscernible from the true sources. This paper describes a nonlinear dipole fit reconstruction algorithm with a new regularization approach for the embedded linear problem, automatically controlled by the noise in the data and the condition of the occuring least square problems. The algorithm is stable with regard to source components which "nearly" lie in the kernel of the projection or lead field operator and it thus gives an estimate of the unknown number parameter. EEG simulation studies in a simulated sulcus structure are

carried out for an instantaneous dipole model and spatial resolution in the sulcus and stability of the new method are compared with a classical reconstruction algorithm without regularization.

17

[Wolters:2006aa] C. H. Wolters, A. Anwander, X. Tricoche, D. Weinstein, M. A. Koch, and R. S. Macleod. Influence of tissue conductivity anisotropy on eeg/meg field and return current computation in a realistic head model: A simulation and visualization study using high-resolution finite element modeling. *Neuroimage*, 30(3):813–826, 2006.

> **Abstract:** To achieve a deeper understanding of the brain, scientists, and clinicians use electroencephalography (EEG) and magnetoencephalography (MEG) inverse methods to reconstruct sources in the cortical sheet of the human brain. The influence of structural and electrical anisotropy in both the skull and the white matter on the EEG and MEG source reconstruction is not well understood. In this paper, we report on a study of the sensitivity to tissue anisotropy of the EEG/MEG forward problem for deep and superficial neocortical sources with differing orientation components in an anatomically accurate model of the human head. The goal of the study was to gain insight into the effect of anisotropy of skull and white matter conductivity through the visualization of field distributions, isopotential surfaces, and return current flow and through statistical error measures. One implicit premise of the study is that factors that affect the accuracy of the forward solution will have at least as strong an influence over solutions to the associated inverse problem. Major findings of the study include (1) anisotropic white matter conductivity causes return currents to flow in directions parallel to the white matter fiber tracts; (2) skull anisotropy has a smearing effect on the forward potential computation; and (3) the deeper a source lies and the more it is surrounded by anisotropic tissue, the larger the influence of this anisotropy on the resulting electric and magnetic fields. Therefore, for the EEG, the presence of tissue anisotropy both for the skull and white matter compartment substantially compromises the forward potential computation and as a consequence, the inverse source reconstruction. In contrast, for the MEG, only the anisotropy of the white matter compartment has a significant effect. Finally, return currents with high amplitudes were found in the highly conducting cerebrospinal fluid compartment, underscoring the need for accurate modeling of this space.

30, 31

[Yamada:1995aa] H. Yamada, T. Tamaki, K. Wakano, A. Mikami, and E. E. Transfeldt. Effect of transcranial magnetic stimulation on cerebral function in a monkey model. *Electroencephalogr Clin Neurophysiol*, 97(2):140–4, 1995.

> **Abstract:** The effect of transcranial magnetic stimulation on higher cerebral function was studied using 3 monkeys. They were trained in a delayed response task which required spatial short-term memory. The task was presented by a computer on a cathode-ray tube and results of the delayed response task, which consisted of the percentage of correct choices, reaction time and trial number, were analyzed. For stimulation, small and large round coils were used as well as a figure 8 configuration. Their maximal B-fields were 3.3 T, 1.9 T and 2.4 T, respectively. A total of more than 7000 stimuli were given to each monkey in various patterns. There was no deficit in the delayed response. Further complications such as epileptic seizures were not observed either. In conclusion, transcranial magnetic stimulation does not appear to have any effect on higher cerebral functions in monkeys.

116, 174

[Yamamoto:1966aa] C. Yamamoto and H. McIlwain. Electrical activities in thin sections from the mammalian brain maintained in chemically-defined media in vitro. *J Neurochem*, 13(12):1333–43, 1966. 83

[Yamamoto:1966ab] C. Yamamoto and H. McIlwain. Potentials evoked in vitro in preparations from the mammalian brain. *Nature*, 210(5040):1055–6, 1966. 83

[Yamamoto:1976aa] T. Yamamoto and Y. Yamamoto. Electrical properties of the epidermal stratum corneum. *Med Biol Eng*, 14(2):151–8, 1976. 17

[Yamamoto:1976ab] T. Yamamoto and Y. Yamamoto. Dielectric constant and resistivity of epidermal stratum corneum. *Med Biol Eng*, 14(5):494–500, 1976. 17

[Yan:1991aa] Y. Yan, P. L. Nunez, and R. T. Hart. Finite-element model of the human head: scalp potentials due to dipole sources. *Med Biol Eng Comput*, 29(5):475–81, 1991.

> **Abstract:** Three-dimensional finite-element models provide a method to study the relationship between human scalp potentials and neural current sources inside the brain. A new formulation of dipole-like current sources is developed here. Finite-element analyses based on this formulation are carried out for both a three-concentric-spheres model and a human-head model. Differences in calculated scalp potentials between these two models are studied in the context of the forward and inverse problems in EEG. The effects of the eye orbit structure on surface potential distribution are also studied.

30

[Yankner:1996aa] B. A. Yankner. Mechanisms of neuronal degeneration in alzheimer's disease. *Neuron*, 16(5):921–32, 1996. 120

[Zangen:2005aa] A. Zangen, Y. Roth, B. Voller, and M. Hallett. Transcranial magnetic stimulation of deep brain regions: evidence for efficacy of the h-coil. *Clin Neurophysiol*, 116(4):775–9, 2005.

> **Abstract:** OBJECTIVE: Standard coils used in research and the clinic for non-invasive magnetic stimulation of the human brain are not capable of stimulating deep brain regions directly. As the fields induced by these coils decrease rapidly as a function of depth, only very high intensities would allow functional stimulation of deep brain regions and such intensities would lead to undesirable side effects. We have designed a coil based on numerical simulations and phantom brain measurements that allows stimulation of deeper brain regions, termed the Hesed coil (H-coil). In the present study we tested the efficacy and some safety aspects of the H-coil on healthy volunteers. METHODS: The H-coil was compared to a regular figure-8 coil in 6 healthy volunteers by measuring thresholds for activation of the abductor pollicis brevis (APB) representation in the motor cortex as a function of distance from each of the coils. RESULTS: The rate of decrease in the coil intensity as a function of distance is markedly slower for the H-coil. The motor cortex could be activated by the H-coil at a distance of 5.5cm compared to 2cm with the figure-8 coil. CONCLUSIONS: The present study indicate that the H-coil is likely to have the ability of deep brain stimulation and without the need of increasing the intensity to extreme levels that would cause a much greater stimulation in cortical regions. SIGNIFICANCE: The ability of non-invasive deep brain stimulation potentially opens a wide range of both research and therapeutic applications.

27

[Zavaglia:2006aa] M. Zavaglia, L. Astolfi, F. Babiloni, and M. Ursino. A neural mass model for the simulation of cortical activity estimated from high resolution eeg during cognitive or motor tasks. *J Neurosci Methods*, 157(2):317–29, 2006.

> **Abstract:** Neural mass models have been used for many years to study the macroscopic dynamics of neural populations in a simple and computationally inexpensive way. In this paper, we modified a model proposed by Wendling et al. [Wendling F, Bartolomei F, Bellanger JJ, Chauvel P. Epileptic fast activity can be explained by a model of impaired GABAergic dendritic inhibition. Eur J Neurosci 2002;15:1499-508] to simulate EEG power spectral density (PSD) in some regions of interest (ROIs) during simple tasks (finger movement or working memory tests). The work consists of two subsequent stages: (1) in the first we evaluated the role of some model parameters (i.e., average gain of synapses and their time constants) in affecting power spectral density. This analysis confirmed the possibility to simulate

various EEG rhythms (in the alpha, beta and gamma frequency ranges) by modifying just the time constants of the synapses. The position of the individual rhythms (i.e., the corresponding peaks in the PSD) can be finely tuned acting on the average gain of fast inhibitory synapses. This analysis suggested that a single neural mass model produces a unimodal spectrum, which can be finely adjusted, but cannot mimic the overall complexity of EEG in an entire cortical area. (2) Hence, in the second stage we built a model of a ROI by combining three neural mass models arranged in parallel. With this model, and using an automatic fitting procedure, we carefully reproduced the PSD of cortical EEG in several ROIs during finger movement, and their temporal changes during a working memory task, by estimating nine parameters. The estimated parameters represent the excitation of each population (mean value and variance of exogenous input noise) and the average gain of fast inhibitory synapses. Cortical EEGs were computed with an inverse propagation algorithm, starting from measurement performed with a high number of electrodes on the scalp (46-96). Results show that the proposed model is able to mimic PSD of cortical activity acting on a few parameters, which represent external activation and short-time synaptic changes. This information may be exploited to reach a quantitative summary of electrical activity in ROIs during a task, and to derive information on connectivity, starting from non-invasive EEG measurements.

66

[Zetterberg:1978aa] L. H. Zetterberg, L. Kristiansson, and K. Mossberg. Performance of a model for a local neuron population. *Biol Cybern*, 31(1):15–26, 1978.

Abstract: A model of a local neuron population is considered that contains three subsets of neurons, one main excitatory subset, an auxiliary excitatory subset and an inhibitory subset. They are connected in one positive and one negative feedback loop, each containing linear dynamic and nonlinear static elements. The network also allows for a positive linear feedback loop. The behaviour of this network is studied for sinusoidal and white noise inputs. First steady state conditions are investigated and with this as starting point the linearized network is defined and conditions for stability is discovered. With white noise as input the stable network produces rhythmic activity whose spectral properties are investigated for various input levels. With a mean input of a certain level the network becomes unstable and the characteristics of these limit cycles are investigated in terms of occurence and amplitude. An electronic model has been built to study more closely the waveforms under both stable and unstable conditions. It is shown to produce signals that resemble EEG background activity and certain types of paroxysmal activity, in particular spikes.

66

[Zheng:1984aa] E. Zheng, S. Shao, and J. G. Webster. Impedance of skeletal muscle from 1 hz to 1 mhz. *IEEE Trans Biomed Eng*, 31(6):477–81, 1984. 17

[Ziemann:1996aa] U. Ziemann, J. C. Rothwell, and M. C. Ridding. Interaction between intracortical inhibition and facilitation in human motor cortex. *J Physiol*, 496 (Pt 3):873–81, 1996.

Abstract: 1. In seven normal subjects, subthreshold transcranial magnetic conditioning stimuli (using a figure-of-eight coil) were applied over the motor cortex in order to evoke activity in intracortical neuronal circuits. The net effect on cortical excitability was evaluated by measuring the effect on the size of EMG responses elicited in the abductor digiti minimi (ADM) muscle by a subsequent suprathreshold test stimulus. 2. A single conditioning stimulus suppressed the size of the test response at interstimulus intervals (ISIs) of 1-4 ms whereas the response was facilitated at ISIs of 6-20 ms. The facilitation could be augmented if pairs of conditioning stimuli were given. 3. Inhibition and facilitation appeared to have separate mechanisms. The threshold for inhibition (0.7 active motor threshold) was slightly lower than that for facilitation (0.8 active threshold). Similarly, the inhibitory effect was independent of the direction of current flow induced in the cortex by the

conditioning shock, whereas facilitation was maximal with posterior-anterior currents and minimal with lateromedial current. 4. Direct corticospinal effects were probably not responsible for the results since facilitation of cortical test responses could be produced by conditioning stimuli which had no effect on the amplitude of H reflexes elicited in active ADM muscle. 5. Inhibition and facilitation appeared to interact in a roughly linear manner, consistent with separate inputs to a common neurone. 6. We suggest that subthreshold transcranial magnetic stimulation is capable of activating separate populations of excitatory and inhibitory interneurones in the motor cortex.

62

[Ziemann:1998aa] U. Ziemann, B. J. Steinhoff, F. Tergau, and W. Paulus. Transcranial magnetic stimulation: its current role in epilepsy research. *Epilepsy Res*, 30(1):11–30, 1998.

Abstract: This paper reviews the current role of transcranial magnetic stimulation (TMS) in epilepsy research. After a brief introduction to the technical principles, the physiology and the safety aspects of TMS, emphasis is put on how human cortex excitability can be assessed by TMS and how this may improve our understanding of pathophysiological mechanisms in epilepsy and the mode of action of antiepileptic drugs (AEDs). Also, potential therapeutical applications of TMS are reviewed. For all aspects of this paper, a clear distinction was made between single-/paired-pulse TMS and repetitive TMS, since these two techniques have fundamentally different scopes and applications.

62

[Ziemann:1998ac] U. Ziemann, F. Tergau, E. M. Wassermann, S. Wischer, J. Hildebrandt, and W. Paulus. Demonstration of facilitatory i wave interaction in the human motor cortex by paired transcranial magnetic stimulation. *J Physiol*, 511 (Pt 1):181–90, 1998.

Abstract: 1. Transcranial magnetic stimulation (TMS) of the human motor cortex results in multiple discharges (D and I waves) in the corticospinal tract. We tested whether these volleys can be explored non-invasively with paired TMS. The intensity of the first stimulus (S1) was set to produce a motor-evoked potential (MEP) of 1 mV in the resting contralateral abductor digiti minimi (ADM) muscle; the second stimulus (S2) was set to 90 1.1-1.5, 2.3-2.9 and 4.1-4.4 ms the MEP elicited by S1 plus S2 was larger than that produced by S1 alone. 2. Varying the S1 intensity between 70 and 130 threshold showed that the threshold for the first MEP peak was ¡= 70 resting motor threshold. The second and third MEP peaks appeared only at higher S1 intensities. The latency of all peaks decreased with increasing S1 intensity. 3. Varying the S2 intensity with S1 held constant to produce a MEP of 1 mV on its own showed that the amplitude of all MEP peaks increased with S2 intensity, but that their timing remained unchanged. 4. Paired TMS in the active ADM (S1 clearly suprathreshold, S2 just above threshold; interstimulus interval, 1 ms) produced strong MEP facilitation. The onset of this facilitation occurred later by about 1.5 ms than the onset of the MEP evoked by S2 alone. No MEP facilitation was seen if the magnetic S2 was replaced by anodal or cathodal transcranial electrical stimulation. 5. It is concluded that the MEP facilitation after paired TMS, at least for the first MEP peak, is due to facilitatory interaction between I waves, and takes place in the motor cortex at or upstream from the corticospinal neurone.

107

[Zimmermann:1996aa] K. P. Zimmermann and R. K. Simpson. "slinky" coils for neuromagnetic stimulation. *Electroencephalogr Clin Neurophysiol*, 101(2):145–52, 1996.

Abstract: Future advances in neuromagnetic stimulation depend significantly on the design of coils with improved focality. Although in the absence of internal current sources, no true focusing of magnetically induced currents is possible, improvements in the focality of current concentrations passing through an area of

biologic tissue are achievable through variations of the shape, orientation and size of neuromagnetic stimulating coils. The "butterfly" and the "4-leaf" coils are two examples of planar designs which achieve improved focality through centralization of the maximum coil current and peripheral distribution of the return currents. We introduce the "slinky" coil design as a 3-dimensional generalization of the principle of peripheral distribution of return currents and demonstrate its advantages over planar designs.

27

[Zyss:1997aa] T. Zyss, Z. Gorka, M. Kowalska, and J. Vetulani. Preliminary comparison of behavioral and biochemical effects of chronic transcranial magnetic stimulation and electroconvulsive shock in the rat. *Biol Psychiatry*, 42(10):920–4, 1997.

> **Abstract:** To confirm the assumption that repetitive rapid-rate transcranial magnetic stimulation (TMS) induces the functional and structural changes analogous to those which are evoked during electroconvulsive shock (ECS), we compared now the effects of treatments with TMS and ECS on the behavioral responses in rats. We also tested the reactivity of the cyclic adenosine monophosphate (AMP) generating system in cerebral cortical slices. TMS similarly to ECS shortened the immobility time in the forced swimming test and produced a depression of responsiveness of the noradrenaline-stimulated cyclic AMP generating system, although the significance of the latter effect was borderline. In contrast to ECT, TMS produced no such immediate behavioral effects as analgesia and depression of the early phase of locomotor activity. The data suggest that TMS produces in rats some responses that are regarded as predictive for antidepressant activity, similar to those produced by ECS, but less adverse effects.

118, 171

[Zyss:1999aa] T. Zyss, J. Mamczarz, A. Roman, and J. Vetulani. Comparison of effectiveness of two schedules of rapid transcranial magnetic stimulation on enhancement of responsiveness to apomorphine. *Pol J Pharmacol*, 51(4):363–6, 1999.

> **Abstract:** Locomotor response to apomorphine (0.5 mg/kg s.c.) was tested in rats pre-treated with multiple rapid transcranial magnetic stimulation (rTMS) or electroconvulsive shock (ECS). rTMS (B = 1.6T, f = 20 Hz, t = 300 s) was delivered 9 times during 18 days (group rTMS1, total number of stimulations 54,000) or 18 times during 18 days (group rTMS2, total number of stimulations 108,000); ECS (I = 150 mA, f = 50 Hz, t = 500 ms) was delivered 9 times at 48 h intervals. Apomorphine given 24 h after the last treatment induced hyperactivity that was significantly more pronounced in rats receiving ECS and rTMS. The effect was most pronounced for electroconvulsive treatment, the least in the rTMS1 group. The results indicate that an increase in the total number of impulses during the rTMS may increase the responsiveness of rats to dopaminergic stimulation to the level comparable with that induced by ECS.

171

[Zyss:1999ab] T. Zyss, J. Mamczarz, and J. Vetulani. The influence of rapid-rate transcranial magnetic stimulation (rtms) parameters on rtms effects in porsolt's forced swimming test. *Int J Neuropsychopharmacol*, 2(1):31–34, 1999.

> **Abstract:** To assess the similarity of the behavioural effects of the rapid transcranial magnetic stimulation (rTMS) to those produced by other antidepressant treatments, in particular to repeated electroconvulsive shock (ECS), we carried out experiments on Wistar rats. The effects of a standard ECS procedure (9 daily treatments; the current parameters: 150 mA, 50 Hz, 0.5 s) were compared with 18 d treatment with rTMS of the same field intensity of 1.6 T but with different stimulation frequency (20 or 30 Hz) and a different number of sessions (9 or 18). Twenty-four hours after the last treatment the forced swimming test was carried out and the immobility time was recorded. The standard ECT reduced the immobility by 50the intensive rTMS (90 or 104 K impulses for the whole period of

treatment) caused a significant effect, although smaller than that induced by ECT (reduction by 20-30sessions to produce a significant effect, while only 9 sessions with stimulation at 30 Hz were sufficient to produce a comparable result. This suggests that the effectiveness of rTMS may be augmented by increasing the number or frequency of rTMS impulses.

118, 171

List of Figures

List of Tables

GLOSSARY

Here we provide a quick reference guide to commonly used terms in this report. Many of them are straight from Wikipedia.

Term/ Acronym	Description
AC/DC	A legendary rock band formed in Sidney in 1973. Alternating Current and Direct Current. In alternating current (AC, also ac) the movement (or flow) of electric charge periodically reverses direction. An electric charge would for instance move forward, then backward, then forward, then backward, over and over again. In direct current (DC), the movement (or flow) of electric charge is only in one direction.
Action poptential	An action potential is a self-regenerating wave of electrochemical activity that allows nerve cells to carry a signal over a distance. It is the primary electrical signal generated by nerve cells, and arises from changes in the permeability of the nerve cell's axonal membranes to specific ions. Action potentials (also known as nerve impulses or spikes) are pulse-like waves of voltage that travel along several types of cell membranes. The best-understood example of an action potential is generated on the membrane of the axon of a neuron, but also appears in other types of excitable cells, such as cardiac muscle cells, and even plant cells. A typical action potential is initiated at the axon hillock when the membrane is depolarized sufficiently (i.e. when its voltage is increased sufficiently). As the membrane potential is increased, both the sodium and potassium ion channels begin to open. This increases both the inward sodium current and the balancing outward potassium current. For small voltage increases, the potassium current triumphs over the sodium current and the voltage returns to its normal resting value, typically -70 mV. However, if the voltage increases past a critical threshold, typically 15 mV higher than the resting value, the sodium current dominates. This results in a runaway condition whereby the positive feedback from the sodium current activates even more sodium channels. Thus, the cell "fires", producing an action potential. Once initiated, the action potential travels through the axon.
Alveus; Fimbria	The alveus of the hippocampus borders the wall of the lateral ventricle and is composed of white, myelinated fibers. The alveus arises from cell bodies in the subiculum and hippocampus, and eventually merges with the fimbria of the hippocampus. The fimbria goes on to become the fornix. These structures are part of the limbic system.
Anode	A term best avoided. An anode is an electrode through which electric charge flows into a polarized electrical device. The flow of electrons is always from anode to cathode outside of the cell or device, regardless of the cell or device type. In the United States, many battery manufacturers regard the positive electrode as the anode, particularly in their technical literature. This is always the case in the electrical stimulation literature (see, e.g., [Manola:2007aa]).

347

Term/ Acronym	Description
Cathode	A term best avoided. In any case, always the opposite of an Anode.
Crank-Nicolson method	In numerical analysis, the CrankNicolson method is a finite difference method used for numerically solving the heat equation and similar partial differential equations.[1] It is a second-order method in time, implicit in time, and is numerically stable. The method was developed by John Crank and Phyllis Nicolson in the mid 20th century.
Chronaxie	In the mathematical description of the functioning of the nervous system, the chronaxie (or chronaxy) is the minimum time over which an electric current double the strength of the rheobase needs to be applied, in order to stimulate a muscle fiber or nerve cell. The terms "chronaxie" and "rheobase" were coined in 1909 by the French physiologist Louis Lapicque.
CSF	Cerebro spinal fluid. Cerebrospinal fluid (CSF), Liquor cerebrospinalis, is a clear bodily fluid that occupies the subarachnoid space and the ventricular system around and inside the brain. Essentially, the brain"floats" in it. More specifically, the CSF occupies the space between the arachnoid mater (the middle layer of the brain cover, meninges) and the pia mater (the layer of the meninges closest to the brain). It constitutes the content of all intra-cerebral (inside the brain, cerebrum) ventricles, cisterns and sulci (singular sulcus), as well as the central canal of the spinal cord. It acts as a "cushion" or buffer for the cortex, providing a basic mechanical and immunological protection to the brain inside the skull.
DT-MRI	Diffusion tensor MRI. A method that produces in vivo images of biological tissues weighted with the local microstructural characteristics of water diffusion.
EPSP, IPSP	An excitatory postsynaptic potential (EPSP) is a temporary depolarization of postsynaptic membrane potential caused by the flow of positively charged ions into the postsynaptic cell as a result of opening of ligand-sensitive channels. They are the opposite of inhibitory postsynaptic potentials (IPSPs), which usually result from the flow of negative ions into the cell or positive ions out of the cell. A postsynaptic potential is defined as excitatory if it makes it easier for the neuron to fire an action potential. EPSPs can also result from a decrease in outgoing positive charges, while IPSPs are sometimes caused by an increase in positive charge outflow. The flow of ions that causes an EPSP is an excitatory postsynaptic current (EPSC). EPSPs, like IPSPs, are graded (i.e. they have an additive effect). When multiple EPSPs occur on a single patch of postsynaptic membrane, their combined effect is the sum of the individual EPSPs. Larger EPSPs result in greater membrane depolarization and thus increase the likelihood that the postsynaptic cell reaches the threshold for firing an action potential.
EEG	Electroencephalography (EEG) is the recording of electrical activity along the scalp produced by the firing of neurons within the brain.
EP	Evoked Potential. An evoked potential (or "evoked response") is an electrical potential recorded from a human or animal following presentation of a stimulus, as distinct from spontaneous potentials as detected by electroencephalograms or electromyograms.
FE	Finite Elements method.The finite element method (FEM) (sometimes referred to as finite element analysis) is a numerical technique for finding approximate solutions of partial differential equations (PDE) as well as of integral equations.
Fimbria	See Alveus.
fMRI	functional magnetic resonance imaging (MRI). A form of magnetic resonance imaging of the brain that registers blood flow to functioning areas of the brain

Term/ Acronym	Description
GABA	γ-Aminobutyric acid (GABA) is the chief inhibitory neurotransmitter in the mammalian central nervous system. It plays an important role in regulating neuronal excitability throughout the nervous system. In humans, GABA is also directly responsible for the regulation of muscle tone. In insect species GABA acts only on excitatory nerve receptors.
Interneuron	An interneuron (also called relay neuron, association neuron or local circuit neuron) is a multipolar neuron which connects afferent neurons and efferent neurons in neural pathways. Like motor neurons, interneuron cell bodies are always located in the central nervous system (CNS).
MEG	Magnetoencephalography (MEG) is an imaging technique used to measure the magnetic fields produced by electrical activity in the brain via extremely sensitive devices such as superconducting quantum interference devices (SQUIDs). These measurements are commonly used in both research and clinical settings.
MEP	Motor evoked potential response
MRI	Magnetic Resonance Imaging. The use of a nuclear magnetic resonance spectrometer to produce electronic images of specific atoms and molecular structures in solids, especially human cells, tissues, and organs. See also fMRI.
NSE	neuro-specific enolase . Enolase 2 (gamma, neuronal), also known as ENO2 and neuron-specific enolase (abbreviated NSE), is a human gene. It makes a phosphopyruvate hydratase. This gene encodes one of the three enolase isoenzymes found in mammals. This isoenzyme, a homodimer, is found in mature neurons and cells of neuronal origin. A switch from alpha enolase to gamma enolase occurs in neural tissue during development in rats and primates. Detection of NSE with antibodies can be used to identify neuronal cells and cells with neuroendocrine differentiation.
PTZ	Pentylenetetrazol (PTZ) is the International Nonproprietary Name of Metrazol and also known as pentetrazol or pentamethylenetetrazol. It is a drug used as a circulatory and respiratory stimulant (another commercial name is Cardiazol). Larger doses cause convulsions, thus it has been used in shock therapy, as discovered by the Hungarian-American neurologist and psychiatrist Ladislas J. Meduna in 1934. It was never considered to be effective, and side-effects such as seizures are difficult to avoid. Its approval by FDA was revoked in 1982. t is considered a GABA antagonist. The mechanism of the epileptogenic action of PTZ at the cellular neuronal level is still unclear. Electrophysiological studies have shown it acts at cell membrane level decreasing the recovery time between action potentials by increasing potassium permeability of the axon. Other studies have implicated an increase in membrane currents of several other ions, such as sodium and calcium, leading to an overall increase in excitability of the neuron membrane.
rTMS	Repetitive transcranial magnetic stimulation is known as rTMS and can produce longer lasting changes. Numerous small-scale pilot studies have shown it could be a treatment tool for various neurological conditions (e.g. migraine, stroke, Parkinsons Disease, dystonia, tinnitus) and psychiatric conditions (e.g. major depression, auditory hallucinations).
TMS	Transcranial magnetic stimulation (TMS) is a noninvasive method to excite neurons in the brain: weak electric currents are induced in the tissue by rapidly changing magnetic fields (electromagnetic induction). This way, brain activity can be triggered with minimal discomfort, and the functionality of the circuitry and connectivity of the brain can be studied.

Term/ Acronym	Description
LFP	Local Field potential. The extracellular recording of simultanuous evoked synaptic potentials in the population of cells. A local field potential (LFP) is a particular class of electrophysiological signals, which is related to the sum of all dendritic synaptic activity within a volume of tissue.
LTP	Long-term potentiation (LTP) is the long-lasting improvement in communication between two neurons that results from stimulating them simultaneously. Since neurons communicate via chemical synapses, and because memories are believed to be stored within these synapses,[3] LTP is widely considered one of the major cellular mechanisms that underlies learning and memory.
LTD	Long-term depression (LTD) is the weakening of a neuronal synapse that lasts from hours to days. It results from either strong synaptic stimulation (as occurs in the cerebellar Purkinje cells) or persistent weak synaptic stimulation (as in the hippocampus). Long-term potentiation (LTP) is the opposing process
Polarization	A loose term used to describe the transmembrane potential state.
Population spike	The extracellular recording of simultaneous evoked action potentials in the population of cells
Population EPSP	The extracellular recording of simultanuous evoked excitatory synaptic potentials in the population of cells.
Pyramidal cell	Pyramidal neurons (pyramidal cells) are a type of neuron found in areas of the brain including cerebral cortex, the hippocampus, and in the amygdala. Pyramidal neurons are the primary excitation units of the mammalian prefrontal cortex and the corticospinal tract. Pyramidal neurons were first discovered and studied by Santiago Ramón y Cajal. See Figure 3.6.
Rheobase	Rheobase is the minimal electric current of infinite duration (practically, a few hundred milliseconds) that results in an action potential or the contraction of a muscle. In the case of a nerve or single muscle cell, rheobase is half the current that needs to be applied for the duration of chronaxie to result in an action potential or muscle twitch. This can be understood better by looking at a strength duration relationship. This is in short the : "Minimal Electrical current that results in an action potential"
tACS	Transcranial alternating current stimulation. A variant of tCS.
tCS	Transcranial Current Stimulation, a general term englobing tDCS, tACS, tRNS
tDCS	Transcranial direct current stimulation (tDCS) is the application of weak electrical currents (1-2 mA) to modulate the activity of neurons in the brain. Several generations of neurophysiological experiments have shown that neurons respond to static (DC) electrical fields by altering their firing rates. Firing increases when the positive pole or electrode (anode) is located near the cell body or dendrites and decrease when the field is reversed. However, when the electrodes are placed on the scalp, the current density produced in the brain is exceedingly small, changing membrane potentials only by a fraction of a millivolt.
Trans- membrane potential	More precisely, Transmembrane potential *difference*. Membrane potential (or transmembrane potential), is the voltage difference (or electrical potential difference) between the interior and exterior of a cell. Because the fluid inside and outside a cell is highly conductive, whereas a cell's plasma membrane is highly resistive, the voltage change in moving from a point outside to a point inside occurs largely within the narrow width of the membrane itself. Therefore, it is common to speak of the membrane potential as the voltage across the membrane.
tRNS	Transcranial random noise stimulation. A variant of tCS.

Project Summary: Could computers someday interact directly with the human brain? The vision of this four-year project is that in the next 50 years we will witness the coming of age of technologies for fluent brain-computer and computer-mediated brain-to-brain interaction. While recent research has delivered important breakthroughs in brain-to-computer transmission, little has been achieved in the other directioncomputer-controlled brain stimulation. The projects goals is to research stimulation paradigms to design, develop and test a new generation of more powerful and controllable non-invasive brain stimulation technologies. Starting from current distribution and multi-scale neuron-current interaction modelling and stimulation experiments using tDCS, TMS, EEG and fMRI in different scenarios, the project will develop multisite transcranial current stimulation technologies implementing real time EEG monitoring and feedback. It explore high-level communication using stimulation, stimulation during different states of consciousness, stimulation and therapy, as well as sense synthesis, that is, the construction of new perceptions deriving from sensors interacting directly with brains through stimulation systemsall with the goal of probing the limits of non-invasive computer-to-brain interfaces. The project will develop biophysical models for multisite stimulation, carry out stimulation experiments with animals and humans, and integrate the results to develop and test new multisite technologies for interaction. It will also organise two international workshops and carry out dissemination and socio-ethical impact analysis tasks. Given the fundamental role of interaction in human experience, advances in this area can deliver breakthrough information society technologies of great value in addition to advancing the state-of-the-art in fundamental neuroscience research, neurology diagnosis and therapy.

- Consortium: Starlab, Charite, Bangor U, Kapodistiran U of Athens, U of Lisbon, INSERM and U Pablo de Olavide

- Coordinator: Giulio Ruffini (Starlab)

- EU Project Officer: Aymard de Touzalin

http://www.hive-eu.org/
The HIVEproject

Released: 09 June, 2009

THE HIVE PROJECT - HYPER INTERACTION VIABILITY EXPERIMENTS

Could computers someday interact directly with the human brain? In the next 50 years we will witness the coming of age of technologies for fluent brain-computer and computer-mediated brain-to-brain interaction. While recent research has delivered important breakthroughs in brain-to-computer transmission, little has been achieved in the other direction – computer-controlled brain stimulation. HIVE is a FET Open FP7 EU project. Our goal is to research stimulation paradigms to design, develop and test a new generation of more powerful and controllable non-invasive brain stimulation technologies. HIVE will develop improved electrical current distribution and multi-scale neuron-current interaction models and carry out stimulation experiments using tDCS, TMS, EEG and fMRI in different scenarios, and based on these develop multisite transcranial current stimulation technologies implementing real time EEG monitoring and feedback. HIVE will also explore high-level communication using stimulation, stimulation during different states of consciousness, stimulation and therapy, as well as 'sense synthesis', that is, the construction of new perceptions deriving from sensors interacting directly with brains through stimulation systems – all with the goal of probing the limits of non-invasive computer-to-brain interfaces. We believe that given the fundamental role of interaction in human experience, advances in this area can deliver breakthrough technologies of great value in addition to advancing the state-of-the-art in fundamental neuroscience research and neurology.

hiVE
HYPER
INTERACTION
VIABILITY
EXPERIMENTS

PRODUCED BY:

Starlab
Living Science